1992

PRESSURE FLUCTUATIONS IN TWO-PHASE FLOWS

Samways, Andrew Leonard

PRESSURE FLUCTUATIONS IN TWO-PHASE FLOWS

Andrew Leonard Samways

B.Eng.(hon)

Submitted to the Council for National Academic Awards
in partial fulfilment for the Degree of Doctor of Philosophy

Sponsoring Establishment:

University of Plymouth
School of Manufacturing, Materials and Mechanical Engineering

Collaborating Establishment:

Schlumberger Cambridge Research Ltd.

July 1992

PRESSURE FLUCTUATIONS IN TWO-PHASE FLOWS

by
Andrew Leonard Samways B.Eng.(hon)

ABSTRACT

Naturally occurring pressure fluctuations have been observed in two-phase flows by a number of researchers for example *Matsui* [1984]. This thesis investigates the nature of these pressure fluctuations within vertically upward bubbly two-phase flows with a view to developing a novel non-intrusive pressure correlation technique for use downhole to monitor the area average dispersed phase velocity, V_g. To date non-intrusive correlation flow monitoring techniques suitable for use downhole exhibit a non-uniform field sensitivity characteristic which when correlated between two points reflects the velocity of the dispersed phase within the stronger sensing region.

Four sources of pressure fluctuations were identified in the present study, these being temporal variations in the average gas void fraction $\alpha(t)$, variations in the convected pressure field surrounding a moving bubble, turbulence generated by the wake of a bubble and background turbulence in the continuous phase. Magnitudes and structure length scales of these pressure sources were evaluated differentially at two points in a continuous fluid using simple models and it was found that pressure fluctuations associated with a bubbles motion close to the measurement points dominate the pressure signal. It was also found that the magnitude of pressure fluctuations associated with a bubble's motion decreases rapidly with increasing distance from the bubble and the structure length scale caused by this effect is of the order of the tapping separation distance.

Using numerical simulation techniques and a recirculating air/water flow loop with a test section diameter of 77.8mm, (both of which were developed in this thesis) differential pressure fluctuations generated by an upwardly flowing bubbly two-phase flow w ere studied. Superficial gas and liquid velocities up to 0.35m/s and 1.5m/s respectively and average gas void fractions up to 25% were covered. It was concluded that pressure fluctuations caused by bubble motion near the pipe wall dominate the differential pressure signal. The autocorrelogram of these signals is considered to be related to the bubble velocity within the entrapped bubble layer near the pipe wall, which are observed to travel at an almost constant velocity independent of the continuous phase velocity. Cross correlation of two pressure signals are indicated to be related to the convected bubble velocity of bubbles outside the entrapped bubble layer which is related to V_g.

CONTENTS

	Page
ABSTRACT	**2**
CONTENTS	**3**
TABLES	**11**
FIGURES	**12**
PREFACE	**20**
ACKNOWLEDGEMENT	**22**
DECLARATION	**23**
NOMENCLATURE	**24**
CHAPTER 1 - AN INTRODUCTION TO TWO-PHASE FLOW AND A DISCUSSION OF THE NEED TO DEVELOP NOVEL MASS FLOW MONITORING TECHNIQUES FOR USE DOWNHOLE	**29**
Chapter summary	29
1.1 An introduction to two-phase flow	30
1.2 Classification of flow regimes found in two-phase flow	30
1.2.1 The bubbly flow regime	31
1.2.2 The slug flow regime	32
1.2.3 The churn/froth flow regime	33
1.2.4 The annular/mist flow regime	34
1.3 Present measurement techniques used in downhole drill stem testing	34
1.3.1 Average gas void fraction measurements (gradiomanometer)	37

1.3.2 Velocity measurements 37
1.3.3 Limitations of the present measurement tools used in downhole DST tests 41

1.4 Aims of this study programme 43

1.4.1 Investigation of the statistical properties of pressure fluctuations in two-phase flow 44
1.4.2 Use of cross correlation techniques on differential pressure fluctuations in a bubbly two-phase flow as a means of measuring the area averaged gas velocity 45

CHAPTER 2 - REVIEW OF PREVIOUS RESEARCH IN TWO-PHASE FLOW MEASUREMENT TECHNIQUES 50

Chapter summary 50

2.1 Methods used to measure average gas void fractions in two-phase flow 51

2.1.1 On-line sampling using quick closing valves 51
2.1.2 Radiation absorption techniques used for measuring void fraction 53
2.1.3 Void fraction measurement using ultrasonics 55
2.1.4 Impedance measurement techniques used to measure average gas void fractions 56
2.1.5 Average gas void fraction measurements made using differential pressure measurements (gradiomanometer) 58

2.2 Local void fraction measurement techniques 59

2.2.1 Local void fraction measurements using a resistive probe 60
2.2.2 Local void fraction measurements using fibre optics 62
2.2.3 Local void fraction measurements using hot-wire/film anemometry 63

2.3 Objective flow regime identification in vertical two-phase flow 65

2.3.1 Flow regime identification using pressure fluctuations 68

2.4 Measurement of the dispersed gas or bubble velocity in vertically upward bubbly two-phase flow 74

2.4.1 Basic principles of random data analysis 75
2.4.2 Previous research into cross correlation as a means of measuring the area averaged dispersed phase velocity 79
2.4.3 Use of pressure fluctuations in the measurement of the dispersed phase velocity 83

CHAPTER 3 - DESIGN AND CONSTRUCTION OF THE EXPERIMENTAL VERTICAL TWO-PHASE FLOW LOOP 101

Chapter summary 101

3.1 Design and general description of the air/water two-phase flow loop 102

3.2 Structural construction details of the air/water flow loop 103

3.3 Techniques and instrumentation for the measurements of superficial gas and liquid velocities 104

3.3.1 Measurement of the superficial gas velocity 104
3.3.2 Measurement of the superficial liquid velocity 108

3.4 Development and implementation of the control algorithm used to regulate the air/water flow loop 110

CHAPTER 4 - COMMISSIONING OF THE AIR/WATER FLOW LOOP AND COMPARISON OF RESULTS OBTAINED FROM THE FLOW LOOP WITH EXISTING TWO-PHASE FLOW THEORY 123

Chapter summary 123

4.1 Measurement of average gas void fraction 124

4.1.1 Measurement of average gas void fraction using quick closing gate valves 124
4.1.2 Measurement of average gas void fraction using the gradiomanometer 125

4.2 Friction factor measurements in the test section of the air/water flow loop 129

4.2.1 Friction factors in single phase flow 130
4.2.2 Measured values of friction factor within two-phase flow in the vertical test section 130
4.2.3 Comparison of theoretical and experimental friction factor values 131

4.3 Comparison of results obtained for the average gas void fractions for the quick closing valves and the gradiomanometer 132

4.4 Area averaged gas and liquid velocities 133

4.4.1 Local velocity distribution in the experimental test section 135
4.4.2 Local gas void fraction distribution $\alpha_l(r)$ in the experimental test section 136

4.5 Comparison of the area averaged gas velocities obtained by the *Zuber/Findlay* theory and experimental results from the quick closing valves and gradiomanometer 138

4.6 General conclusions drawn from initial experiments carried out in the two-phase flow loop 139

CHAPTER 5 - BUBBLE DYNAMICS AND SOURCES OF PRESSURE FLUCTUATIONS IN TWO-PHASE BUBBLY FLOW 150

Chapter summary 150

5.1 Bubbles dynamics 152

5.1.1	Simple dynamics and drag coefficient of a single bubble	152
5.1.2	Terminal rise velocity of a single bubble from simple theory	155
5.1.3	Theoretical critical bubble diameter and velocity	157
5.1.4	Empirical expressions for variations in terminal bubble rise velocity with changing average gas void fraction	160
5.1.5	Comparison of the theoretical terminal rise velocity and nominal bubble diameter with measurements made using high speed photography	161
5.2	Source of pressure fluctuations in bubbly vertical two-phase flow	164
5.2.1	Pressure fluctuations caused by temporal variations in the average gas void fraction	165
5.2.2	Pressure fluctuations caused by variations in the continuous phase velocity profile around a near spherical bubble	170
5.2.3	Pressure fluctuations in the continuous phase caused by the continuous phase background turbulence and the wake generated by a bubble	177
5.3	Development of measurement techniques used to measure differential pressures	182
5.3.1	Differential pressure measurements obtained by subtracting two static pressure signals	182
5.3.2	Measurement of differential pressure fluctuations using a single differential pressure transducer	185
5.3.3	Design and construction of a housing for mounting the differential pressure transducer	189
5.4	Comparison of theoretical and experimental pressure fluctuations	190
5.4.1	Experimental differential pressure fluctuations caused by a moving sphere in a pipe containing stagnant water	191

5.4.2 Experimental differential pressure fluctuations caused by a single stream of bubbles at low frequencies of generation in a pipe containing stagnant water 194

5.4.3 Comparison of theoretical and experimental differential pressure fluctuations in a standing column of water 195

5.5 Conclusions drawn from the theoretical models and experimental results within chapter 5 198

CHAPTER 6 - AUTO AND CROSS CORRELATION OF PRESSURE FLUCTUATIONS IN BUBBLY TWO-PHASE FLOW 229

Chapter summary 229

6.1 An introduction to the pressure correlation principle 231

6.1.1 Conventional frozen and diffused correlation models 233

6.1.2 Correlation techniques of differential pressure measurements 235

6.2 Previous bubbly two-phase flow correlation techniques 239

6.3 Modelling technique used to simulate bubbly two-phase flow in a vertical pipe 245

6.3.1 Contribution from temporal variations in the average gas void fraction 246

6.3.2 Contribution from the convected bubble pressure field 248

6.3.3 Computer modelling techniques used to simulate bubbly two-phase flow 251

6.3.4 Results of two-phase flow modelling 255

6.4 Initial experimental autocorrelations from a single differential pressure transducer 263

6.5 Modifications to experimental apparatus used to measure differential pressure fluctuations for use in cross correlation flow measurement techniques 267

6.5.1 Transducer matching 270

6.6 Experimental results obtained from auto and cross correlation correlograms 272

6.6.1 Auto and cross correlation experimental results 273
6.6.2 Discussion of experimental results 275

6.7 Experimental measurement of the convected bubble velocity in a circular annulus 279

6.7.1 Experimental auto and cross correlation results in a circular annulus 281
6.7.2 Discussion and comparison of experimental convected disturbance velocity measurements made in a circular annulus with those made in a full pipe 283

6.8 Conclusions of experimental results 285

CHAPTER 7 - GENERAL CONCLUSIONS AND FURTHER INVESTIGATIONS 340
Chapter summary 340

7.1 Conclusions drawn from the studies carried out in this thesis relating to the suitability of naturally occuring pressure fluctuations within a bubbly two-phase flow as a means of monitoring the area averaged gas velocity V_g, downhole 341

7.2 Further work 343

7.2.1 The need for further investigation of local void fraction profiles $\alpha_l(r)$ and local gas velocity profiles $v_g(r)$ in vertically upward bubbly two-phase flow 344
7.2.2 Further two-phase flow simulations 345

7.2.3 Possible improvement of the convected disturbance velocity measurement technique 346

APPENDIX 1 - FLOW LOOP INSTRUMENTATION CALIBRATION DETAILS 348

APPENDIX 2 - TWO-PHASE AIR/WATER FLOW LOOP CONTROL SOFTWARE 358

APPENDIX 3 - PSEUDO-RANDOM LOW AVERAGE GAS VOID FRACTION PRESSURE FLUCTUATION SIMULATION SOFTWARE 372

APPENDIX 4 - GENERAL PURPOSE SIGNAL ANALYSIS SOFTWARE 395

LIST OF REFERENCES 426

TABLES

6.1 Ratio of simulated convected disturbance velocity V_{g_1} over the area averaged gas velocity V_g as a function of the local velocity and gas void fraction profile powers m and n respectively 258

6.2 Ratio of simulated convected disturbance velocity V_{g_2} over the area averaged gas velocity V_g as a function of the local velocity and gas void fraction profile powers m and n respectively 259

6.3 Ratio of simulated convected disturbance velocity V_{g_3} over the area averaged gas velocity V_g as a function of the local velocity and gas void fraction profile powers m and n respectively 260

6.4 Experimental results of auto and cross correlation convective velocity measurements for flow in a full pipe 273

6.5 Experimental results of auto and cross correlation convective velocity measurements for flow in a circular annulus 282

FIGURES

Chapter1

1.1 Flow regime map produced from data by *Govier, Radford, & Dunn* [1957] for air/water mixtures in a 1 inch pipe 47

1.2 Typical Slug flow profile in gas/liquid vertically upward two-phase flow 48

1.3 Average gas void fraction measurement using the gradiomanometer technique 49

Chapter2

2.1 Illustration of the quick closing valve technique used to measure average gas void fractions 86

2.2a Schematic diagram of the radiation absorption technique illustrating a hypothetical flow pattern put forward by *Petrick & Swanson* [1958] in which the gas and liquid phases are arranged perpendicular to the collimated beam of radiation 87

2.2b Schematic diagram of the radiation absorption technique illustrating a hypothetical flow pattern put forward by *Petrick & Swanson* [1958] in which the gas and liquid phases are arranged in layers parallel to the collimated beam of radiation (pseudo slug flow) 87

2.3 Illustration of the capacitance average void fraction monitoring transducer developed by *Lucas* [1987] 88

2.4 Principle of local void fraction measurement 89

2.5 Illustration of the resistance probe technique used to measure local void fractions 90

2.6 Fibre optic probe as used by *Lance & Bataille* [1991] to measure local void fractions 91

2.7 Typical signal from a hot-film probe positioned in a two-phase flow when interacting with a discrete bubble 92

2.8 Typical flow regime map produced by objectively discriminating between flow regimes 93

2.9a Probability density function produced by *Jones & Zuber* [1975] of the fluctuations in average gas void fraction α made using an x-ray void fraction technique of vertically upward bubbly two-phase flow within a rectangular duct 94

2.9b Probability density function produced by *Jones & Zuber* [1975] of the fluctuations in average gas void fraction α made using an x-ray void fraction technique of vertically upward annular two-phase flow within a rectangular duct 94

2.9c Probability density function produced by *Jones & Zuber* [1975] of the fluctuations in average gas void fraction α made using an x-ray void fraction technique of vertically upward slug two-phase flow within a rectangular duct 94

2.10 Probability density distribution produced by *Nishikawa* [1969] of the static pressure fluctuations in vertically upward bubbly two-phase flow within a circular pipe 95

2.11 Pressure transducer arrangement used by *Matsui* [1984] in his investigation into flow regime identification using the naturally occuring pressure fluctuations within a two-phase flow 96

2.12 Taitel-type flow regime map produced using an autoregressive moving average (ARMA) model of static and differential pressure measurements developed by *King et al* [1987] 97

2.13 Typical autocorrelation correlogram of a stationary ergodic random signal 98

2.14 Typical cross correlation correlogram of two stationary ergodic random signals 98

2.15 Hypothetical transducer arrangement for use in cross correlation measurements of the area averaged dispersed phase velocity 99

2.16a Decay of the cross correlation coefficient $\rho_{xy}(\tau)$ as a function of transducer separation distance l in experiments carried out by *Ong* [1975] using a pair of ultrasonic transducers 100

2.16b Variation in standard error $\epsilon(\tau)$ (defined by *Ong* [1975]) as a function of transducer separation distance l 100

Chapter 3

3.1 Schematic diagram of the two-phase air/water flow loop constructed at Polytechnic South West 113

3.2 Air/water flow loop nominal pipe diameters 114

3.3 Computer controlled needle valve used to regulate the mass flow rate of air entering the test section 115

3.4 Construction details of sharp edged orifice used to measure the air mass flow rate entering the test section 116

3.5 Experimental set up used to calibrate the air mass flow rate orifice plate 117

3.6 Circuit diagram of the four active arm Wheatstone bridge instrument amplifier used in conjunction with the 1 & 2 Bar pressure transducers 118

3.7 Frequency to voltage converter, amplifier, and low-pass filter circuit used in conjunction with the water volume flow rate turbine type flow transducer 119

3.8 Schematic diagram of computer interfacing with the air/water flow loop 120

3.9 Block diagram of the closed loop control algorithms used to control the two-phase flow loop 121

3.10 Flow chart of software used to control the air/water flow loop 122

Chapter4

4.1 Single phase (water) friction factors in the experimental test section 141

4.2 Two-phase flow friction factors in the experimental test section 142

4.3 Comparison of average gas void fractions measured using the quick closing valve and gradiomanometer techniques 143

4.4 Variation in distribution coefficient C_o produced by *Zuber/Findlay* [1965] 144

4.5 Experimental set up used to measure single phase (water) velocity profiles in the experimental test section 145

4.6 Non-dimensional single phase (water) velocity profile in the experimental test section 146
4.7 Resistive probe technique used in the experimental test section to measure the local gas void fraction profile 147
4.8 Non-dimensional local gas void fraction profile in the experimental test section for average gas void fractions of approximately 5, 11, 18% 148
4.9 Area averaged gas velocity V_g predicted by the *Zuber/Findlay* relationship and the experimental measurements of average gas void fraction using the quick closing valve technique and gradiomanometer 149

Chapter5

5.1 Calculated shape of bubbles as functions of Reynolds and Weber numbers, *Ryskin & Leal* [1985] 201
5.2 Calculated bubble drag coefficients, *Ryskin & Leal* [1985] 202
5.3 Experimental drag coefficient of a solid sphere as a function of the Reynolds number, *Massey* [1968] 203
5.4 Experimental measurement of terminal bubble rise velocity $V_{g\infty}$ as a function of the equivalent bubble diameter for air in water at 20°C, *Clift et al* [1978] 204
5.5 Variation in the superficial gas velocity V_{sg} as a function of the average gas void fraction α, where V is the continuous phase velocity, *Wallis* [1969] 205
5.6 Typical frame of high speed film used to estimate the variation in terminal bubble rise velocity $V_{g\infty}$ in the experimental test section of the present study, $V_{sl} = 0$ and $\alpha < 5\%$ 206
5.7 Single bubbles tracked over 9 consecutive frames of high speed film representing 0.2 seconds 207
5.8 Diagrammatic representation of differential pressure measurements performed in the present study 208
5.9 Theoretical analysis of variation in the local average gas void fraction 209

5.10 Statistical model used to predict the variation in local average gas void fraction assuming a uniform probability density distribution and by estimating the r.m.s. error ϵ in a small sample 209

5.11 Estimated magnitude of r.m.s. pressure fluctuations $\Delta P'$ generated by variations in local average gas void fraction as a function of the average gas void fraction α and tapping separation distance l 210

5.12 Estimated variations in the ratio of r.m.s. pressure fluctuations to the mean differential pressure ($\Delta P'/\Delta P_h$) caused by variations in local average gas void fractions plotted as a function of the average gas void α fraction and tapping separation distance l 211

5.13 *Butlers* sphere theorem for a sphere travelling with a constant velocity through an infinitely large incompressible inviscid fluid 212

5.14 Estimated peak pressure fluctuations P_{peak} caused by the motion of a single sphere as a function of pipe wall to sphere centre separation distance 213

5.15 Diagrammatic representation differential pressure measurement 214

5.16 Recorded pressure signals generated as a sphere of radius a = 3mm travels with a constant velocity, V_∞, past two fixed pressure measuring points, 1 and 2, at a distance R = 4.5mm 215

5.17 Theoretical differential pressure signal generated by a moving sphere derived from *Butlers* sphere, as a function of the pipe wall to sphere centre separation distance 216

5.18 Turbulent intensity in the continuous phase generated by air bubbles in water where the continuous phase has a background turbulence generated by a 40mm grid. Turbulent intensity is plotted as a function of the average gas void fraction and area averaged liquid velocity, *Lance & Bataille* [1991] 217

5.19 Arrangement of Endevco static pressure transducers and associated instrument amplifiers initially used to study differential pressure fluctuations 218

5.20 Diagrammatic representation of the single Validyne differential pressure transducer used in the present study to investigate differential pressure fluctuations 219
5.21 Photograph of Validyne differential pressure transducer mounting facility 220
5.22 Validyne differential pressure transducer housing/mounting facility 221
5.23 Schematic diagram of differential pressure transducer water purging and back flushing arrangement 222
5.24 Experimental apparatus used to measure differential pressure fluctuations generated by the motion of a sphere in a stagnant column of water 223
5.25 Photograph of experimental apparatus used to measure differential pressure fluctuations generated by the motion of a sphere in a stagnant column of water 224
5.26 Differential pressure signal measured experimentally and calculated from equation 5.46 generated by a moving sphere of diameter 6.5mm travelling with a constant velocity of 0.25m/s at a fixed wall to sphere centre separation distance of 4.5mm 225
5.27 Comparison of normalised peak fluctuations in differential pressure generated by a sphere moving at constant velocities of 0.1, 0.25 and 0.4m/s, plotted as a function of the ratio of the pipe wall to sphere centre separation distance over the sphere radius 226
5.28 Arrangement of apparatus used to measure fluctuations in differential pressure generated by a low frequency single stream of bubbles in a stagnant column of water 227
5.29 Comparison of theoretical and experimental fluctuations in differential pressure caused by the motion of a sphere/bead/bubble with a velocity of 0.25m/s 228

Chapter 6

6.1 Frozen pattern correlation model 287
6.2 Diffused pattern model and auto/cross correlation correlogram 288
6.3 Frozen and diffused pattern autocorrelations of pressure fluctuations within a bubbly two-phase flow 289

6.4 Arrangement of the differential pressure tappings 1, 2, 3 and 4 used to measure ΔP_A and ΔP_B in the present study, and the interpretation of a typical cross correlation developed in this study 290

6.5 Observed bubble motion by *Lance*, *Bataille* and *Marie'* at the *Laboratorire de Mecanique des Fluides et d'Acoustique*, *Lyon* 291

6.6 Illustration of local gas velocity and void fraction profiles, $v_g(r)$ and $\alpha_l(r)$ respectively 292

6.7 Illustration of the bubbly two-phase flow correlation simulation model and co-ordinate system developed in the present study 293

6.8 Illustration of temporal variations in the average gas void fraction $\alpha(t)$ in a bubbly two-phase flow 294

6.9 Diagram illustrating the nomenclature used in the evaluation of the pressures measured by two differential pressure transducers, A and B, caused by the convected pressure field surrounding a moving bubble 295

6.10 Illustration of the annular technique used to simulate local gas void fraction profiles $\alpha_l(r)$ within a bubbly two-phase flow 296

6.11 Comparison of magnitudes between the two pressure sources considered in the bubbly two-phase flow simulations 297

6.12 Convected disturbance velocity ratio evaluations from the simulated differential pressure fluctuations displayed as functions of the local gas void fraction and velocity profile powers n and m respectively 298

6.13 Typical autocorrelation correlogram of a simulated bubbly two-phase flow 299

6.14a Measured autocorrelation of differential pressure fluctuations in a stagnant column of liquid with an average gas void fraction $\alpha \simeq 10\%$ 300

6.14b Measured autocorrelation of differential pressure fluctuations, $V_{sl} = 0.64$ m/s, and $\alpha \simeq 10\%$ 301

6.14c Measured autocorrelation of differential pressure fluctuations, $V_{sl} = 1.0$ m/s, and $\alpha \simeq 10\%$ 302

6.14d Measured autocorrelation of differential pressure fluctuations, $V_{sl} = 1.5$ m/s, and $\alpha \simeq 10\%$ 303

6.15 Transducer housing pressure tappings insert machining detail 304
6.16 Transducer housing detail 305
6.17 Variation between the tapping separation distance of transducer A, l_A, and transducer B, l_B 306
6.18 Predicted percentage error in cross correlation convected velocity measurement as a function of the variation in transducer tapping separation distances l_A and l_B 307
6.19 Photograph of the experimental test section showing the differential pressure transducer housing and the eccentric mass used to excite and match the differential pressure transducers 308
6.20 Measured auto and cross correlation correlograms of differential pressure fluctuations in bubbly flow 309
6.35 Convected disturbance velocity ratio V_{g_2}/V_g evaluations for non-zero continuous phase flows plotted as a function of the average gas void fraction α 325
6.37 Illustration of experimental annular two-phase flow setup 326
6.38 Measured auto and cross correlation correlograms of differential pressure fluctuations in bubbly two-phase within an annulus 327
6.50

Appendix 1

A1.1 Orifice plate calibration. Velocity profile of air exhausted from a 1" diameter pipe 356
A1.2 Turbine flowmeter calibration. Volume flow rate of water as a function of the output voltage from the frequency to voltage converter 357

PREFACE

For many years, engineers and scientists in industries such as the nuclear and oil industries have been interested in the properties of two-phase flows which has prompted numerous research studies. In recent years the oil industry has expressed an interest in the measurement of oil/gas/water properties and flow rates 'downhole' in the well, the aim of these measurements being to obtain a better understanding of the well structure and expected life. One of the parameters of particular interest is the mass flow rate of gas in a two-phase gas/liquid flow. The mass flow rate of gas in a steady state two-phase flow can be evaluated as

$$\dot{m}_g = \int\int_A \rho_g \, \alpha_l \, v_g \, dA$$

where ρ_g is the gas density, α_l the local gas void fraction, v_g the local gas velocity and 'A' being the cross-sectional area of the pipe or duct over which the local properties are integrated.

Due to the extremely harsh conditions encountered downhole intrusive flow measurements are not possible, this makes local measurements extremely difficult to monitor. However, if the averaged gas void fraction, α, and the area averaged gas velocity, V_g, could be measured downhole, then an approximation to the mass flow rate of gas could be made from

$$\dot{m}_g = \rho_g \, \alpha \, V_g \, A$$

Using existing technology the average gas void fraction, α, is

currently evaluated downhole using the gradiomanometer technique. The gradiomanometer, which is described in some detail in section 2.1.5, basically relates the differential pressure ΔP measured along a straight pipe to the average gas void fraction α. However, existing non-intrusive measurement techniques of the area averaged gas velocity, V_g, are either toobulky and hence not suitable for downhole use, or appear to be dependent on the local gas velocity profile $v_g(r)$.

Pressure measurements made by differential pressure transducers placed downhole have been found to give reliable and consistent results in the harsh environment they encounter and are made use of by the gradiomanometer. It has been reported by a number of researchers in the field of two-phase flow (see, for example, *Matsui* [1984]) that observed naturally occurring pressure fluctuations within a bubbly two-phase flow are related to the motion of the bubbles within the flow. If pressure fluctuations at one point in the flow could be detected (by correlation techniques) at another point in the flow down-stream of the first, it may be possible to relate the time of flight of the moving convected disturbances within the two-phase flow to the area averaged gas velocity v_g, and hence develop a novel non-intrusive technique for monitoring the area averaged gas velocity.

Consequently, the aims of the thesis are to investigate naturally occurring pressure fluctuations within a bubbly two-phase flow and evaluate the possibility of using correlation techniques as a means of monitoring the area average gas velocity.

ACKNOWLEDGEMENT

I would like to express my thanks to Professor Les Bradbury, who acted as my director of studies, for initiating this project in conjunction with Schlumberger Cambridge Research Ltd. and whose little guidance was immeasurable in the later stages of this project.

I would also like to extend by gratitude to Dr. Phil James who stepped in towards the end of this project and took over as internal supervisor on the retirement of Professor Bradbury, and without whose administrative skills I am sure this thesis would not have been completed.

Dr. Andy Hunt, my industrial supervisor at Schlumberger Cambridge Research Ltd., was of considerable assistance in both providing equipment for this project and financial support in the latter stages of the research programme. I would like to express my appreciation to all the staff of the Fluid Mechanics Department at SCR for their help when visiting the Cambridge site.

I would also like to acknowledge my fellow researchers and members of academic staff in the School of Manufacturing, Materials and Mechanical Engineering at the University of Plymouth. In particular Mr Tony Fell whose many varied and interesting conversations I found particularly stimulating. Dr. Mansel Davis who consistently solved mathematical and computer problems when presented with them, and Mr Peter Nurse who was a constant source of inspiration and whose practical engineering knowledge seemed limitless at times.

I would like to extend my appreciation to all the technical

staff within the department and to the Technical Services Department (Mechanical and Electrical) who I am sure all assisted me at some stage during my time in Plymouth. In particular I would like to thank Mr Rob Crocker, whose excellent technical skills were continuously tested during his almost single handed construction of the experimental apparatus used in this study, and who was forced to enjure my constant nagging throughout this project.

Finally I would like to express my sincere thanks to Dr. Hans Bruun, whose constructive criticism during the preparation of this thesis was both essential and greatly appreciated.

DECLARATION

No portion of the work referred to in this thesis has been submitted in support of an application for another degree or qualification of this or any other university or institute of learning.

NOMENCLATURE

This section contains a list of most of the algebraic symbols used in this thesis. Some symbols have more than one meaning however, the one symbol will not have two different meanings in the same section and where possible the section to which the meaning of a symbol belongs will be indicated.

a	-	Radius of a sphere
d	-	Bubble diameter
d_c	-	Critical bubble diameter
d_o	-	Orifice plate orifice diameter
e_f	-	Frictional loss per kg mass (section 4.1.2)
f	-	Non-dimensional friction factor
g	-	Gravity ($9.81 m/s^2$)
h	-	Gradiomanometer wall pressure tappings separation distance (chapter 4)
h	-	Differential pressure transducer separation distance (chapter 6)
h_t	-	Tracer injection to detection separation distance
k	-	A constant
k_o	-	Orifice plate calibration constant
l	-	Transducer separation distance
l_A	-	Upstream pressure transducer tappings separation distance
l_B	-	Down-stream pressure transducer tappings separation distance
m	-	Local mixture velocity profile power exponent
m	-	Average number of bubbles (section 5.2.1)
$\dot{m}_g$	-	Mass flow rate of gas
n	-	Local gas void fraction profile power exponent
n	-	Number of orifices (section 5.1.3)
p_{21}	-	Wall differential pressure (p_2-p_1) *Nishikawa et al* [1969]
r	-	Radial distance
r.m.s.	-	Root mean square of a signal
t	-	Time
t_g	-	Time spent in gas phase during local gas void fraction measurements

t_t - Total sample time in local gas void fraction measurements

v_b - Bubble velocity

v_b - Volume of bubble (section 5.1.3)

v_b^* - Volume of bubble at generation from an orifice *Yip et al* [1970] (section 5.1.3)

v_g - Volume of gas (chapter 1)

$v_g(r)$ - Local gas velocity as a function of the pipe radius

v_l - Volume of liquid (chapter 1)

v_t - Mixture volume ($v_g + v_l$)

w - Probability density interval width (section 5.2.1)

x(t) - Discrete values in time of a signal x (section 2.4)

y(t) - Discrete values in time of a signal y (section 2.4)

z - Vertical distance from a given point

A - Cross sectional area of the experimental test section

A_{DST} - Internal area of drill stem test tool

B - Signal bandwidth

C_d - Drag coefficient

C_o - Distribution coefficient defined by *Zuber & Findlay* [1965]

D - Internal test section diameter (77.8mm)

F_b - Buoyancy force

F_d - Drag force

F_m - Frictional pressure loss

I_g - Radiation intensity through a column of gas

I_l - Radiation intensity through a column of liquid

I_m - Measured radiation intensity of a two-phase flow

L - Total length (section 5.2.1)

L_t - Ultrasonic transducer separation distance (section 2.1.3)

N - Total number of bubbles (section 5.2.1)

P_r - Amplitude of received pulse of ultrasound

P_t - Amplitude of transmitted pulse of ultrasound

P_{peak} - Peak pressure fluctuation caused by the motion of a single sphere derived from Butlers sphere theorem

P_1 - Initial reservoir pressure (chapter 1)

P_2 - Reservoir pressure during flowing (chapter 1)

P_1 - Wall pressure tapping 1 (most upstream)

P_2 - Wall pressure tapping 2

P_3 - Wall pressure tapping 3

P_4 - Wall pressure tapping 4 (most down-stream)

P_o - Pressure at infinite

R	-	Internal pipe radius (D/2)
R	-	Gas constant (chapter 3)
R.M.S.	-	Root mean square of any signal (section 2.4.1)
Re	-	Reynolds number Vl/ν
Re_b	-	Reynolds number based on bubble diameter $V_g d/\nu$
Re_D	-	Reynolds number based on the inner diameter of the test section $V_l D/\nu$
$R_{xx}(\tau)$	-	The autocorrelation function of a signal x as a function of the time delay τ
$R_{xy}(\tau)$	-	The cross correlation function of two signals x and y as a function of the time delay τ
SD	-	Standard deviation (positive square root of the variance σ^2)
T	-	Sampling time (section 2.4)
T	-	Absolute temperature at the orifice plate (chapter 3)
T_t	-	Time taken for tracer injected at a point upstream to flow down-stream to a second point
V_c	-	Centreline mixture velocity (section 4.4)
V_g	-	Area averaged gas velocity
V_{g_1}	-	Autocorrelation convected disturbance velocity
V_{g_2}	-	Cross correlation convected disturbance velocity evaluated over the shorter 6mm correlation length scale
V_{g_3}	-	Cross correlation convected disturbance velocity evaluated over the longer 25mm correlation length scale
$\dot{V}_g$	-	Volume flow rate of gas
$V_{g\infty}$	-	Terminal rise velocity of a single bubble
V_l	-	Area averaged liquid velocity
V_l	-	Local mixture velocity (section 4.4)
$\dot{V}_l$	-	Volume flow rate of liquid
$\dot{V}_m$	-	Area averaged mixture velocity ($V_{sg} + V_{sl}$)
V_m	-	Mixture volume flow rate
V_r	-	Velocity vector (section 5.2.2)
V_{sg}	-	Superficial gas velocity
V_{sl}	-	Superficial liquid velocity
V_{turb}	-	Turbine flowmeter output voltage
V_θ	-	Velocity vector (section 5.2.2)
V_ψ	-	Velocity vector (section 5.2.2)
$\underline{V}$	-	Magnitude of velocity vectors ($\underline{V}^2 = V_r^2 + V_\theta^2 + V_\psi^2$)
V_∞	-	Uniform velocity (section 5.2.2)

W_b - Weber number based ob bubble diameter $\rho_g V_g^2 d/\sigma$

α - Average gas void fraction

α_c - Chordal-average gas void fraction

$\alpha_l(r)$ - Local gas void fraction as a function of the pipe radius

$\alpha(t)$ - Temporal variations in the average gas void fraction (section 6.3.1)

α_w - Wall gas void fraction defined by *Zuber & Findlay* [1965]

α' - R.m.s fluctuations in the average gas void fraction

θ - Angle of inclination to the flow (section 5.2.2)

ϵ - R.m.s error (chapter 5)

$\epsilon(\tau)$ - Standard error as a function of the correlation time delay τ defined by *Ong* [1975]

ν - Kinematic viscosity

μ - The mean of any signal (section 2.4.1)

π - Pi (3.14159)

ρ_g - Density of gas

ρ_l - Density of liquid

ρ_m - Mixture density

$\rho_m(t)$ - Mixture density as a function of time (section 6.3.1)

ρ_{man} - Density of manometer fluid

ρ_o - Density of air at the orifice plate

$\rho_{xx}(\tau)$ - Normalised autocorrelation coefficient of a signal x as a function of the time delay τ

$\rho_{xy}(\tau)$ - Normalised cross correlation coefficient of two signals x and y as a function of the time delay τ

$\rho_{AA}(\tau)$ - Normalised autocorrelation coefficient of the differential pressure signal $\Delta P_A(t)$

$\rho_{AB}(\tau)$ - Normalised cross correlation coefficient of the differential pressure signals $\Delta P_A(t)$ and $\Delta P_B(t)$

σ - Surface tension of the gas/liquid interface

σ^2 - The variance of a signal

τ - Time delay in auto and cross correlations

τ_1 - Autocorrelation transient time associated with a correlation length scale of 25mm

τ_2 - Cross correlation transient time associated with the shorter 6mm correlation length scale

τ_3 - Cross correlation transient time associated with the longer 25mm correlation length scale

ω - Frequency of bubble generation

Δh - Difference in height of the manometer fluid (section 4.4.1)

Δp_a - Wall differential pressure (p_1-p_2) *Matsui* [1984]

Δp_b - Wall differential pressure (p_3-p_4) *Matsui* [1984]

Δp_c - Wall differential pressure (p_1-p_3) *Matsui* [1984]

Δp_d - Wall differential pressure (p_2-p_4) *Matsui* [1984]

Δt_{AB} - Time spent in the dispersed phase during hot-film anemometry measurements of local gas void fraction

ΔP - Differential pressure

ΔP_A - Upstream differential pressure P_1-P_3

ΔP_B - Down-stream differential pressure P_2-P_4

ΔP_h - Hydrostatic differential pressure

ΔP_m - Mean differential pressure used by the gradiomanometer

ΔP_o - Differential pressure drop measured across the orifice plate

$\Delta P'$ - R.m.s fluctuations in pressure (chapter 5)

ΔZ - Pressure measurement point separation distance (section 5.2.2)

Φ - Velocity potential (section 5.2.2)

Φ - Angular co-ordinate of a bubble within the test section (chapter 6)

Ψ - The mean square (section 2.4.1)

Ω - Flow deviation angle from the vertical

∞ - Infinity

CHAPTER 1 - AN INTRODUCTION TO TWO-PHASE FLOW AND A DISCUSSION OF THE NEED TO DEVELOP NOVEL MASS FLOW MONITORING TECHNIQUES FOR USE DOWNHOLE

Chapter summary

This chapter introduces the concept of two-phase flow and its relevance to the oil producing industries.

In section 1.2 the four main flow regimes that have been observed to exist in a vertically upward two-phase flow are classified. This is followed in section 1.3 by an introduction to drill stem testing (DST) with an overview of the measurement techniques currently used downhole to evaluate the performance of new oil wells. The limitations and drawbacks of present techniques used by oilfield service companies are then discussed.

The chapter concludes with an outline of the project aims and a summary of the study programme.

1.1 An introduction to two-phase flow

The term multiphase flow is defined by *Wallis* [1969] as "the simultaneous flow of several phases", where "a phase is simply one of the states of matter and can be either a gas, liquid, or solid". Two-phase flow is the simplest form of multiphase flow but can still take many forms. One of these is the bubbly flow regime and it is frequently encountered in the oil industry.

Onshore oil wells such as those found in North America produce not only oil but significant quantities of natural gas. In some cases the well yields water instead of natural gas but *Hunt* [1986] reports that it is unusual to find all three phases in a single well. The study of two-phase flow is therefore of direct relevance to the oil producing industry.

The flow type considered in this investigation was vertically upward gas/liquid two-phase flow, and in particular the bubbly flow regime within pipes. The two immiscible fluids used in this study were air for the dispersed phase and tap water for the continuous phase. The selection of these fluids is primarily from a safety point of view and through personal communications with *Dr A.Hunt* it is thought that natural gas dispersed in oil will act in a similar manner to air dispersed in water.

1.2 Classification of flow regimes found in vertical two-phase flow

The fluid dynamics of a two-phase flow is very complex and still, in general, poorly understood. However, visual observations of

two-phase mixtures have identified the existence of different flow regimes. Vertical gas/liquid two-phase flow has been shown to have four main flow regimes, namely

The bubbly flow regime

The slug flow regime

The churn/froth flow regime

The annular/mist flow regime

Figure 1.1 shows the observations made by *Govier, Radford,* and *Dunn* [1957] using an air/water mixture in a 1 inch diameter pipe. Their results show clearly the four main flow regimes as a function of the superficial gas velocity V_{sg} and the superficial liquid velocity V_{sl}. The superficial gas and liquid velocities are the velocities a particular phase would have if it were the only phase present in the pipe. These are defined mathematically as

$$V_{sg} = \frac{\dot{V}_g}{A} \qquad 1.1$$

$$V_{sl} = \frac{\dot{V}_l}{A} \qquad 1.2$$

where $\dot{V}_g$ and $\dot{V}_l$ are the gas and liquid volume flow rates, respectively, and A the cross-sectional area of the pipe or duct.

1.2.1 The bubbly flow regime

Bubbly flow as its name suggests consists of dispersed bubbles of one phase in a continuous second phase. The dispersed phase is

normally less dense than the continuous phase and the size, shape, and rise velocity of the bubbles can vary from small near spherical bubbles to large cap bubbles. The size and shape of a bubble is affected by many factors such as the dispersed and continuous phase velocities, interfacial surface tensions between the phases, relative densities, bubble generation mechanism, etc.

Bubble generation may result from the addition of heat such as in a heat exchanger, a reduction in pressure i.e. cavitation, through a chemical reaction, or from gas or liquid emerging from a porous media into a second phase, such as natural gas in oil. The size of bubbles that are introduced though an orifice may also be dependent on the size of the orifice (see chapter 5).

It should be noted that the size of the bubbles at generation may differ from that of bubbles some distance down-stream. This is due to collision, adherence, and coalescence of bubbles as they flow down-stream. Therefore, the two-phase flow may go through a development period after the bubbles are introduced into the flow (see *Anderson & Quinn* [1970]). This may account for some researchers having observed a transition from bubbly to churn flow with no observation of slug flow, due to an insufficient development length upstream of the observation point.

1.2.2 The slug flow regime

Govier & Aziz [1972] suggest that slug flow is initiated when large cap bubbles agglomerate to form much larger bubbles that have a length at least equal to the diameter of the pipe. These large

bubbles fill the pipe except for a small annulus of water next to the pipe wall, as shown in figure 1.2. As the gas slug develops, the nose of the gas slug becomes near-spherical in shape and smaller bubbles can be seen to detach from the rear of the slug becoming entrained in its wake.

Vertically upward slug flow can occur at all superficial liquid velocities and as the gas bubble travels up the pipe, the continuous phase liquid above the bubble is displaced, resulting in a net downward flow of the liquid in the small annulus between the bubble and the pipe wall. This is described in more detail by *Govier & Aziz* [1972] 'The Flow of Complex Mixtures in Pipes'.

1.2.3 The churn/froth flow regime

Churn or froth flow differs from slug flow in that the gas bubbles become irregular and the wake behind then becomes much richer in small bubbles and is generally more turbulent. Although churn/froth flow is not as ordered as slug flow there is still a pulsating pattern to the flow but it loses its identity very quickly.

Due to their irregular shape discrete bubbles are difficult to identify in this flow regime, and visual observations in transparent pipes indicate that it is by far the most turbulent form of two-phase flow. Consequently little is known of this flow regime, although some research has been carried out by e.g. *Harmathay* [1960], *Zuber* and *Findlay* [1965].

1.2.4 The annular/mist flow regime

Annular/mist flow occurs at very high superficial gas velocities. Gas is now the continuous phase and it occupies most of the pipe cross-section. A thin annular liquid film travelling in waves or ripples up the pipe wall forms most of the liquid phase with dispersed droplets of liquid entrained in the gas. At its limit the annular film disappears leaving only the gas phase with entrained droplets of the liquid rushing up the pipe.

Annular and mist flow are sometimes treated as two separate flow regimes and *Shearer* and *Nedderman* [1965] discuss further sub-classifications. Nevertheless, annular and mist flow are nearly always found together and for given superficial liquid and gas velocities, decreasing the gas velocity increases the thickness of the liquid film and reduces its velocity to a point where churn or froth flow occurs. This is known as the onset of "flooding" and has been extensively studied by *Hewitt* [1986].

1.3 Present measurement techniques used in downhole drill stem testing

In the evaluation of the expected life and performance of any new oil well, several tests are carried out during and after the drilling operation using instrumentation packages that are lowered into the bore hole. These packages are referred to in the oil industry as "tools".

Periodically during the drilling stage, drilling is interrupted

so that a "wireline tool" can be lowered into the bore hole. This tool assesses the physical properties of the rock formations found in the bore hole by making electrical, acoustic, or radiation measurements which are transmitted to the surface via the armoured cable it is lowered on. On encountering a formation that is likely to produce hydrocarbons, drilling is stopped and what is known as a drill stem test (DST) is performed.

In brief a DST tool contains a valve, a pressure sensor, a packer, and a flow measurement device. The DST tool is lowered into the bore hole on the end of a length of hollow tubing known as the drill pipe. On reaching the likely production formation the packer is set in position. The purpose of the packer is to form a hydraulic seal between the heavy drilling mud and the oil bearing rock formation.

There are several stages to the DST. The first stage is to measure the initial reservoir pressure P_1 with the valve in the drill stem tool closed. The valve is then opened allowing the reservoir fluids to flow through the flow measurement instrumentation held in the DST tool and up into the drill pipe. On opening the valve in the DST tool the reservoir pressure is observed to drop suddenly to a new value P_2.

After an appropriate flowing period the valve in the DST tool is closed. At this point the reservoir pressure will start to recover from the flowing pressure measurement P_2 to the natural reservoir pressure P_1. The rate of change in pressure, the overall time taken for the reservoir to recover, and the new reservoir pressure, along with the oil and natural gas flow rates measured during the flowing

stage of the test, enable site engineers to draw conclusions about the permeability of the rock formation (this governs the extraction rate) and the expected production life and extent of the reservoir. This information can prove invaluable to an oil company when deciding whether it would be profitable to extract oil from a new well.

For conclusions to be drawn from the DST it is important that measurements made of pressure changes, and oil and gas flow rates, are reliable in the harsh conditions (temperatures up to 150^{0}C and pressures up to 700 Bar) likely to be encountered downhole. Present technology allows pressure measurements to be made under these conditions. However, current techniques used for downhole measurement of two-phase flow rates are more complex and less reliable.

During the flowing period of the DST test, two parameters must be calculated in order to make an estimation of the mass flow rates of each phase. These are the superficial gas and liquid velocities, V_{sg} and V_{sl} respectively, and the average volumetric gas void fraction α, which is defined as

$$\alpha = \frac{v_g}{v_g + v_l} \qquad 1.3$$

where v_g and v_l are the gas and liquid volumes, respectively, in a total volume $(v_g + v_l)$.

Schlumberger Cambridge Research, which is a section of an oilfield service company and is also the collaborating organisation involved with this project, presently use two instruments in a DST tool to evaluate the average gas void fraction and the superficial gas and liquid velocities.

1.3.1 Average gas void fraction measurements (gradiomanometer)

The gradiomanometer is used to evaluate the average gas void fraction α. The technique utilises a length of straight pipe with two pressure tappings separated by a distance h, as shown in figure 1.3. The pressure difference ΔP_m between these two tappings is used to calculate the average gas void fraction from the following relationship

$$\alpha = \frac{\dfrac{\Delta P_m - F_m}{g\ h\ \cos\ \Omega} - \rho_l}{(\rho_g - \rho_l)} \qquad 1.4$$

in which ρ_g and ρ_l are the gas and liquid densities, respectively, and Ω the flow deviation angle (0^0 for a vertical pipe). The frictional pressure loss F_m between the two tappings can be estimated from the following equation derived from the *Darcy* formula

$$F_m = \frac{2\ \rho_l\ (V_{sl} + V_{sg})^2\ h\ f}{D} \qquad 1.5$$

where f is the non-dimensional friction factor, and D is the bore diameter of the gradiomanometer.

A more detailed description of the gradiomanometer, and the derivation of the equations used to evaluate the average gas void fraction, is given in section 4.1.2

1.3.2 Velocity measurements

Two of the required parameters in the DST test are the gas and

liquid mass flow rates. One way of evaluating the mass flow rates of each phase involves establishing the area averaged gas and liquid velocities V_g and V_l respectively, within a two-phase mixture.

Two techniques are presently used downhole to estimate the area averaged velocities of a two-phase flow.

(i) Tracer injection - This technique involves injecting a radioactive tracer into the continuous phase of the two-phase flow, and it is assumed that the tracer is only associated with the continuous phase. The time T_t taken for the tracer to flow down-stream a known distance h_t is therefore, to a first order, proportional to the time taken for the continuous phase to travel this distance. An estimate of the area averaged liquid velocity can be therefore calculated from

$$V_l = \frac{h_t}{T_t} \qquad 1.6$$

Using the gradiomanometer described in section 1.3.1, the average gas void fraction α can be measured in the DST tool and thus used to evaluate the area averaged gas velocity V_g

$$V_g = \frac{\alpha\, V_l}{(1 - \alpha)} \qquad 1.7$$

However, the actual time of flight of the tracer is not the same as the time it takes the continuous phase to travel this distance. This is due to diffusion of the tracer in the two-phase flow whilst flowing down-stream. Diffusion is a very complex process and the rate of diffusion will be a function of the flow conditions downhole.

(ii) Turbine flowmeter or spinner - Another technique used downhole to evaluate the area averaged liquid and gas velocity V_l and V_g, respectively, involves placing a turbine flowmeter into the two-phase flow. When a turbine flowmeter is used in a single phase flow it gives a pulse train output whose frequency is proportional to the volume flow rate of the measured fluid. In a bubbly two-phase flow, it is common practice to consider the flow to be homogeneous and the output frequency is assumed to be proportional to the volume flow rate of the two-phase mixture.

However, this technique has two major draw backs. Firstly, the turbine is intrusive to the flow, and hence is prone to damage from entrained rock chippings. Secondly, the turbine flowmeter is in principle a single phase device. Hence, when it is used in a two-phase flow to measure mixture volume flow rates $\dot{V}_m$, substantial uncertainties may be introduced in the measured quantity due to the volume of gas, bubble size, and local velocity and void fraction profiles within the flow.

Knowing the internal cross-sectional area of the DST tool, A_{DST}, the area averaged mixture velocity V_m can be evaluated from

$$V_m = \frac{\dot{V}_m}{A_{DST}} \qquad 1.8$$

which is also defined as the sum of the superficial gas and liquid velocities

$$V_m = V_{sg} + V_{sl} \qquad 1.9$$

The area averaged gas velocity V_g is currently determined by the empirical relationship put forward by *Zuber & Findlay* [1965]

$$V_g = C_0(V_{sg} + V_{sl}) + V_{g\infty} \qquad 1.10$$

where $V_{g\infty}$ is the terminal rise velocity of a single bubble due to its own buoyancy, and C_0 is a distribution coefficient defined by

$$C_0 = 1 + \frac{2}{m + n + 2}\left[1 + \frac{\alpha_w}{\alpha}\right] \qquad 1.11$$

where m and n are the exponents of the power law associated with the shape of the velocity and void fraction distributions, respectively, and α_w is the local void fraction at the pipe wall, as described in section 4.1.2.

Equation 1.11 shows that in order to evaluate the distribution coefficient C_0 assumptions must be made about the velocity and void fraction profiles. Other assumptions concerning the interaction between swarms of bubbles and the effect of the pipe wall must also be made when estimating the terminal rise velocity $V_{g\infty}$ as described in section 5.1.4.

The area averaged gas velocity is related to the superficial gas velocity by the equation 1.12 below, where the average gas void fraction α is determined from the gradiomanometer:

$$V_{sg} = \alpha V_g \qquad 1.12$$

Knowing the superficial gas velocity and the mixture velocity, the superficial liquid velocity can be evaluated by re-arranging equation 1.9 to give

$$V_{sl} = V_m - V_{sg} \qquad 1.13$$

and the area averaged liquid velocity V_l can be calculated from

$$V_l = \frac{V_{sl}}{(1 - \alpha)} \qquad 1.14$$

1.3.3 Limitations of the present measurement tools used in downhole DST tests

The gradiomanometer which is used to measure average gas void fractions downhole has several limitations. The major source of error is caused by uncertainty in the frictional pressure loss F_m between the two pressure tappings.

To evaluate the average gas void fraction α by the gradiomanometer an estimation of the pressure loss term F_m must be made using equation 1.5, which contains the superficial gas and liquid velocities. These quantities can be measured with relative ease in the laboratory but evaluation of the downhole superficial gas and liquid velocities currently rely on either the tracer injection or turbine flowmeter techniques to estimate the area averaged liquid velocity. To evaluate F_m it is also necessary to make an estimation of the non-dimensional friction factor f. The friction factor f is not only dependent upon the pipe roughness but is also a function of the flow itself. Using the gradiomanometer in the laboratory it is possible to perform calibration experiments to determine the value of

f (see section 4.1.2). However, the flow conditions downhole are relatively unknown and hence the value of the friction factor f will also be somewhat uncertain.

It should also be noted that the *Darcy* formula, from which F_m is derived (equation 1.5), was originally developed for use in single phase flows. However, research by *Aziz*, *Govier* and *Fogarazi* [1972], and more recently *Hunt* [1987], suggests that this formula may still apply when interpreted correctly.

Having evaluated the average gas void fraction α, it is necessary to make assumptions regarding flow conditions deep in the bore hole such as the flow regime, local velocity and void fraction profiles in order to evaluate the area averaged gas and liquid velocities, using either the tracer injection method or the turbine flowmeter and *Zuber* & *Findlay* relationship.

The accuracy and reliability of these techniques is therefore questionable, partly due to the assumptions made about the flowing fluid with only limited or no information about the average gas void fraction, local velocity and void fraction profiles, etc.

The downhole evaluation of the three fundamental parameters α, V_{sg} and V_{sl} using present instrumentation requires initial assumptions to be made about the flow conditions being measured. Using these initial assumptions the average gas void fraction, and area averaged gas and liquid velocities can be calculated.

From these calculations using the initial assumptions and measurements, it is then possible to make more informed assumptions

about the flow conditions downhole. Therefore, by a process of iteration, the accuracy of the measured average gas void fraction α, and the area averaged gas and liquid velocities V_{sg} and V_{sl} can be improved.

1.4 Aims of this study programme

Due to the complexity of bubbly two-phase flow, a single measurement technique cannot accurately predict all the required parameters. Therefore, a number of measurement techniques must be used downhole, each technique having a weighting based upon its performance when used in particular flow conditions. By analysing the results of each technique it is thought by *Schlumberger* that it will be possible to improve the accuracy of flow measurements in downhole bubbly two-phase flow.

At present the downhole area averaged gas velocity is calculated knowing the area averaged liquid velocity from the tracer injection method and the average gas void fraction from the gradiomanometer. Or the area average gas velocity is calculated from the empirical equation 1.10 proposed by *Zuber* & *Findlay* [1965] using the mixture velocity obtained from the turbine flowmeter and the average gas void fraction from the gradiomanometer. Use of either technique requires some very wide reaching assumptions about the two-phase flow to be made. More reliable downhole flow measurements would be obtained if the area averaged gas velocity could be measured directly.

The aim of this study was therefore to investigate the possibilities of using naturally occurring differential pressure

fluctuations as a means of non-intrusively monitoring the area averaged gas velocity V_g in a vertically upward bubbly two-phase flow. In order to carry out a study in which naturally occurring pressure fluctuations within bubbly two-phase flow are to be investigated a vertical air/water flow loop was designed and constructed in the fluid mechanics laboratory at the University of Plymouth (formerly Polytechnic South West). After the construction, calibration, and commissioning of the air/water flow loop was complete (see chapters 3 & 4), the theoretical and experimental studies were divided broadly into two main areas

Investigation of the statistical properties of pressure fluctuations in a two-phase flow

Use of cross correlation techniques on differential pressure fluctuations in a bubbly two-phase flow as a means of measuring the area averaged gas velocity

1.4.1 Investigation of the statistical properties of pressure fluctuations in two-phase flow

It is well documented in standard texts such as *Massey* [1968], *Milne-Thomson* [1960], that as a sphere moves through a fluid temporal variations occur in the velocity field at fixed observation points due to the fluid being displaced. Corresponding fluctuations in the pressure field can also be observed. It is suggested by *Bradbury* [1988] that small gas bubbles, less than approximately 8mm, will act in a similar manner to solid spheres of the same density when analysed

in theoretical two-phase flow conditions and work carried out initially by *Tutu* [1982] and more recently by *Matsui* [1984] into the identification of two-phase flow regimes using pressure fluctuations suggest this is so.

The initial objective of this project was therefore to investigate the statistical properties of differential pressure fluctuations at the pipe wall caused by vertically upward bubbly two-phase flow. The results of experimental studies in which solid spheres were used to generate pressure waves in a stagnant column of liquid were analysed and compared to the theoretical models developed in this thesis for the fluctuations in pressure generated by a solid sphere in similar flow conditions.

The results of these initial experiments were then used in designing the pressure transducer test section used in the subsequent correlation experiments.

1.4.2 Use of cross correlation techniques on differential pressure fluctuations in a bubbly two-phase flow as a means of measuring the area averaged gas velocity

Cross correlation is a well documented statistical technique for measuring velocities. If the pressure fluctuations produced by bubbles in a two-phase flow were recorded at two locations along a pipe, then the down-stream pressure signal will be a time shifted version of the upstream signal assuming the signal source does not lose its identity. However the source of the pressure signal will vary with time and there will be a finite time period in which the

signals will correlate with each other. If the approximate velocity of the bubbles is known, then the length scale of structures within the flow can be calculated, and hence the maximum transducer spacing can be deduced. Using the information from the statistical study of pressure fluctuations outlined in section 1.4.1, the characteristic length which governs the maximum transducer spacing was calculated from the autocorrelation correlograms of the differential pressure signals. The experimental pressure transducer housing was then constructed with a high degree of confidence that cross correlation velocity measurements could be obtained, and using this device measurements of the convected disturbance velocities were made and compared to the area averaged gas velocity V_g of the two-phase flow.

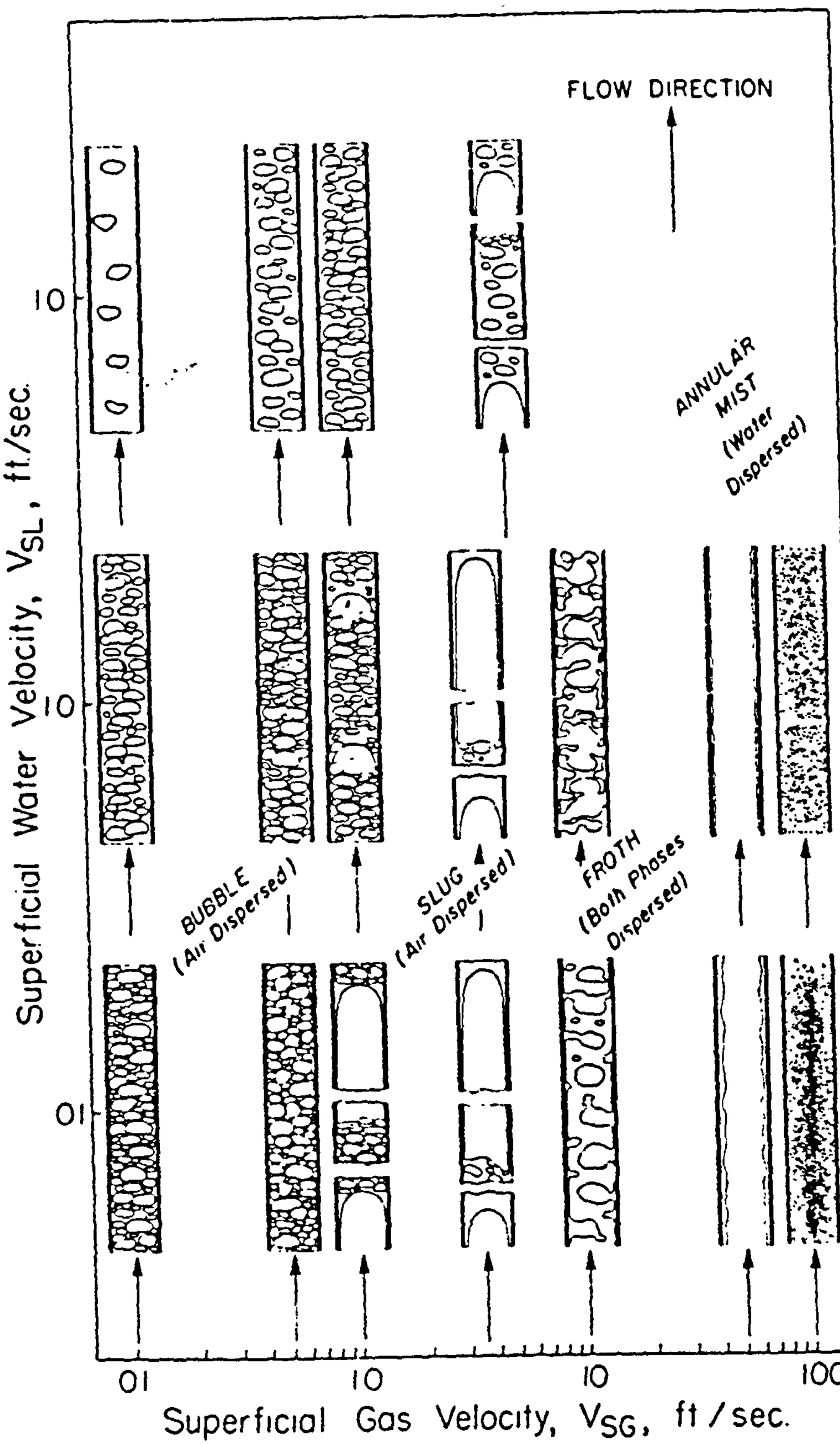

Figure 1.1 Flow regime map produced from data by *Govier, Radford, & Dunn* [1957] for air/water mixtures in a 1 inch pipe

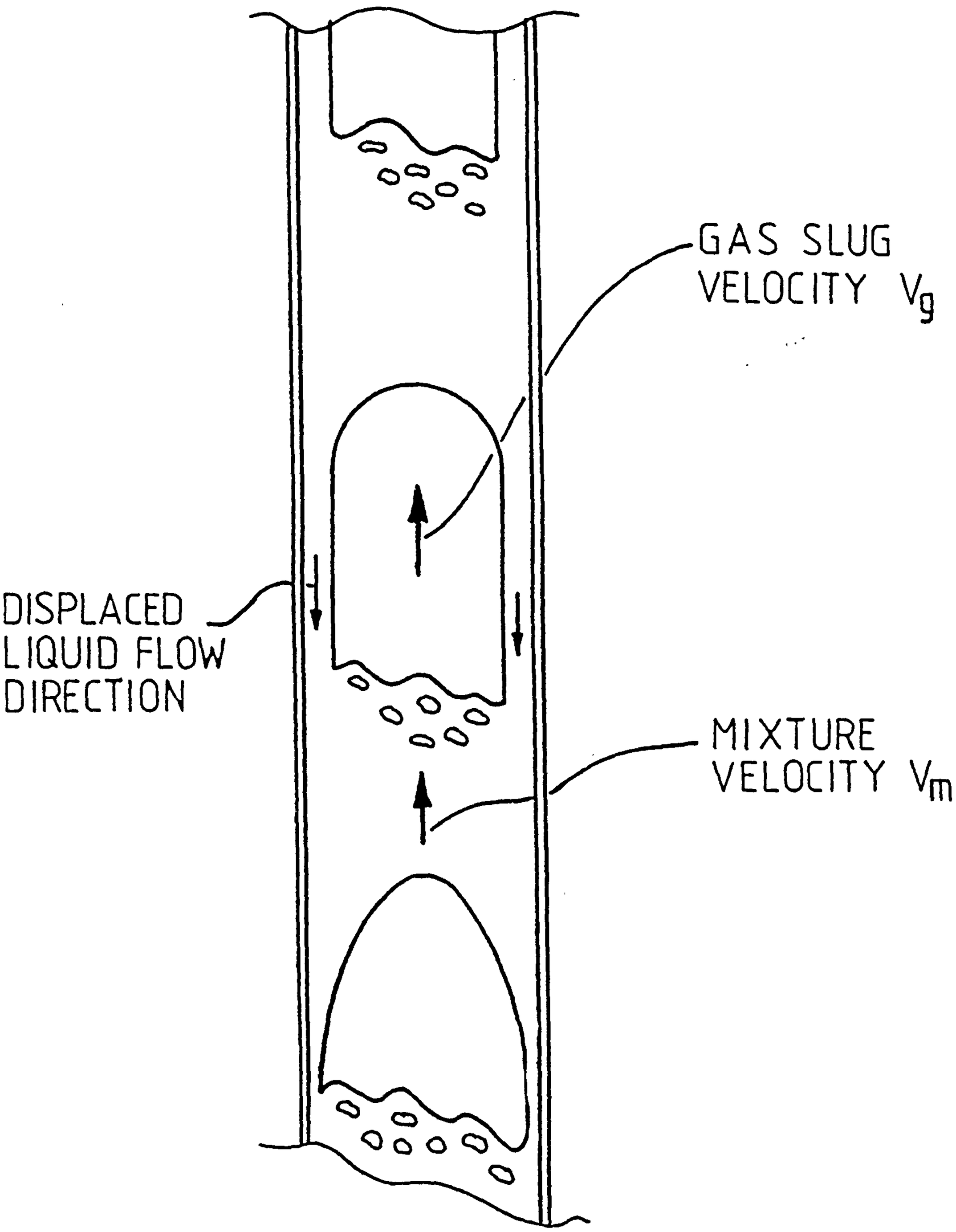

Figure 1.2 Typical Slug flow profile in gas/liquid vertically upward two-phase flow

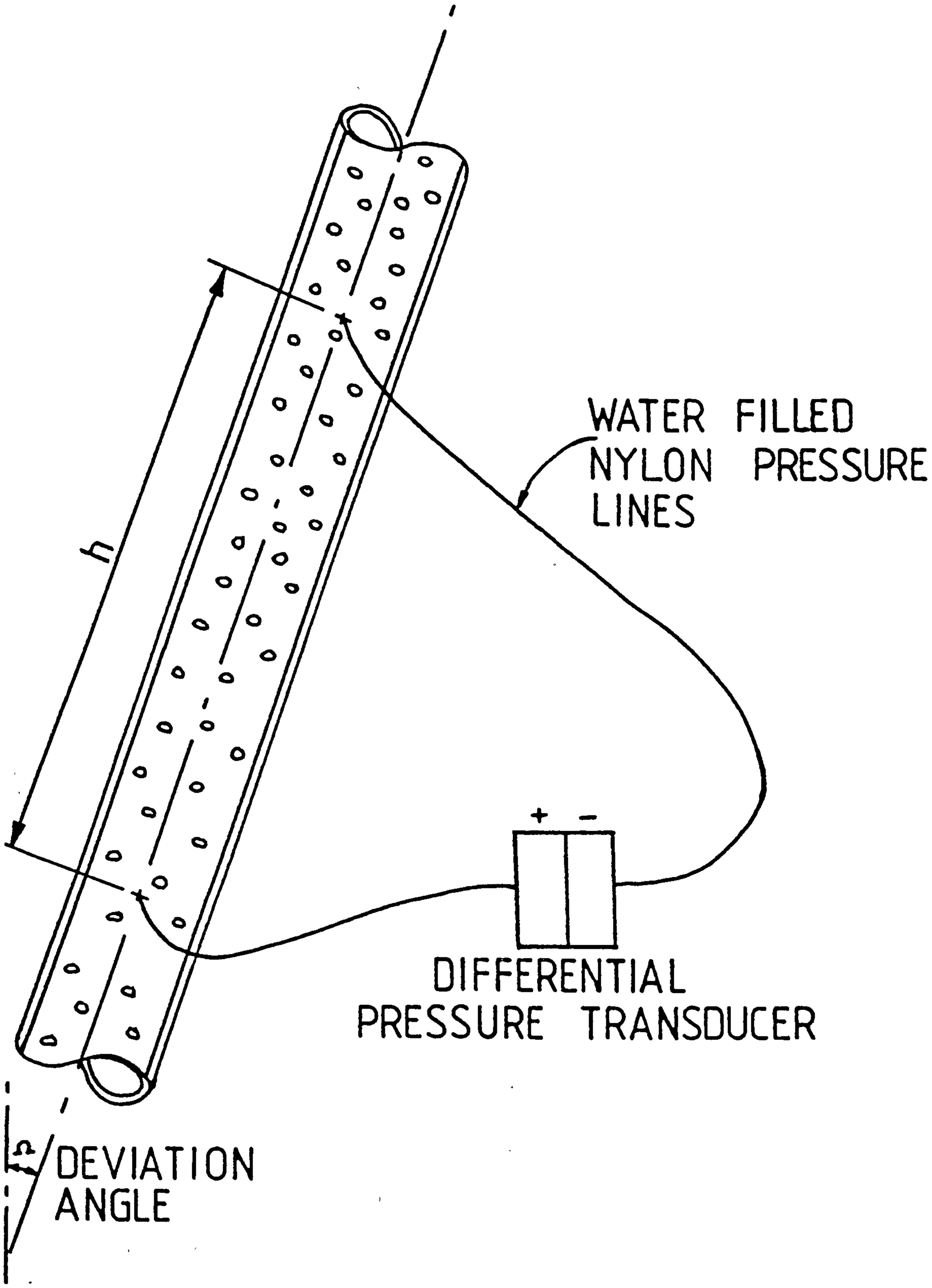

Figure 1.3 Average gas void fraction measurement using the gradiomanometer technique

CHAPTER 2 - REVIEW OF PREVIOUS RESEARCH IN TWO-PHASE FLOW MEASUREMENT TECHNIQUES

Chapter summary

Section 2.1 reviews the techniques developed by previous researchers for the measurements of the average gas void fraction α in a pipe or duct. A brief description of each sensing technique is given together with a summary of its advantages and limitations. This is followed by a discussion of local void fraction α_l measurement techniques in section 2.2.

Section 2.3 covers the techniques that have been developed to discriminate between flow regimes. In particular, analysis of statistical techniques such as those which involve the probability density function (PDF), forms the basis of many of the techniques used for flow regime identification.

Cross correlation techniques have been developed by a number of researchers such as *Lucas* [1986] to measure the area averaged velocity of the dispersed phase within the bubbly flow regime. These are discussed in section 2.4. Many of these non-intrusive dispersed phase velocity monitoring techniques which have been investigated are developements of area average and local void fraction measurement studies.

2.1 Methods used to measure average gas void fractions in two-phase flow

Extensive research has been conducted into the prediction and measurement of the average gas void fraction α. This is one of the fundamental two-phase flow parameters and it is used in nearly all two-phase flow analyses. The most common techniques for the measurement of average gas void fractions in a two-phase flow are summarised below. However, for a more comprehensive overview of the less widely used techniques for measuring void fractions the reader is referred to *Hewitt* [1978].

2.1.1 On-line sampling using quick closing valves

The average gas void fraction α in a gas/liquid two-phase flow is defined in chapter 1, equation 1.3,

$$\alpha = \frac{v_g}{v_g + v_l} \qquad 1.3$$

where v_g is the volume of gas, at any instant in time, that is contained in a representative volume v_t or $(v_g + v_l)$.

The on-line sampling technique is usually incorporated in a section of transparent pipe fitted between two quick closing valves as shown in figure 2.1. The transparent pipe section is normally situated vertically in the flow loop at a position where the flow is considered to be both fully developed and steady. At an appropriate sampling time the quick closing valves are activated simultaneously thus capturing a section of the flowing two-phase fluid.

After natural separation of the two captured phases has taken place, the volume of the gas can be measured as a fraction of the total volume, and assuming both no leakage and the pressure to be near atmospheric, this is then a measurement of the average gas void fraction α.

One source of error which may occur in this technique involves the closure of the valves. The valves must close both simultaneously and relatively quickly compared to the velocity of the flowing fluid. A number of methods have been tried in order to minimise these errors. *Johnson* and *Abou-Sabe* [1952] used spring loaded valves, *Hammer* [1983] used two mechanically linked ball valves, and *Denton* [1987] uses pneumatically operated valves. In this study a pair of pneumatically operated gate valves were specially constructed for this purpose (see section 4.1.1) and have been used successfully by *Hunt* [1987].

A major disadvantage of the quick closing valve technique is that the flow is interrupted whilst measurements are being made. Hence, use of this technique is mainly limited to the laboratory, and it is shown in the literature that it is mainly used as a 'standard' for the comparison of other average gas void fraction measurement techniques.

The quick closing valve technique has been reported to work well in the bubbly flow regime where the flow is considered to be homogeneous. However, in slug and churn flows the distance between the valves needs to be many times larger than the length of the structures that exist in these flow regimes, in order to avoid statistical errors when measuring the average gas void fraction. The corresponding distance between the two valves may therefore exceed the

available length of the experimental test section.

2.1.2 Radiation absorption techniques used for measuring void fractions

Gamma radiation absorption as used by *Jones* and *Zuber* [1975], relies upon the fact that gamma rays are absorbed at different rates by different materials. This technique has been used extensively for determining the chordal-average gas void fraction α_c.

Consider a collimated, monoenergetic radiation source placed on one side of a pipe, and diametrically opposite this source a detector is positioned as shown in figure 2.2. When the pipe contains only the continuous liquid phase, the radiation intensity at the detector will be I_l. Similarly when the pipe contains only gas the radiation intensity at the detector will be I_g.

Petrick & *Swanson* [1958] studied the effect of different distributions of phases within a two-phase flow. Two hypothetical flow patterns were studied, firstly one in which the gas and liquid phases were arranged perpendicular to the collimated radiation beam as shown in figure 2.2a. In this case the chordal-average gas void fraction α_c is given by the equation below, where I_m is the measured radiation intensity at the detector when the two-phase flow is present.

$$\alpha_c = \frac{\ln(I_m/I_l)}{\ln(I_g/I_l)} \qquad 2.1$$

In the second case they considered a 'pseudo slug flow' where the two phases were arranged in layers parallel to the beam of

collimated radiation, as shown in figure 2.2b. In this case the chordal-average gas void fraction α_c is given by equation 2.2 when the signal is averaged over a suitably long time period to eliminate statistical errors.

$$\alpha_c = \frac{I_m - I_l}{I_g - I_l} \qquad 2.2$$

It can be seen by comparing equations 2.1 and 2.2 that the chordal-average gas void fraction α_c when evaluated by radiation absorption technique is strongly dependent upon the distribution of phases within the flow. This is a major limitation to the use of this technique if changes in flow regime are to be encountered in the two-phase flow. Even in the case of a fairly homogeneous two-phase flow such as bubbly two-phase flow, the chordal-average gas void fraction α_c given by equation 2.1 is simply the average gas void fraction measured along a diametrical choard through the pipe. There is no guarantee that this estimated value of chordal-average gas void fraction α_c gives a true representation of the average gas void fraction α, since the two-phase flow may not be symmetrical about its axis which may result in non-uniform radial phase distributions.

Another limitation to the use of gamma radiation attenuation is that many sources of radiation have a range of gamma energies (*Hewitt* [1978]). This can lead to ambiguity in the interpretation of the detected radiation intensity.

Finally, the hazardous nature of gamma radiation cannot be over-looked. The equipment involved in this technique has to be heavily shielded to protect both the operator and surrounding optical and electronic equipment. It should also be noted that there are a number of less widely reported techniques employing radioactive

sources such as x-ray absorption (*Smith* [1985]) and scattered gamma radiation (*Kondic* & *Hahn* [1970]). However these suffer from the same limitations imposed by safety considerations.

2.1.3 Void fraction measurement using ultrasonics

Techniques in which ultrasonics have been used in air/water two-phase flow to measure the gas void fractions are not widely reported. However *Ong* [1975] and more recently *Xu* [1986] have studied the effects of ultrasound on a homogeneous bubbly two-phase flow. *Xu* [1986] proposed a void fraction measuring device which was based on the attenuation of pulsed ultrasound as it passed through a bubbly two-phase flow from the transmitter on one side of the pipe to the receiver mounted diametrically opposite on the other side of the pipe. *Xu* predicted that if the amplitude of the transmitted ultrasound pulse was P_t then the amplitude of the received pulse P_r would be given by

$$P_r = P_t \, e^{(-1.5 L_t \, \alpha_c) \, / \, d} \qquad 2.3$$

where α_c is the chordal-average gas void fraction, L_t the separation distance between the transmitter and receiver (in this case one pipe diameter), and d is the bubble diameter. Experiments showed that P_r decreased exponentially as the chordal-average gas void fraction α_c was increased and that the amplitude of P_r was also dependent on the bubble diameter d as predicted by equation 2.3. However, when the chordal-average gas void fraction α_c was greater than a critical value $\alpha_{c,crit}$, P_r was not reduced further by increasing α_c, indicating that the device had saturated.

For bubbles of the order of 1mm in diameter $\alpha_{c,crit}$ was less

than 0.5%, whereas for bubbles of the order of 5mm in diameter $\alpha_{c,crit}$ was determined to be approximately 5%. The most likely reason why P_r did not decrease as α_c was increased beyond $\alpha_{c,crit}$ is associated with the fact that the receiver not only picked up ultrasound that had travelled directly across the pipe from the transmitter but also picked up a significant amount of scattered ultrasound, the intensity of which increased as α_c was increased. This effect is not accounted for in equation 2.3.

Novel signal processing techniques were developed by *Xu* in an attempt to improve the useful range of this device. Unfortunately only a marginal improvement was achieved. Furthermore, *Xu* was unable to eliminate the dependency of the output on the bubble diameter.

It must therefore be concluded that since bubbly two-phase flow is made up of bubbles of different diameters covering a wide range of average gas void fractions whereas this technique operates over a small range of average gas void fractions, its usefulness as a device for measuring chordal-average gas void fraction is limited.

2.1.4 Impedance measurement techniques used to measure average gas void fraction

Average gas void fraction evaluations using impedance measurements of a two-phase flow have been investigated by a number of researchers. Several of these techniques are, unfortunately, intrusive to the flow and so are unsuitable for downhole flow measurements. However, a number of non-intrusive techniques have been investigated (see, for example, *Lucas* [1987]).

Impedance measurement techniques, broadly speaking, involve placing electrodes in one of many configurations, either in the pipe wall in contact with the fluid or on the outside of the pipe, depending on the two phases present and the type of impedance measurement to be made i.e. capacitive, inductive or resistive. The change in measured impedance is then related to the average gas void fraction after suitable signal processing has been carried out.

These techniques have been used by *Beck et al* [1983], *Bernier* [1981] and many other researchers, with a limited amount of success. *Shu et al* [1982] showed theoretically that, for a given value of average gas void fraction, the measured value of impedance is highly dependent upon the two-phase flow regime. Furthermore, *Bernier* [1981] found that in a vertically upward bubbly two-phase flow, the measured impedance for a given average gas void fraction is dependent upon the the local void fraction distribution which, is affected by the superficial liquid velocity and average gas void fraction. *Bernier* attributes this dependence of measured impedance on the local void fraction distribution to a non-uniform sensing field strength associated with his electrode configuration. *Hammer* [1983] developed a capacitive 'noise' transducer for measuring average gas void fraction concentrations. When used in a vertically upward gas/liquid bubbly two-phase flow he too found that the transducer was very susceptible to variations in the local void fraction profile, which he also suggested was due to a non-uniform field sensitivity.

However, *Lucas* [1987] developed a technique for monitoring the changing average gas void fraction of a two-phase flow using a capacitance measuring transducer. He claimed that the capacitance measuring transducer used had a uniform field sensitivity which was

achieved by incorporating a 'dielectric insert' near the sensing electrodes, as shown in figure 2.3. This transducer was found to be insensitive to variations in superficial velocities, however only limited success was obtained since *Lucas* suggests that his capacitance sensor was more sensitive to the relatively large, fast moving bubbles in the flow.

2.1.5 Average gas void fraction measurements made using differential pressure measurements (gradiomanometer)

The gradiomanometer as presently used in drill stem test (DST) tools (see section 1.3.1, *Hunt* [1987] and *Lucas* [1987]), evaluates the average gas void fraction α. It basically consists of a length of straight pipe with two pressure tappings separated by a distance h as shown in figure 1.3. The pressure difference ΔP_m between these two tappings is used, in equation 1.4, to calculate the average gas void fraction α

$$\alpha = \frac{\dfrac{\Delta P_m - F_m}{g\ h\ \cos\Omega} - \rho_l}{(\rho_g - \rho_l)} \qquad 1.4$$

where ρ_g and ρ_l are the gas and liquid densities, respectively, and Ω is the flow deviation angle. F_m is the frictional pressure loss between the two tappings and is currently estimated using equation 1.5 (derived from the Darcy formula as discussed in section 4.1.2)

$$F_m = \frac{2\ \rho_l\ (V_{sl} + V_{sg})^2\ h\ f}{D} \qquad 1.5$$

where f is the non-dimensional friction factor, and D is the bore

diameter of the gradiomanometer.

This technique is relatively easy to implement and non-intrusive to the flow. However, the application of equation 1.5, which is derived from the empirical Darcy friction formula for a single phase fluid, to the evaluation of the frictional pressure loss F_m in a two-phase flow is open to speculation and interpretation. Research by *Aziz, Govier & Fogorazi* [1972] and more recently by *Hunt* [1987], suggest that the Darcy expression is still applicable if interpreted correctly, and for the bubbly flow regime, where the two-phase flow is considered to be homogeneous, equation 1.5 is reported to give reasonable results.

A more detailed description of this technique, along with a derivation of equations, list of assumptions and a discussion of the limitations is given in section 4.1.2.

2.2 Local void fraction measurement techniques

Local void fraction measurements differ from average gas void fraction measurements in that they are measurements at a point in the flow. which will have a unique radial and longitudinal position within a pipe or duct. Consider the case of a pipe, as shown in figure 2.4 and assume that the local void fraction distribution is fully developed i.e. there is no change in the local void fraction profile along the pipe, then the local void fraction, α_l, can be related to the average gas void fraction α using equation 2.4 below, in which $\alpha_l(r)$ is the local void fraction at radial location r within a pipe of radius R.

$$\alpha = \frac{1}{\pi R^2} \int_0^R \alpha_l(r)\, 2\pi r\, dr \qquad 2.4$$

There are three commonly used techniques for evaluating the local gas void fraction. These are the resistive probe technique, the optical probe technique and the hot-wire/film anemometry technique, each of which is discussed in the following sections. However the basic method underlying each of these techniques is the same. Each technique uses a small probe, inserted into the flow at a known radial position r, to detect, using suitable electronics, which phase is present at its tip. Since bubbles are discrete, an instantaneous measurement will produce a local void fraction measurement of either 100% or 0% depending on which phase the probe is in at the time of the instantaneous measurement. The measurement of local void fraction α_l is therefore normally recorded over a suitably long period of time to avoid statistical errors in the measuring technique. A long sampling period also has the advantage of reducing errors caused by small fluctuations in the local void fraction. Therefore, the ratio of time spent in the dispersed phase t_g to the total sampling period t_t is a measure of the local gas void fraction α_l if the total sampling period t_t is suitably long, as given below.

$$\alpha_l = \frac{t_g}{t_t} \qquad 2.5$$

2.2.1 Local void fraction measurements using a resistive probe

The most commonly reported technique in the literature for the measurment of the local void fraction in a two-phase flow where one of the phases is far more conductive than the other (such as air and water). *Delhaye* & *Chevrier* [1966], *Bergeles*, *Lopina* & *Fiori* [1967],

Bergeles [1969] and others have used this technique which involves inserting a thin, wire-like probe into the flow. The probe is electrically insulated right up to its tip, which is conical in shape, and is the only point which is allowed to make an electrical connection with the two-phase flow. An electrical connection is made to the tip of the probe via the insulated wire, as illustrated in figure 2.5. Another electrical connection is made to the fluid in contact with the pipe wall. When the tip of the probe is in air, the resistance between the tip of the probe and the pipe wall connection is high, and when in water the resistance is low.

To distinguish which phase the tip of the probe is in, a threshold level of resistance must be determined above which the probe is considered to be in the dispersed gas phase. This is necessary because there will be a finite time taken for the resistance of the probe to change from the high to low levels of resistance during wetting and from low to high levels of resistance during drying. The position of the threshold level between the low and high resistance points will alter the measured amount of time t_g, in which the probe is considered to spend in the dispersed gas phase thus altering the local void fraction α_l in equation 2.5. Nevertheless, if a mid-point in the range of change in resistance is taken as the threshold level then the errors will be small over a long time period.

Another problem associated with this technique is surface contamination of the probe tip, which alters the range of resistance measured between the dispersed gas phase and the continuous phase. This in turn alters the position of the threshold level within the range, causing variations in local void fraction readings over a period of time.

2.2.2 Local void fraction measurements using fibre optics

An alternative instrument for the measurement of local void fraction that has been used successfully by many researchers (see, for example, *Lance* & *Bataille* [1991]), is the fibre optic probe. This is very similar in principle to the resistance probe technique in that the fibre optic probe detects which phase is present at its tip.

The fibre optic probe basically consists of an infra-red light source that is shone along a length of optical fibre, the end of which is thinned down to approximately 0.01mm in diameter and positioned in the flow as shown in figure 2.6. At the tip of the fibre optic probe the inferred light beam is either reflected back along the fibre optic, or is allowed to escape out of the probe, depending upon the phase present at the tip of the probe. If the infra-red light beam is reflected back along the optical fibre it is detected by an infra-red sensor which converts it to an analogue voltage signal. The tip of the probe is either conical in shape or square cropped depending on the difference in refractive index between the two phases. For air in water it is conical and for oil in water it is square cropped.

As with the resistance probe, there are two levels of the analogue signal, one of which is associated with the discontinuous phase and the other with the continuous phase. A threshold level is determined between the upper and lower levels to discriminate between phases. The ratio of time the tip of the probe spends in the discontinuous phase, t_g, to the (suitably long) sampling period, t_t, is taken to be the local void fraction α_l, as given in equation 2.5.

There will be, as in the case of the resistive probe, a finite

time period over which there will be some uncertainty as to which of the phases the probe is in during the passage from one phase to the other due to wetting and drying of the optical tip surface. However, due to the very small size of the fibre optic probe (0.01mm in diameter), interference between the probe tip and the discrete phase interface is thought to be less than that for the resistive probe and so this effect is less significant. It is also worth mentioning however that the tip of the fibre optic is prone to contamination with impurities in the flow which will alter the levels of the reflected infa-red signal. Therefore regular and careful cleaning of the probe tip must be carried out using an ultrasonic bath.

2.2.3 Local void fraction measurements using hot-wire/film anemometry

One of the latest techniques has been developed by *Farrar & Bruun* [1989] in which hot-film anemometry is used to measure the local void fraction α_l in vertical bubbly two-phase oil/water and air/water flows. The use of hot-wires/films in two-phase flow is not new (see *Hsu et al* [1963] and *Delhaye* [1969]), however *Farrar & Bruun* have developed a technique to interpret the signal from a cylindrical hot-film as it interacts with discrete spherical bubbles.

Farrar and *Bruun* [1989] showed theoretically how the output signal from a hot-film anemometer would vary as a discrete bubble interacts with a small cylindrical hot-film probe for air in water and oil in water. The theoretical results were compared with experiments using high speed photography and hot-film anemometry and were found to be in good agreement.

A hot-film anemometer is basically a constant temperature device, i.e. the probe is held at constant temperature. The current needed to heat the film probe and keep it at a constant temperature will depend upon the heat transfer properties of the fluid in contact with the probe, and the velocity of this fluid. By calibration of the probe under known conditions the current supplied to the probe can be related to the flow conditions.

Consider a typical signal from a hot-film probe positioned in a two-phase flow, as shown in figure 2.7, each of the large U shaped dips in the signal is associated with a bubble being cut by the hot-film probe. Now consider one of these dips in the signal more carefully, four points can be identified on the signal and can be related to discrete events in the interaction of a bubble with the hot-film probe.

(A) This is the point at which the bubble makes contact with the cylindrical hot-film probe.

(B) At this point the rear of the bubble reaches the cylindrical hot-film probe.

(C) This point is associated with the dynamic overshoot due to the formation of a meniscus around the sensor.

(D) This point represents the position in the signal where the effect of the bubble has passed and the probe reflects the contribution to the signal of the continuous phase only.

From this analysis of the signal it can be seen that the only portion of the signal that needs to be considered to evaluate the local void fraction α_l is the portion of the signal AB. Therefore the local void fraction α_l can be calculated from equation 2.6 as

$$\alpha_l = \frac{\Sigma \Delta t_{AB}}{t_t} \qquad 2.6$$

where t_t is a suitably long period of time.

It is also worth mentioning that *Farrar* & *Bruun's* interpretation of a hot-film signal in a bubbly two-phase flow can be used to obtain much more information than just the local void fraction. Information such as distribution in cut cord bubble diameters, turbulent intensity of the continuous phase and bubble velocity can also be evaluated (although there is some question to the accuracy of the bubble velocity).

2.3 Objective flow regime identification in vertical two-phase flow

In a number of research programmes, flow regime identification has been made by visual observations through transparent pipes or ducts. Unfortunately this method of flow regime identification is subjective, and is impractical in many industrial situations, including downhole flow conditions. A number of alternative techniques have been proposed which objectively discriminate between flow regimes and attempts have been made to produce flow regime maps based on the results obtained by these techniques, as shown in figure 2.8. The majority of the techniques employ statistical analyses of fluctuations in the average gas void fraction α as a basis for discrimination between flow regimes in opaque pipes and ducts.

Jones and *Zuber* [1975] used a fast response linearised X-ray void fraction measurement system to discriminate between flow regimes in air/water flows with mixture velocities up to 37m/s in a vertical

rectangular channel 5mm deep by 63.5mm wide. They demonstrated that by analysing the shape of the probability density function (PDF) produced by fluctuations in the average gas void fraction α, three flow regimes, namely bubbly, slug, and annular, could be distinguished. Each flow regime was shown to have a distinct shape to its respective PDF. Bubbly two-phase flows have a single-peaked PDF at low average gas void fractions (figure 2.9a), annular flows exhibit a single-peaked PDF at high average gas void fractions (figure 2.9b) and slug flows have a twin-peaked PDF with peaks at high and low average gas void fractions (figure 2.9c). However, *Jones* and *Zuber's* technique showed some limitions in distinguishing flow regimes especially at the transitional boundaries and at higher mixture velocities.

Sekoguchi et al [1987], using a constant current probe method for cross-sectional mean void fraction measurement (see *Sekoguchi* [1983]), discriminate between six different flow regimes which they name as bubbly, cap-bubble, plug, froth (F_1, F_2) and annular. Their experiments were carried out in a 26mm diameter transparent pipe containing vertically upward two-phase air/water mixture over a range of superficial gas and liquid velocities up to 30m/s and 1.5m/s, respectively.

The technique adopted by *Sekoguchi et al* [1987] involved selecting six typical void fraction signals, one for each of the flow regimes. These were digitally compared at a sampling frequency of approximately 100Hz to the measured signals from the flowing two-phase mixture using an autoregressive model adapted from previous work by the authors in the areas of voice-recognition (*Kashap* [1978]) and the analysis of human brain-waves (*Inoue* [1983]). When combining the flow

pattern recognition method with an evaluation of the cross-sectional and time averaged void fractions, an 80% success rate in discriminating between the six flow regimes was reported.

Wang et al [1988] identifies four flow regimes in a vertically upward air/water two-phase flow within a 24mm diameter transparent acrylic pipe by analysing the frequency spectra from a single solar cell illuminated diametrically across the transparent pipe by a D.C. light source. The output from the solar cell is low-pass filtered at 50Hz prior to being amplified and sampled at a frequency of 100Hz by a 12 bit analogue to digital converter connected to a microcomputer. The criteria used to identify each flow regime are as follows.

Bubbly flow - The solar cell detects bubbles as high frequency low amplitude fluctuations. Therefore, the contribution of high frequency components in the frequency spectra is more prominent when compared with other flow regimes.

Slug flow - The solar cell detects slug flows as basically a square wave. This is represented in the frequency spectra by a single peak in the low frequency range that is associated with the fundamental frequency of the slug flow, and high frequency components are nearly negligible in comparison.

Churn flow - Churn flow is regarded as a transition between slug flow and annular flow and the solar cell detects both high frequency fluctuations caused by bubbles and low frequency slugs. Therefore, the frequency spectra contains both high and low frequency components. However, it is reported that the low frequency components are dominant, which makes it difficult to distinguish churn flow from slug flow.

Annular flow - The solar cell detects annular flow as low frequency interfacial liquid waves with high frequency droplets entrained in the

gas phase. The combination of these effects produce so-called middle frequency components in the spectra.

Wang et al report that by applying the above frequency spectra based criteria 76% of flows are identified correctly if churn flows are included. However if churn flow is ignored then recognition success rates are increased to 88%. When the average gas void fraction α is considered in conjunction with the frequency spectra data, an 83% success rate is achieved with churn flow included and 96% success rate if churn flow is neglected.

2.3.1 Flow regime identification using pressure fluctuations

Very few attempts have been made to investigate pressure fluctuations in a two-phase flow. In one of the earliest investigations, by *Nishikawa et al* [1969], a detailed study using five static strain gauge pressure transducers connected to tappings at 0.1, 0.25, 0.5, and 1m intervals from the first tapping in a transparent 26mm smooth bore pipe was made. The data from these five channels were recorded simultaneously on oscillograph paper and at a later stage 540 points per channel were digitised and analysed. From the digitised pressure transducer signals, recorded for various flow conditions, the standard deviation, characteristic length of the autocorrelation, probability distribution, and spectral densities were calculated. Based on the statistical data obtained from the fluctuations in static pressure and visual observations in the four flow regimes, namely bubbly, slug, froth and annular, *Nishikawa et al* [1969] claims that each flow regime corresponds to a particular set of statistical properties. However, in the transitional area between

flow regimes it is difficult to draw any conclusions.

In the bubbly flow regime, *Nishikawa et al* concluded that the shape of the probability distribution roughly represents a normal distribution, see figure 2.10, and the values of both standard deviation and characteristic autocorrelation length scale are small. The spectral density of bubbly two-phase flow was found to exhibit peaks at lower frequencies than those associated with the passage of individual bubbles. It was concluded that these low frequency peaks were associated with dense and sparse clouds of bubbles travelling along the pipe periodically.

In most cases of slug and froth flow, *Nishikawa et al* found that the probability distribution was no longer normal in shape but exhibited twin peaks. Furthermore, the standard deviation and characteristic length of the pressure signals are much larger than those found in the bubbly flow regime. The spectral densities of static pressures pulsations in both slug and froth flow were found to be periodic at very low frequencies.

In annular flow, the probability distribution equates approximately to a normal distribution, similar to that found in the bubbly flow regime, which would suggest the existence of random pressure fluctuations. The values of standard deviation and characteristic length are also small, as in the bubbly flow regime.

From the results of this investigation it would appear difficult to discriminate between the bubbly and annular flow regimes. However, *Nishikawa et al* concluded that further investigations of these and other statistical properties would lead to an objective discrimination

technique for flow regime identification. It should be noted, however, that these conclusions were based on measurements of static pressure signals and that the disturbances causing the pressure signals monitored by *Nishikawa et al* may originate from anywhere in the apparatus.

Tutu [1982], using an air/water flow loop with a constant liquid head, investigated the possibility of using the fluctuations in static and differential wall pressures as a means of flow pattern recognition. The experimental test section was approximately 2.5m long with an internal diameter D of 52.2mm. *Tutu* recognised some of the problems affecting the measurements of static pressure fluctuations, such as pump induced pressure pulses, vibration through pipes and pressure pulses due to bubble formation. He attempted to reduce, and hopefully eliminate, these effects by giving careful consideration to the design of the flow loop. The design features included the installation of flexible coupling to isolate the test section from pump vibrations, air being introduced to the flow through a porous plate some distance upstream of the measurement section so as to reduce the magnitude of any pressure pulses caused by bubble formation. In the experimental test section, two Endevco model 8506-5 piezoresistive pressure transducers with a resonant frequency of 65KHz were separated axially by D/2 and flush mounted with the inside pipe wall along the same vertical axis.

Tutu, like *Nishikawa et al* [1969], also made static pressure measurements p_2 and p_1 from upstream and down-stream pressure transducers, respectively, and recorded the results on magnetic tape that has a response frequency range from DC to 5KHz. However, unlike *Nishikawa et al* [1969], the two static pressure signals were also

subtracted using an analogue 'difference' circuit to obtain the differential pressure $p_{21} = (p_2-p_1)$, which was also recorded. Unfortunately, an analogue subtraction technique is very susceptible to electrical noise. Therefore *Tutu* used a 1.6KHz low pass filter with a drop off of 24 dB per octave to reduce electrical noise and prevent aliasing when digitising the signals at a sampling frequency of 3.2KHz.

The data analysis performed evaluated and plotted the PDF, skewness factor and flatness factor of p_{21} for each set of data. Using a discrimination technique based on the skewness and flatness factors, *Tutu* claims that various flow regimes can be objectively identified for vertical two-phase gas liquid flows using a single differential pressure signal. In bubbly, vertically upward air/water two-phase flow he observed that the PDF exhibits a single peak centred approximately around the position of the average gas void fraction α, with skewness and flatness factors of the order of 0.2 and 6 respectively (Equation 1.4 is used to calculate α with F_m set to zero).

Matsui [1984] investigated the statistical properties of differential pressures measured by four static piezoresistive pressure transducers placed in pairs with an axial separation of D/2, where the internal pipe diameter D is given as 22mm. Each pair of transducers are separated axially by 200mm, as shown in figure 2.11, and mounted as near flush as possible with the internal diameter of the transparent pipe. The working fluids were nitrogen gas and water.

The four static pressure signals were amplified using a DC amplifier, with a frequency response of 10KHz, to a suitable level

prior to being low-pass filtered at 20Hz to remove the effects of high frequency disturbances. These signals were then sampled by a 12 bit A/D converter every 10 msec. The differential pressure signals were obtained by subtracting the static pressure signals digitally, unlike *Tutu* [1982] who used analogue techniques, to obtain $\Delta p_a=(p_1-p_2)$, $\Delta p_b=(p_3-p_4)$, $\Delta p_c=(p_1-p_3)$ and $\Delta p_d=(p_2-p_4)$, where p_1, p_2, p_3 and p_4 are the static pressure signals from the four transducers, as shown in figure 2.11. Δp_a and Δp_b are referred to by *Matsui* as the radius or 'R' scales, Δp_c and Δp_d are referred to as the long or 'L' scales. The 'R' and 'L' scales are simply used to distinguish between the two different transducer separation distances when calculating differential pressures, the separation distances being 11mm for the 'R' scales and 200mm for the 'L' scales.

Matsui evaluated the probability density functions, cross correlations, variances, and mean values for both the 'R' and 'L' scales for six flow regimes, bubbly, spherical-cap bubbles, slug, froth, annular, and mist flows. Results obtained in the bubbly flow regime for fluctuations in differential pressures over the shorter 'R' scale, Δp_a and Δp_b, show PDFs to have a near normal type distribution with a single peak centred at a point approximately equal to the average gas void fraction α, which is consistent with *Tutu* [1982] who used a similar axial transducer spacing. *Matsui* also found that flow regimes can be identified using the much longer 'L' scale, and in general it was found that the PDFs associated with differential pressure measurements over the 'L' scale, Δp_c and Δp_d, are more peaked than those obtained from either the 'R' scale or *Tutu's* results. The variance in the bubbly flow regime of Δp_a was quoted as being very small, and in the spherical-cap bubble flow regime it was reported as being of the order of ten times larger.

Flow regime maps have been produced by many researchers from visual observations of flow regimes for known superficial gas and liquid velocities. *King et al* [1988], however, developed a technique using an optimising autoregressive moving average (ARMA) model of static and differential pressure signals, and produced a Taitel-type flow regime map as shown in figure 2.12. Experiments were carried out for air/water flows ranging from 1 - 390L/min and 10 - 190L/min respectively in a 6m long 24mm internal diameter transparent pipe. Two Ohkura model PT3000 pressure transmitters were mounted in the wall of the test section 1.5m apart and 4m down-stream of the inlet. The outputs from the pressure transmitters are reported to have pulsation frequencies below 35Hz. The signals are therefore filtered through a 35Hz low pass filter to reject noise and then amplified to a suitable level using a DC amplifier. The differential pressure signal is obtained by analogue subtraction of the two filtered and amplified static pressure signals. The two static pressure signals and the differential pressure signal are then sampled at 100Hz by the analogue to digital converter of an IBM PC/XT computer. The average gas void fraction α was evaluated using the quick closing valve technique (see section 2.1.1).

Data collected from their experiments was used in a computer algorithm developed by *King et al* to evaluate the so called 'dynamic signature' of six flow regimes they labelled as spherical bubbly flow, bubbly flow, high-velocity bubbly flow, slug flow, churn flow and annular flow. The dynamic signatures of known two-phase flow regimes are then used as comparisons for measured pressure fluctuations in unknown two-phase flows. Using their technique they claim an 85% success rate in flow regime recognition, however, at the transition boundaries, flow regime identification is less accurate.

All of these investigations into flow regime identification were based on the direct measurement of the static pressures. The differential pressure fluctuations, which were used as a means of discriminating between flow regimes, were obtained by the subtraction of static pressure signals either using analogue electronics or digital techniques. However, this approach is very susceptible to errors creeping into the differential pressure signals through a number of sources such as, unmatched transducers and electronics for both static and dynamic measurements, and from electronic noise. *Matsui* [1984], and other authors, have made references to low-pass filtering of the pressure signals, which indicates that problems have been encountered in this approach to differential pressure measurements.

During the literature survey no reference was found to the measurement of differential pressures using a differential pressure transducer. A single differential pressure transducer requires none of the expensive matched electronics associated with the subtraction methods described previously and should provide a true measurement of the difference in pressures at two points in the flow. In this study both methods will be investigated and evaluated for their suitability for use downhole (see chapter 5).

2.4 Measurement of the dispersed gas or bubble velocity in vertically upward bubbly two-phase flow

Cross correlation has been used for many years as a statistical technique for measuring the time of flight between two sensors a known distance apart (see, for example, *Butterfield et al* [1961]). *Beck* &

Plaskowski [1987] have extensively covered the theoretical and practical aspects of cross correlation in their book entitled 'Cross Correlation Flowmeters - their Design and Application'. Nevertheless, a brief summary of statistical techniques used in the analysis of random data is given below.

2.4.1 Basic principles of random data analysis

Any turbulent flow, whether it is single or multi-phase, is considered to be random in its nature. A particular type of random process in which the statistical properties observed in any interval of time are the same as those in any other interval of time is called a 'stationary' random process. Fluctuating differential pressure signals produced by fully developed vertically upward bubbly two-phase flow are considered to be stationary random signals (see, for example, *Lance* & *Bataille* [1991]). They can also be considered to be 'ergodic' random signals, which means that the statistical parameters of the signal e.g. the mean and autocorrelation, evaluated by taking time averages over a single long recording time will be the same as those evaluated by taking ensemble averages.

The statistical parameters used to describe a stationary ergodic random signal x(t) are as follows.

(i) The mean (μ), mean square (Ψ^2), root mean square (RMS), variance (σ) and standard deviation (SD)

The mean value, or the first moment, μ of a random signal is the average of the instantaneous values of that signal, and is defined as

$$\mu = \lim_{T\to\infty} \frac{1}{T} \int_0^T x(t)\, dt \qquad 2.7$$

The mean square value Ψ^2 of a random signal is the average of the squared values of the signal x(t) and is defined as

$$\Psi^2 = \lim_{T\to\infty} \frac{1}{T} \int_0^T x^2(t)\, dt \qquad 2.8$$

The root mean square value RMS of a signal is the positive square root of the mean square value Ψ^2.

The variance σ is the mean square value about the mean. This is effectively the mean square value of the AC component of the signal and hence is not affected by any DC offset:

$$\sigma^2 = \lim_{T\to\infty} \frac{1}{T} \int_0^T (x(t) - \mu)^2\, dt \qquad 2.9$$

The standard deviation SD is the positive square root of the variance σ^2.

(ii) <u>The autocorrelation $R_{xx}(\tau)$</u>

The autocorrelation function $R_{xx}(\tau)$ of a random data signal x(t) describes the general dependence of data values at time t on the data value at time $(t+\tau)$. It can be calculated as the time averaged product of the instantaneous values separated by the time interval τ as shown in figure 2.13 and described by equation 2.10:

$$R_{XX}(\tau) = \lim_{T\to\infty} \frac{1}{T} \int_0^T x(t)\, x(t+\tau)\, dt \qquad 2.10$$

It can be seen from equation 2.10 that the autocorrelation is obtained by averaging the instantaneous product of the two values x(t) and x(t+τ) over a time period T which approaches infinity. However, in practice the observation time T must be finite, i.e.

$$R_{XX}(\tau) = \frac{1}{T} \int_0^T x(t)\, x(t+\tau)\, dt \qquad 2.11$$

The length of the finite sampling time T is determined by the highest and lowest frequency components of the signal that is to be sampled. Nyquist sampling theory for a sequence of N samples, taken at regular time intervals t, states that the frequency resolution is equal to 1/Nt and the number of frequency components is N/2+1, therefore t is set by the highest frequency component to be sampled i.e. there must be at least two samples for each cycle of the highest frequency component. Furthermore the number of samples N in a given record must contain at least one complete cycle of the lowest frequency component of the signal to be sampled. The minimum length of the finite sampling time T is therefore given by Nt, however in practice it is usually many times larger than given by Nt.

The autocorrelation $R_{XX}(\tau)$ can also be shown to be a real-valued even function of τ with a maximum at τ=0, therefore

$$R_{XX}(\tau) = R_{XX}(-\tau) \qquad 2.12$$

$$R_{XX}(0) \geq |R_{XX}(\tau)| \text{ for all } \tau \qquad 2.13$$

Since equation 2.13 is true for all τ a normalised correlation coefficient $\rho_{xx}(\tau)$ is often quoted, where

$$\rho_{xx}(\tau) = \frac{R_{xx}(\tau)}{R_{xx}(0)} \qquad 2.14$$

Another important characteristic of the autocorrelation is that at τ=0 the autocorrelation equals the mean square value of the signal x(t):

$$R_{xx}(0) = \Psi^2 \qquad 2.15$$

and if the signal x(t) has <u>no</u> periodic component then

$$\mu = (R_{xx}(\infty))^{\frac{1}{2}} \qquad 2.16$$

(iii) <u>The cross correlation $R_{xy}(\tau)$</u>

The cross correlation function of two sets of stationary ergodic random data signals describes the general dependency of the values of one data set on another, as shown in figure 2.14. The cross correlation function $R_{xy}(\tau)$ of two signals x(t) and y(t) is defined by

$$R_{xy}(\tau) = \lim_{T\to\infty} \frac{1}{T} \int_0^T x(t)\, y(t+\tau)\, dt \qquad 2.17$$

However, in practice a finite value of T is used as in equation 2.11 for $R_{xx}(\tau)$, therefore

$$R_{xy}(\tau) = \frac{1}{T} \int_0^T x(t)\, y(t+\tau)\, dt \qquad 2.18$$

If the two stationary random ergodic signals were identical, then the cross correlation function would equal the autocorrelation function. However this is seldom the case in practice since the source of the two signals often varies with time (see section 6.2). It can be shown that

$$(R_{xx}(0)\ R_{yy}(0))^{\frac{1}{2}} \geq |R_{xy}(\tau)| \qquad 2.19$$

Equation 2.19 is also true for all τ, and a normalised cross correlation coefficient, $\rho_{xy}(\tau)$, is defined by

$$\rho_{xy}(\tau) = \frac{R_{xy}(\tau)}{(R_{xx}(0)\ R_{yy}(0))^{\frac{1}{2}}} \qquad 2.20$$

2.4.2 Previous research into cross correlation as a means of measuring the area averaged dispersed phase velocity

Many techniques of measuring the area averaged dispersed gas velocity in two-phase flow have been explored. Much of this research has come about as an extension to the development of void fraction measurement systems. It has been well reported that when measuring average gas void fractions, there are always fluctuations caused by the turbulent nature of a two-phase flow.

Consider two void fraction sensors placed an axial distance Δz apart as shown in figure 2.15. If we examine the slug flow regime, when a slug of gas passes a sensor, there will be a dramatic change in void fraction from zero to nearly one. By cross correlating the two void fraction signals over a suitable length of time T, the time taken for a gas slug to travel the distance Δz can be calculated, and hence the dispersed phase velocity can be evaluated. This method is

probably best suited to the slug flow regime.

However, the correlation method of area averaged dispersed phase velocity measurement has been used in conjunction with many void fraction measurement techniques e.g. impedance, capacitance, ultrasonics and pressure fluctuations, for various flow regimes. *Matthes, Riebold,* and *De Cooman* [1970] in vertically upward air/water bubbly two-phase flow, used two laser light beams approximately 1mm in diameter axially separated by one pipe diameter D, where D is the inside diameter of the glass test section (D=10mm). The laser light beams were positioned diametrically opposite two photodiodes. As bubbles passed through the light beams the intensity of light detected by the photodiodes fluctuated due to the scattering of the light beam caused by the bubbles. Cross correlation of the photodiode signals produced very repeatable initial results over a range of gas and liquid volume flow rates of 20 - 100L/hour and 300 - 600L/hour respectively.

Olszowski et al [1976] cross correlated the outputs from two piezoelectric ultrasonic receivers separated by a distance *l*, which in this case is equal to one pipe diameter (D=50.8mm). The ultrasonic receivers were excited by two separate parallel ultrasonic beams transmitted through the wall of the test section diametrically opposite the receivers. The ultrasonic beams are modulated by acoustic impedance changes within the moving two-phase flow. Experiments were carried out in vertical air/water two-phase flow with homogeneous mixture velocities V_m, where V_m is defined as the total volume flow rate divided by the cross-sectional area of the test section, in the range of 1.6 - 4.1m/s, and average gas void fractions α up to 43%. Cross correlation of the two ultrasonic receivers

produced, after suitable amplification, a transit time t_t for the fluid flowing between the two transducers. From this the homogeneous mixture velocity was calculated as $V_m = l/t_t$, which matched the actual mixture velocity with a maximum error of ±10%. An important point to be noted from their work is that a pseudo-homogeneous dispersed flow, such as bubbly two-phase flow, retains an almost frozen flow pattern identity for at least one pipe diameter.

Ong [1975], using ultrasonic transducers, investigated the standard error $\epsilon(\tau)$ of the transit time cross correlation measurement, which is defined below as the squareroot of the normalised variance,

$$\epsilon(\tau) = \sqrt{\frac{\mathrm{var}(\tau)}{\tau^2}} \qquad 2.21$$

as functions of the signal bandwidth B, the correlation integration time T and the normalised cross correlation coefficient $\rho_{xy}(\tau)$, from which the following relationship was developed:

$$\epsilon(\tau) = \frac{k_1}{B^{1.5}\, T^{0.5}} \left[1 + (1/\rho_{xy}(\tau))^2\right]^{0.5} \qquad 2.22$$

where k_1 is a constant.

The volume flow rate $\dot{V}$ obtained using a cross correlation flowmeter, by measurement of the transit time τ, will be of the form

$$\dot{V} = k_2(l/\tau)\, A \qquad 2.23$$

where l is the transducer separation distance, A the pipe cross-sectional area, and k_2 a calibration constant. *Ong* shows that standard

error in volume flow rate $\epsilon(\dot{V})$ is related to $\epsilon(\tau)$ by

$$\epsilon(\dot{V}) \propto \epsilon(\tau)/l \qquad 2.24$$

Ong suggests that since the error in the measured volume flow rate decays as l increases, then the standard error $\epsilon(\tau)$ increases in a non-linear way as the length l increases. Equation 2.24 shows that increasing l can reduce the error in volume flow rate measurement. Therefore, a short transducer separation distance l results in a short transit time τ and a large value of $\epsilon(\tau)$, while an excessively long separation distance l, results in poor correlation of signals. Experiments carried out by *Ong* suggest that there is an optimum range for the transducer separation distance l of between one and six pipe diameters. The way in which the cross correlation function decays as l is increased is shown in figure 2.16a, and the corresponding way in which the standard error varies is shown in figure 2.16b. These results are for water flow in a pipe of diameter 25.4mm and mean velocity of 4.2m/s and were obtained by using ultrasonic transducers with a bandwidth of 1-5KHz and an integration time T of 20 seconds.

Using pulsed ultrasound transducers, *Xu* [1986] obtained, on average, 82% - 85% accuracy in measuring the dispersed gas velocity of air/water bubbly two-phase flows. He also claimed that under certain flow conditions it was possible to determine the continuous phase velocity from the cross correlogram.

Bernier [1981] used impedance sensors to measure the area averaged gas velocity in the bubbly flow regime. He found that the dispersed phase velocity measured by cross correlation techniques was always much lower than the actual area averaged gas velocity. He

concludes that he was measuring the slower moving, large scale structures in the flow known as kinematic waves.

Kinematic waves (see *Lighthill & Whitham* [1955]) are waves within a flowing fluid travelling slower than the area averaged velocity of the fluid. In vertical bubbly two-phase flow, bubbles travelling at a terminal velocity greater than the kinematic wave propagation speed, on reaching the rear of the kinematic wave slow down. After travelling through the wave the bubbles accelerate until they reach their terminal velocity once again. The effect of reducing the bubble velocity at the kinematic wave interface causes a concentration in void fraction, hence kinematic waves also cause dense and sparse regions of void gas fraction within bubbly two-phase flow.

Hammer [1983] and *Lucas* [1987] both used capacitance void fraction sensors, and found, in contradiction to *Bernier's* work, that the cross correlation dispersed phase velocity was always higher than the actual area averaged gas velocity. *Lucas*, using sensors separated by 2 pipe diameters (160mm), suggests that his capacitance void fraction sensors may be more sensitive to the relatively large, faster moving bubbles within the flow.

2.4.3 Use of pressure fluctuations in the measurement of the dispersed phase velocity

Naturally occurring pressure fluctuations in a two-phase flow may be caused by any disturbance in the flow. In the vertically upward bubbly flow regime, phases of different densities travel at different velocities along random paths causing fluctuations in

pressure. These are combined with fluctuations in the effective density of the fluid due to variations in local average gas void fractions, pressure fluctuations caused by the turbulent wake behind a bubble and the background tutbulence present in the continuous phase. Since pressure fluctuations are generally associated with the dispersed phase velocity, cross correlating two fluctuating pressure signals may result in a transit time τ that is associated with the velocity of the dispersed phase.

As reported in section 2.3.1, *Matsui* [1984] investigated the statistical properties of differential pressures fluctuations. He also cross correlated the differential pressures Δp_a and Δp_b as shown in figure 2.11 for the spherical cap bubble flow regime. The position of the temporal delay peak in the cross correlation was assumed to correspond to the time of flight of the dispersed phase and the corresponding gas rise velocity was evaluated as 0.37m/s. This compares well with the average rise velocity measured from serial photographs of 0.36m/s. However, he produced no corresponding correlation results for the bubbly flow regime.

In this study naturally occurring pressure fluctuations within a vertically upward bubbly air/water two-phase pipe flow are monitored by two differential pressure transducers which are separated by a short axial distance l along the pipe. These differential pressure signals ΔP_A and ΔP_B are related to each other since they are generated by the same basic source (the bubbly two-phase flow) and through auto and cross correlations of these pressure signals the velocity of the convected disturbances within the two-phase flow can be evaluated. Convected disturbances within the bubbly two-phase flow will be primarily generated by passage of the dispersed bubbly

phase through the continuous phase, therefore it follows that the convected disturbance velocity of the naturally occurring pressure fluctuations evaluated by correlation techniques will reflect the velocity of the dispersed phase. In this thesis theoretical and experimental studies of naturally occurring pressure fluctuations are carried out with the aim of forming a novel non-intrusive dispersed phase velocity monitoring technique that meets the requirements of the oil industry for use downhole.

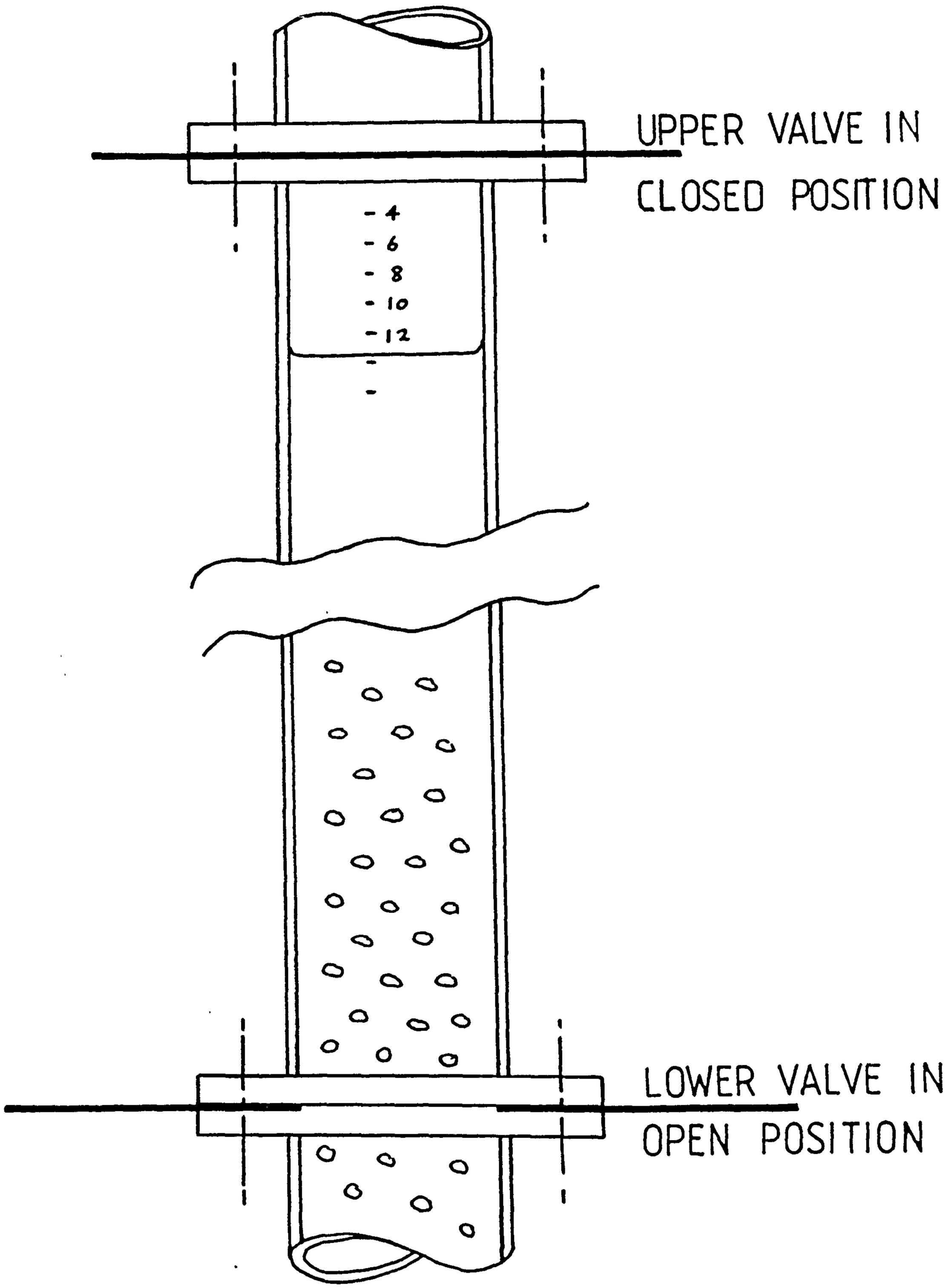

Figure 2.1 Illustration of the quick closing valve technique used to measure average gas void fractions

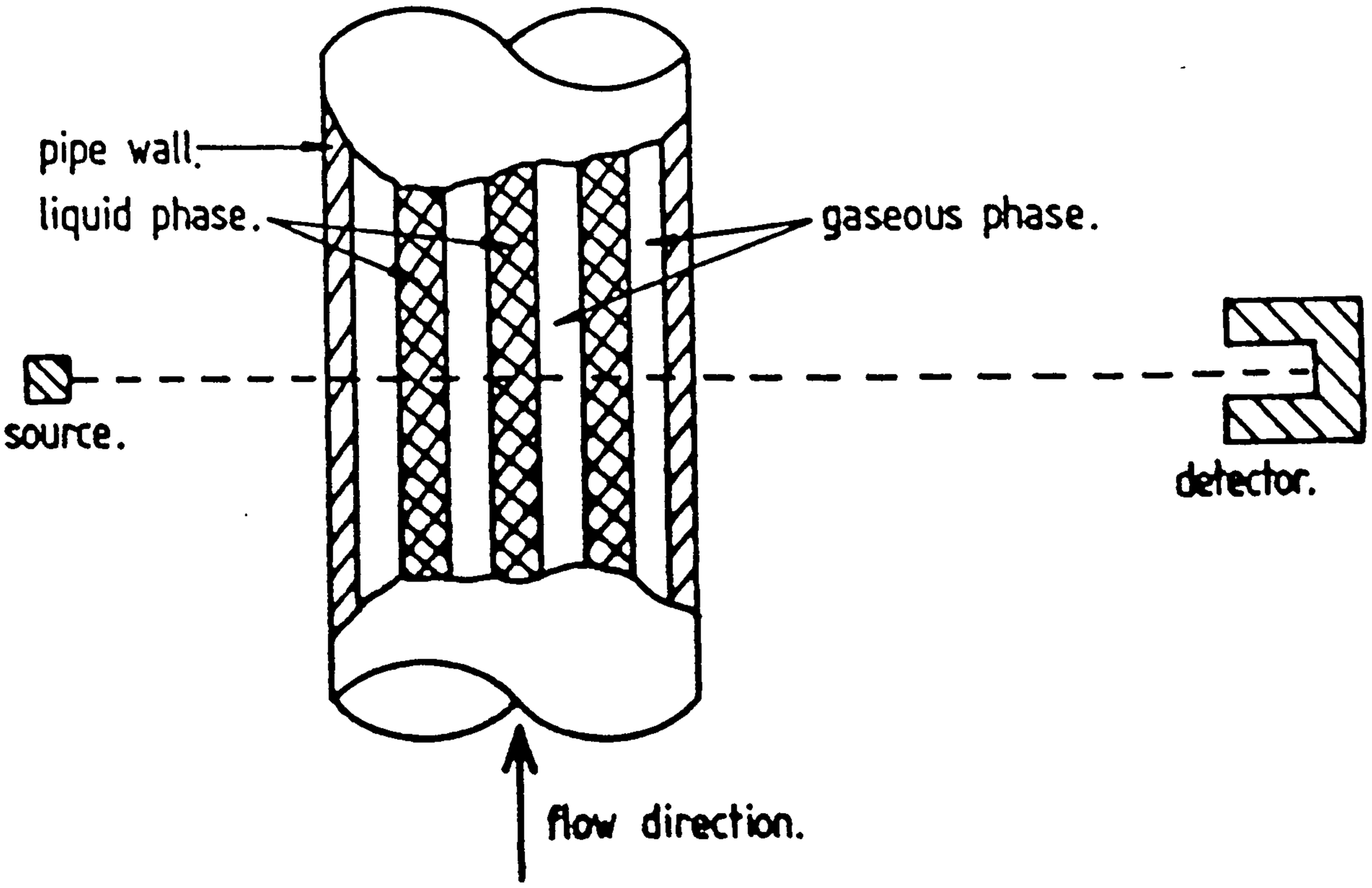

Figure 2.2a Schematic diagram of the radiation absorption technique illustrating a hypothetical flow pattern put forward by *Petrick & Swanson* [1958] in which the gas and liquid phases are arranged perpendicular to the collimated beam of radiation

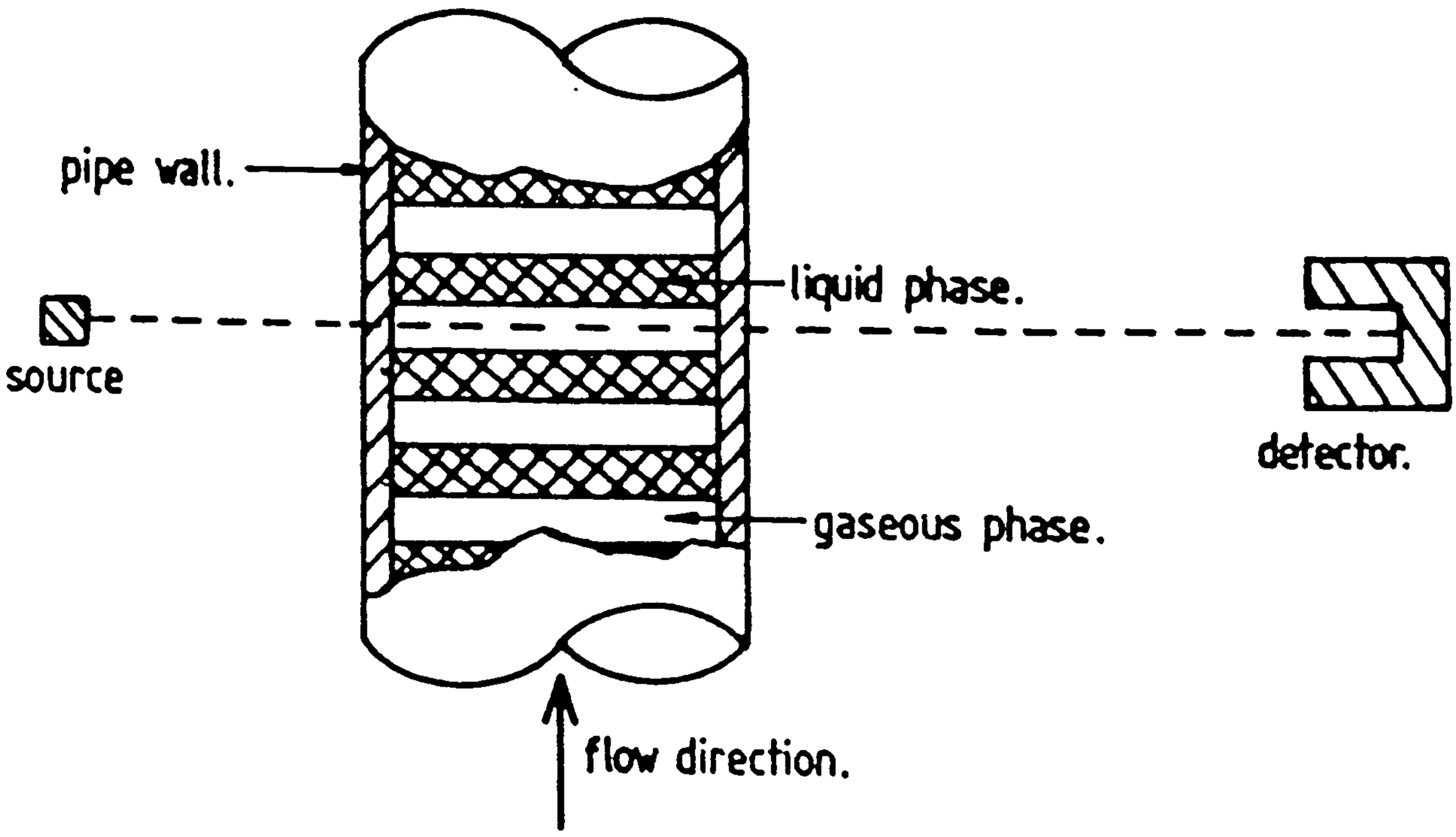

Figure 2.2b Schematic diagram of the radiation absorption technique illustrating a hypothetical flow pattern put forward by *Petrick & Swanson* [1958] in which the gas and liquid phases are arranged in layers parallel to the collimated beam of radiation (pseudo slug flow)

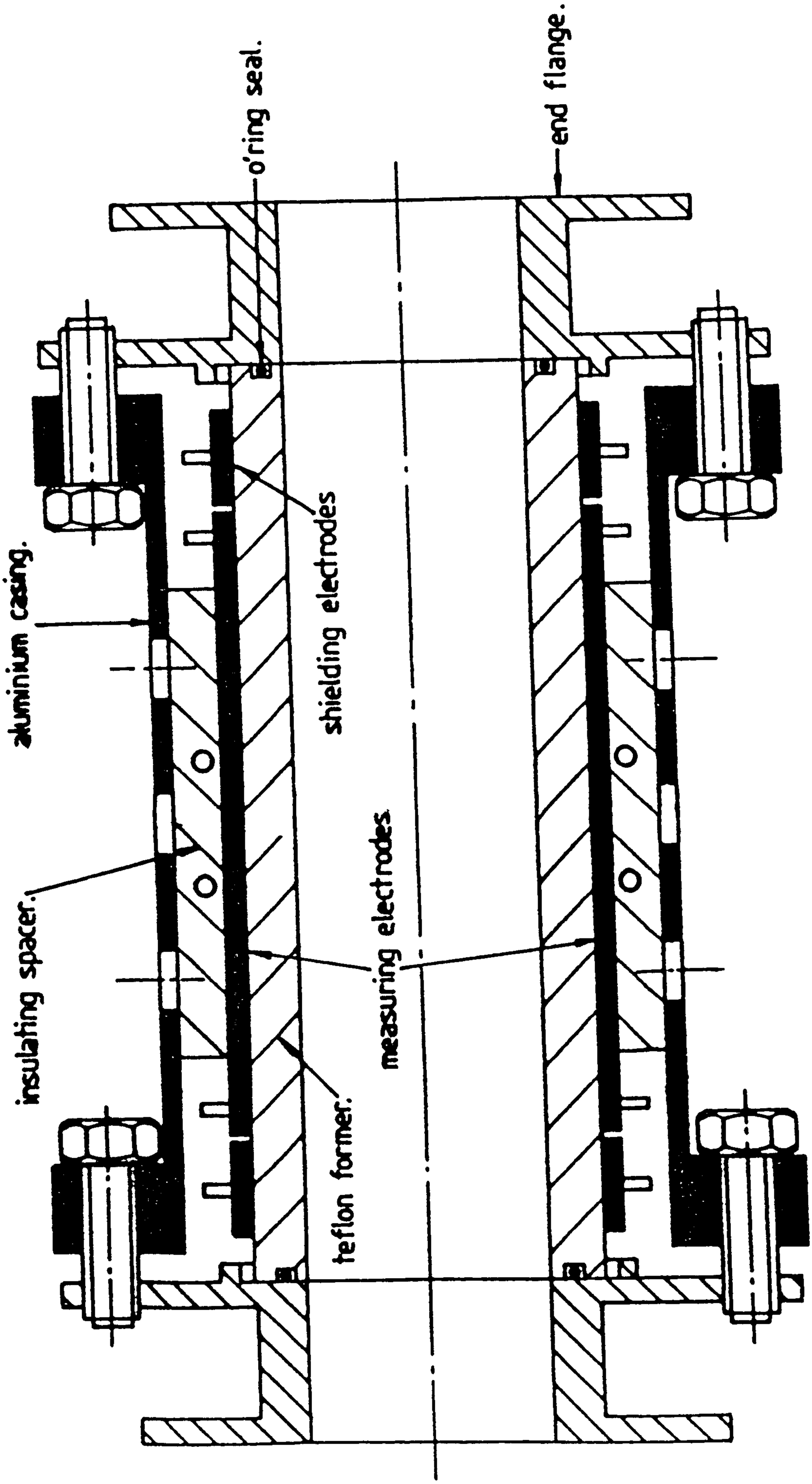

Figure 2.3 Illustration of the capacitance average void fraction monitoring transducer developed by *Lucas* [1987]

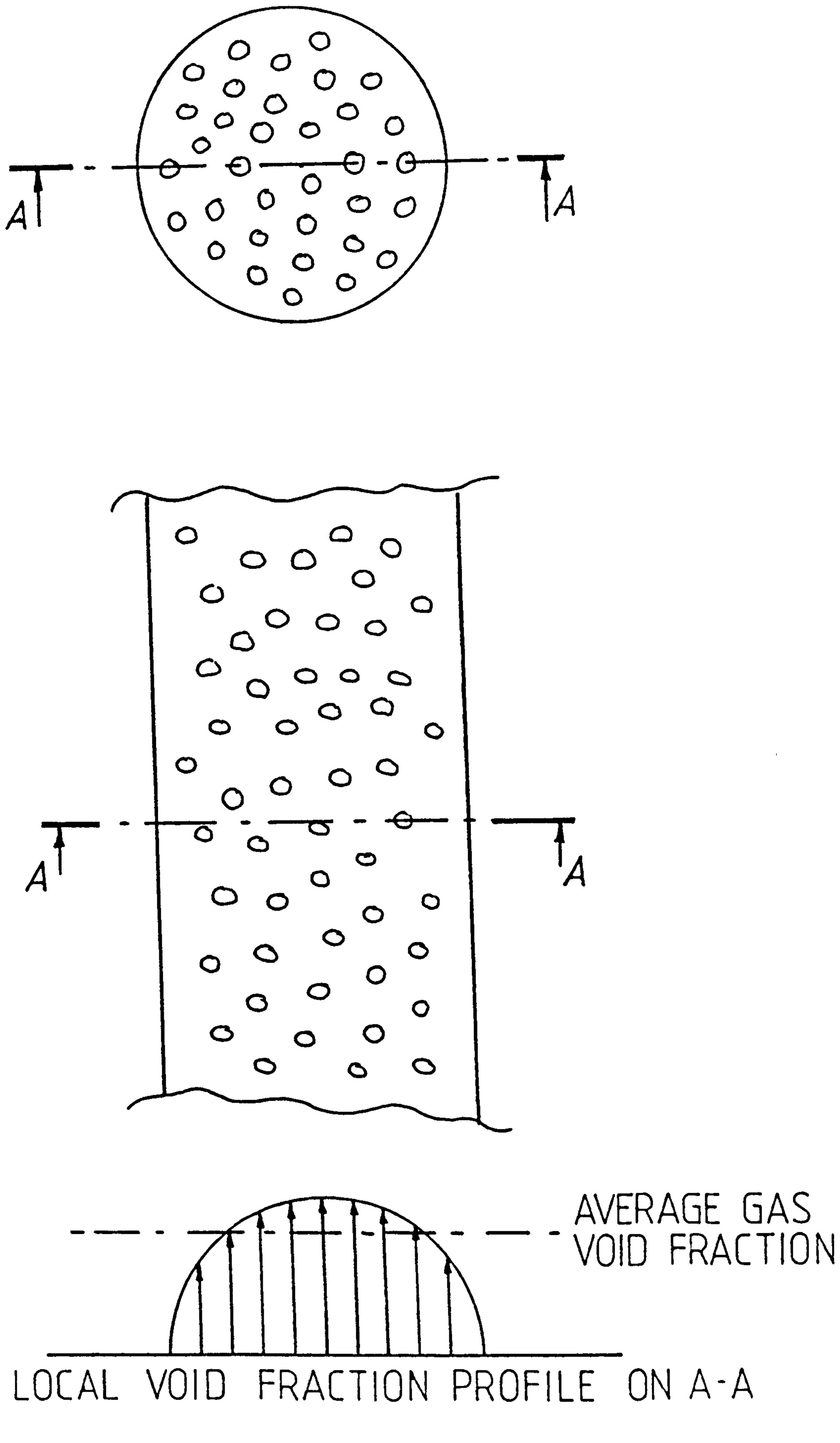

Figure 2.4 Principle of local void fraction measurement

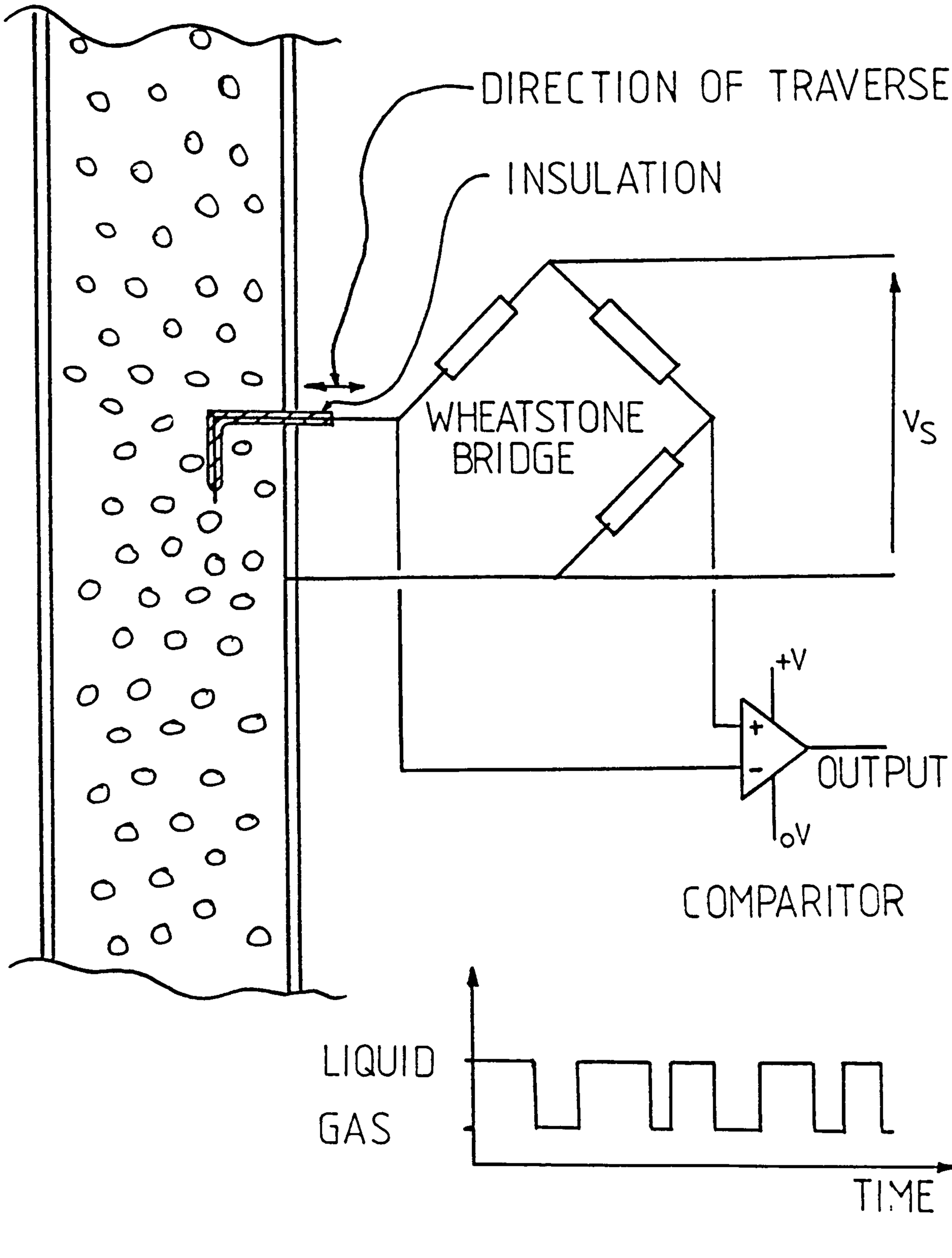

Figure 2.5 Illustration of the resistance probe technique used to measure local void fractions

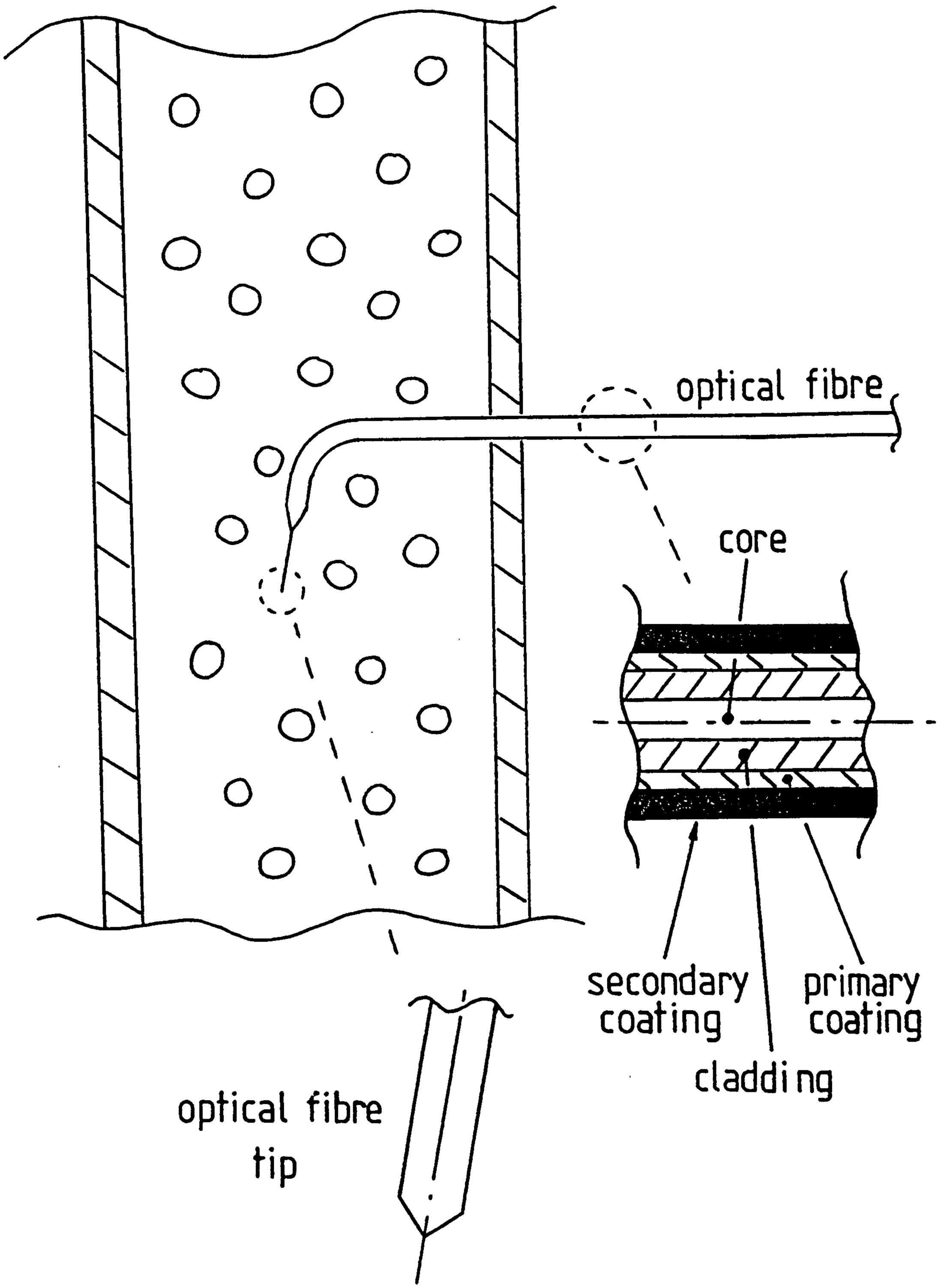

Figure 2.6 Fibre optic probe as used by *Lance & Bataille* [1991] to measure local void fractions

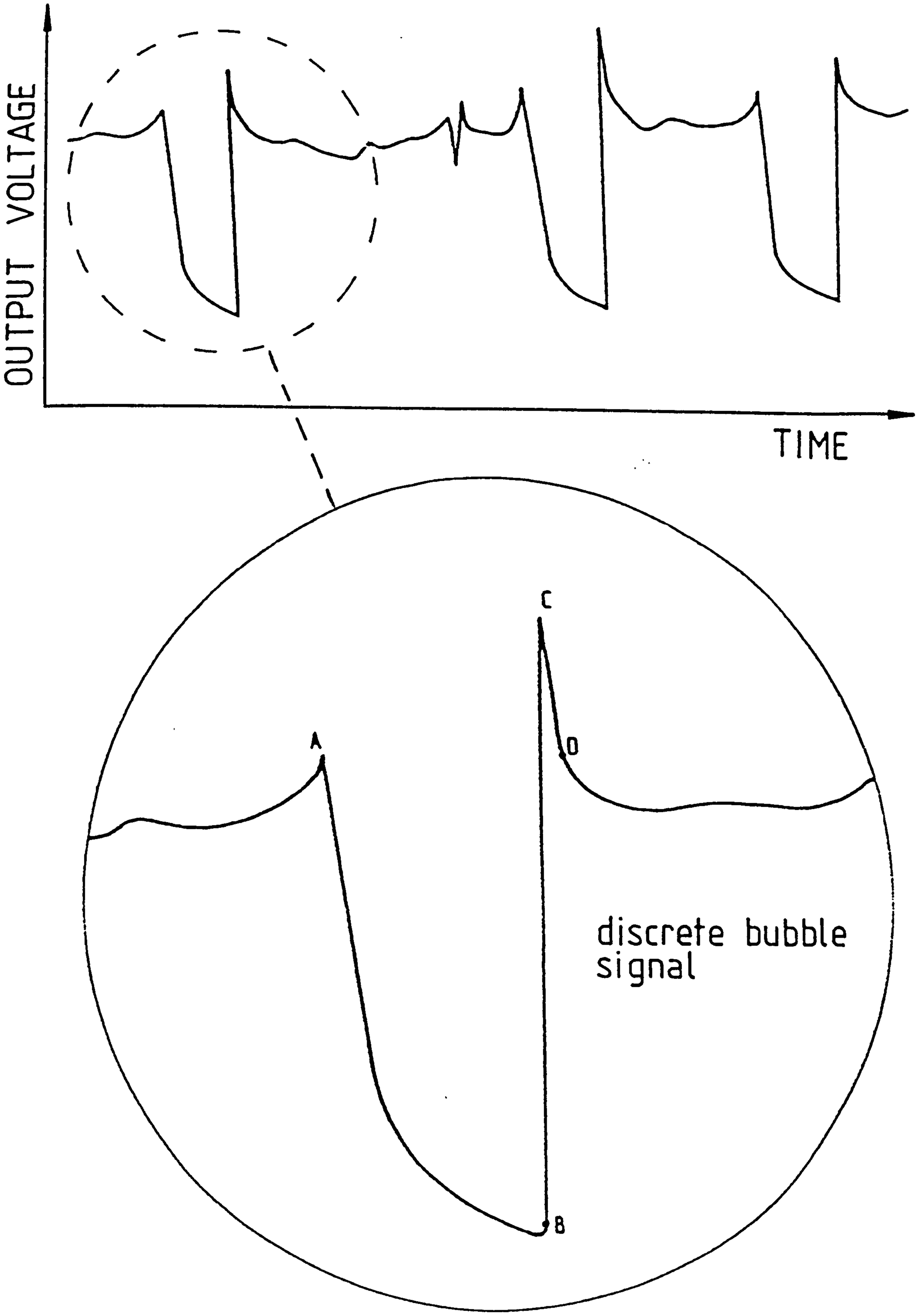

Figure 2.7 Typical signal from a hot-film probe positioned in a two-phase flow when interacting with a discrete bubble

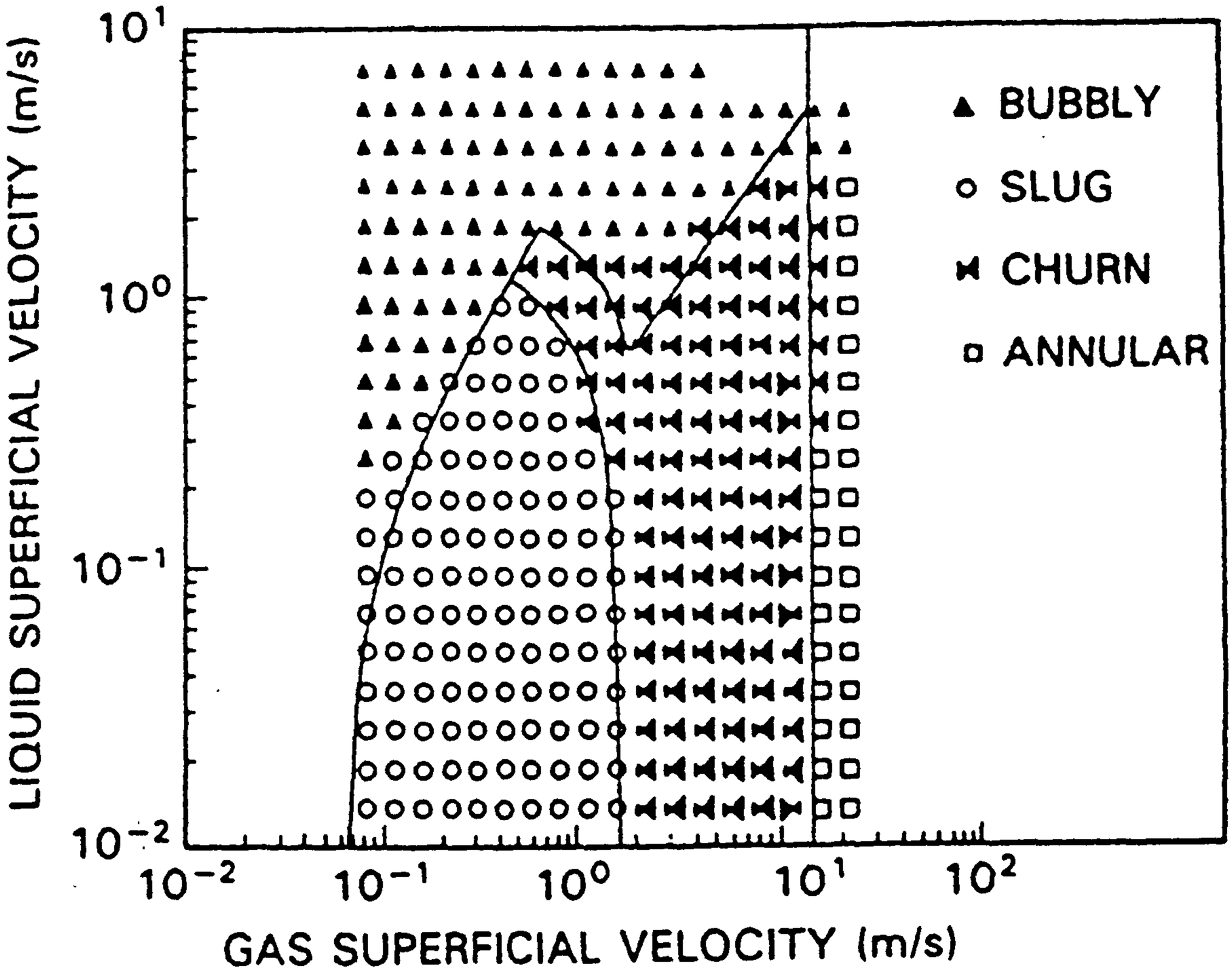

Figure 2.8 Typical flow regime map produced by objectively discriminating between flow regimes

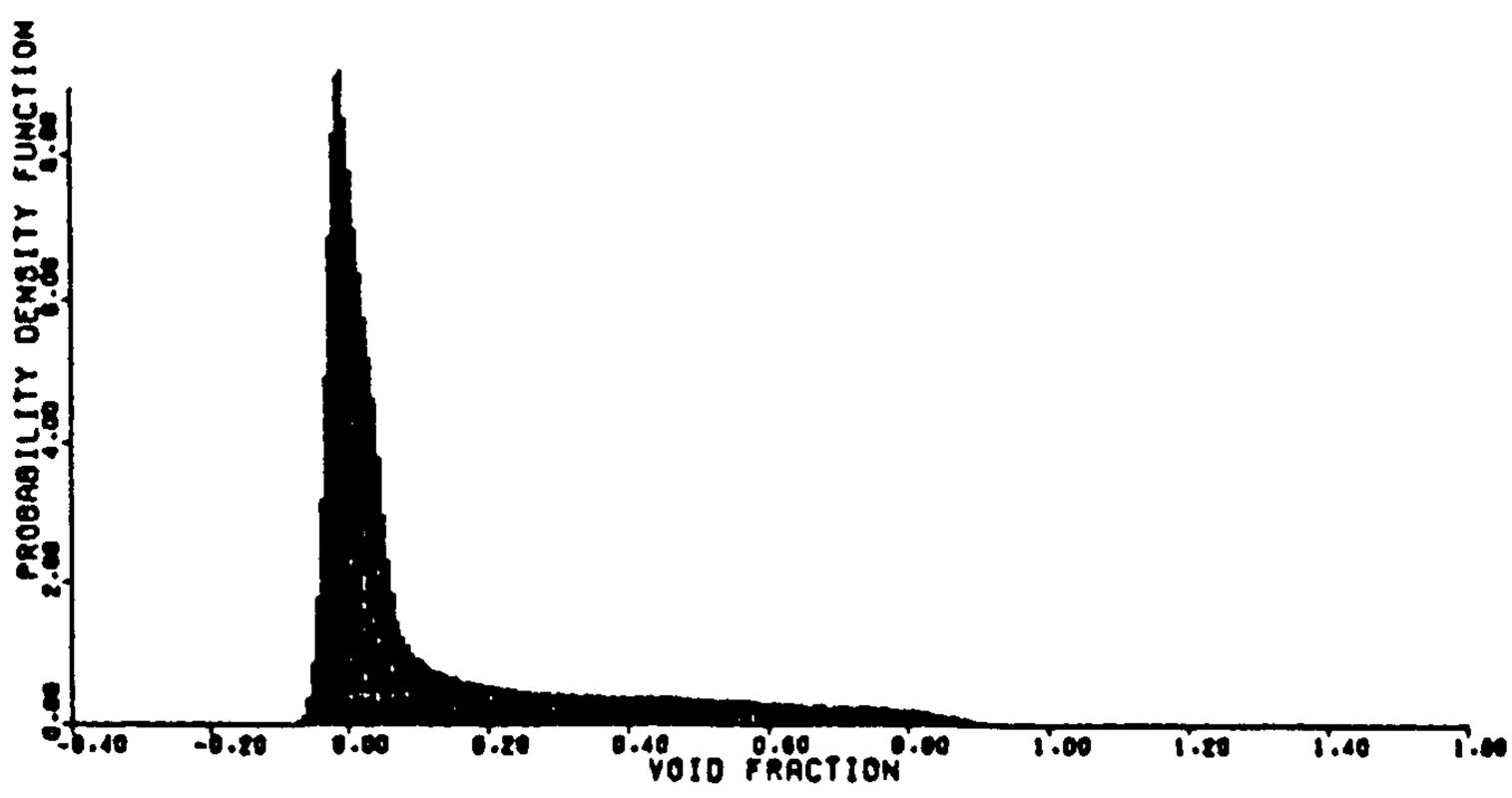

Figure 2.9a Probability density function produced by *Jones & Zuber* [1975] of the fluctuations in average gas void fraction α made using an x-ray void fraction technique of vertically upward bubbly two-phase flow within a rectangular duct

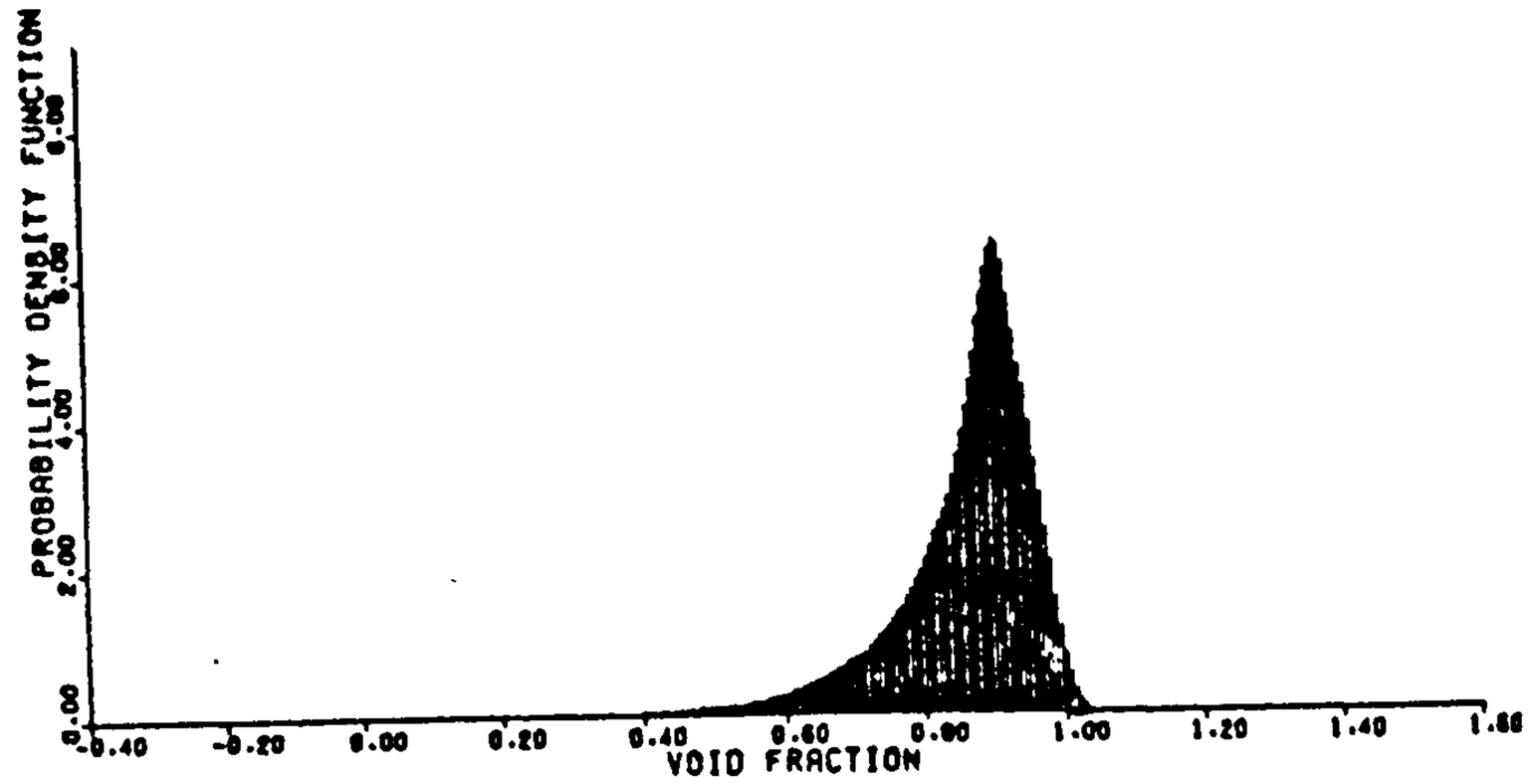

Figure 2.9b Probability density function produced by *Jones & Zuber* [1975] of the fluctuations in average gas void fraction α made using an x-ray void fraction technique of vertically upward annular two-phase flow within a rectangular duct

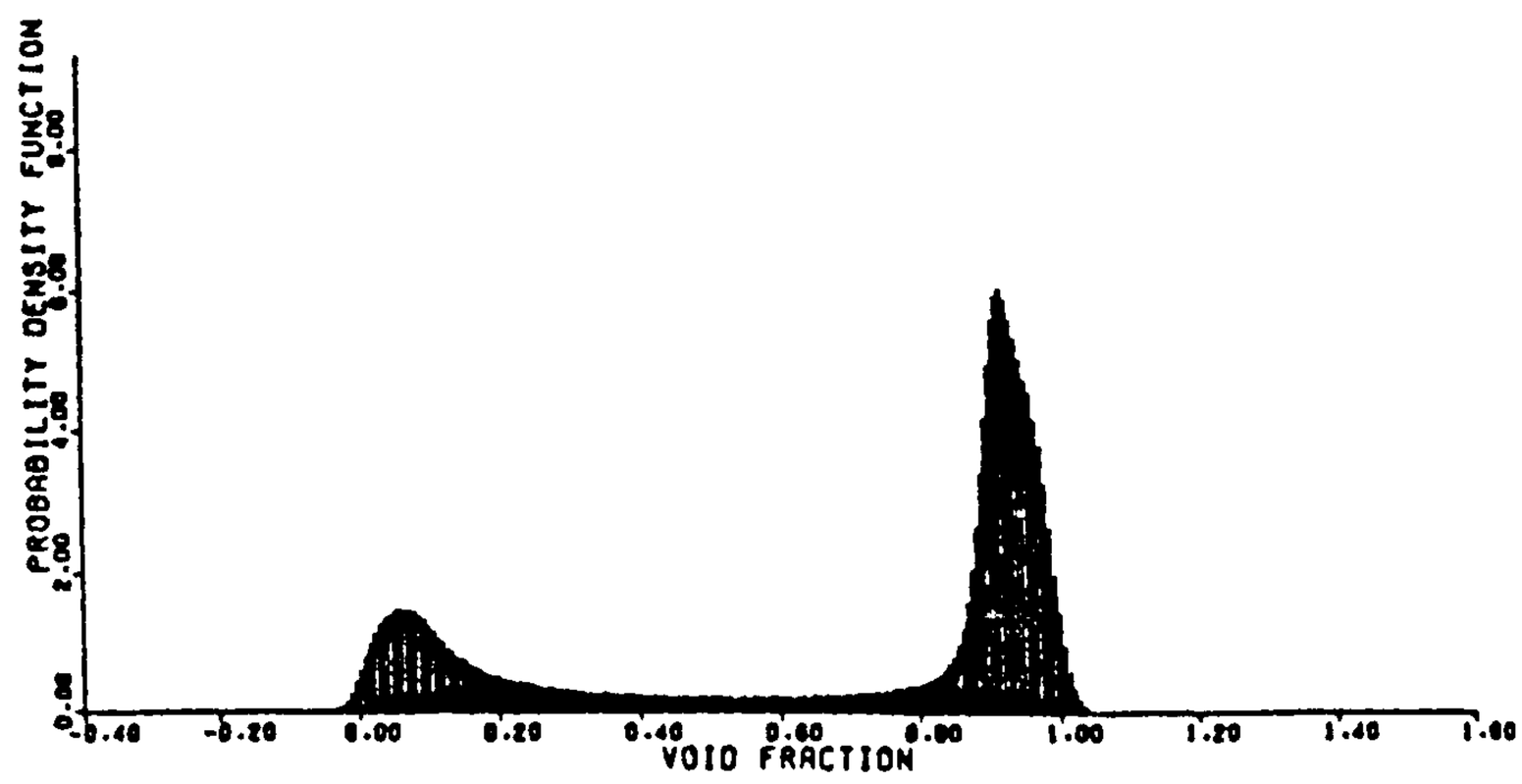

Figure 2.9c Probability density function produced by *Jones & Zuber* [1975] of the fluctuations in average gas void fraction α made using an x-ray void fraction technique of vertically upward slug two-phase flow within a rectangular duct

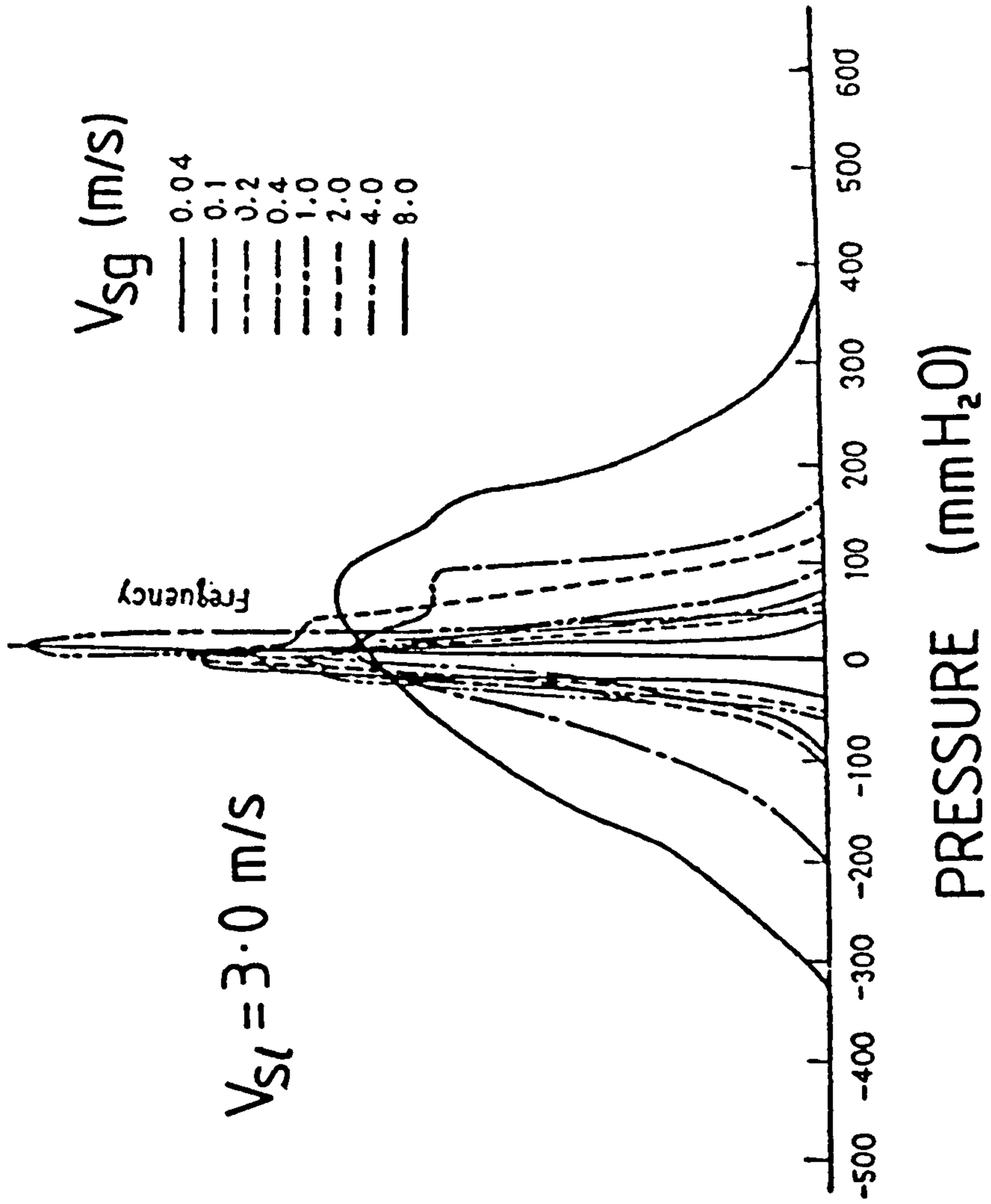

Figure 2.10 Probability density distribution produced by *Nishikawa* [1969] of the static pressure fluctuations in vertically upward bubbly two-phase flow within a circular pipe

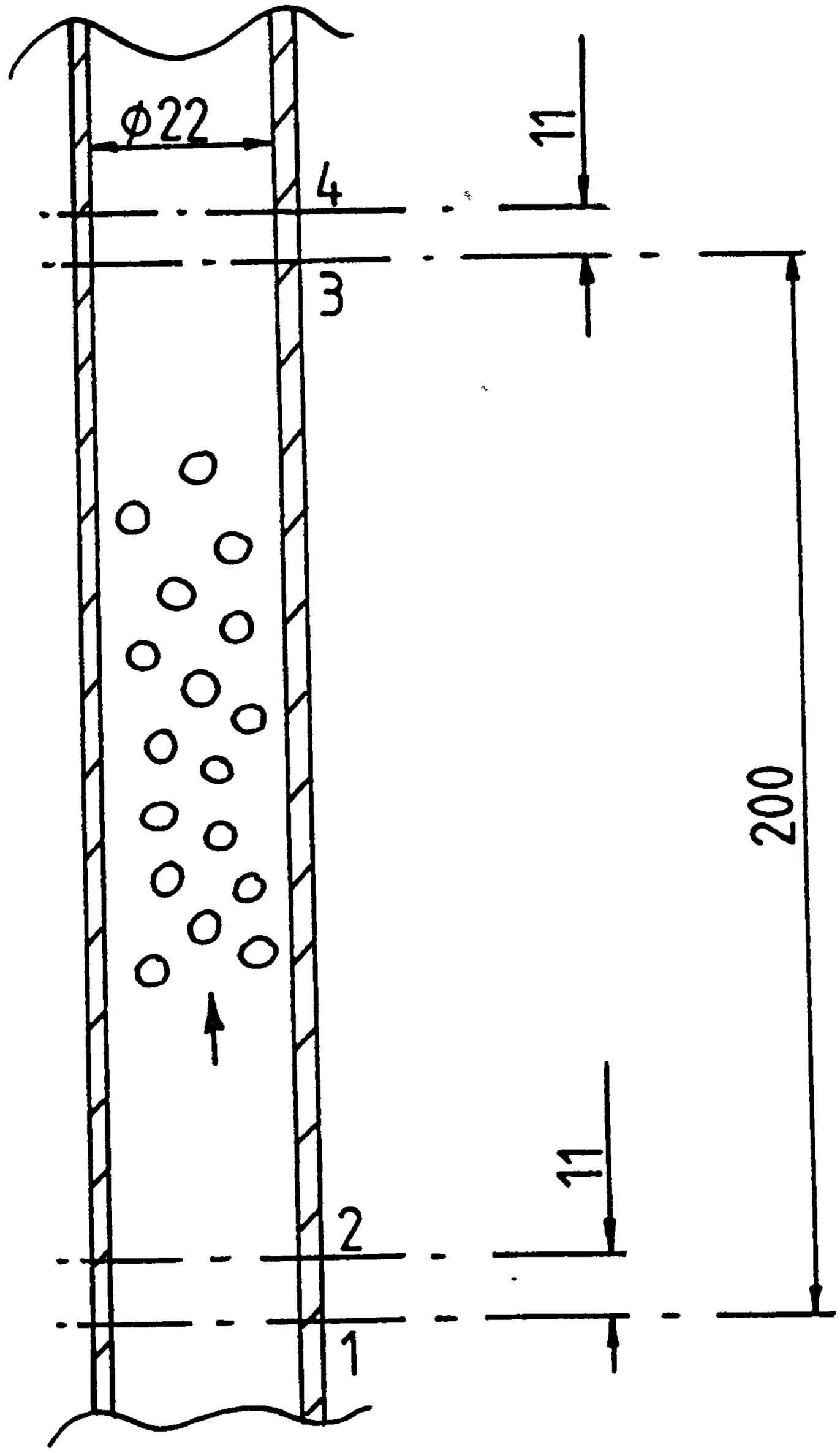

Figure 2.11 Pressure transducer arrangement used by *Matsui* [1984] in his investigation into flow regime identification using the naturally occuring pressure fluctuations within a two-phase flow

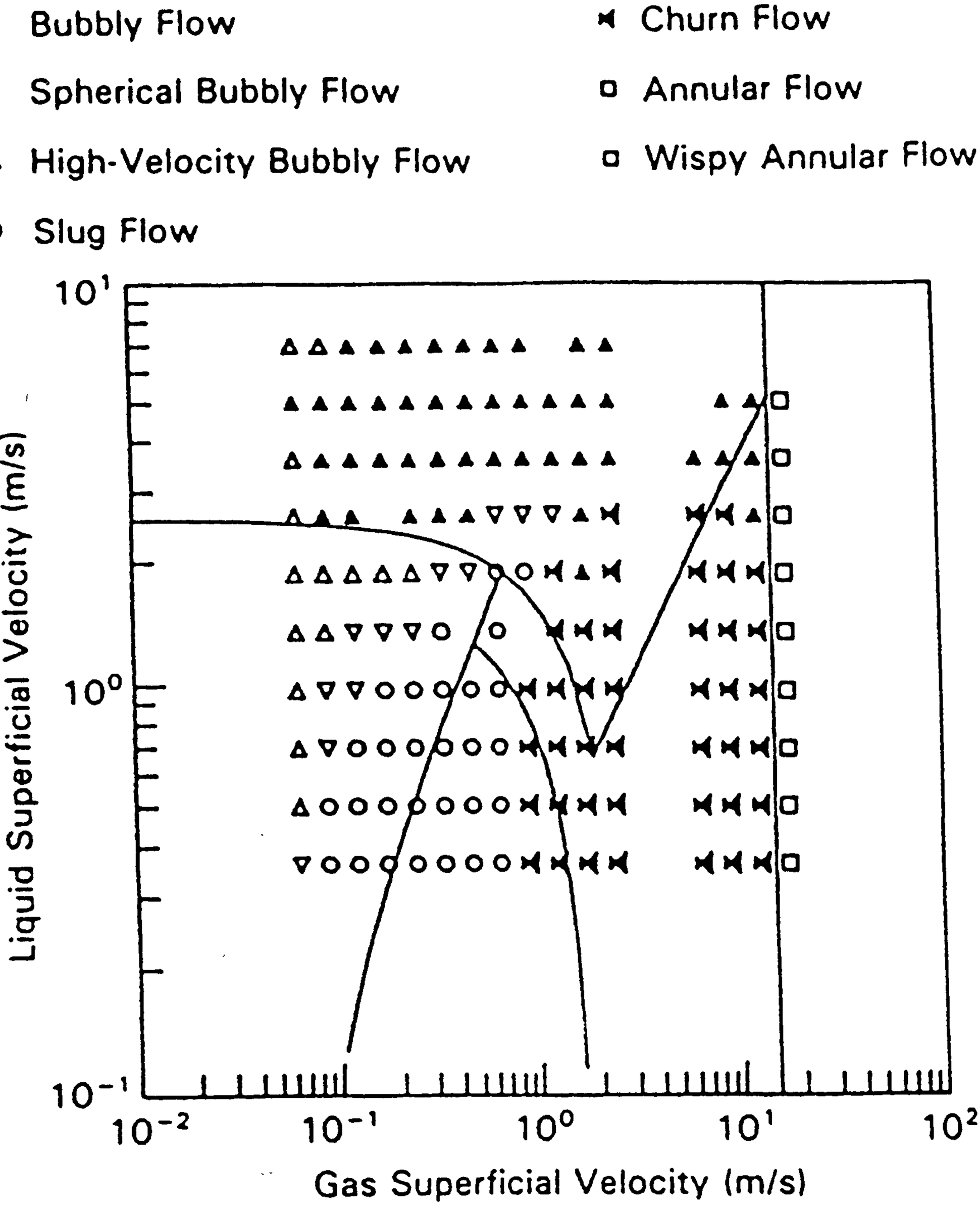

Figure 2.12 Taitel-type flow regime map produced using an autoregressive moving average (ARMA) model of static and differential pressure measurements developed by *King et al* [1987]

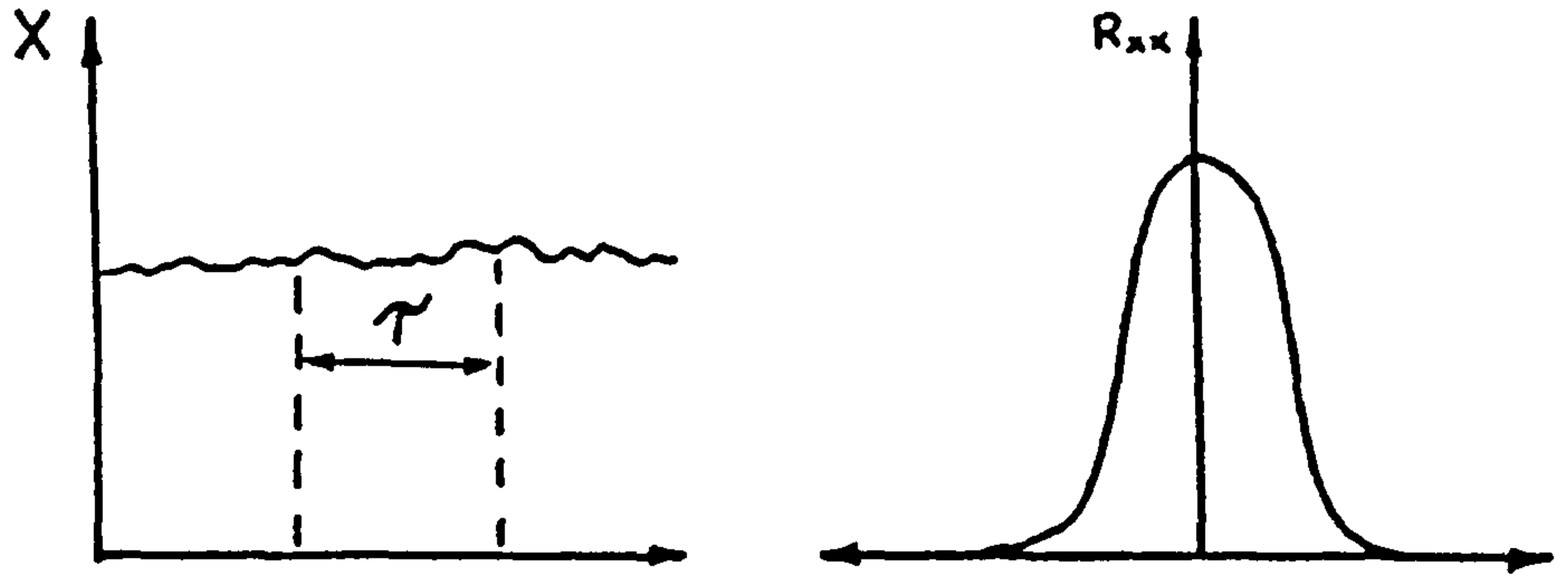

Figure 2.13 Typical autocorrelation correlogram of a stationary ergodic random signal

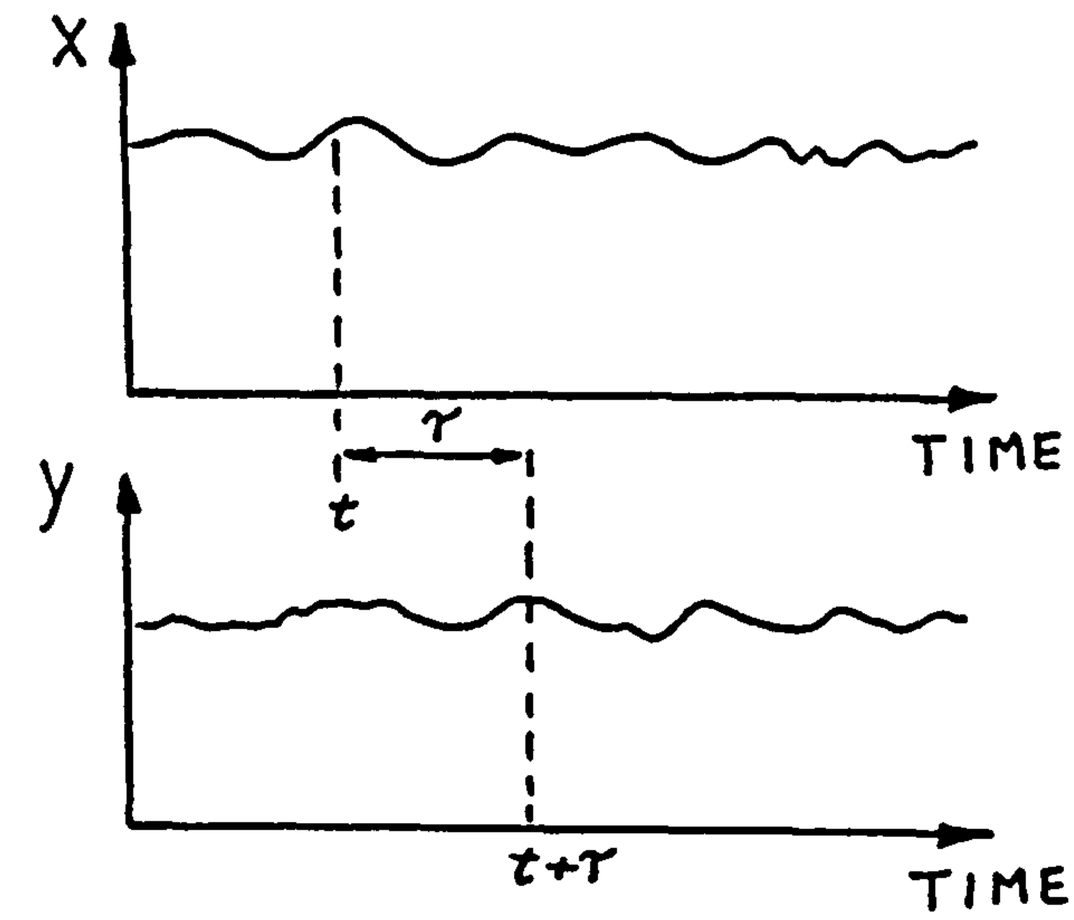

Figure 2.14 Typical cross correlation correlogram of two stationary ergodic random signals

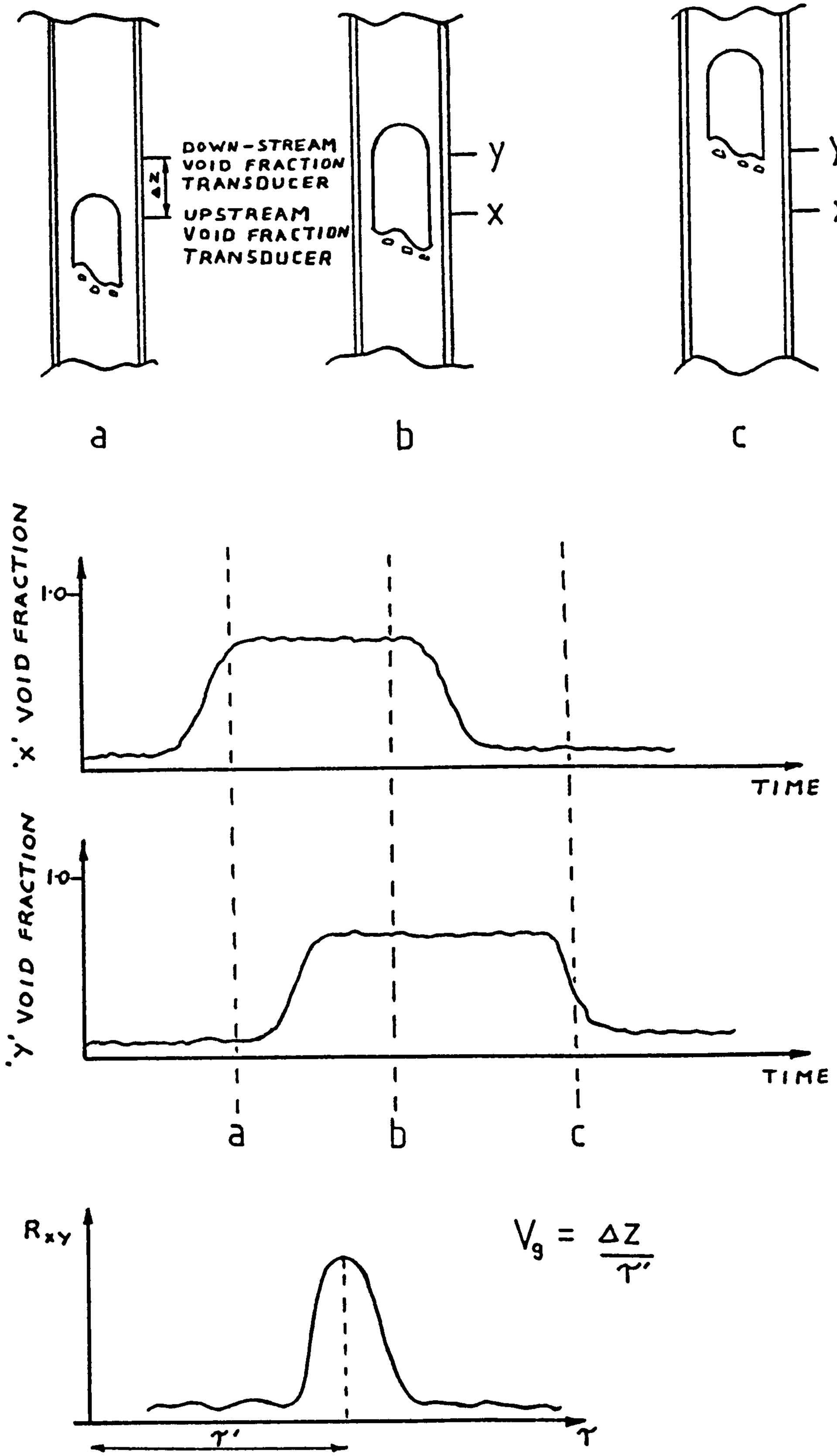

Figure 2.15 Hypothetical transducer arrangement for use in cross correlation measurements of the area averaged dispersed phase velocity

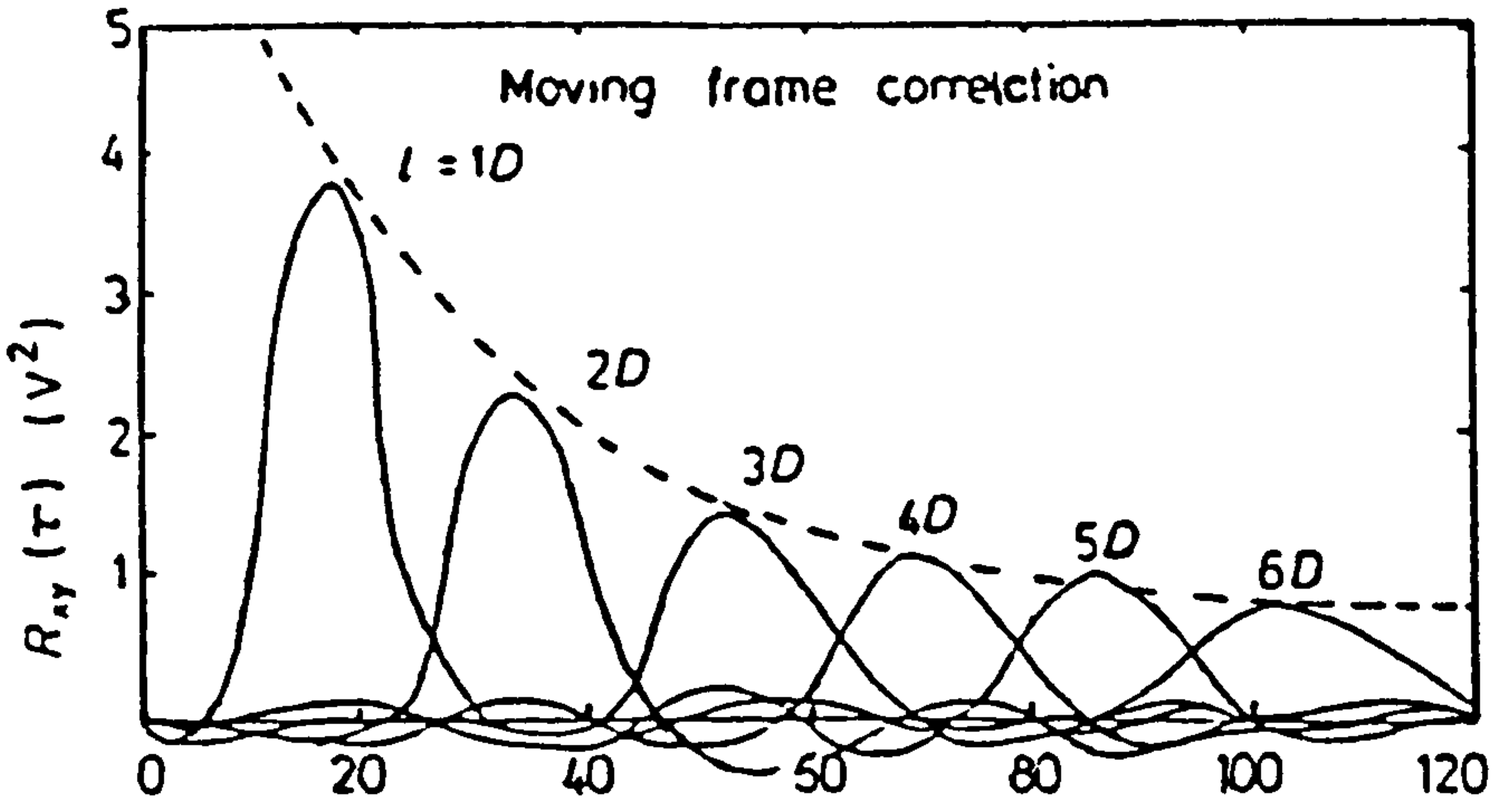

Figure 2.16a Decay of the cross correlation coefficient $\rho_{xy}(\tau)$ as a function of transducer separation distance l in experiments carried out by *Ong* [1975] using a pair of ultrasonic transducers

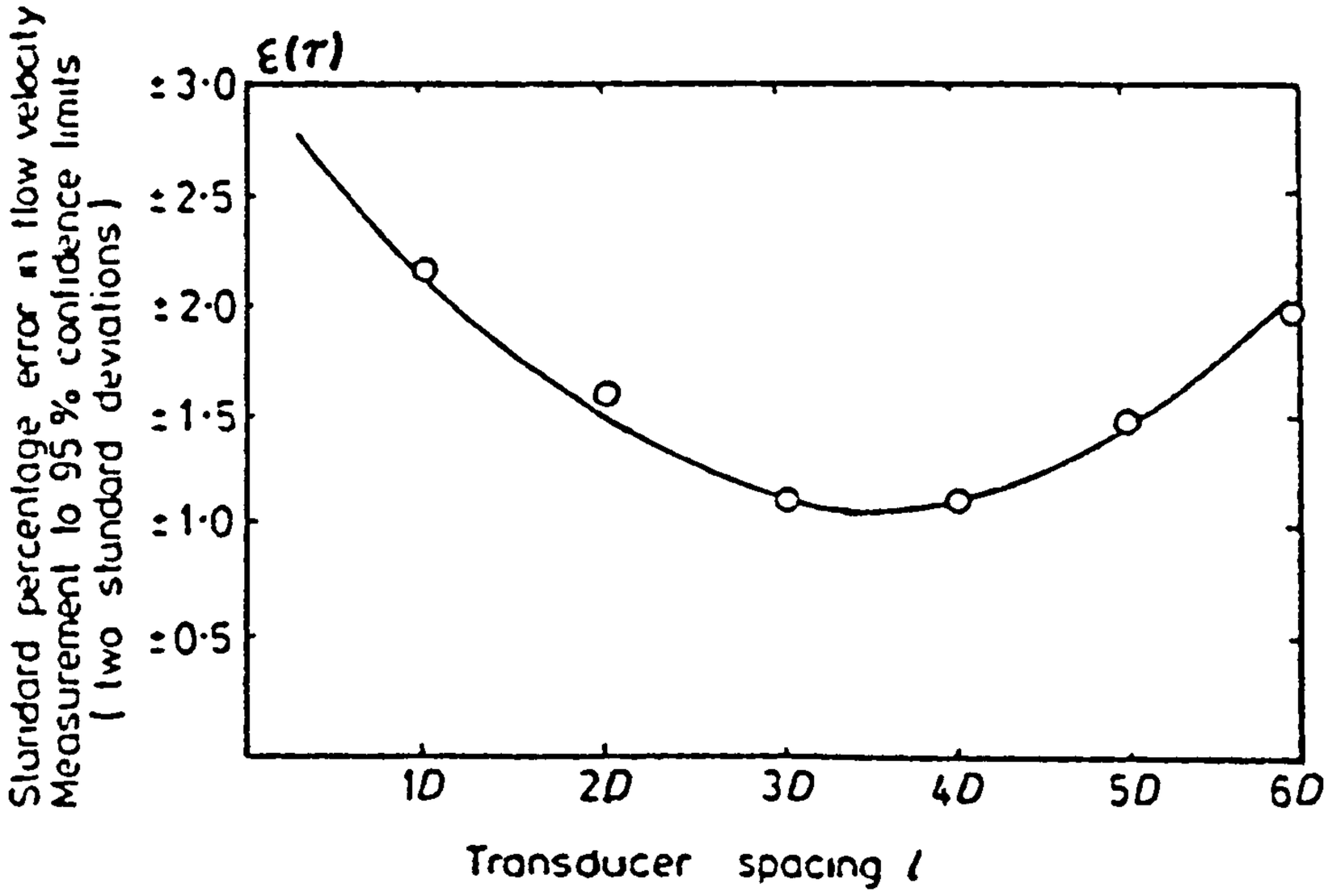

Figure 2.16b Variation in standard error $\epsilon(\tau)$ (defined by *Ong* [1975]) as a function of transducer separation distance l

CHAPTER 3 - DESIGN AND CONSTRUCTION OF THE EXPERIMENTAL VERTICAL TWO-PHASE FLOW LOOP

Chapter summary

This chapter describes the construction and instrumentation used in the air/water two-phase flow loop built for this project. The basic design requirements of the flow loop and the components used are described in sections 3.1 and 3.2. The techniques and instrumentation used for the measurements of the superficial gas and liquid velocities and the related details of the calibration procedures are given in section 3.3. Finally section 3.4 outlines the Proportional + Integral + Differential (PID) controller used to control the conditions in the flow loop whilst experiments were carried out.

3.1 Design and general description of the air/water two-phase flow loop

Figure 3.1 shows a schematic diagram of the flow loop used in this investigation. The main components of the apparatus comprise a pipe work loop, air/water separation tank, centrifugal water pump, air injector and the instrumentation used for measuring and controlling the mass flow rates of the two immiscible fluids prior to mixing.

The operation of the flow loop is as follows. Water leaving the separation tank passes through a filter and enters the centrifugal pump. The pump rotor speed can be adjusted by means of a three phase thyristor controller, which determines the flow rate of water through the test section. On exit from the pump water flows through a turbine flowmeter which is used to monitor the volume flow rate of water through the test section. A short distance down-stream of the flowmeter the water turns through a sharp 90° bend and starts to flow vertically upward. This turning will introduce a rotational component in its velocity about the axis of flow. To eliminate this, the water passes through a flow straightener prior to air injection and mixing.

Bubbles are formed when air is introduced through a number of small orifices by means of a "spoked wheel" type air injector with holes of the order of 0.5 mm in diameter along each of the spokes. The air is supplied to the apparatus by a 14 cubic feet per minute, 10 Bar air compressor and regulated to maintain a constant supply pressure of approximately 1.5 Bar. The flow of air into the air/water mixer is regulated by means of a computer controlled needle valve and the mass flow rate of air entering the flow loop is monitored by an orifice plate meter.

The two immiscible phases form a pseudo-homogeneous flow of bubbles of one phase suspended in the second phase during the passage through a contraction unit prior to entering the vertical test section where the experimental studies are carried out. The contraction was designed by the method of *Whitehead et al* [1951], which gives a rapid change in cross-sectional area with a small adverse pressure gradient and produces a near uniform velocity profile in the test section.

On leaving the test section the air/water mixture is delivered to the separation tank via the return pipe, where the two phases separate naturally with the air being exhausted to the atmosphere and the water recirculated.

3.2 Structural construction details of the air/water flow loop

The structural framework of the flow loop was made from Unistrut P2000, which is made from zinc plated steel and rolled into a 'U' cross-section, and so offers good structural rigidity along with easy assembly and dis-assembly, as requirements change.

The nominal pipe diameters of each section are given in figure 3.2. The majority of the pipe work is manufactured from 'UPVC', the exceptions being the test section and the contraction which are manufactured from centrifugally cast transparent acrylic plastic, and fibre glass mat impregnated with resin respectively. The contraction reduces a 6" nominal bore pipe to a 3" nominal bore pipe through a smooth curve.

The water flow straightener is constructed from a bundle of

plastic drinking straws of approximately 250 mm long with an internal diameter of approximately 3 mm. This was positioned in the flow upstream of the air injector and covers the entire cross-section of a 6" nominal bore pipe. The straws are held in position by a combination of their own friction against the side wall of the pipe and a fine wire mesh.

3.3 Techniques and instrumentation for the measurements of superficial gas and liquid velocities

3.3.1 Measurement of the superficial gas velocity

The superficial gas velocity V_{sg} is defined as the velocity the gas would have if it was the only phase present in the two-phase flow. This quantity can be evaluated using equation 1.1

$$V_{sg} = \frac{\dot{V}_g}{A} \qquad 1.1$$

where $\dot{V}_g$ is the volume flow rate of gas and A is the cross-sectional area of the pipe.

As stated earlier air is delivered to the apparatus at a constant pressure of 1.5 Bar. To control the flow of air going into the test section, a computer controlled needle valve was specially designed and constructed as shown in figure 3.3. This uses a stepper motor to drive a lead screw which actuates linkage to position the needle, and in so doing controls the volume flow rate of air entering the test section. The stepper motor is driven via an interface card, which required two digital inputs from the computer to determine the

direction and step.

To measure the air mass flow rate a sharp edged orifice plate was constructed (see figure 3.4). This was mounted in a machined housing which was inserted in the air delivery pipe work between the control valve and the air injector. The diameter of orifice needed to measure the expected range of flow rates was calculated for a 26mm diameter housing. The required orifice diameter was found to be in the region of 6mm, which is smaller than recommended by British Standard 1042 (1981). It was therefore necessary to obtain experimentally the discharge coefficient k_o in the gas mass flow rate equation

$$\dot{m}_g = \frac{k_o \pi d_o^2}{4} \sqrt{2 \Delta P_o \rho_o} \qquad 3.1$$

where d_o is the diameter of the orifice plate, ΔP_o is the pressure drop across the orifice plate and ρ_o is the density of air at the orifice plate. ρ_o can be calculated using the perfect gas equation

$$P = \rho RT \qquad 3.2$$

$$\rho_o = \frac{P_o}{RT_o} \qquad 3.3$$

where P_o and T_o are the upstream pressure and temperature at the orifice plate.

Two methods were employed to calibrate the orifice plate. First, a small pitot tube was used to measure the velocity profiles in a 1" diameter pipe being exhausted to the atmosphere for various air flow rates (see figure 3.5). By integrating the velocity profile over the cross-sectional area of the pipe and knowing the static pressure

and ambient temperature at the pitot tube, the air mass flow rates were calculated. A more detailed discussion of the calibration procedure and table of results is given in Appendix 1.

In the second method a domestic gas meter was connected to a length of pipe coming from the orifice plate housing. The outlet from the gas meter was exhausted to atmosphere. The time taken to pass a known volume of air was recorded the mass flow rates calculated for a number of settings.

In both of the methods, the pressure drop across the orifice plate was measured using tappings at 1 and 0.5 diameters of the orifice housing on the upstream and the down-stream sides of the orifice plate respectively. In addition to the pressure drop, the upstream static pressure at the orifice plate was recorded as recommended by British Standard 1042. The pressure drop was measured using a Furness Controls Ltd. Micromanometer MDC FC001, which can measure pressures in the range 0 - 1000mm of H_2O. The upstream pressure at the orifice plate was measured by a 0 - 2 Bar piezo-resistive pressure transducer connected to a suitable 4 arm Wheatstone bridge amplifier, as shown in figure 3.6. This pressure transducer was calibrated using a deadweight tester to give a full scale voltage output of 10 volts at a maximum pressure of 2 Bar.

The results, shown in Appendix 1, produced a value of discharge coefficient k_o for the orifice plate of 0.632. This value is similar to results obtained within the covered orifice diameter range of BS 1042.

As stated in equation 1.1, the superficial gas velocity is defined by

$$V_{sg} = \frac{\dot{V}_g}{A} \qquad 1.1$$

However, the air supplied was measured in terms of the mass flow rate $\dot{m}_g$ and the volume flow rate $\dot{V}_g$ must be related to the density ρ, and therefore the pressure P and temperature T, in the test section. Assuming a perfect gas we have

$$P = \rho RT \qquad 3.2$$

$$\dot{m}_g = \rho \dot{V}_g = \frac{P \dot{V}_g}{R T} \qquad 3.4$$

In this equation R is the universal gas constant, T is the absolute temperature of the air, which is assumed to be the same as the water temperature in the test section due to air having a low thermal inertia, and P the absolute static pressure in the test section. Combining equation 1.1 and 3.4 we get

$$V_{sg} = \frac{\dot{V}_g}{A} = \frac{RT\dot{m}_g}{P A} \qquad 3.5$$

From equation 3.1 it follows that

$$V_{sg} = \frac{R T k_o \pi d_o^2}{4 P A} \sqrt{\frac{2 \Delta P_o P_o}{R T_o}} \qquad 3.6$$

Equation 3.6 is used to calculate the superficial air velocity and

thus can be used in the Proportional + Integral + Differential (PID) closed loop control algorithm described in section 3.4.

The static pressure in the test section will not be constant over its entire length due to the change in height and frictional pressure losses. However as the pressure P in equation 3.6 is the absolute pressure, this variation is insignificant. Therefore, an average pressure over the length of the test section (relative to the atmospheric pressure) was measured using a 0 - 1 Bar pressure transducer and amplifier similar to the one used to measure the upstream pressure at the orifice plate (see figure 3.6). To the average static pressure measured in the test section, the absolute pressure was obtained by adding the barometric air pressure, measured by the laboratory's Fortin barometer.

3.3.2 Measurement of the superficial liquid velocity

The superficial liquid velocity V_{sl} is the velocity the liquid would have if it was the only phase present. As described in chapter 1, this quantity is given by equation 1.2

$$V_{sl} = \frac{\dot{V}_l}{A} \qquad 1.2$$

where $\dot{V}_l$ is the volume flow rate of liquid and A is the cross-sectional area of the pipe. As water is virtually incompressible it is possible to evaluate the volume flow rate directly from the metered volume or mass flow rate.

Water was circulated by means of a centrifugal pump whose speed was controlled by an IMO Jaguar VL550 thyristor controller. One disadvantage of this type of thyristor controller was the electrical noise produced at high frequencies. Excess voltages were discarded on to the earth return line causing high voltage spikes on the earth return, and airborne electromagnetic waves were also emitted. To reduce the magnitude of the earth spikes as much as possible a 3-phase in-line filter was fitted to the controller's power supply and to reduce the airborne electromagnetic waves a metal box was placed around the controller and substantial earthing straps were fitted.

The water volume flow rate $\dot{V}_l$ was measured by a Bestobell turbine flowmeter positioned approximately 20 pipe diameters down-stream of the centrifugal pump. This turbine flowmeter has an inductive pick-up that produces a pulse every time the turbine rotates. The frequency of this pulse train is proportional to the volume flow rate through the transducer.

To condition the signal for computer interfacing, it was decided to convert the turbine flowmeter's pulse train output into a DC voltage, V_{turb}, with the output voltage being proportional to the volume flow rate of water through the turbine flowmeter. This conversion was achieved using the circuit shown in figure 3.7, which amplifies the signal from the inductive pick-up, filters out frequencies above 1 KHz using a low-pass active filter and then converts the frequency of the signal to a proportional DC voltage using a frequency to voltage converter chip.

To minimise calibration errors the turbine flowmeter and the frequency to voltage converter unit were calibrated together. This

was achieved by recording the time taken to fill a known volume with water, with the centrifugal pump running at a constant speed. This procedure was repeated several times and the results averaged. The speed of the pump was then altered and the experiment repeated. A more detailed explanation of the calibration procedure and results is given in Appendix 1.

The above method provided a calibration relationship for the volume flow rate of water of the form

$$\dot{V}_l = 1.668\times10^{-3}\ V_{turb} - 0.44\times10^{-3} \quad (m^3/s) \qquad 3.7$$

Inserting equation 3.7 into 1.2, and assuming water to be incompressible in the pressure range found in the test section (less than 1 Bar), an expression is obtained for the superficial liquid velocity V_{sl} in terms of the output voltage from the turbine flowmeter V_{turb} and the cross-sectional area of the test section:

$$V_{sl} = \frac{1.688\times10^{-3}\ V_{turb} - 0.44\times10^{-3}}{A} \quad (m^3/s) \qquad 3.8$$

3.4 Development and implementation of the control algorithm used to regulate the air/water flow loop

To repeat a series of experiments using the air/water flow loop it was considered advantageous if the superficial gas and liquid velocities could be set easily, thus facilitating repeatable flow conditions. This proved difficult to achieve manually due to the constant interaction between the two phases in the test section i.e. making an adjustment to one superficial velocity also affected the

other.

Consequently to aid the control of the flow loop a computer was installed. The computer system used for this purpose was a Control Universal Euro Beeb system. This is an industrial computer based on the 6502 microprocessor with a clock speed of 2MHz. Three types of computer interface were used to connect to the flow loop's instrumentation. These are

(i) 12 bit Analogue to Digital converter (5 channels)

(ii) 16 bit Digital to Analogue converter (1 channel)

(iii) Digital outputs (2 amps @ 25 volts max) (6 channels)

A block diagram of the computer interface connections is given in figure 3.8.

Algorithms were developed not only to control the flow loop but also to perform simple experiments (Appendix 2 contains a listing and brief description of the control software). The software algorithms used to control the the superficial velocities of the flow loop consists of two closed loop Proportional + Integral + Differential (PID) control algorithms. Figure 3.9 shows a block diagram of the closed loop controller used to control the air/water flow loop. To control the water superficial velocity passing through the test section the water volume flow rate was measured by the computer using a turbine flowmeter and its associated frequency to voltage converter electronics (see section 3.3.2) which was situated down-stream of the centrifugal pump used to circulate the water. The computer compares the actual volume flow rate of water with the desired value calculating the error. Based on the magnitude and rate of change of

the error signal monitored by the computer, adjustments are made to the speed of the centrifugal pump, thus altering the volume flow rate of water always trying to achieve a zero error. The mass flow rate of air entering the test section is controlled in a similar manner except that the air mass flow rate is monitored using an orifice plate meter and adjustments to the mass flow rate are made via a stepper motor controlled needle valve designed in this thesis (see section 3.3.1). A simple flow chart showing the control algorithms implementation in software can be found in figure 3.10 and a detailed description of the software is given in Appendix 2.

However, although the control algorithms work satisfactorily it was found that, even at a low average gas void fractions, it was necessary to switch from a computer control mode to a purely monitoring mode which made no adjustments to the flow rates while making experimental measurements. This reduced the scatter on experimental results and thus produced more repeatable experimental data.

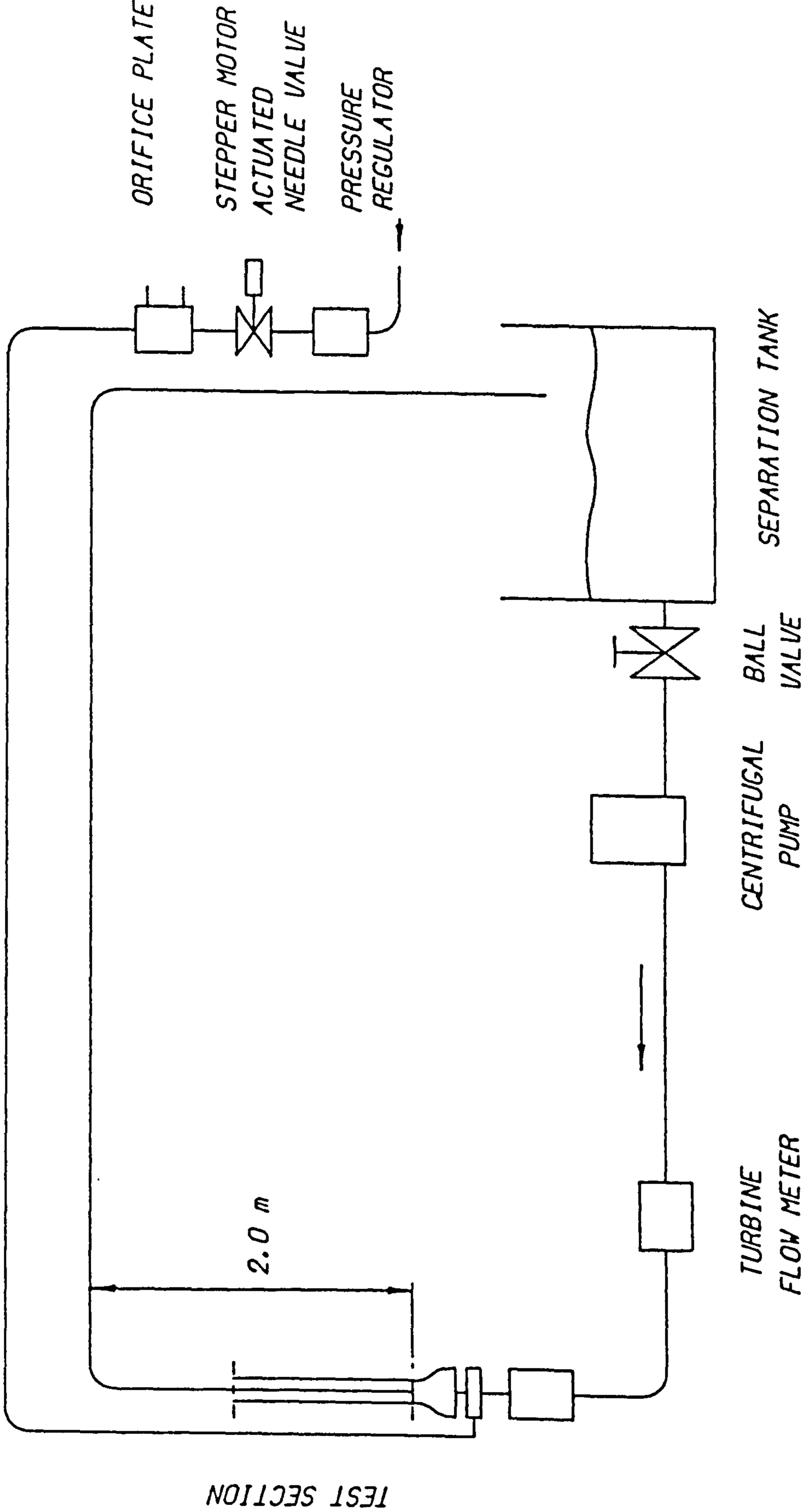

Figure 3.1 Schematic diagram of the two-phase air/water flow loop constructed at Polytechnic South West

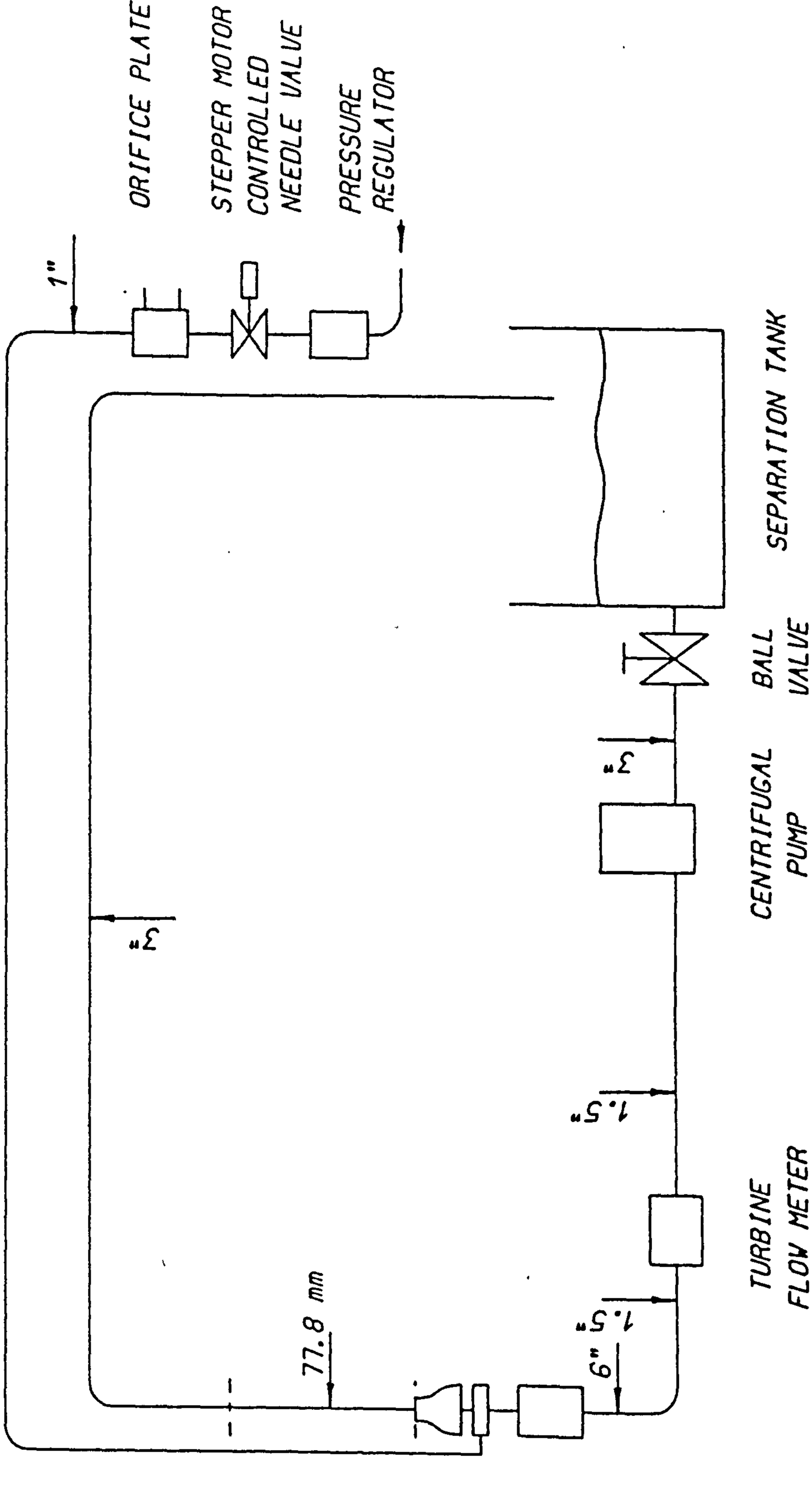

Figure 3.2 Air/water flow loop nominal pipe diameters

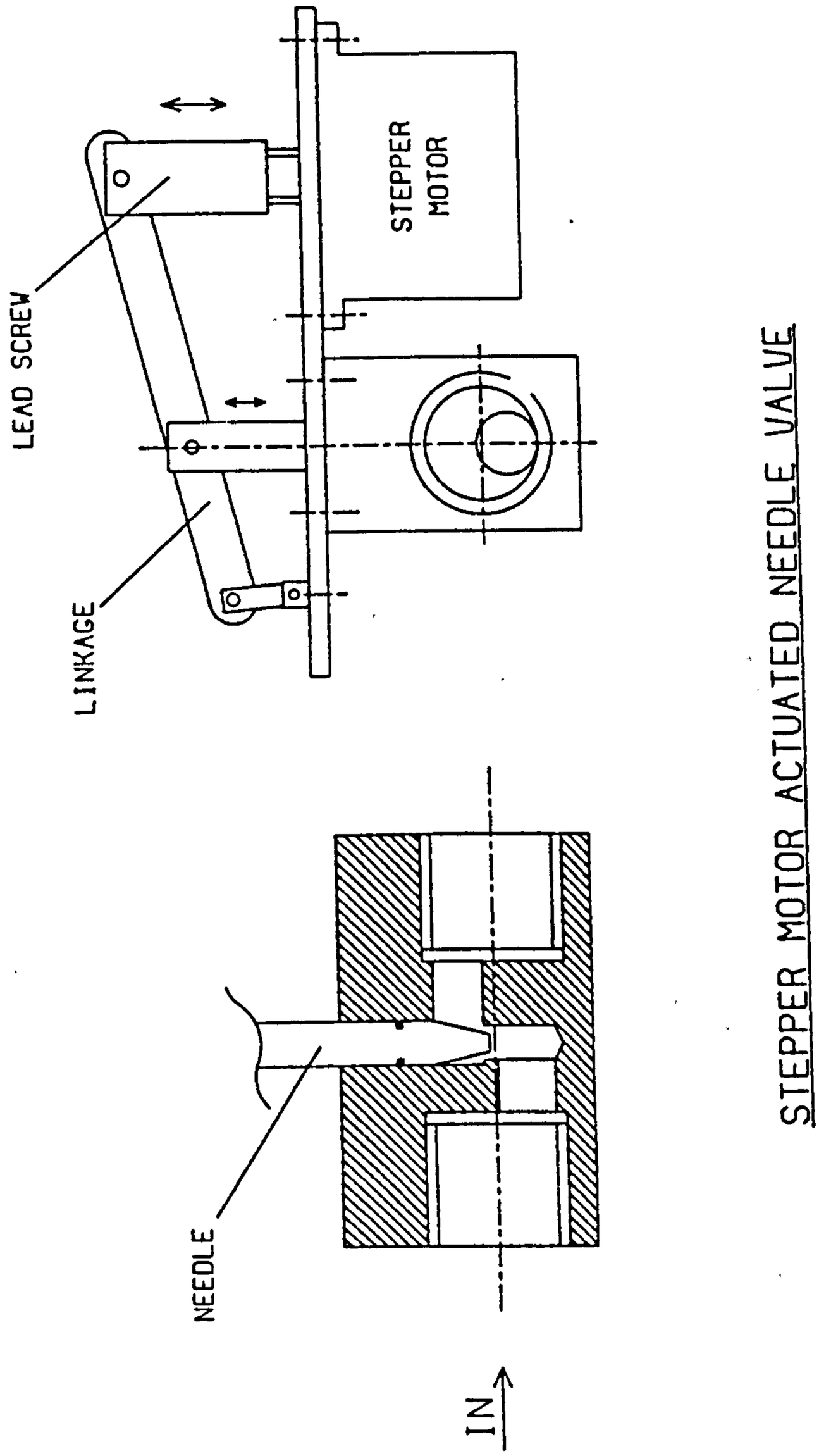

Figure 3.3 Computer controlled needle valve used to regulate the mass flow rate of air entering the test section

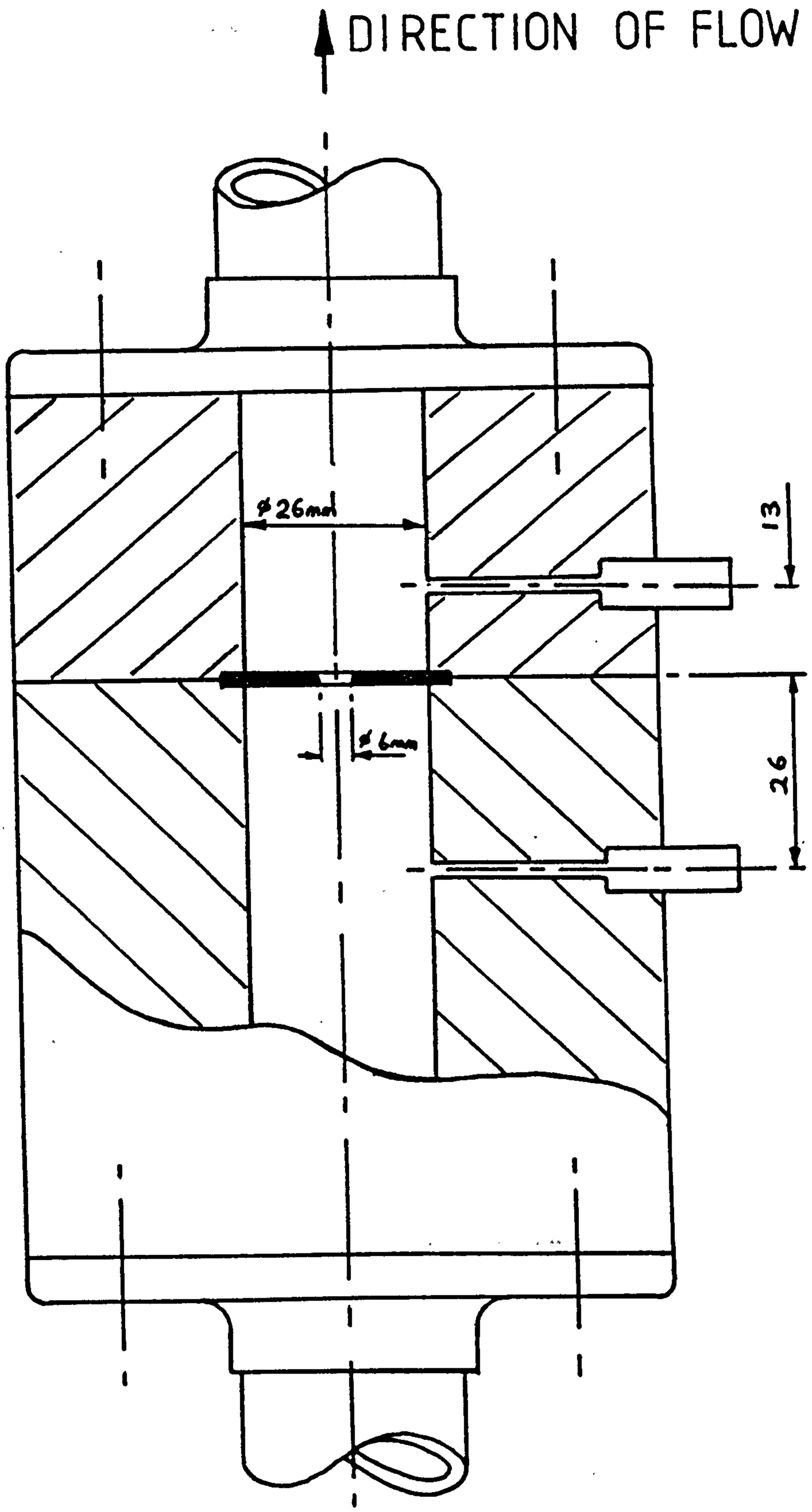

Figure 3.4 Construction details of sharp edged orifice used to measure the air mass flow rate entering the test section

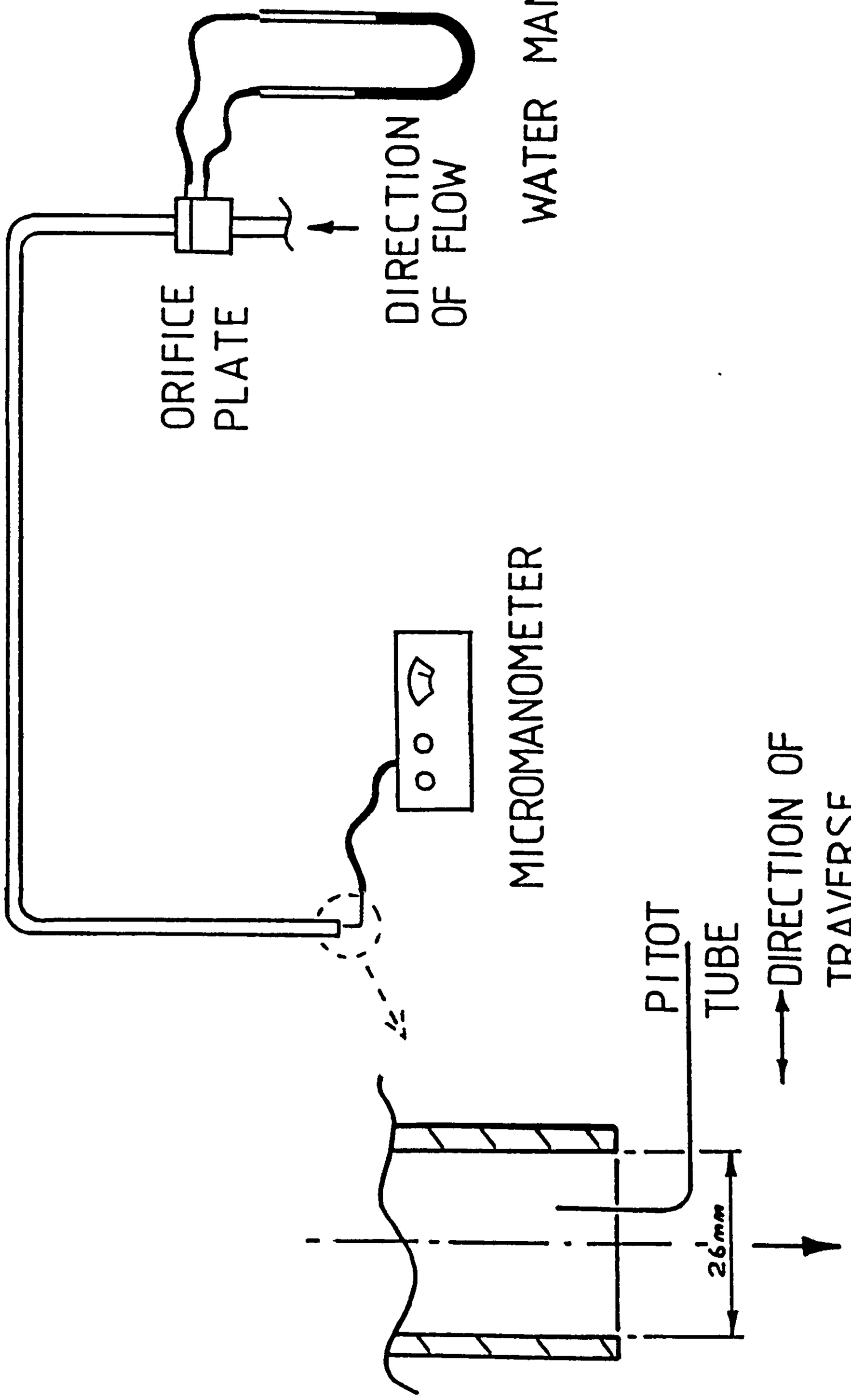

Figure 3.5 Experimental set up used to calibrate the air mass flow rate orifice plate

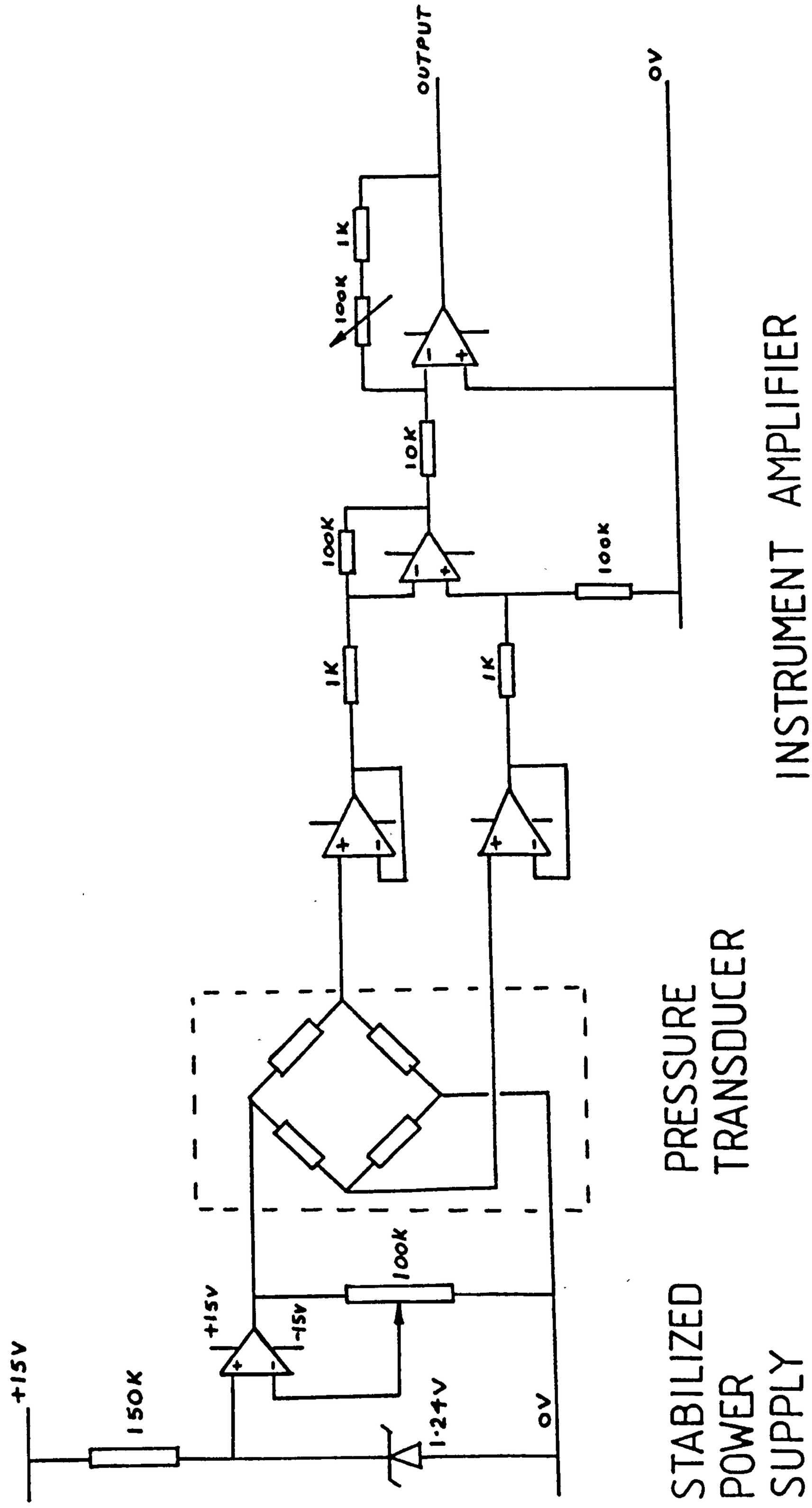

Figure 3.6 Circuit diagram of the four active arm Wheatstone bridge instrument amplifier used in conjunction with the 1 & 2 Bar pressure transducers

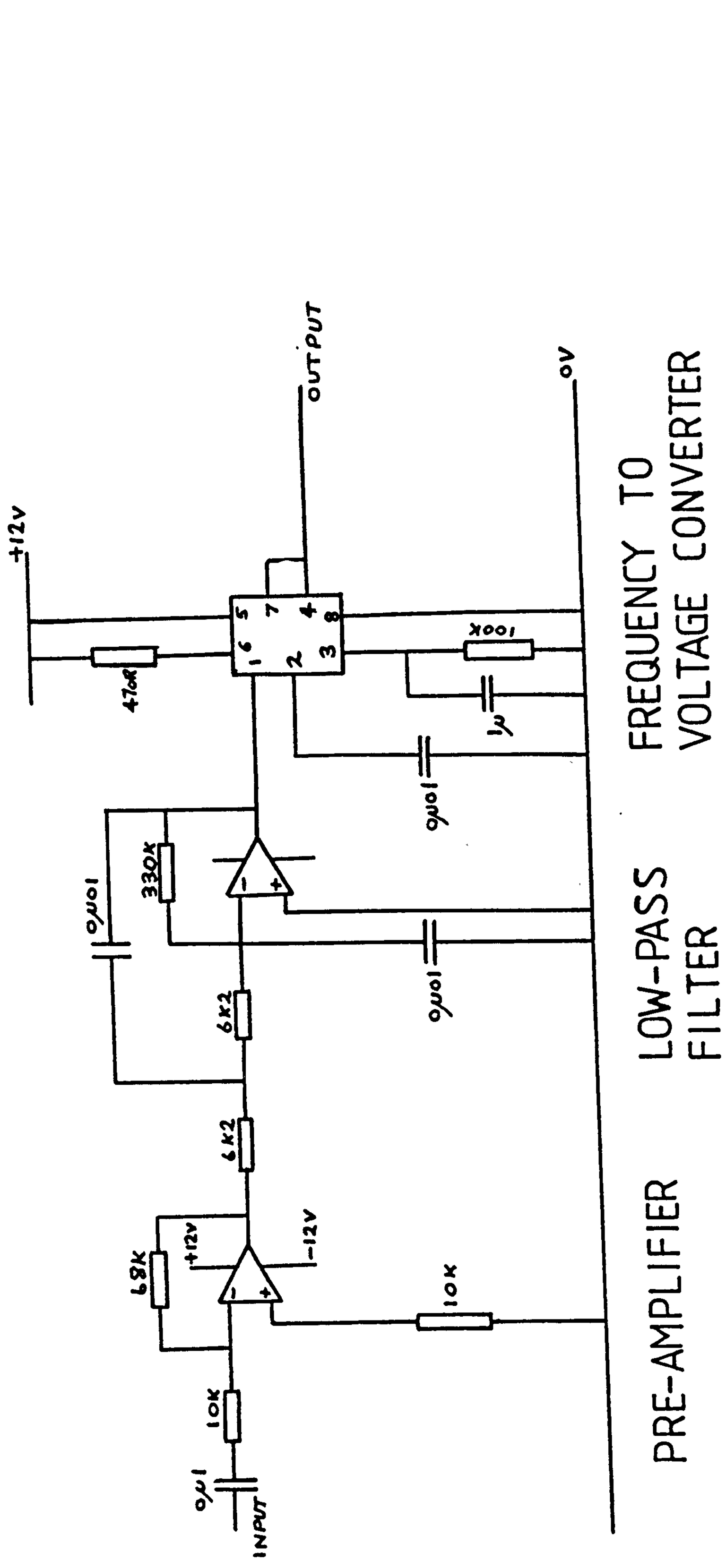

Figure 3.7 Frequency to voltage converter, amplifier, and low-pass filter circuit used in conjunction with the water volume flow rate turbine type flow transducer

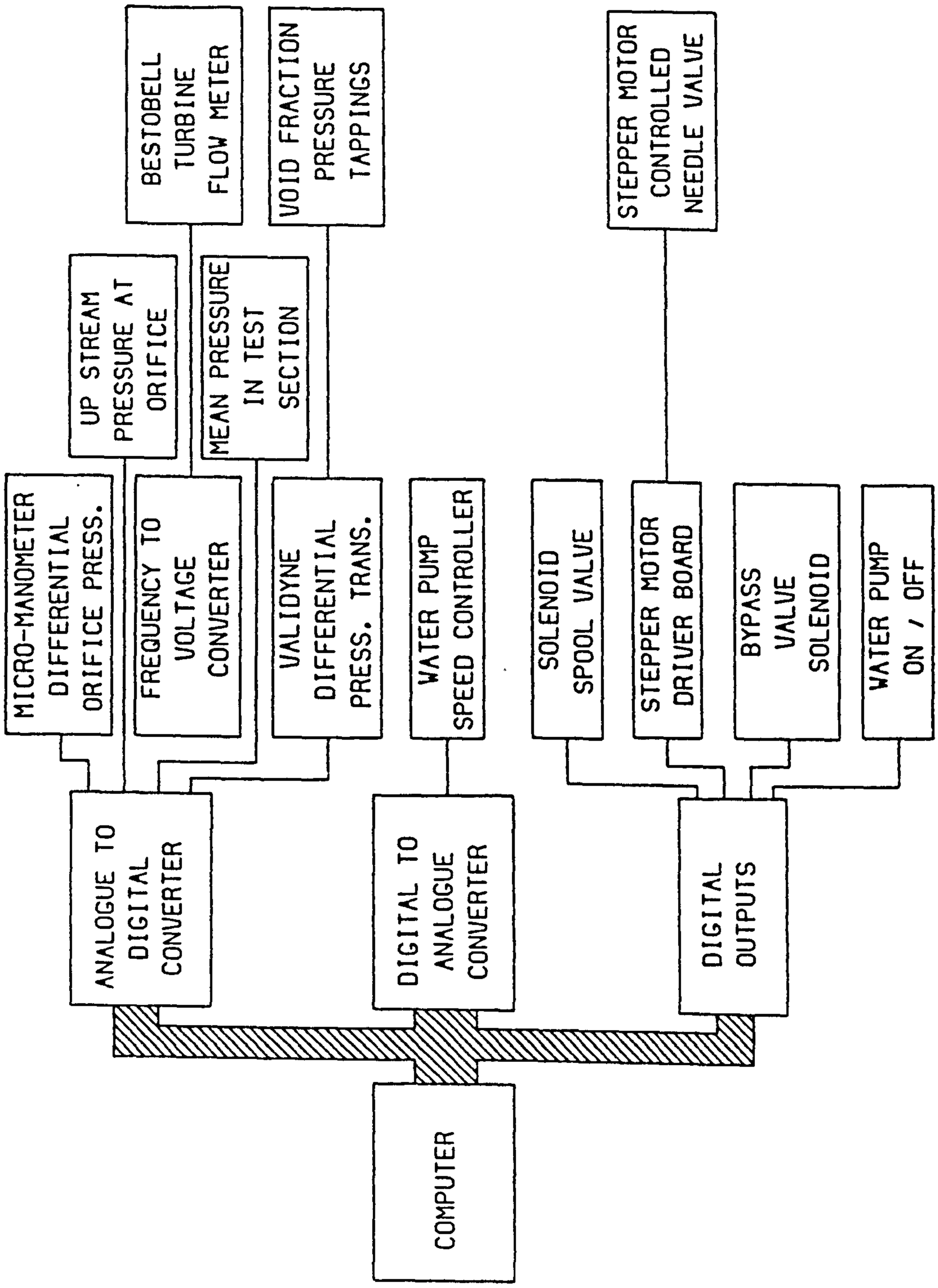

Figure 3.8 Schematic diagram of computer interfacing with the air/water flow loop

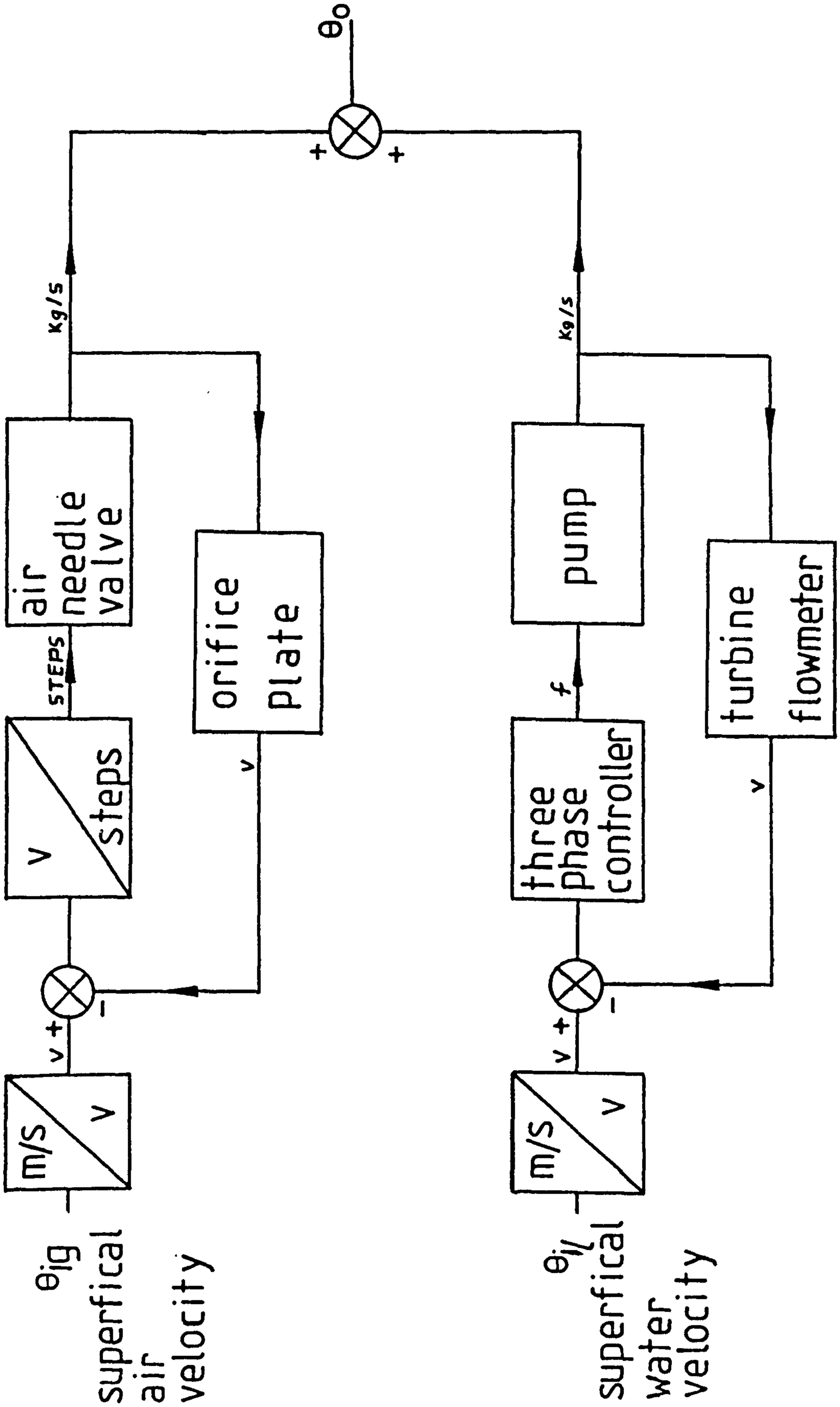

Figure 3.9 Block diagram of the closed loop control algorithms used to control the two-phase flow loop

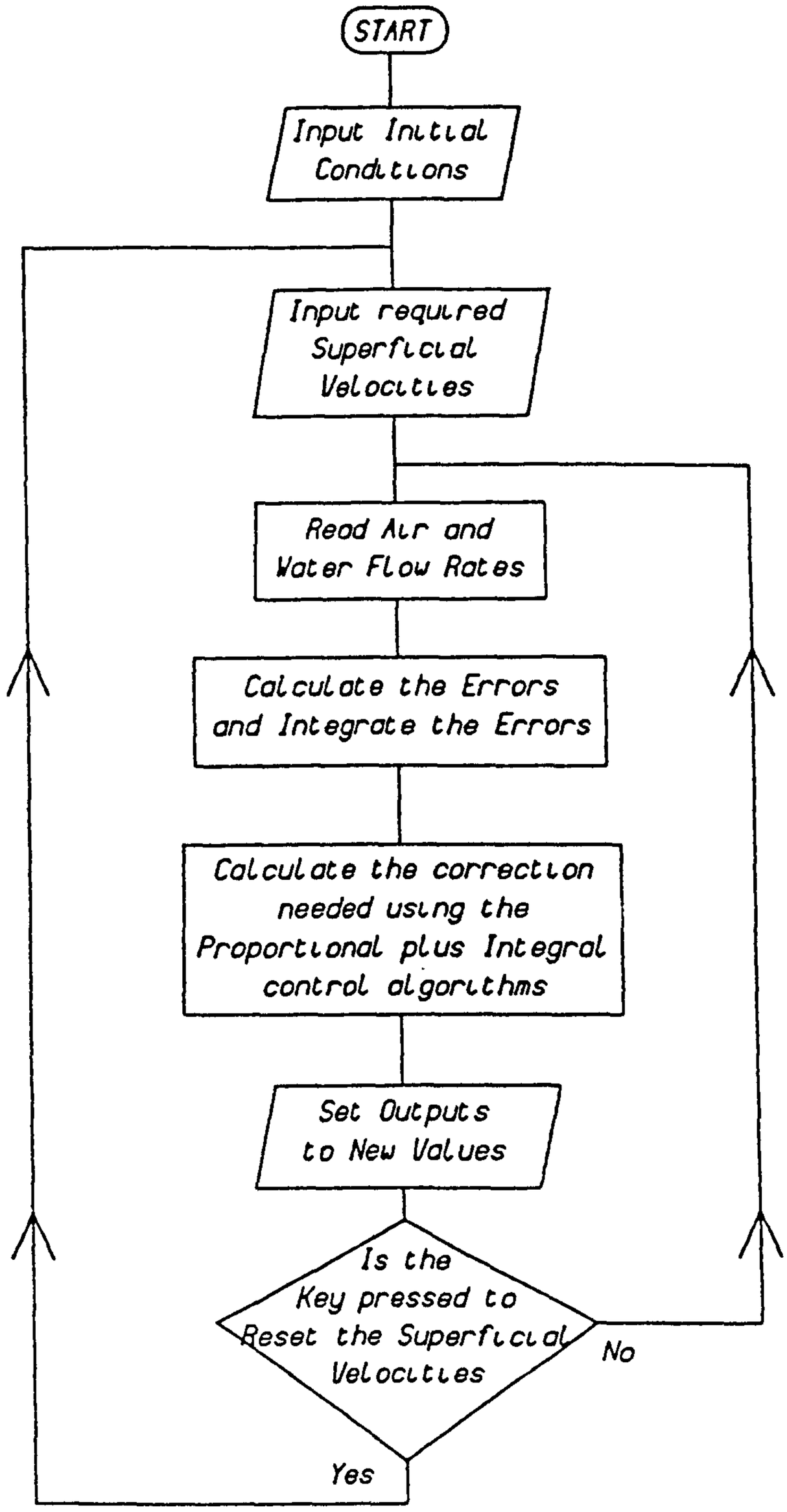

Computer Program Flow Chart

Figure 3.10 Flow chart of software used to control the air/water flow loop

CHAPTER 4 - COMMISSIONING OF THE AIR/WATER FLOW LOOP AND COMPARISON OF RESULTS OBTAINED FROM THE FLOW LOOP WITH EXISTING TWO-PHASE FLOW THEORY

Chapter summary

Section 4.1 outlines the two methods used to determine the average gas void fraction α, namely the quick closing valve technique and the gradiomanometer.

Section 4.2 is concerned with the determination of friction factors in both single and two-phase flows. The two-phase flow friction factor f is then subsequently used in the gradiomanometer method of determining the average gas void fraction α.

Comparisons are made between the quick closing valve technique and the gradiomanometer used to determine α in section 4.3, and reasons are given why only the gradiomanometer is used in subsequent experiments.

Section 4.4 uses the relationship proposed by *Zuber* & *Findlay* [1965] to predict the area averaged gas velocity V_g in a pipe. Comparisons are made in section 4.5 between the *Zuber / Findlay* method of calculating V_g and experimental results using the quick closing valve and gradiomanometer methods to determine V_g.

4.1 Measurement of average gas void fraction

The average gas void fraction α is one of the fundamental parameters in two-phase flow. For steady flow conditions α can be defined either as the fraction of a pipe's cross-sectional area that is occupied by the gas phase *Hewitt* [1978], or as the fraction of a pipe volume that is occupied i.e.

$$\alpha = \frac{v_g}{v_g + v_l} \qquad 1.3$$

where v_g and v_l are the gas and liquid volumes respectively in a total volume v_t $(v_g + v_l)$.

Two techniques have been used in this study to measure the average gas void fraction in the vertical test section. These are on-line sampling using quick closing gate valves and the gradiomanometer as presently used downhole.

4.1.1 Measurement of average gas void fraction using quick closing gate valves

Based on the definition given in the previous section, if a section of two-phase flow is captured and allowed to separate into its two natural phases then, assuming no leakage, the ratio of gas volume to total volume will be a measure of the average gas void fraction.

By positioning two quick closing gate valves, at each end of the test section, as shown in figure 2.1, a section of pipe flow can be sampled. Assuming a constant cross-sectional area in the test

section, the average gas void fraction can be measured by scaling the length of the gas phase to the distance between the valves.

The apparatus used in this study was constructed by *Schlumberger Cambridge Research* and has been used successfully by *Hunt* [1987]. The gate valves are operated by pneumatic cylinders at a pressure of 15 Bar. They are controlled by a solenoid spool valve, which allows the gate valves to close simultaneously in approximately 0.1 seconds.

When the gate valves are actuated the centrifugal water pump and air supplies are also turned off automatically. This induced large pressure transients in the flow loop due to the inertia of the water. This effect was largest at low gas void fractions as would be expected in a mixture whose compressibility is proportional to its average gas void fraction. To overcome this problem a bypass pipe was fitted around the test section in which a solenoid valve could be opened to relieve the build up of pressure at the same time as the gate valves are operated.

It was found difficult to measure accurately void fractions of less than 3 - 4% because the gate valves' sliding mechanism obscured the measurement scale. However, this was not a significant problem since the range of void fractions in this study was typically between 5 and 25 %.

4.1.2 Measurement of average gas void fraction using the gradiomanometer

The gradiomanometer makes use of the fact that the two

immiscible phases have different densities. Using the definition of α based on ratio of pipe cross-sectional area that is occupied by the gas phase, the mean density ρ_m of a two-phase mixture is defined by

$$\rho_m = \rho_g\alpha + \rho_l(1-\alpha) \qquad 4.1$$

where ρ_g and ρ_l are the densities of air and water respectively.

Consider a section of vertical pipe with two tappings separated by a distance h, as shown in figure 1.3. If it is assumed that the air/water mixture behaves like a homogeneous single phase fluid, as suggested by *Hunt* [1987], then the energy equation can be applied to this flow provided ρ_m is used for the density of the mixture:

$$\frac{P_1}{\rho_m} + \frac{V_1^2}{2} + gz_1 = \frac{P_2}{\rho_m} + \frac{V_2^2}{2} + gz_2 + e_f \qquad 4.2$$

Here e_f is the frictional loss per kg mass between position 1 and 2. As $V_1 = V_2$, substituting $h\cos\Omega$ for $z_1 - z_2$ and F_m for $\rho_m e_f$, the pressure difference between the two tappings can be expressed as

$$P_1 - P_2 = \rho_m\, g\, h\cos\Omega + F_m \qquad 4.3$$

In these equations P_1 and P_2 are the static pressures at the upstream and down-stream pressure tappings, respectively, Ω the angle of deviation from the vertical of the test section, and F_m the pressure losses due to friction within the air/water mixture and between the fluid mixture and the wall of the test section. It should be noted that equation 4.3 neglects any compressibility effects that may be associated with the dispersed air phase. These are regarded as being small because the pressure in the test section is near atmospheric.

Inserting equation 4.1 into equation 4.3 and letting $P_1 - P_2 = \Delta P_m$, it follows that

$$\Delta P_m = g\ h \cos \Omega\ (\rho_g \alpha + \rho_l (1 - \alpha)) + F_m \qquad 4.4$$

By rearranging equation 4.4 the average gas void fraction α can be calculated from

$$\alpha = \frac{\dfrac{\Delta P_m - F_m}{g\ h \cos \Omega} - \rho_l}{(\rho_g - \rho_l)} \qquad 1.4$$

In this equation ΔP_m can be measured using a differential pressure transducer of a suitable range. The frictional pressure loss F_m will be a function of the Reynolds number Re, the flow conditions and the pipe surface roughness. To determine the value of F_m the following approach was adopted in this study. The frictional pressure loss F_m for a single phase, fully developed pipe flow can be estimated from the empirical relationship given by *Darcy* (*Massey* [1968])

$$F_m = \rho e_f = \rho \frac{2\ f\ h\ V^2}{D} \qquad 4.5$$

where h is the length of the pipe, ρ the density of the flowing fluid, V the area averaged flow velocity, D the diameter of the pipe and f the non-dimensional friction factor.

Aziz, Govier and *Fogorazi* [1972], state that equation 4.5 can also be applied to two-phase bubbly flow provided that the terms are redefined in the following way. The area averaged velocity V should be replaced by the mixture velocity V_m as defined in equation 1.9

$$V_m = V_{sl} + V_{sg} \qquad 1.9$$

Furthermore, empirical results obtained by *Hunt* [1987] suggest that the term ρ should be replaced by the liquid density ρ_l. Introducing these quantities, equation 4.5 can be rewritten as

$$F_m = \frac{2\ \rho_l\ (V_{sl} + V_{sg})^2\ h\ f}{D} \qquad 4.6$$

To use this equation the value of the dimensionless friction factor f must be determined.

If we insert equation 4.6 into equations 4.4 and solve for the dimensionless friction factor f we get

$$f = \frac{(\Delta P_m - g\ h\ \cos\ \Omega\ (\rho_g \alpha + \rho_l (1-\alpha)))\ D}{2\ \rho_l\ (V_{sl} + V_{sg})^2\ h} \qquad 4.7$$

In a series of experiments (see section 4.2.2) the average gas void fraction α was evaluated using the quick closing gate valve method described in section 4.1.1 for particular values of superficial gas and liquid velocities whilst monitoring the corresponding pressure drop ΔP_m between two pressure tappings separated by an axial distance h.

In the range of mixture velocities considered in this study (V_m < 2.0 m/s) which is associated with a range of Reynolds numbers, based on the internal diameter of the test section $Re_D = \rho D V_m / \mu$ where μ is the viscosity, of approximately 10^4 - 10^5, it would not be unreasonable to make the assumption that the change in friction factor f for fully developed turbulent pipe flow will be small over this range of Reynolds number. Therefore, the friction factors calculated using equation 4.7 over the range of mixture velocities were averaged to obtain an average value of friction factor f (see section 4.2.3).

Having obtained an empirical value for the friction factor, all of the terms in equation 4.6 are now known. Thus combining 4.6 with 1.4 provides an expression for the average gas void fraction in terms of the change in differential pressure ΔP_m:

$$\alpha = \frac{\dfrac{\Delta P_m}{g\ h\ \cos\Omega} - \dfrac{2\ \rho_l\ (V_{sl} + V_{sg})^2\ h\ f\ g}{D} - \rho_l}{(\rho_g - \rho_l)} \qquad 4.8$$

This equation can be used to calculate the average gas void fraction α in the test section and it has the advantage over the rapid closing gate valve technique in that it is non-intrusive to the flow. It can therefore be used to measure the average gas void fraction whilst experiments are being carried out in the test section.

4.2 Friction factor measurements in the test section of the air/water flow loop

As discussed in section 4.1.2, it is necessary to determine the magnitude of the dimensionless friction factor f for the test section in order to use the gradiomanometer to measure the average gas void fraction. Although the friction factor will be a function of the flow conditions and the Reynolds number Re_D it has been argued in section 4.1.2 that over the small range of Reynolds numbers considered in this study it would be exceptable to use an average value of f.

Bubbly two-phase flow is frequently treated as being a homogeneous single phase fluid. If this assumption is made then comparisons can be made between theoretical values of friction factor and experimental values calculated using equation 4.7.

4.2.1 Friction factors in single phase flow

The empirical *Blasius* solutions for fully developed laminar and turbulent pipe flows can be used to give the following expressions for the friction factor f of a homogeneous fluid:

$$f = \frac{16}{Re_D} \qquad \text{(laminar)} \qquad 4.9$$

$$f = 0.079\ Re_D^{-0.25} \qquad \text{(turblent)} \qquad 4.10$$

Using water only, friction factors were calculated from the measured differential pressure ΔP_m over the range of superficial liquid velocities used in this study (up to 1.5 m/s). Figure 4.1 shows a plot of the calculated experimental friction factors f plotted against Reynolds number Re_D. Since the Reynolds numbers of the experimental data are higher than those associated with laminar flow (approximately 2300), the empirical equation 4.10 for fully developed turbulent pipe flow is also plotted and comparisons are made in section 4.2.3.

4.2.2 Measured values of friction factor within two-phase flow in the vertical test section

In the two-phase flow experiments the friction factor f was calculated using equation 4.7 in a bubbly flow regime. The differential pressure measurements ΔP_m were made with an Elect Torr model FA 63120E differential pressure transducer with range of ±20 mBar, and the average gas void fraction α was obtained using the quick closing gate valves. The superficial gas and liquid velocities V_{sg},

and V_{sl} were evaluated using equations 1.1 and 1.2 as described in chapter 1.

The results of these experiments are shown in figure 4.2 where the friction factor f for a bubbly two-phase fluid is plotted against the Reynolds number Re_D. Also plotted is the empirical equation for fully developed turbulent pipe flow, equation 4.10.

4.2.3 Comparison of theoretical and experimental friction factor values

It can be clearly seen from figure 4.1 that although the entry length from the exit of the shaped contraction to the centre of the test section is approximately seven pipe diameters, the friction factors evaluated experimentally from differential pressure measurements ΔP_m in single phase water match the empirical equation 4.10 for fully developed turbulent pipe flow very closely.

Figure 4.2 shows the friction factors f calculated from equation 4.7 for bubbly two-phase flow conditions. Measurements of average gas void fraction were made using the quick closing valve technique and the differential pressure ΔP_m was evaluated using a differential pressure transducer as described in section 4.2.2. Although figure 4.2 shows a considerable amount of scatter generally the friction factors have increased in value from the single phase water experiments which is consistent with a more turbulent flow.

As argued in section 4.2.1, in the range of mixture velocities considered in this study ($V_m < 2.0$ m/s), which is associated with a

range of Reynolds number Re_D of approximately 10^4 - 10^5, it would not be unreasonable to make the assumption that the change in friction factor f for fully developed turbulent pipe flow will be small over the range of Reynolds number. Therefore, the friction factors calculated using equation 4.7 for bubbly two-phase flow were averaged to obtain a friction factor of f = 0.0187 which was subsequently used in equation 4.8 to evaluate the average gas void fraction α using the gradiomanometer.

4.3 Comparison of results obtained for average gas void fractions using the quick closing valves and the gradiomanometer

Figure 4.3 shows a plot of the average gas void fraction α measured using the quick closing valve technique plotted against α measured using the gradiomanometer. The experimental average gas void fraction data α follows the perfect solution, i.e. the average gas void fraction evaluated using the quick closing valve technique equals the average gas void fraction evaluated from the gradiomanometer, very closely over the entire range of average gas void fractions and mixture velocities covered in this study (α < 20%, V_m < 2.0 m/s). However, there is a slight tendency for the average gas void fraction α measured using the gradiomanometer to give higher values of α than those measured using the quick closing valve technique. This is thought to be due to experimental inaccuracies in the two-phase flow friction factor experiments and the assumption that the friction factor f can be considered a constant over the range of Reynolds number Re_D considered in these studies.

Figure 4.3 clearly shows that although is a slight variation in

the measurement of average gas void fraction α using the gradiomanometer and the quick closing valves techniques. However, any inaccuracy due to the gradiomanometer technique is more than compensated for by the advantage of being able to use it whilst the flow loop is in continuous operation.

4.4 Area averaged gas and liquid velocities

Once the superficial gas and liquid velocities V_{sg} and V_{sl}, and the average gas void fraction α have been measured, the area averaged gas and liquid velocities V_g and V_l can be evaluated from

$$V_g = \frac{V_{sg}}{\alpha} \qquad 4.11$$

and

$$V_l = \frac{V_{sl}}{(1 - \alpha)} \qquad 1.14$$

Alternatively, for a vertical two-phase pipe flow, the area averaged gas velocity V_g can be evaluated from the *Zuber & Findlay* [1965] equation

$$V_g = C_0(V_{sg} + V_{sl}) + V_{g\infty} \qquad 1.10$$

where $V_{g\infty}$ is the terminal rise velocity of a single bubble due to buoyancy (which, it is suggested in section 5.1.4, may be dependent on the average gas void fraction α). C_0 is an empirical distribution coefficient defined as

$$C_0 = 1 + \frac{2}{m + n + 2}\left[1 + \frac{\alpha_w}{\alpha}\right] \qquad 1.11$$

where m and n are the exponents of the power law associated with the velocity and local void fraction profiles, as defined in the following equations:

$$\frac{V_l}{V_c} = 1 - \left[\frac{r}{R}\right]^m \qquad 4.12$$

$$\frac{\alpha_l - \alpha_w}{\alpha_c - \alpha_w} = 1 - \left[\frac{r}{R}\right]^n \qquad 4.13$$

V_l and V_c are the local and centreline velocities of the fluid, R is the radius of the pipe, and α_l,α_w and α_c are the local, wall and centreline void fractions respectively. The gas void fraction at the wall, α_w, is assumed to be zero since there is always a film of the continuous liquid phase at the pipe wall.

Zuber & *Findlay* have shown how the value of C_0 varies as a function of the exponents of the velocity and void fraction profiles for an axisymmetric upwardly flowing fluid in a vertical pipe (see figure 4.4). *Zuber* & *Findlay*, using the data of *Petrick* [1962], found that in general the distribution parameter C_0 is not very sensitive to changes in profile shape and that, provided reasonably accurate values for m and n can be found, a good estimation of C_0 will result.

To determine a value for the distribution parameter C_0 for the flow loop used in these studies the procedures described in the following two sub-sections were adopted.

4.4.1 Local velocity distribution in the experimental test section

To utilize the emperical equation 1.10 proposed by *Zuber & Findlay*, it is necessary to estimate the exponent of the power law that best fits the existing velocity profile in the pipe flow. Experiments designed to evaluate the velocity profile of a two-phase mixture within the test section, however these experiments could only be carried out for a single phase fluid due to the unavailability of hot-film anemometry equipment at the experimental stage of this study so that two-phase flow continuous phase velocity measurements could be made. Nevertheless, it is thought that if the velocity profile changes significantly due to the presence of gas bubbles, then the velocity profile will become flatter and hence the value of m will increase.

To measure the velocity profile in the test section a small pitot tube was traversed across the test section as shown in figure 4.5. A static pressure measurement was made from a tapping in the pipe wall just down-stream of the pitot tube. The difference ΔP was measured using an inverted 'U' tube manometer. The corresponding manometer reading Δh can be used to calculate the fluid velocity at any point in the flow, assuming no losses, from the equation

$$V_l = \sqrt{2 \frac{\rho_{man}}{\rho_l} g \Delta h} \qquad 4.14$$

where ρ_{man} is the density of the manometer fluid.

Figure 4.6 shows the measured non-dimensional velocity distributions for area average liquid velocities V_l of 0.3, 0.6, and 1.0 m/s. It can be seen that the velocity profile is very uniform

across most of the test section although the traverse position is only seven pipe diameters (7D) down-stream of the inlet. This is due to the shaped contraction prior to the test section and the flow being turbulent.

A curve fit to the experimental data of the form of equation 4.12 showed that, due to the uniformity of the velocity profile, no power of m fitted the data extremely well. However, since only a reasonable estimation of the power law parameter m is needed to evaluate the distribution coefficient C_0 in equation 1.11, a value for m of eight was found to give a reasonable agreement with the measured velocity profiles in the range of liquid velocities used in this study. Since there is little variation in velocity profiles over the range of area averaged liquid velocities, m = 8 was used in equation 1.11 to evaluate the distribution coefficient C_0.

4.4.2 Local gas void fraction distribution $\alpha_l(r)$ in the experimental test section

To measure the local gas void fraction in the test section, a fine insulated copper wire similar to that used by *Delhaye* and *Chevrier* [1966], as briefly described in section 2.2, was traversed across the test section with only its tip uninsulated. The resistance between the wall of the test section and the tip of the probe will change dramatically when the tip of the probe moves from air to water or vice-versa.

The probe was connected as one of the arms in a Wheatstone bridge circuit, the output from which was connected to a comparitor.

The output from the comparitor was interfaced to the digital input of a BBC micro computer as shown in figure 4.7. The computer was programmed to measure the ratio of time that the probe was in air over a sample period of approximately 1 minute. This ratio is the local gas void fraction α_l, the void fraction at any point in the flow.

The local gas void fraction profiles were measured for average gas void fractions of approximately 5, 11, and 18%. Figure 4.8 shows the non-dimensional results of these experiments plotted as the ratio of local gas void fraction over the centreline gas void fraction (α_l/α_c), against the local radius over the radius of the pipe (r/R).

It can be seen from figure 4.8 that there is little variation in the local gas void fraction profile with changing average gas void fraction. The local gas void fraction profile is seen to be fairly uniform over most of the cross-section. Curve fitting equation 4.13 to the experimental data gives a 'best value' for the power law exponent n of 7. This value gave a reasonable average value for the local gas void fraction distribution over the range of average gas void fractions used in this study.

From these results for m and n and assuming the local gas void fraction at the wall α_w to be zero, since there is always a thin liquid film at the wall, the value of C_0 was calculated as 1.12.

4.5 Comparison of the area averaged gas velocity results obtained by *Zuber / Findlay* theory and experimental results from the quick closing valves and gradiomanometer

For a range of mixture velocities V_m the three methods mentioned above were used to calculate the area average gas velocity V_g. For each experiment the gas and liquid volume flow rates $\dot{V}_g$ and $\dot{V}_l$ were measured, as described in chapter 3, and the corresponding superficial gas and liquid velocities $\dot{V}_{sg} = V_g/A$ and $\dot{V}_{sl} = V_l/A$ were calculated.

The area averaged gas velocity V_g can then be evaluated from equation 4.11. Two techniques, the quick closing valves method and the gradiomanometer method were used to obtain the average gas void fraction α.

The area averaged gas velocity V_g results are presented in figure 4.9. This shows that the area average gas velocity V_g evaluated using the quick closing valve technique and the gradiomanometer give similar results. However, the quick closing valve data exhibits more scatter than the gradiomanometer. Inaccuracies in measuring small values of α due to the construction of the apparatus used in this technique are thought to account for this effect.

Having determined in section 4.4 the value of the distribution coefficient C_0 for the experimental test section to be 1.12 and assuming an average terminal bubble rise velocity $V_{g\infty}$ of 0.29 (see chapter 5), the area averaged gas velocity V_g can also be obtained from the *Zuber / Findlay* relationship.

The result of the *Zuber / Findlay* relationship, equation 1.10 is also shown on figure 4.9 and can be seen to give a reasonable approximation to the area averaged gas velocity V_g for mixture velocities V_m of less than 1 m/s. However, at higher mixture velocities significantly lower values of V_g are predicted by the *Zuber / Findlay* relationship than calculated using both the quick closing valve and gradiomanometer techniques. This may be due to inaccuracies in the evaluation of the local void fraction and mixture velocity profile powers.

4.6 General conclusions drawn from initial experiments carried out in the two-phase flow loop

Comparisons made between the quick closing valve technique and the gradiomanometer, when used to measure average gas void fraction in the test section, give results that match each other very closely. When there is disagreement the gradiomanometer results tend to give higher average gas void fraction. This is thought to be due to experimental inaccuracies in the determination of the friction factor f. However, since both methods produce similar results, subsequent experiments used only the gradiomanometer to measure the average gas void fraction α. This technique is more practical than the quick closing valves since it is non-intrusive to the flow and thus can be used in conjunction with other experiments.

Using the *Zuber / Findlay* relationship described in section 4.4, the area averaged gas velocity V_g can be calculated from the local void fraction and velocity profile powers, the mixture velocity V_m and the terminal bubble rise velocity $V_{g\infty}$. Comparing the results of

experiments in which the area averaged gas velocity V_g is calculated from equation 4.11 using the average gas void fractions α from both the gradiomanometer and the quick closing valves, with the *Zuber / Findlay* relationship (equation 1.10) where $C_0 = 1.12$, figure 4.9 show that the *Zuber / Findlay* relationship tends to give better results than the gradiomanometer for lower mixture velocities, typically less than 1 m/s.

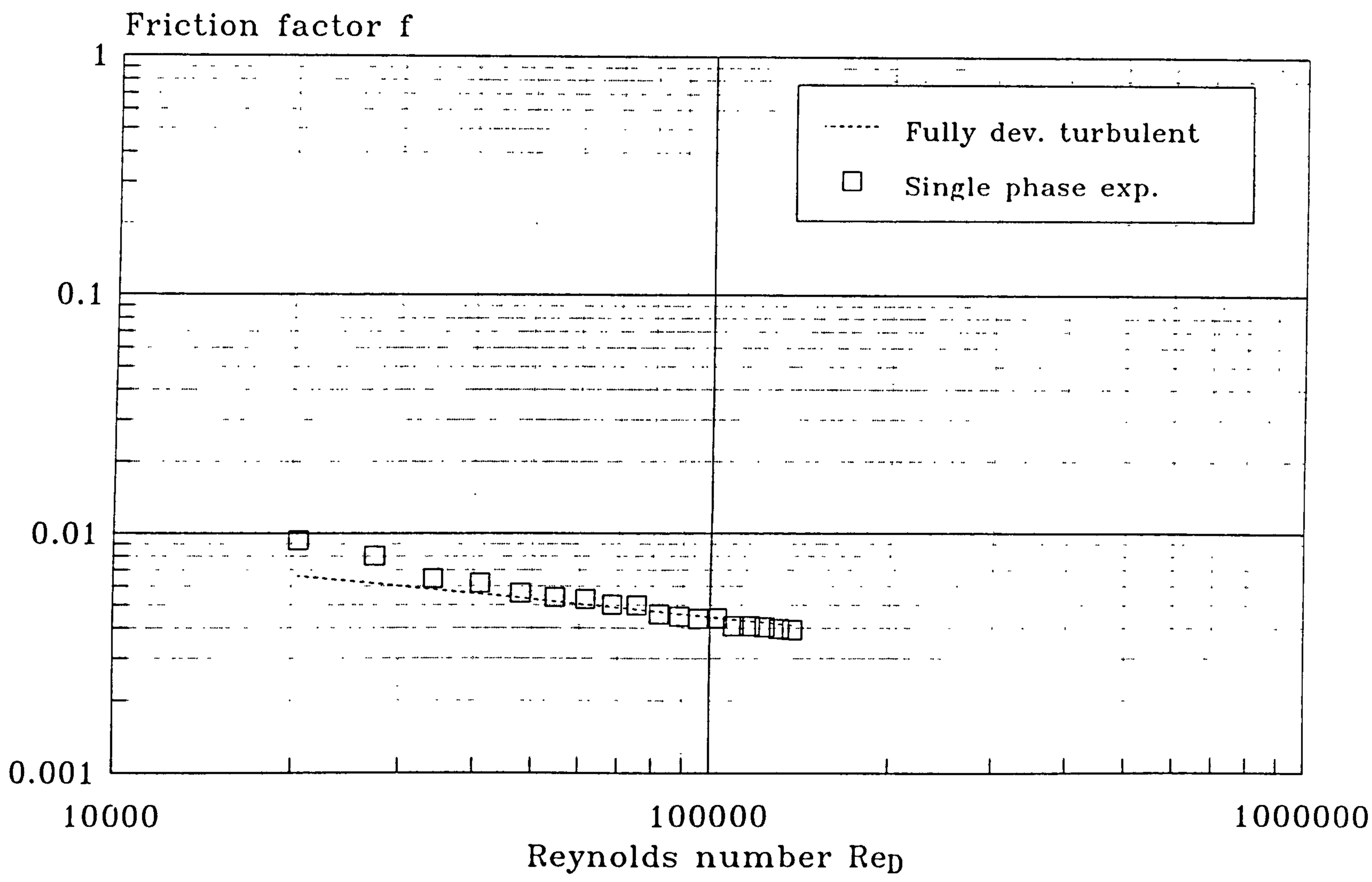

Figure 4.1 Single phase (water) friction factors in the experimental test section

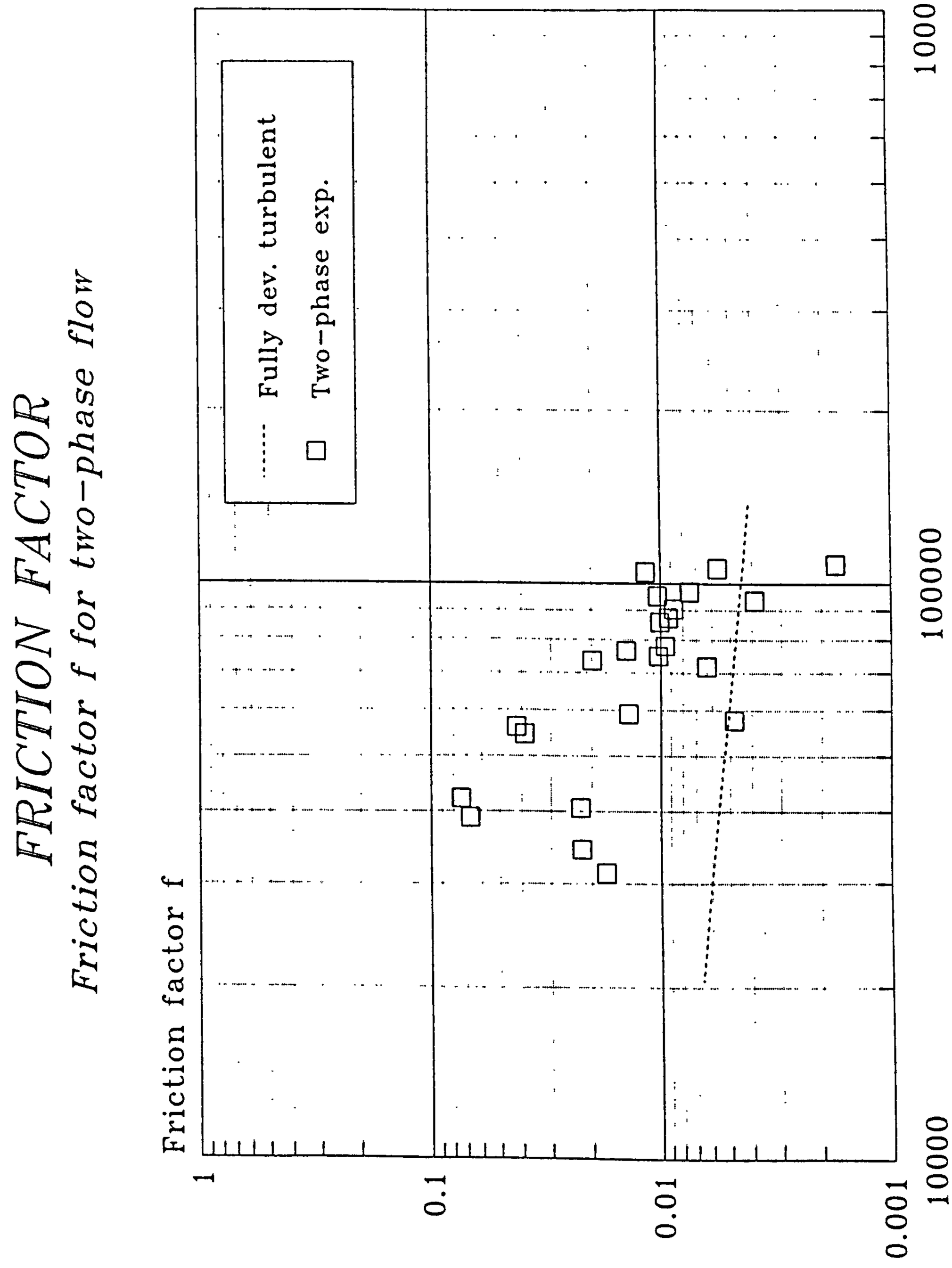

Figure 4.2 Two-phase flow friction factors in the experimental test section

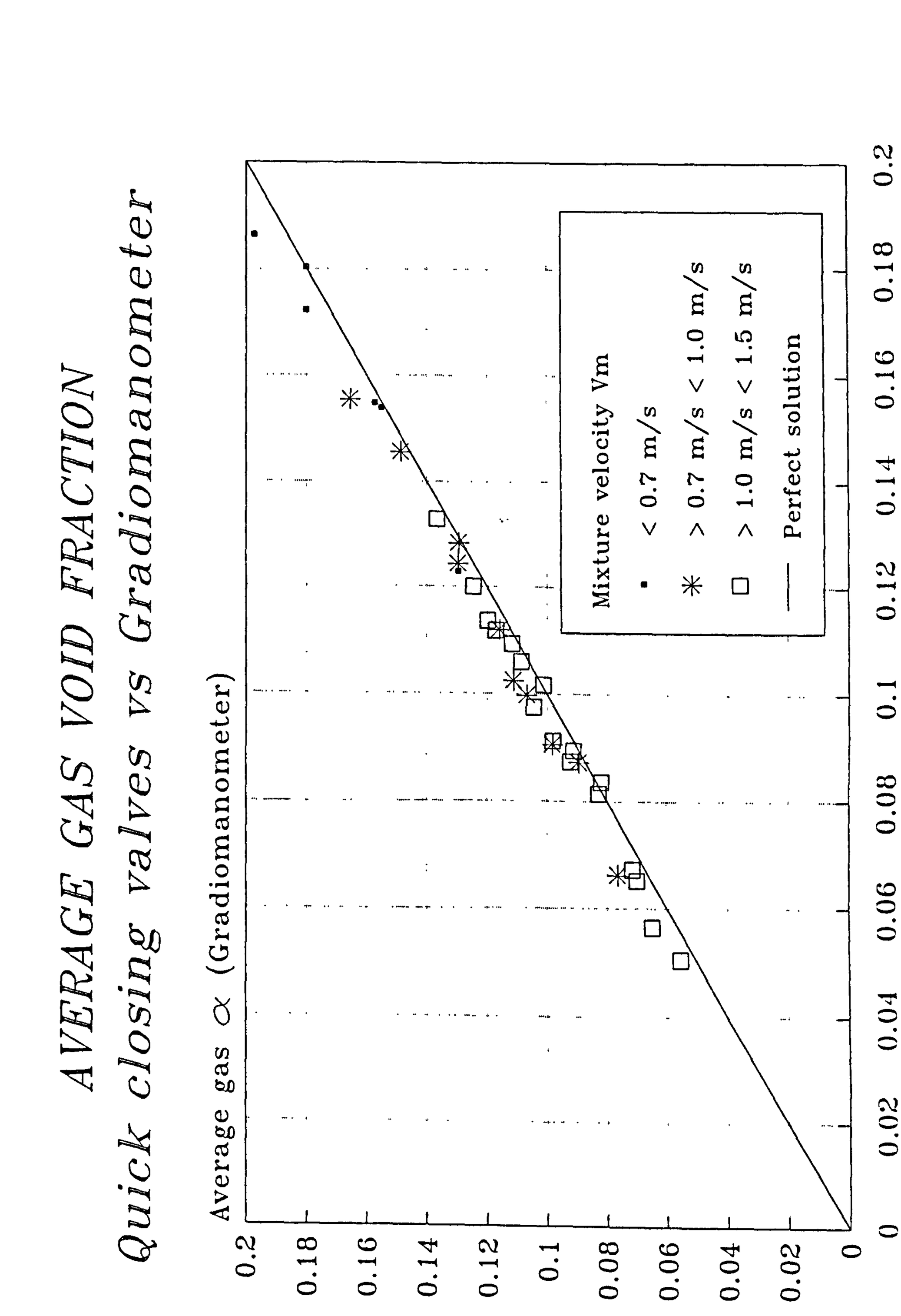

Figure 4.3 Comparison of average gas void fractions using the quick closing valve and gradiomanometer techniques

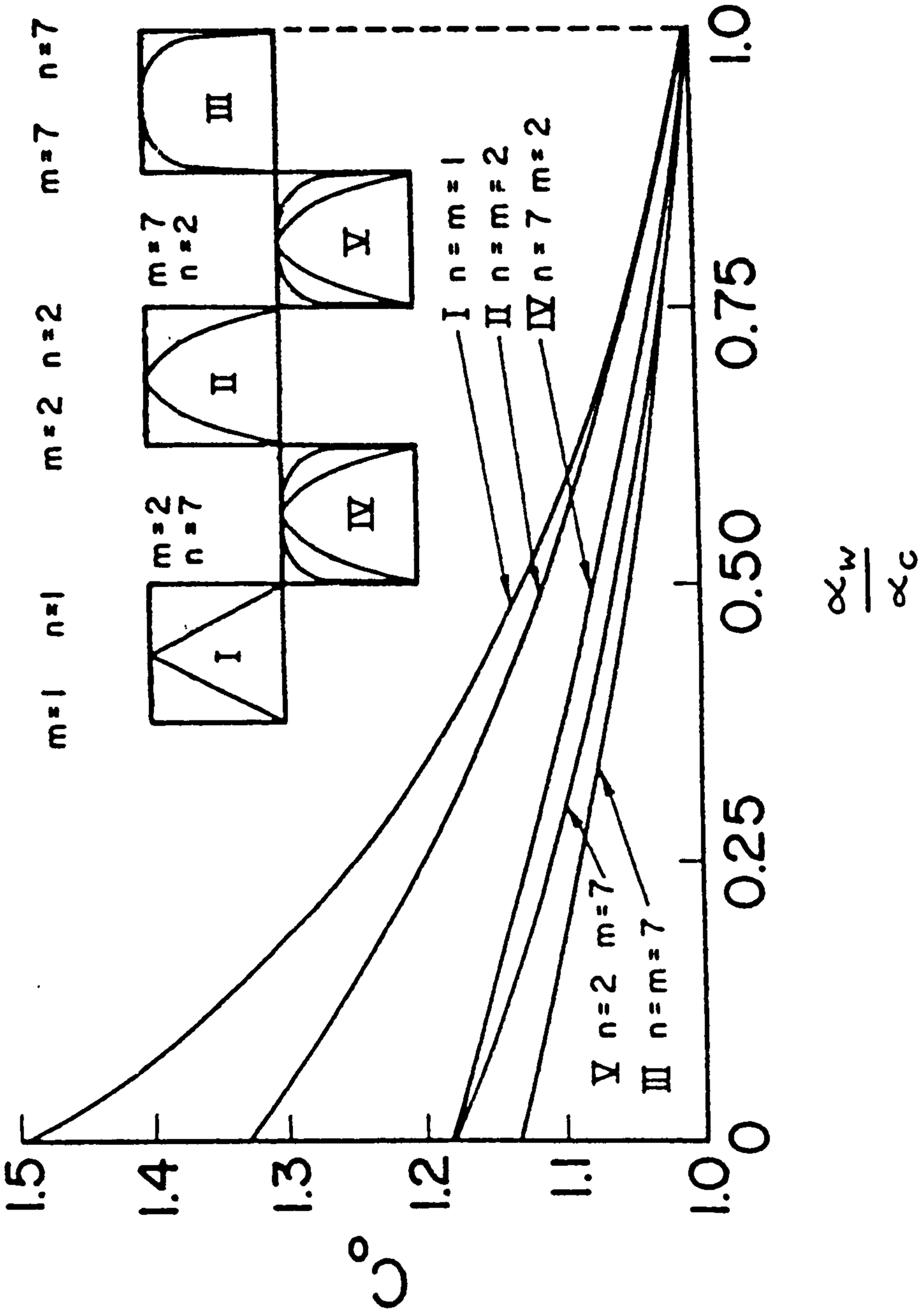

Figure 4.4 Variation in distribution coefficient C_o produced by *Zuber/Findlay* [1965]

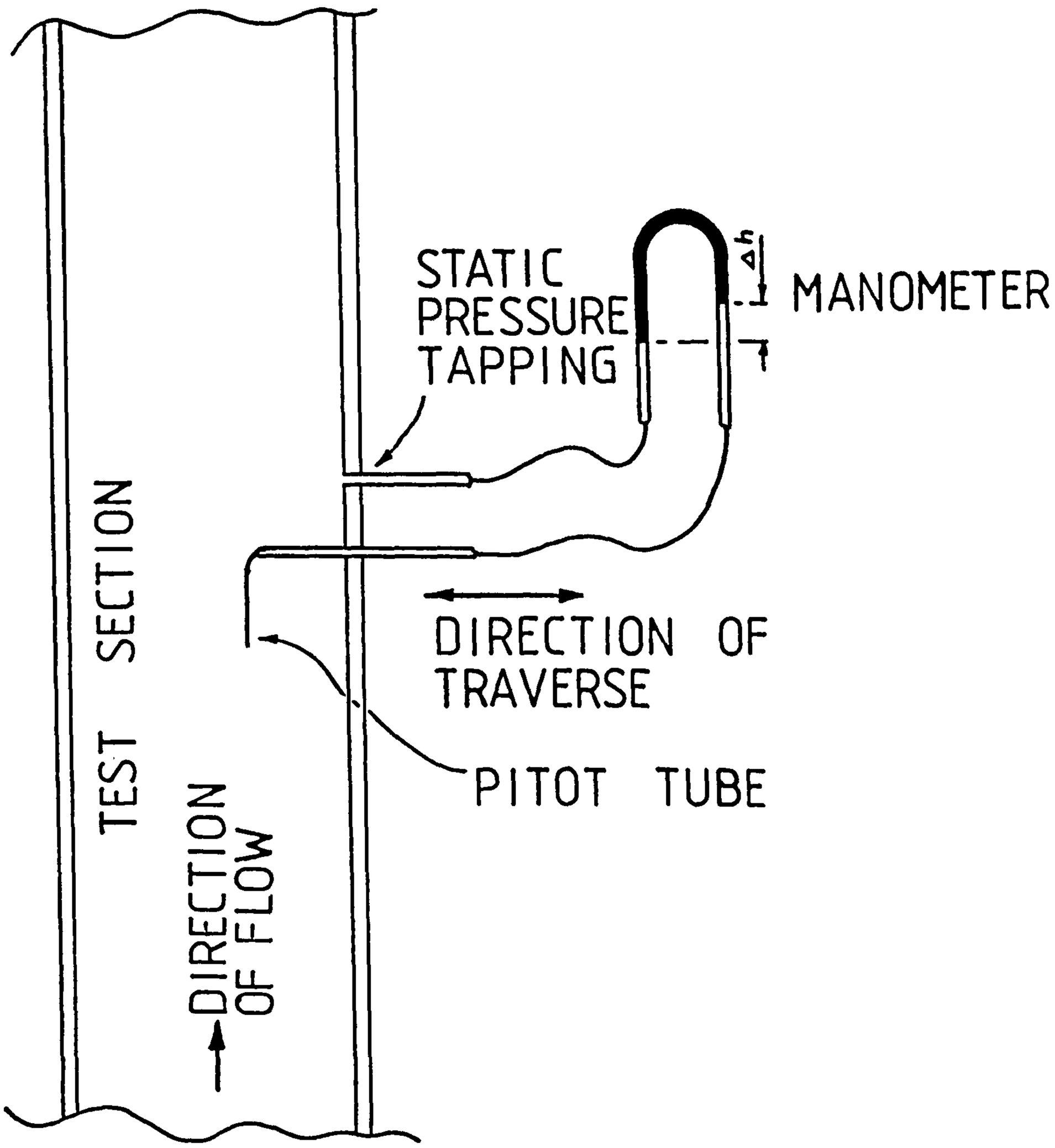

Figure 4.5 Experimental set up used to measure single phase (water) velocity profiles in the experimental test section

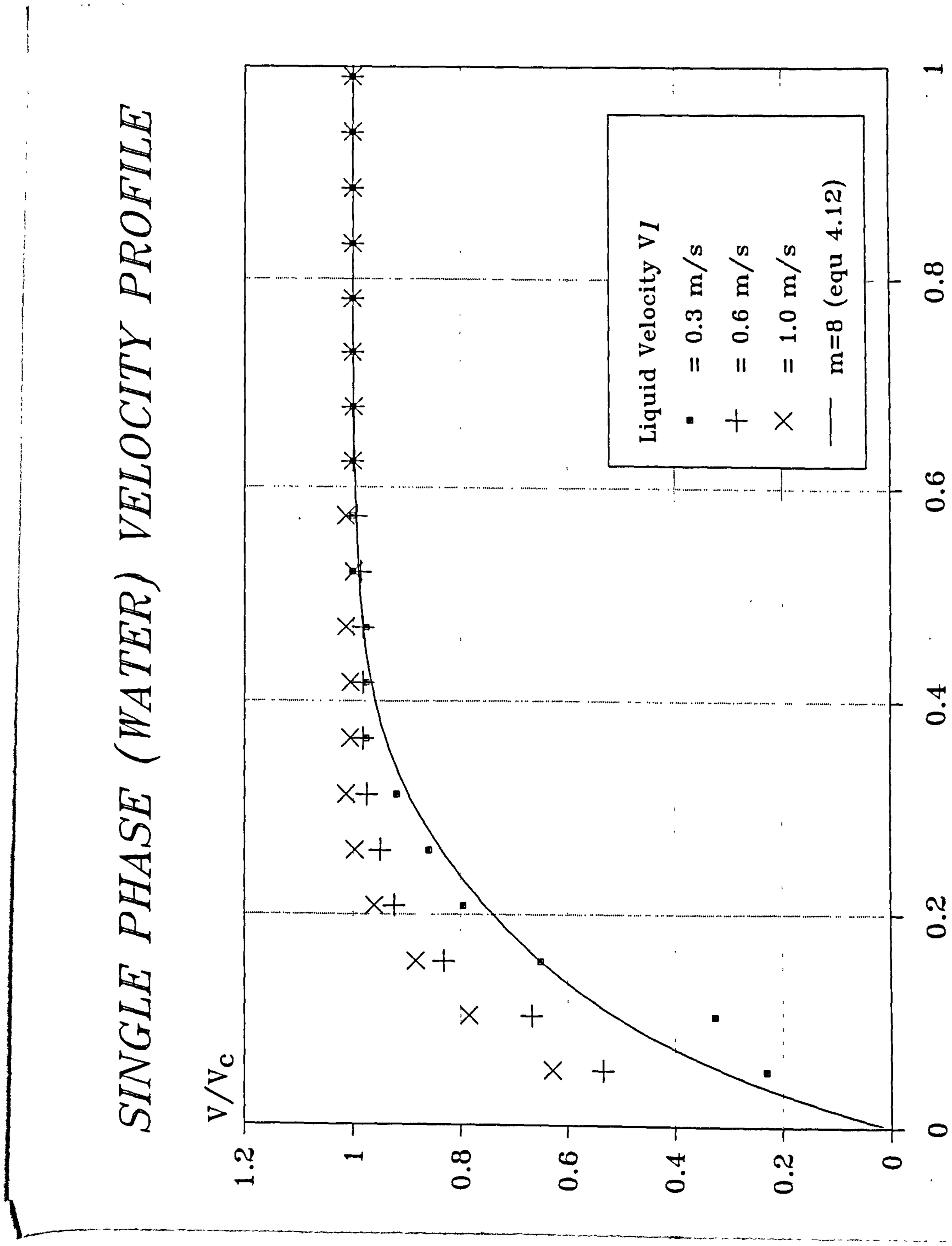

Figure 4.6 Non-dimensional single phase (water) velocity profile in the experimental test section

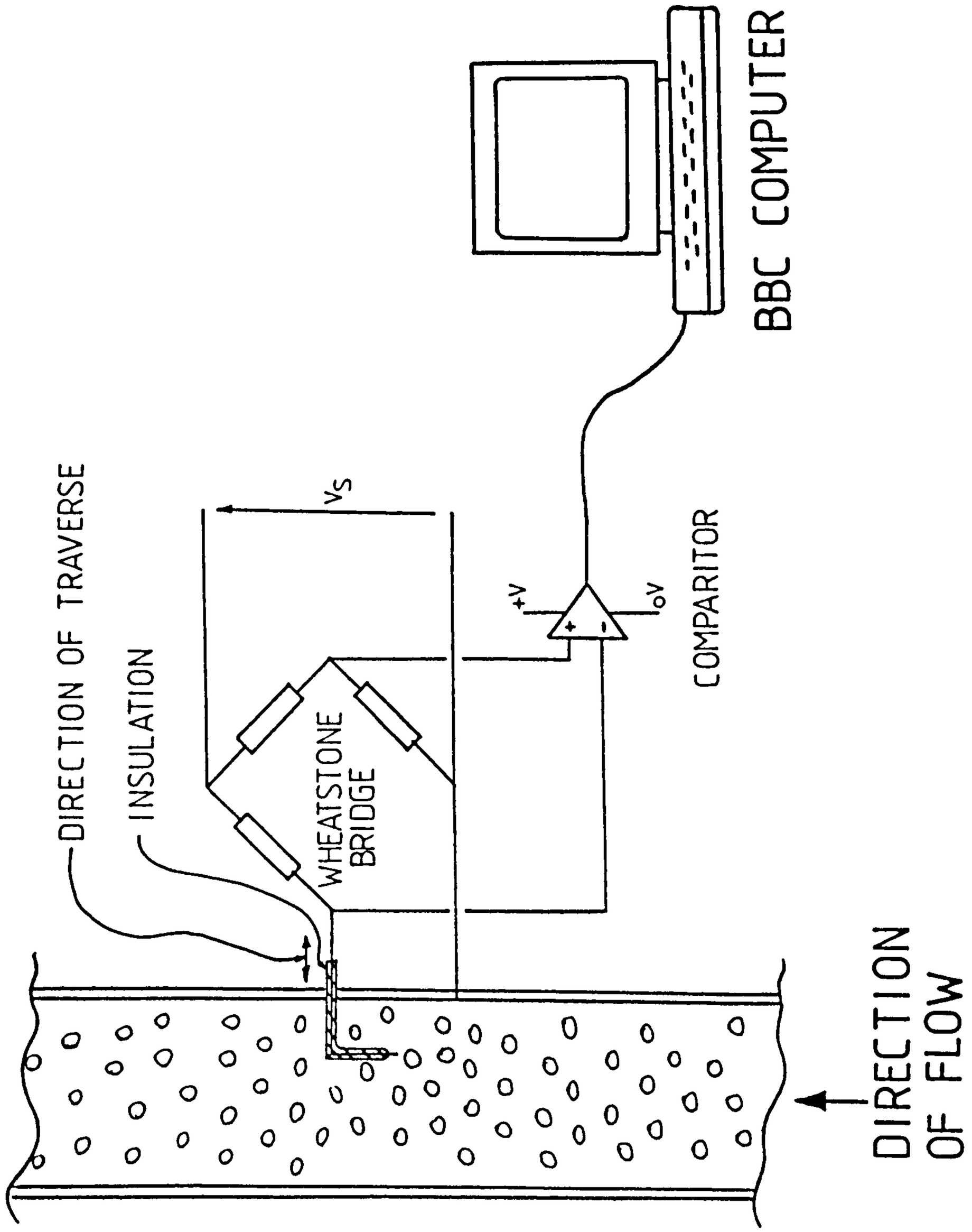

Figure 4.7 Resistive probe technique used in the experimental test section to measure the local gas void fraction profile

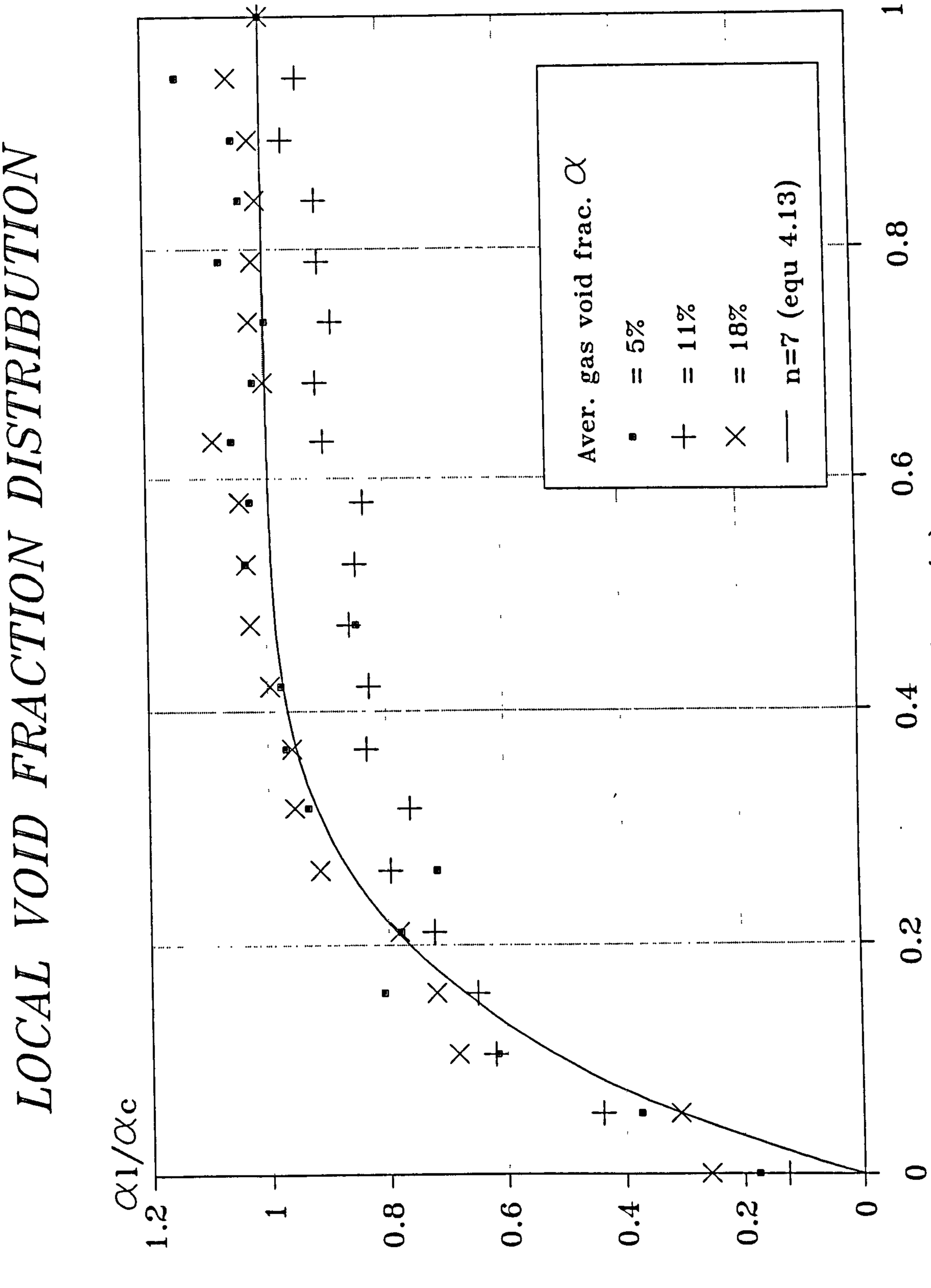

Figure 4.8 Non-dimensional local gas void fraction profile in the experimental test section for average gas void fractions of approximately 5, 11, 18%

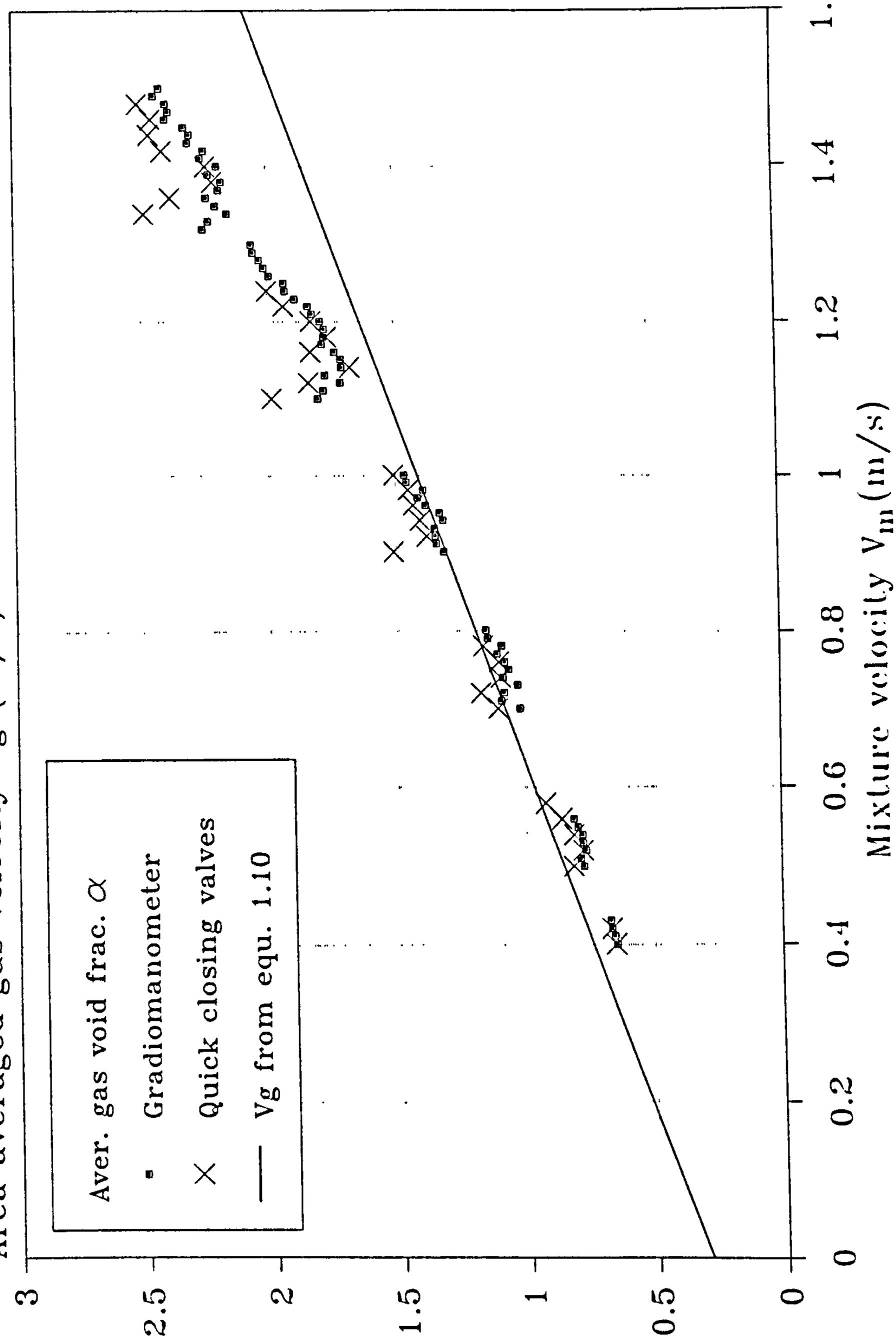

Figure 4.9 Area averaged gas velocity V_g predicted by the *Zuber/Findlay* relationship and the experimental measurements of average gas void fraction using the quick closing valve technique and gradiomanometer

CHAPTER 5 - BUBBLE DYNAMICS AND SOURCES OF PRESSURE FLUCTUATIONS IN TWO-PHASE BUBBLY FLOW

Chapter summary

The aim of this chapter is two fold, firstly to investigate the sources that give rise to pressure fluctuations in a bubbly two-phase flow, in order that subsequent auto and cross correlations produced in this study may be interpreted accurately. Secondly to provide simple models for the main sources of pressure fluctuations which can then be used to predict pressure fluctuations within a bubbly two-phase flow.

The dynamics of bubbles are considered in section 5.1, with bubble shape, size, drag coefficient and terminal velocity being discussed and evaluated using simple theories which are compared with the findings of other researchers.

Section 5.2 describes the four main sources of pressure fluctuations as observed at fixed points in the flow field. These are due to (i) temporal variations in the average gas void fraction, (ii) the convected potential pressure profile around a bubble as it travels through the continuous phase, (iii) the wake generated by a bubble in the continuous phase and (iv) background turbulence present in the continuous phase. Simple models are developed and where possible the magnitude of each source of pressure fluctuation is predicted and its corresponding autocorrelation length scales discussed.

Two techniques were investigated for measuring differential pressure fluctuations and these are described in section 5.3. The first method involved subtracting two static pressure signals. This proved to be unsuitable due to the presence of background noise (both mechanical and electrical) which was found to be difficult to eliminate. The second technique involved the use of a single differential pressure transducer with tappings separated by a short axial distance l.

Section 5.4 describes experimental pressure measurements, made with both a constant velocity bead travelling through a stagnant column of water at a fixed distance from the pipe wall, and a single stream of bubbles injected at a nominal distance from the wall upstream of the differential pressure transducer. These experimental results are compared with theoretical predictions demonstrating good agreement.

5.1 Bubble dynamics

The dynamics of a fluid flowing around gas bubbles in pipes or ducts is very complex since bubbles have flexible boundaries which allow them to change shape, to sub-divide into smaller bubbles, or to coalesce into larger bubbles. Bubble dynamics can be influenced by a number of factors such as surface tension, densities and method of bubble generation. In this study the theoretical analysis of bubbles will treat the bubbles as solid spheres and, where possible, comparisons between experiments involving bubbles, solid spheres and theory will be made to determine the validity of this assumption. Bubble generation in this study will be through a number of small orifices, as this method is thought to be similar to the mechanism by which natural gas bubbles are generated from porous rock downhole.

5.1.1 Simple dynamics and drag coefficient of a single bubble

If we assume that the bubbles are spherical, then it is well reported in standard texts such as *G ovier* and *Aziz* [1972] that the flow about a single bubble as it travels through the continuous phase is a function of two non-dimensional numbers. These are the bubble Reynolds and Weber numbers Re_b and W_b respectively, where

$$Re_b = \frac{V_g\ d}{\nu} \qquad 5.1$$

and

$$W_b = \frac{\rho_l\ V_g^2\ d}{\sigma} \qquad 5.2$$

Here V_g is the bubble velocity, d the bubble diameter, ν the

continuous phase kinematic viscosity, ρ_l the liquid density and σ the surface tension at the gas/liquid interface. The Reynolds number is the ratio of inertia to viscous forces and the Weber number is the ratio of inertia to surface tension forces. Figures 5.1 show how the calculated shape of a bubble changes as a function of both bubble Reynolds and Weber numbers. These calculations were made by *Ryskin & Leal* [1985] who assuming steady axisymmetric bubble flow, obtained numerical solutions to the full Navier-Stokes equations. It will be noted from figure 5.1 that at low Weber numbers, the bubbles are almost spherical in shape due to the dominance of surface tension forces which try to pull the bubble into a spherical shape. At high Weber numbers, the surface tension forces cease to dominate and non-spherical cap bubbles develop. Another non-dimensional number which is a function of both Reynolds and Weber numbers is the drag coefficient C_d which is defined as

$$C_d = \frac{F_d}{\frac{1}{2}\rho_l V_g^2 \left[\frac{\pi d^2}{4}\right]} \qquad 5.3$$

where F_d is the drag force exerted of the bubble, ρ_l the density of the continuous phase, V_g the bubble velocity and d the bubble diameter.

The flow around a bubble at low Reynolds and Weber numbers is strongly dependent on the boundary conditions at the surface of the bubble. In some theoretical calculations on bubbles, a zero tangential stress condition is applied at the bubble boundary. However, in practice when bubbles travel through a liquid such as tap

water, contaminants collect on the surface of the bubble and the interface then behaves more like a solid boundary. *Peebles & Garber* [1953] for example have shown that for bubble diameters of the order of 1mm and Reynolds numbers below two in an almost infinite fluid, the Stokes solution for the drag coefficient of a solid sphere moving in an infinite fluid, neglecting inertia forces (as given in equation 5.4) agrees closely with experimental results.

$$C_d = \frac{24}{Re_b} \qquad 5.4$$

For larger near spherical bubbles that have Reynolds numbers greater than two and placed in an infinite fluid, it is suggested in an unpublished seminar by *Bradbury* [1988] that a value for C_d given by *Hadamard* [1911] of

$$C_d = \frac{16}{Re_b} \qquad 5.5$$

gives better agreement with experimental results.

Many other expressions have been proposed for the drag coefficient. For example an empirical expression by *Peebles & Garber* [1953] is given as

$$C_d = \frac{18.7}{Re_b^{0.68}} \qquad 5.6$$

This expression gives a value of C_d between those obtained from equations 5.4 and 5.5. *Ryskin & Leal* [1985] obtained numerical solutions to the full Navier-Stokes equations, assuming steady state axisymmetric bubble flow, and computed theoretical drag coefficients for a bubble as a function of both the Reynolds and Weber numbers, as shown in figure 5.2. Although it is difficult to make detailed

comparisons between *Ryskin* & *Leal's* calculated drag coefficients and the drag coefficient of a solid sphere, shown in figure 5.3, spot checks at Reynolds numbers up to 20 indicate that *Ryskin* & *Leal's* calculated drag coefficients for higher Weber numbers are very similar to the measured drag coefficients for a solid sphere. The effect of surfactants, universally present in aqueous systems, tends to make the mobile interface of a bubble behave more like a rigid sphere. This suggests that although bubbles have a flexible interface, for simple modelling, the drag coefficient of a bubble can be calculated on the assumption that the bubble interface behaves as a solid sphere.

5.1.2 Terminal rise velocity of a single bubble from simple theory

If we consider a volume containing two immiscible phases flowing in a pipe, one phase will be suspended in the other as bubbles or droplets. In the case of air/water with an average gas void fraction α of less than approximately 25%, air forms into discrete bubbles in a continuous water phase. Air bubbles, being less dense than water try to rise through the continuous water phase at a higher velocity than the continuous and the difference between the continuous phase velocity and the bubble velocity is often referred to as the slip or bubble rise velocity. The terminal velocity at which a bubble rises in still water, $V_{g\infty}$, can be determined by equating the buoyancy to drag forces acting on the bubble.

Consider a bubble in an infinite stagnant liquid with a volume v_b. We can define an equivalent spherical bubble of diameter d

$$d = \left[\frac{6\ v_b}{\pi} \right]^{1/3} \qquad 5.7$$

The buoyancy force F_b on a near spherical bubble is given by

$$F_b = \frac{\pi\ d^3}{6}\ g\ (\rho_l - \rho_g) \qquad 5.8$$

and the drag force F_d on a bubble travelling through the continuous liquid phase can be estimated using equation 5.3 as

$$F_d = C_d \frac{\pi\ d^2}{4} \frac{1}{2}\ \rho_l\ V_{g\infty}^2 \qquad 5.9$$

These two forces will be in equilibrium when a bubble reaches its terminal rise velocity. By combining equations 5.8 and 5.9 the terminal rise velocity of a single near spherical bubble can be expressed as

$$V_{g\infty} = \frac{2}{\sqrt{3}} \left[\frac{g\ (\rho_l - \rho_g)\ d}{\rho_l\ \ C_d} \right]^{\frac{1}{2}} \qquad 5.10$$

The terminal rise velocity of a single bubble could be calculated using their theoretical drag coefficients of *Ryskin* & *Leal* [1985], as a function of both Reynolds and Weber numbers. However, since a real bubble tends to exhibit the drag coefficient properties of a solid sphere when in impure water (see section 5.1.1), *Ryskin* & *Leal's* values of C_d would not necessarily give better results than using the drag coefficient for a simple sphere.

5.1.3 Theoretical critical bubble diameter and velocity

Many researchers have made the observation that only a small range of bubble sizes are observed in the bubbly flow regime. This may be due to the stability of a bubble being governed by interfacial surface tension forces. If a large cap bubble forms on the introduction to the continuous phase, surface tension forces on a bubble of this size are less dominant than drag forces. Therefore, large cap bubbles tend to be unstable, especially in the presence of other bubbles. Break up of the bubble thus occurs until surface tension forces are of the same order as the drag forces and at this point there is no longer a mechanism for further reduction in bubble size thus limiting the observed variation in bubble size.

At the critical bubble size the pressure in a bubble due to the interfacial surface tension

$$\Delta p_1 = \frac{4\,\sigma}{d} \qquad 5.11$$

will balance the pressure exerted on a bubble due to its motion in the continuous phase

$$\Delta p_2 = K\,\frac{1}{2}\,\rho_l\,V_{g\infty}^2 \qquad 5.12$$

where K is a constant of the order of unity. Equating Δp_1 and Δp_2 will give an expression for the critical diameter d_c of a spherical bubble

$$d_c = \frac{8\,\sigma}{K\,\rho_l\,V_{g\infty}^2} \qquad 5.13$$

Equations 5.10 and 5.13 can be used to obtain expressions for $V_{g\infty}$ and

d_c. Elimination of d_c gives

$$V_{g\infty} = 1.81 \left[\frac{g(\rho_l - \rho_g)\sigma}{\rho_l^2} \right]^{\frac{1}{4}} \left[\frac{1}{K\ C_d} \right]^{\frac{1}{4}} \qquad 5.14$$

Equation 5.14 gives the terminal rise velocity of a spherical bubble of critical diameter d_c. By eliminating $V_{g\infty}$ the expression for the critical bubble diameter d_c (defined as the diameter of a bubble at which there is no mechanism for a further reduction in bubble volume) becomes

$$d_c = \left[\frac{6\ \sigma\ C_d}{K\ g\ (\rho_l - \rho_g)} \right]^{\frac{1}{2}} \qquad 5.15$$

If we assume both the constant K and the drag coefficient C_d to be of the order of one, then for air bubbles in water with an interfacial surface tension of σ = 7000dynes/m, $V_{g\infty}$ = 0.293m/s and d_c = 6.5mm.

Equation 5.14 can be compared to the empirical expression put forward by *Harmathay* [1960] which is often used for the terminal rise velocity of a single bubble $V_{g\infty}$ in an infinite fluid

$$V_{g\infty} = 1.53 \left[\frac{g(\rho_l - \rho_g)\sigma}{\rho_l^2} \right]^{\frac{1}{4}} \qquad 5.16$$

Using the above value of σ equation 5.16 gives $V_{g\infty}$ = 0.248m/s. The two values for $V_{g\infty}$ obtained by equations 5.14 and 5.16 are seen to be in reasonable agreement when K and C_d are each taken to be equal to one.

The size of a bubble produced at an orifice is influenced by many factors such as the diameter of the orifice, the interfacial surface tension between the phases and the average volumetric flow rate through the orifice. Work by *Siemes* [1954], *Kauffmann* [1956], and others suggests that when gas is introduced in to a continuous phase at low volumetric flow rates through an orifice of a known diameter d_o, then the volume of the generated bubbles generally remains constant and the frequency of generation ω increases with volumetric flow rate. This remains the case up to a critical bubble generation frequency, beyond which the bubble volume increases. The bubble volume continues to increase at a fixed frequency as the gas volume flow rate increases until discrete bubbles are no longer generated and gas is emitted from the orifice as a continuous jet.

In the bubbly flow regime, bubbles generated from an orifice tend to be in the constant-volume increasing frequency region. In this region

$$\dot{V}_g = n\,\omega\,v_b \qquad 5.17$$

where $\dot{V}_g$ is the total volume flow rate of gas in the pipe, n is the number of orifices, ω the frequency of bubbles generated per orifice and v_b the average bubble volume.

The volume of a single air bubble generated in water at an orifice v_b^* can be estimated from an empirical expression put forward by *Yip* et al [1970] which is consistent with experimental data by *Krevelen & Hoftijzer* [1950],

$$v_b^* = 0.0942 \sinh (1.64\, d_o) \qquad 5.18$$

where d_o is the diameter of the orifice. If we assume the bubble to be spherical, then equation 5.18 can be rewritten to give an estimation of the bubble diameter d

$$d = \left[\frac{0.5652 \sinh (1.64\ d_o)}{\pi} \right]^{1/3} \qquad 5.19$$

Yip also makes a correction for bubble volume when influenced by the inertia of other bubbles, namely,

$$v_b = v_b^* (1 + 0.075\omega) \qquad 5.20$$

where ω is the frequency of bubble generation. Note that the units in equations 5.18 to 5.20 are in units of centimetres and seconds.

For a single bubble generated at an orifice with a diameter d_o = 0.6mm, equation 5.19 gives a nominal bubble diameter of 2.6mm. This is much smaller than the critical bubble diameter 6.5mm calculated from equation 5.15 above. However, as the frequency of bubble generation goes up so will the nominal bubble diameter. Other mechanisms such as coaxiallation between bubbles after generation may also increase the bubble volume.

5.1.4 Empirical expressions for variations in terminal bubble rise velocity with changing average gas void fraction

The calculations in section 5.1.2 for the terminal rise velocity of a single bubble assume that there is no influence upon any one

bubble from other bubbles or solid boundaries. In practice this is seldom the case and it has been found empirically that a correction factor is needed in order to estimate the terminal rise velocity of swarms of bubbles.

Peebles & Garber [1953] have suggested the use of the following equation to calculate the terminal rise velocity of the discontinuous phase with an average volume fraction α in a liquid-liquid system:

$$V_\infty = 1.18\ (1 - \alpha)^2 \left[\frac{g(\rho_1 - \rho_2)\sigma}{\rho_l^2} \right]^{\frac{1}{4}} \qquad 5.21$$

where ρ_1 and ρ_2 are the continuous and discontinuous phase densities respectively. For gas-liquid systems *Harmathay* [1960] has proposed that equation 5.16 should be modified to

$$V_{g\infty} = 1.53\ (1 - \alpha)^2 \left[\frac{g(\rho_l - \rho_g)\sigma}{\rho_l^2} \right]^{\frac{1}{4}} \qquad 5.22$$

Equations 5.21 and 5.22 are compared using $V_{sg}=\alpha V_{g\infty}$ with experimental data by *Shulman & Molstad* [1950] by *Wallis* [1969] in figure 5.5, which shows, as one would expect, that *Harmathay's* equation 5.22 gives the better approximation to the terminal rise velocity for gas bubbles in a liquid with average gas void fractions in the range of 5 - 25%.

5.1.5 Comparison of theoretical terminal rise velocity and nominal bubble diameter with measurements made using high speed photography

Using high speed photography, a film was made of bubbles rising

through a stagnant column of water in the experimental test section of the two-phase flow loop constructed in this project. The bubbles were injected through a number of small orifices as described in chapter 3 into a column of stagnant water with an average gas void fraction α less than 5%. At higher average gas void fractions individual bubbles could not be distinguished between when consecutive frames were examined. The high speed camera was set to 1000 frames per second and timing marks were placed optically on the film at intervals of 0.1 seconds. Using prints (see figure 5.6) of consecutive frames from this film individual bubbles were tracked. By measuring the axial distance travelled by an individual bubble over a known time period, and assuming the bubble is travelling at a constant velocity, its speed can be evaluated. The equivalent bubble diameters can also be estimated from these still frames by averaging the difference between the major and minor axis of the ellipsoidal bubble.

It should be noted however that since the film is two-dimensional and has a large depth of field over the cross-section of the test section, no estimation of the distance a bubble is from the wall can be made except for bubbles that are close to the edge of the pipe, as shown in the prints. Therefore, it can only be assumed that a bubble is nearer the centre of the test section.

Figure 5.7 shows plots of individual bubbles that have been tracked over 9 frames for a time period of 0.2 seconds. The terminal rise velocity $V_{g\infty}$ and diameter d can be estimated for bubbles that are identified as being close to the wall and for those that are assumed to be near the centre of the pipe. Bubbles that are known to be near the wall of the pipe can be seen to travel slower than those we assume to be nearer the centre. This is probably due to

friction effects near to the wall of the test section caused by bubble motion.

Variations in terminal bubble rise velocity $V_{g\infty}$ in the test section range from approximately 0.28m/s, at what is assumed to be the centre of the pipe, to 0.19m/s at the wall. This compares well with the calculated value of terminal bubble rise velocity $V_{g\infty}$ in section 5.1.3 where, using a value of σ = 7000dynes/m for the interfacial surface tension in equation 5.14 and assuming the constant K and drag coefficient C_d to be of the order of unity, a value for $V_{g\infty}$ of 0.293m/s was calculated for a single air bubble in an infinite expanse of water. This is slightly higher than that measured but, considering the simplicity of the theoretical model, the assumption that the constant K and drag coefficient C_d are both unity and that no allowance has been made in the model for the effects of other bubbles or the pipe wall, the agreement is very good.

It is not easy to estimate the average bubble diameter by averaging the difference between the major and minor axes of the ellipsoidal bubbles from figure 5.6. However, on average, the equivalent bubble diameter is approximately 7mm. This estimate compares well with a calculated bubble diameter of 6.5mm using equation 5.15 in which the constant K and the drag coefficient C_d are considered to be unity and the interfacial surface tension σ = 7000 dynes/m. Figure 5.6 also shows that, in general, the bubbles are not spherical in shape but are more ellipsoidal.

5.2 Sources of pressure fluctuations in bubbly vertical two-phase flow

If we consider any point in the two-phase flow contained in the vertical test section, then the pressure at this point can be affected by disturbances to the flow loop which may be caused by the nature of the two-phase flow itself, pressure pulsations from pumps, restrictions/intrusions to the flow or from vibrations acting upon the flow loop from external forces. Let us consider the pressures at two points 1 and 2 at cross-sections separated by a short axial distance *l* as shown in figure 5.8. If the two static pressures are subtracted to obtain the differential pressure $\Delta P = P_1 - P_2$, then although the two static pressures will still be affected by the sources of pressure fluctuations mentioned above, when subtracted any variations in pressure that are common to both P_1 and P_2 such as changes in hydrostatic head will in effect be cancelled out. However, pressure fluctuations that are not common to both P_1 and P_2 such as those caused by bubbles as they flow from the upstream to the down-stream pressure measurement points, P_1 and P_2 respectively, will result in a fluctuation in the differential pressure signal ΔP. It should also be noted that pressure waves travelling through the fluid caused by pump pulsation or external vibrations will take a finite time to travel from 1 to 2 thus resulting in short time duration differential pressure fluctuations which will be much shorter in duration than those caused by the bubbly flow. However, such effects as external vibrations and pump pulsation will contaminate the pressure signals naturally generated by bubbles as they travel in a two-phase flow and thus attempts have been made in this study to minimise these effects and are described in section 5.4.3.

Naturally occurring pressure fluctuations in a bubbly two-phase flow are caused by a combination of many effects. The four main contributors will be discussed in the following sections

5.2.1 Pressure fluctuations caused by temporal variations in the average gas void fraction

5.2.2 Pressure fluctuations caused by variations in the continuous phase velocity profile around a near spherical bubble

5.2.3 Pressure fluctuations in the continuous phase caused by the continuous phase background turbulence and the wake generated by a bubble

The contribution that each of these effects has to the overall fluctuations in differential pressures are investigated using simple models developed in each section and estimates of their relative importance are made.

5.2.1 Pressure fluctuations caused by temporal variations in the average gas void fraction

Consider a length of pipe of diameter D containing a liquid in which spherical bubbles of constant diameter d are dispersed randomly and uncorrelated with one another as shown in figure 5.9. In any measurement volume, which we will defined as a slice through the pipe of thickness l, the average number of bubbles per unit length will be termed m. The variation in the average number of bubbles per unit length in each small interval is directly proportional to the variation in average gas void fraction α, if incompressibility is

assumed. The variation in α leads to a variation in the mixture density ρ_m (defined by equation 4.1) which can be used to calculate the corresponding magnitude of pressure fluctuations. In this way, knowledge of the variation in m allows the magnitude of the pressure fluctuations caused by this effect to be predicted.

Due to the assumption of randomness in discrete bubble positions within the pipe, the variation in the average number of bubbles per unit length is one of assessing the r.m.s. error in an estimate of the probability density distribution of a random signal with a uniform probability density distribution. Consider the problem of estimating the probability density of a uniform distribution in the range from 0 to 1 as shown in figure 5.10. If a total of N samples are taken and an estimate is made of the probability density in an interval of width w, it is a well known standard result (see *Bajpai* et al [1978]) that the r.m.s. error in the density estimate is given by

$$\epsilon = \frac{1}{\sqrt{N\,w}} \qquad 5.23$$

Bradbury [1988] states that the r.m.s. error in a sample from the total number of samples N is given by

$$\epsilon = \frac{\Delta n}{N\;w} \qquad 5.24$$

where Δn is r.m.s. error of samples within a slot of width w from the average value within any slot of width w (see figure 5.10). Combining equations 5.23 and 5.24 gives

$$\Delta n = \sqrt{N\ w} \qquad 5.25$$

Returning to the case of bubbly flow and applying the result above, consider a very long length of pipe L with m bubbles per unit length. In equation 5.25 N can be substituted by

$$N = m\ L \qquad 5.26$$

and the interval w by

$$w = \frac{l}{L} \qquad 5.27$$

then we obtain an expression for predicting the r.m.s. error Δn in a large number of samples N, which in this case represents the variation in the average number of bubbles contained within a small interval of length l in a much longer length L as shown in figure 5.9.

$$\Delta n = \sqrt{m\ l} \qquad 5.28$$

Equation 5.28 can now be used as the basis of a model in which we can predict the magnitude of fluctuations in pressure due to the variations in the average gas void fraction α. For the case shown in figure 5.9, the average gas void fraction α in a slice through the pipe of thickness l is given by

$$\alpha = \frac{\text{bubble volume}}{\text{total volume}} = \frac{\frac{\pi\ d^3}{6}\ m\ l}{\frac{\pi\ D^2}{4}\ l}$$

$$\alpha = \frac{2\ d^3\ m}{3\ D^2} \qquad 5.29$$

The r.m.s. fluctuation in the average gas void fraction, α', in the measurement slice of length l is then given by

$$\alpha' = \frac{\frac{\pi\ d^3}{6}\ \Delta n}{\frac{\pi\ D^2}{4}\ l}$$

Using equations 5.26 and 5.28 we get

$$\alpha' = \sqrt{\frac{2\ \alpha\ d^3}{3\ l\ D^2}} \qquad 5.30$$

As shown by *Bradbury* [1988] the corresponding r.m.s. fluctuation in the hydrostatic pressure, $\Delta P'$, for a low average gas void fraction bubbly two-phase flow due to average bubble number fluctuations will therefore be of the order of $\alpha' \rho_l g l$ or

$$\Delta P' = \frac{\frac{\pi\ d^3}{6}\ \Delta n\ \rho_l\ g}{\frac{\pi\ D^2}{4}}$$

$$\Delta P' = \rho_l\ g \sqrt{\frac{2\ \alpha\ l\ d^3}{3\ D^2}} \qquad 5.31$$

From equation 5.31 it would appear that the r.m.s. fluctuations in pressure will increase without limit as the slice thickness l increases. However, it should be noted that the average hydrostatic pressure ΔP_h is given by

$$\Delta P_h = \rho_m \, g \, l \qquad 5.32$$

which, if we assume the density of air to be negligible when compared to the density of water, the mixture density can be approximated to $\rho_l(1 - \alpha)$ and thus equation 5.32 becomes

$$\Delta P_h = \rho_l(1 - \alpha) \, g \, l \qquad 5.33$$

Combining equations 5.31 and 5.33 then gives us

$$\frac{\Delta P'}{\Delta P_h} = \frac{1}{(1 - \alpha)} \sqrt{\frac{2 \, \alpha \, d^3}{3 \, l \, D^2}} \qquad 5.34$$

Using equation 5.31, figure 5.11 shows how the magnitude of the r.m.s. pressure fluctuation $\Delta P'$ (evaluated in mm H_2O) is expected to vary with increasing average gas void fraction α and the measurement slice thickness l (see figure 5.9). Figure 5.12 shows, however, that the ratio of $\Delta P'/\Delta P_h$ will decrease with increasing average gas void fraction and the measurement slice thickness. From figure 5.12 it can be seen that for a measurement slice thickness l of 25mm an acceptable ratio of fluctuating to average pressure, $\Delta P'/\Delta P_h$, is achieved over the range of average gas void fractions considered in the present study ($\alpha \simeq 5 - 20\%$).

It should be noted that in practice the measurement slice thickness will be the separation distance between two pressure tappings 1 and 2. It should also be noted that the model derived in this section neglects the possibility of random bubble positions overlapping with one another and is therefore only valid for low average gas void fractions where the diameter of the spherical bubbles are much smaller than the diameter of the pipe i.e. $d/D \ll 1$.

It will be shown in section 5.2.2 that the magnitude of pressure fluctuations caused by the temporal variations in the average gas void fraction are small compared to pressure fluctuations generated by a bubble's motion. Consequently the length scale of structures in the flow associated with the temporal variations in the average gas void fractions will have little effect on the measured autocorrelation length scale of a bubbly two-phase flow.

5.2.2 Pressure fluctuations caused by variations in the continuous phase velocity profile around a near spherical bubble

To estimate the amplitude of pressure waves created by a bubble's motion as it disturbs the continuous phase it is flowing through, consider the problem where the continuous phase is stagnant and bubbles rise through the continuous phase with a constant velocity V_∞. As discussed in section 5.1.1, a near spherical air bubble in a continuous water phase tend to act like a solid sphere due to the collection of contaminates at the interface (see *Peebles & Garber* [1953]). However, it has been observed in this study that the bubbles are ellipsoidal in shape, nevertheless it is not unreasonable to treat a discrete bubble, in this case, as a solid sphere of diameter d so that calculations may be made to estimate the amplitude of the pressure fluctuation caused by a bubble's motion.

Using this comparison, *Butler's* [1953] sphere theorem (see, for example, *Milne-Thomson* [1960]) for a stationary sphere in an infinite fluid having a uniform velocity can be translated to describe a sphere travelling at a constant velocity through a stationary fluid. Using *Butler's* sphere theorem in this form the pressure field surrounding a

moving bubble can be calculated and hence the amplitude of the pressure fluctuation caused by a bubble's motion can be estimated.

Consider the motion of a solid sphere of radius a and travelling at a velocity V_∞ in a stationary infinitely large incompressible inviscid fluid, as shown in figure 5.13. If we assume the flow of the fluid displaced by the sphere to be both axisymmetric and irrotational about the axis of the spheres motion, then *Butler's* sphere theorem gives the velocity potential Φ for this case as

$$\Phi = V_\infty \left[r + \frac{a^3}{2\ r^2} \right] \cos\theta \qquad 5.35$$

where θ is the angle between the axis of bubble motion, in the direction of bubble motion, and a point n in the infinite fluid at a distance r from the centre of the sphere. Using this result provided by *Butler* for the velocity potential Φ for the flow surrounding a moving sphere, the amplitude of a differential pressure measured between two fixed points in an infinite fluid is derived below.

Using spherical polar co-ordinates, the r and θ velocity components are given by

$$V_r = -\frac{\partial\Phi}{\partial r} = -V_\infty \left[1 - \frac{a^3}{r^3} \right] \cos\theta \qquad 5.36$$

$$V_\theta = -\frac{1}{r}\frac{\partial\Phi}{\partial\theta} = -\frac{V_\infty}{r} \left[r + \frac{a^3}{2\ r^2} \right] \sin\theta \qquad 5.37$$

and if we assume the velocity field surrounding the sphere to be symmetrical about the axis of motion

$$V_\psi = -\frac{1}{\sin\theta}\frac{\partial\Phi}{\partial\psi} = 0 \qquad 5.38$$

The magnitude of the velocity vector is defined by

$$\underline{V}^2 = V_r^2 + V_\theta^2 + V_\psi^2 \qquad 5.39$$

and so

$$\underline{V}^2 = V_\infty^2\left[1 + \frac{a^3}{r^3}\left[1 - 3\cos^2\theta\right] + \frac{a^6}{4\,r^6}\left[1 + 3\cos^2\theta\right]\right] \qquad 5.40$$

The pressure P and magnitude of velocity V at any point can be related to the pressure at infinity (where V=0) by Bernoulli's equation

$$P = P_0 - \frac{1}{2}\rho_l\,\underline{V}^2 \qquad 4.41$$

where P_0 is the pressure at infinity. Therefore

$$P = P_0 - \frac{1}{2}\rho_l V_\infty^2\left[1 + \frac{a^3}{r^3}\left[1-3\cos^2\theta\right] + \frac{a^6}{4\,r^6}\left[1+3\cos^2\theta\right]\right] \qquad 5.42$$

The velocity potential between any point on the sphere's surface and any point in the infinite fluid can be shown to be a maximum on a plane perpendicular to the axis of bubble motion ($\theta = 90^0$) passing through the centre of the sphere. Therefore, by setting $\theta = 90^0$ in equation 5.42 we obtain a solution for the peak pressure P_{peak} seen by any fixed point in the infinite fluid on a plane perpendicular to the axis of flow at a distance r from the centre of the sphere.

$$P_{peak} = (P - P_0) = -\frac{1}{2}\rho_l V_\infty^2\left[\left[1 + \frac{a^3}{2\,R^3}\right]^2 - 1\right] \qquad 5.43$$

where R is the perpendicular distance, with respect to the sphere trajectory, from the centre of the sphere to the fixed measuring point.

For a sphere of radius a = 3mm, travelling at a constant velocity V_∞ = 0.250m/s in water (ρ = 1000kg/m^3), figure 5.14 shows how the magnitude of peak pressure P_{peak} (evaluated in mm H_2O) due to this effect is expected to vary as a function of the perpendicular distance R from the centre of the sphere's trajectory to the measuring point in an infinite fluid. Using the analogy derived above to describe the motion of a bubble travelling at a constant velocity, figure 5.14 clearly shows that any pressure fluctuation caused by a bubble's motion will diminish rapidly with increasing bubble to measuring point perpendicular separation distance. It should be noted at this time that equation 5.43 is for a sphere travelling through an infinite fluid and therefore does not allow for the effect of a pipe wall.

For two fixed points, 1 and 2, in the fluid the theoretical differential pressure ΔP between these two points caused by the bubble's motion is given by

$$\Delta P = P_1 - P_2 \qquad 5.44$$

It is assumed that the sphere is travelling at a constant velocity V_∞ along a fixed trajectory which is at a constant perpendicular distance R from the two points 1 and 2, and 1 and 2 are separated by a distance l which is parallel to the trajectory of the sphere. Assuming the pressure field to be irrotational, as shown in figure 5.15, then by substituting equation 5.42 into equation 5.44 for the pressures P_1 and P_2 we obtain

$$\Delta P = \frac{1}{2}\rho_l V_\infty^2 \left[\left[1+\frac{a^3}{r_2^3}\left[1-3\cos^2\theta_2 \right] + \frac{a^6}{4r_2^6}\left[1+3\cos^2\theta_2 \right] \right] \right.$$

$$\left. - \left[1+\frac{a^3}{r_1^3}\left[1-3\cos^2\theta_1 \right] + \frac{a^6}{4r_1^6}\left[1+3\cos^2\theta_1 \right] \right] \right] \qquad 5.45$$

where $r_1 = R/\sin\theta_1$ and $r_2 = ((r_1\cos\theta_1+l)^2 + R^2)^{\frac{1}{2}}$ 5.46

where the angles θ_1 and θ_2 are the angles between the points 1 and 2 and the centre of the sphere along its trajectory respectively.

It is instructive to look at the calculated pressures $P_1(t)$ and $P_2(t)$ and the differential pressure $\Delta P(t) = P_1(t) - P_2(t)$ as a sphere travels past the pressure tappings 1 and 2. This is illustrated in figure 5.16 for a sphere of radius a = 3mm travelling past point 1 and 2 with a perpendicular distance R = 4.5mm. The time t = 0 corresponds to the sphere being directly opposite tapping number 1. The normalised pressures $P_1(t)/\frac{1}{2}\rho_l V_\infty^2$, $P_2(t)/\frac{1}{2}\rho_l V_\infty^2$ and $(P_1(t)-P_2(t))/\frac{1}{2}\rho_l V_\infty^2$ are shown in curves a, b and c of figure 5.16 respectively. To facilitate the interpretation of the correlation method described in chapter 6, the autocorrelation function for the differential pressure $P_1(t) - P_2(t)$ is included in curve d of figure 5.16. For a sphere moving at a constant velocity, V_∞, the translation between the temporal t and spacial z coordinates is

$$V_\infty = \frac{z}{t} \qquad 5.47$$

In this equation it is assumed that z = 0 at tapping 1 and t = 0 when the sphere is opposite tapping 1.

From the autocorrelation plot, curve d of figure 5.16, a clear negative peak 'c' can be identified corresponding to the time τ, which

can be used to evaluate the sphere velocity V_∞ as

$$V_\infty = \frac{l}{\tau} \qquad 5.48$$

where l is the axial spacing between tappings 1 and 2. In a practical experiment the additional peaks a, b and d will be smoothed out due to fluctuations in bubble velocities and deviations in the bubble paths, consequently these peaks will not be used for any data correlation.

For a sphere of radius a = 3mm, the resulting set of curves corresponding to equation 5.45 for discrete values of R and as a function of l have been plotted in figure 5.17. The two fixed measuring points 1 and 2 are located at 0 and 1 pressure tapping intervals respectively and the sphere is travelling in the direction from measuring point 1 to 2. The fluctuations in differential pressures ΔP have been normalised in the following way

$$\text{Normalised pressure} = \frac{\text{measured or predicted differential pressure}}{\frac{1}{2}\rho_l \left[\text{bubble, bead, or sphere velocity}\right]^2} \qquad 5.49$$

It can be clearly seen from figure 5.17 that the pressure wave created by a moving sphere observed by the differential pressure $\Delta P = P_1 - P_2$, is an inversely symmetrical curve about a point mid way between the measuring points 1 and 2, at $l/2$, or 0.5 tapping intervals. The amplitude of the differential pressure ΔP can be seen to decrease as R, the perpendicular distance between the sphere's centreline trajectory and the measurement points 1 and 2, increases.

It can seen from figure 5.14 that the predicted maximum

amplitude of this source of pressure fluctuation can be up to 10 times larger than predicted in section 5.2.1 from the variations in the average gas void fraction (see figure 5.11). It is also observed from figure 5.17 that the maximum amplitude of the pressure wave occurs when one of the two fixed measurement points, 1 or 2, is perpendicularly opposite the centre of the sphere with respect to the sphere's trajectory. The existence of this convective pressure wave will be utilised in the auto and cross correlation results discussed in detail within chapter 6.

The above results have clearly indicated that bubbles close to the pressure tappings will dominate the pressure signal, since the magnitude of pressure fluctuations caused by the motion of a bubble decreases as the perpendicular distance R increases. If many bubbles traveling along fixed parallel trajectories at different values of R, then it is expected that the autocorrelation signal of the differential pressure ΔP measured at two fixed points 1 and 2 will be dominated by the pressure fluctuations of spheres associated with small values of R.

The simple model developed above is for the motion of a solid sphere in an infinite fluid, and from the arguments put forward in section 5.1.1, a bubble is expected to exhibit similar properties to that of a solid sphere and therefore the predictions made in this section are thought to be valid for the motion of a single bubble. However, the influence of the test section's pipe wall will be to modify the amplitude of pressure signal and reduce the velocity of bubbles close to the wall. the autocorrelation technique illustrated in curve d of figure 5.16 may be used to evaluate the corresponding bubble velocity as described in chapter 6.

5.2.3 Pressure fluctuations in the continuous phase caused by the continuous phase background turbulence and the wake generated by a bubble

In fully developed turbulent single phase flow within a pipe, which has been shown to exist in section 4.2.1 for water in the experimental test section, there will be fluctuations in the velocity of the fluid measured at any point caused by the turbulent motion of the flow. The ratio of the fluctuations in velocity to the area averaged velocity of the fluid is often used as a measure of the magnitude of turbulence in the flow, this is known as the turbulent intensity and will be of the order of 0.01 for a fully developed single phase turbulent pipe flow (see, for example, *Ward-Smith* [1980]). However this could not be measured in the experimental flow loop with the equipment available. The turbulent intensity of the continuous phase in a bubbly two-phase flow however will also be affected by the wake generated behind a bubble as it travels through the continuous phase.

Consider a bubble of diameter d moving with a constant slip or terminal bubble velocity $V_{g\infty}$ through a continuous phase which is also flowing in the same direction with a uniform velocity V_l. A wake will be generated in the continuous phase behind the bubble caused by the shedding of vortices as the boundary layer separates from the rear of the bubble. This will add to some extent to the turbulent intensity of the continuous phase flow and is termed the 'excess turbulent intensity' by *Lance & Bataille* [1991]. *Lance & Bataille* report that *Moore* [1963] suggested that for a pure liquid the wake is thin and can be neglected in a first approximation. However in the case of tap water, surface contaminants at the air/water interface of a bubble

cause separation of the flow at the bubble wall and the turbulent kinetic energy is significantly increased.

Lance & *Bataille* found that the turbulent kinetic energy in the continuous phase increases strongly with increasing average gas void fraction and that, broadly speaking, there exist two distinct regimes in which the magnitude of the turbulent kinetic energy of the continuous phase varies. The first is at low average gas void fractions where α is less than 1% and the hydrodynamic interaction between bubbles is negligible. In this case the turbulent kinetic energy in the continuous phase of such a two-phase flow is simply the sum of the single phase turbulent kinetic energy and the kinetic energy associated with the motion of a cloud of non-interactive bubbles. The latter's contribution can be correctly evaluated using the inviscid potential flow model for oblate spheroidal bubbles in spiralling motions (see *Lamb* [1932] and *Saffman* [1956]). *Lance* and *Bataille* found that the second regime occurs at critical average gas void fractions α_c of the order of 1%. In this case the turbulence in the continuous phase is strongly amplified by the hydrodynamic interaction between bubbles.

Lance and *Bataille* using Laser Doppler Anemometry (LDA) performed experiments in an air/water two-phase flow loop which had a square cross-sectioned experimental test section. Single phase turbulence was generated in the continuous phase by a 40mm grid upstream of the air injectors and area averaged liquid velocities V_l ranged from 0 - 1.2m/s. Bubble diameters of up to 5mm were recorded with average gas void fractions of less than 3%. Figure 5.18 produced by *Lance* & *Bataille* shows how the turbulent intensity varies as a function of the area averaged liquid velocity and the average gas void

fraction α. The results were taken at a distance of 1.456m down-stream of the 40mm grid used to generate the single phase turbulence, at which point the flow was considered to be almost fully developed. It can be clearly seen from figure 5.18 that for water only (α = 0) the turbulent intensity is almost constant over the range of area averaged liquid velocities used in their study (0.3 - 1.2m/s). The value of the grid-generated turbulent intensity is of the order of 0.017 which, as expected, is higher than for a circular cross-sectioned pipe without a grid.

Figure 5.18 also shows the measured continuous phase turbulent intensity for average gas void fractions α up to 3% in increments of 0.5%. The increase in turbulent intensity for each increment in average gas void fraction α appears very uniform in each of the two kinetic energy regimes described by *Lance* and *Bataille*. In the experiments performed in this thesis, average gas void fractions will always be higher than the critical average gas void fraction α_c quoted by *Lance* & *Bataille*, therefore the magnitude of the continuous phase turbulent kinetic energies in the present study will fall into the second more turbulent higher average gas void fraction regime defined by *Lance* and *Bataille*. Although *Lance* and *Bataille's* experiments have average gas void fractions of less than 3%, from the uniformity of the results plotted in figure 5.18 for the higher void fraction regime it would not be unreasonable to assume that, if experiments had been performed for higher average gas void fractions within the bubbly flow regime, a similar trend would have been observed. Unfortunately the use of LDA in bubbly two-phase flow is not practical at higher average gas void fractions since the number of bubbles present in the flow does not allow the laser to penetrate into the flow. Assuming the turbulent intensity increases in a similar manner, then the turbulent

intensity of a bubbly two-phase flow with average gas void fractions in the range of 5 - 20% would be expected to be of the order of 0.1 to 0.4. However, *Lance* and *Bataille* suggest that the excess turbulence generated by the bubbles is a function of the single phase turbulence in the higher void fraction regime. Therefore, in the case of a circular cross-sectioned pipe without a grid to generate turbulence in the continuous phase, the excess turbulence generated by the bubbles would be expected to be less than 0.1 to 0.4 predicted from the work of *Lance* and *Bataille*. Hence the turbulent intensity measured in such a two-phase flow would be much lower than that measured in similar experiments with higher initial single phase turbulence levels.

In order to estimate the relative magnitude of pressure fluctuations generated by turbulent fluctuations in the area averaged liquid velocity caused by the combined single phase turbulence and the turbulence caused by the wake behind a bubble, consider the worst case of a low area average liquid velocity of, say, 0.25m/s with a high average gas void fraction of, say, 15 - 20%. Then by extrapolating the results of *Lance* and *Bataille* [1991] the turbulent intensity for such a two-phase flow is expected to be of the order of 0.4. The r.m.s. amplitude of pressure fluctuations $\Delta P'$ would therefore be of the order $\Delta P' = \frac{1}{2} \rho_l (0.4 V_l)^2 = 5$ N/m^2 or 0.51mm H_2O, whereas from section 5.2.1 and 5.2.2 the predicted r.m.s. amplitude of pressure fluctuations caused by temporal variations in the average gas void fraction will be of the order of 0.2 - 0.3mm H_2O and the predicted peak magnitude of pressure fluctuations generated by the motion of a single bubble will be of the order of 2 - 3mm H_2O.

The autocorrelation length scale of the turbulent structures in a two-phase flow can be broken down into the single/continuous phase

turbulent structure and the turbulent structure generated by a bubble's wake. Turbulent structures in the single/continuous phase may range up to several pipe diameters in length depending of flow conditions such as Reynolds number, surface friction factors and entry length. However, the magnitude of the pressure fluctuations associated with the single/continuous phase is expected to be small compared to other sources of pressure fluctuations and therefore the contribution of this effect to the autocorrelation correlogram is also expected to be small.

If we assume the bubble to be a solid sphere then the wake generated by a solid sphere in the continuous phase will be of the form of a series of vortex rings (see, for example, *Douglas et al* [1979]). A vortex ring forms for a sphere when the Reynolds number is approximately greater than 10 and becomes unstable at $200 < Re < 2000$ when it tends to separate from the sphere and is immediately replaced by a new ring. However, unlike a circular cylinder, this process is not periodic and therefore the length scale of these structures will not be constant. Experiments by *Lance* and *Bataille* [1991] found the fluctuations in the bubble wakes become decorrelated within a spacial distance of 0.8d, which for a bubble diameter of say 6mm equates to approximately 4.8mm. An autocorrelation length scale of the order of 0.8d is relatively short when compared with the selected distance l = 25mm between the two pressure tappings, the corresponding measured differential pressure is therefore dominated by the convected pressure field associated with the bubble motion. However, in the cross correlation measurements made in the present study the transducer separation distance is only 6mm and therefore, cross correlation correlograms may be affected by shorter structure lengths in the flow, this will be discussed further in chapter 6.

From the arguments put forward in this section, which have been based largely on the work of *Lance* and *Bataille* [1991], the estimated magnitude of pressure fluctuations caused by turbulence in the continuous phase of a bubbly two-phase flow is expected to be small. The autocorrelation length scale is also shorter than those associated with the other two sources of pressure fluctuations. The short autocorrelation length scale combined with the small magnitude of predicted pressure fluctuations associated with this source of pressure fluctuation therefore leads to this effect being neglected in subsequent calculations within this thesis.

5.3 Development of measurement techniques used to measure differential pressures

Two basic techniques were investigated for the measurement of differential pressure fluctuations between two tappings in the wall of a vertical pipe separated by an axial distance l.

5.3.1 Differential pressure measurements obtained by subtracting two static pressure signals

Matsui [1984] used four piezoresistive pressure transducers with a response frequency of 600 Hz to measure the static pressures at four wall locations. These signals were subsequently subtracted to obtain differential pressure signals, which were used to study the statistical properties of differential pressure fluctuations in vertical two-phase flow. The static pressure signal from each transducer was first amplified using DC amplifiers and then passed

through 10 Hz low-pass filters. The conditioned signals were sampled using a 12 bit A/D converter and stored in the memory of a digital computer. The A/D converter had a conversion time of 15 μs with a sampling interval of 10 ms. The differential pressure signals were obtained by taking the difference between two of the digital static pressure signals thus removing the common reference component of the signals and hence leaving only the differential pressure fluctuations.

This technique was investigated in the present study using two Endvco piezoresistive pressure transducers with a range of ±2 psi and a response frequency of 70 KHz, which were mounted as near flush as possible with the inside wall of the test section without penetrating into the flow, at a separation distance l = 25mm, as shown in figure 5.19. Each transducer is internally electrically connected to form a four active arm Wheatstone bridge circuit. Each transducer is then connected to its own instrument amplifier as shown in figure 5.19. The transducers were calibrated using a deadweight tester to give a full range output of 10 volts for a maximum pressure of 2 psi.

The outputs from the instrument amplifiers were sampled by an A/D converter with a conversion time of 25 μs, with a sampling interval of 100 μs. These two static pressure signals were subtracted digitally to eliminate the common mode component of the signals leaving only the fluctuating component of the differential pressure signal. Unfortunately, it was found that although this method of measuring differential pressure fluctuations is very simple, implementation of the technique has a number of major drawbacks.

(i) Electrical noise proved to be a very significant problem. This was due partially to the thyristor controller (see section 3.3.2) used

to control the speed of the centrifugal water pump. Shielding of cables and components resulted in a slight improvement but the signals from the transducers were swamped by the noise at low average gas void fractions. Fortunately however, as the noise source was common to both signals, when the pressure signals were subtracted the noise was significantly reduced.

(ii) Any variation in the calibration of the transducers and amplifier assembly will cause a zero shift of the differential pressure signal. This will also cause errors in the magnitude of the pressure fluctuations. However, the r.m.s. values of the two static signals should be equal if measured over a suitably long period of time due to the fact that the transducers are being subjected to the same sources of pressure separated by a small axial distance which results in a short time delay between the signals. To minimise any calibration errors, the two static pressure signals were scaled to make the r.m.s. values of each signal equal prior to subtraction. However, using this technique the true values of differential pressure measurements are suspect due to the scaling factors involved.

(iii) It was also found that both the transducers and signal processing equipment had slightly different response characteristics. The effect of this is discussed in more detail in chapter 6 but briefly the result is a filtering out of some of the higher frequency components on one of the two static pressure signals. Therefore, when the signals are subtracted, a high frequency ripple appears on the differential pressure signal giving false results. This was overcome to some extent by low-pass filtering each of the signals. The low-pass filtering can be achieved by using carefully matched analogue filters, but in the present study it was decided to use a digital

filter programmed into the computer and to carry out the filtering prior to subtracting the two static pressure signals.

(iv) One advantage of using physically small pressure transducers such as these, with very low displacement volumes, is that they are relatively insensitive to vibration of the apparatus. However, they are subject to pressure pulses present in the flow generated for instance by the centrifugal water pump.

After extensive trials using the two Endevco pressure transducers in the experimental test section of the flow loop, it was decided to investigate the direct measurement of the differential pressure signals using a single differential pressure transducer. Then, by comparing the advantages and disadvantages of each technique an informed decision could be made as to the most suitable transducer configuration for the application under investigation.

5.3.2 Measurement of differential pressure fluctuations using a single differential pressure transducer

In this technique two tappings, a short axial distance *l* apart, are connected to two identical chambers which are separated by a thin diaphragm, as shown in figure 5.20. Any change in pressure on either side of the diaphragm that is not common to both will cause the diaphragm to be displaced. Over the operational range of the transducer, the displacement will be linearly proportional to the differential pressure between the two tappings.

Validyne Engineering Corporation manufacture a range of variable

reluctance differential pressure transducers of a very robust nature. These can measure differential pressures in the range of ±2.22 inches of H_2O to ±220 Bar depending upon the diaphragm fitted to the transducer. A single Validyne DP15 differential pressure transducer with a number 22 diaphragm, which has a range of ±5.5 inches of H_2O, was initially connected, using nylon pipes, to two tappings in the test section separated by an axial distance l = 25mm. The diaphragm of the transducer was positioned in the vertical plane as shown in figure 5.20, in order to eliminate any gravitational effects.

For use in water flows it is necessary to bleed the air from the transducer and the associated pressure lines. This proved to be very difficult due to the internal design of the transducer pressure chambers, which it is thought were designed for gases. Nevertheless, after considering the problem of eliminating air traps in the design of the transducer, the transducer chambers were modified by elongating the bleed holes to allow any air to be bled from the transducer without having to tilt or move the transducer in any way.

Unfortunately, it was found that any vibration of the nylon pressure lines resulted in the fluid contained within these pipes being displaced, thus causing inertia forces to act on the diaphragm. The inertia forces of the water in the pressure lines generated far greater differential pressure fluctuations than those caused by the bubbles. To reduce the magnitude of this effect the nylon pressure lines were replaced by much stiffer pressure lines manufactured from copper. This reduced the magnitude of the noise fluctuations but not sufficiently to make this transducer arrangement a satisfactory one.

As a result of these findings it was decided to manufacture a

more substantial transducer mounting facility from aluminium alloy containing the pressure lines from the test section to the differential pressure transducer. The aluminium housing, which was fitted between two flanges in the test section, allows for rigid mounting of the differential pressure transducer and pressure lines to the experimental test section, as shown in the photograph in figure 5.21. The design and construction of the differential pressure transducer housing are described in detail in section 5.3.3. As the differential pressure transducer was now rigidly mounted, any vibrations will be common to both sides of the transducer diaphragm and hence cancel each other out. Therefore, differential pressure fluctuations caused by the bubbles in the test section can be measured without being swamped by high levels of noise.

The transducer measures the change in displacement of the diaphragm inductively. Validyne engineering manufacture a 'carrier demodulation amplifier' specifically for use in conjunction with their range of pressure transducers. The combined pressure transducer and amplifier fitted with a number 22 diaphragm was initially zeroed and statically calibrated to give a voltage output of ±10 volts for a static pressure of ±5.5 inches of H_2O.

By experiment, using the impact hammer of a Bruel & Kjaer model 2034 dual channel analogue signal analyser to excite the transducer housing and transducer in situ in the experimental test section and connecting the output from the transducer amplifier into the frequency analyser, it was found that a Validyne pressure transducer and housing had a frequency response of the order of 400 Hz. This is much lower than the Endevco pressure transducers. However, *Matsui* [1984] and others have found that the frequency spectrum, of a pressure signal

from a bubbly two-phase flow with superficial gas and liquid velocities in the range covered in the present study, contains little energy at frequencies higher than 100 Hz.

After some initial trials, this technique proved to be successful in detecting differential pressure fluctuations in a bubbly two-phase flow over a wide range of average gas void fractions. However, two disadvantages of this technique are:

(i) Due largely to the transducer having a relatively large flexible diaphragm of approximately 30 mm in diameter, the transducer is very susceptible to vibration forces from both external movements as well as pressure pulses. This being the case, great care needs to be exercised when orientating the transducer so as to minimise the effect of vibrations including those in the flow loop.

(ii) Purging of the transducer with water, and thus bleeding the air from the pressure lines and chambers, proved to be difficult. Fortunately, with careful redesign, this was successfully achieved by a combination of back flushing and bleeding along angled pressure lines.

Nevertheless, when steps are taken to minimise these drawbacks this technique provided a stable and repeatable differential pressure signal which could easily be interfaced to signal analysers and computers without the need for additional complex electronics and computer analysis of the raw data as was needed with the subtraction method described in section 5.3.1.

After considering the advantages and disadvantages of both

methods, it was decided that the most suitable technique for use in this application would be the method described in this section. Therefore, the fluctuations in differential pressures in the present study were measured using a Validyne DP15 differential pressure transducer fitted with a number 22 diaphragm.

5.3.3 Design and construction of a housing for mounting the differential pressure transducer

To minimise the problem of vibration discussed in section 5.3.2, a special housing was designed and manufactured from aluminium alloy. This contained not only the pressure lines from the wall tappings to the differential pressure transducer but also acted as a rigid mounting for the pressure transducer, as can be seen in figure 5.22. The housing was designed to be robust, in order to eliminate independent vibration of components, and to facilitate the bleeding of air from the system. As discussed earlier, vibration of the pressure lines caused pressure fluctuations due to the inertia of the water in these lines displacing the transducer diaphragm. By incorporating the pressure lines into a solid body, any vibration will be common to both sides of the transducer diaphragm and so, to a large extent, will cancel out.

Air, being a compressible fluid, acts like a spring when subjected to pressure pulses. This results in magnification and frequency phase changes in the fluctuating pressure signals, which give rise to corresponding changes in the frequency spectrum of the signals. It is therefore essential to eliminate all the air from the measurement system. To facilitate the bleeding of air from the

transducer and the associated pressure lines, all pressure lines have been reamed to make them smooth and machined at an angle to allow the air to bleed out naturally. Screw threads in pressure line fittings can also trap air, therefore all bleed ports have been sealed using blanking plates rather than screw plugs. It was also found that back flushing of the transducer, as shown in figure 5.23, with mains water aided air elimination.

The internal bore of the transducer housing is the same as the bore of the test section (77.8 mm) and it was designed to fit between two flanges. The housing was positioned approximately 0.6m down-stream from the contraction in approximately the middle of the experimental test section. Two axially in-line pressure tappings 1mm in diameter are separated by a distance l of 25mm. This distance was chosen for two reasons. Firstly the predicted $\Delta P'/\Delta P_h$ ratio for l = 25mm is reasonably constant (see section 5.2.1) over the range of average gas void fractions α considered in the present experimental study (approximately 5 - 20%). Secondly, size limitations, cost, availability of material and manufacturing difficulties associated with the machining of small smooth bore holes (for the pressure lines) in the aluminium alloy housing lead to a tapping separation distance l of 25mm being chosen.

5.4 Comparison of theoretical and experimental pressure fluctuations

Two experiments were designed to make comparisons between theoretical differential pressure fluctuations, derived from *Butlers* sphere theorem in section 5.2.2, and measured differential pressure fluctuations. Differential pressure fluctuations were measured and

calculated first for a sphere moving at constant velocity through a stagnant column of liquid in a pipe and, secondly, for a single stream of bubbles also in stagnant column of water. From the results of these experiments, conclusions were drawn about the validity of modelling the bubbles as solid spheres.

5.4.1 Experimental differential pressure fluctuations caused by a moving sphere in a pipe containing stagnant water

A 6.5mm diameter bead was attached to a thin nylon cord and strung between two pulleys as shown in figure 5.24. Attached to this nylon cord loop was a second nylon cord which was wound around a pulley fixed to a stepper motor. The bead was strung tightly between the two fixed pulleys and could therefore only move along the fixed path at constant velocity. Knowing the diameter of the pulley fitted to the stepper motor, the frequency of the stepper motor corresponding to various constant bead velocities could be calculated.

The 'bead' apparatus described above was positioned in a short section of transparent pipe similar to that used in the test section of the flow loop. The transducer housing (section 5.3.3) with a single Validyne differential pressure transducer attached, used to measure differential pressure fluctuations in the experimental test section, was also positioned in this section of pipe, as shown in the photograph, figure 5.25.

The combined short test section was set up and the air bled from the differential pressure transducer. The required stepper motor frequencies were calculated to drive the bead at constant velocities

of 0.1, 0.25, and 0.4 m/s. The output from the differential pressure transducer amplifier was connected to a Bruel & Kjaer model 2034 dual channel analogue signal analyser. A computer programme was written to interface the the output from the Bruel & Kjaer's IEEE488 parallel port with a similar port on an IBM compatible computer. This computer link was used to store measured data from the signal analyser on to computer discs for further analysis.

Differential pressure fluctuations were measured for wall to bead centre separations ranging from 4.5 - 25.5mm at the three constant bead velocities of 0.1, 0.25, and 0.4m/s. A typical measured differential pressure signal, which has been normalised using equation 5.49, is shown in figure 5.26, for a wall to bead centre distance of 4.5mm, at a constant bead velocity of 0.25m/s. Also plotted on figure 5.26 is the predicted shape of the pressure wave caused by the motion of a sphere derived from *Butler's* sphere theorem in section 5.2.2, equation 5.45. The differential pressure signal ΔP predicted by equation 5.45 has also been normalised using equation 5.49 and the conditions used in equation 5.45 are the same as those for the constant velocity bead i.e. pipe wall to sphere centre separation distance R = 4.5mm, sphere velocity V_∞ = 0.25m/s, the distance between the two fixed measuring points, l = 25mm and a sphere radius a = d/2, where d = 6.5mm. It is noticed that for this condition the maximum amplitude of the measured and calculated pressure fluctuations are similar. It should be noted that variations between the calculated and measured pressure signals may be due to the influence of the pipe wall on the measured signal which is not accounted for in the theoretical calculations. Although the measured differential pressure wave from the constant velocity bead experiment is not as well defined and generally the peaks are broader than the calculated pressure wave,

the peak pressures occur at the same time (or space) location. This confirms the ability of the correlation technique to evaluate bubble velocities.

In section 5.2.3 it was predicted that the wake generated by a sphere will be small, comparing the noise levels on the measured signal before the bead reaches the pressure transducer, with the magnitude of the signal after the bead has passed the pressure transducer in figure 5.26, in which time increases from left to right, there would appear to be very little difference. This, to some extent, indicates that as predicted in section 5.2.3 the effect of the wake is almost negligible when compared to the magnitude of pressure fluctuations generated by the convected pressure field surrounding a moving sphere.

Figure 5.27 shows the measured peak differential pressures, normalised using equation 5.49, plotted as a function of the ratio between the pipe wall to bead centre separation distance over the bead radius, R/a, for three constant bead velocities 0.1, 0.25 and 0.4 m/s. Although showing some experimental scatter when the bead is close to the pipe wall, the normalised differential pressures can be seen to have the same basic trend with magnitudes which are dependent on the bead's velocity and the pipe wall to bead centre separation distance. It can also be clearly seen that as predicted by the theoretical calculations in section 5.2.2, the contribution to fluctuations in differential pressure from a bead/bubble diminishes rapidly with increasing pipe wall to bead/bubble centre separation distance. If we assume a terminal bubble rise velocity of the order of 0.25m/s, then at a pipe wall to bead centre separation distance of approximately 3 - 4 bead diameters, the contribution to fluctuations in differential pressure becomes virtually insignificant.

5.4.2 Experimental differential pressure fluctuations caused by a single stream of bubbles at low frequencies of generation in a pipe containing stagnant water

In this experiment the basic experimental arrangement described in section 5.4.1 was used, but with the bead assembly removed and a small pipe inserted through the wall of the short test section into the column of stagnant water approximately 100mm below the first pressure tapping, as shown in figure 5.28. From an orifice 0.8mm in diameter in the small pipe a single stream of bubbles was generated with a similar size range to those produced by the 'spoked wheel' air injector used in the flow loop. The bubbles were generated with a frequency of the order of 0.5Hz. The radial position R of the orifice used to generate the bubbles could be varied by moving the small pipe, thus providing a means for measuring the differential pressure fluctuations as a function of the pipe wall to bubble generation separation distance. Again the results were measured using the Bruel & Kjaer model 2034 dual channel analogue signal analyser and stored on computer discs.

As discussed in section 5.1.1, bubbles tend to wander as they make their ascent. This makes it extremely difficult to be certain of the actual pipe wall to bubble centre separation distance at the location of the differential pressure transducer. To obtain useful data from this experiment, the normalised peak fluctuation in differential pressures are plotted as a function of the pipe wall to injection point separation distance. The peak recorded fluctuation in differential pressure from a single bubble was normalised using equation 5.49, assuming a terminal bubble rise velocity $V_{g\infty}$ of 0.25m/s. Because the differential pressure measurements are plotted

as a function of the pipe wall to injection point separation distance and not the actual wall to bubble separation distance at the location of the transducer, it is thought that since a bubble near the wall tends to migrate towards the wall causing a region of high void fraction at the pipe wall, the peak value of differential pressure fluctuations measured here are likely to be associated with an actual pipe wall to bubble separation distance which is less than the pipe wall to injection point separation distance. Therefore, for a given wall to bubble centre separation distance, the measured fluctuations in differential pressure in this experiment are expected to be slightly higher than those obtained from the bead experiment and those calculated theoretically. Hence, it is thought that these results will form the upper limit to the magnitude of pressure fluctuations caused by a bubbles motion.

5.4.3 Comparison of theoretical and experimental differential pressure fluctuations in a standing column of water

The peak differential pressure for a moving sphere in an infinite fluid can be predicted from equation 5.43 which is derived from *Butler's* sphere theorem. A comparison can be made between the theoretical predictions and the experimental results obtained from the peak differential pressure measurements obtained from constant velocity bead experiments, and from the low frequency bubble stream experiments, see sections 5.4.1 and 5.4.2 respectively. In figure 5.29 the theoretical predictions from equation 5.43 are plotted with the two sets of experimental data from the constant velocity bead experiments and low frequency bubble stream experiments. The differential pressure fluctuations are all normalised using equation

5.49, using a constant bubble/bead/sphere velocity of 0.25m/s. The three data sets are plotted as a function of the ratio of the pipe wall to bubble/bead/sphere centre separation distance over the bead radius, R/a, where a = 3.25mm.

It can be seen from figure 5.29 that although many assumptions have been made in the derivation of equation 5.43, the calculations and the experimental constant velocity bead data exhibit similar trends. It is clearly shown in figure 5.29 that the theoretical peak differential pressure fluctuations predicted for a sphere in an infinite fluid give the lowest values for fluctuations in differential pressure and the magnitude of these fluctuations die away more rapidly with increasing distance from the fixed pressure measurement points than is exhibited by either of the experimental data sets. The variation between the theoretical predictions and the constant velocity bead experiments is likely to be largely due to the assumption of an infinite fluid in the theoretical predictions whereas the constant velocity bead experiments are performed in a pipe of diameter D = 77.8mm, i.e. the effect of the pipe wall and the wake generated by a moving bubble have been neglected in the theoretical predictions. As shown by figure 5.26 this change is primarily reflected as a change in amplitude, with no detectable significant change in the signal phase information.

It can also be seen that, as predicted in section 5.4.2, the normalised peak differential pressure fluctuations caused by the low frequency single stream of bubbles give the highest magnitude of differential pressure fluctuations for most values of R/a, and that the magnitude of these pressure fluctuations die away less rapidly with increasing wall to bubble centre separation distance than shown

by either the theory or the constant velocity bead experiments. This is likely to be due to the wandering/migration effect of free bubbles which tend to travel towards the pipe wall. In presenting the bubble results in the form given by equation 5.49 ($\Delta P/\frac{1}{2}\rho_l V_\infty^2$), two effects will distort this presentation. Firstly, the bubble results have been plotted as a function of their injection distance from the wall, but a significant number of bubbles released in the region 1 - 6 bubble radius from the wall will end up closer to the wall than their initial release positions giving rise to a larger ΔP than would have been recorded if the bubble had remained the same distance from the wall. A secondary effect would be the deviation of the bubble velocity near the wall from the assumed $V_{g\infty}$ = 0.25m/s. An additional factor that may affect the amplitude of the differential pressure fluctuations may be the constantly changing shape of bubbles as they travel through the stagnant liquid phase, which may cause the pressure field around a bubble to vary from that of a sphere.

Although the experiments described in sections 5.4.1 and 5.4.2 were carried out in stagnant water where there is no initial background/continuous phase turbulence, the effect of the background/continuous phase turbulence is expected to result in only slightly higher magnitude of measured differential pressure fluctuations. Although the length scale of structures in the background turbulence may be of the order of several pipe diameters they are not expected to have much of an effect on the main feature of autocorrelation correlogram of differential pressure fluctuations since the magnitude of the background turbulence pressure fluctuations are small when compared to other sources of pressure fluctuations in a bubbly two-phase flow.

From the arguments put forward above it is therefore expected that the results of the constant velocity bead experiments will best approximate the effect of variation in the convected pressure field surrounding a bubble generated by its motion at its true pipe wall to bubble centre separation distance. In making this observation the main reason why the bubble experiments could not be interpreted correctly was the significant uncertainty in the bubble position from the wall, not in the pressure signal generated by these bubbles.

5.5 Conclusions drawn from the theoretical models and experimental results within chapter 5

Comparisons made between the theoretical analysis and experimental work in this chapter has considerably enhanced our knowledge of pressure fluctuations within a bubbly two-phase flow. This knowledge will be invaluable in the subsequent interpretations of the fluctuating differential pressure signals in the remaining investigations. In summary, from the simple theory presented in section 5.1, the terminal rise velocity and critical bubble diameter of a single bubble were calculated. These estimates have been compared with theoretical and experimental work of other researchers as well as measurements made using high speed photography undertaken in the present study. In general, good agreement has been found with variations being due largely to velocity and void fraction profiles within the two-phase flow.

Measurement of small differential pressure fluctuations that are of the order of 1 - 25mm of H_2O is best achieved using a single differential pressure transducer. Drawbacks associated with this

technique which have been encountered are pressure pulses caused by external vibrations and bleeding of air from the transducer while purging with water. However, this technique proved to be more successful than the subtraction of static pressure measurements used by *Matsui* [1984.

Four main sources of pressure fluctuations were initially identified within a bubbly two-phase flow, namely

(i) Temporal variations in the average gas void fraction

(ii) Variations in the pressure field around a moving bubble

(iii) Turbulence generated by the wake of a bubble in the continuous phase

(iv) Background turbulence in the continuous phase

Using simple theoretical analysis and experimental results obtained from the constant velocity bead experiments and the low frequency single bubble stream, comparisons of the differential pressure fluctuations have been made. Figure 5.26 shows a typical measured differential pressure signal produced by a moving bead and the corresponding theoretical calculation derived from *Butler's* sphere theorem. The curves exhibit very similar results in both magnitude and shape. It can also be seen from figure 5.26 that, as predicted by the derivation from *Butler's* sphere theorem, the maximum fluctuation in differential pressure occurs when the bead's centre is perpendicular to one of the pressure tappings with respect to the pipe wall.

The autocorrelation, curve d in figure 5.16, indicates that the main feature of this curve can be used, when interpreted correctly, to measure the velocity of a single bubble travelling close to the pressure tappings at the pipe wall. This result will be used and extended in chapter 6 to cover the situation where many bubbles are flowing in the pipe at different velocities and how the auto and cross correlation correlograms can be interpreted to evaluate the bubble velocity.

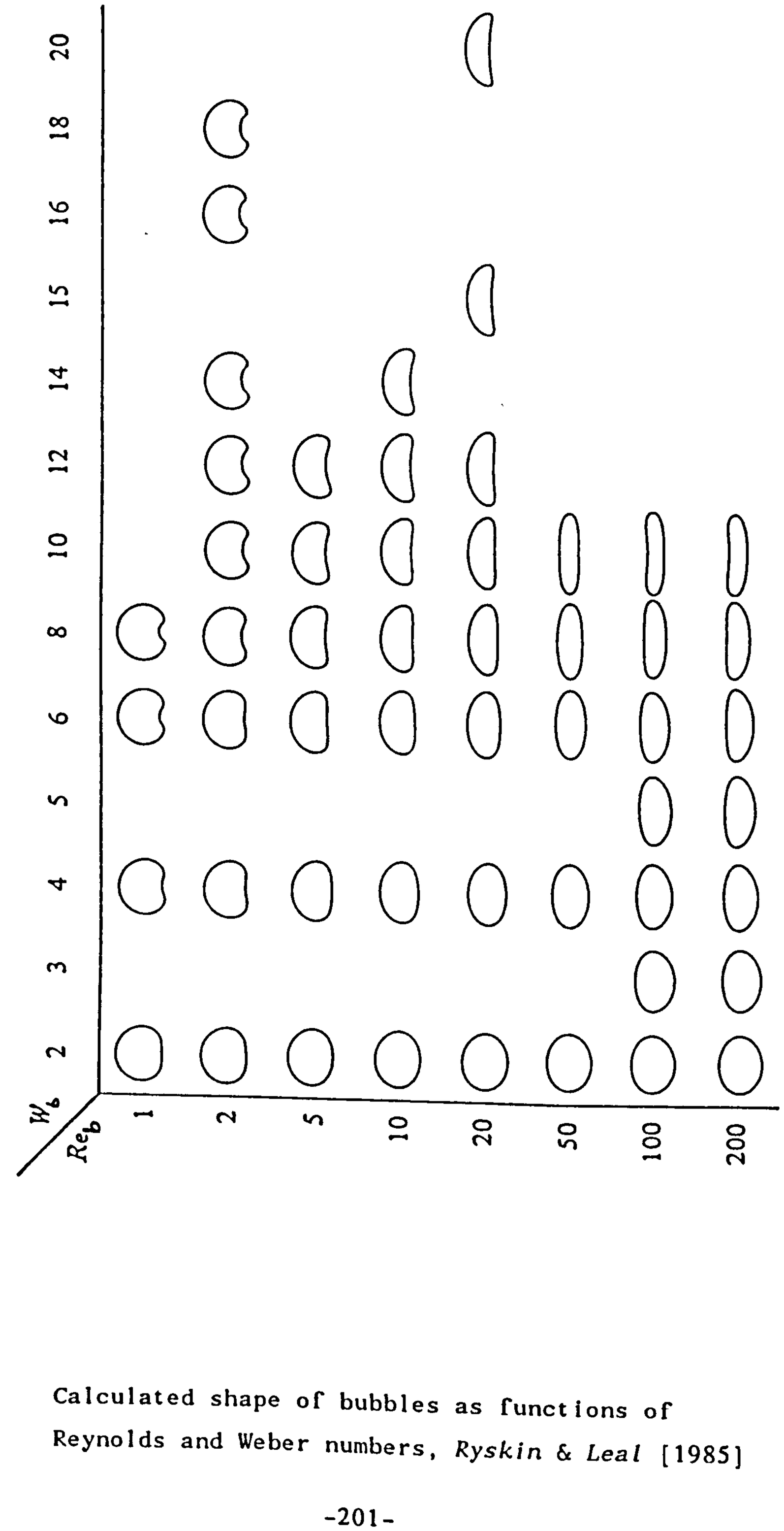

Computed steady, axisymmetric shapes of rising bubbles as a function of Re_b and W_b.

Figure 5.1 Calculated shape of bubbles as functions of Reynolds and Weber numbers, *Ryskin & Leal* [1985]

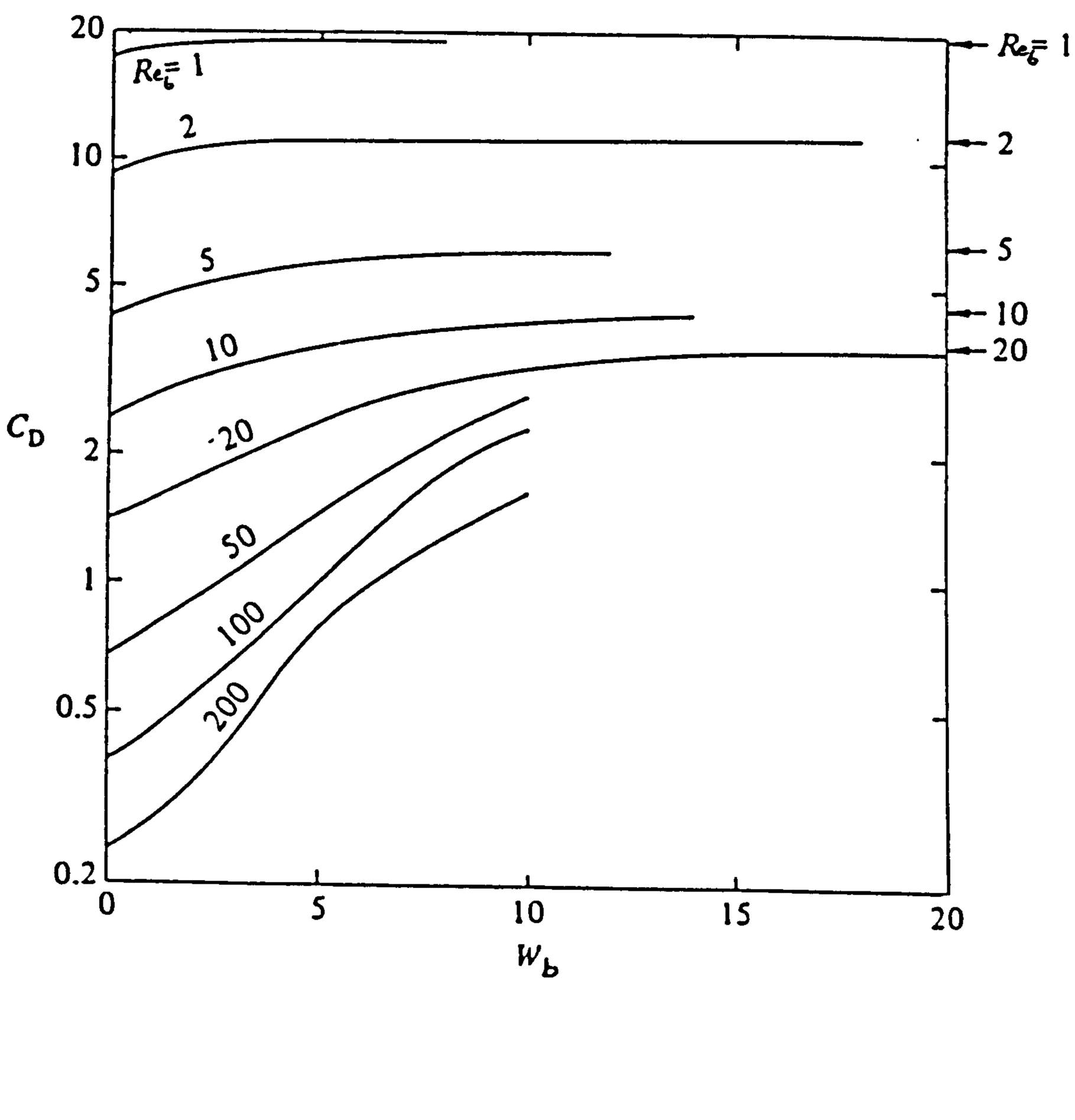

Figure 5.2 Calculated bubble drag coefficients, *Ryskin & Leal* [1985]

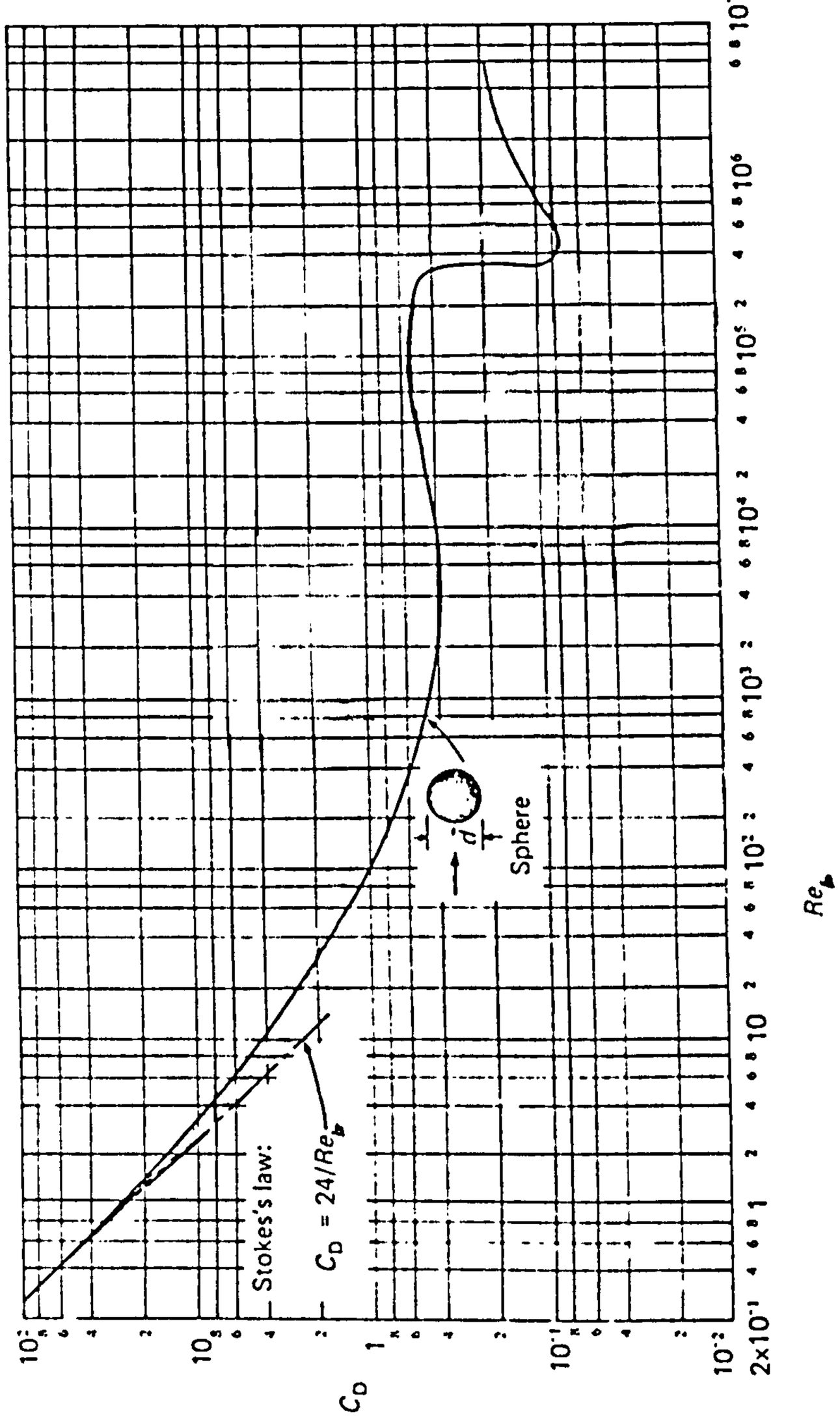

Figure 5.3 Experimental drag coefficient of a solid sphere as a function of the Reynolds number, *Massey* [1968]

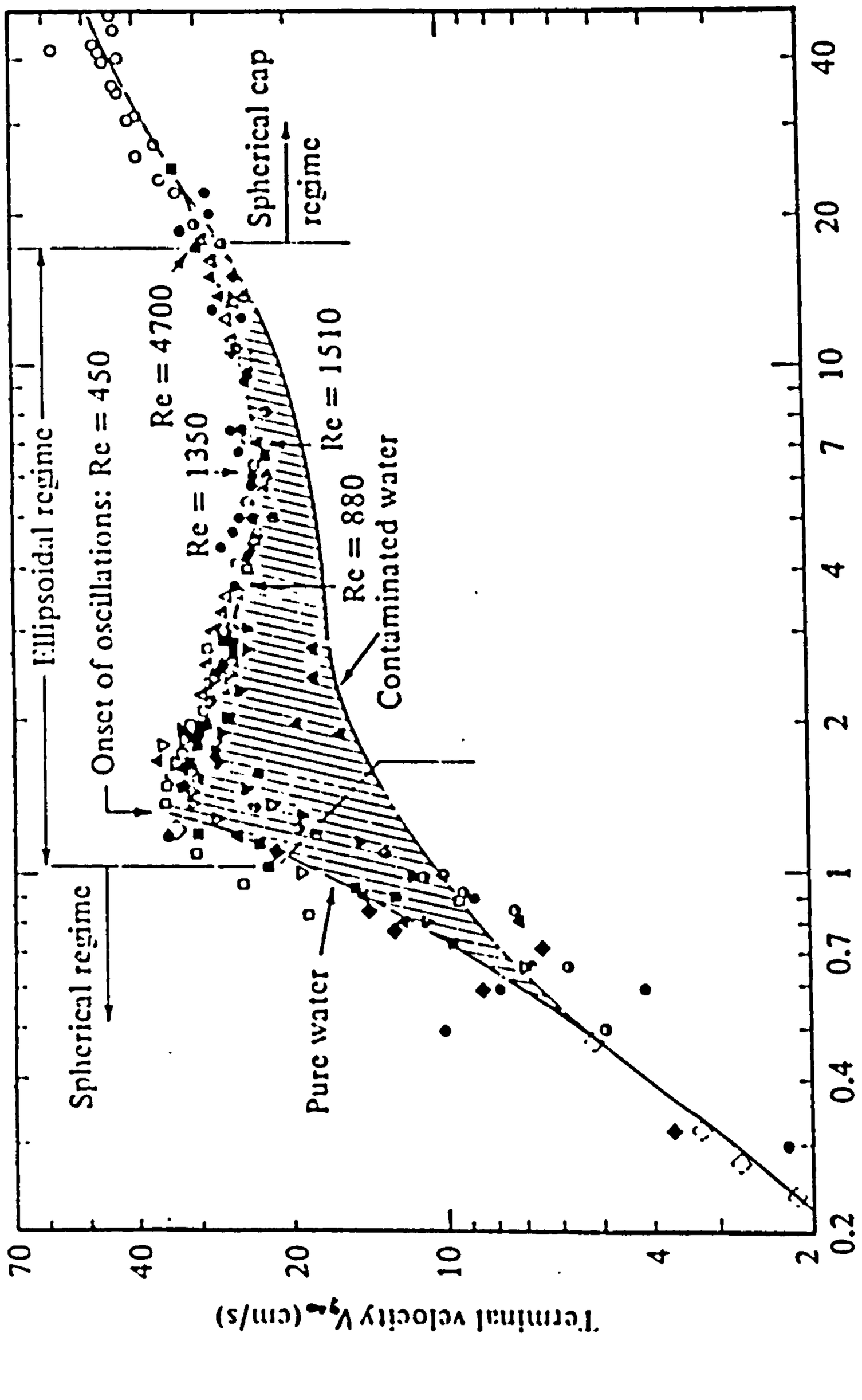

Figure 5.4 Experimental measurement of terminal bubble rise velocity $V_{g\infty}$ as a function of the equivalent bubble diameter for air in water at 20°C, *Clift et al* [1978]

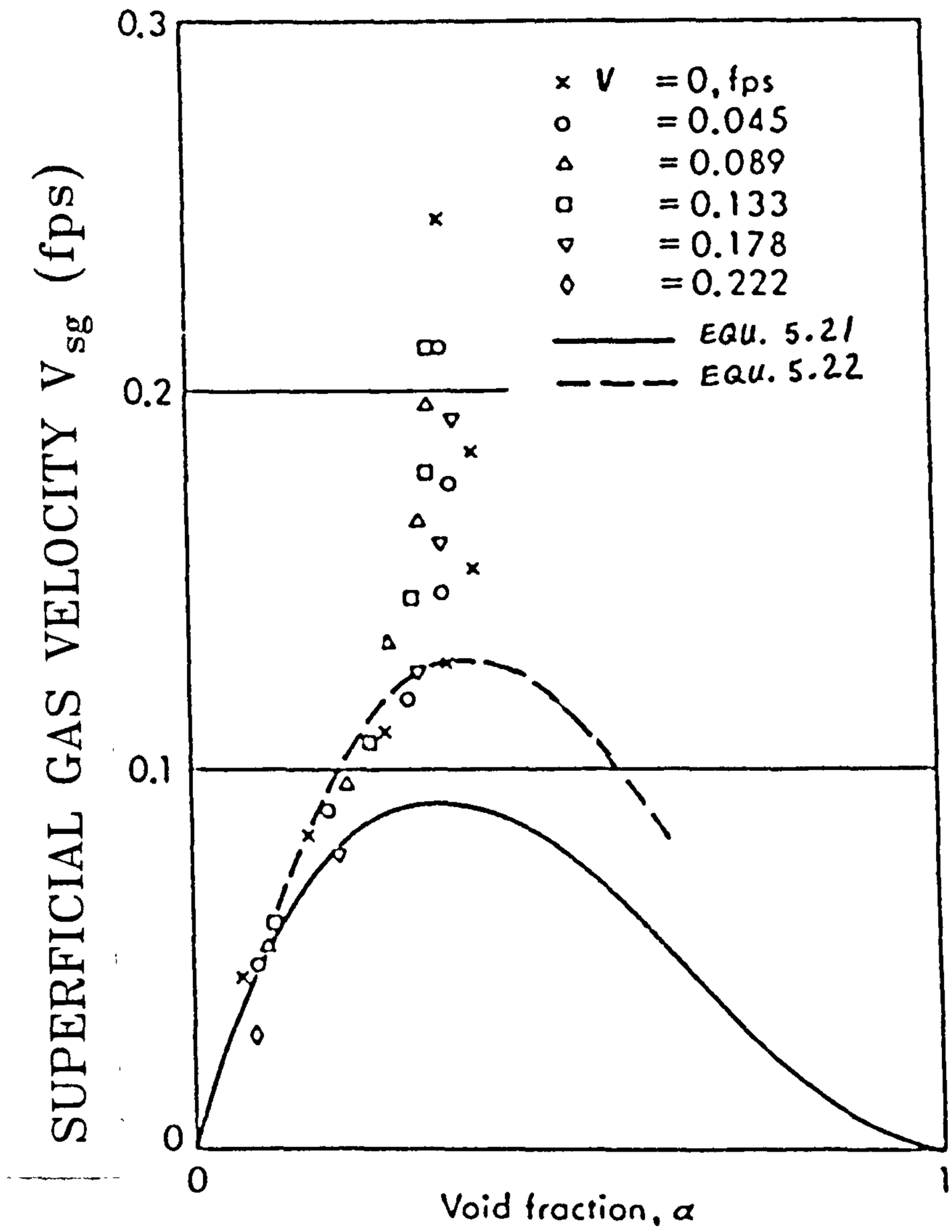

Figure 5.5 Variation in the superficial gas velocity V_{sg} as a function of the average gas void fraction α, where V is the continuous phase velocity, *Wallis* [1969]

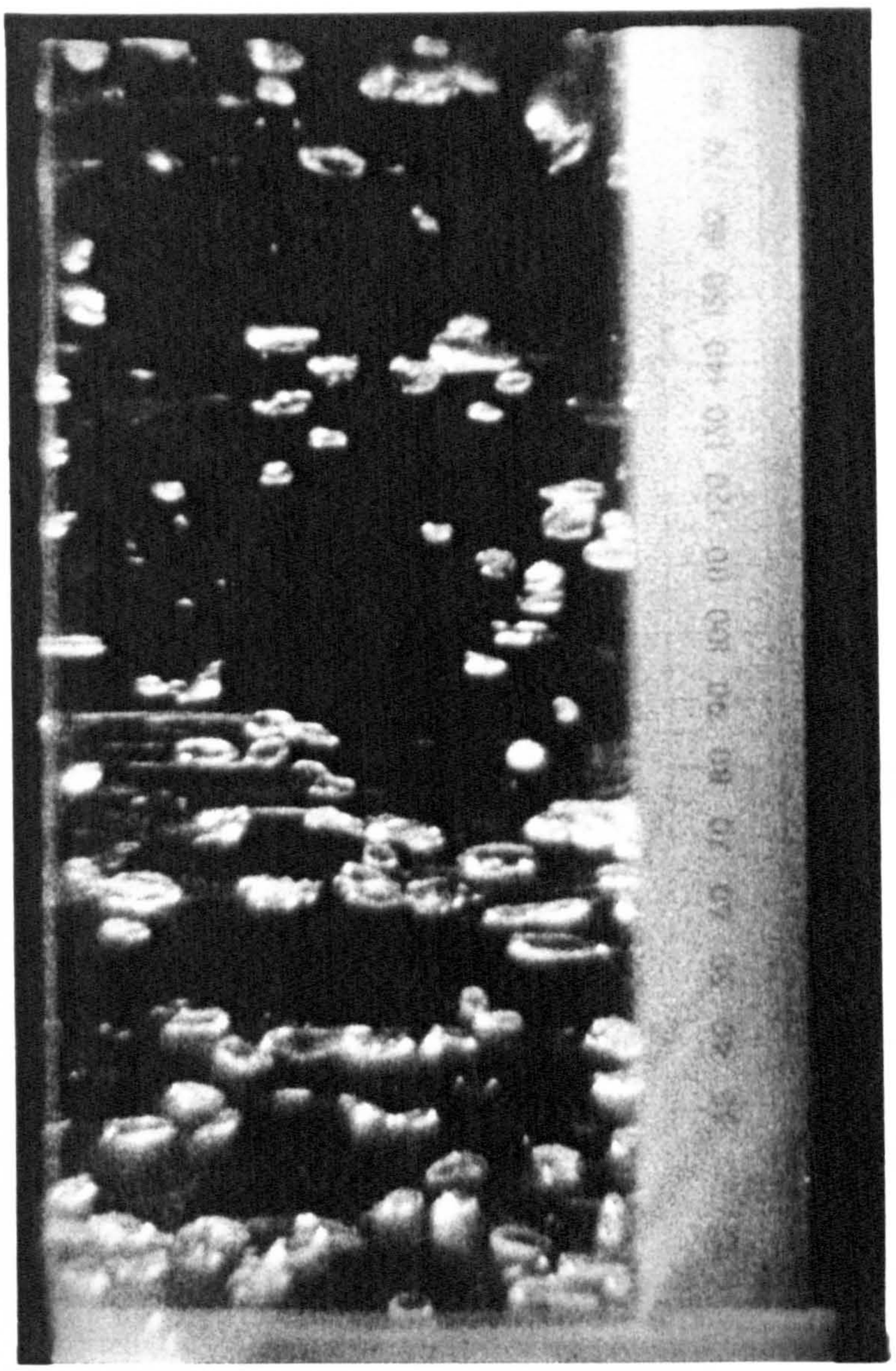

Figure 5.6 Typical frame of high speed film used to estimate the variation in terminal bubble rise velocity $V_{g\infty}$ in the experimental test section of the present study, $V_{sl} = 0$ and $\alpha < 5\%$

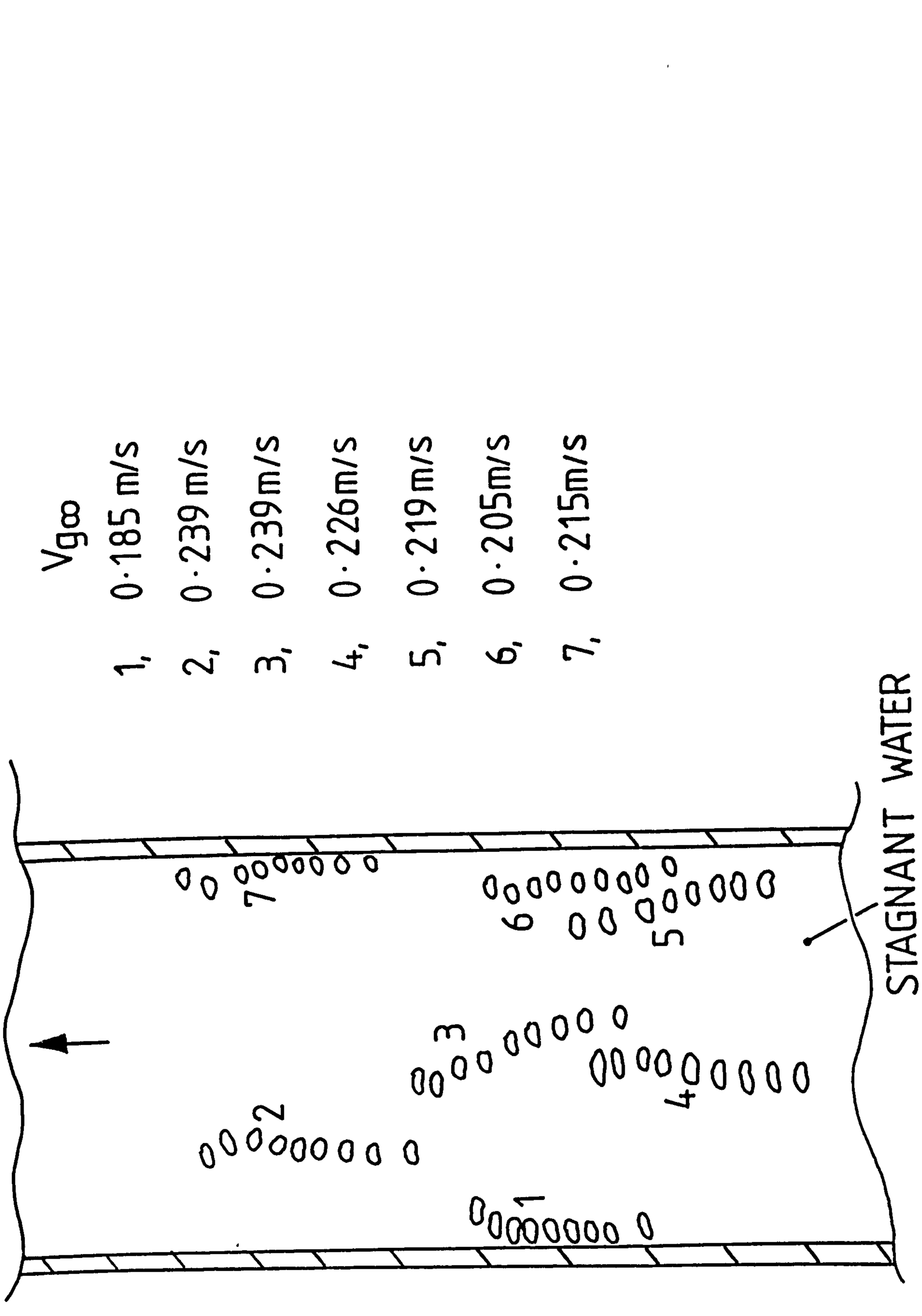

Figure 5.7 Single bubbles tracked over 9 consecutive frames of high speed film representing 0.2 seconds

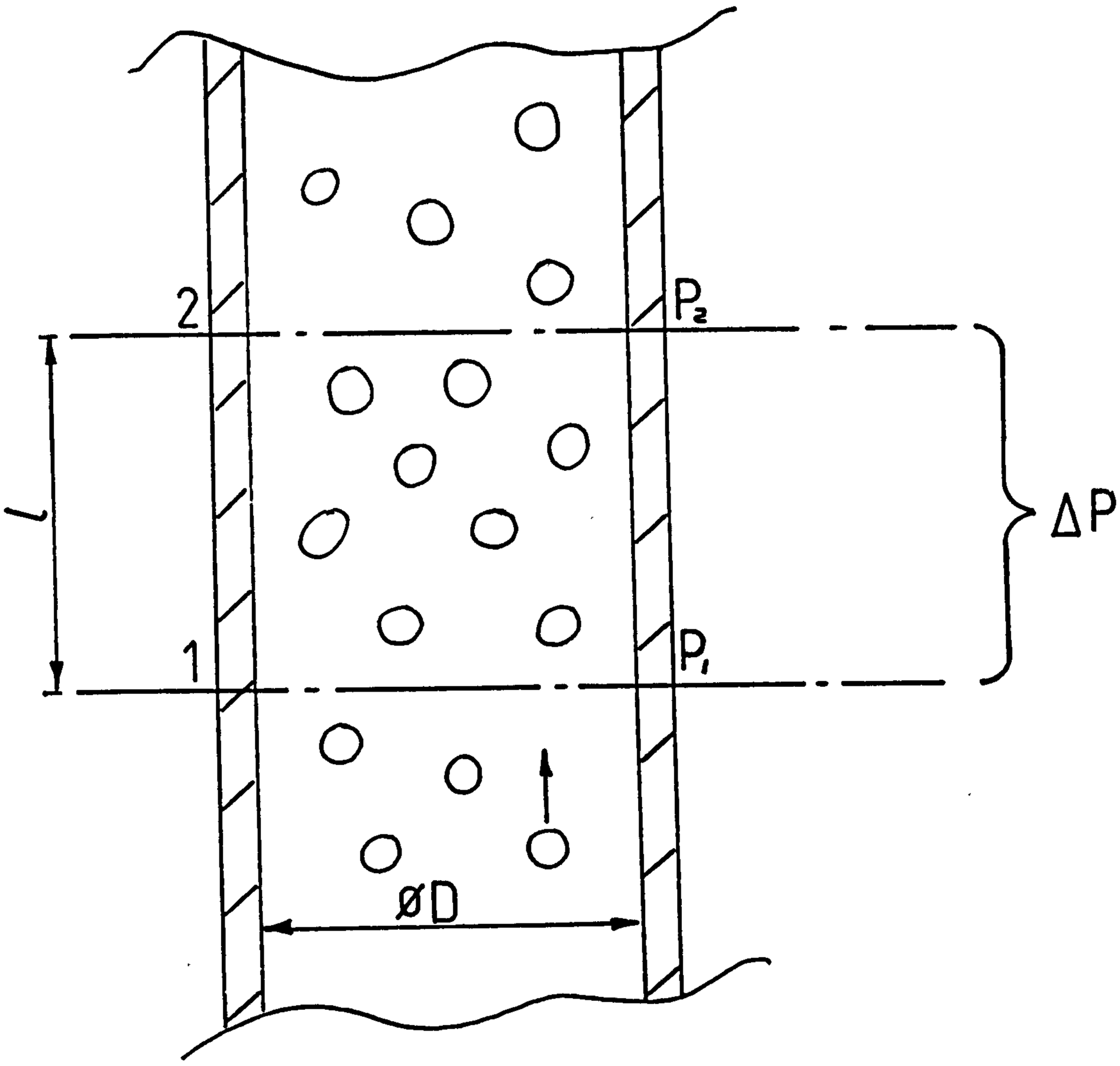

EXPERIMENTAL TEST SECTION

Figure 5.8 Diagrammatic representation of differential pressure measurements performed in the present study

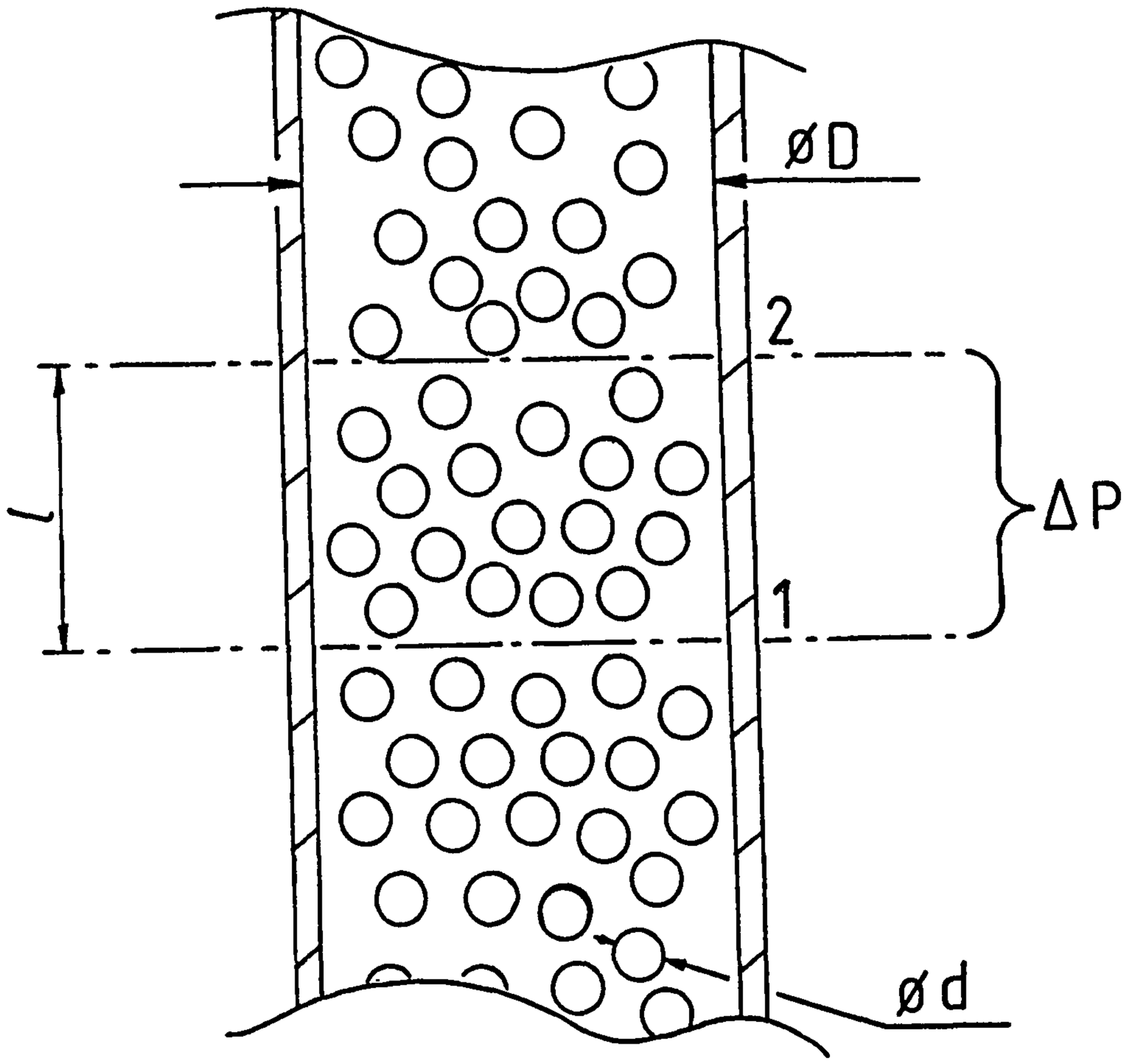

Figure 5.9 Theoretical analysis of variation in the local average gas void fraction

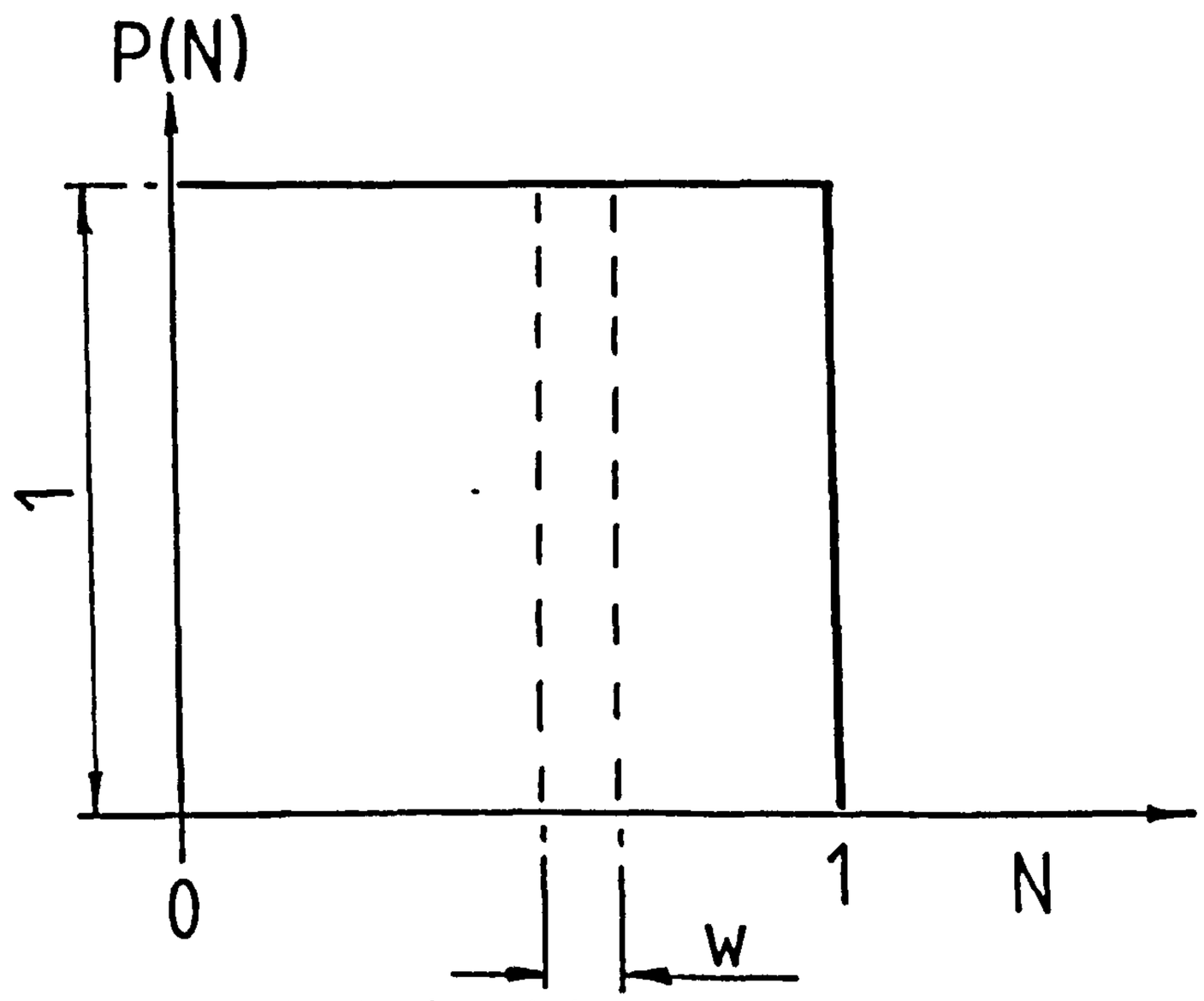

Figure 5.10 Statistical model used to predict the variation in local average gas void fraction assuming a uniform probability density distribution and by estimating the r.m.s. error ϵ in a small sample

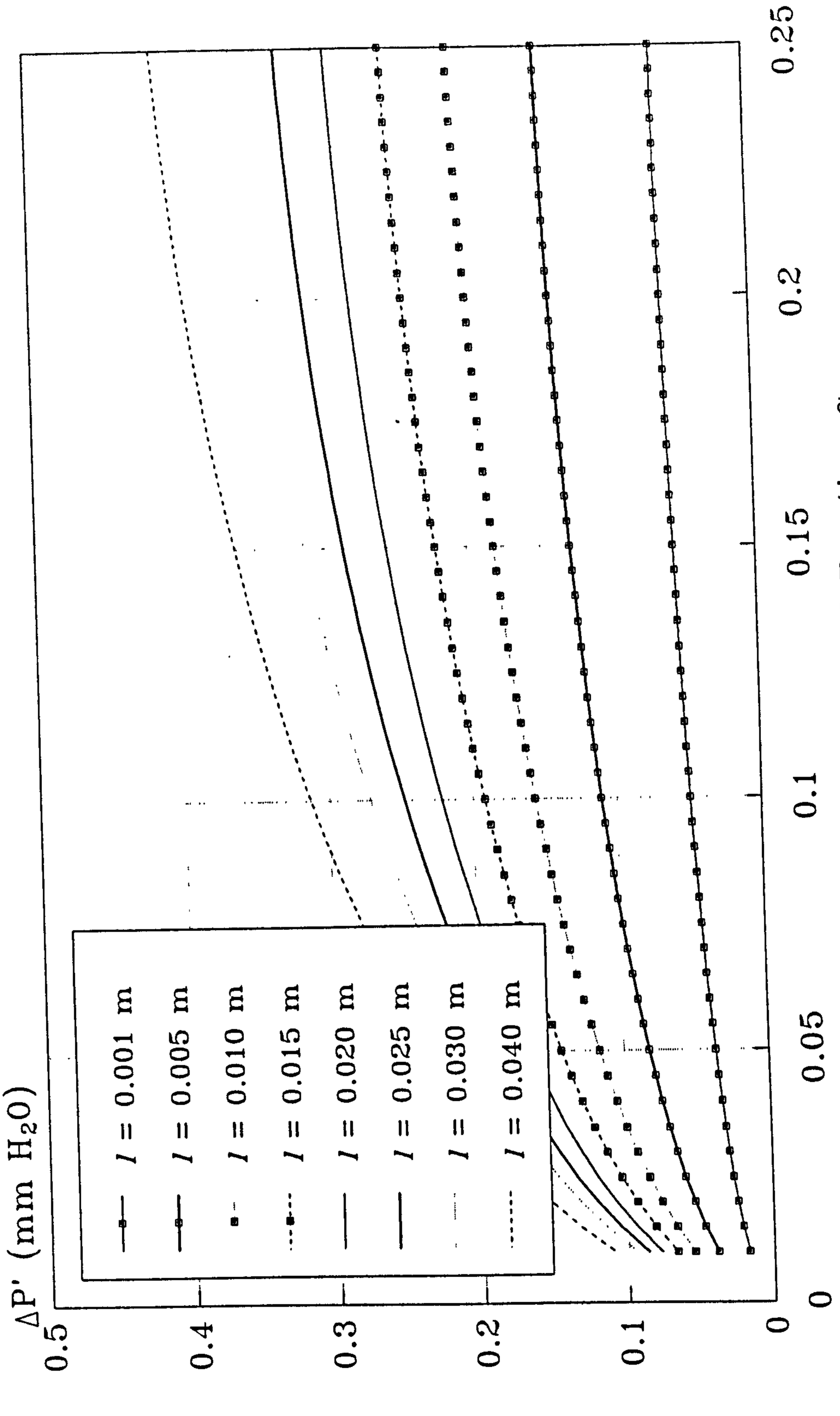

Figure 5.11 Estimated magnitude of r.m.s. pressure fluctuations $\Delta P'$ generated by variations in local average gas void fraction as a function of the average gas void fraction α and tapping separation distance l

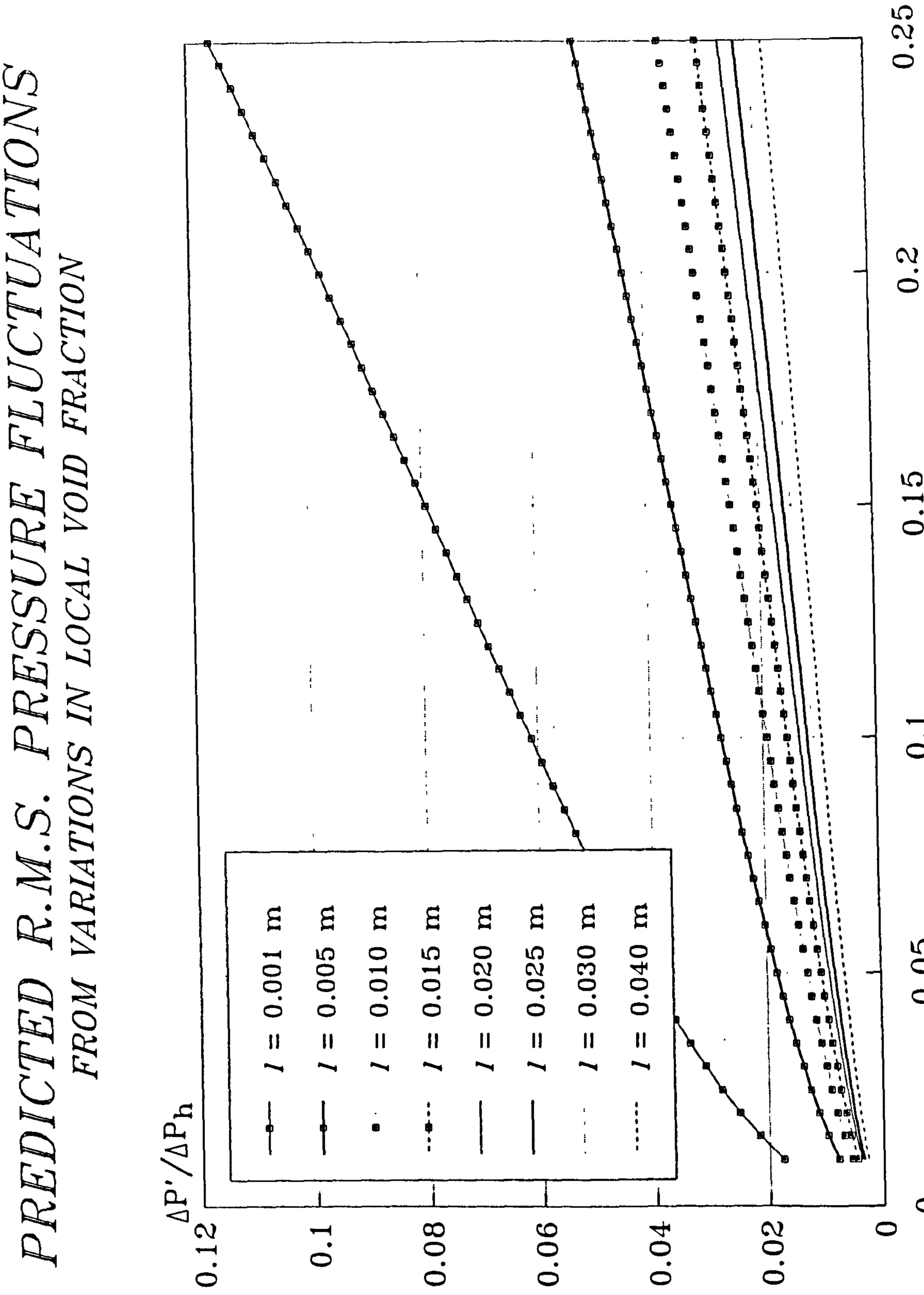

Figure 5.12 Estimated variations in the ratio of r.m.s. pressure fluctuations to the mean differential pressure ($\Delta P'/\Delta P_h$) caused by variations in local average gas void fractions plotted as a function of the average gas void α fraction and tapping separation distance l

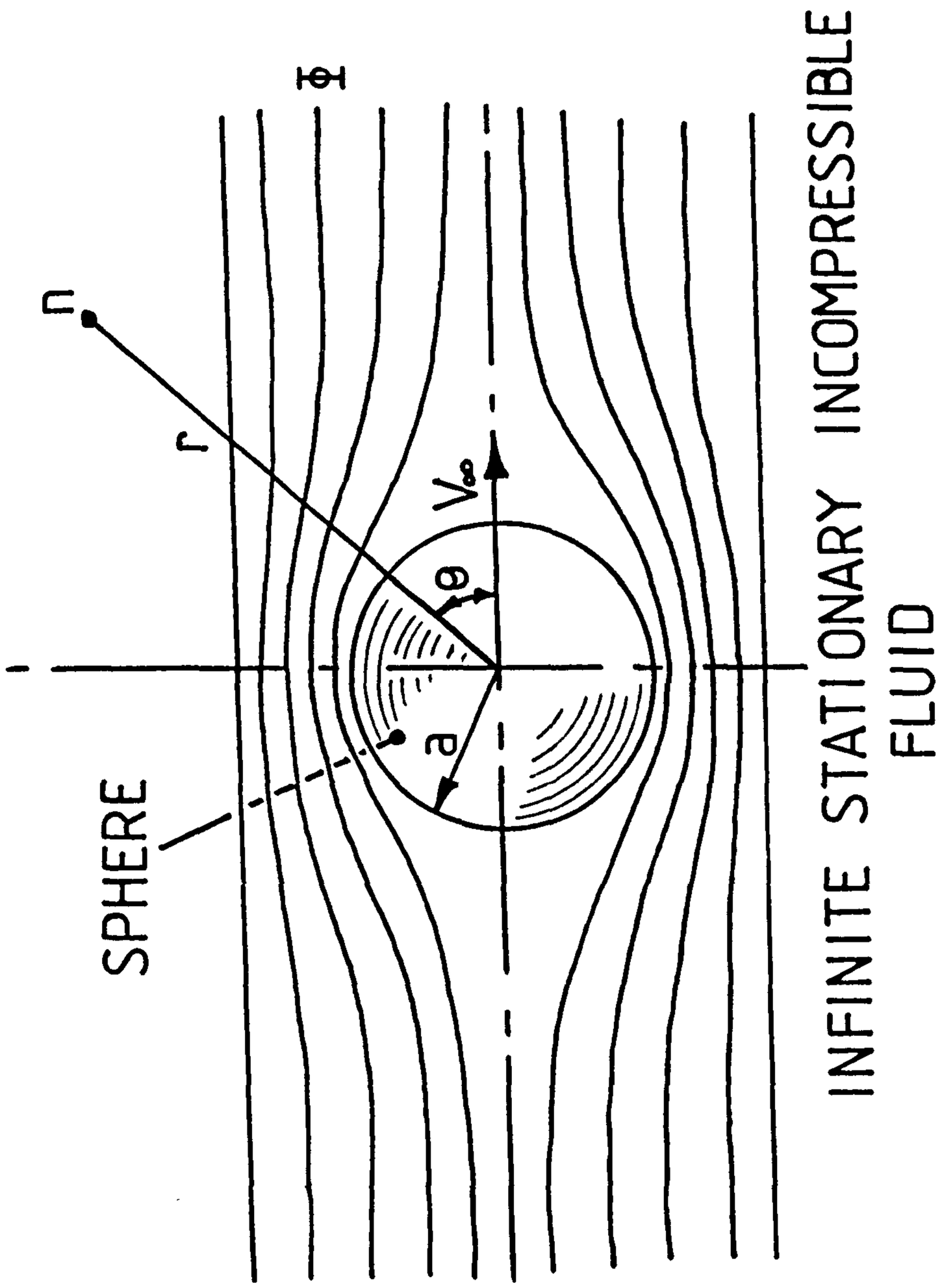

Figure 5.13 *Butlers* sphere theorem for a sphere travelling with a constant velocity through an infinitely large incompressible inviscid fluid

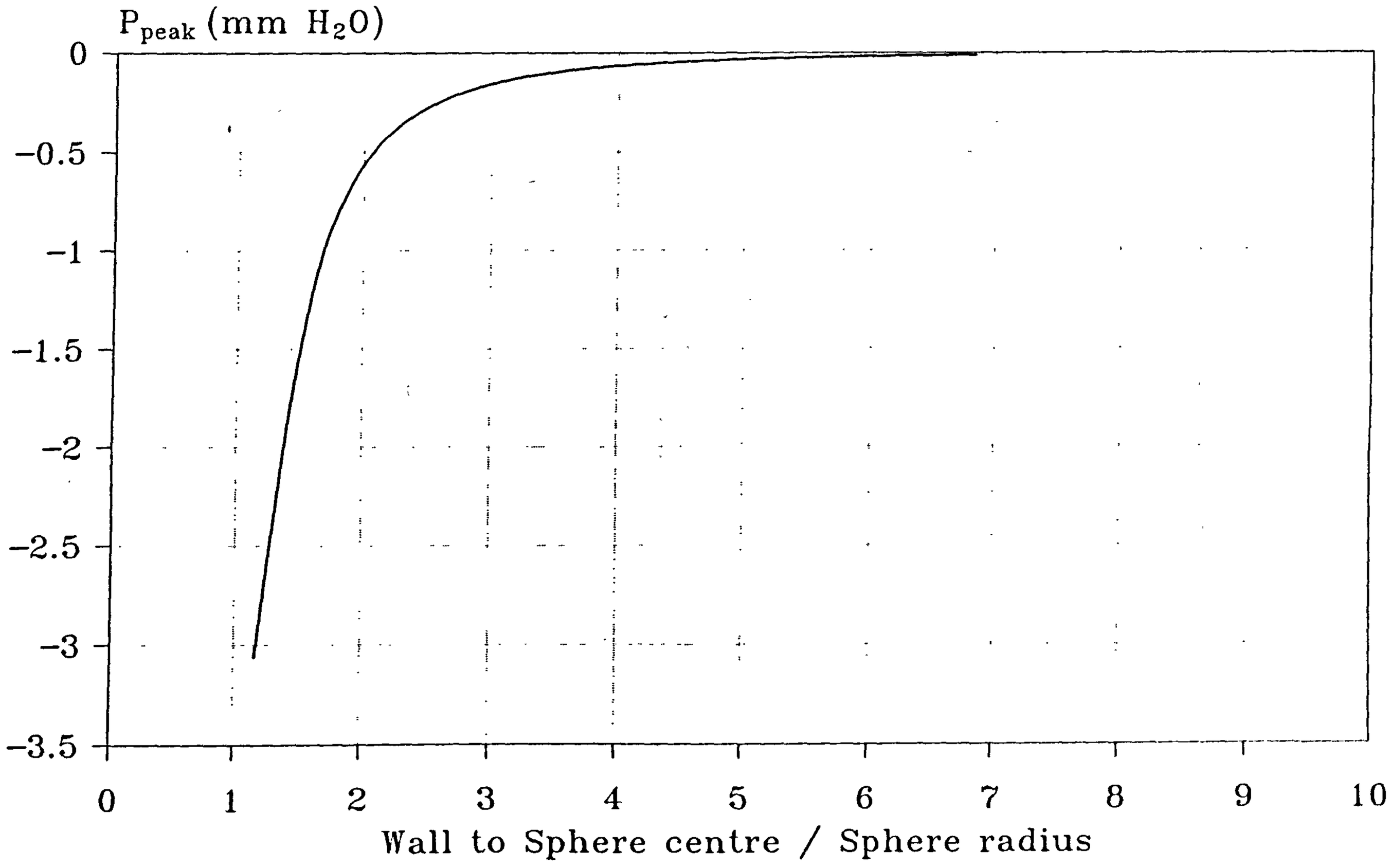

Figure 5.14 Estimated peak pressure fluctuations P_{peak} caused by the motion of a single sphere as a function of pipe wall to sphere centre separation distance

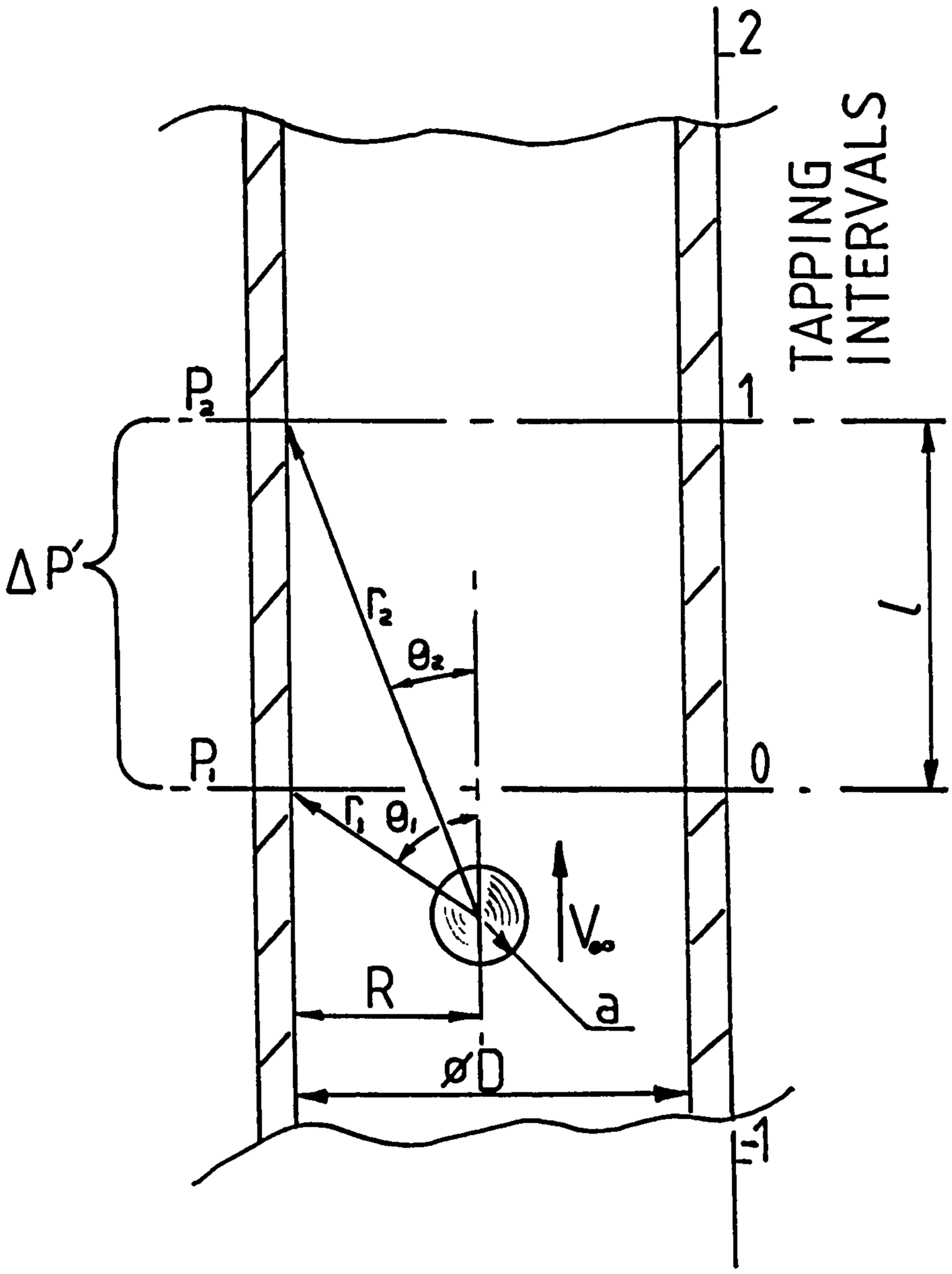

Figure 5.15 Diagrammatic representation differential pressure measurement

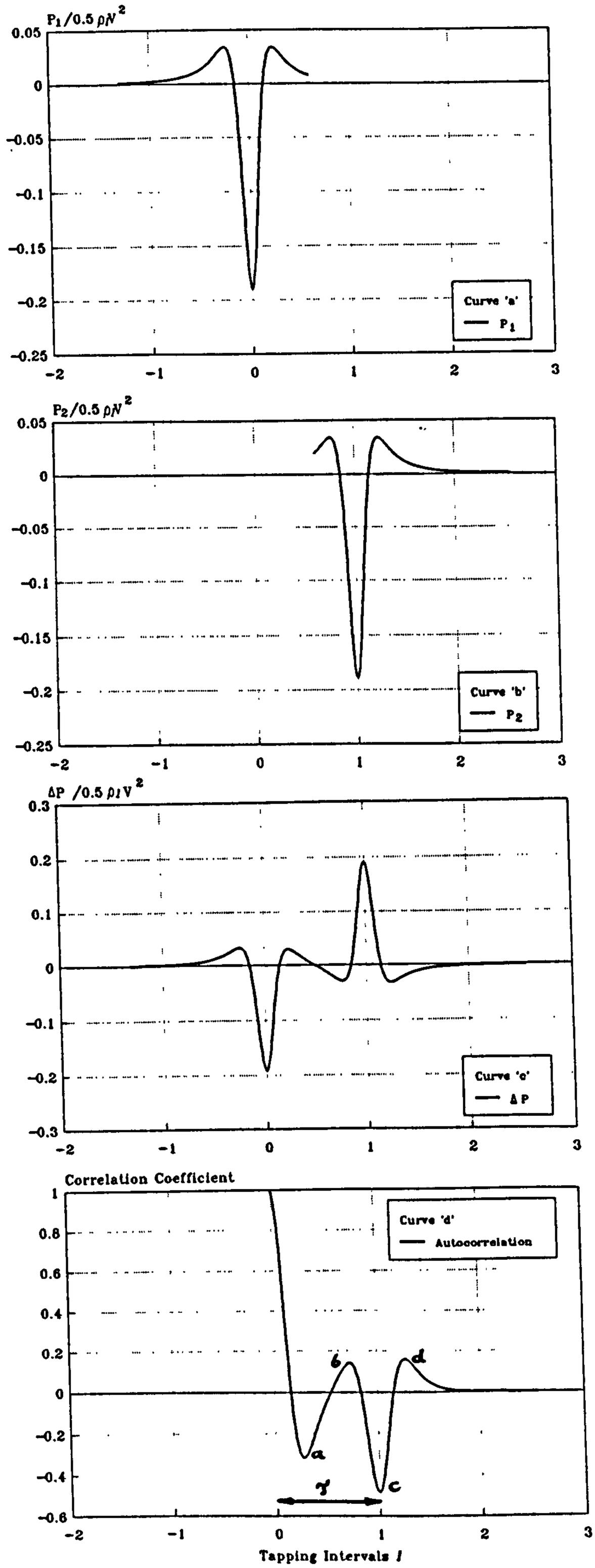

Figure 5.16 Recorded pressure signals generated as a sphere of radius a = 3mm travels with a constant velocity, V_∞, past two fixed pressure measuring points, 1 and 2, at a distance R = 4.5mm

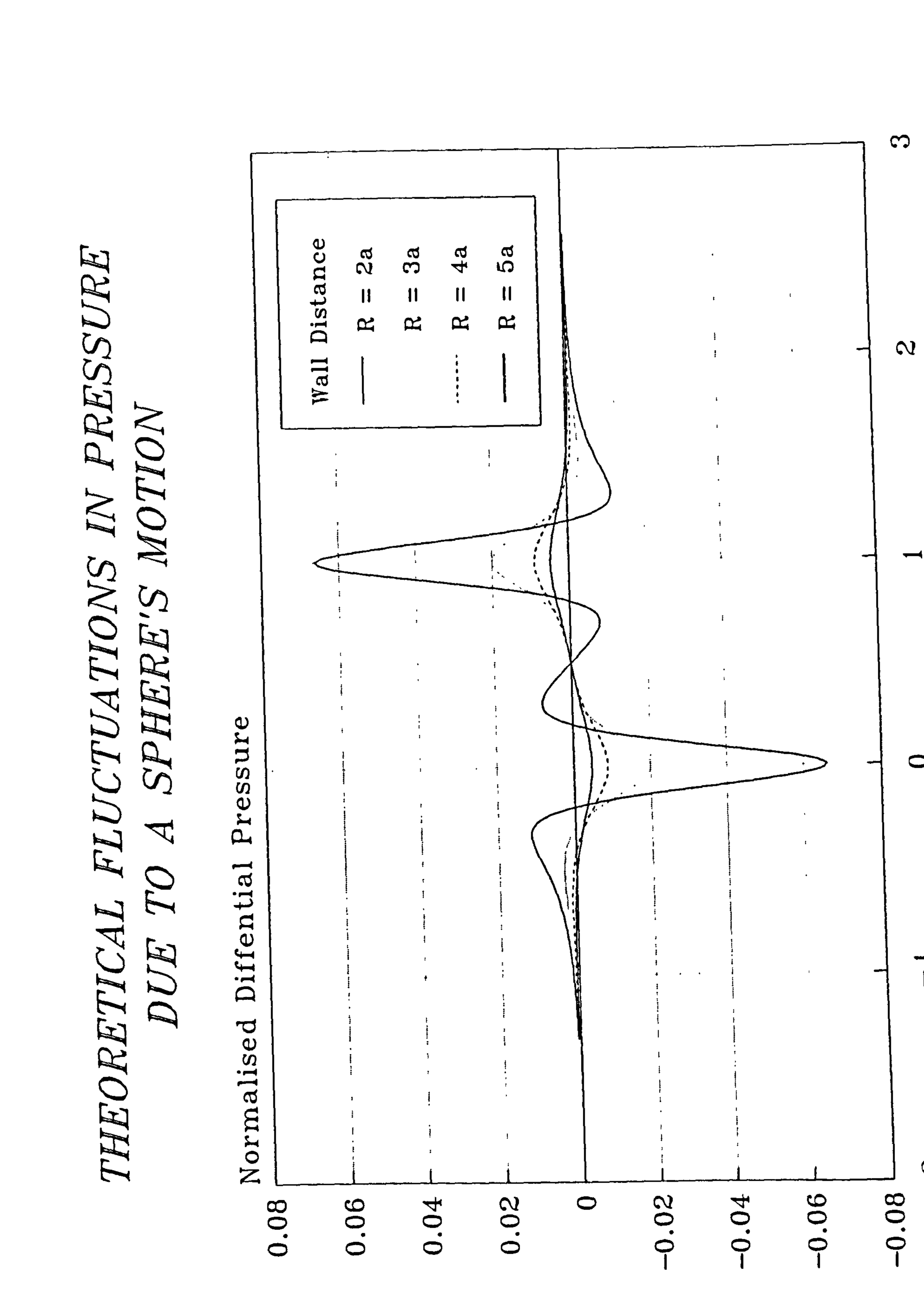

Figure 5.17 Theoretical differential pressure signal generated by a moving sphere derived from *Butlers* sphere, as a function of the pipe wall to sphere centre separation distance

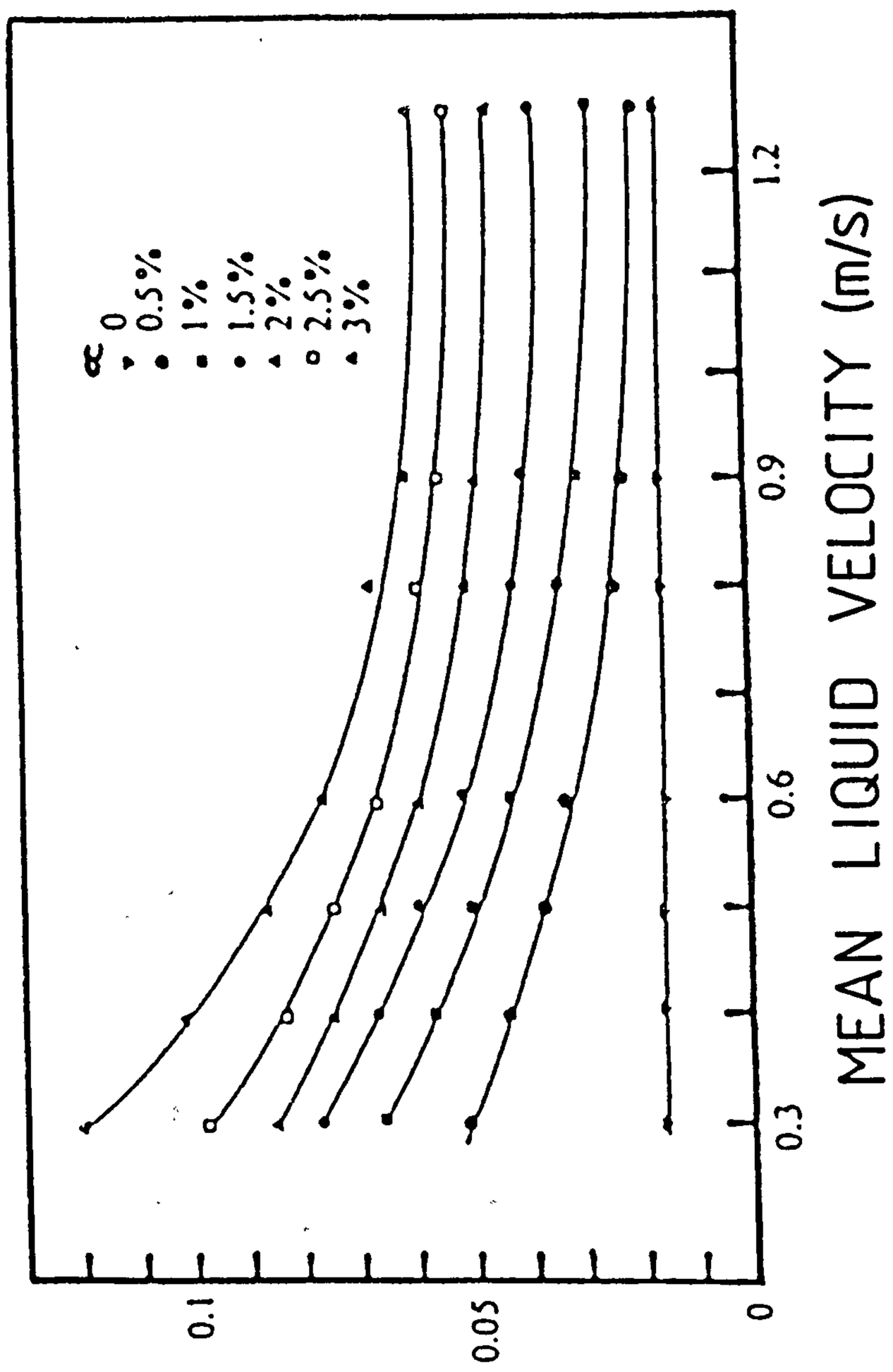

Figure 5.18 Turbulent intensity in the continuous phase generated by air bubbles in water where the continuous phase has a background turbulence generated by a 40mm grid. Turbulent intensity is plotted as a function of the average gas void fraction and area averaged liquid velocity, *Lance & Bataille* [1991]

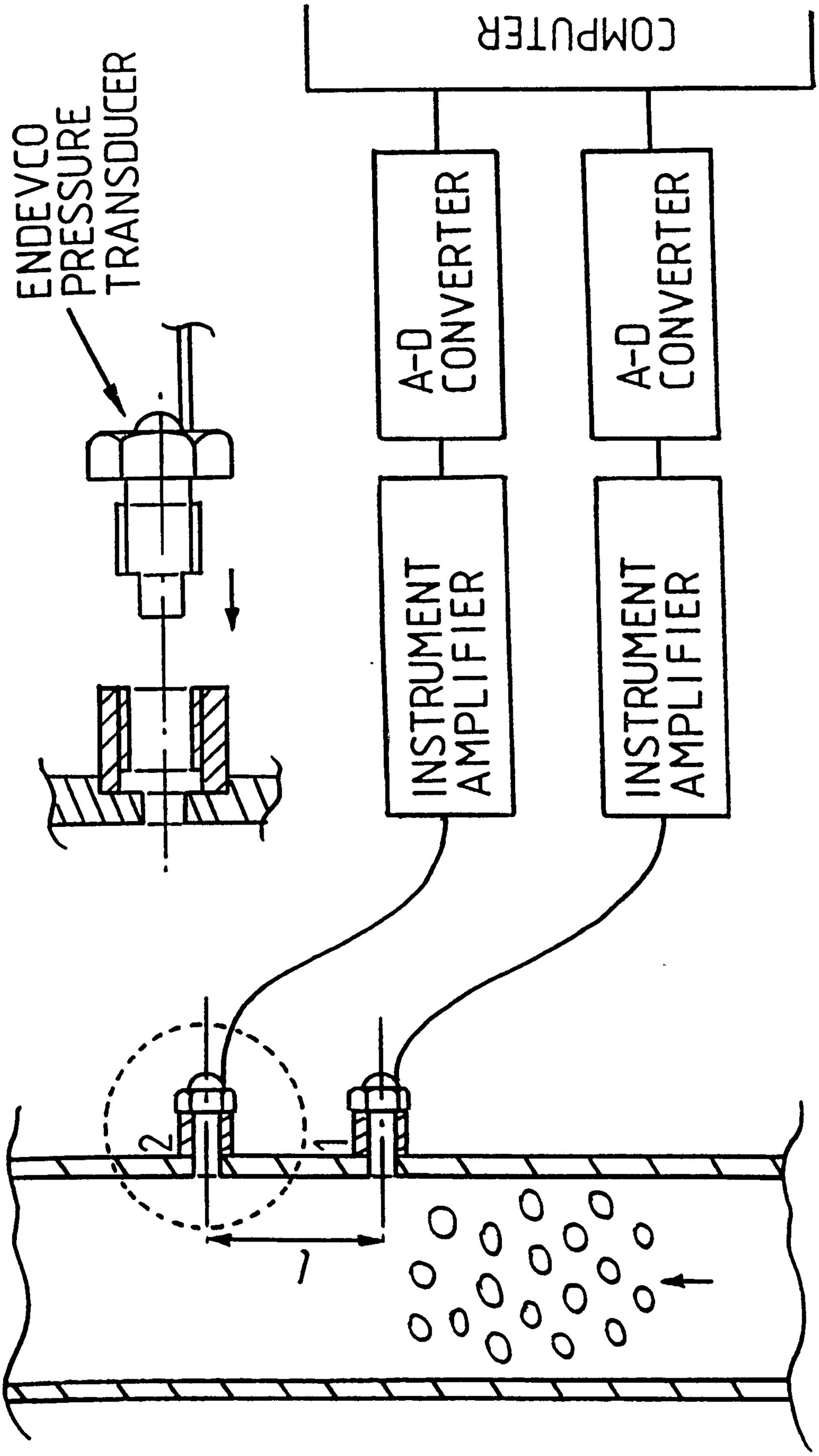

Figure 5.19 Arrangement of Endevco static pressure transducers and associated instrument amplifiers initially used to study differential pressure fluctuations

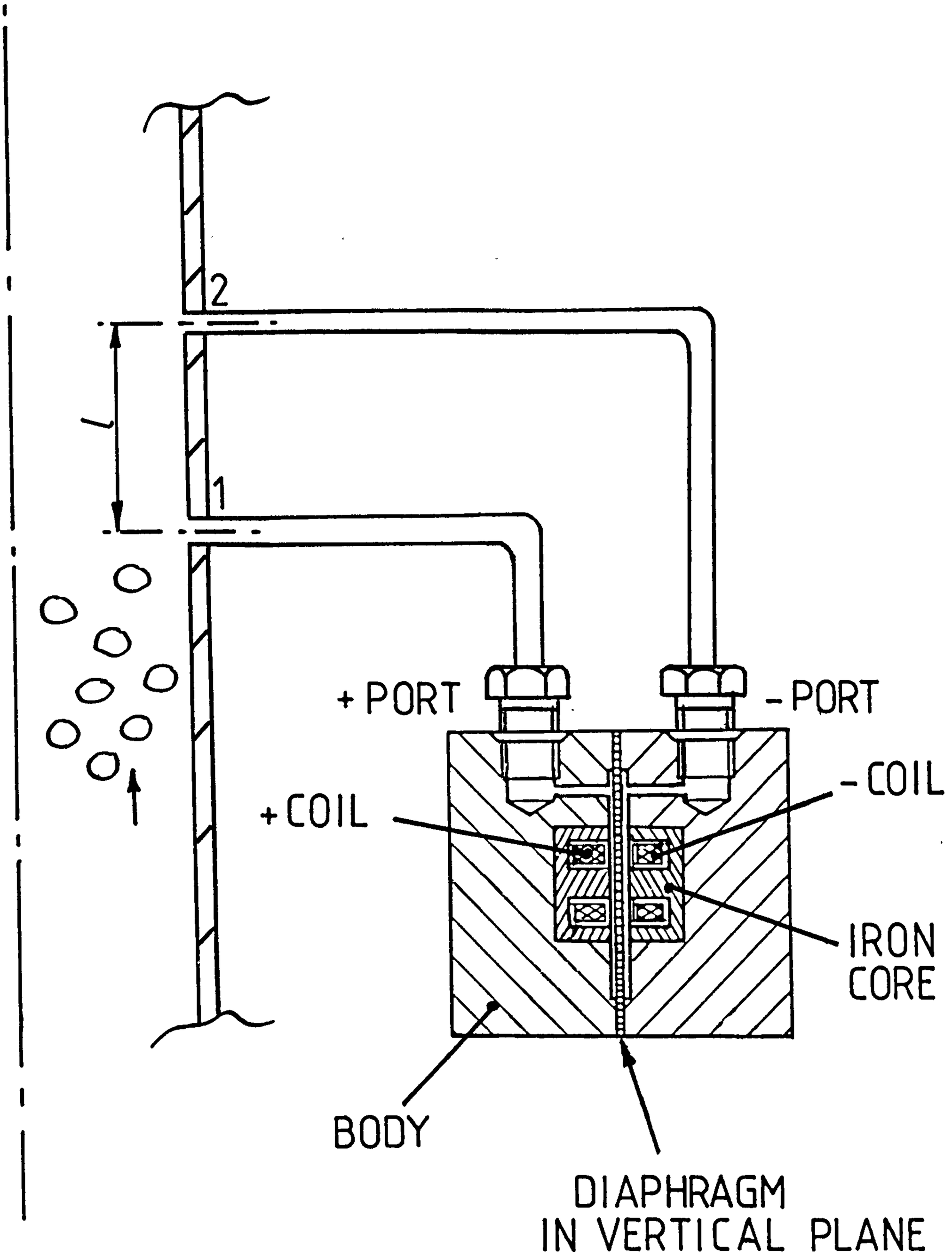

Figure 5.20 Diagrammatic representation of the single Validyne differential pressure transducer used in the present study to investigate differential pressure fluctuations

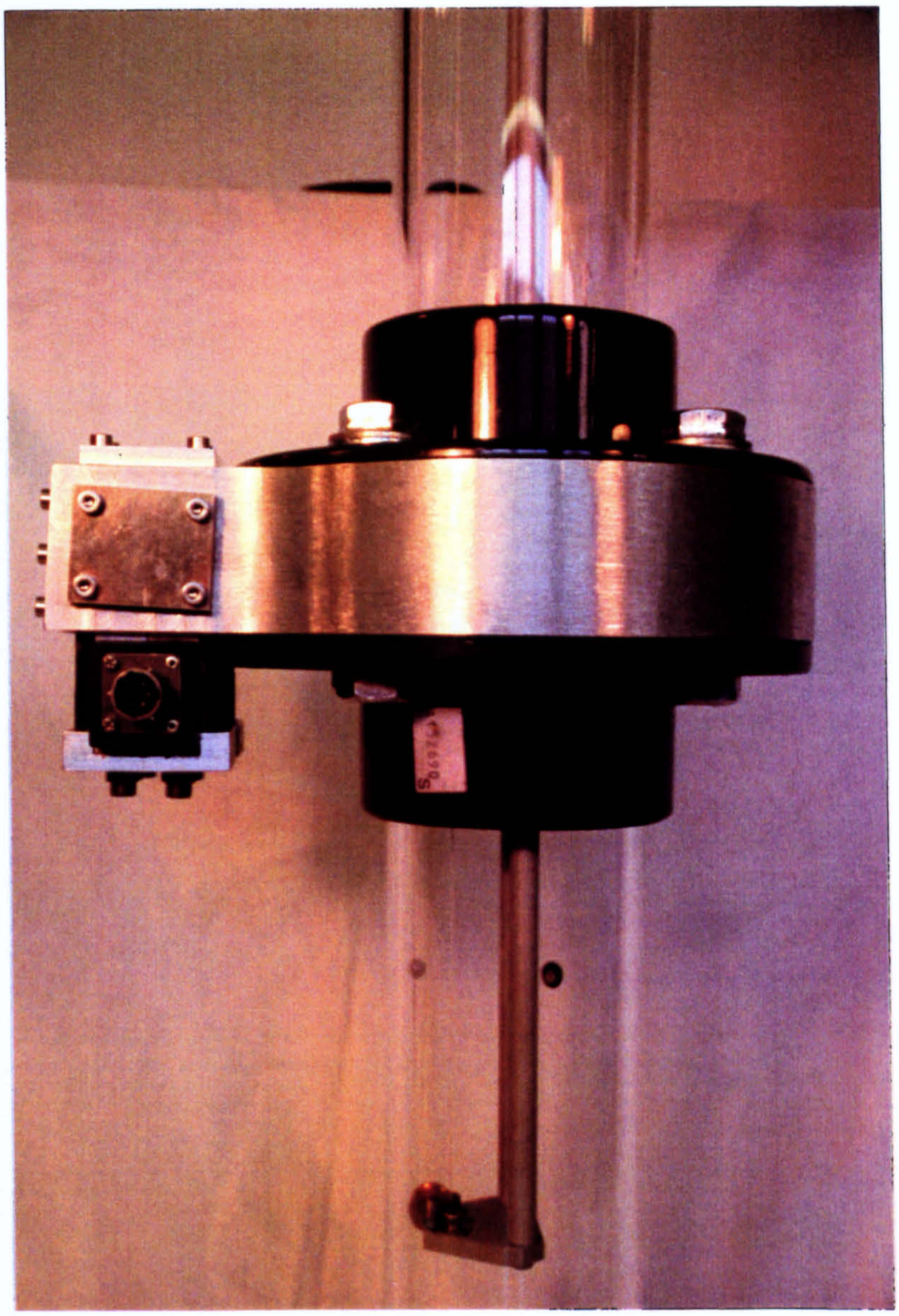

Figure 5.21 Photograph of Validyne differential pressure transducer mounting facility

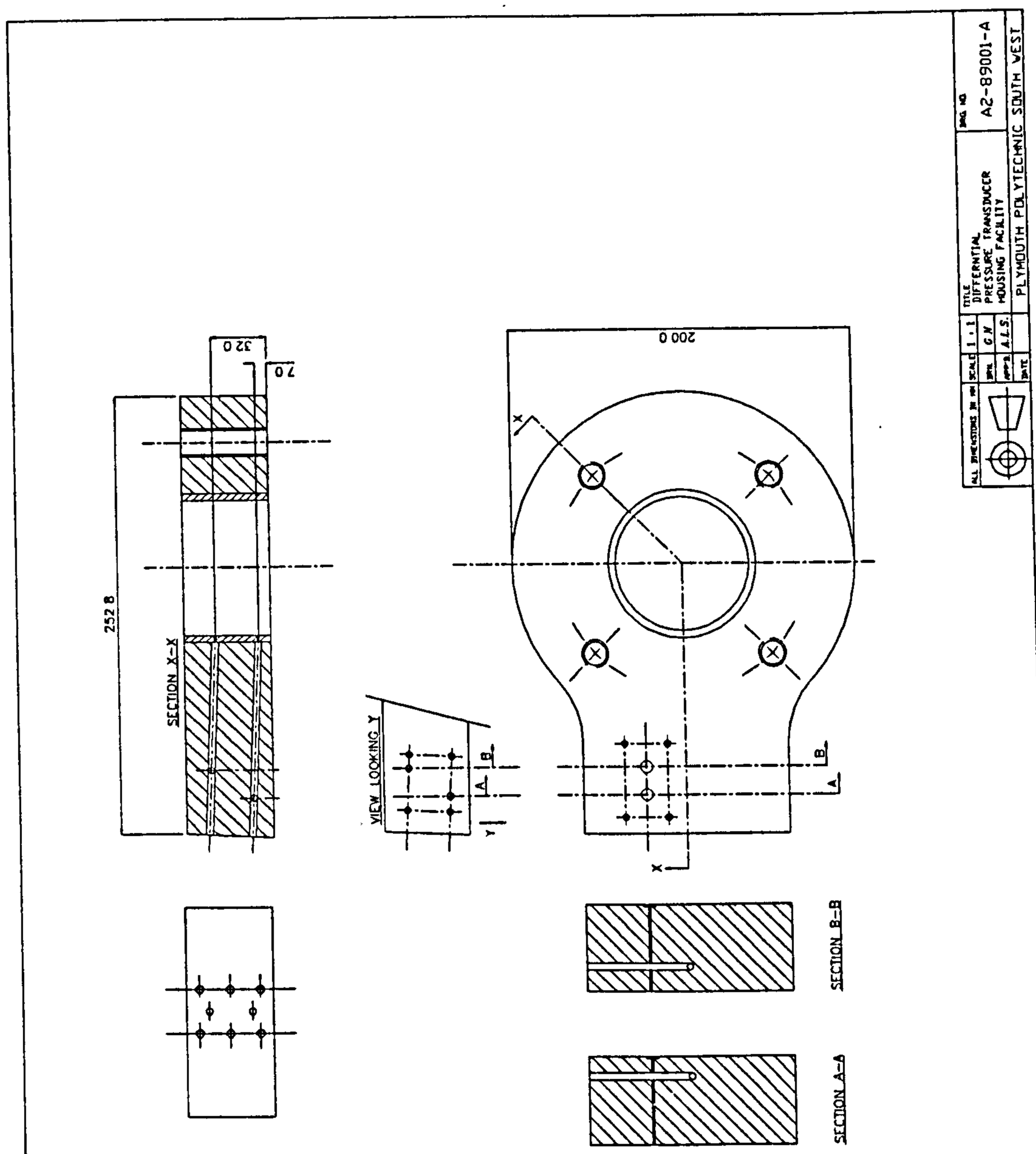

Figure 5.22 Validyne differential pressure transducer housing/mounting facility

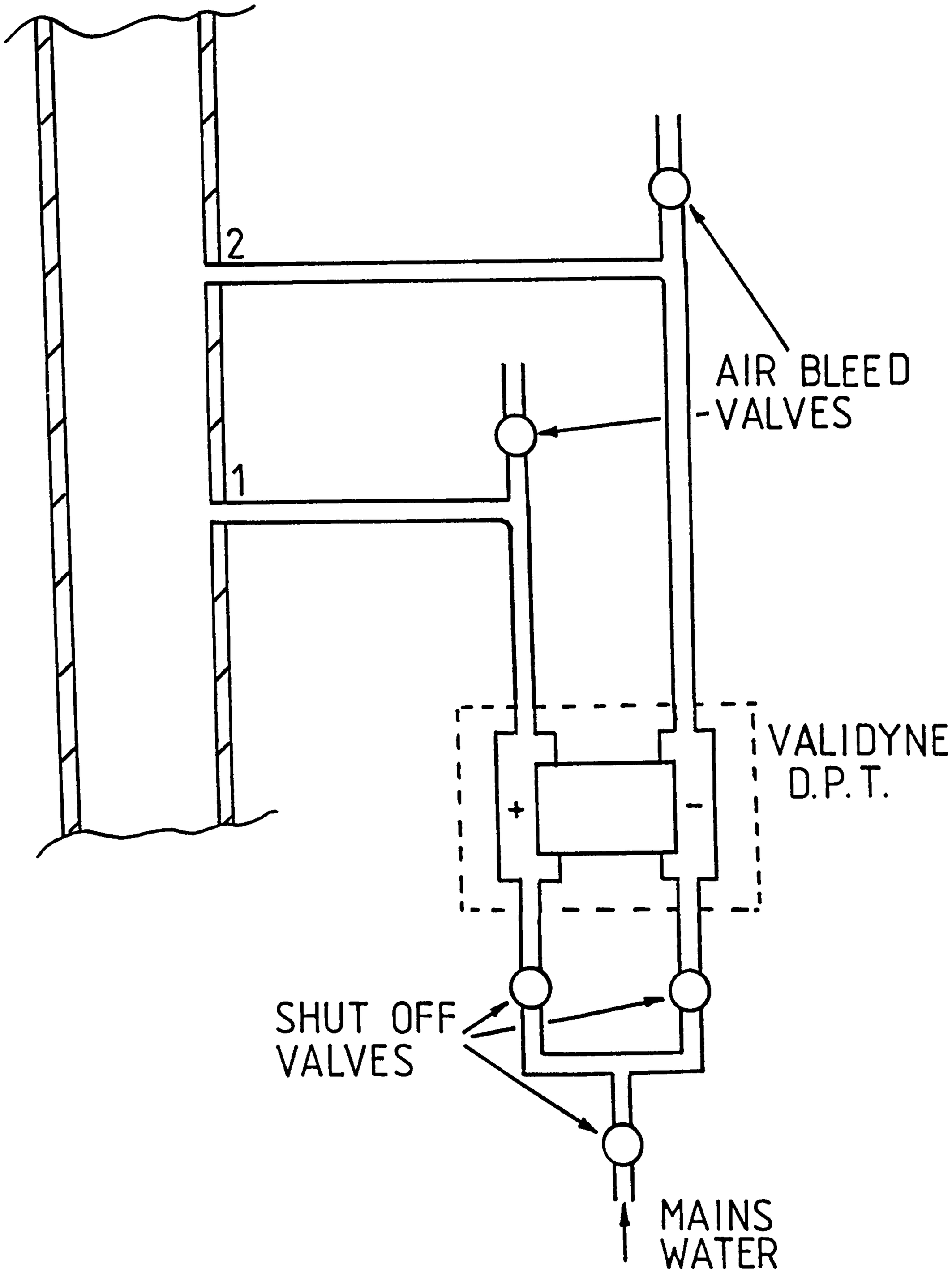

Figure 5.23 Schematic diagram of differential pressure transducer water purging and back flushing arrangement

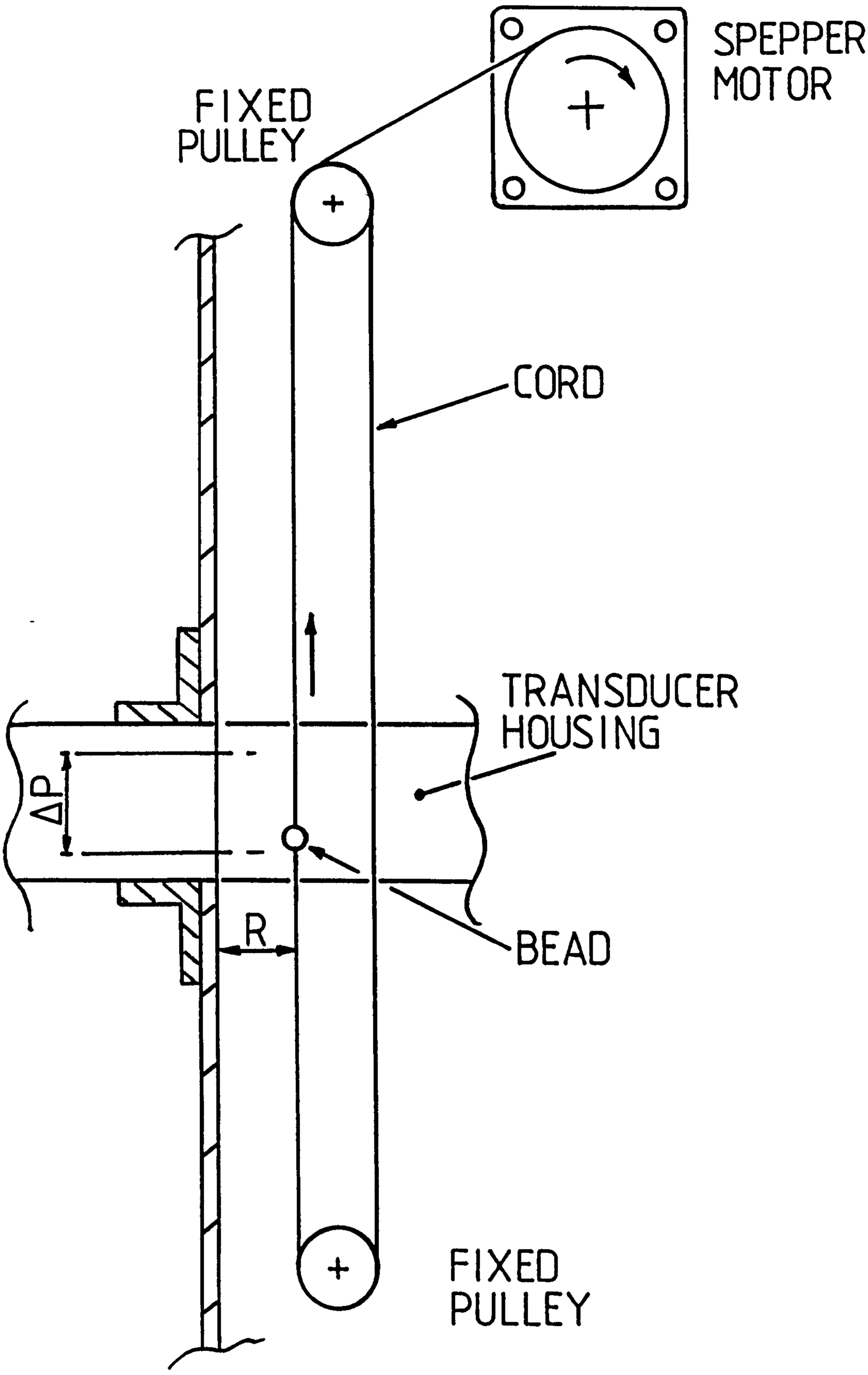

Figure 5.24 Experimental apparatus used to measure differential pressure fluctuations generated by the motion of a sphere in a stagnant column of water

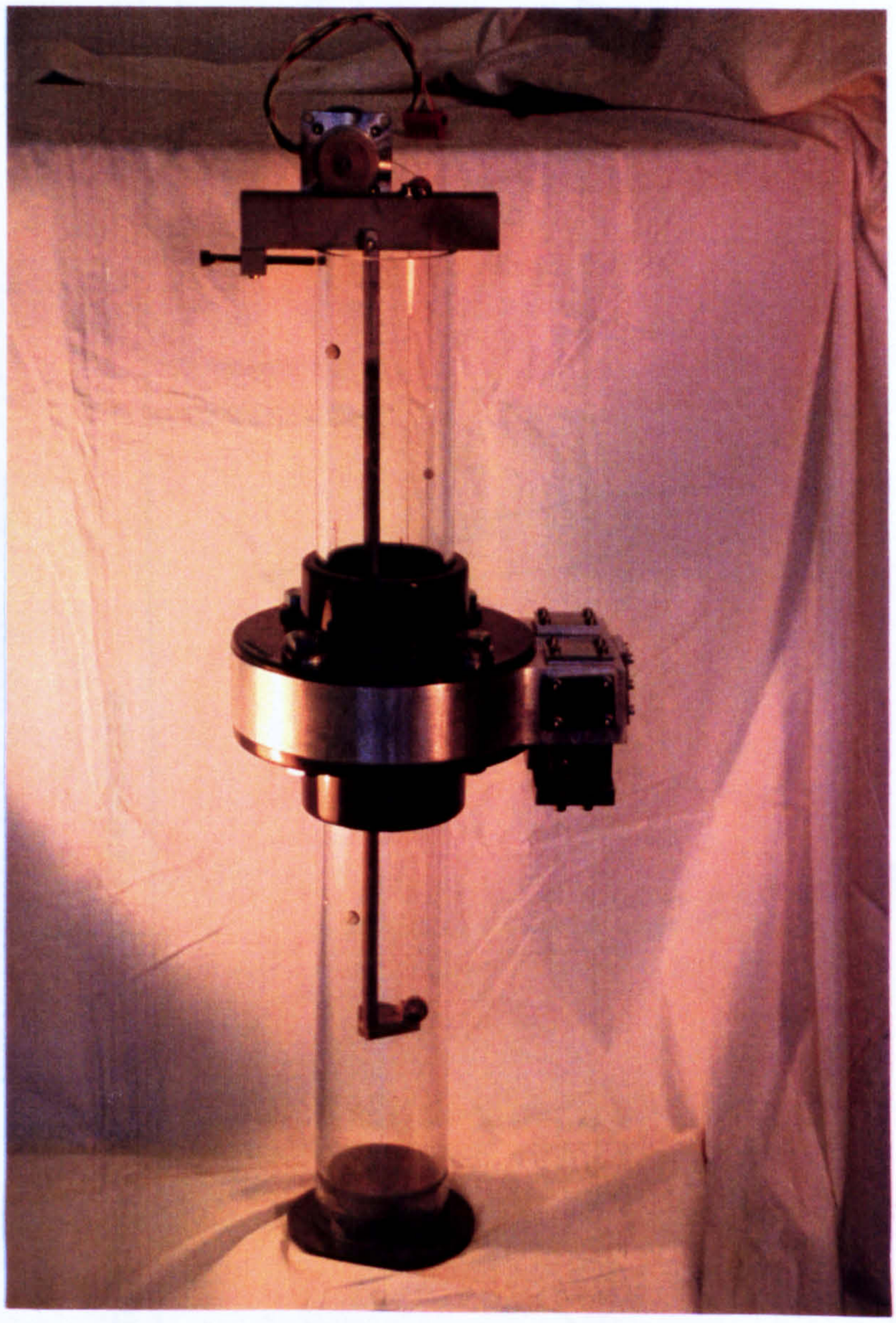

Figure 5.25 Photograph of experimental apparatus used to measure differential pressure fluctuations generated by the motion of a sphere in a stagnant column of water

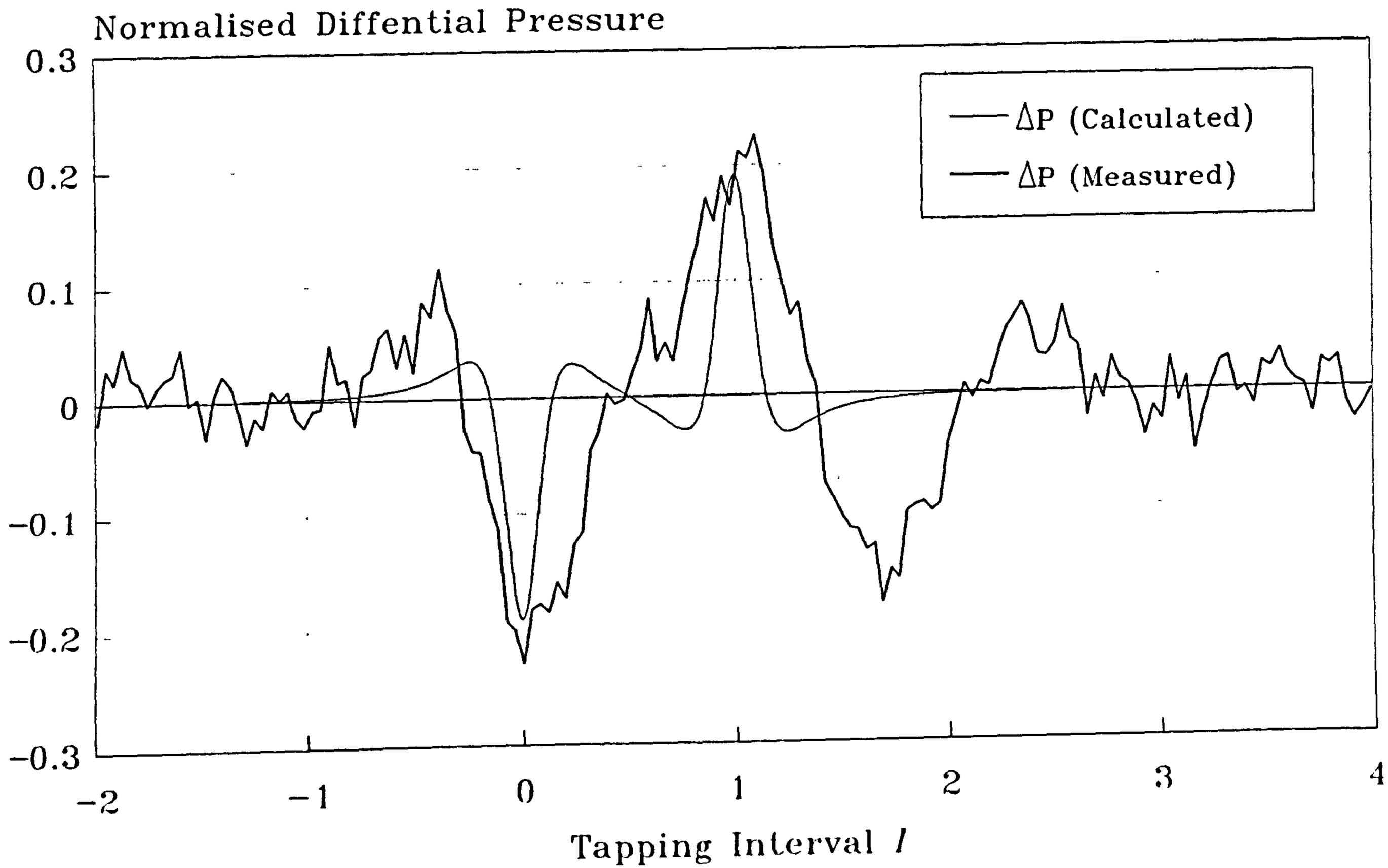

Figure 5.26 Differential pressure signal measured experimentally and calculated from equation 5.46 generated by a moving sphere of diameter 6.5mm travelling with a constant velocity of 0.25m/s at a wall to sphere centre separation distance of 4.5mm

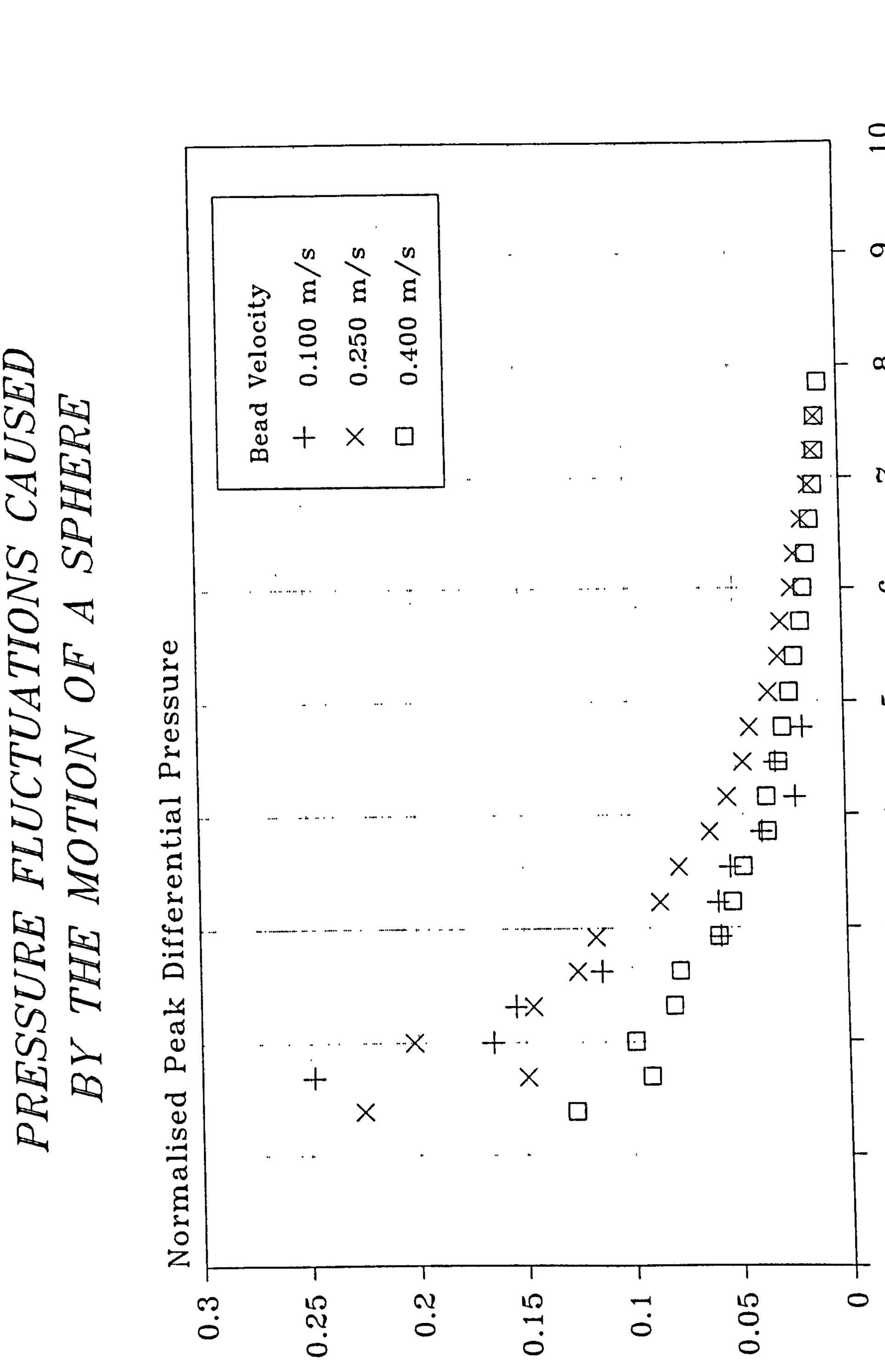

Figure 5.27 Comparison of normalised peak fluctuations in differential pressure generated by a sphere moving at constant velocities of 0.1, 0.25 and 0.4m/s, plotted as a function of the ratio of the pipe wall to sphere centre separation distance over the sphere radius

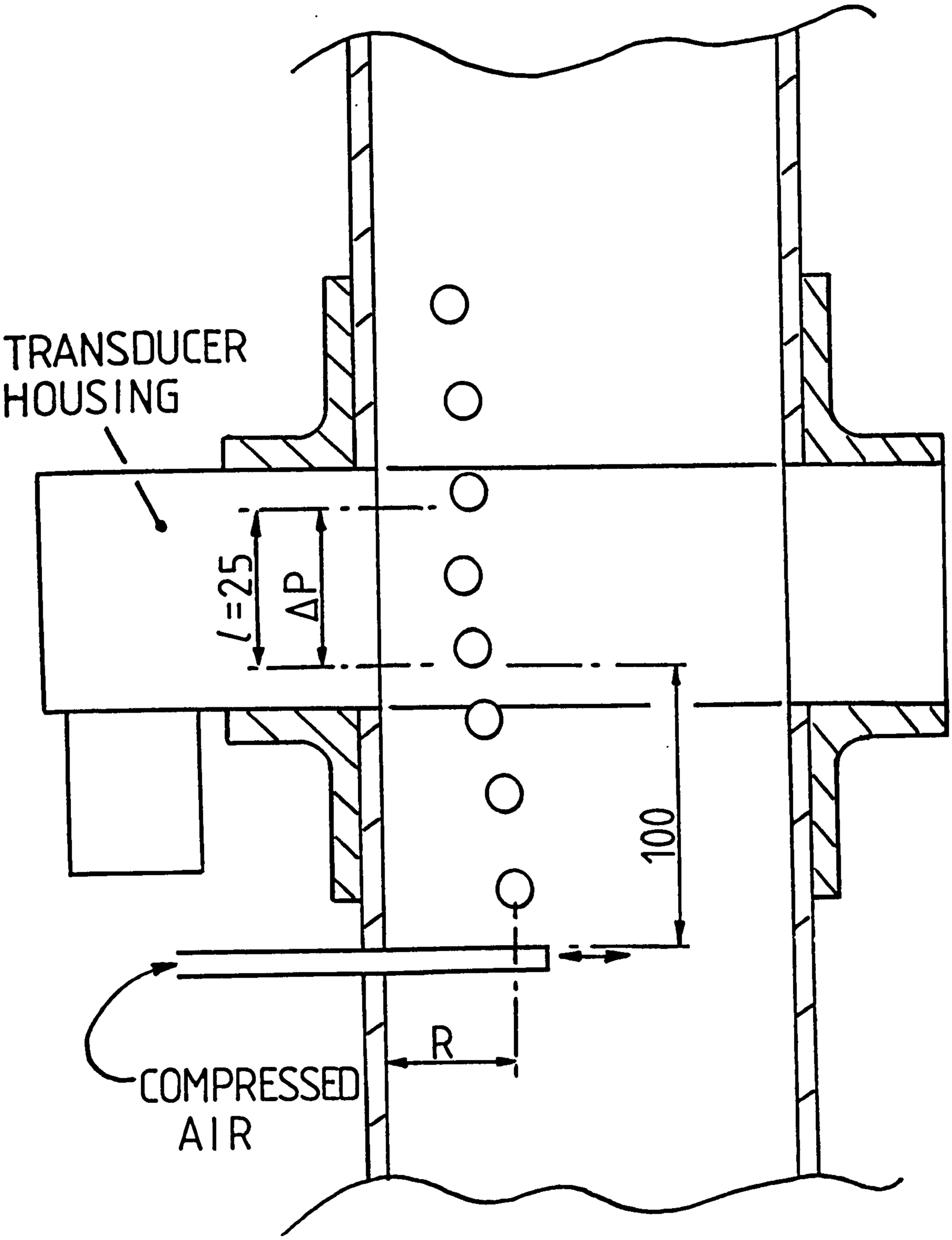

Figure 5.28 Arrangement of apparatus used to measure fuctuations in differential pressure generated by a low frequency single stream of bubbles in a stagnant column of water

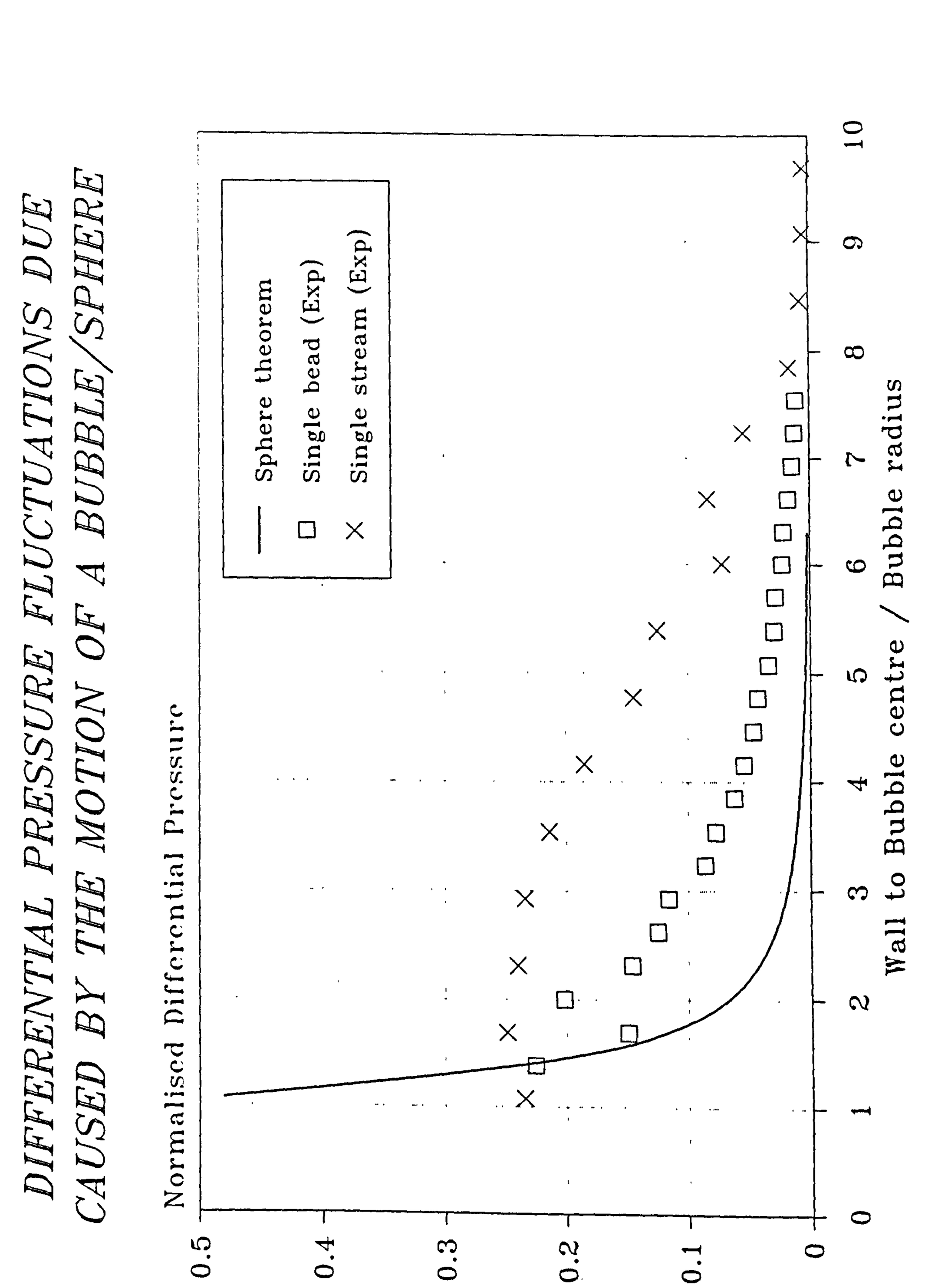

Figure 5.29 Comparison of theoretical and experimental fluctuations in differential pressure caused by the motion of a sphere/bead/bubble with a velocity of 0.25m/s

CHAPTER 6 - AUTO AND CROSS CORRELATION OF PRESSURE FLUCTUATIONS IN BUBBLY TWO-PHASE FLOW

Chapter summary

This chapter is concerned with both the computer simulation and experimental measurement of convected pressure disturbances within a bubbly two-phase flow. It is shown that the velocity of bubbles close to the pressure tappings can be evaluated by interpreting the auto and cross correlation correlograms of the naturally occurring pressure fluctuations that exist within a vertically upward bubbly two-phase flow.

The chapter initially introduces the concept of conventional auto and cross correlation models i.e. the frozen and diffused correlation models. This leads on to a description of bubbly flow phenomena which is known to exist and a description of the correlation model used in the present study. In section 6.2, previously researched velocity measurement techniques are discussed in which the cross correlation of two axially separated void fraction measuring transducers are used to evaluate the dispersed phase velocity of a bubbly two-phase flow and reasons for variations in experimental results are examined.

Section 6.3 describes the computer model developed in the present study to simulate a low average gas void fraction bubbly

two-phase flow. The computer model considers the possibility of local void fraction and velocity profiles, $\alpha_l(r)$ and $v_g(r)$ respectively and generates pseudo-random bubble positions that do not over lap. Two sources of pressure fluctuations are considered in the computer model, namely, pressure fluctuations generated by temporal variations in the average gas void fraction $\alpha(t)$, and pressure fluctuations generated by the convected pressure field surrounding a moving bubble. It is subsequently concluded that the simulated auto and cross correlation convected disturbance velocities are dominated by the velocity of bubbles near the pressure tappings, and that for a realistic practical bubbly two-phase flow with a velocity profile power, m, of 2 to 4 and a near flat local gas void fraction profile power, the predicted correlation velocity will be of the order of 0.5 of the area averaged gas velocity V_g.

Initial autocorrelations are made using a single differential pressure transducer in section 6.4 and modifications to the differential pressure transducer housing/mounting used to measure a single differential pressure signal to one which is suitable for measuring two differential pressure signals are described along with the problems associated with the matching of transducers in section 6.5.

Sections 6.6 and 6.7 are devoted to covering the experimental measurement of the convected disturbance velocities V_{g_1}, V_{g_2} and V_{g_3} for flow within a circular cross-sectioned pipe and within a circular annulus. Results are interpreted and discussed and conclusions drawn from these experimentals are summarised in section 6.8.

6.1 An introduction to the pressure correlation principle

As discussed in section 5.2, there are four main sources from which pressure fluctuations have been identified to emanate, these being (i) variations in the average gas void fraction, (ii) variations in the convected pressure field surrounding a moving bubble, (iii) the turbulence in the continuous phase generated by the wake of a bubble, and by (iv) the background turbulence present in the continuous phase. Pressure fluctuations generated by the wake and background turbulence have been argued in section 5.2 to be small in magnitude compared with pressure fluctuations associated with the dispersed phase, and it has also been observed that the wake turbulence has a very short decorrelation length scale. Therefore, in the computer model developed in section 6.3, only pressure fluctuations generated by temporal variations in the average gas void fraction and pressure fluctuations generated by the convected pressure field surrounding a moving bubble, sections 5.2.1 and 5.2.2 respectively, are considered. Results from this computer simulation demonstrate that the pressure fluctuations from the variation in local average gas void fraction is small compared with that of the convected pressure field surrounding the moving bubbles. This enables the measured pressure field to be interpreted in terms of integrated effect of many bubbles and related to the convected pressure field surrounding a single bubble.

The convected pressure field is recorded at pressure tappings separated in the longitudinal direction by a distance l in the vertical pipe. To facilitate the interpretation of both the simulation results in section 6.3 and the experimental results in section 6.5, the following conclusions concerning the pressure field

surrounding a single moving bubble should be noted.

The pressure fluctuations generated by variations in the pressure field surrounding a moving bubble (see section 5.2.2) rapidly diminish in amplitude with increasing distance from the bubble and become insignificant at distances greater than 3-4 bubble diameters. This means that bubbles further than 3-4 bubble diameters, d, from a pressure transducer tapping will contribute to the total fluctuating pressure only as a variation in local average gas void fraction, and no contribution will be detected that can be associated with bubble's motion. This information can be applied to two pressure tappings 1 and 2, separated by a distance $l > 4d$ in the flow direction, and connected to a differential pressure transducer A. The corresponding differential pressure is denoted as $\Delta P_A(t) = P_1(t) - P_2(t)$. If at any time t_1 a single bubble is located close to pressure tapping 1 then $P_1(t_1)$ will record the convected pressure associated with a distortion in the pressure field surrounding this bubble caused by its motion, while the corresponding pressure at point 2, $P_2(t_1)$, will be unchanged since point 2 is more than 4d away. If we assume the bubble moves with a velocity V_∞ in a straight line past the tapping points 1 and 2 then at a later time, t_2, tapping 2 will record the convected bubble pressure signal, $P_2(t_2)$, while the corresponding signal at 1, $P_1(t_2)$, will now be unaffected by this bubble. This is illustrated in figure 5.16 in section 5.2.2, where the simple transformation equation 5.48

$$V_\infty = \frac{l}{\tau} \qquad 5.48$$

has been applied to the autocorrelation of the differential pressure signal shown by curve d. This principle will be extended to auto and cross correlation techniques for differential pressures caused by the

integrated effect of many bubbles in section 6.1.2.

The interpretation of correlation results is therefore a complex matter, since the measured pressure signal convection time is the integrated effect of disturbances (in this case bubbles) which are distributed throughout the pipe section and which are contributing in a non-linear manner to the recorded pressure fluctuations. This chapter deals with the development of a numerical simulation to the above problem and the analysis of experimental results aimed at providing answers to the above problem.

6.1.1 Conventional frozen and diffused correlation models

In correlation flowmeter techniques, relating the transient time τ, which is the time it takes for the integrated effect of disturbances travelling with the flowing fluid to travel a distance l separating an upstream from a down-stream transducer, to the velocity of the flowing fluid requires some knowledge or assumptions to be made with regards to the velocity distribution or diffusion process of the fluid being monitored. Two conventional modelling techniques are used in cross correlation flowmeters, these are the frozen and diffused pattern models.

The basic concept behind the frozen pattern model when applied to cross correlation flowmeters assumes that some fixed pattern travels with the moving flow stream without distortion between the upstream and down-stream measurement transducers, as shown in figure 6.1. The cross correlation method of flow measurement is based upon the determination of the transit time of measurable disturbances e.g.

$P_1(t)$ and $P_2(t)$, between two points separated by a known distance l (in this discussion it is assumed P_1 and P_2 are measured separately). By evaluating the cross correlation coefficient using equation 2.20, and identifying $\rho_{12}(\tau) = 1$, then the value of τ is the time taken for the convected disturbances to travel from the upstream measurement point to the down-stream measurement point. Since there is no distortion in the fixed pattern of the signal the velocity of the convected disturbance, V, is given by an equation of the form

$$V = \frac{l}{\tau} \qquad 6.1$$

Since the frozen model assumes no distortion of the signal between the two transducers, both signals must be identical except for the time delay τ and hence a cross correlation coefficient of 1 is recorded at the peak of the curve. This being the case, then the cross correlation function is simply the autocorrelation function time shifted by τ, as shown in figure 6.1.

However, in practice, real convected flow patterns/disturbances deviate from the frozen pattern model. This is due both to the existence of velocity profiles and to turbulence within the flowing fluid. In the diffused model, the pattern that exists at the upstream measurement transducer will change as the fluid flows down-stream to the second transducer (see figure 6.2). Hence the signal at the upstream and down-stream transducers will be slightly different. The effect of this difference in signals between locations 1 and 2 will be to flatten out the cross correlation function as shown in figure 6.2, reducing the amplitude of the cross correlation coefficient i.e. $\rho_{12}(\tau) < 1$.

6.1.2 Correlation techniques of differential pressure measurements

In the present study the signals $P_1(t)$ and $P_2(t)$ from the two pressure tappings 1 and 2, which are separated by a distance l in the flow direction, were applied to a differential pressure transducer A giving a single differential pressure signal $\Delta P_A(t) = P_1(t) - P_2(t)$. The correlation techniques used to evaluate convected disturbance velocities within a bubbly two-phase flow are as follows.

(i) Autocorrelation

Consider a single bubble moving past two fixed points 1 and 2. As the recorded pressure from each tapping is a minimum when the centre of the bubble is opposite a pressure tapping (see curves a and b of figure 5.16), ΔP_A (curve c of figure 5.16) will be of maximum amplitude in the negative direction when the bubble is at measurement point 1 and a maximum positive when at point 2. Consequently evaluating the autocorrelation $\rho_{AA}(\tau)$ for the passing of a single bubble will result in a correlogram of the form of curve d in figure 5.16. When ΔP_A is evaluated for the integrated effect of many bubbles the form of the autocorrelation will be as shown in figure 6.3, where curve a corresponds to the ideal frozen correlation model, which is similar to curve d in figure 5.16, and curve b represents the experimentally observed diffusion result. From figure 6.3 the convected bubble velocity V_{g_1} can be evaluated as

$$V_{g_1} = \frac{l}{\tau_1} \qquad 6.2$$

(ii) Cross correlation

These results were obtained using two differential pressure transducers A and B, with A connected to pressure tappings 1 and 2 and B connected to 3 and 4, as shown in figure 6.4. As can be seen transducer B is shifted by a small distance h in the flow direction relative to transducer A. The two sets of pressure tappings 1, 2 and 3, 4 for each differential pressure transducer have the same tapping separation distance l = 25mm. In the present study the transducer separation distance h of 6mm has been chosen which is of the order of one bubble diameter d in this study. The cross correlation of the signal from pressure transducer A with that from pressure transducer B produces a correlogram of the form shown in figure 6.4. Two convected bubble velocities, V_{g_2} and V_{g_3}, can be evaluated from the cross correlation correlogram, these correspond to a correlation length scale of the shorter transducer separation distance h = 6mm and longer tapping separation distance l = 25mm, respectively. The two convected bubble velocities can be evaluated as

$$V_{g_2} = \frac{h}{\tau_2} \qquad 6.3$$

$$V_{g_3} = \frac{l}{\tau_3} \qquad 6.4$$

where τ_2 and τ_3 are the time delays associated with the convected bubble velocities V_{g_2} and V_{g_3}, respectively, evaluated from the cross correlation correlogram shown in figure 6.4.

Over the short distance h, deviation from the frozen pattern will be small compared to that measured over the tapping separation distance l, which is approximately 4 bubble diameters. However, the

velocity and trajectories of bubbles within a bubbly two-phase flow may affect the convected bubble velocity evaluated by V_{g_1}, V_{g_2} and V_{g_3} in the following way.

It is well known that bubbles wander in a spiralling motion during their ascent through an unbounded fluid. However, initial results from work currently being conducted by *Lance*, *Bataille* and *Marie'* [1992] using high speed video techniques, indicate that a typical bubbly two-phase flow exhibits a phenomenon in which bubbles migrate towards the test section wall where some are entrapped within a layer near the wall and others appear to travel into the layer and then 'bounce' away on a new trajectory as shown in figure 6.5. Theoretical work by *Lance*, *Bataille* and *Marie'* indicates that bubble migration is due to lift forces acting on a bubble as it travels through the continuous phase causing it to move towards the test section wall, and if a bubble velocity and size is similar to that of other bubbles near the wall then the bubble becomes entrapped in the layer near the wall causing the characteristic high local void fraction region near the test section wall as shown by curve a of figure 6.6. It has also been noticed that bubbles that 'bounce' away from the wall are both larger and travel at higher velocities than those entrapped near the wall.

The effect of the above observations by *Lance*, *Bataille* and *Marie'* on the convected autocorrelation velocity V_{g_1}, which is evaluated over the longer 25mm correlation length scale, will be that bubbles not remaining near the pipe wall i.e. the bubbles that 'bounce' away, will have little or no effect on the corresponding evaluation of the convected bubble velocity. This is because a bubble that moves in and out of the entrapped bubble layer will do so in an

axial distance which is much shorter than the correlation length scale of 25mm. However, a faster moving bubble, which generates a higher magnitude of pressure fluctuation, will affect the convected bubble velocity V_{g_2}, which is evaluated over the shorter 6mm length scale, if it enters and leaves the entrapped bubble layer near either pressure tappings 1 and 3, or 2 and 4. Consequently the evaluated convected bubble velocity V_{g_2} is expected to be higher than the convected bubble velocity evaluated from the autocorrelation V_{g_1} but lower than the velocity of bubbles in the main flow which 'bounce' away from the entrapped bubble layer. The extent to which V_{g_2} will be affected by these 'bouncing' bubbles will be a function of the number of bubbles that pass near the pressure tappings during the sampling period. The evaluation of V_{g_3} will also be affected, to some extent, by the number of bubbles that 'bounce' close to the pressure tappings since τ_3 (see figure 6.4) is the time shift between the maximum positive peak, which is associated with the 6mm correlation length scale, and the maximum negative peak. Once again the extent to which the evaluation of V_{g_3} will be affected will be a function of the number of bubbles that pass near the pressure tappings during the sampling period.

Since the observations of *Lance*, *Bataille* and *Marie'* are thought to be associated with lift forces acting on a bubble causing it to migrate towards the pipe wall, it is expected that for bubbles rising through a stagnant column the effects described above will be greatly reduced and that evaluated convected bubble velocities may not be consistent with those of a flowing continuous phase due to the absence of an entrapped bubble layer at the pipe wall from reduced lift forces acting on bubbles as they ascend through a stagnant continuous phase and therefore not causing bubble migration towards the wall. It is also expected that the amplitude of cross correlation coefficients

will be much lower since the bubbles will no longer be entrapped in a region near the pipe wall and will therefore wander during their ascent past the pressure tappings enhancing the diffusion effect.

6.2 Previous bubbly two-phase flow correlation techniques

Cross correlation of fluctuations in a bubbly two-phase flow at location, 1, with another location, 2, further down-stream have been attempted by a number of researchers (see, for example, *Bernier* [1981] and *Lucas* [1987]). The most common technique involves the monitoring of fluctuations in the average void fraction at points 1 and 2, subsequent cross correlation of these two signals is then used to evaluate the area averaged convected disturbance velocity from the known distance l between the measuring locations over the time shift τ between the signals (equation 6.1). Fluctuations in the average void fraction can be monitored by a number of techniques such as radiation absorption, light absorption, impedance or capacitance techniques. Of these the two most common techniques are the impedance and capacitance techniques which were described in section 2.1.4, however, conflicting convected dispersed phase velocity results have been observed from these two techniques and reasons for the discrepancies are discussed below.

It is well known that within a bubbly two-phase flow there will exist both a local void fraction profile and a corresponding local dispersed phase velocity profile across the test section, similar to those shown in figure 6.6. From the work currently being carried out by *Lance, Bataille* and *Marie'* at the *Laboratorire de Mecanique des Fluides et d'Acoustique* in Lyon, (mentioned in section 6.1.2) a

typical bubbly two-phase flow tends to show regions of high local void fraction near the test section walls as shown by curve a in figure 6.6. *Lance, Bataille* and *Marie'* believe the reason for this region of high local void fraction near the pipe wall to be due to migrating bubbles becoming entrapped within a layer at the pipe wall.

A typical corresponding local dispersed phase velocity profile is shown in curve b of figure 6.6. Curve b indicates that bubbles near the pipe wall travel significantly slower than bubbles near the centre of the test section. The reason for this velocity profile is thought to be primarily due to friction effects at the pipe wall where the velocity of the continuous phase approaches zero. If we therefore consider a bubble which is travelling close to the pipe wall, its velocity will be less than the area averaged dispersed bubble velocity, similarly if a bubble is away from the wall near the centre of the pipe its velocity will be greater than the area averaged velocity.

Let us return then to the case of the dispersed bubble velocity measurements evaluated from the cross correlation of void fraction fluctuation, with the above description of a bubbly two-phase flow in mind. It is not difficult to appreciate that if the void fraction transducer being used to monitor fluctuations performs in a way that spatially filters the flow within the pipe i.e. the transducer does not have a uniform sensitivity and is therefore more sensitive to a particular region or event within the flow, then the result of cross correlating such signals will be to reflect the velocity of disturbances within this region or event (see *Hammer* & *Green* [1982]). For example consider a void fraction monitoring transducer with a non-uniform sensitivity across the diameter of the test section, which

is more sensitive to fluctuations in void fraction nearer the centre of the test section. Then cross correlation of signals from two such transducers will result in the evaluation of a higher than average dispersed bubble velocity. Similarly if the transducer is more sensitive to fluctuations near the pipe wall, this will be reflected in the evaluation of lower than area averaged dispersed bubble velocities. The spacial filtering effect may also be extended to cover void fraction monitoring transducers that are more sensitive to particular ranges of void fractions, such as high or low, and therefore, cross correlation of these signals will reflect the velocity of bubbles within that particular void fraction region.

Lucas [1987] cross correlated the measurements of two axially separated, so termed, 'uniform field strength' capacitance void fraction monitoring transducers in vertically upward and inclined bubbly air/water two-phase flow. Superficial gas and liquid velocities, V_{sg} and V_{sl} respectively, were calculated using equations 1.1 and 1.2 knowing the two volume flow rates entering the test section and the cross-sectional area of test section whose diameter D = 77.8mm. The average gas void fraction α was monitored using the gradiomanometer technique described in section 4.1.2, and local gas void fractions $\alpha_l(r)$ were measured using hot-film anemometry (see section 2.2.3). In this study the axial separation l between the two transducers was 160mm or $l \simeq 2D$. Cross correlation of the two signals produced correlograms whose peak positions were used to evaluate the transit time of the signal τ, and the corresponding convection velocity was evaluated using equation 6.1.

The cross correlation convected bubble velocities were compared with high speed serial photography of the bubbly two-phase flows, and

area averaged gas velocity calculated from equation 1.12. *Lucas* found that in vertically upward bubbly two-phase flows, the convection velocity obtained by his cross correlation measurement technique gave results which were always in excess of the actual area average dispersed phase velocity. He suggests that the reason for the cross correlation velocity measurements being higher than those expected is caused by his transducer being more sensitive to the larger faster moving bubbles which were present in his experimental apparatus near the centre of his test section, and so spatially filter out the slow moving bubbles near the pipe wall.

Hammer [1983] performed a series of cross correlation measurements in vertically upward, bubbly air/water two-phase flows also using two capacitance noise transducers. *Hammer*, like *Lucas*, measured cross correlation velocities which were substantially faster than the actual area averaged dispersed bubble velocity. *Hammer* also observed that as the average gas void fraction increased, the difference by which the cross correlation velocity exceeds the area averaged dispersed phase velocity increased rapidly. *Hammer* [1983] and *Lucas* [1987] both account for their respective discrepancies in the measured area averaged bubble velocities by suggesting that their respective capacitance transducers are more sensitive to detecting larger faster moving bubbles in the centre of the flow which are generally travelling quicker than the actual area averaged bubble velocity.

However, experiments carried out by *Bernier* [1981] in which he attempted to measure the average velocity of structures in vertically upward bubbly air/water two-phase flows using two flush mounted impedance monitoring void fraction transducers, which were axially

separated by a distance *l*, found, in contradiction to *Hammer* [1983] and *Lucas* [1987], that evaluated cross correlation velocities were always lower than the actual area averaged bubble velocity. In this study by *Bernier*, he assumes the flow to be both one-dimensional and under steady state conditions. In *Berniers* analysis of a theoretical bubbly two-phase flow, he considered the possibility of a long section of flow, at any instant in time, being divided up into discrete regions of constant average gas void fraction, however, the value of average gas void fraction within each region may vary from region to region. These regions of constant average gas void fraction, he suggests, are separated by structures in the flow and from experimental work he concludes that his impedance cross correlation technique does not measure the area average bubble velocity of the flow but actually measures the velocity of these structured waves, which he termed 'infinitesimal kinematic waves'.

Bernier [1981] suggests that his 'infinitesimal kinematic waves' are similar to those of *Lighthill* and *Whitham* [1955] in which the propagation of traffic flow disturbances along major arterial roads were studied. An analogy can be drawn between discrete bubbles flowing along a pipe in a bubbly two-phase flow and discrete cars all travelling in the same direction along a crowded road. It is reported by *Lighthill* and *Whitham* that the propagation speed of a kinematic wave will be less than the average velocity of the vehicles and that vehicles will have to decrease their speed when entering the wave and can only increase their speed gradually on leaving the wave, hence causing a concentration within the flow around the wave. This is similar to the situation considered by *Bernier* described above.

Bernier goes on to state that for a given average gas void fraction and superficial liquid velocity, the cross correlation velocity agreed closely with the infinitesimal kinematic wave speed, however, the measured cross correlation velocities were always lower than the actual area average gas velocity which is calculated from the volume flow rate of gas and the average gas void fraction using equations 1.1 and 1.12. *Kyatomaa* [1987] using the same flow loop as *Bernier* conducted a series of cross correlation experiments using virtually identical impedance transducers to *Bernier* except *Kytomaa* employed shielding electrodes on either side of the measurement electrodes. *Kyatomaa's* experiments tend to confirm *Bernier's* findings and both agree that impedance cross correlation measurements in bubbly two-phase flows reflect the propagation velocity of the infinitesimal kinematic waves and not the area averaged velocity of the dispersed bubbles.

Although *Bernier* [1981] and *Kyatomaa* [1987] concluded that they are measuring the kinematic wave speed and not the area averaged bubble velocity, the discrepancies observed between the evaluated cross correlation velocity and the actual area averaged bubble velocity can also be explained from a spatial filtering point of view. For example, if their respective impedance monitoring void fraction transducers do not have a uniform field sensitivity and are more sensitive to the slower moving bubbles near the pipe wall, filtering out the faster moving bubbles near the centre of the pipe, then the cross correlation velocity will reflect the velocity of the bubbles near the pipe wall. Since these bubbles tend to travel slower than the area averaged bubble velocity, this could also account for the discrepancies observed by *Bernier* [1981] and *Kyatomaa* [1987].

Correlation of pressure fluctuations have been attempted most recently by *Matsui* [1984]. He investigated the statistical properties of pressure fluctuations in two-phase flows, but could obtain no cross correlation for the bubbly flow regime. One reason for this may be due to the large transducer separation distance of 200mm. Unfortunately, *Matsui* did not reproduce any autocorrelation correlograms to support the theory that his transducers are separated by a distance larger than the correlation length scales of structures in the flow (see chapter 5). It should also be noted that, the cross correlation of fluctuations in two static pressure measurements, as attempted by *Matsui* [1984], may generate large errors in the position of the correlation peak caused by test section vibration and transducer mis-matching as discussed in section 5.3.

It is also worth mentioning that the transducer separation distances, l, used by *Bernier* [1981], *Kyatomaa* [1987], *Hammer* [1983], and *Lucas* [1987] are all in the order of two pipe diameters, $l \simeq 2D$, which is much larger than found acceptable in this study (see section 5.5). This would indicate that impedance and capacitance void fraction measuring transducers are more sensitive to much larger scale structures in the bubbly two-phase flow than those being detected in the present study using differential pressure fluctuations.

6.3 Modelling technique used to simulate bubbly two-phase flow in a vertical pipe

The mathematical modelling of a turbulent process such as the movement of bubbles in bubbly two-phase flow is extremely complex. Therefore, a simpler, but not unrealistic, approach to modelling this

phenomenon has been developed in the present study in order to help evaluate experimental data gathered in this investigation. In the computer simulation only pressure fluctuations generated by temporal variations in the average gas void fraction and variations in the convected pressure field surrounding a bubble are included.

The convective velocities of the pressure field related to disturbances caused by temporal variations in the average gas void fraction and by the motion of bubbles were evaluated in the following way.

The pressure field created by the moving bubbles were monitored by two differential pressure transducers A and B which were connected to the pressure tappings 1 to 4 as shown in figure 6.4. In the computer simulation the contribution to the differential pressures at any instant in time t from the two pressure sources were evaluated for a pipe of length L and diameter D with spherical bubbles of a constant diameter d pseudo-randomly positioned (see section 6.3.3) in the r, Φ, and z co-ordinate system as shown in figure 6.7 and none of these spheres occupy the same space in the pipe.

6.3.1 Contribution from temporal variations in the average gas void fraction

Assuming the two phases to be inviscid and incompressible, the magnitude of differential pressure $\Delta P_A(t)$ and $\Delta P_B(t)$ associated with temporal variations in the average void fraction, $\alpha(t)$, for a differential pressure transducer. $\alpha(t)$ will be defined as being the average gas void fraction of the fluid contained within the control

volume bounded by the pipe wall and cross-sections associated with the pressure transducer tappings P_1 & P_2 or P_3 & P_4, as shown in figure 6.4, at any instant in time t. $\alpha(t)$ can be related to the local mixture density $\rho_{ml}(t)$ contained within the control volume by

$$\rho_{ml}(t) = \rho_g\alpha(t) + \rho_l(1-\alpha(t)) \qquad 6.5$$

where ρ_g and ρ_l are the gas and liquid densities respectively. The corresponding differential pressure between tappings separated by a distance l is given by *Bradbury* [1988] as

$$\Delta P(t) = \rho_{ml}(t)\ g\ l \qquad 6.6$$

for either transducer A or transducer B.

In order to simulate this source of pressure fluctuation it is necessary to determine the magnitude of $\alpha(t)$ at any instant in time. If we consider an elemental slice, A, of width l, through the pipe as shown in figure 6.8, then the ratio of volume occupied by the spheres in this elemental slice to the total volume of the elemental slice is a measure of the temporal average gas-void fraction $\alpha(t)$ at that instant in time. The value of average gas void fraction for transducer A, $\alpha_A(t)$, at time t can then be used in equations 6.5 and 6.6 to evaluate the differential pressure measured by transducer A, $\Delta P_A(t)$, within the elemental slice that contributes to the total differential pressures measured by transducer A at that moment in time. Consider further a second elemental slice, B, also of width l, positioned down-stream of slice A by a distance h so that they over lap by an amount l-h as shown in figure 6.8. Then the temporal value of average gas void fraction $\alpha_{lB}(t)$ for transducer B can be evaluated

at the same instant in time t and consequently the contribution in differential pressure, $\Delta P_B(t)$, to the total differential pressure measured by transducer B can also be evaluated.

6.3.2 Contribution from the convected bubble pressure field

If the flow is assumed to be axisymmetrical and irrotational then the differential pressures $\Delta P_A(t)$ and $\Delta P_B(t)$, at any instant in time t, caused by the convected pressure field surrounding a single bubble was estimated for a moving sphere in an infinite fluid in section 5.2.2. The differential pressure, $\Delta P = P_1 - P_2$, was derived from *Butlers* sphere theorem, between two wall pressure tappings which were axially separated by a distance *l*. The equations derived in section 5.2.2 can be applied to two differential pressure transducers, A and B, which are positioned a short distance, h, apart (where $h \simeq d$) as shown in figure 6.9. If a bubble is travelling with a constant velocity $V_{g\infty}$, and we assume there to be no interaction between bubbles in the flow, and no interaction with the pipe wall, then at an instant in time t a gas bubble's position will be given by the polar rectangular co-ordinates r, Φ, and z as shown in figure 6.9. The differential pressures measured by transducers A and B at time t, $\Delta P_A(t)$ or $\Delta P_B(t)$, generated by the convected pressure field surrounding this bubble will be given by

$$\Delta P_A(t) = \frac{1}{2}\rho_l V_{g\infty}^2 \left[\left[1 + \frac{a^3}{r_2^3}\left[1-3\cos^2\theta_2 \right] + \frac{a^6}{4r_2^6}\left[1+3\cos^2\theta_2 \right] \right] - \left[1 + \frac{a^3}{r_1^3}\left[1-3\cos^2\theta_1 \right] + \frac{a^6}{4r_1^6}\left[1+3\cos^2\theta_1 \right] \right] \right] \qquad 6.7$$

where ρ_l is the liquid density, 'a' the radius of the bubble, and r_1,

r_2, θ_1, and θ_2 are given below as

$$r_1 = \sqrt{\left[\frac{(D/2) - r\cos\Phi}{\sin\theta_1}\right]^2 + \left[r\sin\theta_1\right]^2} \qquad 6.8$$

$$r_2 = \sqrt{\left[\frac{(D/2) - r\cos\Phi}{\sin\theta_2}\right]^2 + \left[r\sin\theta_2\right]^2} \qquad 6.9$$

$$\theta_1 = \tan^{-1}\left[\frac{(D/2) - r\cos\Phi}{z_1 - z}\right] \qquad 6.10$$

$$\theta_2 = \tan^{-1}\left[\frac{(D/2) - r\cos\Phi}{(z_1 + l) - z}\right] \qquad 6.11$$

and

$$\Delta P_B(t) = \frac{1}{2}\rho_l V_{g\infty}^2\left[\left[1+\frac{a^3}{r_4^3}\left[1-3\cos^2\theta_4\right]+\frac{a^6}{4r_4^6}\left[1+3\cos^2\theta_4\right]\right] - \left[1+\frac{a^3}{r_3^3}\left[1-3\cos^2\theta_3\right]+\frac{a^6}{4r_3^6}\left[1+3\cos^2\theta_3\right]\right]\right] \qquad 6.12$$

where r_3, r_4, θ_3, and θ_4 as given below

$$r_3 = \sqrt{\left[\frac{(D/2) - r\cos\Phi}{\sin\theta_3}\right]^2 + \left[r\sin\theta_3\right]^2} \qquad 6.13$$

$$r_4 = \sqrt{\left[\frac{(D/2) - r\cos\Phi}{\sin\theta_4}\right]^2 + \left[r\sin\theta_4\right]^2} \qquad 6.14$$

$$\theta_3 = \tan^{-1}\left[\frac{(D/2) - r\cos\Phi}{(z_1 + h) - z}\right] \qquad 6.15$$

$$\theta_4 = \tan^{-1}\left[\frac{(D/2) - r\cos\Phi}{(z_1 + h + l) - z}\right] \qquad 6.16$$

By summing the individual contributions in differential pressure to $\Delta P_A(t)$ and $\Delta P_B(t)$ from all of the bubbles in the pipe assuming they all travel only in the z direction and each having an individual bubble velocity, $V_{g\infty}$, that is a function of its radial position, r, within the pipe (see section 6.3.3). Then the total differential pressure (from all the bubbles) between the tappings P_1-P_2 = $\Delta P_A(t)$ and P_3-P_4 = $\Delta P_B(t)$ can be predicted mathematically at any instant in time t provided the size and position of bubbles within the two-phase flow are known at that instant in time.

However, it has been shown in section 5.2.2 that pressure fluctuations generated by the movement of a sphere becomes insignificant at distances greater than approximately 3-4 bubble diameters. Consequently since the test section diameter D used in this model (and in experimental studies) is in the order of 12 bubble diameters, only bubbles within one pipe radius (approximately 6 bubble diameters) of the pressure tappings will be considered in the computer simulation to reduce computation time.

Consequently, using the model described above and adding the contributions to the differential pressures $\Delta P_A(t)$ and $\Delta P_B(t)$ from the two pressure sources, an evaluation of the total differential pressures measured by transducers A and B can be made at any instant in time t. However, after a short time interval Δt, the position of the bubbles will have changed. Hence repeating the calculation for the total differential pressure for the two transducers A and B, for t = t+Δt, N number of times, will result in a time series history of

discrete total differential pressure values for transducers A and B.

6.3.3 Computer modelling techniques used to simulate bubbly two-phase flow

The software used in the modelling of pressure fluctuations in bubbly two-phase flow was split into two programs which can be found in appendix 3 & 4 respectively. The first program is used to generate the random bubble co-ordinates within a modelled test section and used to simulate two-phase flow conditions such as local void fraction profiles $\alpha_l(r)$ and dispersed phase velocity profiles $v_g(r)$ and evaluating the differential pressures $\Delta P_A(t)$ and $\Delta P_B(t)$ at discrete time intervals Δt. Two channels of simulated discrete differential pressure signals representing $\Delta P_A(t)$ and $\Delta P_B(t)$, as shown in figure 6.4, are generated and stored in files on computer discs. These files can then be analysed using the second program which is a general purpose signal analysis package written to analyse the auto and cross correlations of experimental or modelled pressure transducer data. This section describes in some detail the theory behind the generation of random bubble co-ordinate data with known local void fraction profiles $\alpha_l(r)$, and flow simulations in which the differential pressures signals $\Delta P_A(t)$ and $\Delta P_B(t)$ are evaluated in the present study.

Consider a section of pipe, L long and of internal diameter D, that is divided radially into a series of six annular tubes that fit inside of each other. Each annulus has a thickness of one bubble diameter d, which has been chosen in this simulation to be 6.5mm as shown in figure 6.10. Then for a given average gas void fraction α

over the length of the pipe L, and the shape of the local void fraction profile $\alpha_l(r)$, then the gas void fraction contained in each of the annular tubes can be calculated to maintain the local void fraction profile $\alpha_l(r)$ across the diameter of the pipe. This produces a step like simulated local void fraction profile as shown in figure 6.10. In this simulation only power law void fraction profiles of the form given in equation 6.17 are considered where α_c is the centreline local gas void fraction.

$$\alpha_l(r) = \alpha_c \left[1 - \left[\frac{r}{(D/2)} \right]^n \right] \qquad 6.17$$

For a given α and n the centreline local void fraction α_c were evaluated from

$$\alpha = \frac{1}{\pi R^2} \int_0^R \alpha_l(r)\, 2\pi r\, dr \qquad 6.18$$

Knowing the desired gas void fraction for each of the annular tubes, spherical bubbles of diameter d are distributed randomly throughout both the axial length L of the annulus and angularly within the annulus, ensuring that no two bubbles occupy the same space, until the desired annular void fraction is reached. Annular tubes filled with bubbles were generated with random z, and Φ co-ordinates, with radial r co-ordinates corresponding to the mid annular radial position of each annulus respectively. Consequently, when the annular tubes are observed as a complete pipe, bubbles are seen to be located pseudo-randomly with a known average gas void fraction α over the whole pipe with a known local void fraction profile $\alpha_l(r)$ across the diameter of the pipe that is constant throughout the length of the pipe i.e. simulating fully developed two-phase bubbly flow with a local void fraction profile $\alpha_l(r)$.

In the computer simulation, the initial position of bubble centres generated as described above are stored in a three dimensional array containing z, r, and Φ co-ordinates. The contents of this array can be stored on computer disc as a simulated bubble data file which can be re-loaded time and time again so that variations in the bubble velocity profile can be studied using the same bubble/void fraction data.

Using generated bubble/void fraction data with the required average gas void fraction α and local void fraction profile $\alpha_l(r)$, flow of the two-phase fluid is simulated in a series of discrete time steps of interval Δt. Δt can be considered to be similar to the sampling time interval when recording discrete experimental data from an analogue source. If we assume that bubbles only travel in the z direction, then for a known bubble velocity profile $v_g(r)$ and area averaged gas velocity V_g, the bubble velocity at any radial position r can be calculated. In the present study only power law bubble velocity profiles of the form

$$v_g(r) = V_c \left[1 - \left[\frac{r}{(D/2)} \right]^m \right] \qquad 6.19$$

are considered where V_c is the centreline bubble velocity. For a given V_g and m the centreline bubble velocity V_c was evaluated from

$$V_g = \frac{1}{\pi R^2} \int_0^R v_g(r)\, 2\pi r\, dr \qquad 6.20$$

Having evaluated the velocity of a particular bubble, $v_g(r)$, at radius r, the axial distance Δz the bubble will travel in the time interval Δt, assuming a constant velocity, is simply $\Delta z(r) = v_g(r)\Delta t$. The distance Δz can then be added to the current position of the bubble, z, contained in the three dimensional array to obtain a new

bubble z position for use in subsequent calculations. This procedure is carried out for all bubbles in the simulation, hence, giving the appearance of bubble movement in discrete time steps. Initially when bubble centre co-ordinates are generated, it is defined that no two bubbles can occupy the same space within the simulated test section, since all the bubbles within a particular annulus of the simulated test section will travel with the same velocity, since they have the same radial position r, this initial requirement will be maintained throughout the whole simulation. In this model coalescence of bubbles causing variations in bubble diameter/volume which would affect the velocity and convected pressure field surrounding a bubble are not considered, bubble break up is also not considered. To make efficient use of the generated bubble/void fraction data, if the z co-ordinate of a bubble becomes greater than the length of the pipe L, L is subtracted from z thus giving the appearance of the bubble re-circulating to re-enter the bottom of the test section.

In the computer simulation pressure fluctuations are evaluated at four simulated wall tappings 1, 2, 3 and 4 which are axially in line and arranged as shown in figure 6.9, the position of pressure tapping 1 in the simulated test section being at a distance of L/2 from the inlet. The differential pressures $\Delta P_A = P_1-P_2$ and $\Delta P_B = P_3-P_4$ are evaluated, at each time interval Δt, from the co-ordinates of bubble centres contained in the three dimensional array using equations 6.5 through 6.16 which are defined in sections 6.3.1 and 6.3.2. The simultaneous evaluation of differential pressures ΔP_A and ΔP_B which are axially separated by short distance h = 6mm, at time interval Δt, generates a simulated time history of differential pressures $\Delta P_A(t)$ and $\Delta P_B(t)$ for a particular set of bubbly two-phase flow conditions. In the computer model L = 1m, D = 78mm, d = 6.5mm,

the tapping separation distance l = 25mm between P_1,P_2 and P_3,P_4, and the transducer separation distance h = 6mm. These sizes have been chosen since they represent the experimental conditions present in this study. However, in the computer model these can be varied easily and quickly to accommodate other theoretical conditions.

Using the model described above two channels of discrete differential pressure signals $\Delta P_A(t)$ and $\Delta P_B(t)$ were simulated and stored on computer disc for subsequent correlation evaluation. The record length of the discrete pressure signals being equal to the product of the number of samples N, multiplied by the sample time interval Δt.

The computer system on which both the naturally occuring pressure fluctuations in bubbly two-phase flows were simulated and the statistical analysis package was developed was an Acorn Archimedes 440 computer with 4 MBytes of ram which is more than adequate for the large data arrays generated. This machine, with its Reduced Instruction Set (RISC) microprocessor, exploits the high speed processing power (≃4 Mips) of the relatively new RISC based computer systems. Its ability to run high level compiled languages both quickly and efficiently makes it an ideal choice for this simulation. The software language chosen in this application was 'ANSI C'. This is a modern compiled language that is particularly suitable for high speed numerical computation and has the ability to be portable between computer systems with the minimum of source code modifications.

6.3.4 Results of two-phase flow modelling

Using the computer model described previously in sections 6.3 for vertically upward bubbly air/water two-phase flow, a series of simulations were conducted for an average gas void fraction α of approximately 5%, and local void fraction profiles, $\alpha_l(r)$, specified by the power n (defined in equation 6.16) in the range 1 - 7, and the special case of a flat local void fraction profile where $n = \infty$. It is assumed that the superposition theory applies in the case of a moving continuous phase and therefore a stagnant column of liquid was assumed in these simulations since increasing the superficial liquid velocity V_{sl} will simply shorten the cross correlation transient time measurements in this model. Bubble velocity profiles, $v_g(r)$, were calculated using values of m in the range from 1 - 7 and a bubble velocity specified by an area averaged gas velocity $V_g = 0.25$m/s which is frequently used as the terminal bubble rise velocity for bubbles in a stagnant infinite fluid (see section 5.1). N, the number of discrete sample points within the simulation equalled 4096 (2^{12}) in these simulations with a sample time interval $\Delta t = 0.4$ms, giving a record length of approximately 1.64 seconds.

Initial simulations were carried out to compare the magnitudes of the two simulated pressure sources caused by (i) temporal variations in the average gas void fraction, $\alpha(t)$, and (ii) by the convected pressure field surrounding a bubble generated by its motion. Figure 6.11 shows a plot of the fluctuations in pressure caused by these two simulated pressure sources (evaluated in mm H_2O) for a bubbly two-phase flow of approximately 5% with local bubble velocity and void fraction profile powers, m and n, of 7 and 7 respectively, and an area average gas velocity $V_g = 0.25$m/s. It is clearly shown

from figure 6.11 that the magnitude of pressures associated with the motion of bubbles within this simulated two-phase flow is significantly larger than the magnitude of pressures associated with the temporal variation in the average gas void fraction. It is also observed from figure 6.11 that the shape of the fluctuating pressure signal associated with a bubbles motion resembles those observed for a single bubble (curve c of figure 5.16), the deviation from the single bubble curve being due to the integrated effect of many bubbles.

The results of these initial simulations described above clearly demonstrate that in simulated low void fraction bubbly two-phase flow, which is expected to model a realistic bubbly two-phase flow, differential pressures will be dominated by pressure fluctuations generated by the motion of bubbles. It has been argued in section 5.2.2 that these bubbles must be close to the pressure tappings and hence the pipe wall since the magnitude of the convected pressure field surrounding a bubble diminishes rapidly with increasing distance from the bubble centre and at a distance of 3-4 bubble diameters becomes insignificant. It is therefore predicted that in both numerical simulations and experimental measurements the differential pressures evaluated by two transducers A and B will be dominated by pressure fluctuations associated with a bubbles motion close to the pipe wall, which when auto and cross correlated, the convection velocities evaluated using equations 6.2, 6.3 and 6.4 will reflect the velocity of bubbles near the pipe wall.

Subsequently simulated differential pressure records $\Delta P_A(t)$ and $\Delta P_B(t)$ were statistically analysed using the auto and cross correlation signal analysis program detailed in appendix 4. The corresponding calculated convection velocities were evaluated as

described in section 6.1.2 as

$$V_{g_1} = \frac{l}{\tau_1} \qquad 6.2$$

$$V_{g_2} = \frac{l}{\tau_2} \qquad 6.3$$

$$V_{g_3} = \frac{l}{\tau_3} \qquad 6.4$$

where τ_1, τ_2 and τ_3 are the time delays associated with the convected bubble velocities V_{g_1}, V_{g_2} and V_{g_3}, evaluated from the auto and cross correlation correlogram shown in figures 6.3 and 6.4 respectively. The tabulated results given below are displayed in terms of the local bubble velocity and void fraction profile powers, m and n respectively and have been normalised by the area averaged gas velocity V_g.

Table 6.1 shows how the predicted convected disturbance velocity V_{g_1} evaluated from the autocorrelation using equation 6.2, varies in the simulation as a function of the velocity and local void fraction profile powers m and n respectively.

$\alpha_l(r)_n$ \ $v_g(r)_m$	1	2	3	4	5	6	7
Flat	0.382	0.491	0.574	0.639	0.721	0.769	0.818
7	0.410	0.547	0.623	0.689	0.784	0.843	0.876
6	0.376	0.531	0.610	0.683	0.772	0.876	0.921
5	0.643	0.546	0.867	0.736	1.096	1.172	1.108
4	0.627	0.569	0.787	0.722	1.043	1.018	1.061
3	0.529	0.539	0.836	0.779	1.077	1.111	1.062
2	0.406	0.489	0.595	0.676	0.724	0.787	0.813
1	0.364	0.423	0.384	0.805	0.550	0.455	0.471

Table 6.1 $\dfrac{\text{Autocorrelation convected disturbance velocity}}{\text{Area averaged gas velocity}}$ $\dfrac{V_{g_1}}{V_g}$

Table 6.2 shows how the predicted convected disturbance velocity V_{g_2} evaluated from the cross correlation over the 6mm length scale using equation 6.3, varies in the simulation as a function of the velocity and local void fraction profile powers m and n respectively.

$\alpha_l(r)_n$ \ $v_g(r)_m$	1	2	3	4	5	6	7
Flat	0.397	0.507	0.575	0.657	0.711	0.764	0.813
7	0.400	0.507	0.605	0.683	0.753	0.788	0.854
6	0.392	0.502	0.610	0.674	0.753	0.800	0.854
5	0.400	0.488	0.617	0.692	0.764	0.813	0.868
4	0.404	0.502	0.602	0.679	0.742	0.813	0.868
3	0.394	0.528	0.602	0.683	0.748	0.826	0.868
2	0.394	0.507	0.595	0.683	0.711	0.800	0.854
1	0.413	0.556	0.625	0.711	0.753	0.840	0.883

Table 6.2 $\dfrac{\text{Cross correlation (6mm scale) convected velocity}}{\text{Area averaged gas velocity}}$ $\dfrac{V_{g_2}}{V_g}$

Table 6.3 shows how the predicted convected disturbance velocity V_{g_3} evaluated from the cross correlation over the 25mm length scale using equation 6.4, varies in the simulation as a function of the velocity and local void fraction profile powers m and n respectively.

$\alpha_l(r)_n$ \ $v_g(r)_m$	1	2	3	4	5	6	7
Flat	0.381	0.487	0.574	0.633	0.710	0.768	0.819
7	0.404	0.552	0.623	0.683	0.769	0.829	0.860
6	0.365	0.535	0.598	0.661	0.740	0.841	0.910
5	0.601	0.574	0.918	0.733	1.102	1.205	1.147
4	0.388	0.490	0.825	0.717	0.749	1.018	1.083
3	0.557	0.686	0.575	0.718	1.038	1.178	1.059
2	0.393	0.491	0.585	0.672	0.715	0.774	0.799
1	0.428	0.463	0.414	0.759	0.580	0.487	0.553

Table 6.3 $\frac{\text{Cross correlation (25mm scale) convected velocity } V_{g_3}}{\text{Area averaged gas velocity } V_g}$

On first examination of the three tables above, it would seem that the local gas void fraction profile $\alpha_l(r)$ has little effect on the magnitude of the convected disturbance velocities, and for a given local void fraction and velocity profile power, n and m, the three convected disturbance velocities, V_{g_1}, V_{g_2} and V_{g_3}, are very similar. This is illustrated in figure 6.12 which is extracted from the table above showing the predicted convected disturbance velocity V_{g_2} for values of n of 2 and 7. These results are consistent with the conclusions drawn from the two simulated differential pressure sources earlier in this section, in which it was predicted that differential pressure signals would be dominated by the motion of bubbles near the pipe wall and

correlation techniques would reflect the velocity of bubbles near the pipe wall. Therefore, as the local velocity profile power m increases, generating a more uniform bubble velocity across the test section, the velocity of bubbles near the pipe wall will increase, as shown by the extract of table 6.2 in figure 6.12.

Note that on closer inspection it can be seen that the data exhibits some scatter which is thought to be a consequence statistical errors associated with a short simulated record length (1.64 seconds) and no averaging over a number of auto and cross correlations. However, the variation between the convected disturbance velocity V_{g_1} in table 6.1 and the convected disturbance velocity V_{g_3} in table 6.3, which are both evaluated over the 25mm correlation length scale, show similar results over the local bubble velocity and void fraction profile powers covered in this simulation (m = 1→7, n = 1→7, and n = ∞). On further examination of the two cross correlation convected disturbance velocities V_{g_2} and V_{g_3}, the averaged variation in the velocity ratios of tables 2 and 3 over the range of profile powers indicated above, shows convected disturbance velocities evaluated over the 25mm length scale (V_{g_3}) to be approximately 7%† larger than those evaluated over the 6mm length scale (V_{g_2}). The small variations observed between the convected disturbance velocities evaluated over the 6mm and 25mm length scales is thought to be due to the 6mm correlation length scale being affected by structures in the flow which have a similar length scale to that of the 6mm correlation length scale. It has been indicated in section 5.2.1 that structures of this length scale (of the order of a bubble diameter) are associated with temporal variations in the average gas void fraction $\alpha(t)$. This source of pressure fluctuation may occur at any radial distance from the pipe wall and the effect on the cross correlation

† Although the difference is 35% for n=5

correlogram will be to shift its peak position to a smaller value of τ_2 if the fluctuation in pressure is near the centre of the pipe since these bubbles are travelling faster than those at the pipe wall.

A typical autocorrelation of the differential pressure signal $\Delta P_A(t)$ is shown in figure 6.13. As expected from earlier discussions in this section, the shape of this autocorrelation is similar to that generated by a single bubble from pressure fluctuations associated with a single bubble's motion (curve d of figure 5.16). The magnitude of the autocorrelation coefficient, $\rho_{AA(\tau)}$, at the peak position corresponding to τ_1 in figure 6.3, is approximately -0.4, this compares with a single bubble anti-phase autocorrelation coefficient of -0.5. The variation being due to the diffusion effect of bubbles travelling at different velocities depending upon their radial position r within the flow ($v_g(r)$). The relatively small difference in shape and magnitude of the autocorrelation correlograms for a single bubble and the simulated two-phase flow tends to confirm the predictions made earlier in this section i.e. that the simulated bubbly two-phase flow pressure fluctuations will be dominated by the motion of bubbles near the pipe wall.

The conclusions drawn from the bubbly two-phase flow simulations tend to indicate that the evaluation of the convected disturbance velocity, either by auto or cross correlation techniques, will be strongly dependent upon the bubble velocity profile, $v_g(r)$, within the flow. This is because the fluctuating pressure signals when correlated are dominated by pressure fluctuations caused by the motion of bubbles which are near to the pressure tappings and hence the pipe wall.

In the simulations carried out in this section, power law local gas velocity and void fraction profiles have been used for simplicity of modeling. However, in a practical bubbly two-phase flow this is seldom the case, and it has been suggested by many researches (see, for example, *Lance* and *Bataille* [1991]) that bubble migration occurs towards the wall of the test section causing peaks in local void fraction profile $\alpha_l(r)$ near the wall. Since pressure fluctuations measured at the pipe wall are dominated by the motion of bubbles near the pipe wall, and not the distribution of void fraction, it is thought that this will have little effect on the simulations conducted in this section.

Increasing the average gas void fraction α may reduce the dominance of the pressure fluctuations caused by bubble motion, and the increased bubble density may cause bubble interaction, thus increasing the complexity of the computer model beyond the scope of the simple approach adopted in the present study. Nevertheless, experimental results are obtained for higher average gas void fractions than considered here.

6.4 Initial experimental autocorrelations from a single differential pressure transducer

Autocorrelations can be used to measure the dependency of a signal at any point in time t on any other point in time $t+\tau$. In the case of differential pressure fluctuations generated by a bubbly two-phase flow measured between two fixed locations, 1 and 2, in the pipe wall of the experimental test section, the autocorrelation can be used to detect the passage of convected pressure disturbances

generated by bubbles as they flow down-stream.

In sections 5.2 four main sources of pressure fluctuations were identified in a bubbly two-phase flow and of these four sources it has been argued that the most dominant in terms of both magnitude and structure length scale, when measured differentially, will be pressure fluctuations generated by a the motion of a bubble. It has been shown in section 5.4.1 that the predicted shape of the autocorrelation correlogram for a single bubble resembles quite closely that of the differential pressure signal associated with the motion of a single bubble (see figure 5.16). The anti-phase correlation coefficient peak magnitude is approximately -0.5, which indicates a high degree of correlation over this time period. Similarly it has been shown in section 6.3.4 that the autocorrelation of many bubbles in a simulated bubbly two-phase flow also resembles the autocorrelation of a simulated single bubble's motion, however the magnitude of the anti-phase correlation coefficient is reduced to approximately -0.4, still indicating a high degree of correlation. It has been concluded from these results that simulated pressures evaluated differentially by a single pressure transducer will be dominated by pressures associated with the motion of bubbles near the pressure tappings and hence the pipe wall. It therefore follows that if the modelling of a bubbly two-phase flow in section 6.3 has been successful, then the autocorrelation of an experimental bubbly two-phase flow will exhibit similar autocorrelation results.

Using a single differential pressure transducer and housing described in section 5.3.3, positioned in the experimental test section of the flow loop approximately 0.6m down-stream of the contraction, differential pressure measurements $\Delta P_A(t)$ have been made

as a function of time, t, over a range of superficial gas and liquid velocities, V_{sg} and V_{sl}, respectively. Average gas void fractions α were also recorded simultaneously. Autocorrelations correlograms of the recorded differential pressure signals are shown in figures 6.14a - 6.14d for superficial gas velocities, V_{sl}, of 0, 0.64, 1.0 and 1.5m/s, each with an average gas void fraction α of approximately 10%. The pressure signals were A.C. coupled, and therefore the autocorrelations generated are for the fluctuating component of the differential pressure signal only.

Figures 6.14a - 6.14d show that, as predicted, the general shape of the autocorrelation correlograms closely resemble the autocorrelation of a simulated differential pressure signal $\Delta P_A(t)$ as shown in figure 6.13. The time τ_1 (defined by figure 6.3) taken for the experimental autocorrelation correlograms to reach complete anti-phase would appear to be almost constant. The convected bubble velocity, V_{g_1}, which can be calculated from equation 6.2, ranges from 0.41m/s for bubbles travelling through a stagnant column of water to 0.51m/s for bubbles travelling through water which has a superficial liquid velocity, V_{sl}, of 1.5m/s. These results show only a small change in the convected bubble velocity, V_{g_1}, evaluated from the autocorrelation for a large change in the area averaged gas velocity V_g. This effect is consistent with the interpretation of the autocorrelation correlogram put forward in section 6.1, since the velocity of the fluid in contact with the pipe wall approaches zero and viscous fluid effects within the fluid will generate a local velocity profile and hence for a given local velocity profile, a large change in the area averaged bubble velocity, V_g, will cause little change in the velocity of bubbles near the pipe wall.

It should also be noted that the magnitude of the autocorrelation coefficient, $\rho_{AA}(\tau)$, when the pressure signal is in complete anti-phase is approximately -0.45, indicating a high degree of correlation over the time τ_1. This was also shown to be the case in the autocorrelations of a simulated differential pressure signal, $\Delta P_A(t)$, which had autocorrelation coefficients of the order of -0.5 and -0.4 for a single bubble and many bubbles respectively.

The autocorrelation length scale in which decorrelation of the pressure signal occurs is difficult to determine from the correlograms shown in figure 6.14 since each signal oscillates over a number of cycles. This oscillation is caused by the differential pressure signal being dominated by the convected pressure waves generated by the motion of many bubbles. However, from section 5.2 the shortest flow structure length scales are thought to be those associated with a bubbles wake. *Lance* and *Bataille* [1991] found, the structure length scales associated with a bubbles wake to be of the order of 0.8 bubble diameters, which in the present study equates to approximately 4.8mm. It should, however, be noted that in *Lance* and *Bataille's* experiments the average gas void fraction was much lower than those in the present study. Subsequent cross correlation of two differential pressure signals separated by a short axial distance, h, which is much shorter than the transducer tapping separation distance, *l*, may detect structures in the flow other than those associated with the convected pressure field surrounding a moving bubble that is entrapped in a layer near the pipe wall i.e. the 'bouncing' bubble effect described in section 6.1.2. Therefore, in the present study a cross correlation transducer separation distance of the order of a single bubble diameter d was chosen, h = 6mm, and will be discussed in more detail in section 6.5.

6.5 Modifications of experimental apparatus used to measure differential pressure fluctuations for use in cross correlation flow measurement techniques

Section 5.3.3 covered the design and construction of a special housing used to mount a single Validyne differential pressure transducer and which contained integral pressure lines. This housing/mounting facility was used to rigidly locate the differential pressure transducer, pressure lines, and experimental test section together. The housing was machined from aluminium alloy with special care being taken to eliminate all possible air traps. The design was found suitable for use in the present study programme and was used successfully to make differential pressure measurements using a single differential pressure transducer at the pipe wall of a bubbly two-phase flow. Autocorrelations of experimental results were studied in section 6.4 which aid the interpretation of the measured pressure signal.

However, for cross correlation experiments to be performed two differential pressure signals $\Delta P_A(t)$ and $\Delta P_B(t)$ are required arranged as shown in figure 6.4 where $\Delta P_A = P_1-P_2$ and $\Delta P_B = P_3-P_4$ where P_1 through P_4 are the wall pressure tappings. Note that the wall pressure tappings need to be axially in line since the pressure tapping to bubble centre separation distance can affect the magnitude of the pressure signal generated by the motion of a bubble (see section 5.2.2). The transducer separation distance, h, between the two differential pressure transducers A and B, has been chosen to be 6mm which is of the order of a single bubble diameter. This value of transducer separation distance has been chosen after considering the following points from chapters 5 & 2 respectively, (i) it is of the

order of the shortest structure length scale expected to be present in a bubbly two-phase flow (see section 5.2), (ii) it was reported by *Olszowski et al* [1976] that bubbly two-phase flows retain their identity for at least one pipe diameter, which is much larger than 6mm in this case. It should be noted that with a transducer separation distance h = 6mm, a high degree of correlation between the two transducer signals is expected since 6mm is much shorter than the 25mm transducer tapping separation distance *l* over which a single bubble's motion can be identified (see section 5.2.2).

Based on these preliminary experiments modifications to the existing differential pressure transducer housing were made to accommodate a second differential pressure transducer B with pressure tappings 3 and 4 positioned 6mm down-stream of the tappings 1 and 2, respectively, as shown in figure 6.4. To ensure the distance between the tappings were accurately spaced and axially in line, a stainless steel ring was machined and inserted into the housing with 1mm diameter tapping positioned as shown in figure 6.15. This was then located in the bore of the transducer housing, being secured and sealed in position using Loctite 261 as indicated in the detailed drawing figure 6.16.

As described in section 5.3.3, all pressure lines were reamed smooth and machined at an angle to facilitate the bleeding of air. Care was also taken to ensure that the two diaphragms, one in each differential pressure transducer, were orientated in the same way when mounted on the housing. Thus minimising the effects of vibrations by ensuring that any vibration of the aluminium housing caused by the experimental flow loop would be common to both differential pressure transducers which when cross correlated may show up as a small peak

with zero time displacement which could then be ignored.

The presented theory assumes that the transducer tapping separation distance l between each pair of differential pressure transducer tappings, P_1, P_2 and P_3, P_4, are equal. However in practice the two tapping separations distances, which will be referred to as l_A and l_B and are associated with ΔP_A and ΔP_B respectively, may not be identical due to machining inaccuracies. This effect was simulated for the configuration of differential pressure transducers considered in the present study, using equations 5.45 and 5.46 for the variation in pressure at any point generated by a moving sphere derived from *Butlers* sphere theorem, where l was replaced by l_A and l_B for ΔP_A and ΔP_B respectively. Simultaneous evaluation of the pressure signal from ΔP_A, with a fixed tapping separation, l_A, and ΔP_B for discrete values of l_B, as shown in figure 6.17, was carried out as a sphere travelled along a fixed path parallel to the pressure tappings with a constant velocity V_∞, at a known bubble centre to pipe wall separation distance, R. Assuming a frozen pattern model, the cross correlation of $\Delta P_A(t)$ with $\Delta P_B(t)$, as a function of time, can be used to determine the variation in transient time τ as a function of the variation in the tapping separation distance (l_B-l_A). Figure 6.18 shows the predicted percentage error in velocities as a result of cross correlating two such pressure signals against the percentage variation in tapping separation distance (l_B-l_A) using a frozen pattern model for the motion of a single sphere. It can be seen that as the variation in tapping separation distance (l_B-l_A) increases so does the error in convected velocity measurement.

Since the major contributor to experimental differential pressure fluctuations is caused by the motion of bubbles close to the

pressure tappings, it is likely that the errors in cross correlation velocity measurements caused by machining errors in the tapping separation distances ($l_A \neq l_B$) will be similar to the predicted values given in figure 6.18. However, since the variation between the tapping separation distances l_A and l_B is expected to be less than 2% using C.N.C. machines, the error in cross correlation convected velocity measurements due to this effect is hoped to be no more than 3-4%.

6.5.1 Transducer matching

Consider two transducers which are subjected to the same basic signal but have different response characteristics. Although being subjected to the same source they will produce two different signals containing different frequency components. When these two signals are cross correlated assuming a frozen pattern model described in section 6.1.1, the transient time τ, measured from the peak position of the cross correlation correlogram, may not represent the actual time it took for the convected disturbances to travel from upstream to down-stream transducer, thus introducing an error in the cross correlation velocity measurements V_{g_2} and V_{g_3} evaluated from equations 6.3 and 6.4 respectively.

To ensure that this effect is minimised in the experimental portion of the present study, the two differential pressure transducers, aluminium housing, and experimental test section were all subjected to the same simultaneous excitation vibration after being mounted in position in the flow loop. The vibrations were generated by a rotating eccentric mass mounted on the supporting framework of

the test section as shown in the photograph figure 6.19. This was carried out prior to experimental measurements being made but after the air had been bleed from the transducers and their associated pressure lines.

The output from the two transducer amplifiers were displayed simultaneously on a dual channel oscilloscope. Visually it could be observed if the response from the pressure transducers were similar, and that no time delay existed between the two signals. Levels of gain and zero shift were also adjusted at this stage. When matching the transducer responses the autocorrelation can also be of use. In theory, the two transducers, when subjected to the same signal, should produce identical autocorrelations. However, in practice there are bound to be slight differences due mainly to the accuracy to which the transducer tapping separation distances could be machined (see section 6.5), and differences in the mechanical properties of the differential pressure transducers caused by variations in the tolerance on diaphragm thickness and stiffness.

It was found that variations in the response of the Validyne differential pressure transducers used in the present experimental study was not only caused by trapped air in the transducer and/or pressure lines, but also by fine particle contamination of the small gap between the transducer diaphragm and the over load protection stops, defective or damaged diaphragms and uneven tightening torques on the transducer locating bolts. Matching of the transducers played a critical part in the experimental study phase of this project, and many tedious hours were spent matching transducers prior to making measurements.

6.6 Experimental results obtained from auto and cross correlation correlograms

Using the apparatus described in section 6.5, a series of experiments were undertaken covering a range of superficial gas and liquid velocities. In these experiments auto and cross correlations were evaluated using a Hewlett Packard digital correlator model 3721A. All the auto and cross correlation correlograms are the averaged sum of 32000 separate correlations, thus giving a sufficiently long sampling period to obtain a true picture of the correlation properties of a particular set of bubbly two-phase flow conditions. The evaluated auto and cross correlation correlograms were transferred to a BBC model B micro computer using the parallel communication port on the Hewlett Packard correlator and stored on computer disc.

Autocorrelation correlograms, $\rho_{AA}(\tau)$ and $\rho_{BB}(\tau)$, from both the upstream and down-stream differential pressure transducers, A and B, respectively, were recorded along with the cross correlation correlogram, $\rho_{AB}(\tau)$. The range of superficial gas and liquid velocities, V_{sg} and V_{sl}, were 0.018 - 0.35 m/s and 0 - 1.5 m/s, respectively, covering a range of average gas void fractions α of approximately 5 - 25 %. The superficial gas and liquid velocities were evaluated from equations 3.6 and 3.8 using information from the air mass flowrate orifice meter and the water turbine flow meter as described in section 3.3. The average gas void fraction α was continuously monitored using the gradiomanometer technique described in section 4.1.2, and the area averaged gas velocity, V_g, of bubbles in the experimental test section was calculated using equation 1.12 from the superficial gas velocity, V_{sg}, and the average gas void fraction α.

6.6.1 Auto and cross correlation experimental results

The convected bubble velocities V_{g_1}, V_{g_2} and V_{g_3}, defined by equation 6.2, 6.3 and 6.4, respectively, were evaluated from the autocorrelation (of transducer A, $\Delta P_A(t)$) and cross correlation correlograms as described in section 6.1.2. The results are displayed in table 6.4 as ratios of the area averaged gas velocity V_g. For each experiment tabulated below, autocorrelations $\rho_{AA}(\tau)$ and $\rho_{BB}(\tau)$ of differential pressures $\Delta P_A(t)$ and $\Delta P_B(t)$, respectively, and their associated cross correlation $\rho_{AB}(\tau)$, are shown in figures 6.20 - 6.35.

V_{sl} (m/s)	V_g (m/s)	α	V_{g_1} (m/s)	$\frac{V_{g_1}}{V_g}$	$\frac{V_{g_2}}{V_g}$	$\frac{V_{g_3}}{V_g}$
0.00	0.175	10.0	0.395	2.257	0.674	†
0.00	0.170	16.5	0.375	2.205	0.600	†
0.00	0.160	22.5	0.395	2.469	0.594	†
0.00	0.159	24.8	0.395	2.484	0.566	†
0.43	0.779	6.1	0.417	0.535	0.497	0.465
0.64	1.039	10.3	0.406	0.391	0.427	0.362
0.62	1.040	12.5	0.406	0.390	0.640	0.334
0.58	0.982	16.8	0.429	0.437	0.581	0.386
0.48	0.915	20.0	0.406	0.444	0.525	0.411
1.00	1.824	5.1	0.417	0.229	0.520	†
1.00	1.743	10.5	0.442	0.254	0.544	†
1.00	1.823	13.0	0.442	0.242	0.482	†
1.00	1.923	14.2	0.442	0.230	0.521	†
1.48	2.940	6.7	0.469	0.160	0.557	†
1.50	2.882	9.3	0.484	0.168	0.500	†
1.50	2.556	13.5	0.469	0.183	0.522	†

† - Duration of cross correlation correlogram is too short to determine the convected disturbance velocity V_{g_3}

Table 6.4 - Experimental auto and cross correlation results

Throughout the experimental autocorrelations of $\Delta P_A(t)$ and $\Delta P_B(t)$ shown in figures 6.20 - 6.35, a slight variation can be seen in the two autocorrelation time scales which was found to be independent of the differential pressure transducers and does not vary significantly with either variations in superficial liquid velocity, V_{sl}, or average gas void fraction α. It was therefore concluded to be a function of the transducer housing. Elimination of the variations in autocorrelation could not be achieved in the experiments carried out in this study and from the discussion in section 6.5.1 on the mis-matching of transducers it is thought that the most likely explanation for this effect is a variation in the two transducer tapping separation distances l_A and l_B associated with the differential pressure transducers A and B respectively.

If we assume l_A to be exactly 25mm, and from figures 6.20 - 6.35 we estimate the variation in autocorrelation time τ_1 (see figure 6.3) to be approximately 5ms, from figure 6.18 the transducer tapping separation distance l_B is calculated to be approximately 26mm. However, this is difficult to measure accurately on the transducer housing facility, but it is true that l_B is found to be longer than l_A by approximately 0.5mm. The source of this error may have been caused by the wandering effect of small drills when drilling the 1mm transducer tapping holes in the stainless steel insert (see section 6.5). In the analysis of these experiments we have assumed l_A to be exactly 25mm, and therefore, only considered the autocorrelations of ΔP_A when evaluating the convected bubble velocity V_{g_1}. It has also been assumed that pressure tapping 3 is exactly 6mm down-stream of pressure tapping 1 and it is also recognised that the variation in transducer tapping separation distances l_A and l_B will affect the two convected disturbance velocities evaluated from the cross correlation

correlograms. Nevertheless, over the 6mm correlation length scale this is expected to be negligible, and over the 25mm correlation length scale the variation in tapping separation distance will cause the convected disturbance velocity V_{g_3} to be slightly smaller than measured.

6.6.2 Discussion of experimental results

(i) Zero continuous phase flow

On examination of figures 6.20 - 6.23, it can be clearly seen that the cross correlation correlograms, and hence, the evaluated convected bubble velocities evaluated for no continuous phase flow conditions i.e. a stagnant water column, $V_{sl} = 0$, are very different than those evaluated when the continuous phase is flowing ($V_{sl} \neq 0$).

The convected bubble velocity V_{g_1}, evaluated from the autocorrelation over the 25mm correlation length scale, can be seen from table 6.4 to be almost constant with a value of approximately 0.38. Interpretation of the convected bubble velocity V_{g_1} in section 6.1.2 indicates that V_{g_1} reflects the velocity of bubbles travelling close to the pipe wall, and the results would suggest that for zero continuous phase flow conditions the velocity of bubbles near the pipe wall are approximately twice as high as the area averaged gas velocity. The convection velocity V_{g_2} evaluated from the cross correlation over the 6mm correlation length scale gives convected bubble velocities V_{g_2}, which from the arguments put forward in section 6.1.2 are expected to be influenced by the velocity of bubbles which wander close to the pipe wall and then deviate away. The measured

results indicate a convection velocity of these bubbles of approximately 0.6 the area averaged gas velocity V_g. From continuity considerations this is consistent with bubbles near the pipe wall moving quicker than the area averaged gas velocity V_g.

These results would suggest that bubbles near the pipe wall travel at an almost constant velocity of 0.38m/s (which can also be seen to be almost independent of the continuous phase velocity), and that bubbles away from the pipe wall travel slower than those at the wall for air bubbles travelling through a stagnant water column. However it should be noted that the cross correlation coefficients shown in figures 6.20 - 6.23 are much lower than those predicted by the numerical simulation and observed for bubbly two-phase flows with a non-zero continuous phase velocity which would indicate a more random flow structure and greater diffusion making it more difficult to determine the actual correlogram peak position. As discussed in section 6.1.2, one reason for a greater diffusion effect to be observed in the zero continuous phase flow conditions will be the absence of an entrapped bubble layer near the pipe wall due to a reduced lift force acting on bubbles as they ascend through a stagnant continuous phase and therefore not causing bubbles to migrate towards the wall.

(ii) <u>With continuous phase flow</u>

Analysing the data tabulated in table 6.4, for conditions other than zero continuous phase flows, it can be seen that as predicted in section 6.1.2 and observed in section 6.4 the autocorrelation convected bubble velocity V_{g_1} changes little over the range of superficial liquid velocities covered in this study (0.5 - 1.5m/s).

This indicates that bubbles near the pipe wall are travelling at a constant velocity of approximately 0.4m/s and is consistent with the velocity of bubbles close to the pipe wall travelling much slower than the area averaged or free stream bubble velocity. Figures 6.24 - 6.35 exhibit high degrees of correlation for both auto and cross correlation coefficients, typically 0.8 - 0.9 for cross correlations and as predicted by the two-phase flow simulations in section 6.3 approximately -0.5 for the autocorrelation anti-phase correlation peak. It should also be noted that the shape of the cross correlation curve resembles very closely that of the autocorrelation curves, which is to be expected for highly correlated signals, and that these both resemble the shape of the differential pressure signal generated by the motion of a single bubble close to two fixed pressure tappings (see figure 5.16).

The convected bubble velocity V_{g_2} defined in equation 6.3 evaluated over the shorter 6mm correlation length scale are shown in table 6.4 as the ratio V_{g_2}/V_g, and for continuous phase velocities other than zero are plotted in figure 6.36 as a function of the average gas void fraction α. These ratios can be seen to exhibit some scatter ranging from 0.640 as a maximum to 0.427 as a minimum with an average of 0.55. The ratio V_{g_2}/V_g can be seen to be almost constant (approximately 0.55) over the continuous phase velocity range considered in this study which indicates that the convected bubble velocity V_{g_2} is influenced by the velocity of the continuous phase whereas the corresponding autocorrelation convected bubble velocities, V_{g_1}, are not and remain almost constant at approximately 0.4m/s. This suggests that correlation velocities of convected disturbances evaluated over the 25mm correlation length scale i.e. V_{g_1}, reflect the almost constant velocity of entrapped bubbles near the wall ($V_{g_1} \simeq$

0.4), whereas convection velocities evaluated over the shorter 6mm correlation length scale i.e. V_{g_2}, are influenced by faster moving bubbles than those at the pipe wall and the convected bubble velocity V_{g_2} reflects a velocity which is approximately 0.55 that of the area averaged bubble velocity V_g. From the discussion in section 6.1.2, the convected bubble velocity V_{g_2} is expected to be influenced by bubbles which are travelling through the continuous phase away from the entrapped bubble layer near the wall as they deviate into this layer and then 'bouncing' out again. Hence the convected pressure field surrounding these bubbles generated by their motion, which is generally faster than those at the wall, will be detected by pressure tappings 1 and 3 or 2 and 4 but not at 1 and then at 2 (see figure 6.5) and therefore are not detected on the autocorrelation correlogram.

The effect described above would be expected to become more significant at higher void fractions where there would be more bubbles entering and leaving the entrapped bubble layer. Therefore the cross correlation bubble velocities, V_{g_2}, over the 6mm correlation length scale would be influenced more by the velocity of these bubbles which are entering and leaving the entrapped bubble layer. In the experiments where the continuous phase is flowing, bubbles in the free stream away from the wall travel faster than those at the wall and a slight upward trend can be seen in the data plotted in figure 6.36 indicating that, as expected, the convected bubble velocity V_{g_2} is affected by higher average gas void fractions.

In the cases where the convected bubble velocity V_{g_3} could be evaluated, for a particular set of flow conditions the ratio of V_{g_3}/V_g are always slightly lower than the ratios of V_{g_1}/V_g which are both

evaluated over the same correlation length scale of 25mm. This is because the peak position of the cross correlation correlogram, over the 6mm correlation length scale, are being influenced by the motion of bubbles which are not travelling in the entrapped bubble layer near the pipe wall. Since the time shift τ_3 associated with the convected bubble velocity V_{g_3} is determined by the time difference between the in phase and anti-phase cross correlation peaks as shown in figure 6.4, interpretation of the convected bubble velocity V_{g_3} becomes dubious.

6.7 Experimental measurement of the convected bubble velocities in a circular annulus

To study the effect of variations in local void fraction profiles $\alpha_l(r)$ and variations in bubble velocity profiles $v_g(r)$ experimentally, ideally the local void fraction and bubble velocity profiles would be modified and then measured whilst simultaneously evaluating the convected bubble velocities V_{g_1}, V_{g_2} and V_{g_3} from the auto and cross correlations. This would be carried out over a range of area averaged gas velocities and average gas void fractions. Unfortunately, as stated earlier, in the experimental phase of this study, two-phase flow velocity measurements could not be made due to the un-availability of specialist hot-film anemometry equipment. However, reducing the diameter of the test section will create a more uniform gas velocity profile $v_g(r)$ across the diameter of the test section, unfortunately this too causes problems. As discussed in section 5.3.2, vibration of the pressure lines sets the fluid within the pressure lines into motion, the mass of the fluid causes inertia forces to act on the differential pressure transducer diaphragm

generating a signal of magnitude that swamps the naturally occurring pressure fluctuations within a bubbly two-phase flow. To reduce the swamping effect of vibrations, an aluminium alloy housing was constructed to contain all the pressure lines and mount the two differential pressure transducers to the experimental test section. However, for each diameter of test section a corresponding transducer housing/mounting facility would need to be designed and manufactured. This would be both very time consuming and beyond the budget of the present project.

Therefore, the problem outlined above was approached in a different way, by restricting the two-phase fluid to flow within a small circular annulus inside the existing experimental test section, as shown in figure 6.37, would produce a more uniform bubble velocity profile $v_g(r)$, across the width of the annulus, than would be found in the full pipe flow experiments of section 6.6. By reducing the variation in local bubble velocities in the experimental test section by using an annulus, the velocity of bubbles near the pressure tappings will be similar to the velocity of bubbles anywhere else in the annulus. Evaluation of the convected bubble velocities are therefore expected to produce values that are closer to the area averaged gas velocity V_g than those evaluated in the full pipe flow experiments.

However, it is worth noting that bubbles away from the pressure tappings, further around the annulus, will have less of an effect on the differential pressure measurements. Therefore we will assume the flow in the annulus to be symmetrical about its axis.

6.7.1 Experimental auto and cross correlation results in a circular annulus

Where possible the flow conditions described in section 6.6 for two-phase flow in a full pipe have not been changed, the range of superficial liquid velocities covered being V_{sl} = 0 - 1.5m/s, with average gas void fractions α covering a range of approximately 5 - 25%. The inside diameter D of the experimental test section remains at D = 77.8mm, the inner diameter of the annulus D_{ann} = 42.1mm, this gives an annular thickness of 17.8mm, which is approximately three bubble diameters as opposed to approximately 12d in the full pipe flow. The superficial gas and liquid velocities were evaluated from equations 3.6 and 3.8 using the air mass flowrate orifice meter and the water turbine flow meter respectively, however the new cross-sectional area of the annulus was used in these calculations. The average gas void fraction α was continuously monitored using the gradiomanometer technique described in section 4.1.2, and the area averaged gas velocity V_g of the bubbles in the experimental test section was calculated from equation 1.12 using the measurement of superficial gas velocity V_{sg} and average gas void fraction α.

The convected bubble velocities V_{g_1}, V_{g_2} and V_{g_3} defined by equation 6.2, 6.3 and 6.4 respectively, were evaluated from the auto and cross correlations of the differential pressure fluctuations in a circular annulus and the results are displayed in table 6.5 as ratios of the area averaged gas or bubble velocity V_g. For each experiment tabulated in table 6.5, the two autocorrelation correlograms $\rho_{AA}(\tau)$ and $\rho_{BB}(\tau)$ and their associated cross correlation correlogram $\rho_{AB}(\tau)$, are shown in figures 6.38 - 6.50.

V_{sl} (m/s)	V_g (m/s)	α	V_{g_1} (m/s)	$\frac{V_{g_1}}{V_g}$	$\frac{V_{g_2}}{V_g}$	$\frac{V_{g_3}}{V_g}$
0.00	0.172	9.3	0.385	2.238	1.145	†
0.00	0.169	18.3	0.395	2.337	0.757	†
0.00	0.161	23.0	0.395	2.453	0.882	†
0.00	0.159	29.0	0.395	2.484	0.654	†
0.69	0.940	5.0	0.417	0.734	0.638	0.479
0.86	1.370	8.1	0.395	0.288	0.626	0.221
0.82	1.252	14.3	0.395	0.315	0.685	0.302
1.00	1.485	6.6	0.395	0.266	0.783	†
1.00	1.563	11.2	0.395	0.253	1.153	†
1.00	1.662	14.2	0.455	0.274	0.904	†
1.50	3.095	6.3	0.417	0.135	0.529	†
1.50	2.988	8.9	0.442	0.148	0.928	†
1.50	2.838	11.7	0.469	0.165	0.635	†

† - Duration of cross correlation correlogram is too short to determine the convected disturbance velocity V_{g_3}

Table 6.5 - Experimental auto and cross correlation results of flow in a circular annulus

On examination of figures 6.38 - 6.50, it can be clearly seen, that like the full pipe flow experiments of section 6.6, the cross correlation correlograms have a similar shape as the autocorrelation correlograms and both the auto and cross correlograms exhibit high degrees of correlation. As discussed in section 6.6.1, throughout the experimental autocorrelations of $\Delta P_A(t)$ and $\Delta P_B(t)$ a slight variation can be seen in the two autocorrelation time scales which was concluded to be a fault in the machining of the tapping separation distances l_A and l_B in the transducer housing facility. In the analysis of these experiments we have assumed l_A to be exactly 25mm, and hence only considered the autocorrelations of ΔP_A when evaluating the convected

bubble velocity V_{g_1}. It has also been assumed that the pressure tapping 3 is exactly 6mm down-stream of the pressure tapping 1, which are the same assumptions made for the full pipe experiments in section 6.6.

6.7.2 Discussion and comparison of experimental convected bubble velocity measurements made in a circular annulus with those made in a full pipe

(i) Zero continuous phase flow

We shall discriminate between zero and non-zero continuous phase flow conditions, as done in the full pipe flow experiments. Initial inspection of the data tabulated in table 6.5 indicates that for zero continuous phase flow conditions the convected bubble velocity V_{g_1}, evaluated from the autocorrelation over the 25mm length scale, as expected, is almost constant with a velocity value of approximately 0.39m/s which is similar to that evaluated within the full pipe flow experiments. It can also be seen that the convected bubble velocity V_{g_1} appears to be independent of the continuous phase velocity as was found for the continuous pipe flow experiments.

The convected bubble velocity V_{g_2}, which is evaluated from the cross correlation over the 6mm correlation length scale and is displayed in table 6.5 as the ratio V_{g_2}/V_g, shows that for increasing average gas void fraction the corresponding ratio of V_{g_2}/V_g decreases from 1.14 to 0.66. It can be seen from figure 6.38, which corresponds to the highest ratio of V_{g_2}/V_g = 1.14, that the cross correlation coefficient, $\rho_{AB}(\tau)$, is approximately 0.5 which indicates a high

degree of correlation between the two signals and is much higher than exhibited by other zero continuous phase velocity cross correlations. The reason for this high correlation at a relatively low average gas void fraction may indicate that fewer bubbles wandered near and then away from the pressure tappings during the sampling period. This is also consistent with a more uniform velocity profile across the annulus, at lower average gas void fraction, than is exhibited in the full pipe flow experiments and as the average gas void fraction increases the gas velocity profile across the annulus changes to become more like those of the full pipe flow experiments with a zero continuous phase velocity.

(ii) <u>With continuous phase flow</u>

Examination of the cross correlation convected bubble velocity V_{g_2}, for a non-zero continuous phase velocity, indicates that, as expected, the reduced area in which bubbles can flow pushes more faster moving bubbles into and then out of the entrapped bubble layer at the outer edge of the annulus. This can be seen as an increase in the ratios of convected bubble velocities over area average gas velocities, V_{g_2}/V_g, over those evaluated under similar conditions in full pipe flow experiments. It can also be seen that, as found in the full pipe flow experiments, the convected bubble velocity V_{g_1}, which has been argued in section 6.6.1 reflects the velocity of bubbles near the pressure tappings and hence the pipe wall, gives velocities that are almost independent of the continuous phase velocity with a value of approximately 0.4m/s.

The results in this section tend to confirm the interpretation of auto and cross correlation convected velocity measurements made in

section 6.6. To summarise, evaluation of the convected bubble velocity V_{g_1}, indicates that bubbles near the pressure tappings and hence near the outer annulus pipe wall, rise at a velocity of approximately 0.4m/s and would appear to be independent of the continuous phase flow conditions. For a flow in which the continuous phase is also moving the cross correlation convected bubble velocity V_{g_2} is influenced by the faster moving bubbles entering and then leaving the entrapped bubble layer at the outer annulus pipe wall, giving results, which are higher than those measured in the full pipe flow experiments (approximately $0.55V_g$), of approximately 0.7 the corresponding area averaged gas velocity. This effect becomes slightly more dominant with increasing average gas void fraction, thus increasing the ratio V_{g_2}/V_g, suggesting that more bubbles in the flow are interacting with the entrapped bubble layer.

6.8 Conclusions of experimental results

It has been clearly shown that the use of differential pressure measurements can provide useful information directly relating to the convected bubble velocity, and the experimental results of sections 6.6 and 6.7 are summarised below with reference to a full pipe flow.

Evaluation of the autocorrelation convected bubble velocity V_{g_1}, indicates that bubbles near the pressure tappings and hence near the pipe wall, rise at a velocity of approximately 0.4m/s and would appear to be independent of the continuous phase flow velocity.

However, for a stagnant column of water i.e. $V_{sl} = 0$, evaluation of the cross correlation convected bubble velocity V_{g_2}, which is.

evaluated over the 6mm correlation length scale, indicates that bubbles away from the wall generally travel slower than the area averaged gas velocity V_g.

For a flow in which the continuous phase is also moving i.e. $V_{sl} \neq 0$, the cross correlation convected bubble velocity V_{g_2} is influenced by faster moving bubbles entering and then leaving the entrapped bubble layer at the pipe wall, giving rise to results which are approximately half (0.55) the corresponding area averaged gas velocity. This effect becomes slightly more dominant with increasing average gas void fraction, thus increasing the ratio V_{g_2}/V_g, since there are more bubbles in the flow which may interact with the entrapped bubble layer.

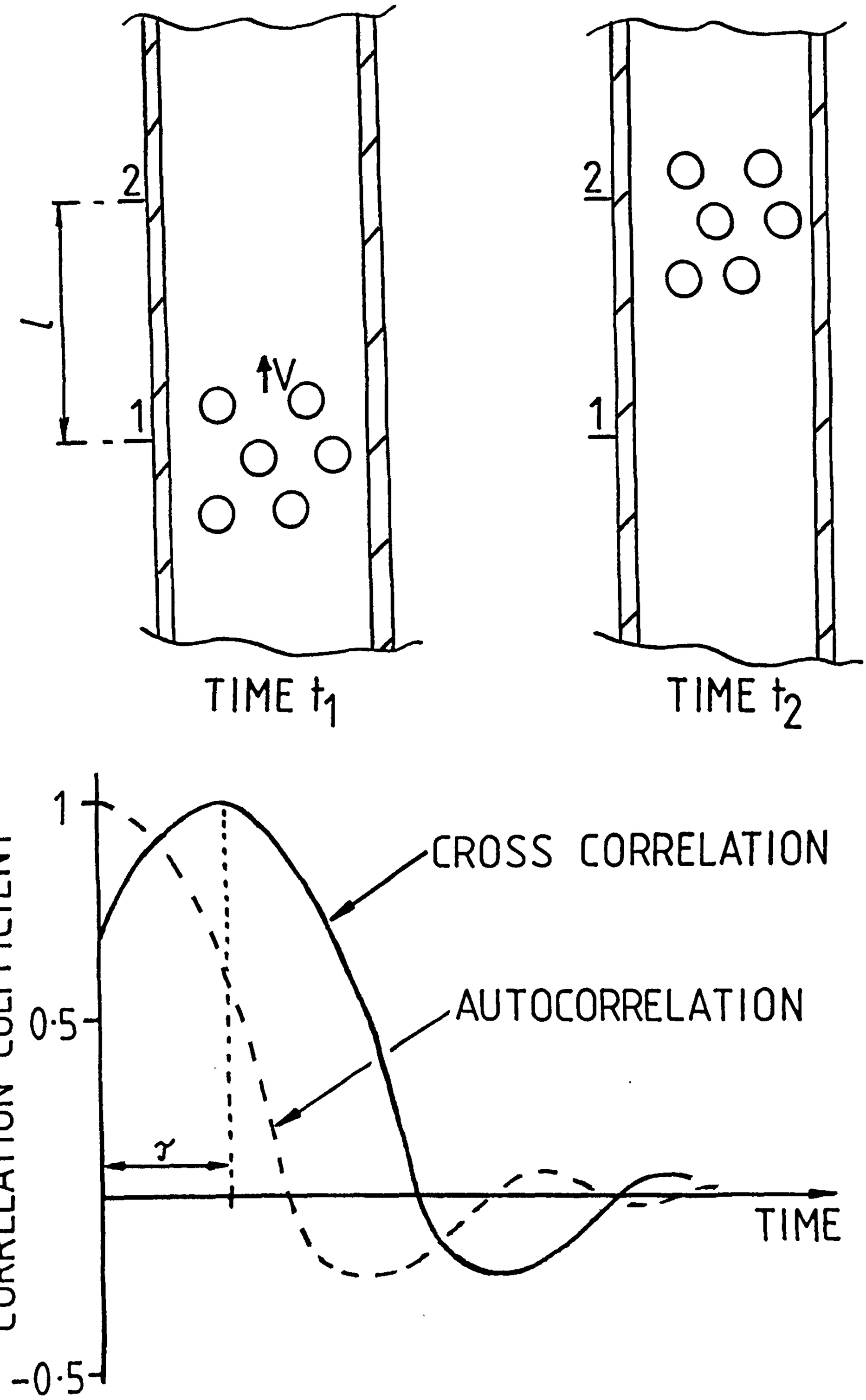

Figure 6.1 Frozen pattern correlation model

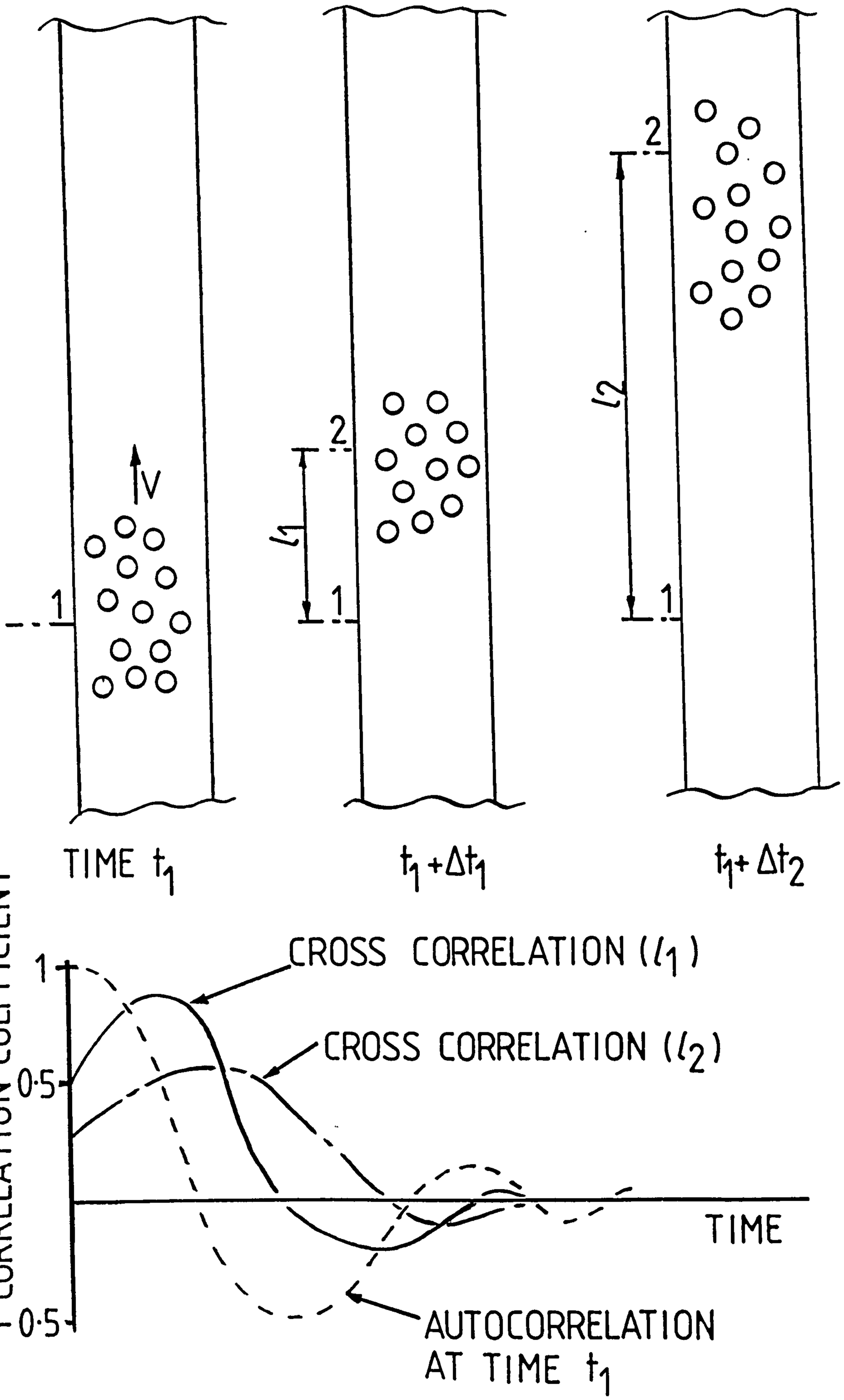

Figure 6.2 Diffused pattern model and auto/cross correlation correlogram

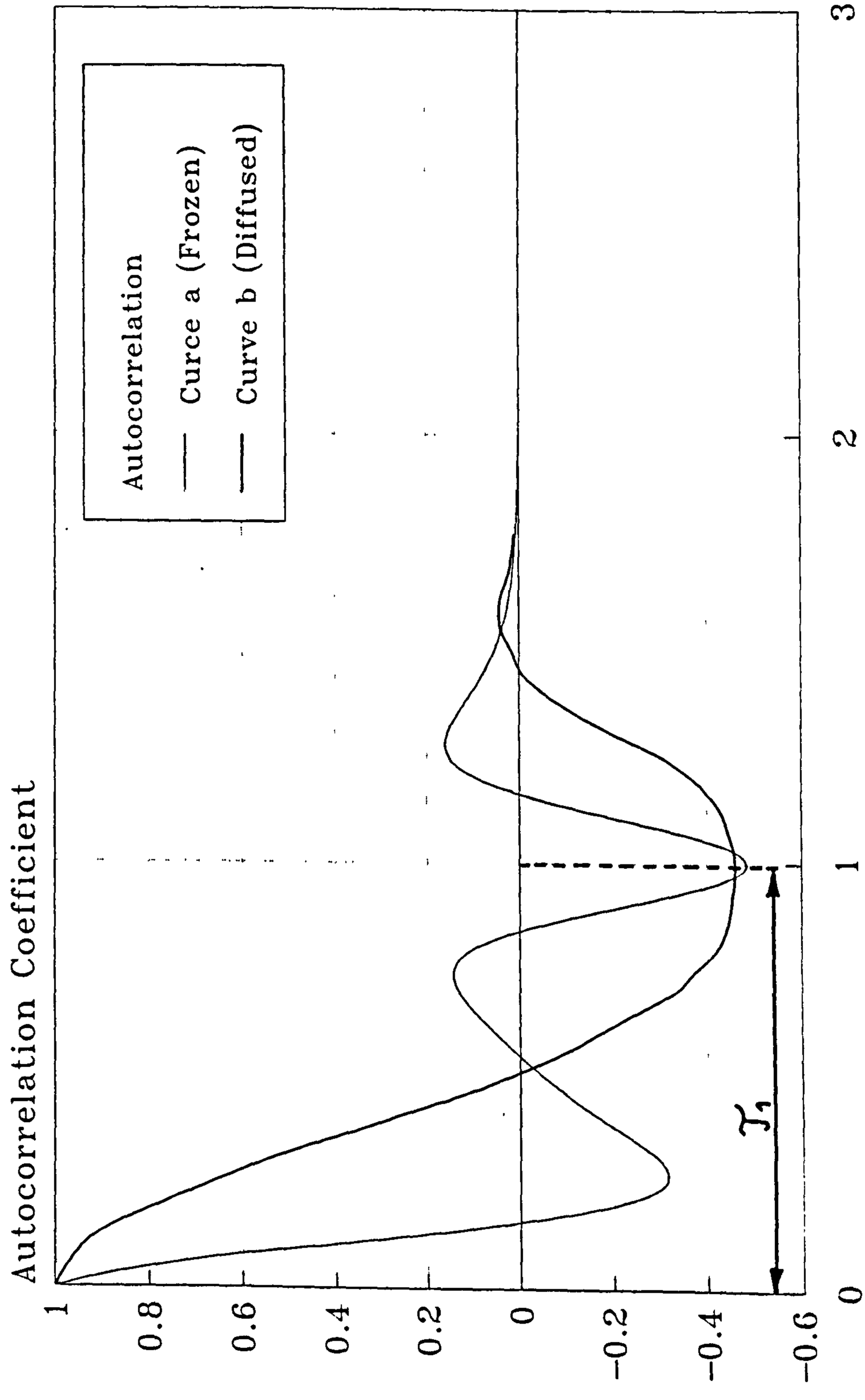

Figure 6.3 Frozen and diffused pattern autocorrelations of pressure fluctuations within a bubbly two-phase flow

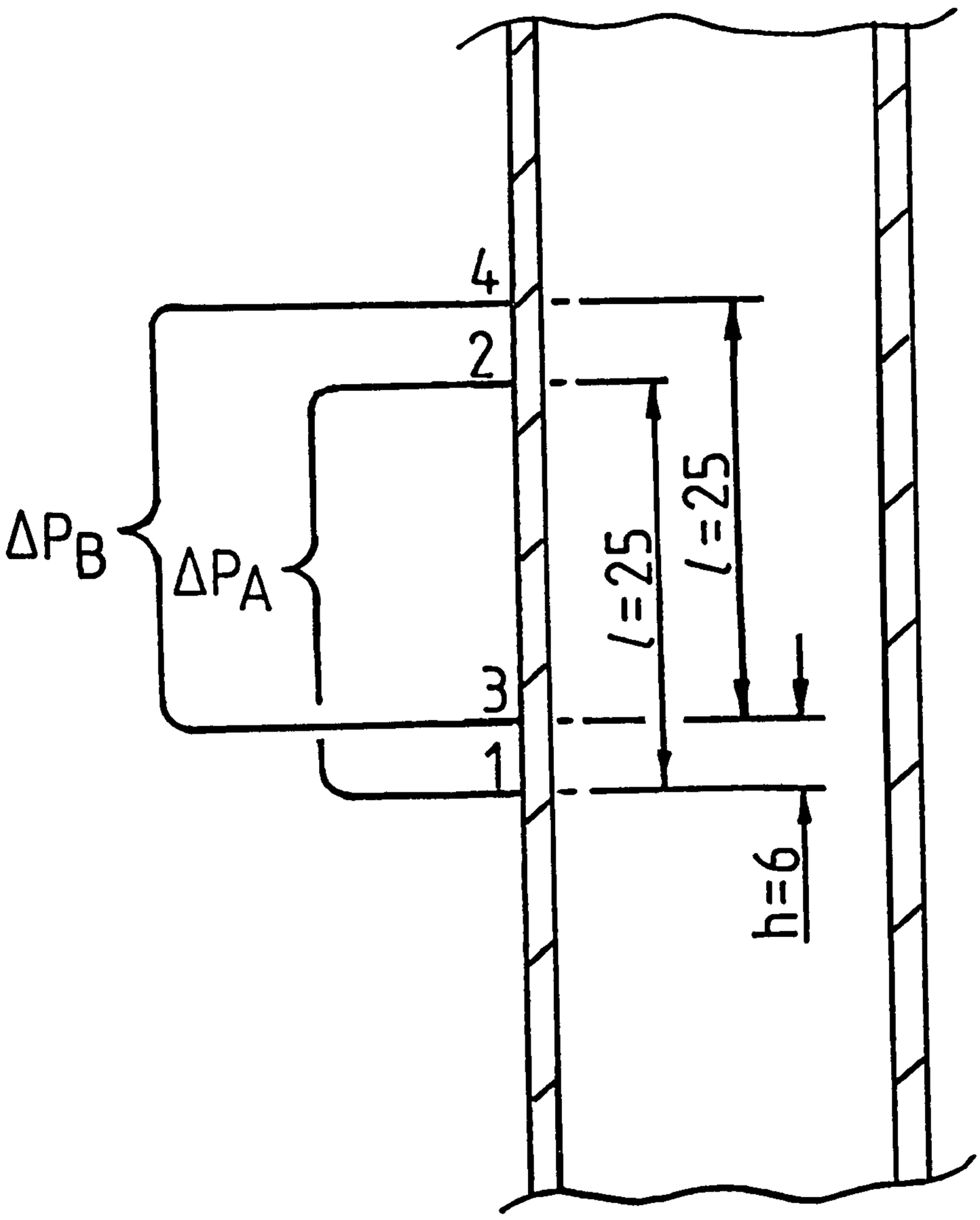

TRANSDUCER TAPPING ARRANGEMENT FOR CROSS CORRELATION MEASUREMENTS

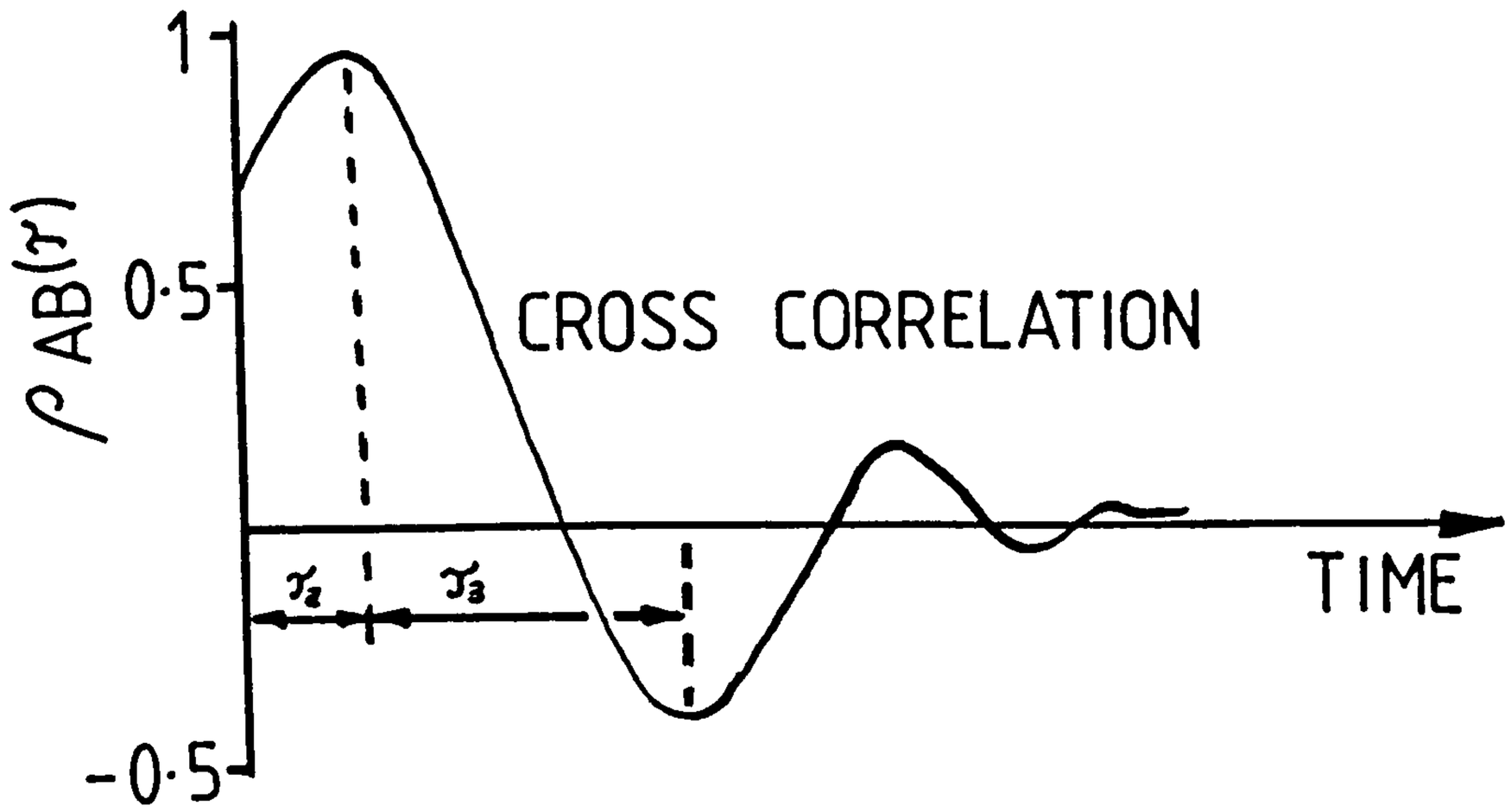

Figure 6.4 Arrangement of the differential pressure tappings 1, 2, 3 and 4 used to measure ΔP_A and ΔP_B in the present study, and the interpretation of a typical cross correlation developed in this study

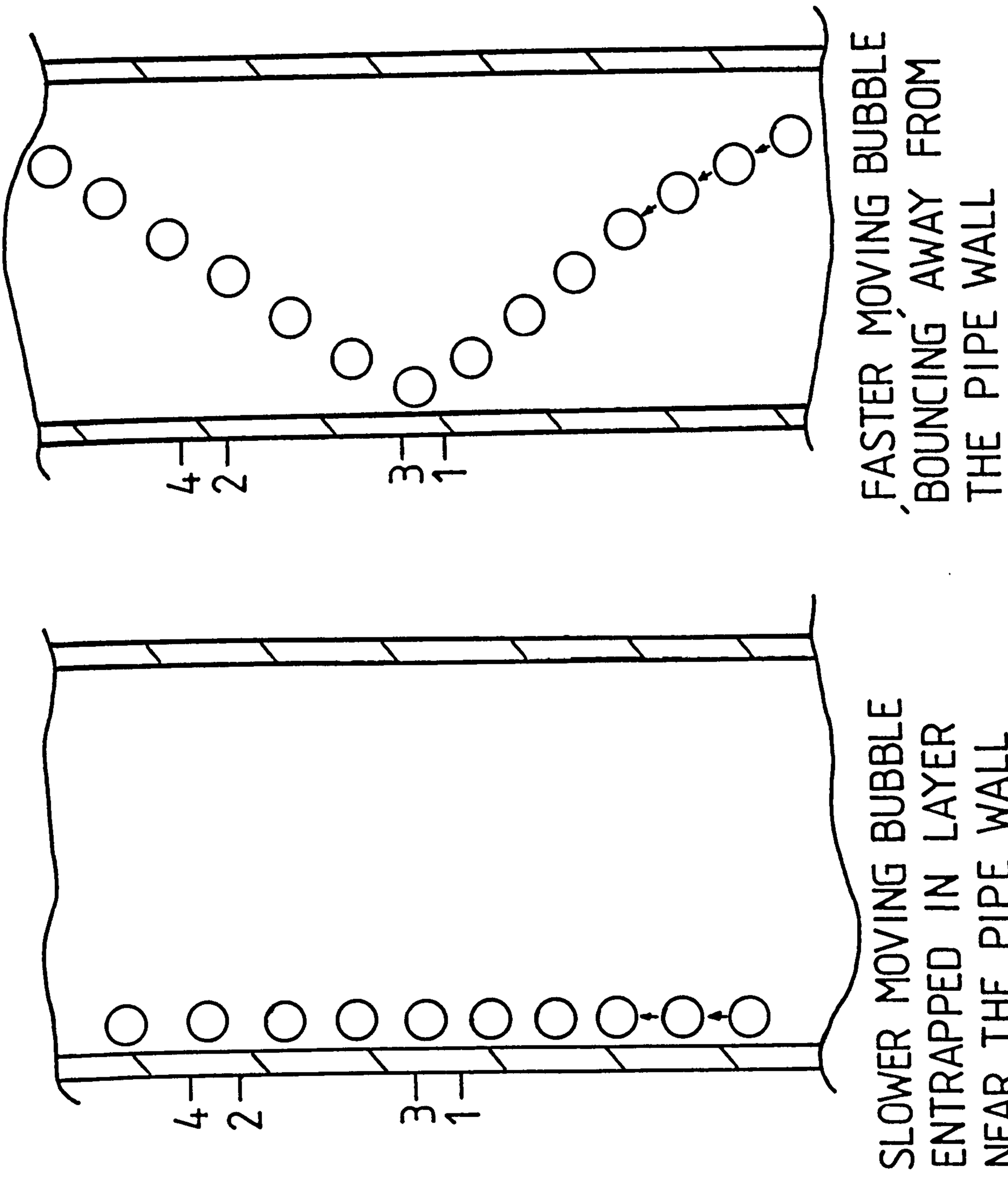

Figure 6.5 Observed bubble motion by *Lance, Bataille* and *Marie'* at the *Laboratorire de Mecanique des Fluides et d'Acoustique, Lyon*

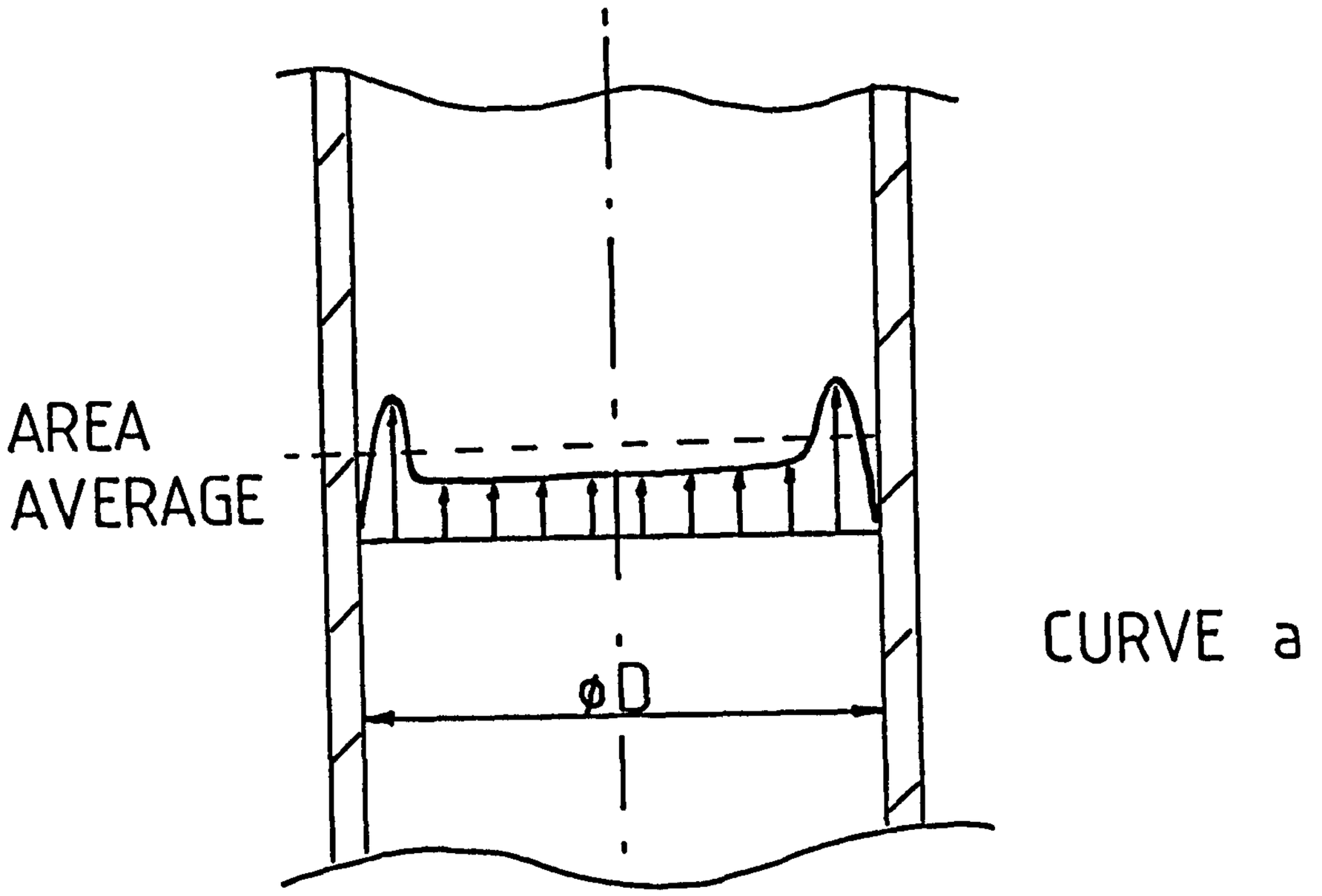

Figure 6.6 Illustration of local gas velocity and void fraction profiles, $v_g(r)$ and $\alpha_l(r)$ respectively

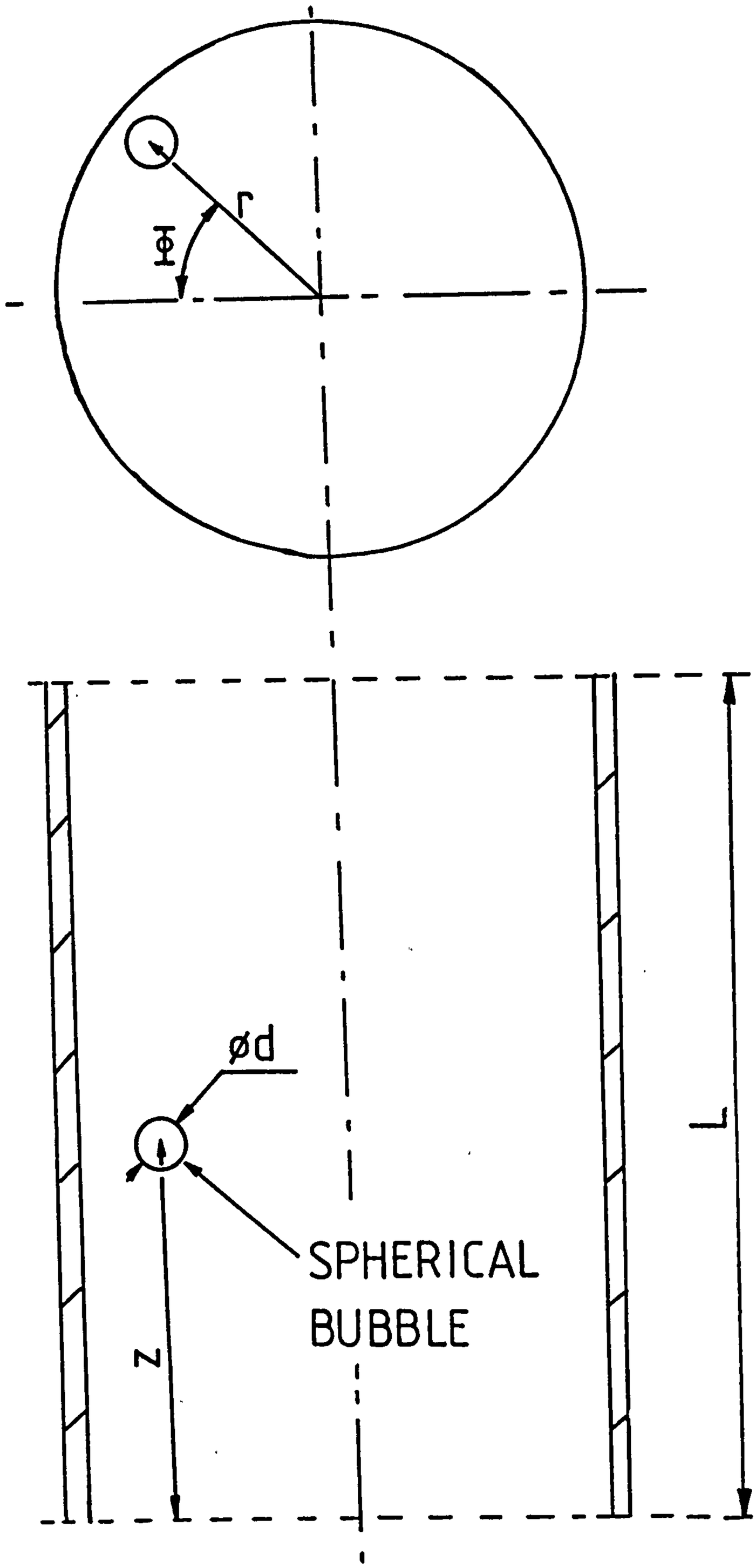

Figure 6.7 Illustration of the bubbly two-phase flow correlation simulation model and co-ordinate system developed in the present study

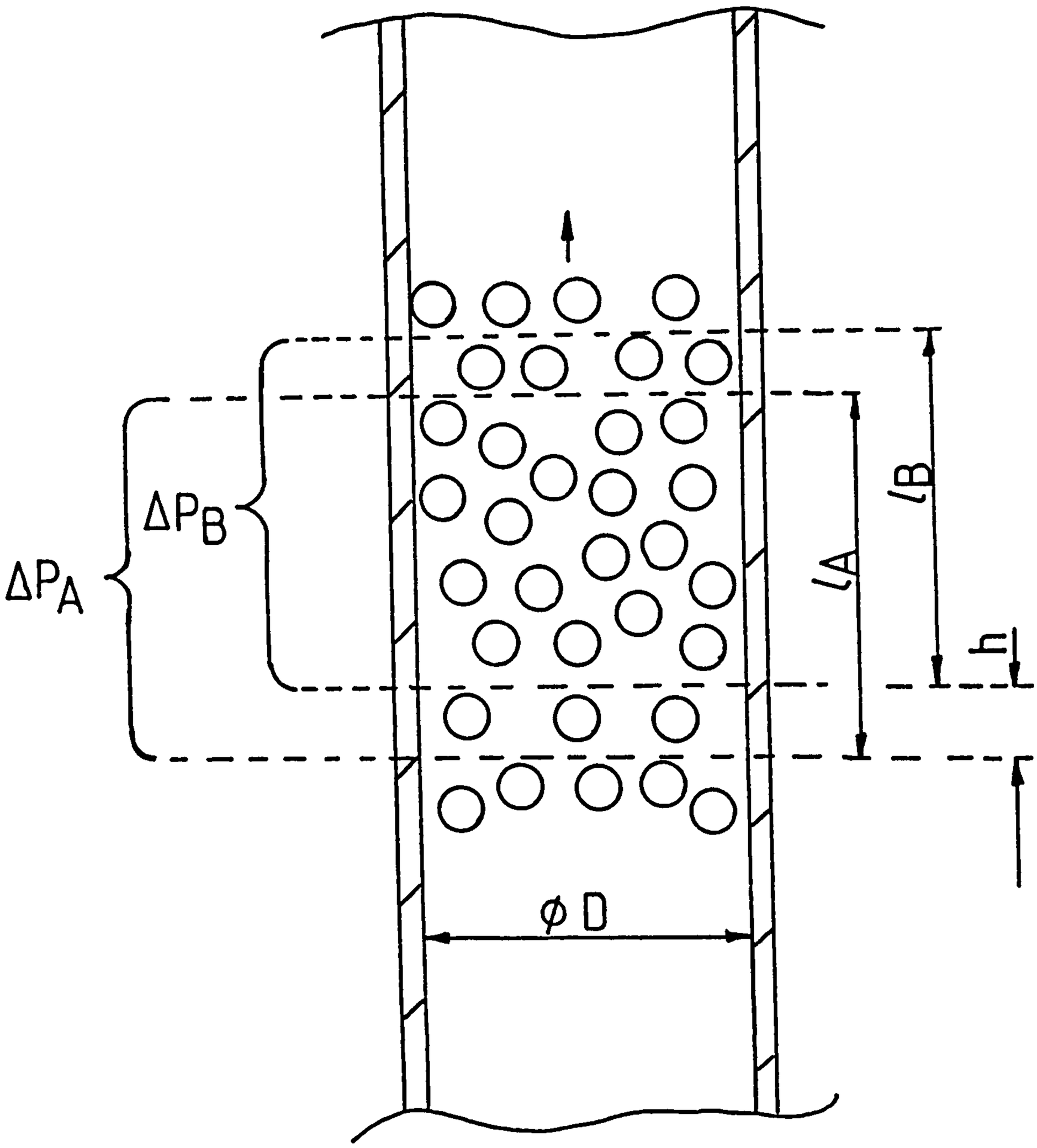

BUBBLE VOLUME WITHIN l_A

$$\alpha_A(t) = \frac{\text{BUBBLE VOLUME WITHIN } l_A}{\frac{\pi D^2 l_A}{4}}$$

BUBBLE VOLUME WITHIN l_B

$$\alpha_B(t) = \frac{\text{BUBBLE VOLUME WITHIN } l_B}{\frac{\pi D^2 l_B}{4}}$$

Figure 6.8 Illustration of temporal variations in the average gas void fraction $\alpha(t)$ in a bubbly two-phase flow

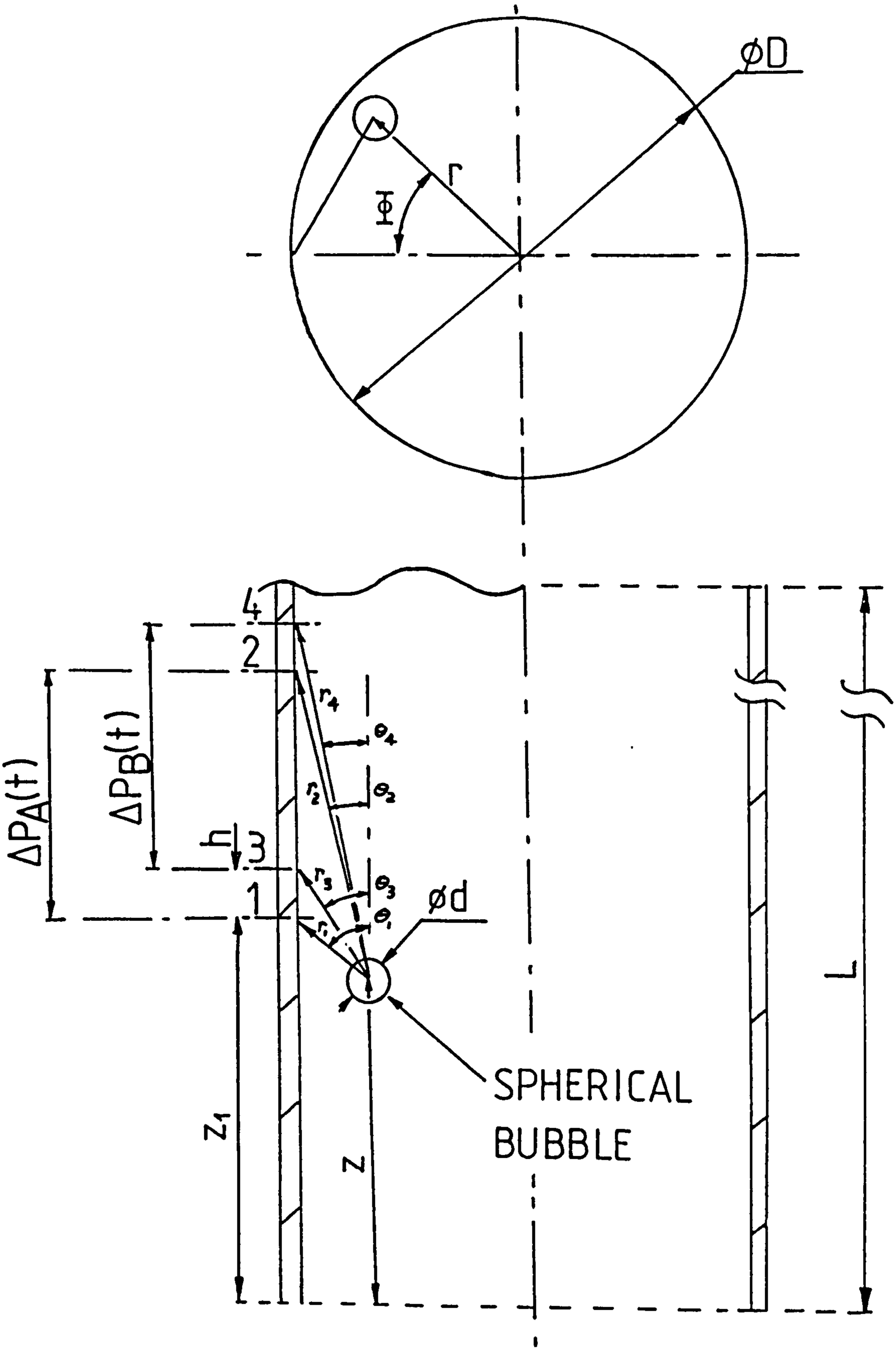

Figure 6.9 Diagram illustrating the nomenclature used in the evaluation of the pressures measured by two differential pressure transducers, A and B, caused by the convected pressure field surrounding a moving bubble

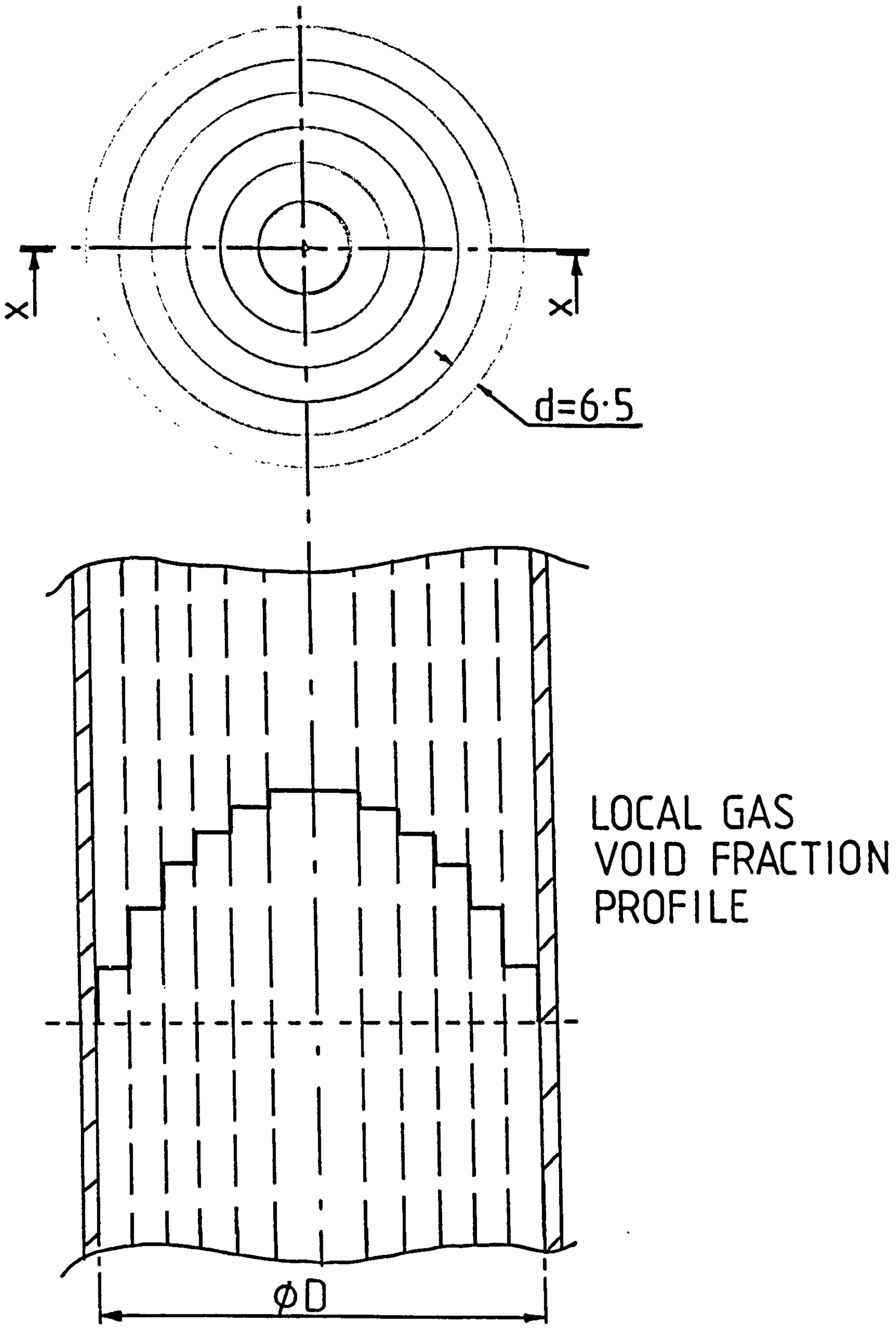

Figure 6.10 Illustration of the annular technique used to simulate local gas void fraction profiles $\alpha_l(r)$ within a bubbly two-phase flow

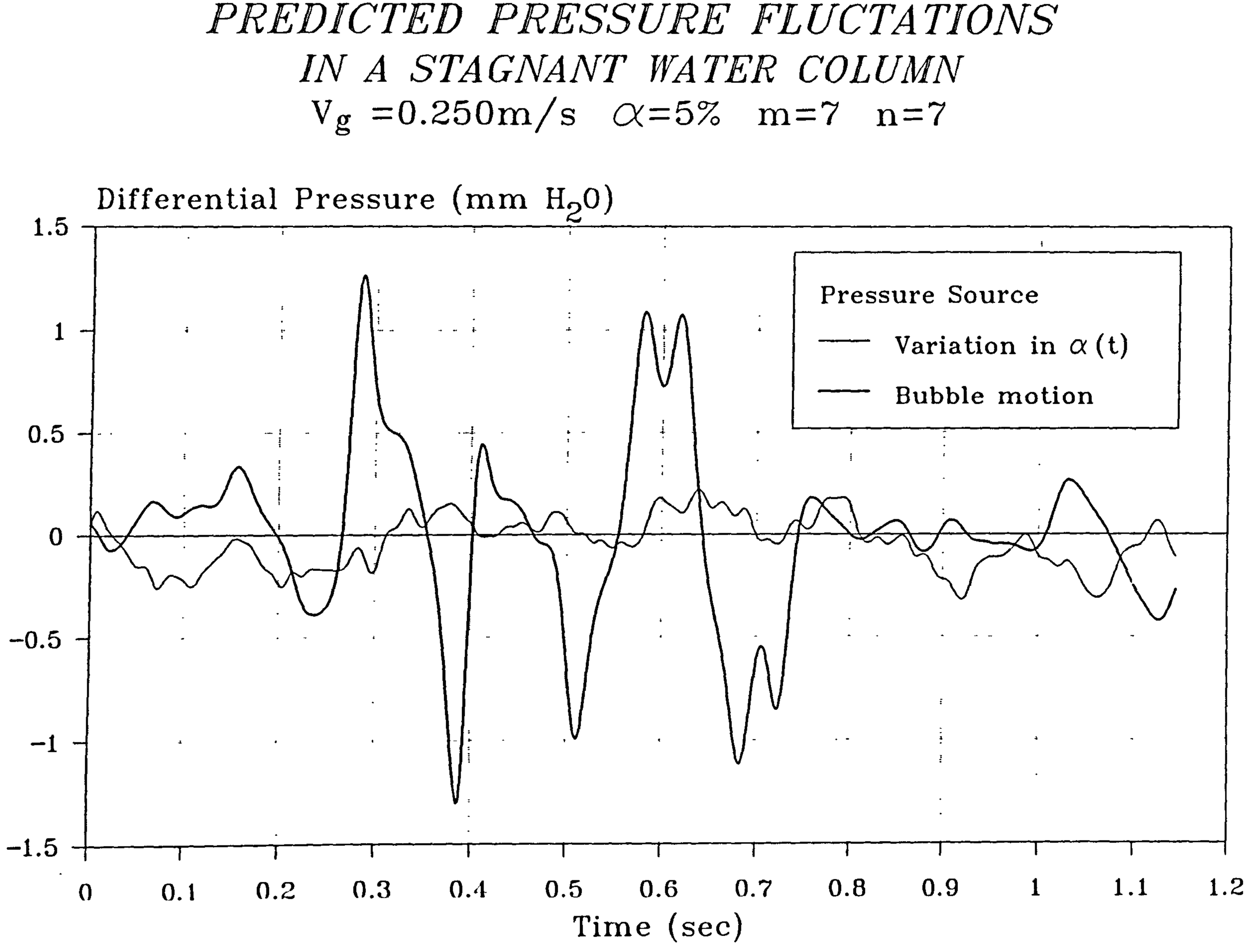

Figure 6.11 Comparison of magnitudes between the two pressure sources considered in the bubbly two-phase flow simulations

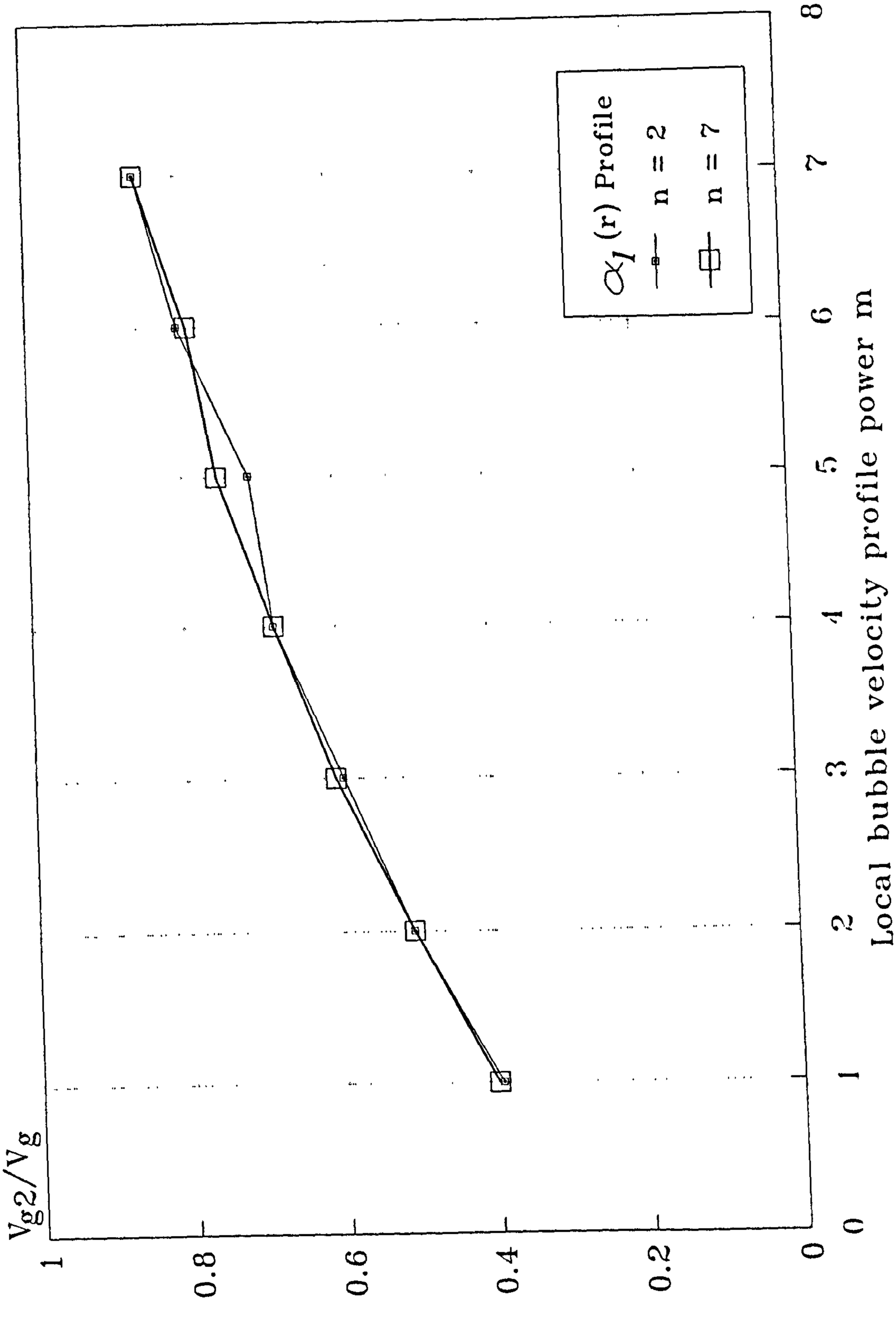

Figure 6.12 Convected disturbance velocity ratio evaluations from the simulated differential pressure fluctuations displayed as functions of the local gas void fraction and velocity profile powers n and m respectively

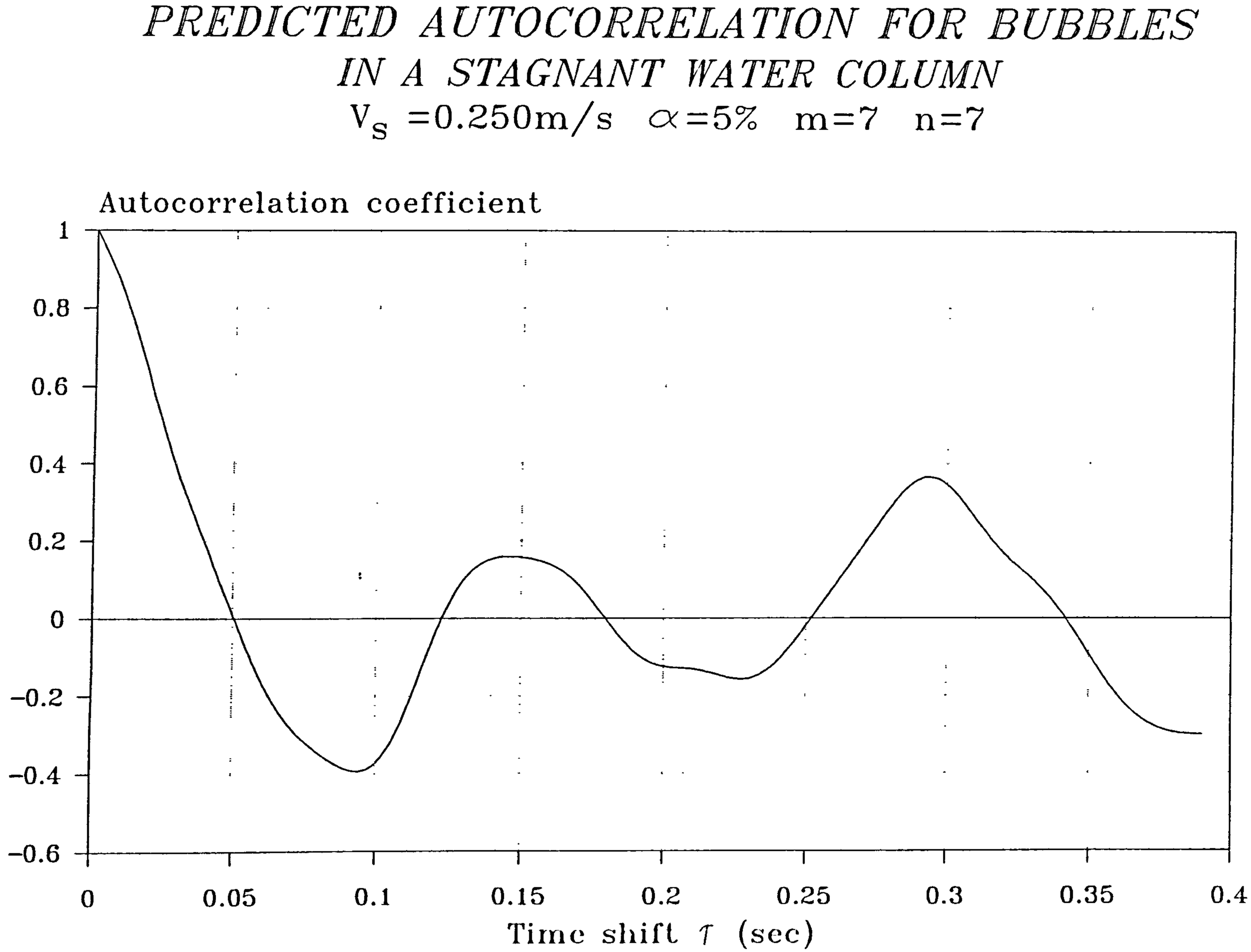

Figure 6.13 Typical autocorrelation correlogram of a simulated bubbly two-phase flow

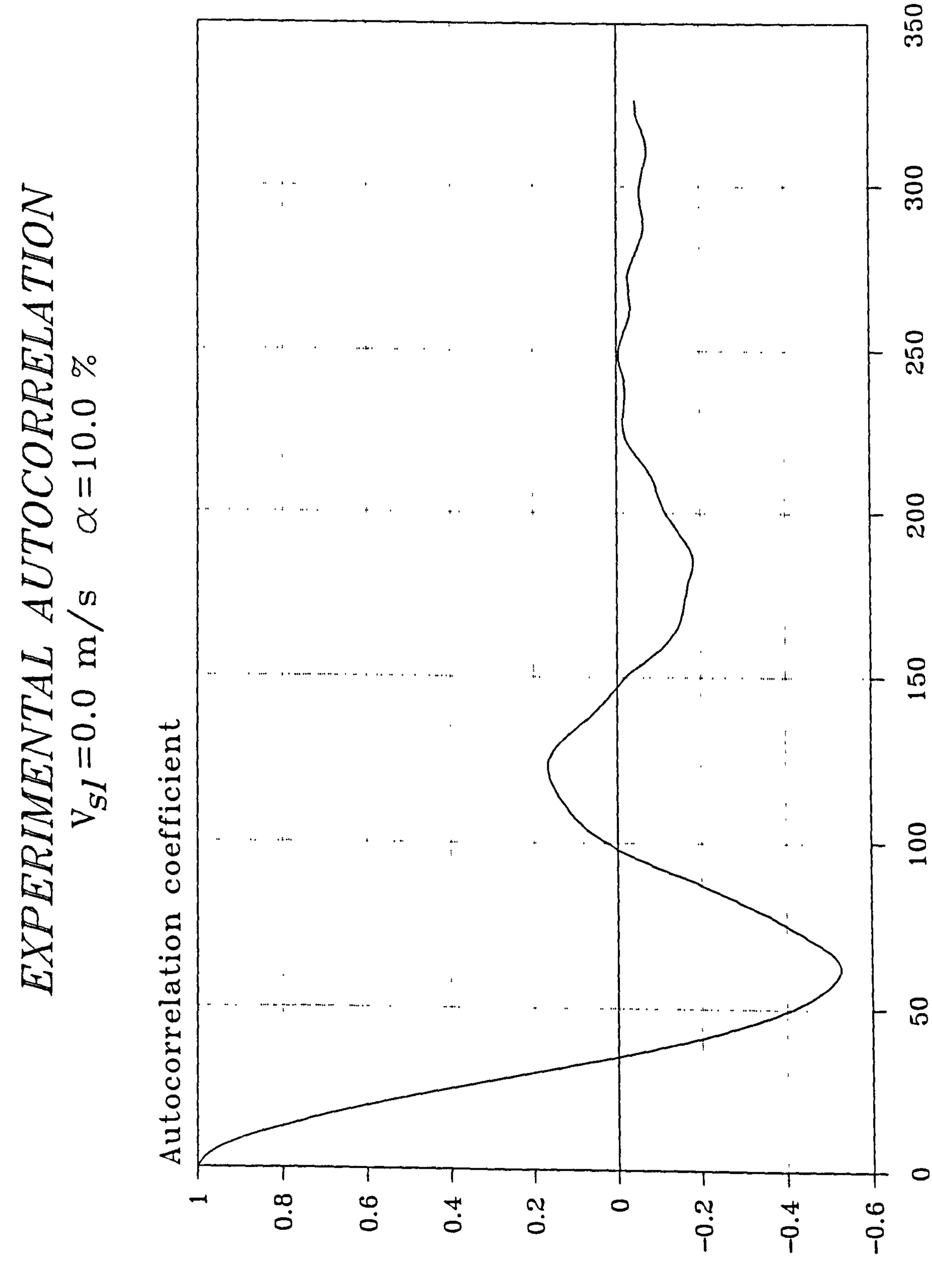

Figure 6.14a Measured autocorrelation of differential pressure fluctuations in a stagnant column of liquid with an average gas void fraction $\alpha \simeq 10\%$

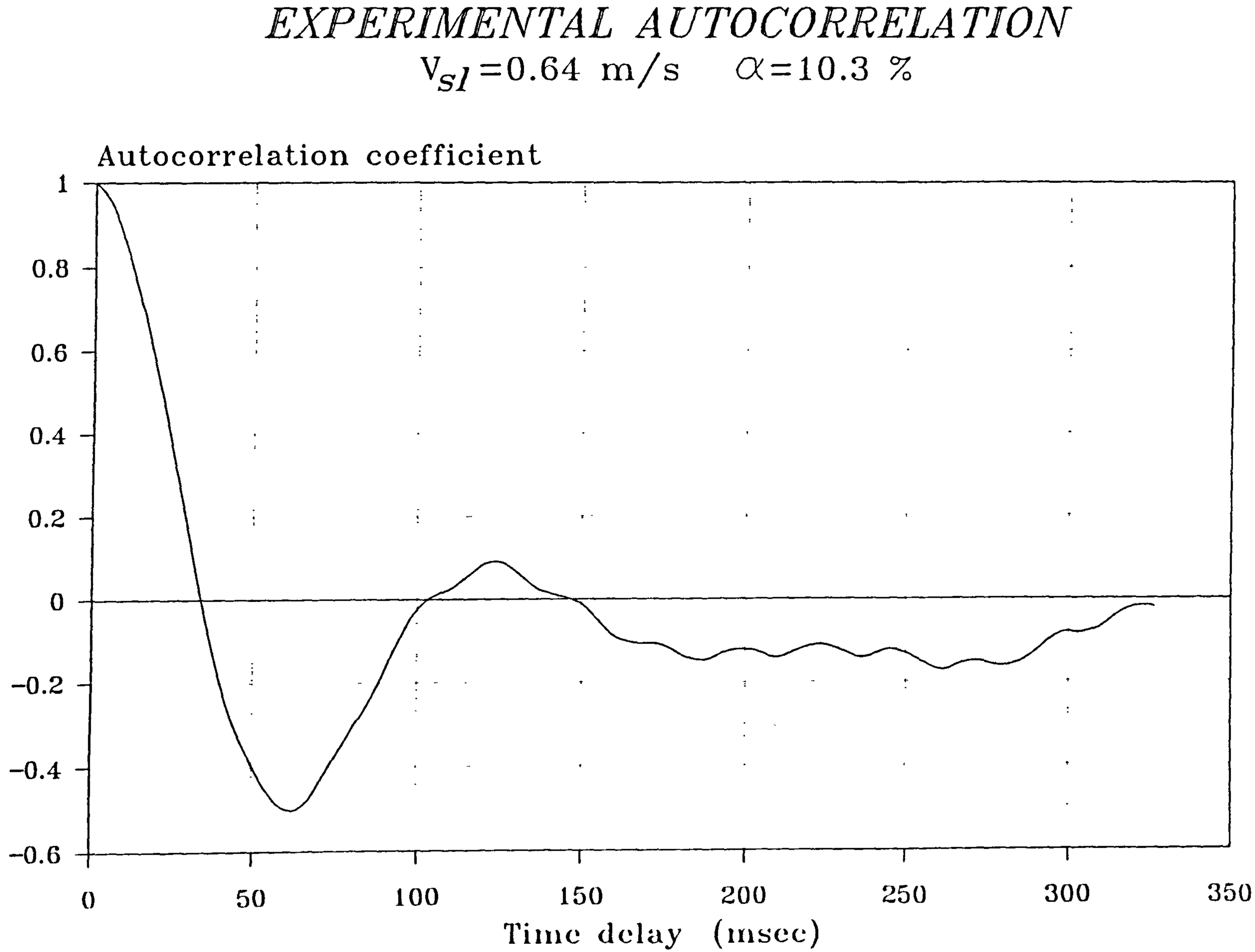

Figure 6.14b Measured autocorrelation of differential pressure fluctuations, V_{sl} = 0.64 m/s, and α ≈ 10%

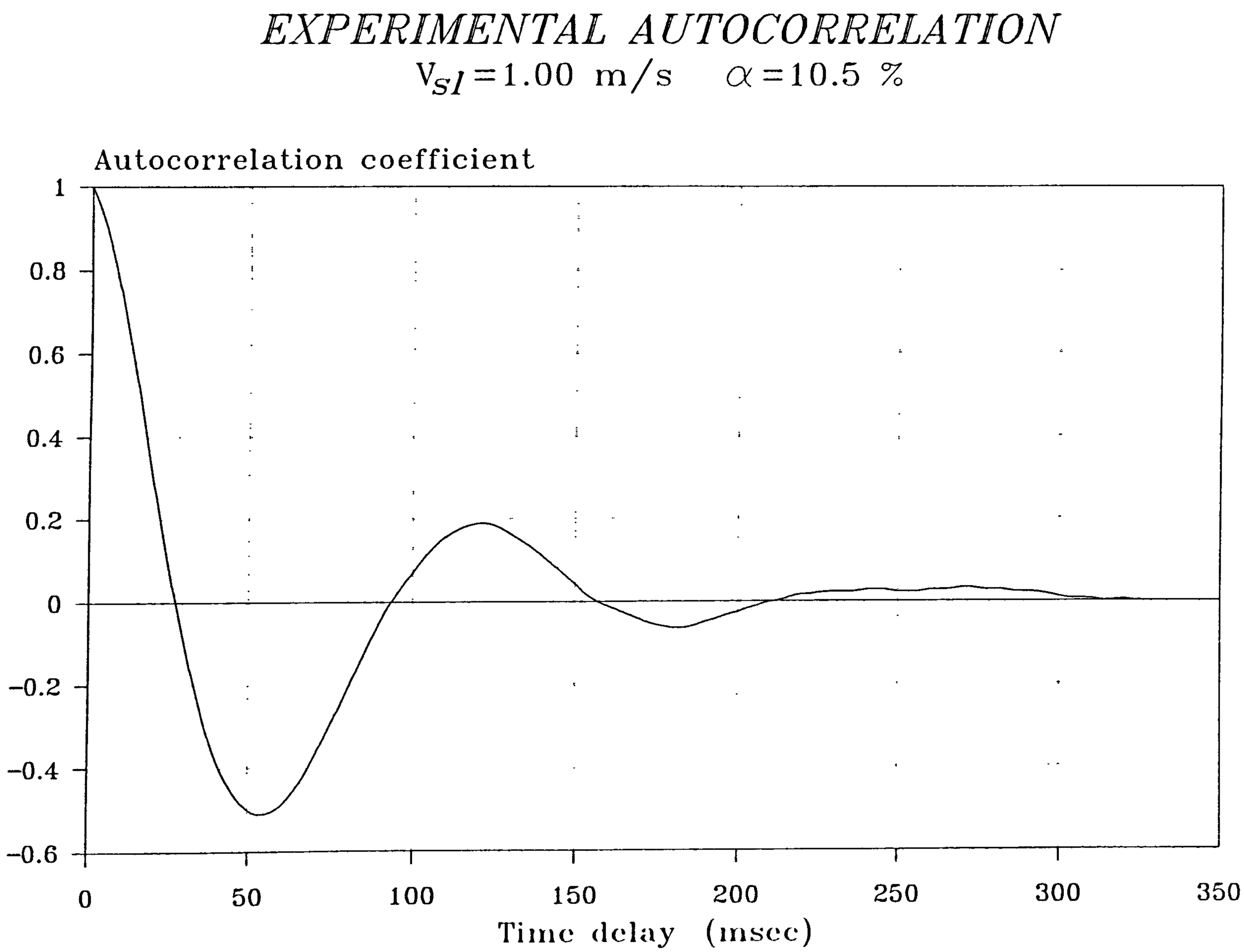

Figure 6.14c Measured autocorrelation of differential pressure fluctuations, V_{sl} = 1.0 m/s, and $\alpha \approx 10\%$

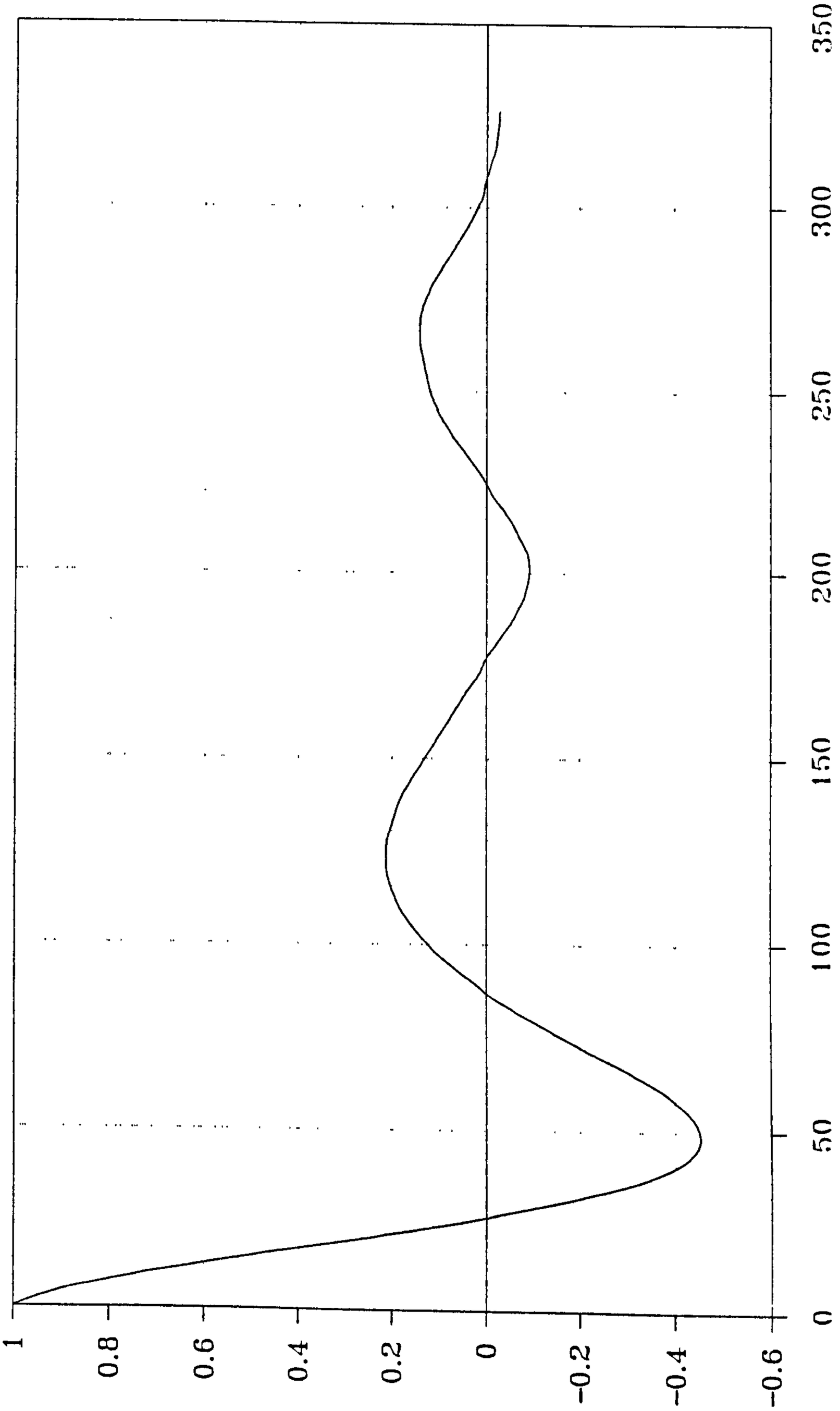

Figure 6.14d Measured autocorrelation of differential pressure fluctuations, V_{sl} = 1.5 m/s, and $\alpha \simeq 10\%$

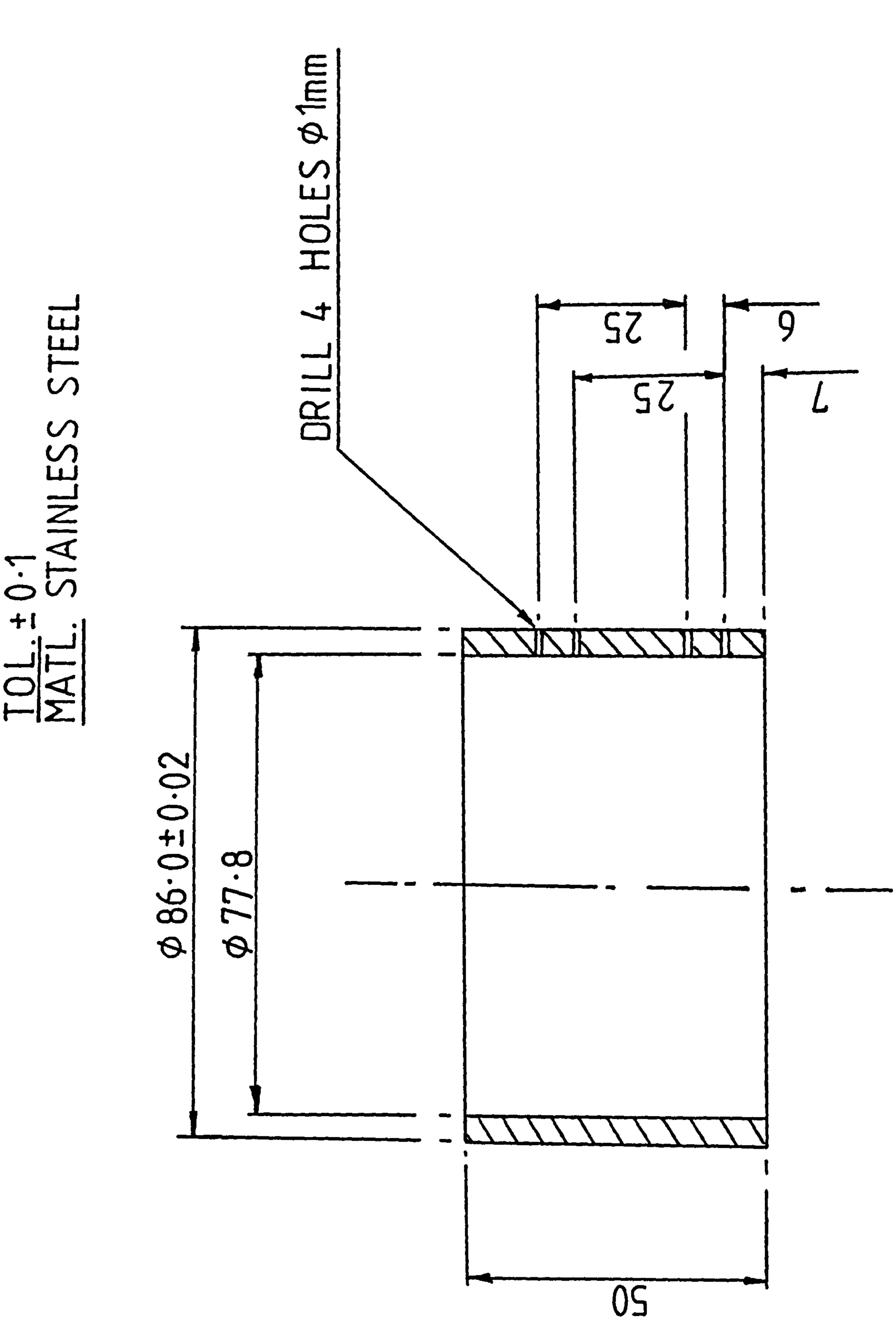

Figure 6.15 Transducer housing pressure tappings insert machining detail

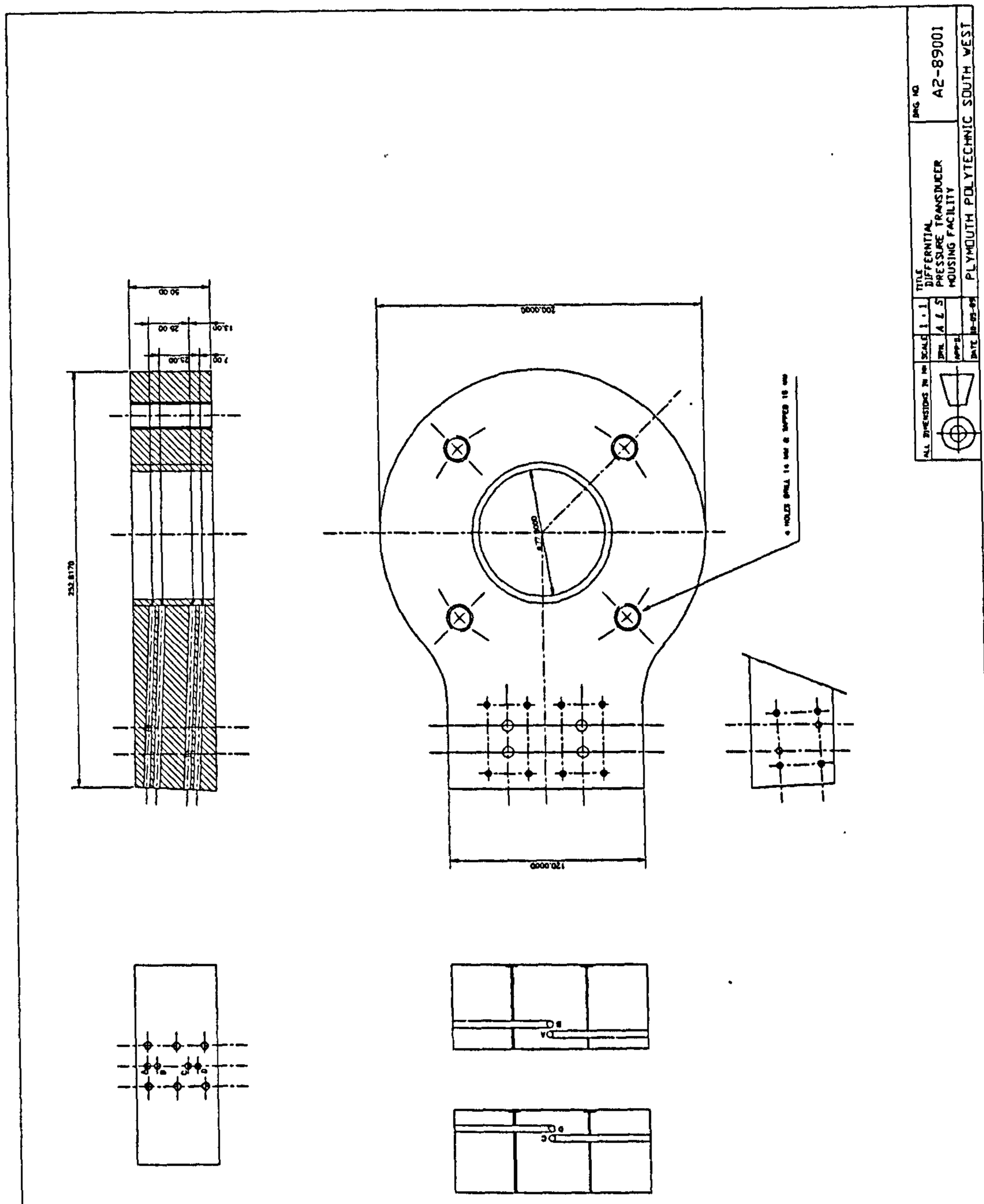

Figure 6.16 Transducer housing detail

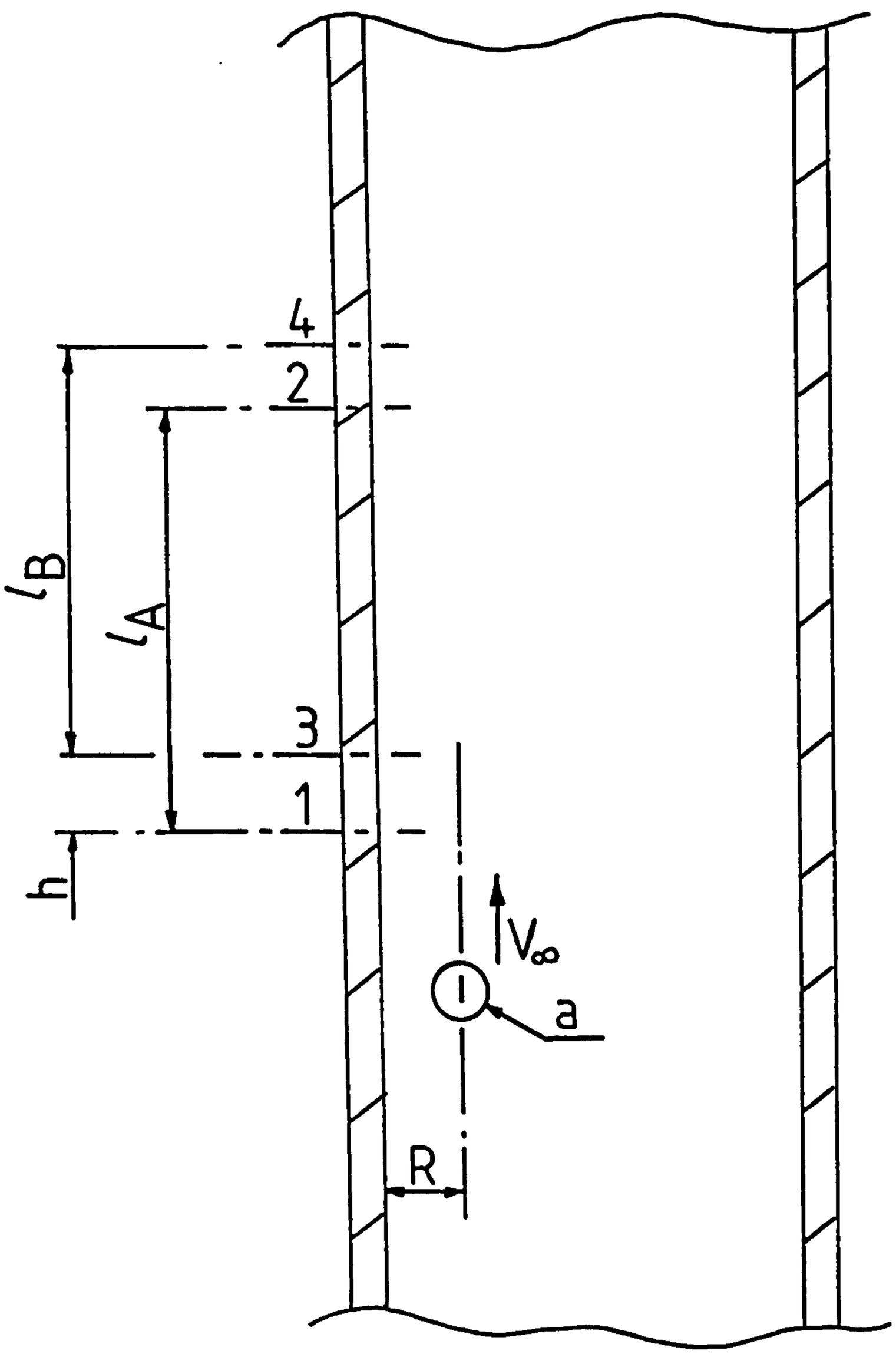

Figure 6.17 Variation between the tapping separation distance of transducer A, l_A, and transducer B, l_B

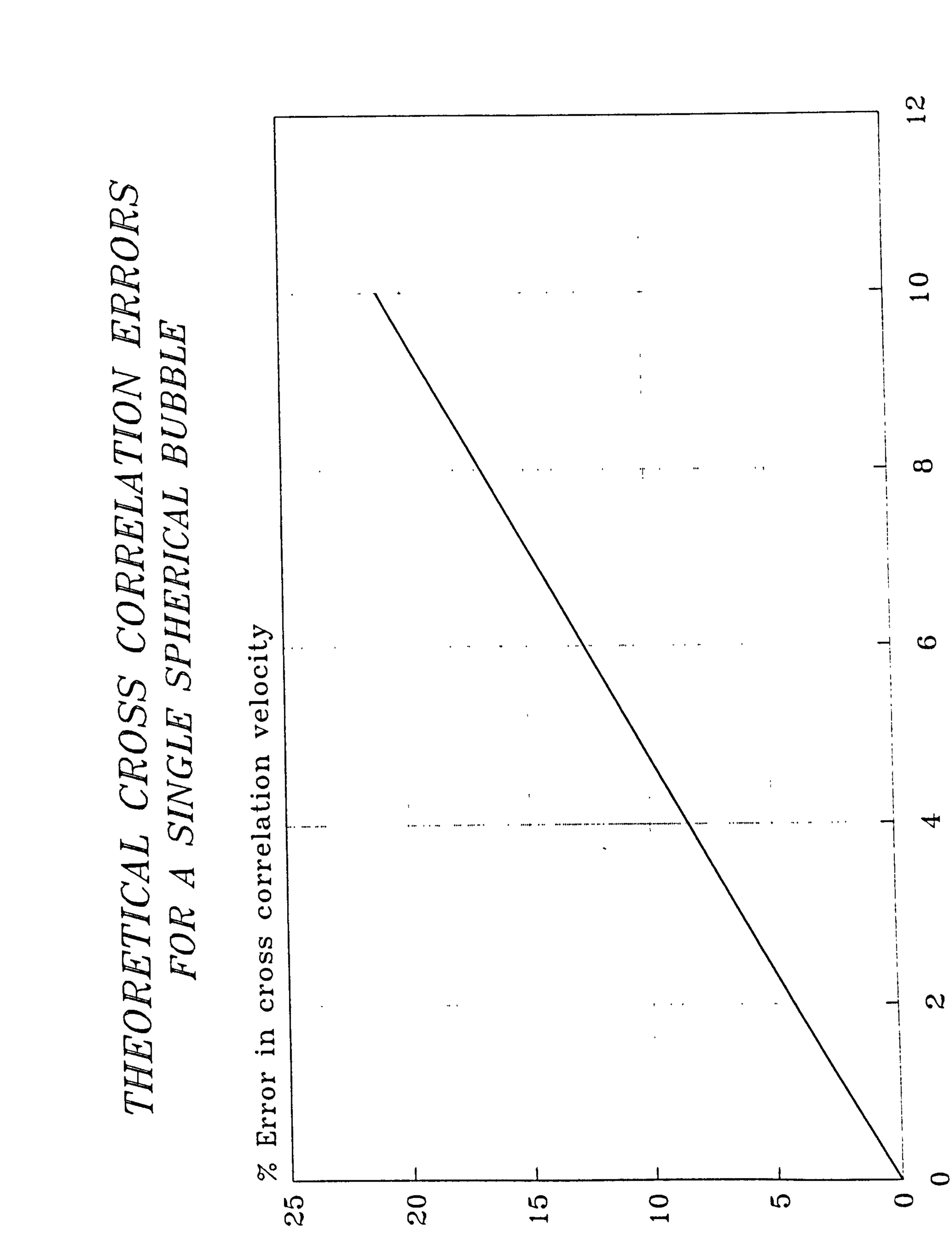

Figure 6.18 Predicted percentage error in cross correlation convected velocity measurement as a function of the variation in transducer tapping separation distances l_A and l_B

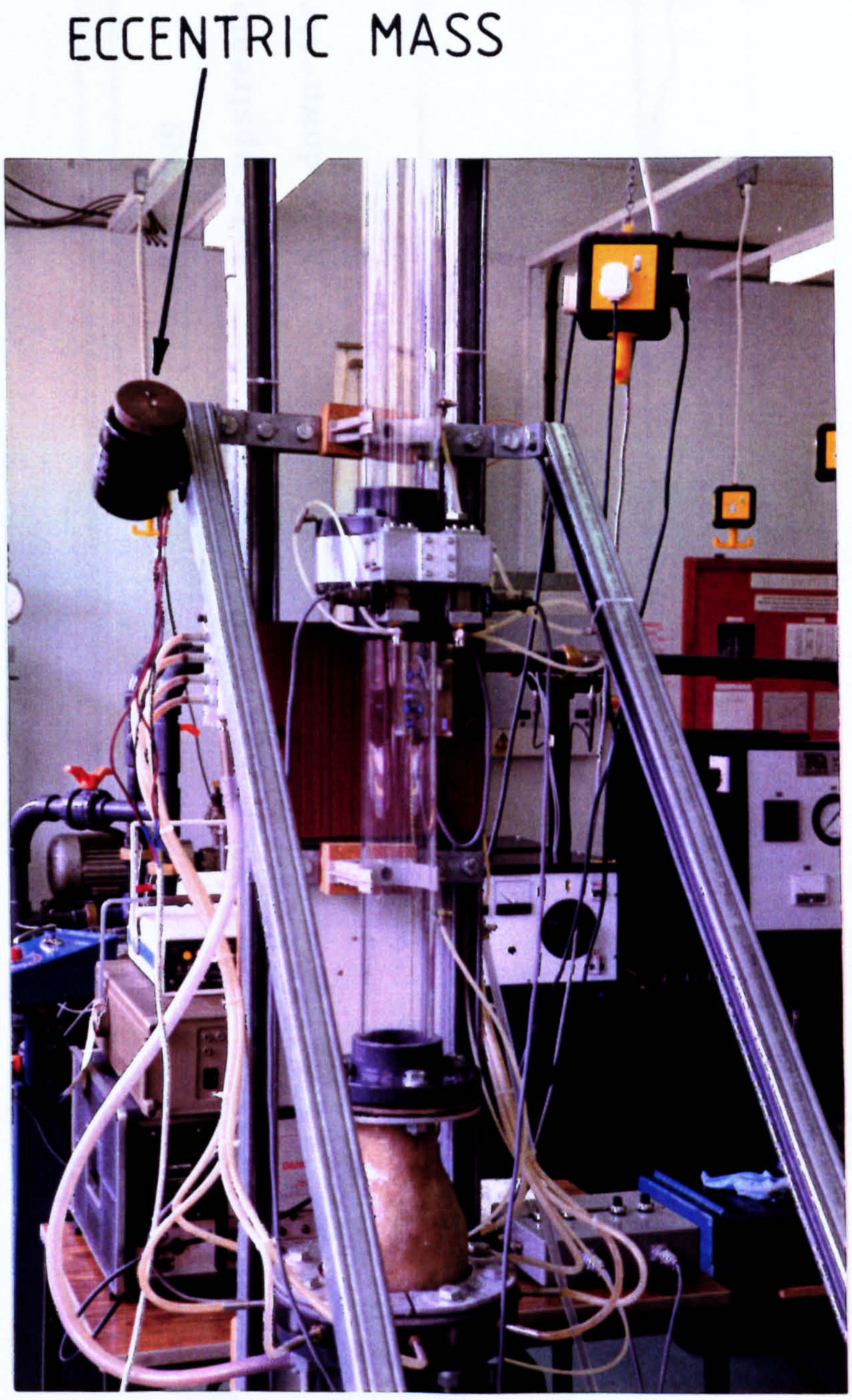

Figure 6.19 Photograph of the experimental test section showing the differential pressure transducer housing and the eccentric mass used to excite and match the differential pressure transducers

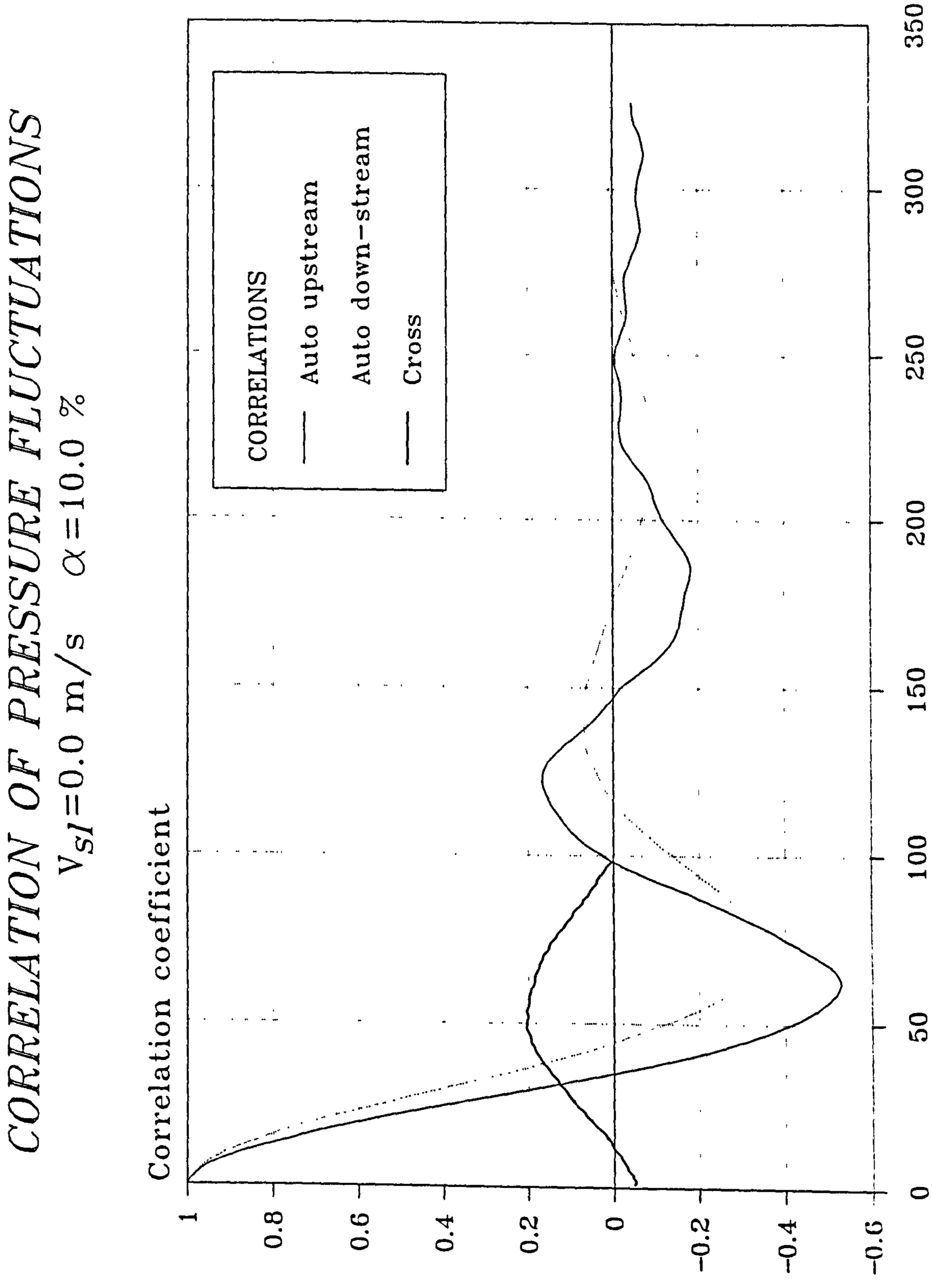

Figure 6.20 Measured auto and cross correlation correlograms of differential pressure fluctuations in bubbly flow

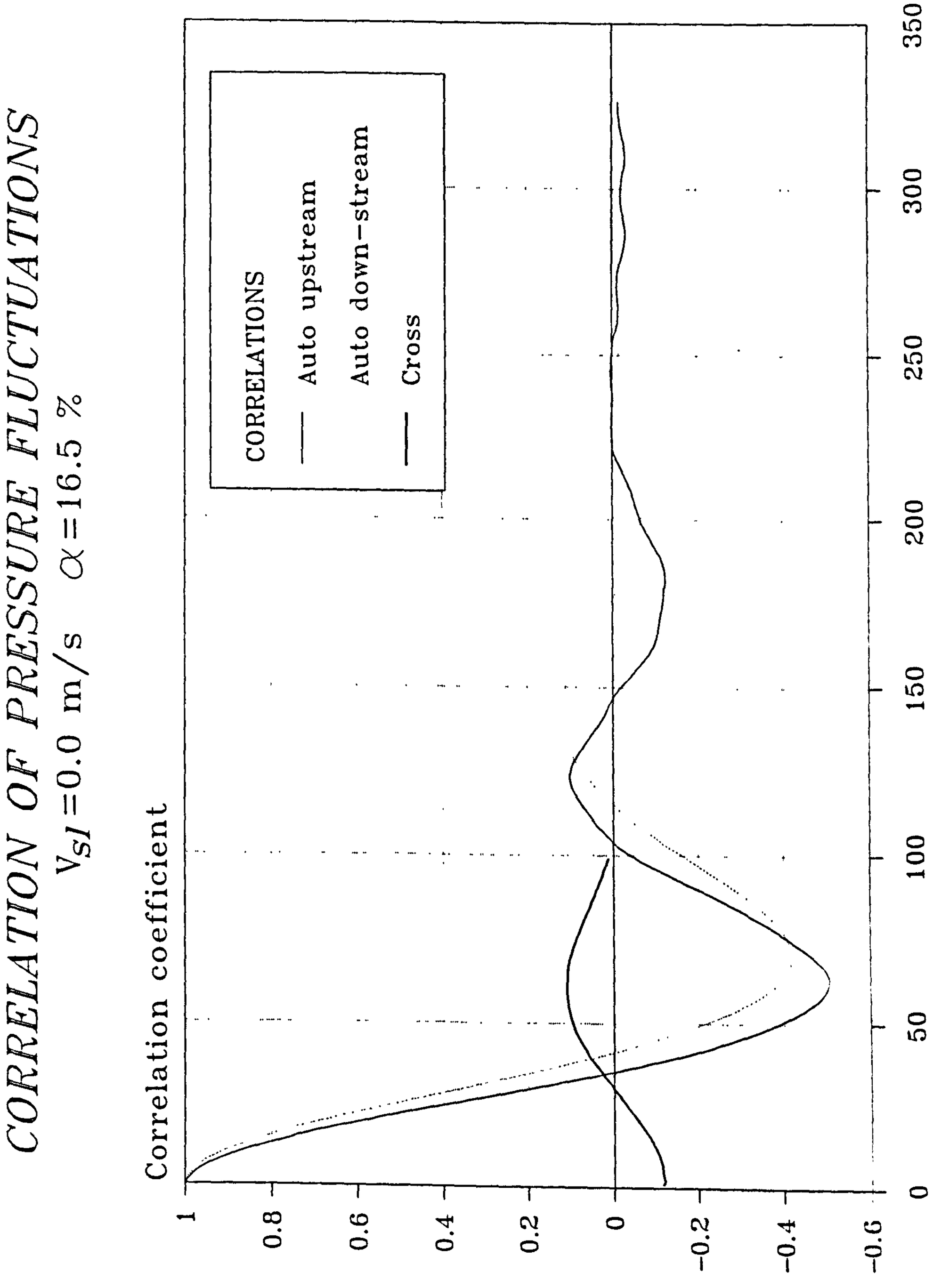

Figure 6.21 Measured auto and cross correlation correlograms of differential pressure fluctuations in bubbly flow

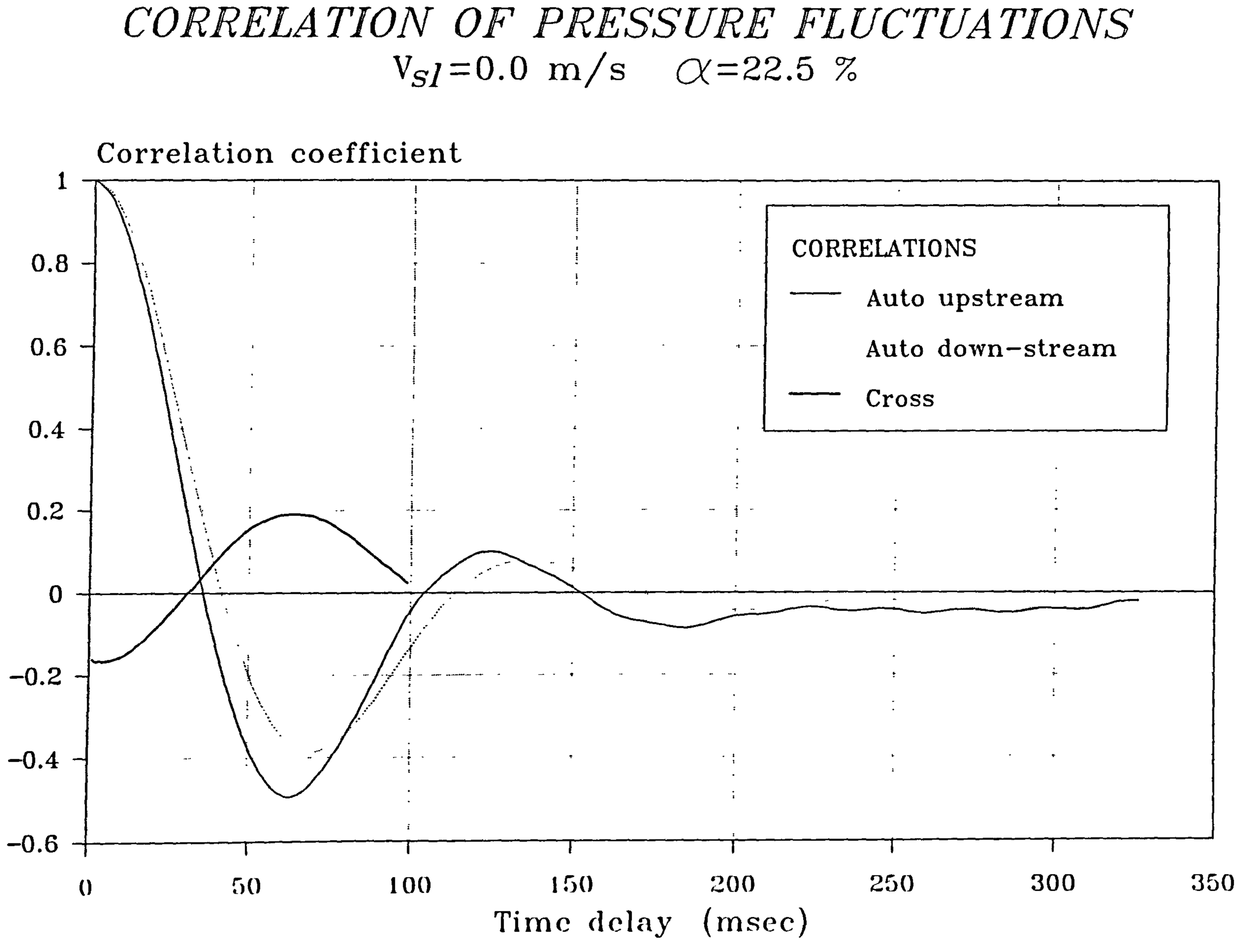

Figure 6.22 Measured auto and cross correlation correlograms of differential pressure fluctuations in bubbly flow

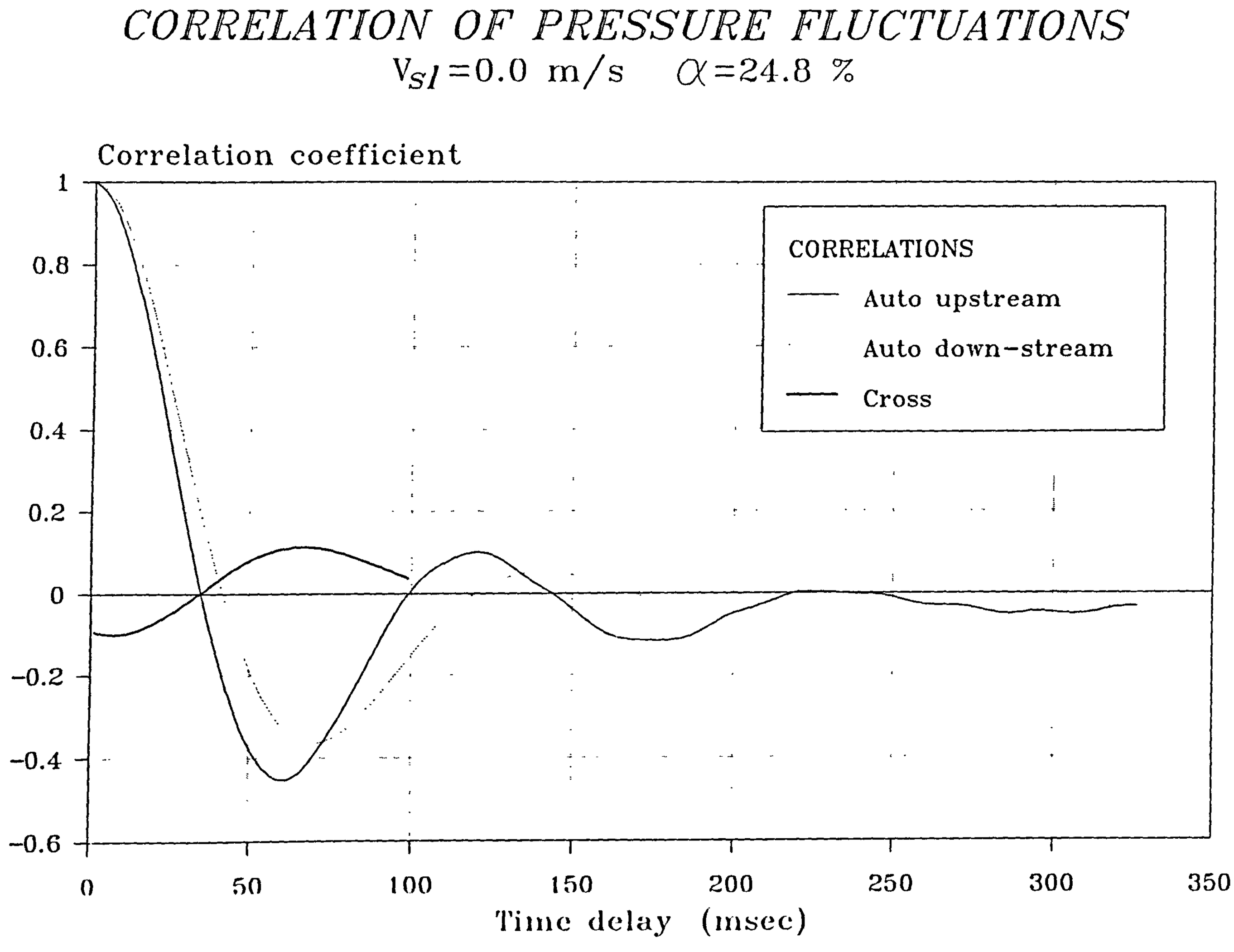

Figure 6.23 Measured auto and cross correlation correlograms of differential pressure fluctuations in bubbly flow

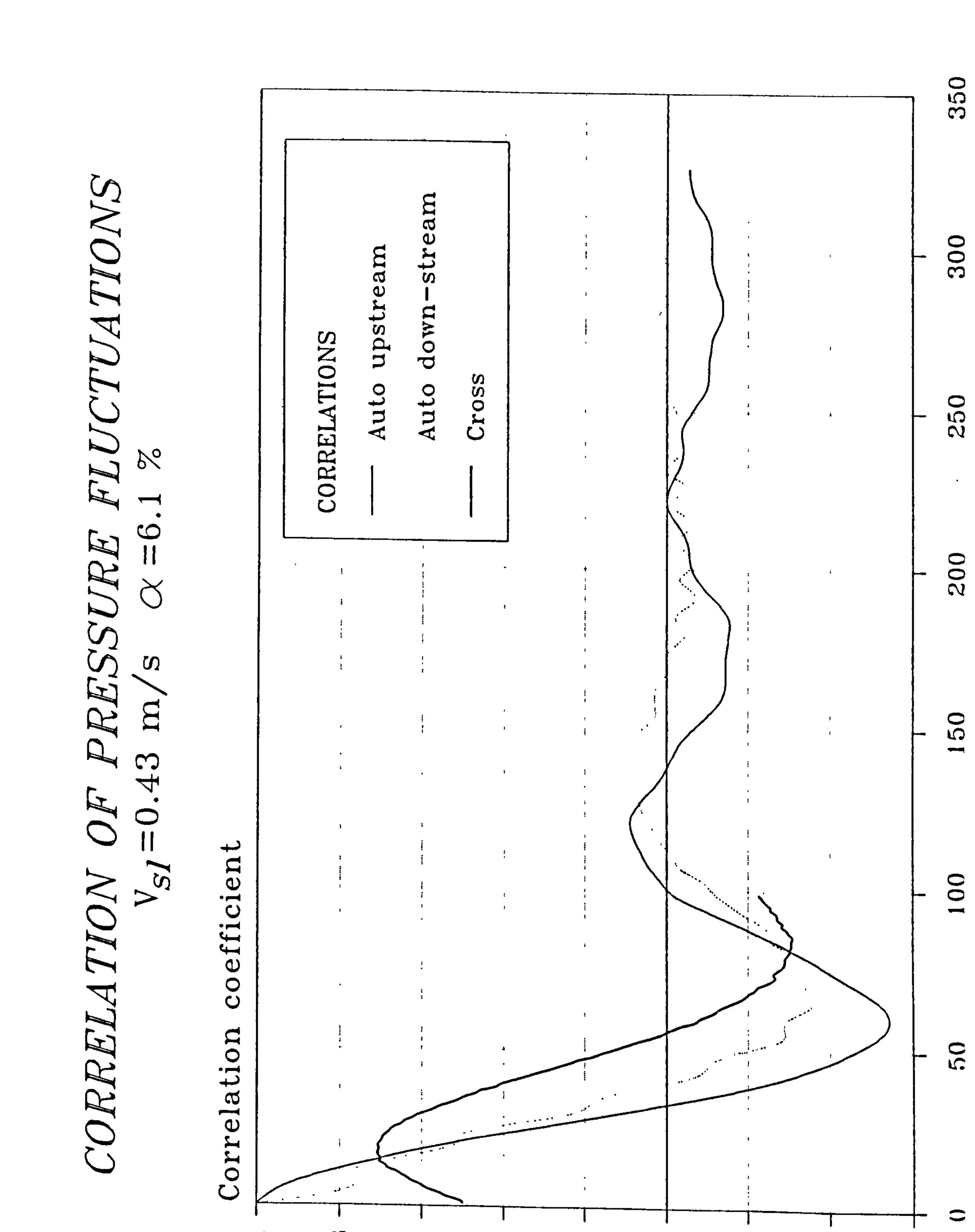

Figure 6.24 Measured auto and cross correlation correlograms of differential pressure fluctuations in bubbly flow

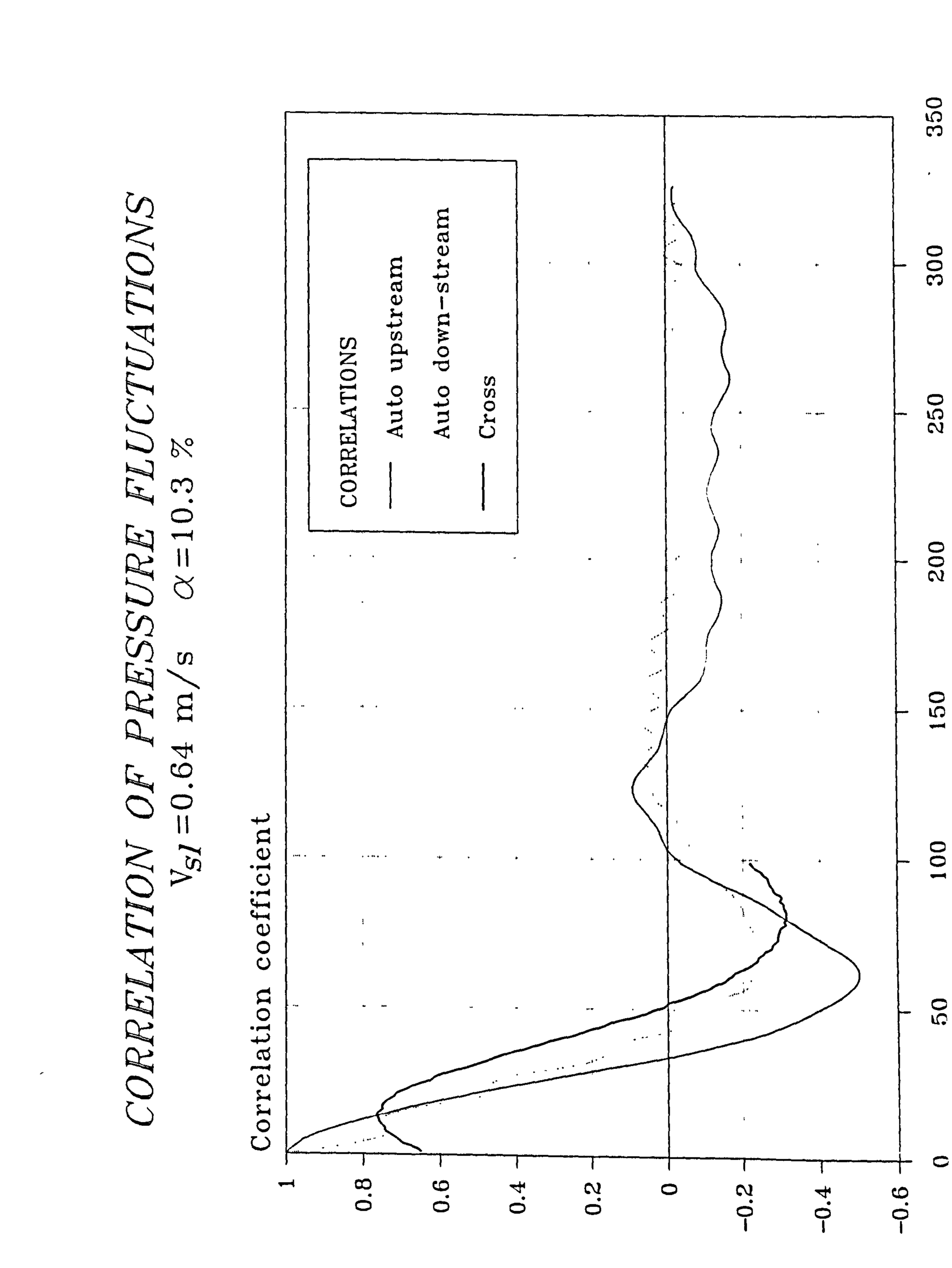

Figure 6.25 Measured auto and cross correlation correlograms of differential pressure fluctuations in bubbly flow

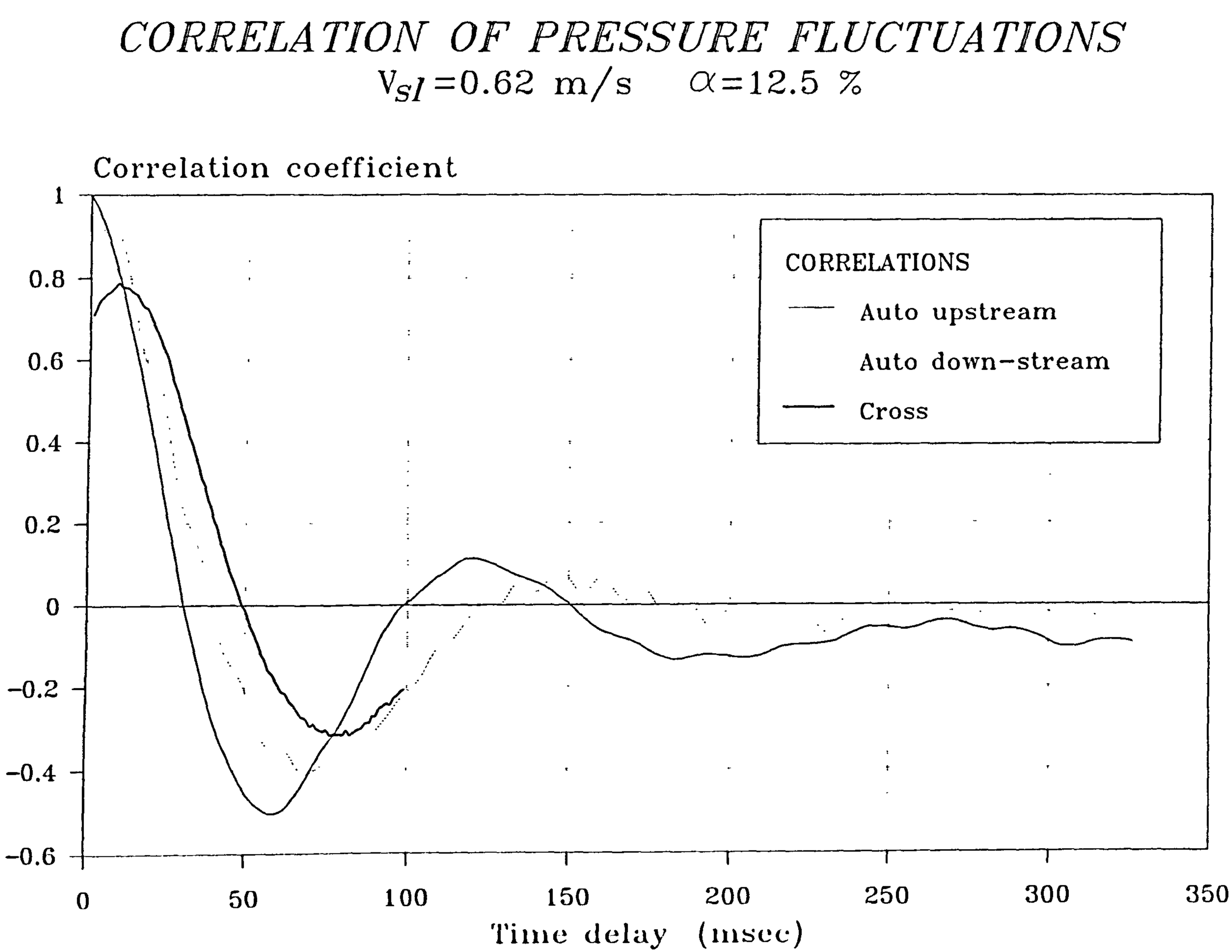

Figure 6.26 Measured auto and cross correlation correlograms of differential pressure fluctuations in bubbly flow

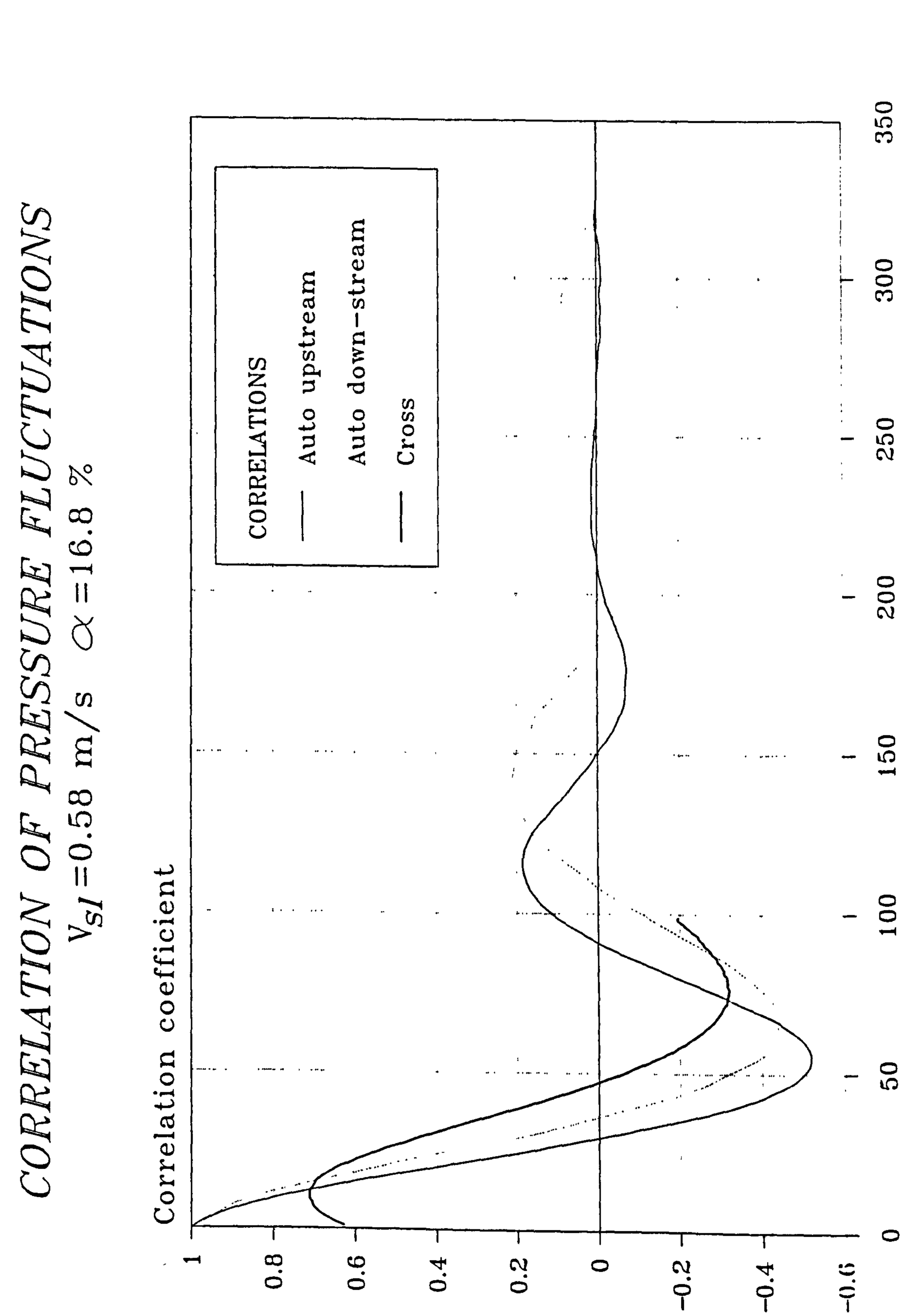

Figure 6.27 Measured auto and cross correlation correlograms of differential pressure fluctuations in bubbly flow

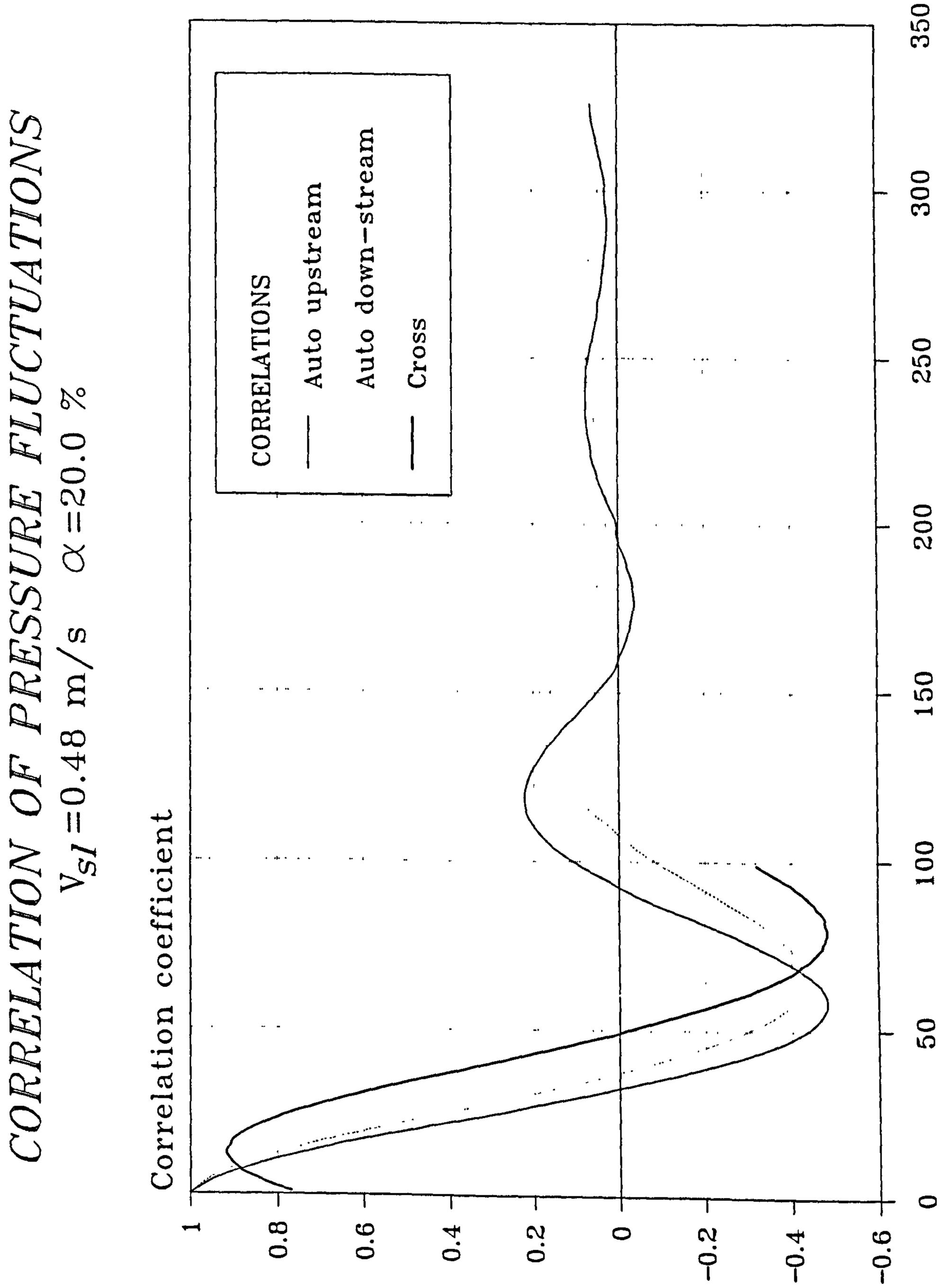

Figure 6.28 Measured auto and cross correlation correlograms of differential pressure fluctuations in bubbly flow

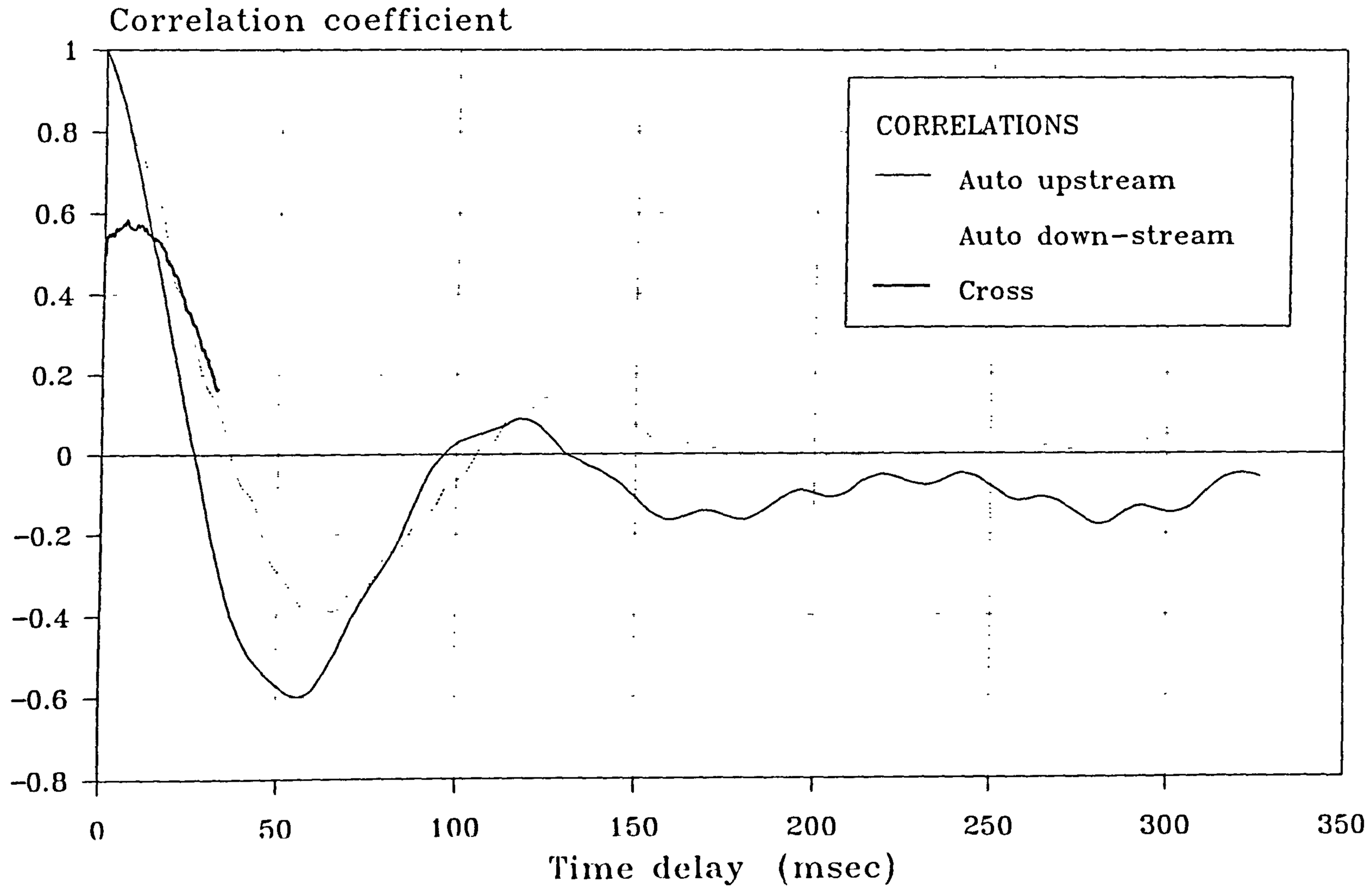

Figure 6.29 Measured auto and cross correlation correlograms of differential pressure fluctuations in bubbly flow

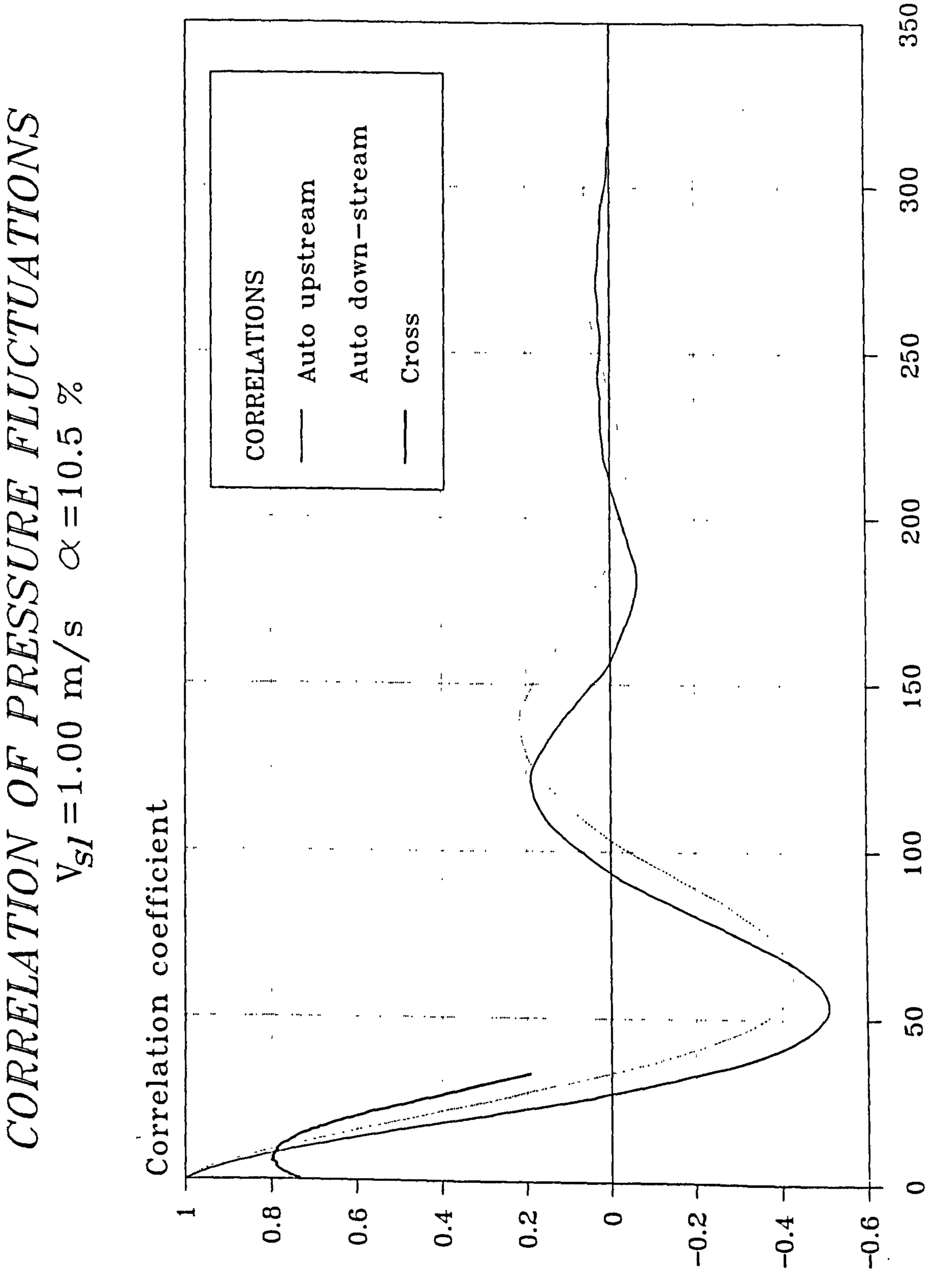

Figure 6.30 Measured auto and cross correlation correlograms of differential pressure fluctuations in bubbly flow

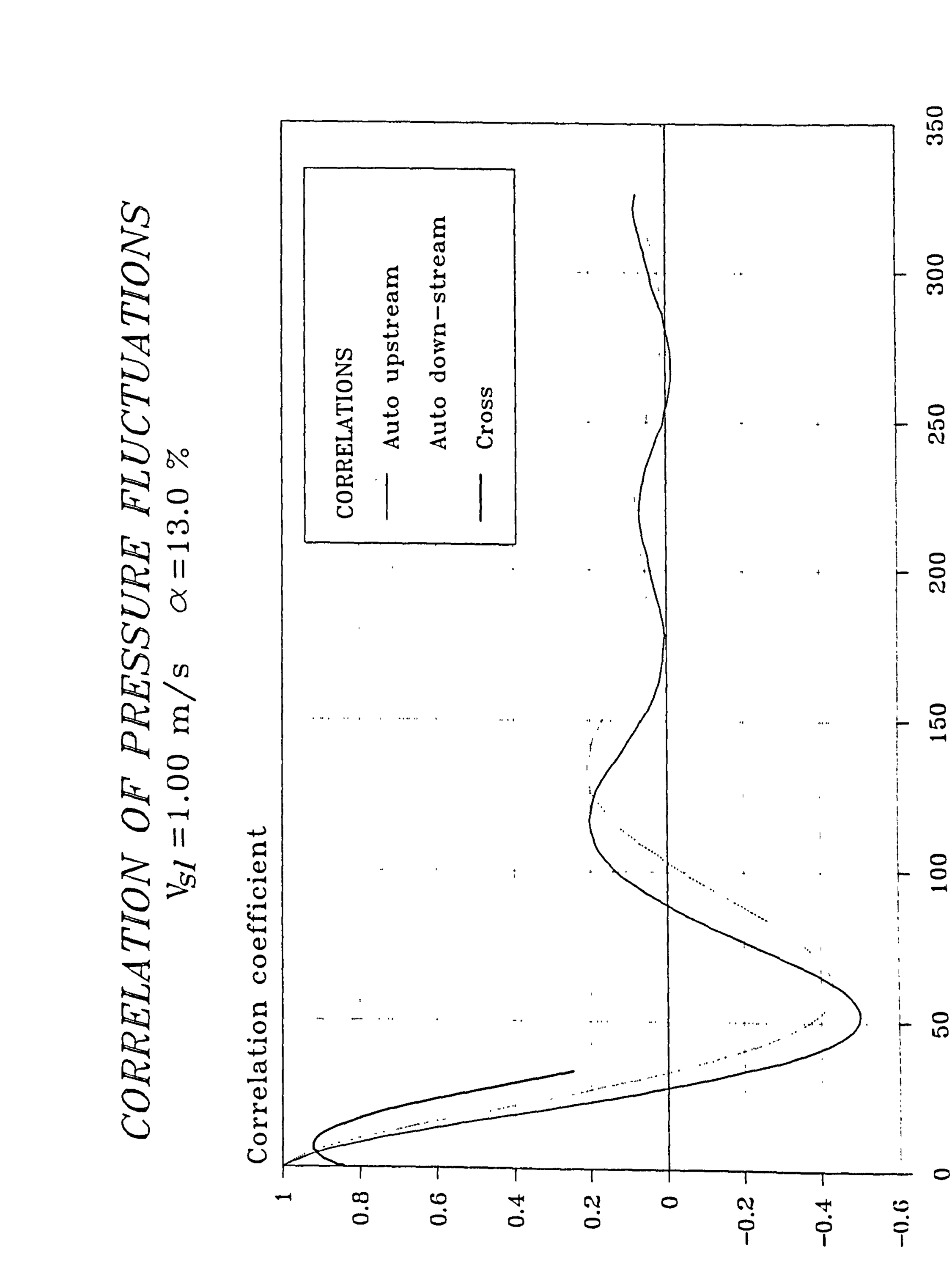

Figure 6.31 Measured auto and cross correlation correlograms of differential pressure fluctuations in bubbly flow

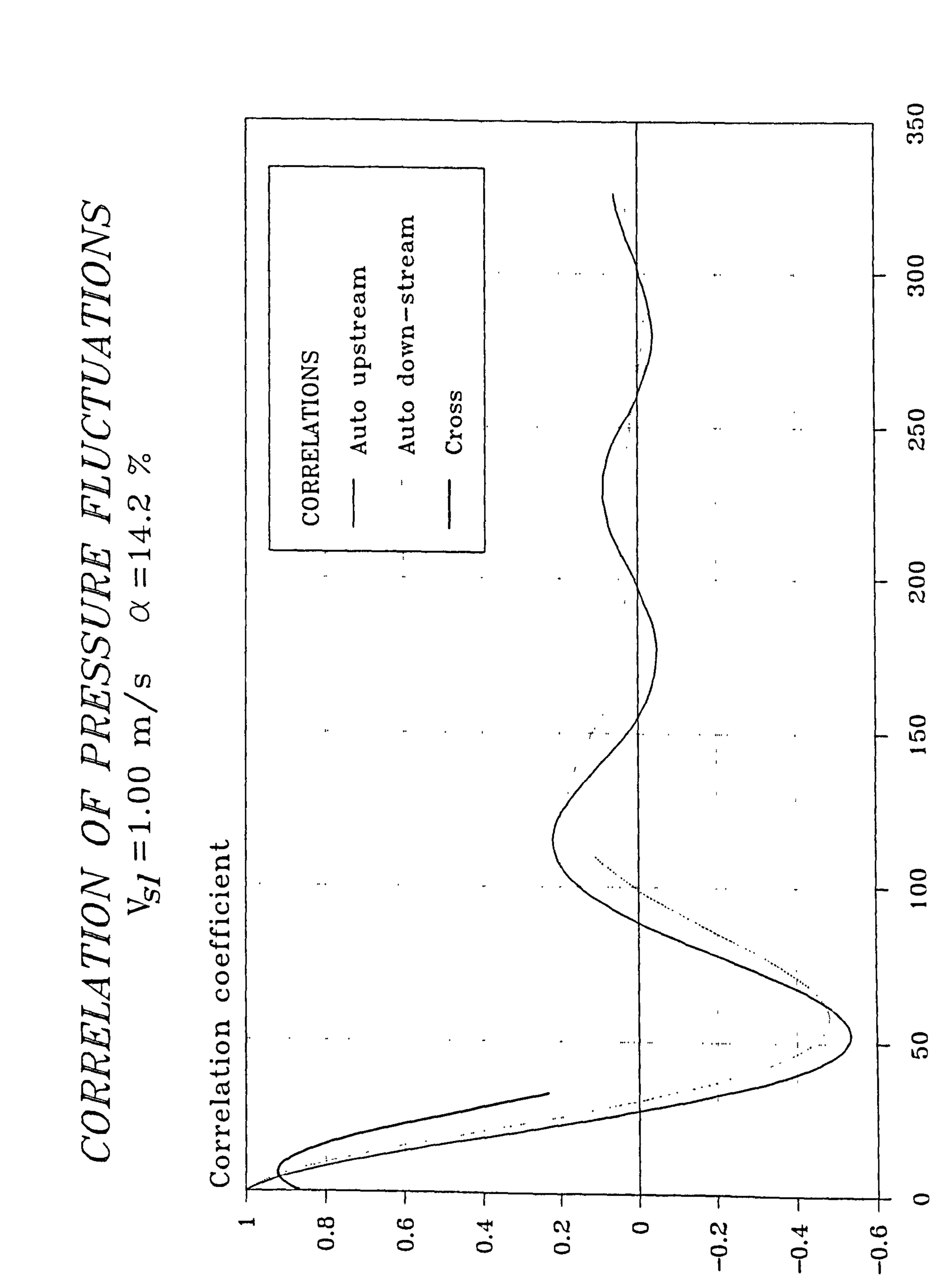

Figure 6.32 Measured auto and cross correlation correlograms of differential pressure fluctuations in bubbly flow

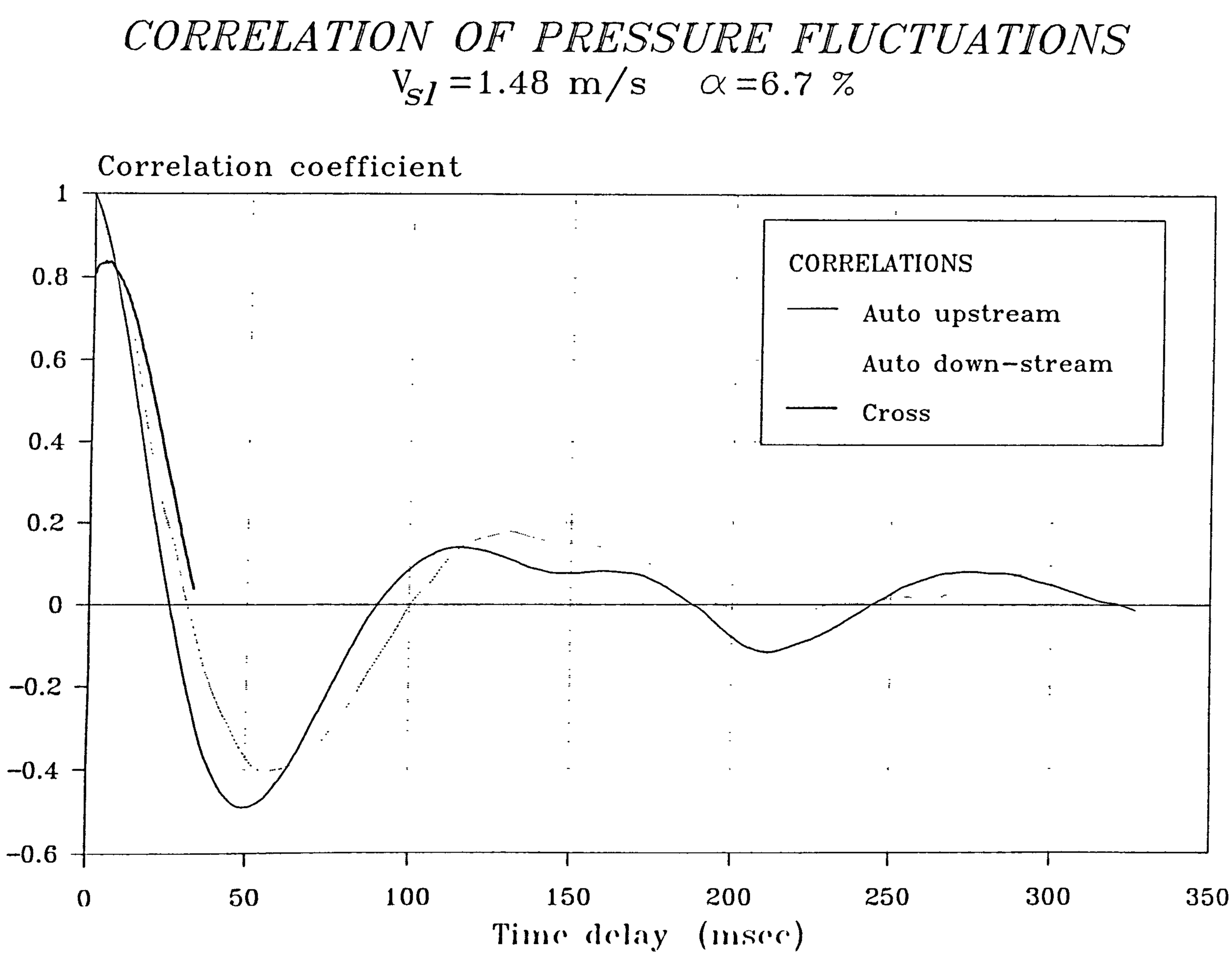

Figure 6.33 Measured auto and cross correlation correlograms of differential pressure fluctuations in bubbly flow

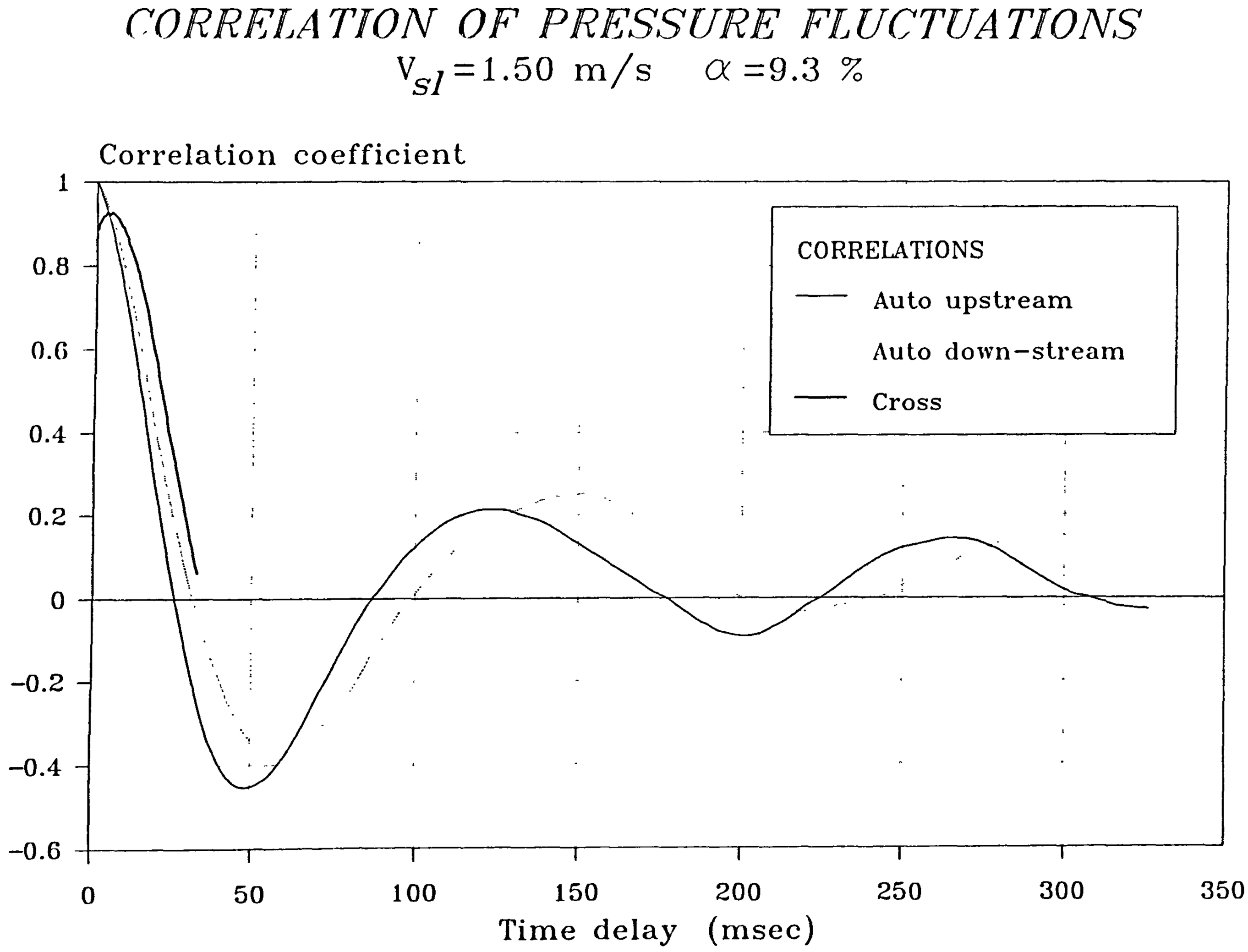

Figure 6.34 Measured auto and cross correlation correlograms of differential pressure fluctuations in bubbly flow

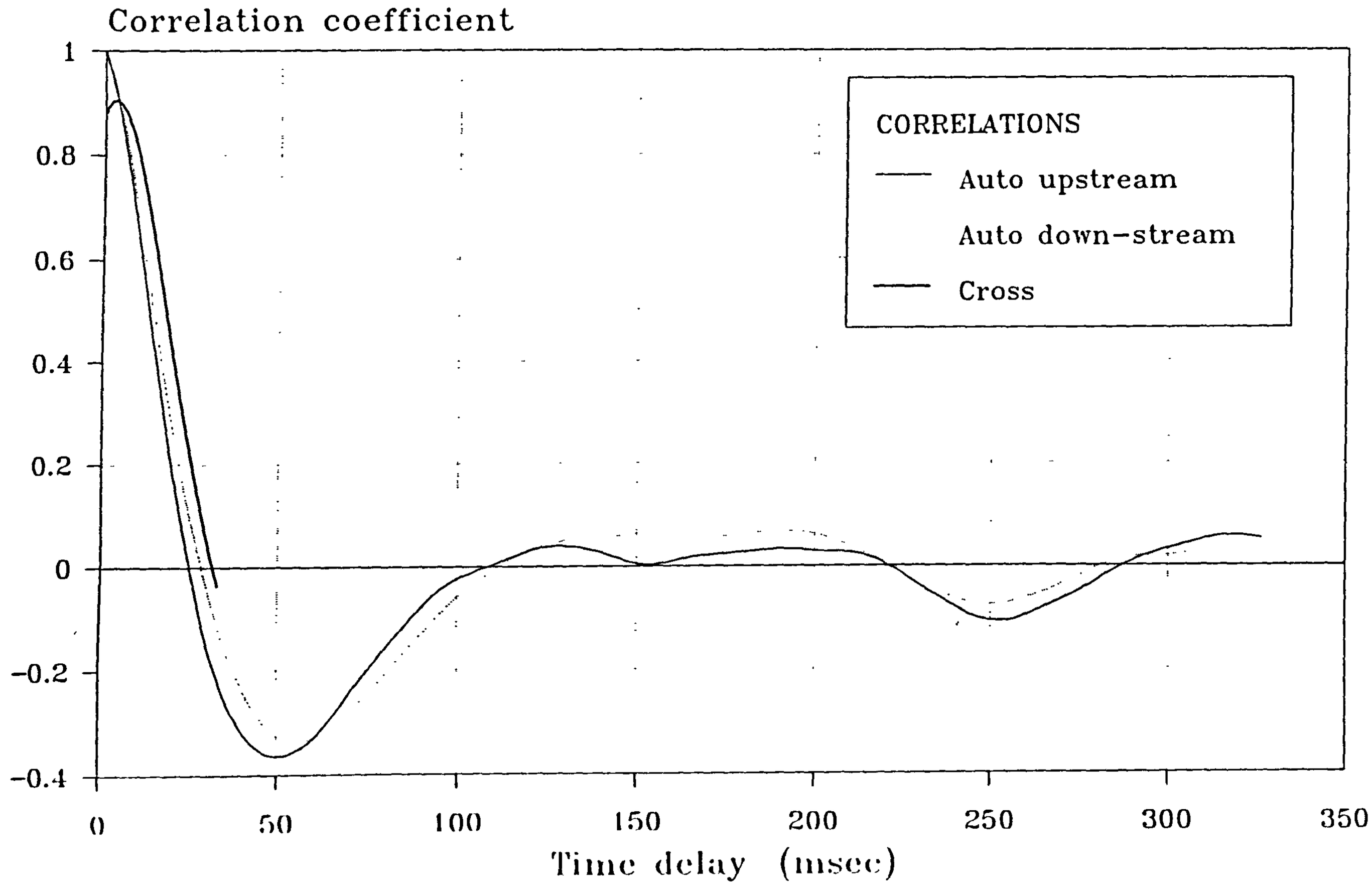

Figure 6.35 Measured auto and cross correlation correlograms of differential pressure fluctuations in bubbly flow

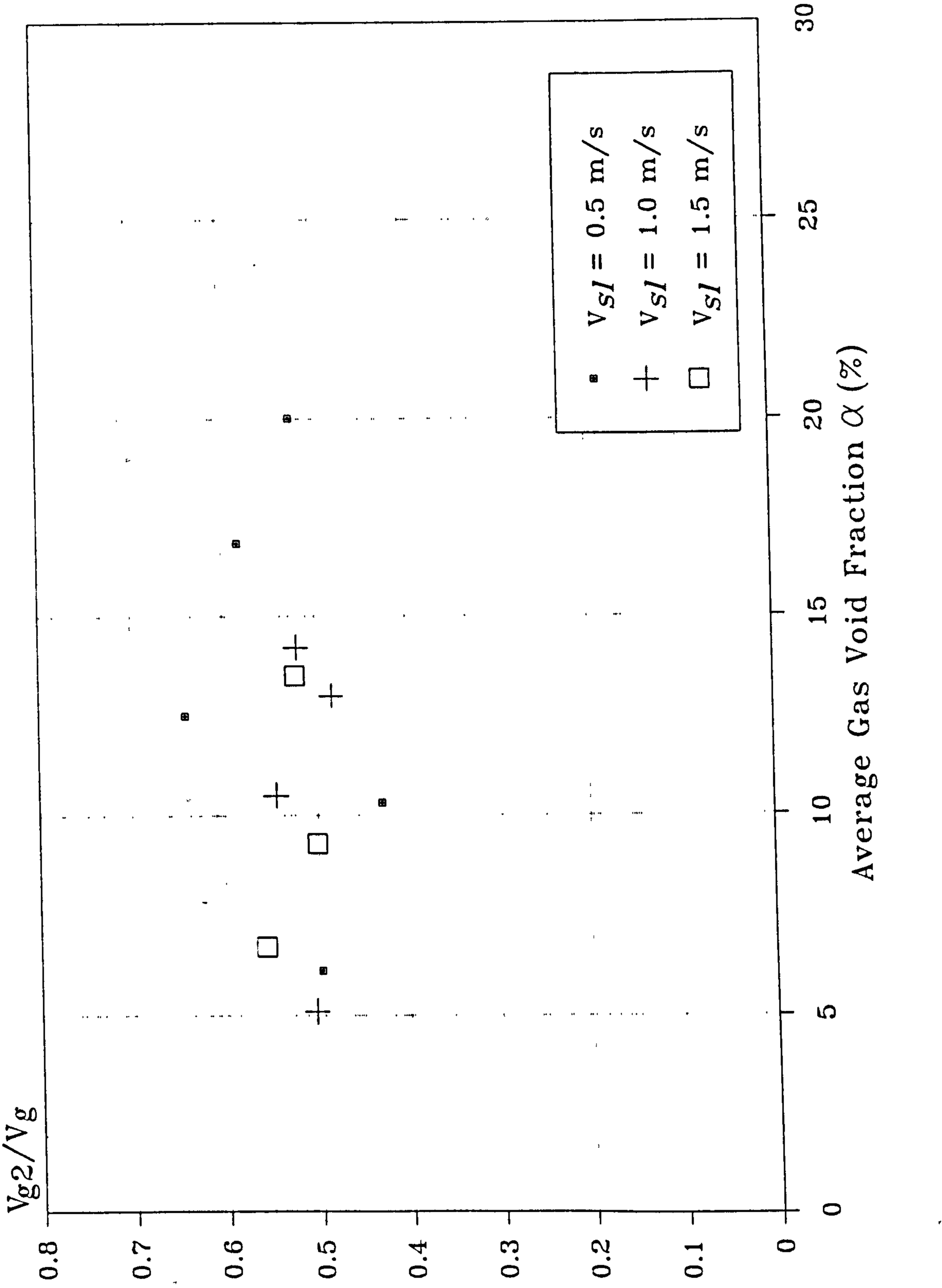

Figure 6.36 Convected disturbance velocity ratio V_{g_2}/V_g evaluations for non-zero continuous phase flows plotted as a function of the average gas void fraction α

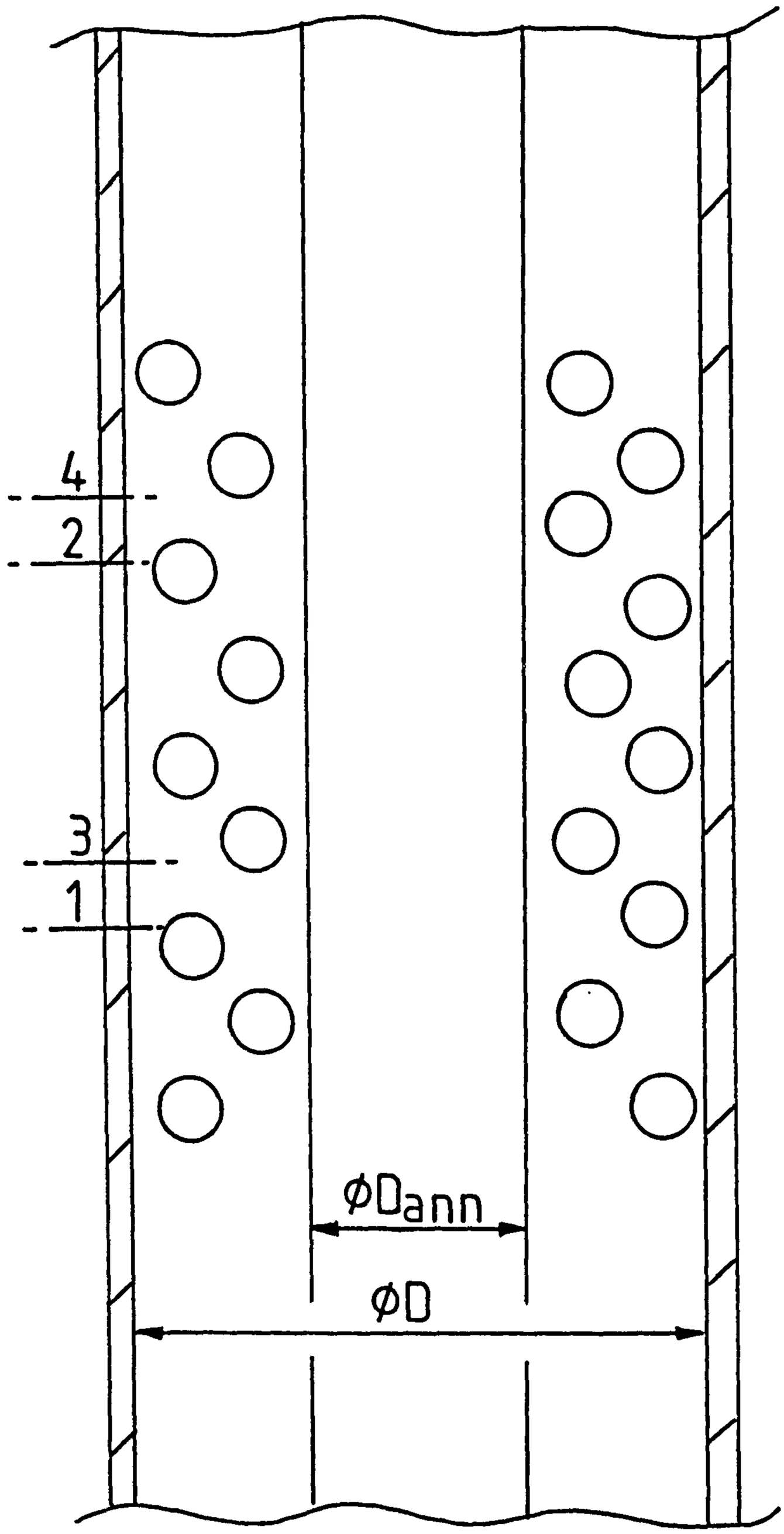

Figure 6.37 Illustration of experimental annular two-phase flow setup

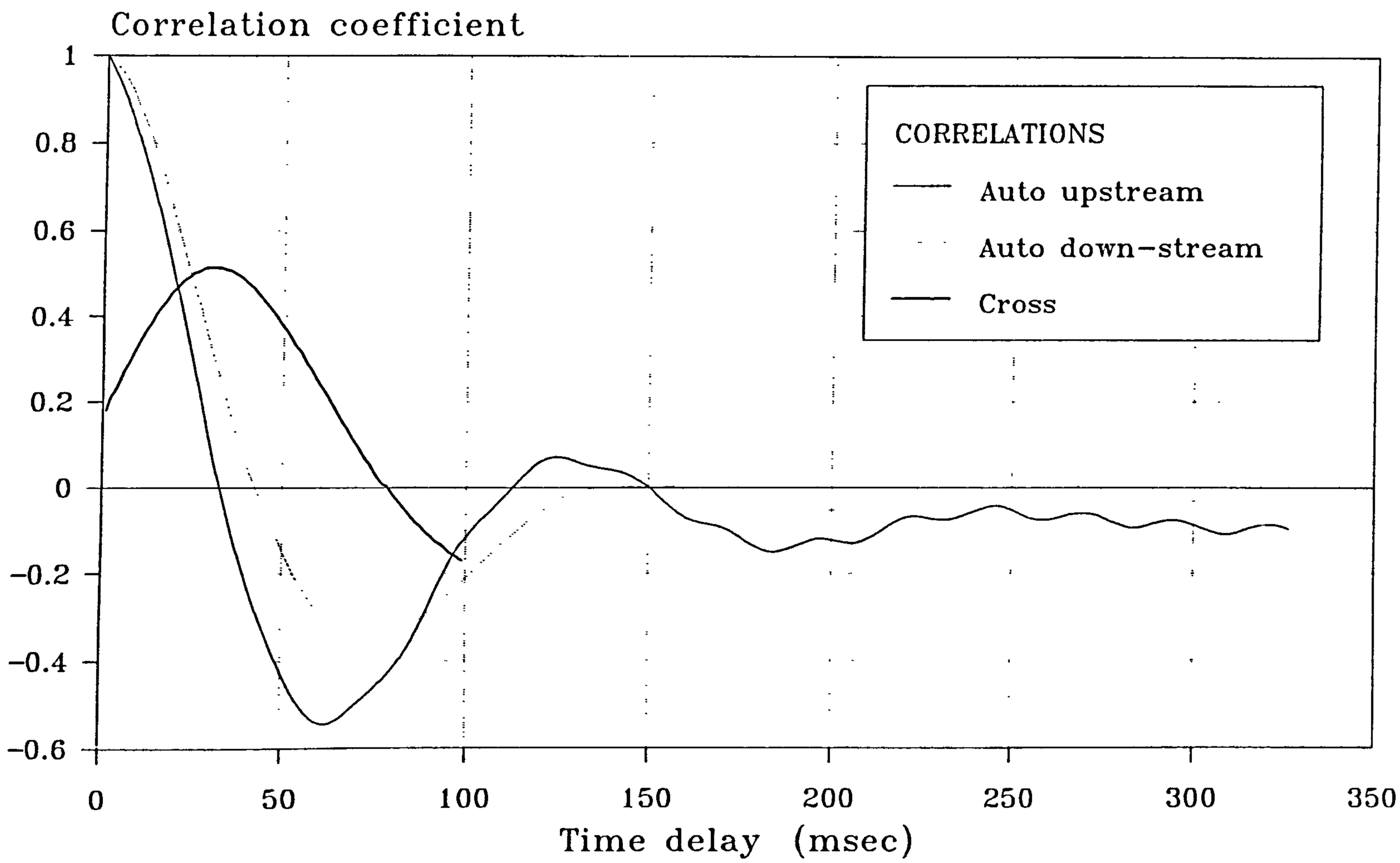

Figure 6.38 Measured auto and cross correlation correlograms of differential pressure fluctuations in bubbly two-phase within an annulus

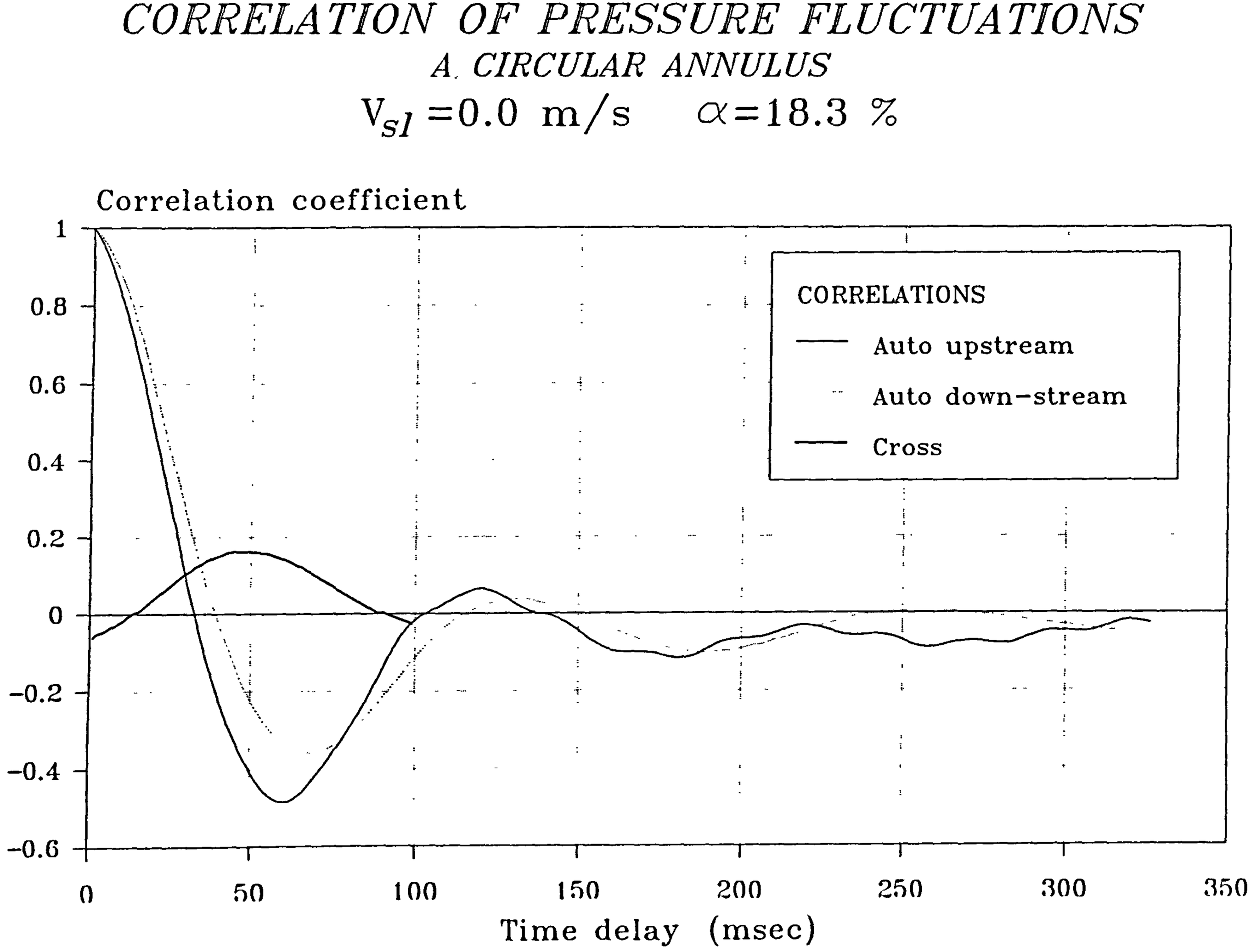

Figure 6.39 Measured auto and cross correlation correlograms of differential pressure fluctuations in bubbly two-phase within an annulus

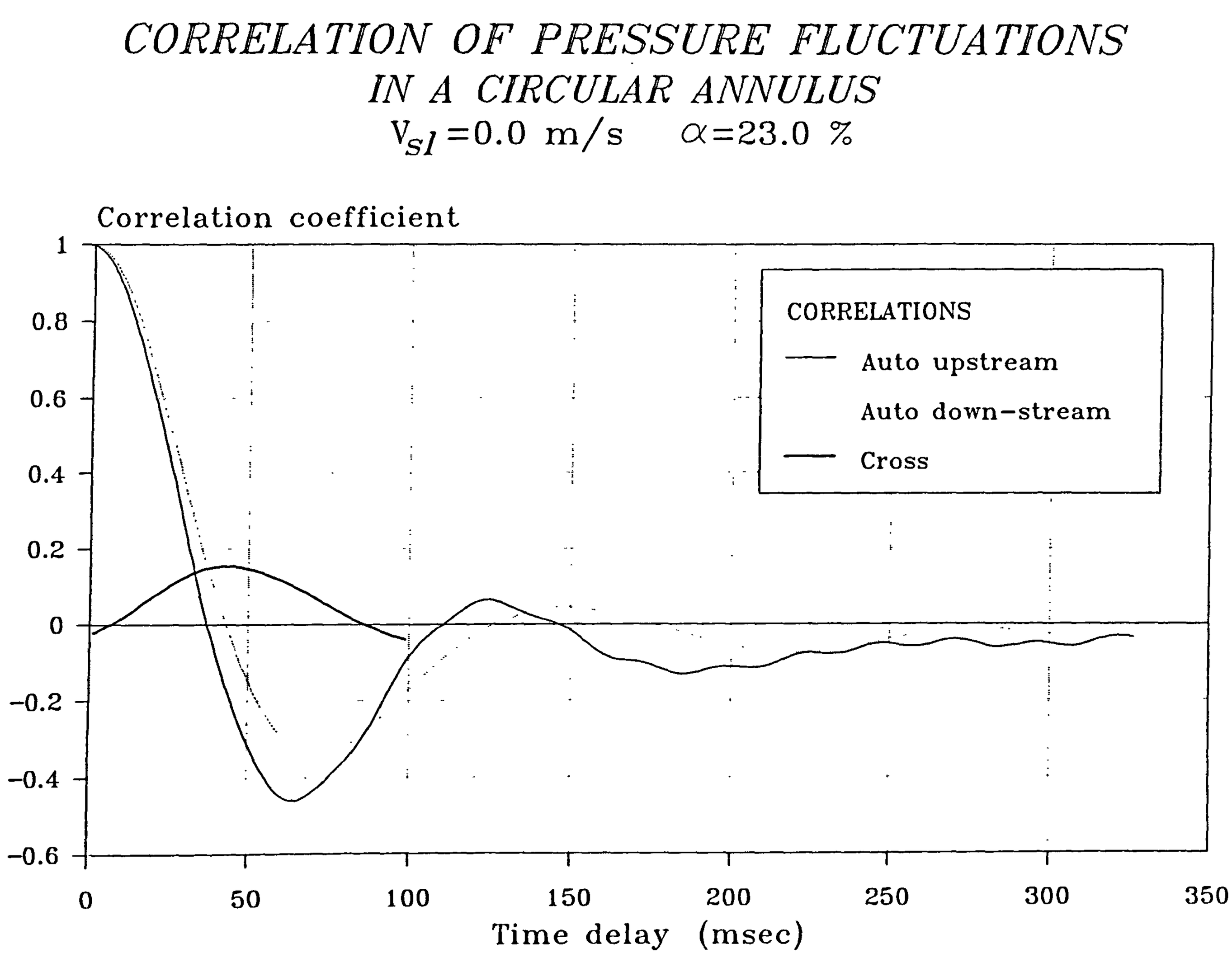

Figure 6.40 Measured auto and cross correlation correlograms of differential pressure fluctuations in bubbly two-phase within an annulus

Figure 6.41 Measured auto and cross correlation correlograms of differential pressure fluctuations in bubbly two-phase within an annulus

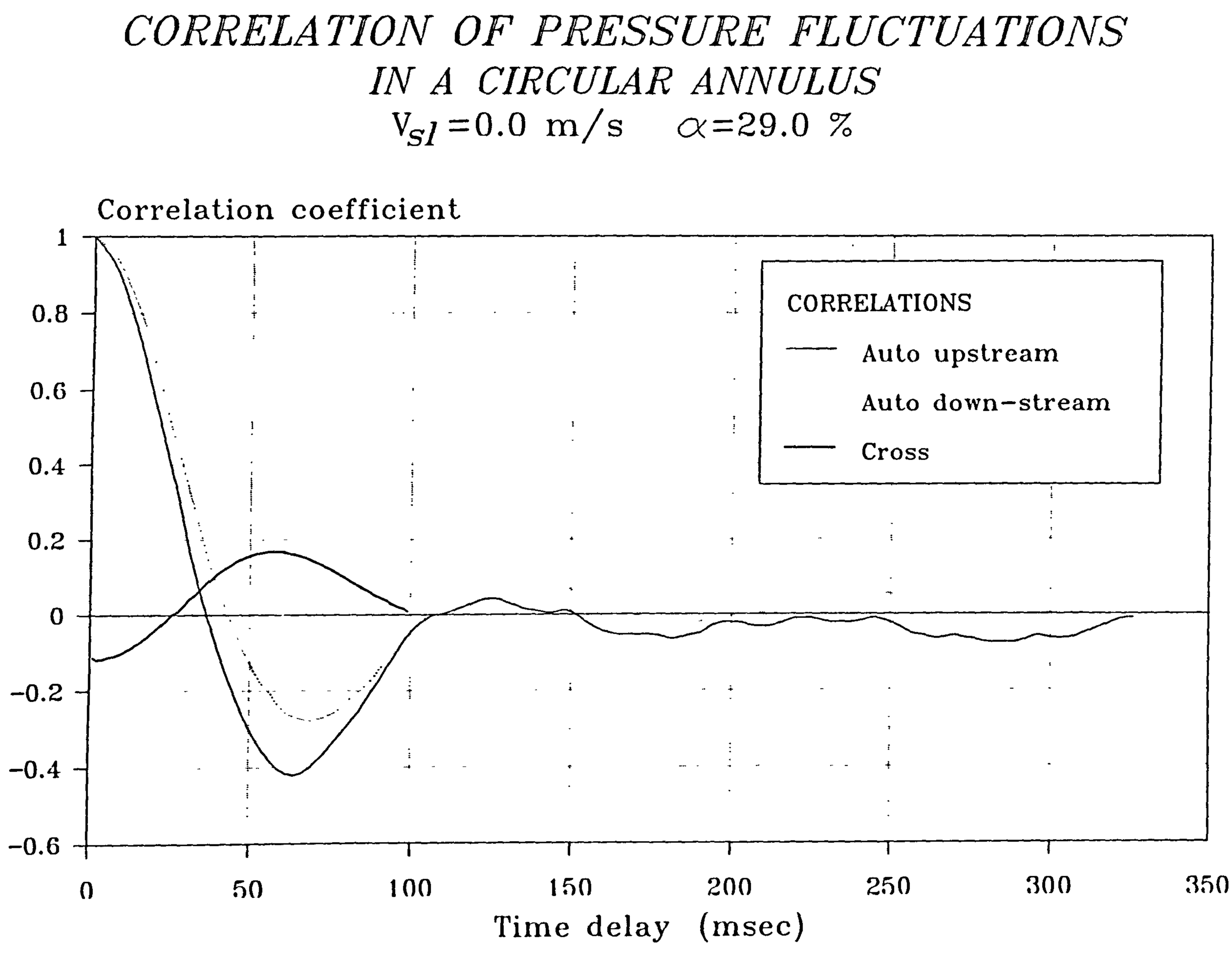

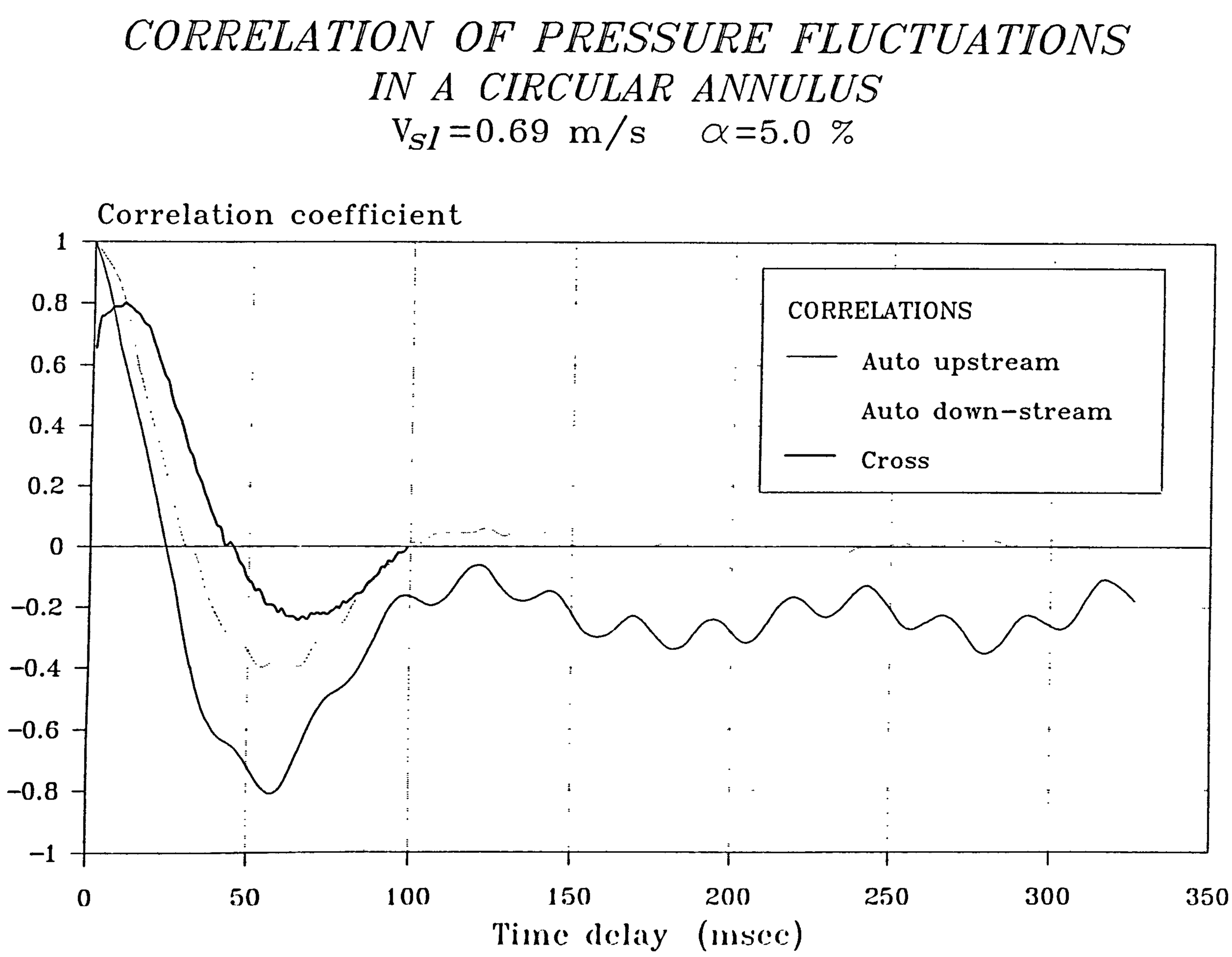

Figure 6.42 Measured auto and cross correlation correlograms of differential pressure fluctuations in bubbly two-phase within an annulus

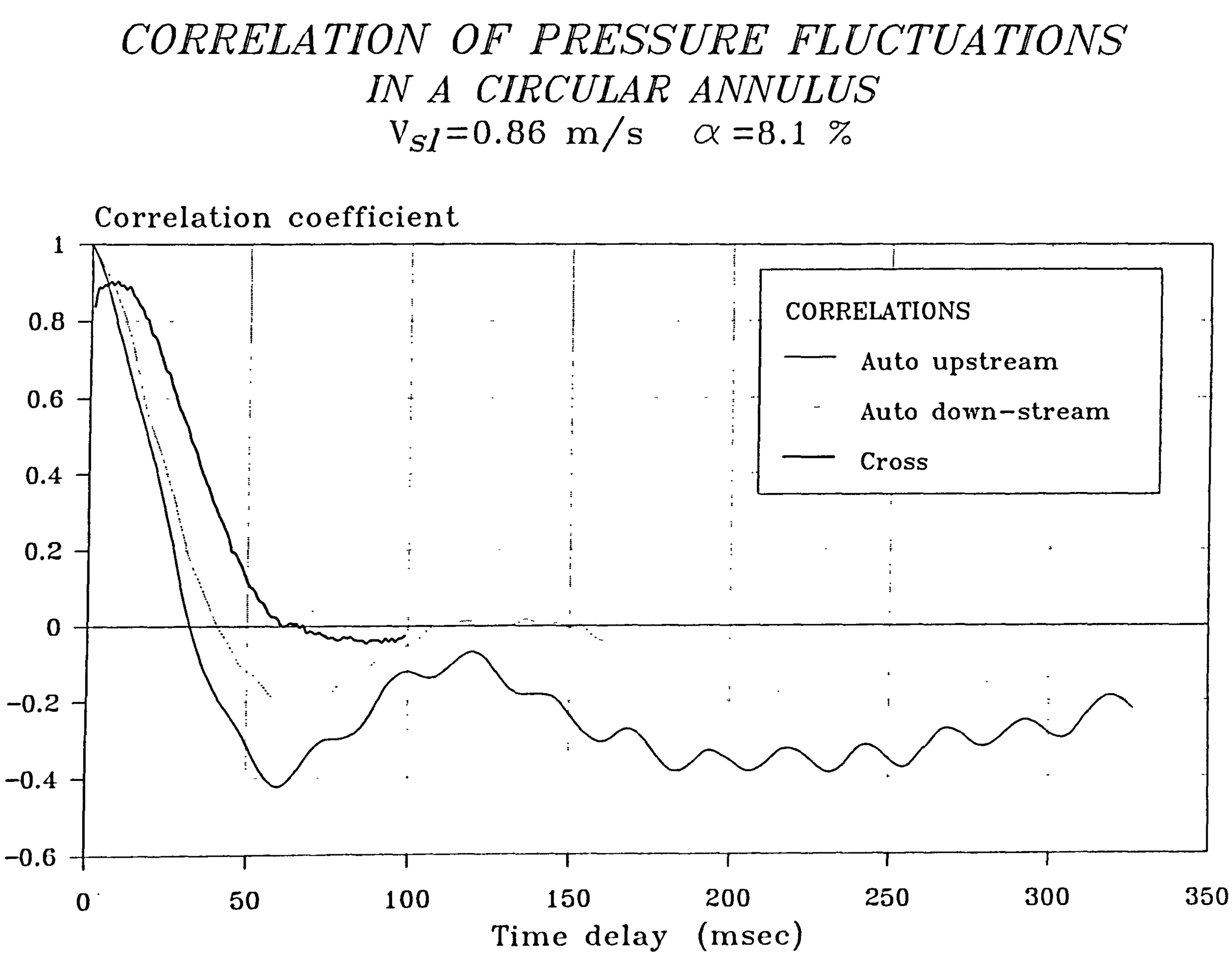

Figure 6.43 Measured auto and cross correlation correlograms of differential pressure fluctuations in bubbly two-phase within an annulus

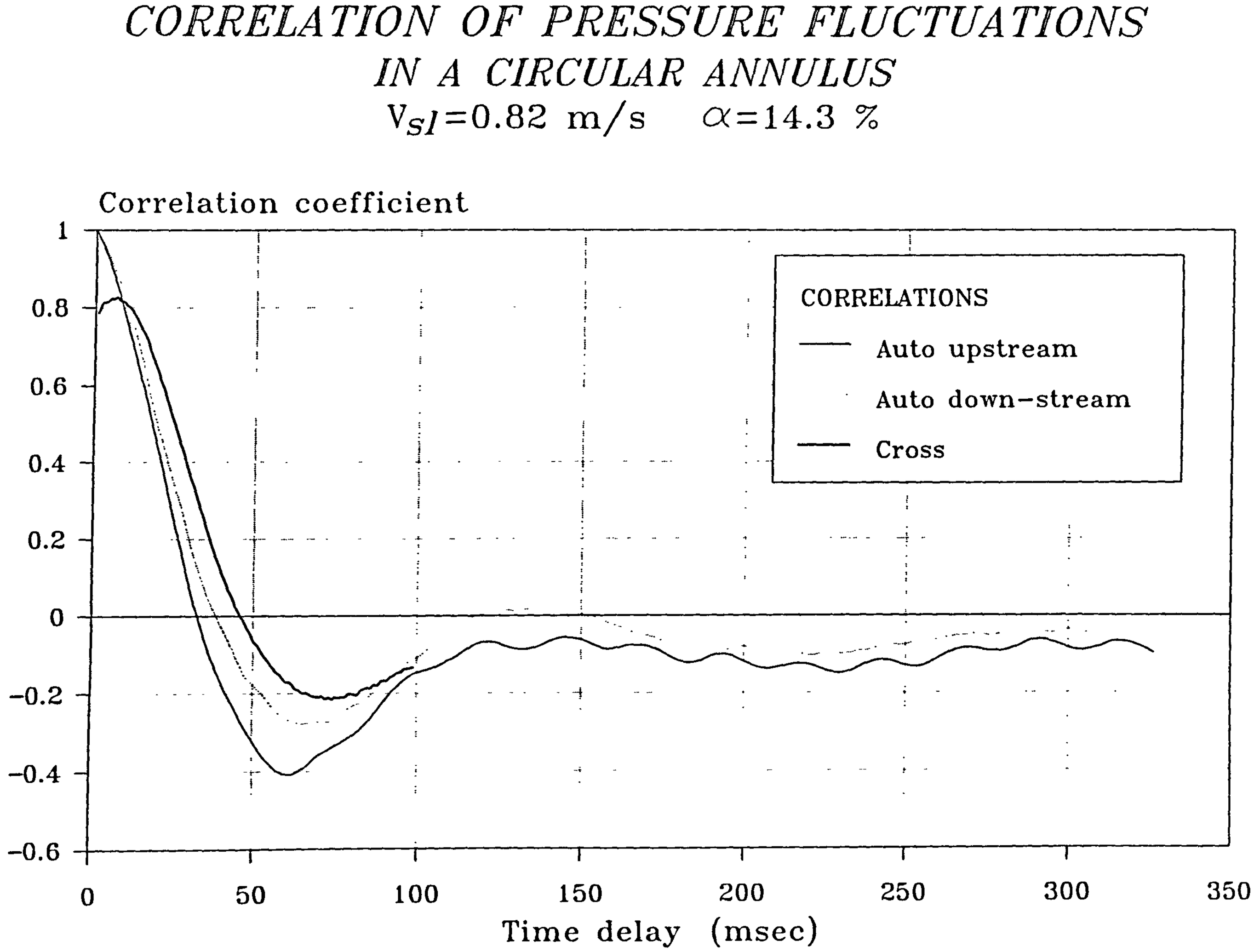

Figure 6.44 Measured auto and cross correlation correlograms of differential pressure fluctuations in bubbly two-phase within an annulus

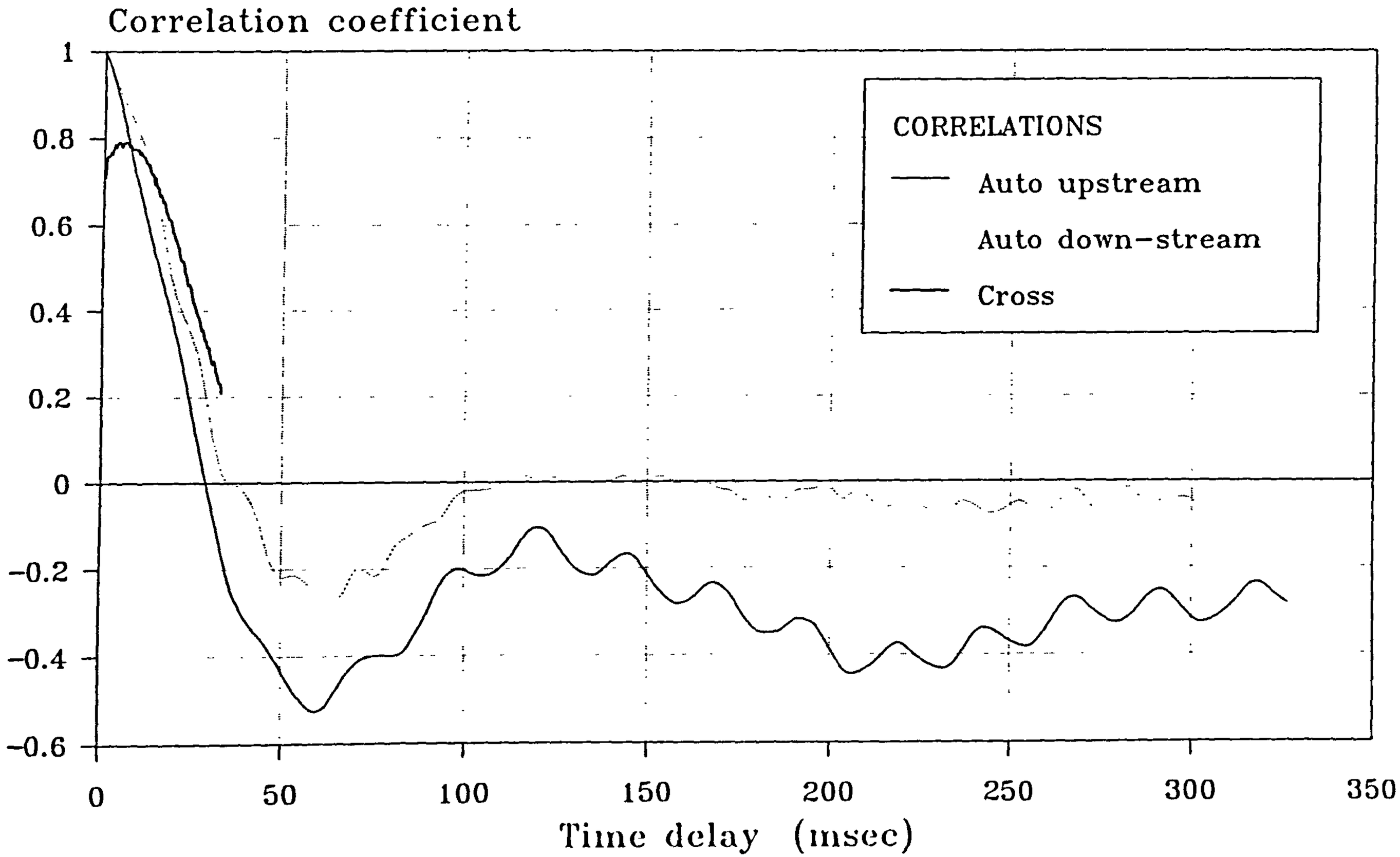

Figure 6.45 Measured auto and cross correlation correlograms of differential pressure fluctuations in bubbly two-phase within an annulus

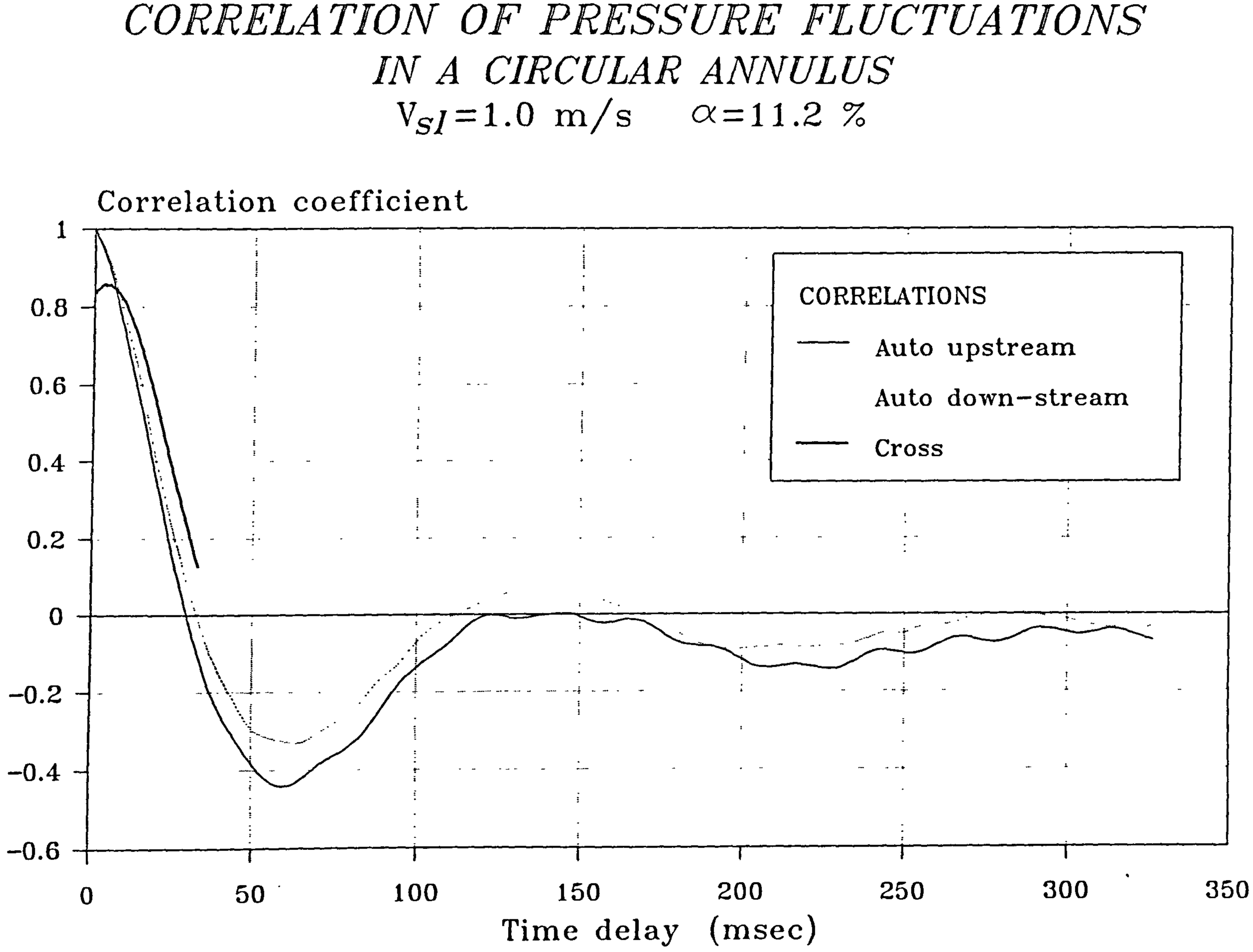

Figure 6.46 Measured auto and cross correlation correlograms of differential pressure fluctuations in bubbly two-phase within an annulus

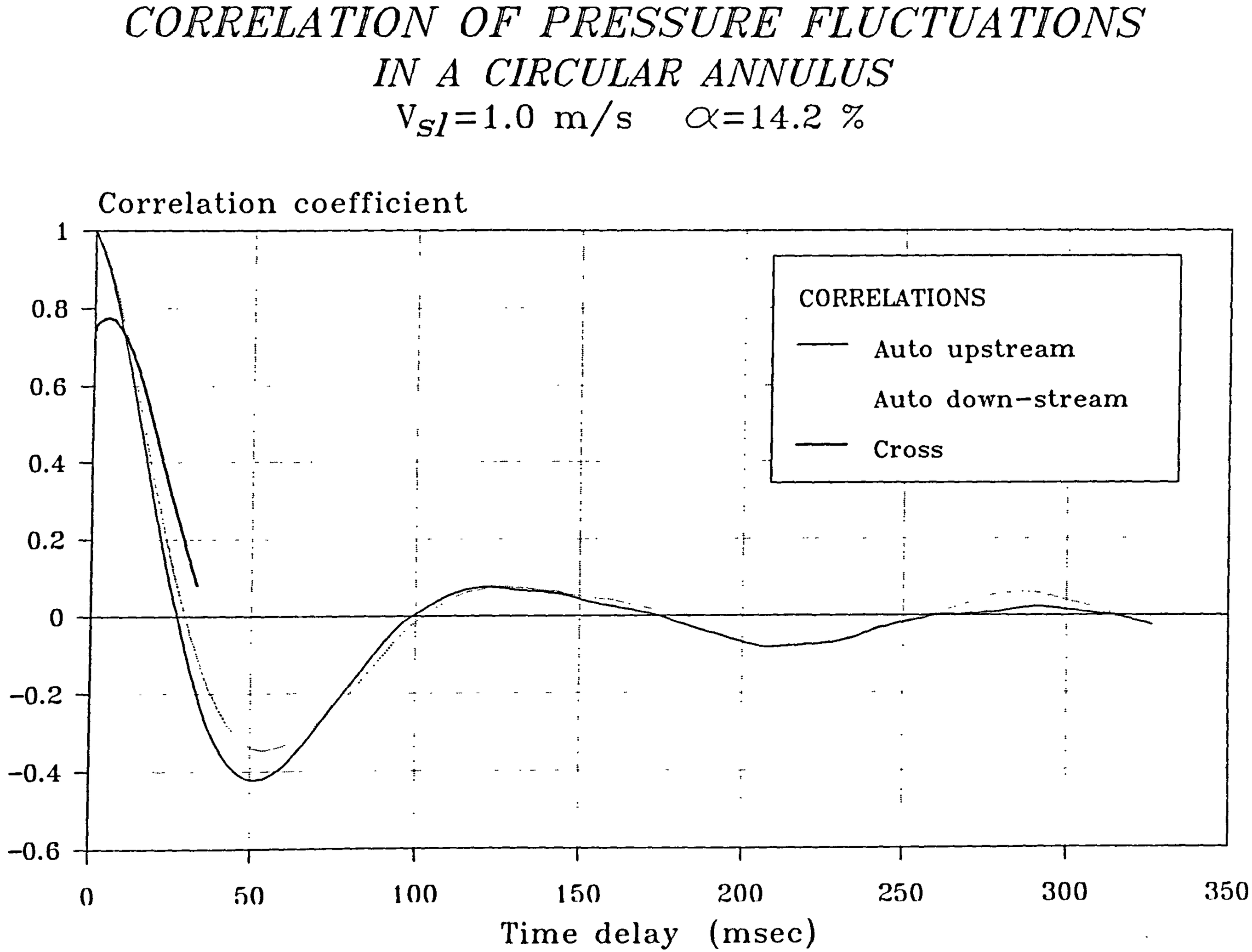

Figure 6.47 Measured auto and cross correlation correlograms of differential pressure fluctuations in bubbly two-phase within an annulus

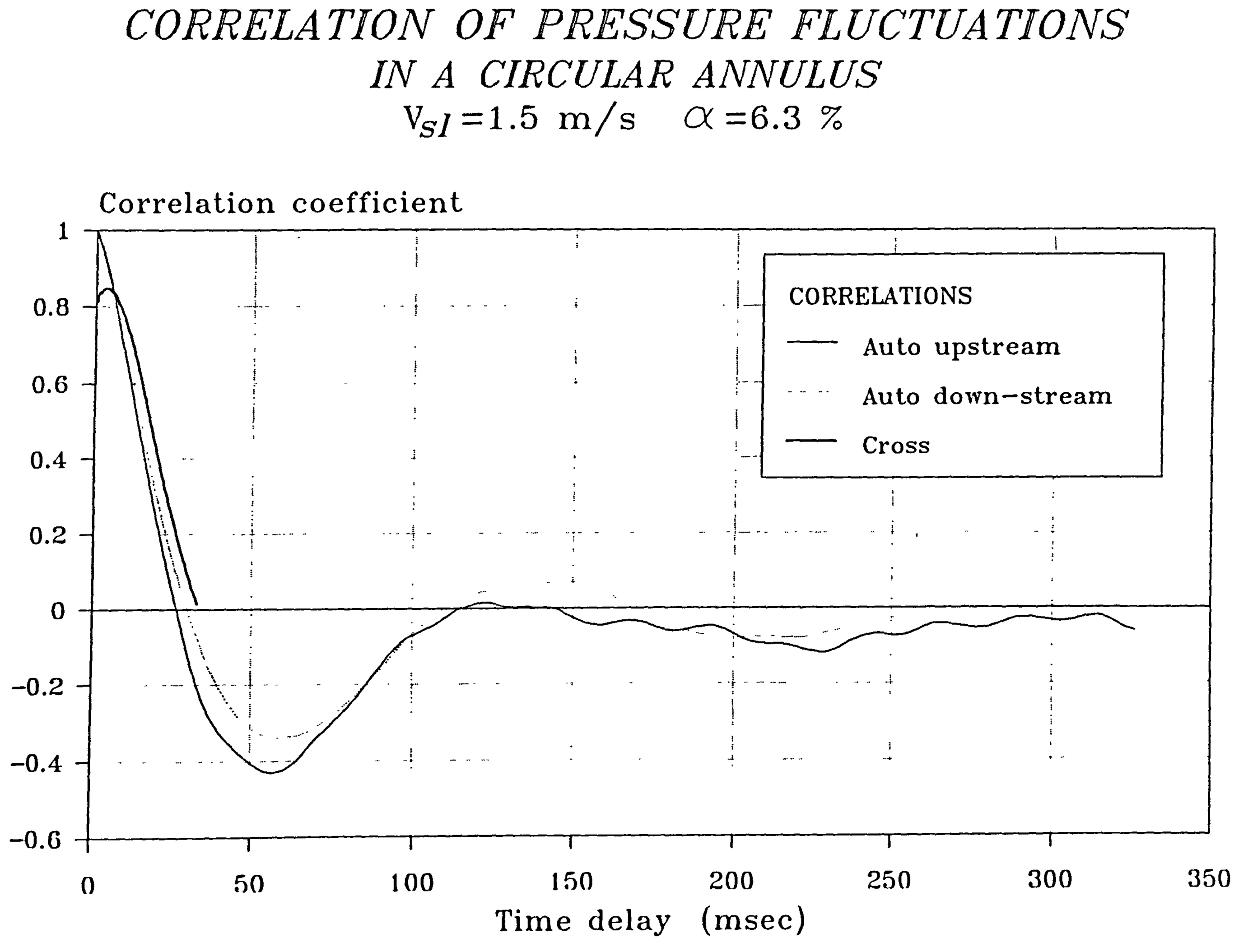

Figure 6.48 Measured auto and cross correlation correlograms of differential pressure fluctuations in bubbly two-phase within an annulus

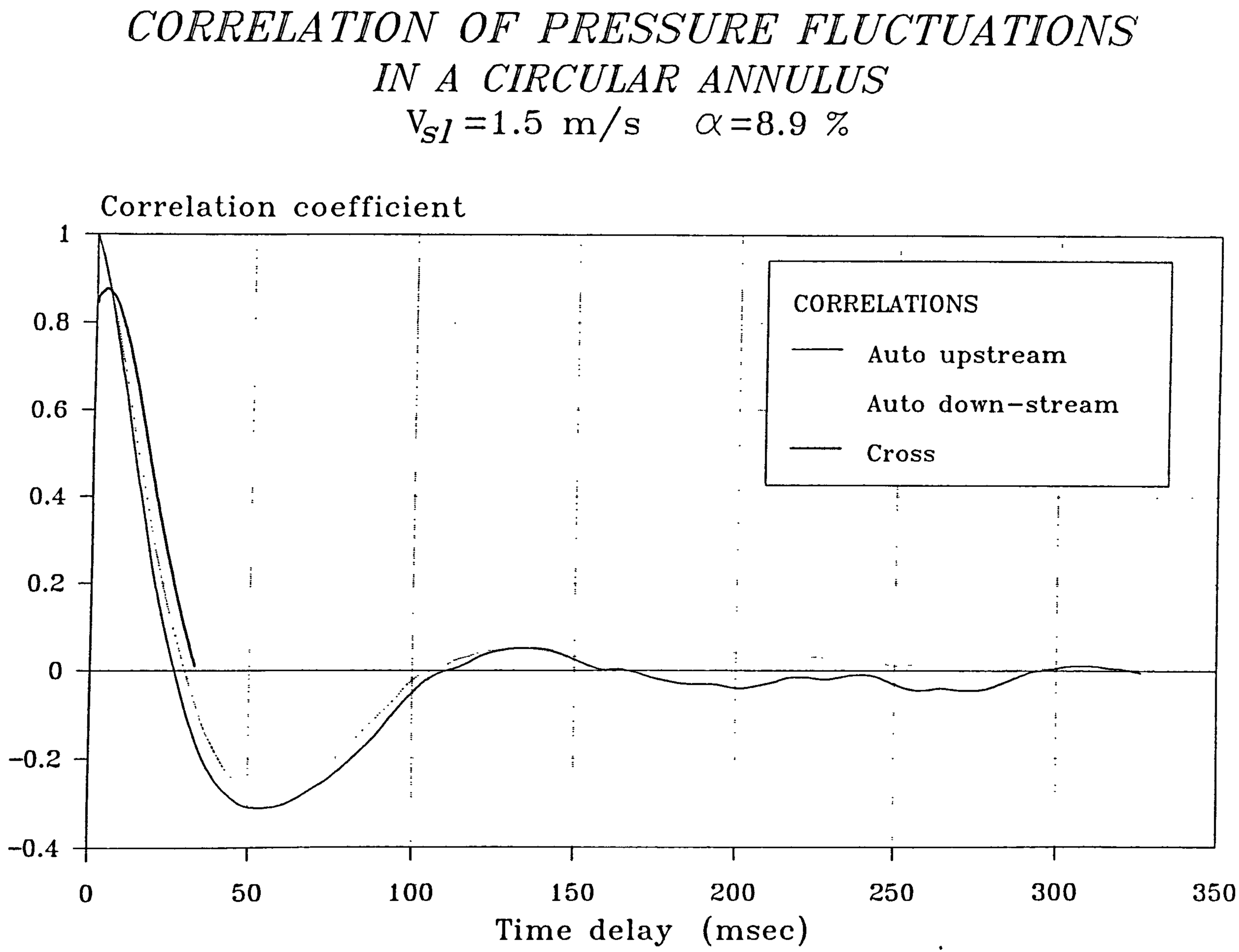

Figure 6.49 Measured auto and cross correlation correlograms of differential pressure fluctuations in bubbly two-phase within an annulus

Figure 6.50 Measured auto and cross correlation correlograms of differential pressure fluctuations in bubbly two-phase within an annulus

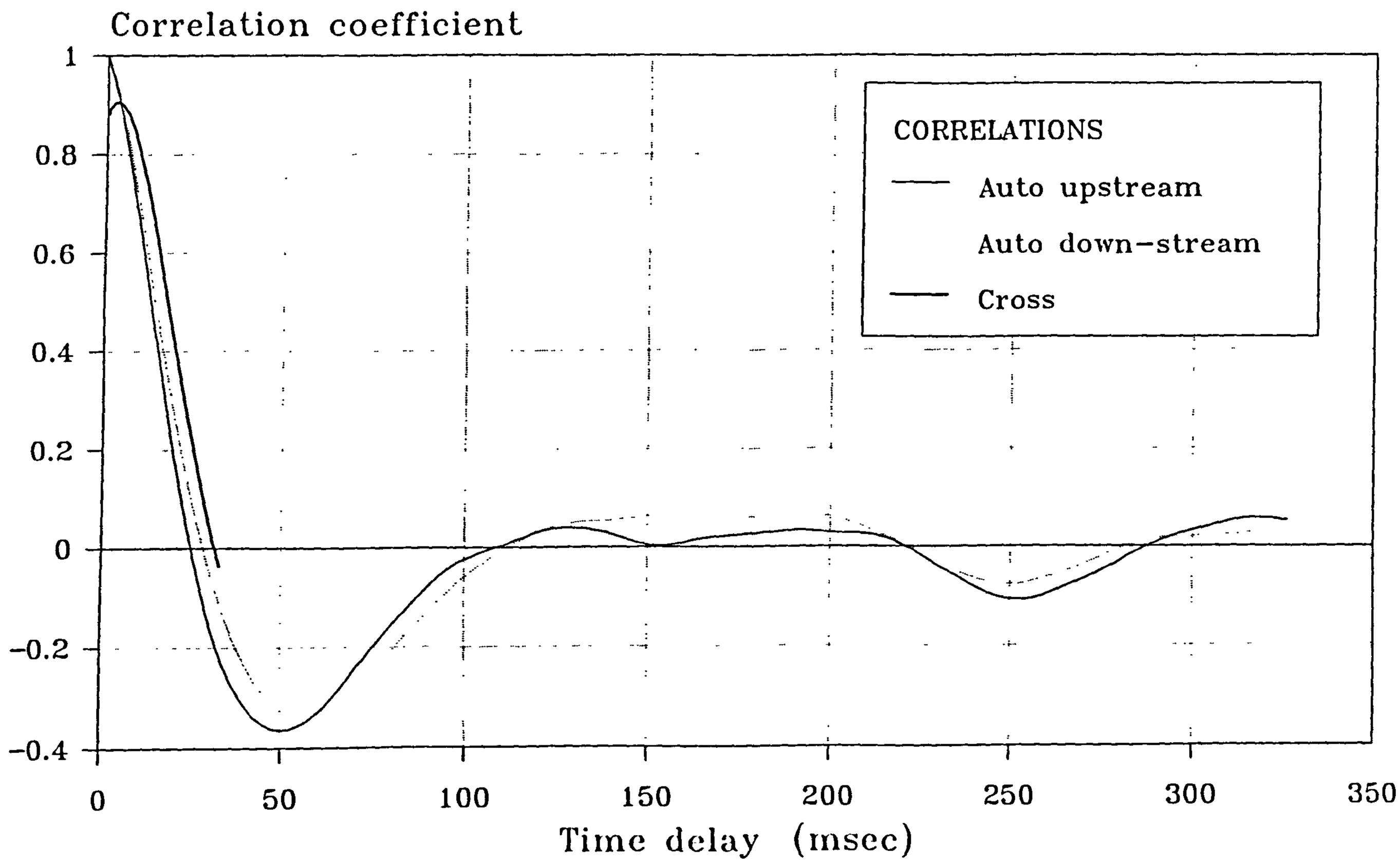

CHAPTER 7 - GENERAL CONCLUSIONS AND FURTHER INVESTIGATIONS

Chapter summary

This chapter draws general conclusions relating to the convected bubble velocities evaluated from the experimental auto and cross correlation correlograms of differential pressure fluctuations within a bubbly two-phase flow and considers its suitability for use downhole. It is also recognised that further studies need to be carried out in the following areas.

(i) Observing the effects of variations in local gas void fraction and velocity profiles, $\alpha_l(r)$ and $v_g(r)$ respectively, on the correlation measurement of the convected bubble velocities V_{g_1}, V_{g_2} and V_{g_3} within a bubbly two-phase flow.

(ii) Modifications to the low average gas void fraction vertically upward bubbly two-phase flow numerical simulation model to facilitate the input of realistic local gas void fraction and velocity profiles.

(iii) Further development of the experimental techniques described in this thesis for monitoring the naturally occurring differential pressure fluctuations within a bubbly two-phase flow.

7.1 Conclusions drawn from the studies carried out in this thesis relating to the suitability of naturally occuring pressure fluctuations within a bubbly two-phase flows as a means of monitoring the area averaged gas velocity V_g, downhole

One of the aims of this thesis was to evaluate the possible use of naturally occurring pressure fluctuations known to exist in bubbly two-phase flows in a novel non-intrusive correlation flowmeter for use downhole to monitor the area averaged gas velocity V_g. Previous studies using non-intrusive correlation flowmeters in a bubbly two-phase flow have displayed limited success with some discrepancy between the cross correlated convected bubble velocity and the actual area averaged gas velocity V_g. For example, in studies undertaken by *Bernier* [1981] and *Kytomaa* [1987] using impedance void fraction monitoring void fraction transducers in similar flow loops, cross correlation evaluation of the dispersed phase velocity was always lower than the actual area averaged dispersed phase velocity. They both conclude that their respective impedance void fraction monitoring transducers were more sensitive to large scale changes in the flow which they termed as a series of infinitesimal kinematic waves. Furthermore, *Bernier* states that it is not possible to derive the area averaged gas velocity from the kinematic wave speed since kinematic waves may be a function of the experimental apparatus. However studies carried out by *Hammer* [1983] and *Lucas* [1987] using capacitance monitoring void fraction techniques, when cross correlated always produced dispersed phase velocities higher than the actual dispersed phase velocity. *Hammer* and *Lucas* both account for their discrepancies by suggesting that their respective capacitance monitoring transducers are more sensitive to detecting larger faster moving bubbles in the flow and thus spacially filtering the flow.

In the present study in which naturally occurring pressure fluctuations within a vertically upward bubbly two-phase flow have been monitored using two axially separated differential pressure transducers, two distinct bubble velocity measurements have been observed. These are, the velocity of bubbles which are entrapped in a layer close to the pipe wall and the velocity of bubbles at a short distance from the pipe wall which enter and then 'bounce' away from the entrapped bubble layer. The velocity of bubbles within the entrapped bubble layer close to the pipe wall can be determined using the autocorrelation convected bubble velocity V_{g_1} over the 25mm correlation length scale, and are observed to travel at an almost constant velocity of approximately 0.4m/s which would appear to be independent of the continuous phase velocity. The velocity of bubbles slightly away from the pipe wall that are thought to enter into and then 'bounce' away from the entrapped bubble layer can be evaluated using the cross correlation convected bubble velocity V_{g_2} over the shorter 6mm correlation length scale. The ratio of the convected bubble velocity over the area averaged gas velocity, V_{g_2}/V_g, gives results that are approximately half (0.55) the area averaged gas velocity over the range of continuous phase velocities covered in the present study. This would indicate a velocity profile is present in the bubbly two-phase flow and that the convected bubble velocity V_{g_2} can be directly related to the area averaged gas velocity, V_g, of the flow.

It is concluded in this thesis that at this stage in our understanding of naturally occurring pressure fluctuations within a bubbly two-phase flow, the technique of non-intrusive monitoring of downhole dispersed phase velocities using pressure fluctuation correlation techniques developed in this thesis requires further

study. It is thought that further research relating local gas velocity profiles, $v_g(r)$, to both the correlation convected bubble velocity measurements and the area averaged gas velocity may aid our understanding of this technique to a point where this technique may be suitable.

7.2 Further work

The correlation of naturally occurring pressure fluctuations investigated in this study as a means of monitoring the dispersed phase velocity downhole, may prove to be too sensitive to vibrations and local variations in the flow conditions to ever be developed commercially as a flow monitoring technique. Nevertheless, this investigation has drawn together the findings of other researchers in the field of dispersed phase flow monitoring and generally it has been found that all non-intrusive flow monitoring correlation techniques investigated to date have had the short coming of a non-uniform field strength within the two-phase flow, which when correlated reflects the velocity of the more dominant portion of the flow rather than area averaged velocity. With this in mind, it is concluded from the studies carried out in this thesis that rather than try to develop a uniform field strength monitoring technique that could then be correlated to obtain area averaged velocity measurements, it would be more beneficial to study flow conditions and relate these conditions to measured correlation velocities, thus introducing flow condition coefficients to correct for the non-uniform field strength.

7.2.1 The need for further investigation of local void fraction profiles $\alpha_l(r)$ and local gas velocity profiles $v_g(r)$ in vertically upward bubbly two-phase flow

As a result of the conclusions drawn in section 7.1, there are certain areas in which further investigations into the phenomena of naturally occurring pressure fluctuations may prove beneficial to the understanding of the results presented in the present thesis. One key area of interest that could not be covered in this thesis due to equipment limitations, is the effect of variations in local gas void fraction and velocity profiles $\alpha_l(r)$ and $v_g(r)$ respectively, on the correlation measurement of convected bubble velocities V_{g_1}, V_{g_2} and V_{g_3}.

In section 4.4.1 single phase local velocity measurements were made using a pitot tube, however local velocity measurements of two-phase flows, of either the dispersed or continuous phase, could not be made in this study. Nevertheless according to *Farrar* [1988] using hot-film anemometry techniques it is possible to evaluate the local dispersed phase velocity, the continuous phase velocity, and the local void fraction using only a single cylindrical hot-film sensor positioned in the two-phase flow. The interpretation of the signal produced by a cylinderical hot-film probe when interacting with a bubbly two-phase flow has been discussed in section 2.2.3, where the technique developed by *Farrar* and *Bruun* [1989] for evaluating the local void fraction was described. It is also reported by *Farrar* [1988] that by careful calibration of the hot-film probe it is also possible to evaluate the local continuous and dispersed phase velocities from the same signal.

Using the technique of *Farrar* and *Bruun* [1989], it is possible to obtain accurate information on developing, and fully developed, local gas void fraction and velocity profiles, $\alpha_l(r)$ and $v_g(r)$ respectively, for a bubbly two-phase flow. From a knowledge of the interaction between local gas velocity profiles $v_g(r)$ and the correlation convected bubble velocities it may be possible to introduce correction factors in order to calibrate the pressure correlation technique developed in the present thesis for known local gas velocity profiles, such as those produced at entry conditions. The importance of such work has been recognised and a study programme is currently being conducted into pressure fluctuations within oil/water and air/water bubbly two-phase flows and their interaction with local void fraction and velocity profiles at the University of Bradford.

7.2.2 Further two-phase flow simulations

The numerical simulation model developed in the present thesis for low void fraction bubbly two-phase flow (see section 6.3), could also benefit from further development work. In particular, the ability to easily enter realistic local void fraction and gas velocity profiles would enhance the software. The effect of 'bouncing' or bubbles with a spiralling motion may also be included. After fine tuning the model by comparing known experimental flow conditions with those predicted by the model, it would be then possible to use the model to both aid in the evaluation of calibration constants for the pressure correlation technique, and could also be used to simulate the affect on correlation convected bubble velocity measurements for variations in flow conditions such as pipe diameters and local void

fraction and velocity profiles. Likewise, the simulation software could also be used to study the effects of non-symmetrical flow profiles such as those encountered in non-vertical flows i.e. flows in deviated bore hole.

7.2.3 Possible improvement of the convected disturbance velocity measurement technique

To improve the technique described in the present thesis for the measurement and subsequent correlation of naturally occuring pressure fluctuations within a bubbly two-phase flow, it is proposed that a study be undertaken in which both the transducer pressure tapping separation distance l and the transducer separation distance h are varied in order to optimise these distances. It is recognised that due to the rigid mounting of the differential pressure transducers and their associated pressure lines in order to make these measurements (see section 5.3.3) that such a study would be both time consuming and expensive in both material and labour costs. However, optimising these separation distances may improve the performance of the pressure correlation technique developed here.

Another area in which further investigations may prove beneficial to aid the understanding of the results presented in the present study, would consist of a detailed investigation into the ascent of a bubble through both a stagnant and flowing continuous phase, and the effect on the rise velocity of a bubble close to the pipe wall in such cases. It has been indicated in the present study that a bubble in the conditions described above travels with a constant velocity which is higher than the expected terminal velocity

of a bubble and independent of the continuous phase velocity. Clarification of this phenomena could be used in both the numerical simulation and aid in our general understanding of a bubbly two-phase flow.

APPENDIX 1 - AIR AND WATER FLOW RATE CALIBRATION DETAILS

Appendix summary

Contained in this appendix are details of the procedures adopted in this study to calibrate the fundamental instrumentation used in the experimental two-phase flow loop to monitor the air and water mass flow rates. Air and water flow rate monitoring instrumentation consists of an orifice plate meter and turbine flowmeter respectively. Calibration data is tabulated and contained within the text and calibration constants are calculated for both instruments.

A1.1 Air mass flow rate orifice plate calibration details

Air is delivered to the experimental facility at a constant pressure of approximately 1.5 Bar. The volume flow rate of air entering the experimental flow loop is metered by an orifice plate flowmeter and regulated by a computer controlled needle valve. These form the major parts of the Proportional + Integral + Differential (PID) closed loop controller used to control the mass flow rate of air entering the flow loop.

The diameter of the orifice plate needed to measure the expected range of flow rates was calculated for a 26mm diameter housing as shown in figure 3.4 in accordance with British Standard 1042 (1981). However, the required diameter of orifice was calculated to be in the order of 6mm which is smaller than recommended by B.S. 1042. It was therefore necessary to obtain experimentally the discharge coefficient k_o in the gas mass flow rate equation

$$\dot{m}_g = \frac{k_o \pi d_o^2}{4} \sqrt{2 \Delta P_o \rho_o} \qquad 3.1$$

where d_o is the diameter of the orifice plate, ΔP_o the pressure drop across the orifice plate, and ρ_o the density of air at the orifice plate. ρ_o can be calculated using the perfect gas equation

$$P = \rho R T \qquad 3.2$$

$$\rho_o = \frac{P_o}{RT} \qquad 3.3$$

where P_o and T are the upstream pressure and temperature at orifice plate.

The volume flow rate of air $\dot{V}_a$ is then given by equation A1.1

$$\dot{V}_a = \frac{k_o \pi d_o^2}{4 \rho_0} \sqrt{2 \Delta P_o \rho_o} \qquad \text{A1.1}$$

To calibrate the orifice plate a small pitot tube was used to measure the velocity profiles across a 1" nominal bore pipe being exhausted to the atmosphere at two arbitrary air flow rate settings (see figure 3.5). By integrating the velocity profile over the cross-sectional area of the pipe and knowing the upstream pressure P_0 and temperature T at the orifice plate, the air mass flow rates can be calculated and hence, the discharge coefficient k_0 can be evaluated as follows.

A sharp edged orifice with an orifice diameter d_0 of 6mm was positioned in the flow of a 1" nominal bore pipe, and held in a housing with a bore diameter D_0 of 26mm and pressure tappings at $0.5D_0$ and $1D_0$ as recommended by B.S. 1042. A small pitot tube was carefully traversed across the 1" nominal bore pipe near to its exit to atmosphere at two radial positions separated by an angle of 90° for two arbitrary flow rates the results of which are shown below.

Experimental Results		Experiment 1	Experiment 2
Upstream pressure	P_0	110.25 KN/m²	103.99 KN/m²
Orifice temperature	T	295 K	295 K
Orifice pressure drop	ΔP_0	9.47 KN/m²	2.68 KN/m²

Radial position pitot tube from centre in mm	Average pitot tube pressure over two traverses at 90° to each other in mm H_2O	Average pitot tube pressure over two traverses at 90° to each other in mm H_2O
0.64	1.44	0.435
1.91	1.43	0.433
3.18	1.38	0.418
4.45	1.33	0.400
5.75	1.26	0.380
6.99	1.18	0.358
8.26	1.09	0.335
9.53	0.98	0.288
10.80	0.87	0.225
12.07	0.60	0.115
13.34	0.35	0.090

The velocity U measured at each point by the small pitot tube can be calculated from equation A1.2 (see *Massey* [1968])

$$U = \sqrt{\frac{2\,\rho_{water}\,g\,h}{\rho_{air}}} \qquad A1.2$$

Figure A1.1 shows the non-dimensional velocity profile for the two experiments U/U_C, where U_C is the centreline velocity, as a function of the non-dimensional position within the 1" nominal bore pipe r/R, where R is the radius of the pipe. These approximate

closely to a $1/7^{th}$ power law curve as would be expected.

The volume flow rate of air $\dot{V}_a$ measured across the 1" nominal bore pipe near the exit where the pitot tube measurements were made can be calculated by integrating of the velocity profile over the area of the pipe, we assume this point to be at atmospheric pressure.

$$\dot{V}_a = 2\,\pi \int_0^r r\ U(r)\ dr \qquad \text{A1.3}$$

The volume flow rate $\dot{V}_a$ can then be substituted into equation A1.1 which can then be re-arranged to determine the discharge coefficient k_o

$$k_o = \frac{4\,\rho_o\,\dot{V}_a}{\pi\,d_o^{\,2}\,\sqrt{2\,\Delta P_o\,\rho_o}} \qquad \text{A1.4}$$

Using equations A1.3 and A1.4, and the experimental data in the the table above, discharge coefficients k_o for experiments 1 and 2 were found to be 0.654 and 0.625 respectively. If we assume the discharge coefficient k_o remains a constant over the range of air mass flow rates used in this study then the two values of k_o can be summed and averaged to produce a discharge coefficient k_o for the 6mm orifice plate used in this study of $k_o = 0.632$.

A1.2 Water volume flow rate turbine flowmeter calibration details

The superficial liquid velocity V_{sl} is the velocity the liquid would have if it was the only phase present. As described in chapter 1, this quantity is given by equation 1.2

$$V_{sl} = \frac{\dot{V}_l}{A} \qquad 1.2$$

where $\dot{V}_l$ is the volume flow rate of liquid, and A is the cross-sectional area of the pipe. Water is circulated by means of a centrifugal pump whose speed is controlled by an IMO Jaguar VL550 thyristor controller. As water is virtually incompressible it is possible to evaluate the volume flow rate directly from the metered volume or mass flow rate.

The water volume flow rate $\dot{V}_l$ measured by a Bestobell turbine flow meter model N^0. M9F/1500/150A(150) was positioned approximately 20 pipe diameters down-stream of the centrifugal pump. This turbine flowmeter has an inductive pick-up that produces a pulse every time the turbine rotates. The frequency of this pulse train is proportional to the volume flow rate though the transducer. The pump/speed controller and the turbine flow meter are both connected to a micro computer which form the major parts of the Proportional + Integral + Differential (PID) closed loop controller used to control the volume flow rate of water entering the flow loop.

To condition the signal from the turbine flowmeter for computer interfacing, it was decided to convert the turbine flowmeters pulse train output into a DC voltage, with the output voltage being

proportional to the volume flow rate of water through the turbine flow meter. This conversion was achieved using the circuit shown in figure 3.7, which amplifies the signal from the inductive pick-up, filters out frequencies above 1 KHz using a low pass active filter, and then converts the frequency of the signal to a proportional DC voltage using a frequency to voltage converter chip.

To minimise calibration errors the turbine flowmeter and the frequency to voltage converter unit were calibrated together. This was achieved by recording the time taken to fill a known volume (48 litres) with water, with the centrifugal pump running at a constant speed. This procedure was averaged over four measurements, the speed of the pump was then altered and the experiment repeated. For each experiment the output voltage from the frequency to voltage converter V_{turb} was also monitored and recorded as shown in the table of results below.

Time taken to fill 48 litre tank in seconds				Averaged time (s)	$\dot{V}_l$ ($\times 10^{-3}$ m^3/s)	output voltage V_{turb} (V)
1	2	3	4			
19.0	18.7	18.5	18.3	18.6	2.58	1.79
13.0	13.2	12.9	13.4	13.1	3.66	2.48
10.1	10.0	10.0	10.4	10.1	4.74	3.11
8.0	8.4	8.3	8.2	8.2	5.84	3.81
6.6	6.5	6.9	6.8	6.7	7.16	4.45
6.0	5.8	6.0	5.8	5.9	8.14	5.17

To obtain a relationship for the volume flow rate of liquid $\dot{V}_l$ in terms of the output voltage form the frequency to voltage converter V_{turb} that conditions the signal from the turbine flowmeter for interfacing with the micro computer, plotting the output voltage

against the volume flow rate of liquid will produce a straight line for this linear relationship as shown in figure A1.2. Appling a least squares fit algorithm to this date we obtain the flowing equation for the volume flow rate of liquid in terms of the measured output voltage from the turbine flowmeter and associated signal conditioning electronics.

$$\dot{V}_l = 1.668\times10^{-3}\ V_{turb} - 0.44\times10^{-3} \quad (m^3/s) \qquad A1.5$$

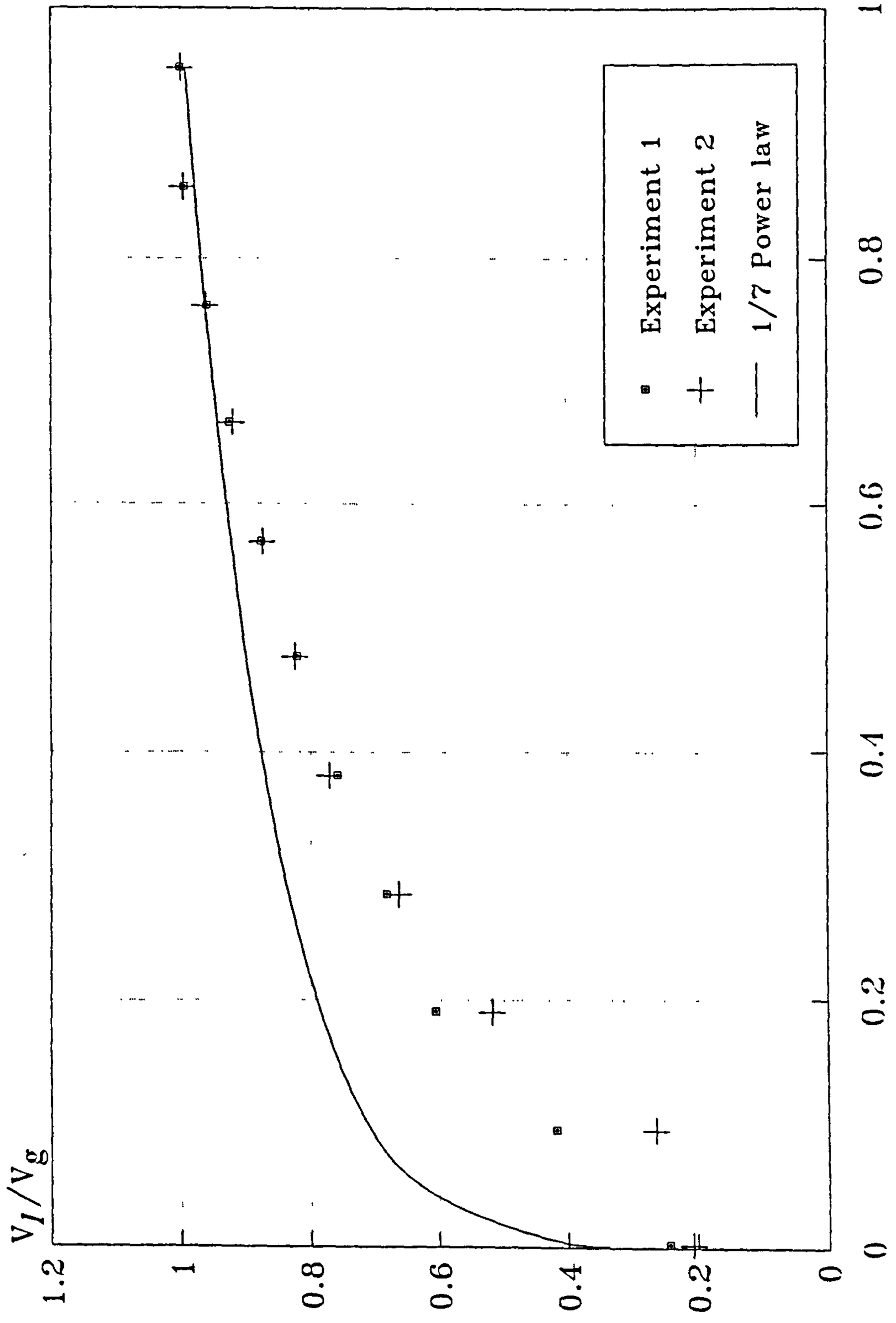

Figure A1.1 Orifice plate calibration. Velocity profile of air exhausted from a 1" diameter pipe

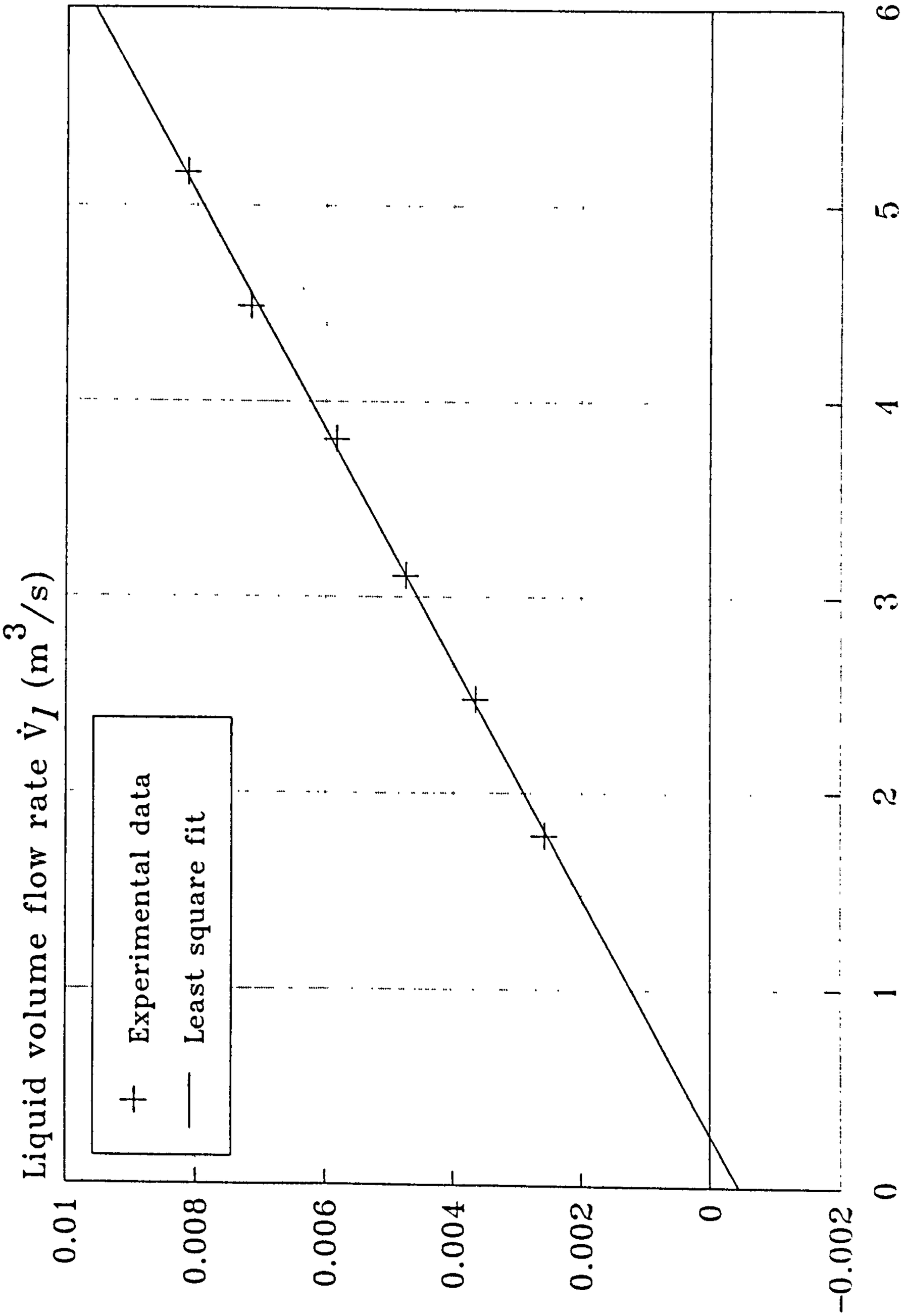

Figure A1.2 Turbine flowmeter calibration. Volume flow rate of water as a function of the output voltage from the frequency to voltage converter

APPENDIX 2 - TWO-PHASE AIR/WATER FLOW LOOP CONTROL SOFTWARE

Appendix summary

Contained in this appendix is a listing of the two-phase air/water flow loop control software developed in this study to control and monitor the air and water mass flow rates in the experimental two-phase flow loop and to perform simple experiments.

Two-phase flow loop control software

Listed below are the procedures used in the flow loop control software and brief descriptions of their functions within the software.

PROCinit	-	Initialisation of variables and constants used in the software
PROCwater-wind-flowrate	-	Set superficial air/water flow rates and other flow loop parameters
PROCwater	-	Superficial water velocity entry
PROCwind	-	Superficial air velocity entry
PROCtube-dia	-	Experimental test section diameter micro manometer settings, and atmospheric temperature and pressure entry
PROCdisplay	-	Display superficial air and water velocities and average gas void fraction
PROCread-flowrates	-	Evaluate mass flow rates of air and water from orifice plate flowmeter and turbine flowmeter respectively
PROCerror-calc	-	Calculate errors between the desired and the actual air/water superficial velocities using the PID algorithm
PROCset-flowrate	-	Adjust the air/water controllers appropriately
PROCtestmenu	-	Average gas void fraction and friction factor test menu

PROCvoid-fraction	-	Quick closing valves average gas void fraction experiment
PROCError	-	Software error trap safe equipment shut down procedure
PROCDiff-press	-	Gradiomanometer average gas void fraction experiment
PROCsetdp	-	Initiate differential pressure transducer
PROCConst-water	-	Gradiomanometer experiments for constant water velocity
PROCConst-air	-	Gradiomanometer experiments for constant air velocity
PROCprinter	-	Printer output routine
PROCSkin-friction	-	Friction factor evaluation experiments
PROCfile	-	Save data to disc
PROCmanometer	-	Evaluate differential pressure measured by the micromanometer connected to the orifice plate flowmeter
PROCvfcalc	-	Evaluate average gas void fraction using the gradiomanometer technique

```
 10 REM ********************************
 20 REM *                              *
 30 REM *    Two phase flow loop       *
 40 REM *      control software        *
 50 REM *                              *
 60 REM *            by                *
 70 REM *                              *
 80 REM *        A.L.Samways           *
 90 REM *                              *
100 REM * To run on the C/U.Cube       *
110 REM * (A-D,Cumem,Power50)           *
120 REM * Date15-11-89                 *
130 REM * Bi-polar,20vrange,samp        *
140 REM ********************************
150 CLOSE#0
160 PROCinit
170 REPEAT
180 VDU23,1,1,0;0;0;0;
190 PROCwater-wind-flowrate
200 VDU23,1;0;0;0;0;
210 PROCdisplay
220 TURNOFF2:TURNOFF5:FORI=0TO1000:NEXTI
230 REPEAT
232 IFINKEY(0)=&31THENFlag%=Flag%*(-1)
240 PROCread-flowrates
250 PROCvfcalc
260 PROCerror-calc
265 IFFlag%=1THENPRINTTAB(0,0);CHR$(129);"M":GOTO280
    :ELSEPRINTTAB(0,0);CHR$(130);"C"
270 PROCset-flowrates
280 UNTILINKEY(0)=&20 :REM Space Bar
290 UNTIL FALSE
300 END
310
320 DEFPROCinit
322 Flag%=-1
330 DIM Voidfraction(50,5)
340 Ko=0.6316 :REM Orifice constant
350 K1=500000 :REM Water const Prop
360 K2=5000 :REM Water const Int
370 K3=70000:REM Air const Prop
380 K4=1200 :REM Air const Int
390 ONERRORPROCError:STOP
400 Pform=&20406
410 @%=Pform
420 Sample=0.07
430 Samplenu=10
440 RoeW=1000
450 Rgas=287
460 h=0.580
470 Ltapping=h
480 OrDia=0.006
490 Manrange=1.00 :REM"Micro-Man"
500 WaterV=0
510 WaterVel=0
520 IntErrorW=0
530 AirV=0
540 AirVel=0
550 IntErrorA=0
560 Inairerr=0
```

```
570 PumpS=0
580 Printer=0
590 Dia=0.0778
600 Flag=0
610 BASE'=&D000
620 OUTCH 0 TO 15
630 TURNON 15
640 TURNON 1
650 TURNOFF 2 :TURNOFF 5
660 TURNON 0 :FOR I=0 TO 1000:NEXT I:TURNOFF 0
670 DAC#0=0
680 ENDPROC
690
700 DEFPROCwater-wind-flowrate
710 CLS
720 TURNOFF 2
730 PRINTTAB(4,1);CHR$(141);CHR$(131);"Two Phase Flow Loop Control"
740 PRINTTAB(4,2);CHR$(141);CHR$(130);"Two Phase Flow Loop Control"
750 PRINTTAB(0,5);CHR$(134);"1) Enter Water Superficial Velocity"
760 PRINTTAB(0,7);CHR$(134);"2) Enter Air Superficial Velocity"
770 PRINTTAB(0,9);CHR$(134);"3) Enter section dia and man setting"
780 PRINTTAB(0,11);CHR$(134);"4) Test Menu"
790
800 PRINTTAB(0,13);CHR$(134);"5) Control Flow Loop"
810 PRINTTAB(3,15);"Enter Number";
820 G=GET:G=G-48
830 IF G=1 THEN PROCwater:GOTO 710
840 IF G=2 THEN PROCwind :GOTO 710
850
860 IF G=3 THEN PROCtube-dia :GOTO 710
870 IF G=4 THEN PROCtestmenu :GOTO 710
880 IF G=5 THEN ENDPROC
890 GOTO 820
900 ENDPROC
910
920 DEFPROCwater
930 PRINTTAB(0,5);CHR$(136)
940 IF WaterVel>0 THEN PRINTTAB(0,17);CHR$(134)"Previous Sup. Vel.
    =";WaterVel;"m/sec"
950 PRINTTAB(0,19);CHR$(134);"Enter New Superficial Velocity in
    m/sec"
960 PRINTTAB(0,20);CHR$(134);"(min 0.3 - max 2.4)";CHR$(131);:INPUT"
    "WaterVel:WaterV=WaterVel*(PI*(Dia↑2)/4)
970 ENDPROC
980
990 DEFPROCwind
1000 PRINTTAB(0,7);CHR$(136)
1010 IF AirVel>0 THEN PRINTTAB(0,17);CHR$(134)"Previous Sup. Vel.
    =";AirVel;"m/sec"
1020 PRINTTAB(0,19);CHR$(134);"Enter New Superficial Velocity in
    m/sec"
1030 PRINTTAB(0,20);CHR$(134);"(min 0.01 - max
    0.6)";CHR$(131);:INPUT" "AirVel:AirV=AirVel*(PI*(Dia↑2)/4)
1040 ENDPROC
1050
1060 DEFPROCtube-dia
1070 PRINTTAB(0,9);CHR$(136)
1080 IF Dia>0 AND Dia<>0.0778 THEN PRINTTAB(0,17);CHR$(134)"Previous
    Tube Diameter =";Dia;"m"
1090 IF Dia=0.0778 THEN PRINTTAB(0,17);CHR$(134)"Default Tube
```

```
     Diameter =";Dia;"m"
1100 PRINTTAB(0,19);CHR$(134);"Enter New Working Section Diameter
     (m)"
1110 PRINTTAB(7,20);" ";CHR$(131);:INPUT" "Dia
1120 IF Dia=0 THEN Dia=0.0778
1130 PRINTTAB(0,17);"                                              "
1140 PRINTTAB(0,19);CHR$(134);"Enter Micro Man range"
1150 PRINTTAB(0,20);CHR$(131);"(1,0.3,0.1,0.03,0.01) ";:INPUT"
     "Manrange
1160 IF Manrange=0 THEN Manrange=1
1170 PRINTTAB(0,19);CHR$(134);"Enter Atmospheric air pressure in"
1180 PRINTTAB(0,20);CHR$(134);"                                    "
1190 PRINTTAB(0,20);CHR$(134);"mm of Hg";:INPUT" "Atmos
1200 Atmos=13.6*RoeW*9.81*Atmos/1000
1210 PRINTTAB(0,19);CHR$(134);"Enter Atmospheric temperature in "
1220 PRINTTAB(0,20);CHR$(134);"                                    "
1230 PRINTTAB(0,20);CHR$(134);"deg 'C'";:INPUT" "Temp
1240 PROCmanometer
1250 ENDPROC
1260
1270 DEFPROCdisplay
1280 CLS
1290 PRINTTAB(4,1);CHR$(141);CHR$(131);"Two Phase Flow Loop Control"
1300 PRINTTAB(4,2);CHR$(141);CHR$(130);"Two Phase Flow Loop Control"
1310 PRINTTAB(0,23);CHR$(134);"(PressSPACE BARto Enter New Values)"
1320 PRINTTAB(0,12);CHR$(134);"Void Fraction"
1330 PRINTTAB(0,4);CHR$(134);"Required Superficial Velocity"
1340 PRINTTAB(0,5);CHR$(134);"of Water (m/sec)"
1350 PRINTTAB(0,8);CHR$(134);"Actual Superficial Velocity"
1360 PRINTTAB(0,9);CHR$(134);"of Water (m/sec)"
1370 PRINTTAB(0,14);CHR$(134);"Required Superficial Velocity"
1380 PRINTTAB(0,15);CHR$(134);"of Air (m/sec)"
1390 PRINTTAB(0,18);CHR$(134);"Actual Superficial Velocity"
1400 PRINTTAB(0,19);CHR$(134);"of Air (m/sec)"
1410 PRINTTAB(0,6);CHR$(129):PRINTTAB(34,6);CHR$(255);CHR$(255)
1420 PRINTTAB(0,16);CHR$(129):PRINTTAB(34,16);CHR$(255);CHR$(255)
1430 PRINTTAB(30,4);CHR$(134);WaterVel
1440 PRINTTAB(30,14);CHR$(134);AirVel
1450 PRINTTAB(30,12);CHR$(134);" 0.00 %"
1460 ENDPROC
1470
1480 DEFPROCread-flowrates
1490 SAMPLE Samplenu,Sample*1E6,&098000,0 TO 4
1500 REPEAT:UNTIL SAMPLE 0,0=0 :REM Waits for sample to finish
1510 Sampup=0 :Sampmean=0
1520 FOR I%=1 TO Samplenu
1530 Sampup=Sampup+(((SAMPLE I%,3)-&FFFF/2)-Inuperr)
1540 Sampmean=Sampmean+(((SAMPLE I%,4)-&FFFF/2)-Inmeanerr)
1550 NEXT I%
1560 Sampup=Sampup/Samplenu
1570 Sampmean=Sampmean/Samplenu
1580 Roeup=(Atmos+(Sampup*2*20*100000/(10*&FFFF)))/
     (Rgas*(Temp+273.15))
1590 Roemean=(Atmos+(Sampmean*20*100000/(10*&FFFF)))/
     (Rgas*(Temp+273.15))
1600 ActualW=0
1610 IntErrorW=0
1620 ActualA=0
1630 IntErrorA=0
1640 FOR I%=1 TO Samplenu
```

```
1650 ActualW=ActualW+((((SAMPLE I%,0)-(&FFFF/2))*20*0.001668/&FFFF)
     -0.0004388)
1660 IntErrorW=IntErrorW+(WaterV-((((SAMPLE I%,0)-(&FFFF/2))
     *20*0.001668/&FFFF)-0.0004388))*Sample
1670 REM "Air flow rate calcs
1680 Samp=((SAMPLE I%,1)-&FFFF/2)-Inairerr
1690 IF Samp<0 THEN Samp=0
1700 ActualA=ActualA+(Ko*PI*(OrDia↑2)*SQR(2*9.81*((Samp*20/&FFFF)
     *1000*Manrange)*Roeup)/(4*Roemean))
1710 IntErrorA=IntErrorA+(AirV-((Ko*PI*(OrDia↑2)*SQR(2*9.81
     *((Samp*20/&FFFF)*1000*Manrange)*Roeup)/(4*Roemean))))*Sample
1720 NEXT I%
1730 ActualW=ActualW/Samplenu
1740 ActualA=ActualA/Samplenu
1750 ENDPROC
1760
1770 DEFPROCerror-calc
1780 IF ActualW<0 THEN PRINTTAB(30,8);CHR$(134);"0.0000":GOTO 1800
1790 PRINTTAB(30,8);CHR$(134);ActualW/(PI*(Dia↑2)/4)
1800 ErrorW=WaterV-ActualW
1810 IncrW=INT(K1*ErrorW+K2*IntErrorW)
1820 IF WaterV=0 THEN 1840
1830 IF ABS(ErrorW/WaterV)<=0.05 THEN PRINTTAB(0,6);CHR$(130)
     ;(ErrorW/WaterV)*100 :ELSE PRINTTAB(0,6);CHR$(129)
     ;(ErrorW/WaterV)*100
1840 IF ActualA<0 THEN PRINTTAB(30,18);CHR$(134);"0.0000":GOTO 1860
1850 PRINTTAB(30,18);CHR$(134);ActualA/(PI*(Dia↑2)/4)
1860 ErrorA=AirV-ActualA
1870 IncrA=INT(K3*ErrorA+K4*IntErrorA)
1880 IF AirV=0 THEN 1900
1890 IF ABS(ErrorA/AirV)<=0.05 THEN PRINTTAB(0,16)
     ;CHR$(130);(ErrorA/AirV)*100 :ELSE PRINTTAB(0,16)
     ;CHR$(129);(ErrorA/AirV)*100
1900 ENDPROC
1910
1920 DEFPROCset-flowrates
1930 PumpS=PumpS+IncrW
1940 IF PumpS>(&FFFF-4000) THEN PumpS=(&FFFF-4000)
1950 IF PumpS<-4000 THEN PumpS=-4000
1960 DAC#0=(PumpS+4000)
1970 IF IncrA>0 THEN TURNON 3 ELSE TURNOFF 3
1980 FOR I=0 TO ABS(IncrA):TURNON 4:FOR J=0 TO 10:NEXT J
     :TURNOFF 4:FOR J=0 TO 10:NEXT J:NEXT I
1990 ENDPROC
2000
2010 DEFPROCtestmenu
2020 CLS
2030 PRINTTAB(11,1);CHR$(141);CHR$(131);"Test Menu"
2040 PRINTTAB(11,2);CHR$(141);CHR$(131);"Test Menu"
2050 PRINTTAB(0,5);CHR$(134);"1) Void Fraction Measurement"
2060 PRINTTAB(0,7);CHR$(134);"2) Differtential Pressure"
2070 PRINTTAB(0,9);CHR$(134);"3) Set DP Transducer"
2080 PRINTTAB(3,15);"Enter Number";
2090 VDU23,1,1;0;0;0;:G=GET:G=G-48:VDU23,1,0;0;0;0;
2100 IF G=1 THEN PROCprinter:PROCvoid-fraction:ENDPROC
2110 IF G=2 THEN PROCDiff-press:ENDPROC
2120 IF G=3 THEN PROCsetdp:ENDPROC
2130 IF G=4 THEN ENDPROC
2140 IF G=5 THEN ENDPROC
2150 GOTO 2090
```

```
2160 ENDPROC
2170
2180 DEFPROCvoid-fraction
2190 IF Printer=1 AND Flag=0 THEN VDU2:PRINT"AirSV  : WaterSV :
     %VF   : MeanV  : TrueGV":VDU3
2200 Flag=1
2210 PRINTTAB(0,5);CHR$(136)
2220 VDU23,1,1;0;0;0;
2230 PRINTTAB(0,17);CHR$(134);"Enter the number of runs"
     ;CHR$(131);:INPUT""Numb
2240 IF Numb<1 OR Numb>20 THEN PRINTTAB(0,17);"                    "
     :GOTO 2230
2250 VDU23,1,0;0;0;0;
2260 Total=0
2270 FOR Void=1 TO Numb
2280 PROCdisplay
2290 TURNOFF 2 :TURNOFF 5:FOR I=0 TO 10000:NEXT I
2300 TIME=0
2310 REPEAT
2320 PROCread-flowrates
2330 PROCerror-calc
2340 PROCset-flowrates
2350 UNTIL (TIME>1000 AND ABS(ErrorA/AirV)<=0.02 AND
     ABS(ErrorW/WaterV)<=0.02)
2360 TURNON 2 :TURNON 5
2370 DAC#0=0 :PumpS=0
2380 TURNOFF 3:FOR I=0 TO 1800 :TURNON 4 :FOR J=0 TO 5:NEXT J
     :TURNOFF 4 :FOR J=0 TO 5:NEXT J:NEXT I
2390 CLS
2400 PRINTTAB(0,4);CHR$(134);"Enter the Void Fraction"
     ;CHR$(131);:INPUT""Voidfrac
2410 Total=Total+Voidfrac
2420 PRINTTAB(0,6);CHR$(134);"The average Void Fraction so far is"
2430 PRINTTAB(10,7);Total/Void
2440 PRINTTAB(4,23);CHR$(134);"(PressSPACE BARto Continue)"
2450 G=GET
2460 NEXT Void
2470 CLS
2480 IF Printer=1 THEN VDU2 ELSE PRINT"AirSV WaterSV %VF MeanV
     TrueGV"
2490 REM"AirSupVel WaterSupVel VoidFrac MeanVel TrueGasVel"
2500 IF Printer=1 THEN PRINT"       :          :          :       :"
2510 PRINTAirVel;" : ";WaterVel;"  : ";Total/Numb;" : "
     ;AirVel+WaterVel;" : ";AirVel/(Total/(100*Numb))
2520 VDU3
2530 PRINTTAB(4,23);CHR$(134);"(PressSPACE BARto Continue)"
2540 G=GET
2550 ENDPROC
2560
2570 DEFPROCError
2580 TURNOFF 0
2590 TURNOFF 1
2600 TURNOFF 2 :TURNOFF 5
2610 DAC#0=0
2620 TURNOFF 3
2630 FOR I=0 TO 2000 :TURNON 4 :FOR J=0 TO 10:NEXT J:TURNOFF 4
     :FOR J=0 TO 10:NEXT J:NEXT I
2640 TURNOFF 15
2650 @%=&90A
2660 REPORT
```

```
2670 ENDPROC
2680
2690 DEFPROCDiff-press
2700 PRINTTAB(0,7);CHR$(136)
2710 TURNOFF 2 :TURNOFF 5
2720 PRINTTAB(0,17);CHR$(134);"Remember to OPEN the valves"
2730 FOR Wait=0 TO 2000 :NEXT Wait
2740 VDU23,1,1;0;0;0;
2750 PRINTTAB(0,17)"                                                    "
2760 PRINTTAB(0,17);CHR$(134);"Skin friction Test, Constant Air or"'
     "Water (S, A or W)";CHR$(131);:INPUT""A$
2770 IF A$="A" OR A$="a" THEN PROCConst-air:ENDPROC
2780 IF A$="W" OR A$="w" THEN PROCConst-water:ENDPROC
2790 IF A$="S" OR A$="s" THEN PROCSkin-friction:ENDPROC
2800 GOTO 2750
2810 ENDPROC
2820
2830 DEFPROCsetdp
2840 PRINTTAB(0,9);CHR$(136)
2850 TURNOFF 2 :TURNOFF 5
2860 PRINTTAB(0,17);CHR$(134);"Remember to OPEN the valves"
2870 FOR Wait=0 TO 2000 :NEXT Wait
2880 CLS
2890 PRINTTAB(0,7);CHR$(134);"Close Water Valve when Test Section is"
2900 PRINTTAB(0,8);CHR$(134);"Floaded. Then press any key to take"
2910 PRINTTAB(0,9);CHR$(131);"Measurment"
2920 DAC#0=7000
2930 G=GET
2940 DAC#0=0
2950 TIME=0
2960 REPEAT:UNTIL TIME>=2000
2970 SAMPLE Samplenu,Sample*1E6,&098000,0 TO 2
2980 REPEAT:UNTIL SAMPLE 0,0=0 :REM Waits for sample to finish
2990 FOR I%=1 TO Samplenu
2991 FOR I%=1 TO Samplenu
2992 Vf=Vf+(4.02965*(((SAMPLE I%,2)
     -(&FFFF/2))*20/&FFFF)-5.4583E-2)*100
2993 NEXT I%
2994 Vf=Vf/Samplenu
2995 Voidfraction(0,0)=Vf
2996 PRINTTAB(0,12);CHR$(134)"Open Water Valve"
2997 PRINTTAB(0,13);CHR$(131)"Then Press any key to continue"
2998 G=GET
2999 ENDPROC
3000
3010 DEFPROCConst-water
3020 CLS
3030 PRINTTAB(2,1);CHR$(141);CHR$(131);"Differential Pressure
     Measurement"
3040 PRINTTAB(2,2);CHR$(141);CHR$(130);"Differential Pressure
     Measurement"
3050 PRINTTAB(0,4);CHR$(134);"Enter Constant Water Sup:
     Velocity";';SPC(15);CHR$(131);
     :INPUT""WaterVel:WaterV=WaterVel*(PI*(Dia↑2)/4)
3060 PRINTTAB(0,7);CHR$(134);"Enter Start Air Sup:
     Velocity";';SPC(15);CHR$(131);:INPUT""StartA
3070 PRINTTAB(0,10);CHR$(134);"Enter End Air Sup: Velocity";'
     ;SPC(15);CHR$(131);:INPUT""EndA
3080 PRINTTAB(0,13);CHR$(134);"Enter Step size";'
     ;SPC(15);CHR$(131);:INPUT""Size
```

```
3090 PRINTTAB(0,16);CHR$(134);"Enter the number of runs"
     ;CHR$(131);:INPUT""Runs
3100 IF Runs<1 OR Runs>20 THEN PRINTTAB(0,16);"                    "
     :GOTO 3090
3110 VDU23,1,0;0;0;0;
3300 PROCsetdp
3310 N=1
3320 FOR AirVel=StartA TO EndA STEP Size
3330 AirV=AirVel*(PI*(Dia↑2)/4)
3340 PROCdisplay
3350 FOR Test=1 TO Runs
3360 REPEAT
3370 PROCread-flowrates
3380 PROCvfcalc
3390 PROCerror-calc
3400 PROCset-flowrates
3410 UNTIL (ABS(ErrorA/AirV)<=0.02 AND ABS(ErrorW/WaterV)<=0.02)
3420 PRINTTAB(0,20);CHR$(134);"Test Number";CHR$(131);(Test+1)
3430 Vf=0
3440 FOR I%=1 TO Samplenu
3450 Vf=Vf+(4.02965*(((SAMPLE I%,2)
     -(&FFFF/2))*20/&FFFF)-5.4583E-2)*100
3460 NEXT I%
3470 Vf=(Vf/Samplenu)-Voidfraction(0,0)
3480 Vf=100-(((Vf/(9.81*h))-RoeW)/(Roemean-RoeW))*100
3490 Voidfraction(N,Test)=Vf
3500 NEXT Test
3510 Vf=0
3520 FOR I%=1 TO Runs
3530 Vf=Vf+Voidfraction(N,I%)
3540 NEXT I%
3550 Voidfraction(N,0)=Vf/Runs
3560 N=N+1
3570 NEXT AirVel
3580 DAC#0=0 :PumpS=0
3590 TURNOFF 3:FOR I=0 TO 1800 :TURNON 4 :FOR J=0 TO 5:NEXT J
     :TURNOFF 4 :FOR J=0 TO 5:NEXT J:NEXT I
3600 CLS
3610 N=1
3620 PROCprinter:IF Printer=1 THEN VDU2 ELSE VDU14
3630 PRINT " Vsg       Vsw          %VF          Vm        Vgt       Rew"
3640 PRINT " (m/s)     (m/s)                     (m/s)     (m/s)"
3650 PRINT" "
3660 FOR AirVel=StartA TO EndA STEP Size
3670 PRINT AirVel;" : ";WaterVel;" : ";(Voidfraction(N,0));" :
     ";(AirVel+WaterVel);" : ";(AirVel*100/(Voidfraction(N,0)));" :
     ";
3680 Pform=@%:@%=&10406:PRINT;(WaterVel*Dia/1.14E-6):@%=Pform
3690 N=N+1
3700 NEXT AirVel
3710 VDU3:VDU15
3720 PRINT'';CHR$(134);"Press 'F' to file the results or any"
3730 PRINT;CHR$(134);"other key to continue"
3740 G$=GET$
3750 IF G$="F" OR G$="f" THEN PROCfile(2)
3760 ENDPROC
3770
3780 DEFPROCConst-air
3790 CLS
3800 PRINTTAB(2,1);CHR$(141);CHR$(131);"Differential Pressure
```

```
     Measurement"
3810 PRINTTAB(2,2);CHR$(141);CHR$(130);"Differential Pressure
     Measurement"
3820 PRINTTAB(0,4);CHR$(134);"Enter Constant Air Sup: Velocity"
     ;';SPC(15);CHR$(131);:INPUT""AirVel:AirV=AirVel*(PI*(Dia↑2)/4)
3830 PRINTTAB(0,7);CHR$(134);"Enter Start Water Sup: Velocity"
     ;';SPC(15);CHR$(131);:INPUT""StartW
3840 PRINTTAB(0,10);CHR$(134);"Enter End Water Sup: Velocity"
     ;';SPC(15);CHR$(131);:INPUT""EndW
3850 PRINTTAB(0,13);CHR$(134);"Enter Step size";';SPC(15)
     ;CHR$(131);:INPUT""Size
3860 PRINTTAB(0,16);CHR$(134);"Enter the number of runs"
     ;CHR$(131);:INPUT""Runs
3870 IF Runs<1 OR Runs>20 THEN PRINTTAB(0,16);"      ":GOTO 3090
3880 VDU23,1,0;0;0;0;
4070 PROCsetdp
4080 N=1
4090 FOR WaterVel=StartW TO EndW STEP Size
4100 WaterV=WaterVel*(PI*(Dia↑2)/4)
4110 PROCdisplay
4120 FOR Test=1 TO Runs
4130 REPEAT
4140 PROCread-flowrates
4150 PROCvfcalc
4160 PROCerror-calc
4170 PROCset-flowrates
4180 UNTIL (ABS(ErrorA/AirV)<=0.02 AND ABS(ErrorW/WaterV)<=0.02)
4190 PRINTTAB(0,20);CHR$(134);"Test Number";CHR$(131);(Test+1)
4200 Vf=0
4210 FOR I%=1 TO Samplenu
4220 Vf=Vf+(4.02965*(((SAMPLE I%,2)
     -(&FFFF/2))*20/&FFFF)-5.4583E-2)*100
4230 NEXT I%
4240 Vf=(Vf/Samplenu)-Voidfraction(0,0)
4250 Vf=100-(((Vf/(9.81*h))-RoeW)/(Roemean-RoeW))*100
4260 Voidfraction(N,Test)=Vf
4270 NEXT Test
4280 Vf=0
4290 FOR I%=1 TO Runs
4300 Vf=Vf+Voidfraction(N,I%)
4310 NEXT I%
4320 Voidfraction(N,0)=Vf/Runs
4330 N=N+1
4340 NEXT WaterVel
4350 DAC#0=0 :PumpS=0
4360 TURNOFF 3:FOR I=0 TO 1800 :TURNON 4 :FOR J=0 TO 5:NEXT J
     :TURNOFF 4 :FOR J=0 TO 5:NEXT J:NEXT I
4370 CLS
4380 N=1
4390 PROCprinter:IF Printer=1 THEN VDU2 ELSE VDU14
4400 PRINT " Vsg      Vsw        %VF        Vm       Vgt      Rew"
4410 PRINT " (m/s)    (m/s)                 (m/s)    (m/s)"
4420 PRINT" "
4430 FOR WaterVel=StartW TO EndW STEP Size
4440 PRINT AirVel;" : ";WaterVel;" : ";(Voidfraction(N,0));" :
     ";(AirVel+WaterVel);" : ";(AirVel*100/(Voidfraction(N,0)));" :
     ";
4450 Pform=@%:@%=&10406:PRINT;(WaterVel*Dia/1.14E-6):@%=Pform
4460 N=N+1
4470 NEXT WaterVel
```

```
4480 VDU3:VDU15
4490 PRINT'''';CHR$(134);"Press 'F' to file the results or any"
4500 PRINT;CHR$(134);"other key to continue"
4510 G$=GET$
4520 IF G$="F" OR G$="f" THEN PROCfile(3)
4530 ENDPROC
4540
4550 DEFPROCprinter
4560 REM"Check to see if printer is connected"
4570 IF Printer=1 ENDPROC
4580 PRINT;CHR$(134)"Is a print out required (Y or N) ";:G$=GET$
4590 IF G$="Y" OR G$="y" THEN Printer=1 ELSE Printer=0
4600 *FX15,1
4610 ENDPROC
4620
4630 DEFPROCSkin-friction
4640 CLS
4650 PRINTTAB(5,1);CHR$(141);CHR$(131);"Skin Friction Measurement"
4660 PRINTTAB(5,2);CHR$(141);CHR$(130);"Skin Friction Measurement"
4670 VDU23,1,0;0;0;0;
4850 PROCsetdp
4860 AirV=0
4870 N=1
4880 FOR WaterVel=0.3 TO 2.1 STEP 0.1
4890 WaterV=WaterVel*(PI*(Dia↑2)/4)
4900 PROCdisplay
4910 FOR Test=1 TO 4
4920 TIME=0
4930 REPEAT
4940 PROCread-flowrates
4950 PROCerror-calc
4960 PROCset-flowrates
4970 UNTIL (TIME>=2000 AND ABS(ErrorW/WaterV)<=0.02)
4980 PRINTTAB(0,20);CHR$(134);"Test Number";CHR$(131);(Test+1)
4990 Vf=0
5000 FOR I%=1 TO Samplenu
5010 Vf=Vf+(4.02965*(((SAMPLE I%,2)-(&FFFF/2))*20/&FFFF)-5.4583E-2)
5020 NEXT I%
5030 Vf=Vf/Samplenu
5040 Voidfraction(N,Test)=Vf
5050 NEXT Test
5060 Vf=0
5070 FOR I%=1 TO 4
5080 Vf=Vf+Voidfraction(N,I%)
5090 NEXT I%
5100 Voidfraction(N,0)=(Voidfraction(0,0)-(Vf/4))
5110 N=N+1
5120 NEXT WaterVel
5130 DAC#0=0 :PumpS=0
5140 CLS
5150 N=1
5160 Ls1=0:Ls2=0:Ls3=0:Ls4=0
5170 PROCprinter:IF Printer=1 THEN VDU2 ELSE VDU14
5180 Pform=@%
5190 PRINT;"  Vsw     delta P        Tor          Cf          Re"
5200 PRINT;" (m/s)      (mbar)"
5210 PRINT'"0.0000   :   ";Voidfraction(0,0)
5220 FOR WaterVel=0.3 TO 2.1 STEP 0.1
5230 PRINTWaterVel;"   :   ";Voidfraction(N,0);"   :   "
     ;(Voidfraction(N,0)*Dia*100/(4*Ltapping));"   :   ";
```

```
      :@%=&10406:PRINT;((Voidfraction(N,0)*Dia*100/(4*Ltapping))
      /(0.5*RoeW*(WaterVel↑2)));"   :   "
      ;(WaterVel*Dia/1.14E-6):@%=Pform
5240  Ls1=Ls1+WaterVel*Voidfraction(N,0)
5250  Ls2=Ls2+WaterVel
5260  Ls3=Ls3+Voidfraction(N,0)
5270  Ls4=Ls4+(WaterVel)↑2
5280  N=N+1
5290  NEXT WaterVel
5300  Ls5=(18*Ls1-Ls2*Ls3)/(18*Ls4-Ls2↑2)
5310  Ls6=(Ls3*Ls4-Ls1*Ls2)/(18*Ls4-Ls2↑2)
5320  PRINT''"Delta P = ";Ls5;" x Vsw +";Ls6;" (mbar)"
5330  VDU3:VDU15
5340  PRINT'''';CHR$(134);"Press 'F' to file the results or any"
5350  PRINT;CHR$(134);"other key to continue"
5360  G$=GET$
5370  IF G$="F" OR G$="f" THEN PROCfile(1)
5380  ENDPROC
5390
5400  DEFPROCfile(Section)
5410  CLS
5420  VDU23,1,1;0;0;0;
5430  PRINTTAB(0,7);CHR$(134);"Enter File name";CHR$(131);:INPUT" "F$
5440  PRINTTAB(0,9);CHR$(134);"Enter Comment";CHR$(131);:INPUT" "Com$
5450  VDU23,1,0;0;0;0;
5460  F$=":2.D."+F$
5470  Out=OPENOUT F$
5480  ON Section GOTO 5490,5600,5710
5490  REM"Section = 1
5500  Nrow=18
5510  Ncol=5
5520  PRINT#Out,Com$,Nrow,Ncol,"Vsw       ","dP        ","Tor   "
      ,"Cf        ","Re        "
5530  N=1
5540  FOR WaterVel=0.3 TO 2.1 STEP 0.1
5550  PRINT#Out,WaterVel,Voidfraction(N,0),(Voidfraction(N,0)
      *Dia*100/(4*Ltapping)),((Voidfraction(N,0)*Dia*100/
      (4*Ltapping))/(0.5*RoeW*(WaterVel↑2))),(WaterVel*Dia/1.14E-6)
5560  N=N+1
5570  NEXT WaterVel
5580  CLOSE#Out
5590  ENDPROC
5600  REM"Section = 2
5610  Nrow=INT((EndA-StartA)/Size)
5620  Ncol=6
5630  PRINT#Out,Com$,Nrow,Ncol,"Vsg       ","Vsw       ","Vf    "
      ,"Vm        ","Vgt       ","Rew       "
5640  N=1
5650  FOR AirVel=StartA TO EndA STEP Size
5660  PRINT#Out,AirVel,WaterVel,(Voidfraction(N,0)),
      (AirVel+WaterVel),(AirVel*100/(Voidfraction(N,0))),
      (WaterVel*Dia/1.14E-6)
5670  N=N+1
5680  NEXT AirVel
5690  CLOSE#Out
5700  ENDPROC
5710  REM"Section = 3
5720  Nrow=INT((EndW-StartW)/Size)
5730  Ncol=6
5740  PRINT#Out,Com$,Nrow,Ncol,"Vsg       ","Vsw       ","Vf    ",
```

```
      "Vm          ","Vgt         ","Rew         "
5750 N=1
5760 FOR WaterVel=StartW TO EndW STEP Size
5770 PRINT#Out,AirVel,WaterVel,(Voidfraction(N,0)),
     (AirVel+WaterVel),(AirVel*100/(Voidfraction(N,0)))
     ,(WaterVel*Dia/1.14E-6)
5780 N=N+1
5790 NEXT WaterVel
5800 CLOSE#Out
5810 ENDPROC
5820
5830 DEFPROCmanometer
5840 SAMPLE Samplenu,Sample*1E6,&098000,0 TO 4
5850 REPEAT:UNTIL SAMPLE 0,0=0 :REM Waits for sample to finish
5860 Samp=0
5870 Sampmean=0
5880 Sampup=0
5890 FOR I%=1 TO Samplenu
5900 Samp=Samp+((SAMPLE I%,1)-&FFFF/2)
5910 Sampup=Sampup+((SAMPLE I%,3)-&FFFF/2)
5920 Sampmean=Sampmean+((SAMPLE I%,4)-&FFFF/2)
5930 NEXT I%
5940 Inairerr=Samp/Samplenu
5950 Inuperr=Sampup/Samplenu
5960 Inmeanerr=Sampmean/Samplenu
5970 ENDPROC
5980
5990 DEFPROCvfcalc
6000 Vf=0
6010 FOR I%=1 TO Samplenu
6020 Vf=Vf+(4.02965*(((SAMPLE I%,2)
     -(&FFFF/2))*20/&FFFF)-5.4583E-2)*100
6030 NEXT I%
6040 Vf=(Vf/Samplenu)-Voidfraction(0,0)
6050 Vf=100-(((Vf/(9.81*h))-RoeW)/(Roemean-RoeW))*100
6060 Pform=@% :@%=&20204
6070 PRINTTAB(30,12);CHR$(131);-Vf;" %"
6080 @%=Pform
6090 ENDPROC
```

APPENDIX 3 - PSEUDO-RANDOM LOW AVERAGE GAS VOID FRACTION PRESSURE FLUCTUATION SIMULATION SOFTWARE

Appendix summary

Contained in this appendix is a listing of the software developed in this study to simulate differential pressure signals within low average gas void fraction vertical bubbly two-phase flows.

Pseudo-random low average gas void fraction pressure fluctuation numerical simulation software

Listed below are the functions written in 'C' used in the simulation software and a brief description of each function.

main()	-	Menu display
randomdata()	-	Generate pseudo-random bubble co-ordinate positions for a given local void fraction profile and average gas void fraction
analyse()	-	Generate simulated differential pressure signals from the pseudo-random bubble co-ordinates and local gas velocity profile using algorithms derived in chapter 6
velocitypro()	-	Local gas velocity profile evaluation routine
savesig()	-	Save two channels of generated simulated differential pressure signals
saveplt()	-	Save a plot file for exporting to Harvard Graphics
box()	-	Draws simple border
grid()	-	Generates grid displays on graphs
skipgarb()	-	Input/output keyboard entry routine
load()	-	Load previously generated pseudo-random bubble/void fraction data
save()	-	Save generated pseudo-random bubble/void fraction data
printout()	-	Display void fraction data whilst generating pseudo-random bubble positions

defa()	-	Default variable settings display and entry point for variables associated with the performance of the analysis software
symbol()	-	Plotting symbols
display()	-	Graphical display routine
motionpressure()	-	Evaluation of pressure caused by a bubbles motion
voidfraction()	-	Evaluate local void fraction $\alpha_l(t)$ between differential pressure transducer tappings
partbub()	-	Evaluate contribution to local gas void fraction $\alpha_l(t)$ for part of a bubble
vfmeasured()	-	Evaluate average gas void fraction when generating pseudo-random bubble positions
vfprofile()	-	Display local void fraction profile
*filename()	-	Filename entry point

```
/* -> $.!C.user.c.Bubble2 */
/*  Bubble simulation     */
/*          BY            */
/*    A.L.Samways         */

#include <stdio.h>
#include <string.h>
#include <ctype.h>
#include <math.h>
#include <stdlib.h>
#include "bbc.h"

#define pi        3.141592654
#define g         9.81
#define roeair    1.28                  /*  Roe of air                */
#define roewater 1000.0                 /*  Roe of water              */

void randomdata(void);
void analyse(void);
void velocitypro(void);
void savesig(void);
void saveplt(int,int);
void box(int,int,int,int);
void grid(int,int,int,int,int,int);
void skipgarb(void);
void load(void);
void save(void);
void printout(void);
void defa(void);
void symbol(int,int,int);
void display(void);
double motionpressure(int,double);
double voidfraction(int,double);
double partbub(double);
double vfmeasured(double);
void vfprofile(void);

char *filename(char*);

int rlength;
int count = 0;
                                        /*  Defaults                  */
double length = 1.0;                    /*  Length of pipe            */
double dpipe = 0.08155;                 /*  Pipe diameter             */
double bdia = 0.0065;                   /*  Bubble diameter           */
double tappings = 0.025;                /*  Tapping distance          */
double distance = 0.006;                /*  Distance between transducers */
double walldist = 0.040;                /*  Max dist from tapping     */
double vwater = 0.000;                  /*  Superficial water velocity */
double vbubble = 0.293;                 /*  Terminal velocity of bubble */
double timint = 0.0004;                 /*  Time interval             */
double vf = 0.05;                       /*  Required void fraction    */

double ampgain1 = 10.33;                /*  amp 1 gain 1v = 23.72 mm h2o */
double ampgain2 = 10.33;                /*  amp 2 gain 1v = 23.72 mm h2o */
double fiddle = 10.0;                   /*  to give better resolution */

int n = 7;                              /*  Velocity power law        */
int m = 7;                              /*  Void fraction profile     */
```

```
int array[4096] [2];
double sample[10000] [3];
double plot[240] [8];

int samplemax = 4096;


char *pathvf  = ":0.$.vfdata.";
char *pathsig = ":0.$.data.";
char *pathplt = ":0.$.plt.";

int main()

{                                          /*  Menu  */
 int true=0;

 char ch;

 bbc-mode(12);
 bbc-colour(132);
 bbc-cursor(0);
 while (true == 0)
  {
   bbc-cls();
   bbc-tab(0,4);
   printf("                                Random Bubble Simulation
Program\n");
   bbc-move(380,850);
   bbc-draw(900,850);
   bbc-tab(0,7);
   printf("                          Generate random data\n");
   printf("                          Save random data to disk\n");
   printf("                          Load random data from disk\n");
   printf("                          Analyse pressure signals\n");
   printf("                          Display pressure signal\n");
   printf("                          Pressure signal save\n");
   printf("                          Change defaults\n");
   printf("                          Void fraction profile\n");
   box(50,50,1220,975);
   bbc-tab(18,17);
   switch (ch = toupper(getchar()))
    {
     case 'G' : randomdata();
                break;
     case 'S' : save();
                break;
     case 'L' : load();
                break;
     case 'A' : analyse();
                break;
     case 'D' : display();
                break;
     case 'P' : savesig();
                break;
     case 'C' : defa();
                break;
     case 'V' : vfprofile();
    }
```

```
  }
 return (0);
}


void randomdata()

{
 int flag = 1;
 int index;
 int count1 = 0;

 double volume;
double vfrac = 0.0;
double vfl,vfracl;
double x;
double r;
double theata;
double a;
double b = 1.0;
double randmax = 2147483647;

char ch;

volume = pi*pow(dpipe,2.0)*length/4;
bbc-cls();
bbc-move(820+(int)(5000.0*(dpipe/2)),60);
bbc-draw(820+(int)(5000.0*(dpipe/2)),900+60);
bbc-move(820-(int)(5000.0*(dpipe/2)),60);
bbc-draw(820-(int)(5000.0*(dpipe/2)),900+60);
for (r=bdia/2; r<=((dpipe/2)-(bdia/2)); r+=bdia)
 {
  vfracl=0.0;
  count1=count;
  vfl=vf;
  while (vfracl <= vfl)
   {
    flag = 1;
    while (flag != 0)
     {
      flag = 0;
      x = ((double) rand())*length/randmax;
      theata = (((double) rand())/randmax)*2*pi;
      for (index=count1; index<count; index++)
       {
        a = pow((sample[index] [1]),2.0)+pow(r,2.0)-(2*sample[index]
            [1]*r*cos((theata-sample[index] [2])));
     b = sqrt(a+pow(sample[index] [0]-x,2.0));
     if (bdia > b)
      {
       flag = 1;
      }
    }
  }
sample[count] [0] = x;
sample[count] [1] = r;
sample[count] [2] = theata;
bbc-tab(4,3);
printf("Number of bubbles  : %u",count);
bbc-tab(4,5);
```

```
      printf("Aver Void fraction : %5.3g",vfrac*100);
      bbc-tab(4,7);
      printf("Local Vf           : %5.3g",vfrac1*100);
      bbc-tab(4,9);
      printf("X                  : %4.3f",x);
      bbc-tab(4,11);
      printf("R                  : %4.3f",r);
      bbc-tab(4,13);
      printf("Theta              : %5.2f",theata*360.0/(2*pi));
      bbc-plot(69,820+(int)(5000.0*sample[count] [1]*cos(sample[count]
[2])),(int)(sample[count] [0]*900.0)+60);
      count++;
      if (count > 10000)
        {
         printf(" Array size to small !!!!");
        }
       vfrac1 = voidfraction((count-count1),(pow((r+(bdia/2)),2.0)
                -pow((r-(bdia/2)),2.0))*pi*length);
       vfrac = voidfraction(count,volume);
      }
   }
  vf=voidfraction(count,volume);
  skipgarb();
  bbc-tab(4,28);
  printf("Press RETURN to continue");
  box(50,50,1220,975);
  ch=getchar();
}

/*
void randomdata()

{
 int flag = 1;
 int index;
 int count1 = 0;

 double volume;
 double vfrac = 0.0;
 double vc;
 double vf1,vfrac1;
 double x;
 double r;
 double theata;
 double a;
 double b = 1.0;
 double randmax = 2147483647;

char ch;

volume = pi*pow(dpipe,2.0)*length/4;
bbc-cls();
bbc-move(820+(int)(5000.0*(dpipe/2)),60);
bbc-draw(820+(int)(5000.0*(dpipe/2)),900+60);
bbc-move(820-(int)(5000.0*(dpipe/2)),60);
bbc-draw(820-(int)(5000.0*(dpipe/2)),900+60);
vc=vf*((double)m+2.0)/(double)m;
for (r=bdia/2; r<=((dpipe/2)-(bdia/2)); r+=bdia)
 {
  vfrac1=0.0;
```

```
count1=count;
vf1=vc*(1-(pow((r/(dpipe/2)),m)));
while (vfracl <= vf1)
 {
  flag = 1;
  while (flag != 0)
   {
    flag = 0;
    x = ((double) rand())*length/randmax;
    theata = (((double) rand())/randmax)*2*pi;
    for (index=count1; index<count; index++)
     {
      a = pow((sample[index] [1]),2.0)+pow(r,2.0)-(2*sample[index]
          [1]*r*cos((theata-sample[index] [2])));
     b = sqrt(a+pow(sample[index] [0]-x,2.0));
     if (bdia > b)
      {
       flag = 1;
      }
    }
 }
sample[count] [0] = x;
sample[count] [1] = r;
sample[count] [2] = theata;
bbc-tab(4,3);
printf("Number of bubbles  : %u",count);
bbc-tab(4,5);
printf("Aver Void fraction : %5.3g",vfrac*100);
bbc-tab(4,7);
printf("Local Vf           : %5.3g",vfracl*100);
bbc-tab(4,9);
printf("X                  : %4.3f",x);
bbc-tab(4,11);
printf("R                  : %4.3f",r);
bbc-tab(4,13);
printf("Theta              : %5.2f",theata*360.0/(2*pi));
bbc-plot(69,820+(int)(5000.0*sample[count] [1]*cos(sample[count]
        [2])),(int)(sample[count] [0]*900.0)+60);
count++;
if (count > 10000)
 {
  printf(" Array size to small !!!!");
 }
vfracl = voidfraction((count-count1),(pow((r+(bdia/2)),2.0)
         -pow((r-(bdia/2)),2.0))*pi*length);
vfrac = voidfraction(count,volume);
    }
  }
 vf=voidfraction(count,volume);
 skipgarb();
 bbc-tab(4,28);
 printf("Press RETURN to continue");
 box(50,50,1220,975);
 ch=getchar();
}
*/

double voidfraction(int numb,double volume)

{
```

```
 double bubvol;

 bubvol = ((double)numb)*pi*pow(bdia,3.0)/6;
 return(bubvol/volume);
}


void analyse()

{
 int index1,index2;

 double i;
 double mean;
 double meanvf;
 double tappingvol;
 double elementvol1;
 double elementvol2;
 double elementvf1;
 double elementvf2;
 double elementroe1;
 double elementroe2;

 tappingvol = (pi*tappings*pow((dpipe/2.0),2.0));
 mean =
((double)count)*4.0*pi*pow((bdia/2),3.0)/(3.0*(length/tappings));
 meanvf = mean/tappingvol;
 for (index1=0; index1<samplemax; index1++)
  {
   elementvol1=0.0;
   elementvol2=0.0;
   for (index2=0; index2<count; index2++)
    {
     i=length/2;
     if ((sample[index2] [0]>=(i+(bdia/2))) && (sample[index2]
                [0]<=(i+tappings-(bdia/2))))
      {
       elementvol1=elementvol1+(4.0*pi*pow((bdia/2),3.0)/3.0);
      }
     if ((sample[index2] [0]>(i-(bdia/2))) && (sample[index2] [0]<i))
      {
       elementvol1=elementvol1+partbub((sample[index2] [0]-i));
      }
     if ((sample[index2] [0]>i) && (sample[index2] [0]<(i+(bdia/2))))
      {
       elementvol1=elementvol1+partbub((sample[index2] [0]-i));
      }
     if ((sample[index2] [0]>(i+tappings)) && (sample[index2]
                [0]<(i+tappings+(bdia/2))))
      {
       elementvol1=elementvol1+partbub((i+tappings
                  -sample[index2] [0]));
      }
     if ((sample[index2] [0]>(i+tappings-(bdia/2))) &&
        (sample[index2] [0]<(i+tappings)))
      {
       elementvol1=elementvol1+partbub((i+tappings
                  -sample[index2] [0]));
      }
```

```
i=i+distance;
if ((sample[index2] [0]>=(i+(bdia/2))) && (sample[index2]
          [0]<=(i+tappings-(bdia/2))))
 {
  elementvol2=elementvol2+(4.0*pi*pow((bdia/2),3.0)/3.0);
 }
if ((sample[index2] [0]>(i-(bdia/2))) && (sample[index2] [0]<i))
 {
  elementvol2=elementvol2+partbub((sample[index2] [0]-i));
 }
if ((sample[index2] [0]>i) && (sample[index2] [0]<(i+(bdia/2))))
 {
  elementvol2=elementvol2+partbub((sample[index2] [0]-i));
 }
if ((sample[index2] [0]>(i+tappings)) && (sample[index2]
          [0]<(i+tappings+(bdia/2))))
 {
  elementvol2=elementvol2+partbub((i+tappings
            -sample[index2] [0]));
 }
if ((sample[index2] [0]>(i+tappings-(bdia/2))) &&
    (sample[index2] [0]<(i+tappings)))
 {
  elementvol2=elementvol2+partbub((i+tappings
            -sample[index2] [0]));
 }

 }
elementvf1=elementvol1/tappingvol;
elementvf2=elementvol2/tappingvol;
elementroe1=roeair*elementvf1+roewater*(1-elementvf1);
elementroe2=roeair*elementvf2+roewater*(1-elementvf2);
array[index1] [0]=2048+(int)(2048.0*((1000.0*((roewater
            -elementroe1-motionpressure(1,walldist))*fiddle
            *tappings/roewater))/ampgain1)/10.0);
array[index1] [1]=2048+(int)(2048.0*((1000.0*((roewater-elementroe2
            -motionpressure(2,walldist))*fiddle*tappings
            /roewater))/ampgain2)/10.0);
array[index1] [2]=0;
bbc-tab(10,16);
printf("Average void fraction %g ",meanvf*100);
bbc-tab(10,21);
printf("%5d        %5.3f        %5.3f        %5d        %5d"
      ,index1,elementvf1*100,elementvf2*100
      ,array[index1] [0],array[index1] [1]);
velocitypro();
}

void velocitypro()

{
 int index;

 double u,ul,c,d;

 /* dbub=vbubble*timint; */
 u=(n+2)*(vwater+vbubble)/(n*(1.0-vf));
 c=u/(pow((dpipe/2),(double)n));
```

```
 for (index=0; index<count; index++)
  {
   ul=u-(c*pow(sample[index] [1],(double)n));
   d=ul*timint;
   sample[index] [0]=sample[index] [0]+d;
   if (sample[index] [0] > 1.0)
    {
     sample[index] [0]=sample[index] [0] - length;
    }
  }
}

/*
void velocitypro()

{
 int index;

 double dbub,u,d;

 dbub=vbubble*timint;
 u=vwater/(1.0-vf);
 d=utimint;
 for (index=0; index<count; index++)
  {
   sample[index] [0]=sample[index] [0]+d+dbub;
   if (sample[index] [0] > 1.0)
    {
     sample[index] [0]=sample[index] [0] - length;
    }
  }
}
*/

double partbub(double b)

{
 double part;

 part = pi*(pow((bdia/2),2.0)*(b+(bdia/2))-((pow((bdia/2),3.0)
        +pow(b,3.0))/3.0));
 return(part);
}


void load()

{
 int index;

 FILE *fp;

 char comment[255];
 char ch;

 bbc-cls();
 bbc-tab(31,4);
 printf("Load from Disk");
 bbc-move(490,850);
 bbc-draw(720,850);
```

```
box(50,50,1220,975);
if ((fp = fopen (filename(pathvf),"r")) == NULL)
 {
  bbc-tab(18,12);
  printf("File could not be found");
  bbc-tab(18,14);
  printf("Press RETURN to continue");
  ch=getchar();
 }
else
 {
  bbc-tab(18,12);
  printf("Random data loading");
  fscanf(fp,"%[^\n]s ",&comment);
  fscanf(fp,"%d %le\n",&count,&vf);
  for (index=0; index < count; index++)
   {
    fscanf(fp,"%le %le %le\n", &sample[index] [0], &sample[index]
          [1], &sample[index] [2]);
   }
  bbc-tab(18,14);
  printf("Comment : %s",comment);
  bbc-tab(18,20);
  printf("Press RETURN to continue");
  ch=getchar();
  if (fclose(fp) != 0)
   {
    bbc-tab(18,12);
    printf("File did not exist !!!\n");
    bbc-tab(18,14);
    printf("Press RETURN to continue");
    ch=getchar();
   }
  }
}


void save()

{
 int index;

 FILE *fp;

 char comment[255];
 char ch;

 bbc-cls();
 bbc-tab(32,4);
 printf("Save to Disk");
 bbc-move(510,850);
 bbc-draw(700,850);
 box(50,50,1220,975);
 printout();
 bbc-tab(18,8);
 skipgarb();
 printf("Enter comment : ");
 scanf("%[^\n]s",&comment);
 skipgarb();
 if ((fp = fopen (filename(pathvf),"w")) == NULL)
```

```
 {
  bbc-tab(18,12);
  printf("File could not be opened");
  bbc-tab(18,14);
  printf("Press RETURN to continue");
  ch=getchar();
 }
else
 {
  bbc-tab(18,12);
  printf("Random data saving");
  fprintf(fp, "Vsl=%5.3f m/s, Vtb=%4.3f m/s, Vf=%4.3f, D=%5.2f mm,
          d=%4.2f mm, Tapping dist=%5.2f mm,
          Transducer spacing=%5.2f mm, Vel profile power=%2d
          ,Vf profile power=%2d,%s\n",vwater,vbubble,vf,dpipe*1000.0
          ,bdia*1000.0,tappings*1000.0,distance*1000.0,n,m,comment);
   fprintf(fp, "%d %g\n",count,vf);
   for (index=0; index < count ; index++)
    {
     fprintf(fp, "%g %g %g\n",sample[index] [0], sample[index] [1]
             ,sample[index] [2]);
    }
   index=fclose(fp);
  }
}


void savesig()

{
int index,ncol=3;

FILE *fp;

char comment[255];
char ch;

bbc-cls();
bbc-tab(32,4);
printf("Save to Disk");
bbc-move(510,850);
bbc-draw(700,850);
box(50,50,1220,975);
printout();
bbc-tab(18,8);
skipgarb();
printf("Enter comment : ");
scanf("%[^\n]s",&comment);
skipgarb();
if ((fp = fopen (filename(pathsig),"w")) == NULL)
 {
  bbc-tab(18,12);
  printf("File could not be opened");
  bbc-tab(18,14);
  printf("Press RETURN to continue");
  ch=getchar();
 }
else
 {
  bbc-tab(18,12);
```

```
printf("Data saving");
rlength=(int) ((double)samplemax*1000.0*timint);
fprintf(fp, "Vsl=%5.3f m/s, Vtb=%4.3f m/s, Vf=%4.3f, D=%5.2f mm,
        d=%4.2f mm, Tapping dist=%5.2f mm
        , Transducer spacing=%5.2f mm, Vel profile power=%2d
        ,Vf profile power=%2d,%s\n",vwater,vbubble,vf,dpipe*1000.0
        ,bdia*1000.0,tappings*1000.0,distance*1000.0,n,m,comment);
fprintf(fp, "%d %d ""Channel A ""Channel B ""Channel C ""%d \n"
        ,samplemax,ncol,rlength);
for (index=0; index < samplemax; index++)
 {
  fprintf(fp, "%d %d ""0""\n",array[index] [0], array[index] [1]);
 }
   index=fclose(fp);
  }
}

void saveplt(int points, int n)

{
 int index,index2;

 FILE *fp;

 char comment[255];
 char ch;

 bbc-cls();
 bbc-tab(31,4);
 printf("Save plot data");
 bbc-move(500,850);
 bbc-draw(710,850);
 box(50,50,1220,975);
 printout();
 bbc-tab(18,8);
 skipgarb();
 printf("Enter legend name : ");
 scanf("%[^\n]s",&comment);
 skipgarb();
 if ((fp = fopen (filename(pathplt),"w")) == NULL)
  {
   bbc-tab(18,12);
   printf("File could not be opened");
   bbc-tab(18,14);
   printf("Press RETURN to continue");
   ch=getchar();
  }
 else
  {
   bbc-tab(18,12);
   printf("Data saving");
   fprintf(fp, "%s\n",comment);
   for (index=0; index <= points; index++)
    {
     fprintf(fp, "%g",plot[index] [0]);
     for (index2=1; index2<=n; index2++)
      {
       fprintf(fp, ",%g",plot[index] [index2]);
      }
```

```
      fprintf(fp, "\n");
     )
    index=fclose(fp);
   )
)


void printout()

{
 bbc-tab(4,16);
 printf("Bubble diameter      : %5.3g m",bdia);
 bbc-tab(4,18);
 printf("Pipe diameter        : %5.3g m",dpipe);
 bbc-tab(4,20);
 printf("Aver Void fraction   : %5.3g",vf*100);
 bbc-tab(4,22);
 printf("Tapping distance     : %5.3g m",tappings);
 bbc-tab(4,24);
 printf("Transducer spacing   : %5.3g m",distance);
 bbc-tab(4,26);
 printf("Super water Vel      : %5.3g m/s",vwater);
 bbc-tab(4,28);
 printf("Terminal bubble Vel  : %5.3g m/s",vbubble);
 bbc-tab(40,16);
 printf("Vel profile power    : %2d",n);
 bbc-tab(40,18);
 printf("Vf profile power     : %2d",m);
}

void defa()

{
 char ch,ch2;

 bbc-cls();
 bbc-tab(0,4);
 printf("                                Random data Defaults\n");
 bbc-move(400,850);
 bbc-draw(750,850);
 bbc-tab(0,7);
 printf("                          Water superficial velocity\n");
 printf("                          Required void fraction\n");
 printf("                          VOid fration profile power\n");
 printf("                          VElocity profile power\n");
 printf("                          Amplifier gains\n");
 printf("                          Pipe diameter\n");
 printf("                          Bubble diameter\n");
 printf("                          TApping spacing\n");
 printf("                          Distance between tappings\n");
 printf("                          TErminal velocity of a bubble\n");
 printf("                          TIme interval\n");
box(50,50,1220,975);
skipgarb();
bbc-tab(14,19);
switch (ch = toupper(getchar()))
 {
  case 'W' : bbc-tab(14,19);
             printf("Present superficial water velocity = %5.3f
```

```
                    m/s",vwater);
                bbc-tab(14,21);
                printf("Enter new superficial water velocity im m/s");
                bbc-tab(14,23);
                skipgarb();
                scanf("%le",&vwater);
                break;
    case 'R' : bbc-tab(14,19);
                printf("Present void fraction = %3.1f percent"
                    ,vf*100.0);
                bbc-tab(14,21);
                printf("Enter new percentage void fraction");
                bbc-tab(14,23);
                skipgarb();
                scanf("%le",&vf);
                vf=vf/100.0;
                break;
    case 'V' : ch2 = toupper(getchar());
                if (ch2 == 'O')
                 {
                  bbc-tab(14,19);
                  printf("Present void fraction profile is a power law
                        of order %d",m);
                  bbc-tab(14,21);
                  printf("Enter new void fraction profile m");
                  bbc-tab(14,23);
                  skipgarb();
                  scanf("%d",&m);
                 }
                if (ch2 == 'E')
                 {
                  bbc-tab(14,19);
                  printf("Present velocity profile is a power law of
                        order %d",n);
                  bbc-tab(14,21);
                  printf("Enter new velocity profile n");
                  bbc-tab(14,23);
                  skipgarb();
                  scanf("%d",&n);
                 }
                break;
    case 'A' : bbc-tab(14,19);
                printf("Present gain of amp1 = %5.3f mm H2O/Volt"
                    ,ampgain1);
                bbc-tab(14,21);
                printf("Enter new gain in mm H2O/Volt");
                bbc-tab(14,23);
                skipgarb();
                scanf("%le",&ampgain1);
                bbc-tab(14,25);
                printf("Present gain of amp2 = %5.3f mm H2O/Volt"
                    ,ampgain2);
                bbc-tab(14,27);
                printf("Enter new gain in mm H2O/Volt");
                bbc-tab(14,29);
                skipgarb();
                scanf("%le",&ampgain2);
                break;
    case 'P' : bbc-tab(14,19);
                printf("Present pipe diameter = %5.4f m",dpipe);
```

```
                bbc-tab(14,21);
                printf("Enter new pipe diameter in metres");
                bbc-tab(14,23);
                skipgarb();
                scanf("%le",&dpipe);
                break;
    case 'B' : bbc-tab(14,19);
                printf("Present bubble diameter = %5.4f m",bdia);
                bbc-tab(14,21);
                printf("Enter new bubble diameter in metres");
                bbc-tab(14,23);
                skipgarb();
                scanf("%le",&bdia);
                break;
       case 'T' : ch2 = toupper(getchar());
                if (ch2 == 'A')
                 {
                  bbc-tab(14,19);
                  printf("Present tapping spacing = %5.4f m",tappings);
                  bbc-tab(14,21);
                  printf("Enter new tapping spacing in metres");
                  bbc-tab(14,23);
                  skipgarb();
                  scanf("%le",&tappings);
                 }
                if (ch2 == 'E')
                 {
                  bbc-tab(14,19);
                  printf("Present terminal velocity of a bubble = %5.3f
m/s",vbubble);
                  bbc-tab(14,21);
                  printf("Enter new terminal velocity in m/s");
                  bbc-tab(14,23);
                  skipgarb();
                  scanf("%le",&vbubble);
                 }
                if (ch2 == 'I')
                 {
                  bbc-tab(14,19);
                  printf("Present sample time interval = %6.5f
seconds",timint);
                  bbc-tab(14,21);
                  printf("Enter new sample time interval in seconds");
                  bbc-tab(14,23);
                  skipgarb();
                  scanf("%le",&timint);
                 }
                break;
       case 'D' : bbc-tab(14,19);
                  printf("Present distance between transducers = %5.4f m"
                         ,distance);
                  bbc-tab(14,21);
                  printf("Enter new transducer spacing in meters");
                  bbc-tab(14,23);
                  skipgarb();
                  scanf("%le",&distance);
                  break;

    }
}
```

```
void vfprofile()

{
 int index,point;

 double index2=0.0;
 double scaledx,scaledy,vc,vfl;

 char ch;

 scaledx = 1000.0/1000.0;
scaledy = 800.0/(vf*2.0);
bbc-cls();
box(100,100,1100,900);
grid(100,100,1100,900,4,4);
bbc-gcol(0,2);
bbc-move(100,100);
vc=vf*((double)m+2.0)/((double)m);
point=0;
for (index=0; index<=1000; index++)
 {
  vfl=vc*(1-pow((index/1000.0),(double)m));
  bbc-plot(5,100+(int)(index*scaledx),100+(int)(vfl*scaledy));
  if ((index%5) == 0)
   {
    plot[point] [0] = index/1000;
    plot[point] [2] = vfl;
    point++;
   }
 }
bbc-move(650,940);
bbc-draw(750,940);
bbc-gcol(0,1);
bbc-move(100,100);
point=0;
for (index2=(bdia/2); index2<=((dpipe/2)-(bdia/2)); index2+=bdia)
 {
  vfl=vfmeasured(index2);
  symbol(1,100+(int)(index2*1000*scaledx*2/dpipe)
         ,100+(int)(vfl*scaledy));
  plot[point] [0] = index2/(dpipe/2);
  plot[point] [1] = vfl;
  point++;
 }
plot[point] [0] = 1.0;
plot[point] [1] = 0.0;
point++;
bbc-move(300,940);
bbc-draw(400,940);
bbc-gcol(0,7);
bbc-tab(1,4);
printf("%3.1f",(vf*2.0*100));
bbc-tab(6,2);
printf("Measured 'Vf'");
bbc-tab(28,2);
printf("Theory 'Vf'");
bbc-tab(5,29);
printf("0.000");
```

```
bbc-tab(1,16);
printf("Vf");
bbc-tab(36,29);
printf("r/R");
bbc-tab(68,29);
printf("1");
bbc-tab(6,31);
printf("Press 'P' RETURN to save data points to file or RETURN to
       continue ");
skipgarb();
ch=toupper(getchar());
if (ch == 'P')
 {
  saveplt(point-1,1);
 }
}


double motionpressure(int updown , double maxdist)

{
 int index;
 double z,z1,z2,angle1,angle2,lp1,lp2,localpress=0.0;

 if (updown==1)
  {
   for (index=0; index<count; index++)
    {
     if ((sample[index] [0] <= ((length/2.0)+tappings+maxdist)) &&
         (sample[index] [0] >= ((length/2.0)-maxdist)))
     {
      z=sqrt(pow((dpipe/2.0),2.0)+pow(sample[index] [1],2.0) -
        (dpipe*sample[index] [1] * cos(sample[index] [2])));
      if (z <= maxdist)
       {
        z1=sqrt(pow(((length/2.0)-sample[index] [0])
           ,2.0)+pow(z,2.0));
        z2=sqrt(pow(((length/2.0)+tappings-sample[index] [0])
           ,2.0)+pow(z,2.0));
        if ((z1 <= maxdist) || (z2 <= maxdist))
         {
          angle1=cos(((length/2.0)-sample[index] [0])/z1);
          angle2=cos(((length/2.0)+tappings-sample[index] [0])/z2);
          bbc-tab(10,19);
          printf("%5.5f   %5.5f   %5.5f   %5.5f",z1,z2
                 ,(360.0*acos(angle1)/(2.0*pi)),(360.0
                 *acos(angle2)/(2.0*pi)));
          lp1=-0.5*roewater*pow((vwater+vbubble),2.0)
              *(1.0+((pow((bdia/2.0),3.0)/(pow(z1,3.0)))
              *(1.0-3.0*pow(angle1,2.0)))+((pow((bdia/2.0),6.0)
              /(4.0*pow(z1,6.0)))*(1.0+3.0*pow(angle1,2.0))));
          lp2=-0.5*roewater*pow((vwater+vbubble),2.0)
              *(1.0+((pow((bdia/2.0),3.0)/(pow(z2,3.0)))
              *(1.0-3.0*pow(angle2,2.0)))+((pow((bdia/2.0),6.0)
              /(4.0*pow(z2,6.0)))*(1.0+3.0*pow(angle2,2.0))));
          localpress=localpress+(lp1-lp2);
          bbc-tab(10,23);
          printf("%5.5f    %5.5f     %5.5f",lp1,lp2,localpress);
         }
       }
     }
```

```
      }
    }
  }
else
  {
   for (index=0; index<count; index++)
    {
     if ((sample[index] [0] <= ((length/2.0)+tappings+maxdist
          +distance)) && (sample[index] [0] >= ((length/2.0)
          -maxdist+distance)))
      {
       z=sqrt(pow((dpipe/2.0),2.0)+pow(sample[index] [1],2.0)
         - (dpipe*sample[index] [1] * cos(sample[index] [2])));
       if (z <= maxdist)
        {
         z1=sqrt(pow(((length/2.0)+distance-sample[index] [0])
            ,2.0)+pow(z,2.0));
         z2=sqrt(pow(((length/2.0)+tappings+distance-sample[index]
            [0]),2.0)+pow(z,2.0));
         if ((z1 <= maxdist) || (z2 <= maxdist))
          {
           angle1=cos(((length/2.0)+distance-sample[index] [0])/z1);
           angle2=cos(((length/2.0)+tappings+distance
                  -sample[index] [0])/z2);
           lp1=-0.5*roewater*pow((vwater+vbubble),2.0)
               *(1.0+((pow((bdia/2.0),3.0)/(pow(z1,3.0)))
               *(1.0-3.0*pow(angle1,2.0)))+((pow((bdia/2.0),6.0)
               /(4.0*pow(z1,6.0)))*(1.0+3.0*pow(angle1,2.0))));
           lp2=-0.5*roewater*pow((vwater+vbubble),2.0)
               *(1.0+((pow((bdia/2.0),3.0)/(pow(z2,3.0)))
               *(1.0-3.0*pow(angle2,2.0)))+((pow((bdia/2.0),6.0)
               /(4.0*pow(z2,6.0)))*(1.0+3.0*pow(angle2,2.0))));
            localpress=localpress+(lp1-lp2);
          }
        }
      }
    }
  }
 return(localpress/(g*tappings));
}


double vfmeasured(double radius)

{
 int index;
double localvf=0.0;

for (index=0; index<count; index++)
 {
  if (sample[index] [1] > (radius-(0.1*bdia)) && sample[index] [1]
      < (radius+(0.1*bdia)))
   {
    localvf=localvf+(pi*pow(bdia,3.0)/6);
   }
 }
localvf=localvf/((pow((radius+(bdia/2)),2.0)
        -pow((radius-(bdia/2)),2.0))*pi*length);
return(localvf);
```

```
}

void display()

{
 int index,point,divider,sigmax=0;
 double scaledx,scaledy;
 char ch;
 for (index=0; index < samplemax; index++)
 {
  if (fabs(array[index] [0]) > sigmax)
   {
    sigmax = (int) fabs(array[index] [0]);
   }
  if (fabs(array[index] [1]) > sigmax)
   {
    sigmax = (int) fabs(array[index] [1]);
   }
 }
scaledx = 1000.0/samplemax;
scaledy = 400.0/sigmax;
bbc-cls();
box(100,100,1100,900);
grid(100,100,1100,900,4,4);
bbc-move(1100,500);
bbc-draw(100,500);
bbc-gcol(0,1);
divider=samplemax/200;
point=0;
bbc-move(100,500+(int)(array[0] [0]*scaledy));
for (index = 0; index < samplemax; index++)
 {
  bbc-plot(5,100+(int)(index*scaledx),500+(int)(array[index] [0]
          *scaledy));
  if (index%divider == 0)
   {
    plot[point] [0] = index*timint;
    plot[point] [1] = ((double)array[index] [0] - 2048.0)
                      *10.0/(2048.0*fiddle);          /* mm h2o */
    point++;
   }
 }
bbc-move(300,940);
bbc-draw(400,940);
bbc-gcol(0,2);
point=0;
bbc-move(100,500+(int)(array[0] [1]*scaledy));
for (index = 0; index < samplemax; index++)
 {
  bbc-plot(5,100+(int)(index*scaledx),500+(int)(array[index] [1]
          *scaledy));
  if (index%divider == 0)
   {
    plot[point] [2] = ((double)array[index] [1] - 2048.0)
                      *10.0/(2048.0*fiddle);          /* mm h2o */
    point++;
```

```
    }
  }
bbc-move(650,940);
bbc-draw(750,940);
bbc-gcol(0,7);
bbc-tab(1,4);
printf("%3.2f",(sigmax/4096.0));
bbc-tab(8,2);
printf("Signal 'A'");
bbc-tab(27,2);
printf("Signal 'B'");
bbc-tab(1,16);
printf("0.00");
bbc-tab(5,29);
printf("0.0000");
bbc-tab(35,29);
printf("Time");
bbc-tab(64,29);
printf("%6.4f sec",(rlength/1000.0));
bbc-tab(6,31);
printf("Press 'P' RETURN to save data points to file or RETURN to
       continue ");
skipgarb();
ch=toupper(getchar());
if (ch == 'P')
 {
  saveplt(point-1,2);
 }
}

void box(int x1,int y1,int x2,int y2)

{
 bbc-move(x1,y1);
 bbc-draw(x2,y1);
 bbc-draw(x2,y2);
 bbc-draw(x1,y2);
 bbc-draw(x1,y1);
}


void grid(int x1,int y1,int x2,int y2,int xsize,int ysize)

{
 int xspace,yspace,index,index2;

xspace=(x2-x1)/xsize;
yspace=(y2-y1)/ysize;
for (index=x1+xspace; index < x2-xspace/2; index += xspace)
 {
  bbc-move(index,y1);
  for (index2=y1; index2 < y2; index2 += 16)
   {
    bbc-draw(index,index2+8);
    bbc-move(index,index2+16);
   }
 }
for (index=y1+yspace; index < y2-yspace/2; index += yspace)
 {
```

```
    bbc-move(x1,index);
    for (index2=x1; index2 < x2; index2 += 16)
     {
      bbc-draw(index2+8,index);
      bbc-move(index2+16,index);
     }
   }
}


void symbol(int n, int x, int y)

{
 bbc-gcol(0,n);
 bbc-plot(4,x-10,y+10);
 bbc-plot(5,x+10,y-10);
 bbc-plot(4,x+10,y+10);
 bbc-plot(5,x-10,y-10);
}


void skipgarb()

{
 while (getchar() != '\n')
   {
   }
}

char *filename(char path[12])

{
 char buffer[255];
 static char *filenm = ".......................";

 while (strlen(filenm) == 0);
 {
   bbc-tab(18,10);
   printf("Enter filename : ");
   scanf("%24s",filenm);
   skipgarb();
  }
 strcpy(buffer,path);
 strcat(buffer,filenm);
 return (buffer);
}
```

APPENDIX 4 - GENERAL PURPOSE SIGNAL ANALYSIS SOFTWARE

Appendix summary

Contained in this appendix are details of the general purpose signal analysis software written to analyse differential pressure signals generated by both the low average gas void fraction vertical bubbly two-phase flow simulation software and experimental differential pressure signals from the two-phase flow loop.

General purpose signal analysis software

Listed below are the functions written in 'C' used in the signal analysis software and a brief description of each function.

main()	-	Menu display
box()	-	Draws simple border
grid()	-	Generates grid displays on graphs
skipgarb()	-	Input/output keyboard entry routine
correlate()	-	Correlation algorithm used correlate two data arrays stored in memory
record()	-	Records up to three channels of experimental signals simultaneously
load()	-	Loads pre-recorded signals or data generated by the simulation software
save()	-	Save recorded signals to disc
saveplt()	-	Save a plot file for exporting to Harvard Graphics
defaults()	-	Default variable settings display and entry point for variables associated with the performance of the analysis software
display()	-	Signals display menu
disp()	-	Graphical display of up to two signals stored in memory
filter()	-	Digital filter menu
filtfft()	-	Digital filter algorithm

fft()	-	Fast Fourier Transform algorithm
dft()	-	Discrete Fourier Transform menu
rms()	-	Root Mean Squared calculation of a signal stored in memory
crosscorrelation()	-	Signal correlation menu
curs()	-	Moving cursor used to evaluate graphical displaces
calibration()	-	Calibration of pressure transducers and associated amplifiers
pdfunction()	-	Probability Density Function menu
pdf2()	-	PDF evaluation for a signal stored in memory
subtract()	-	Subtraction routine used to subtract two signals stored in memory
*filename()	-	Filename entry point

```
/* -> $.!c.user.c.sig   */
/*  Signal analysis     */
/*        BY            */
/*   A.L.Samways        */

#include <stdio.h>
#include <string.h>
#include <ctype.h>
#include <time.h>
#include <math.h>
#include "bbc.h"
#include "samsio.h"

void box(int,int,int,int);
void grid(int,int,int,int,int,int);
void skipgarb(void);
void correlate(int,int,char*);
void record(void);
void load(void);
void save(void);
void saveplt(int,int);
void defaults(void);
void display(void);
void disp(int,int,int);
void filter(void);
void filtfft(int);
void fft(int,int,char*);
void dft(void);
void rms(void);
void crosscorrelation(void);
void curs(double,double,double,double);
void calibration(void);
void pdfunction(void);
void pdf2(int,char*);
void subtract(void);

char *filename(char*);

int pdf[32769];
int rlength;

double cross [16000];

int array [32769] [6];                    /*  Defaults  */
int samplemax = 4096;
int slot = 3;
int delaymax = 14;
int power=12;
int tdisplace=200;

double ampgain1 = 10.33;
double ampgain2 = 10.33;
double ampgain3 = 10.33;

double Ff[32769] [2];
double plot[240] [8];

char *pathdata = ":0.$.data.";
char *pathplt  = ":0.$.plt.";
```

```
int main()

{                                                    /*  Menu  */
 int true=0;

 char ch,ch2;

 while (true == 0)
  {
   bbc-mode(12);
   bbc-colour(132);
   bbc-cls();
   bbc-cursor(0);
   bbc-tab(0,4);
   printf("                                  Signal Analysis Program\n");
   bbc-move(400,850);
   bbc-draw(770,850);
   bbc-tab(0,7);
   printf("                          Record data from A to D converter
         interface\n");
   printf("                          DIsplay signals\n");
   printf("                          SAve data to disk\n");
   printf("                          Load data from disk\n");
   printf("                          DEfault conditions\n");
   printf("                          Filter signals in memory\n");
   printf("                          Auto scale RMS of the signals in
         memory\n");
   printf("                          SUbtract one signal from another\n");
   printf("                          CRoss correlation of signals\n");
   printf("                          Pdf of signals\n");
   printf("                          DFt\n");
   printf("                          CAlibrate\n");
   box(50,50,1220,975);
   bbc-tab(18,20);
   switch (ch = toupper(getchar()))
    {
     case 'R' : record();
                break;
     case 'S' : ch2 = toupper(getchar());
                if (ch2 == 'A')
                 {
                  save();
                 }
                if (ch2 == 'U')
                 {
                  subtract();
                 }
                break;
     case 'L' : load();
                break;
     case 'D' : ch2 = toupper(getchar());
                if (ch2 == 'E')
                 {
                  defaults();
                 }
                if (ch2 == 'I')
                 {
                  display();
                 }
                if (ch2 == 'F')
```

```
                {
                 dft();
                }
               break;
        case 'F' : filter();
               break;
        case 'A' : rms();
               break;
        case 'C' : ch2 = toupper(getchar());
               if (ch2 == 'R')
                {
                 crosscorrelation();
                }
               if (ch2 == 'A')
                {
                 calibration();
                }
               break;
            case 'P' : pdfunction();
          }
        }
       return (0);
      }


      void record()

      {
       int index,delay,timeint,wast,outofrange=0;
       int adc1=0,adc2=0,adc3=0;
       int *point1,*point2,*point3;

       char ch;

       point1=&adc1;
       point2=&adc2;
       point3=&adc3;
       bbc_cls();
       bbc_tab(31,4);
       printf("Record Signals");
       bbc_move(490,850);
       bbc_draw(710,850);
       box(50,50,1220,975);
       bbc_tab(18,10);
       skipgarb();
       printf("Press RETURN to take %6d samples",samplemax);
       ch=getchar();
       bbc_tab(18,12);
       printf("Sampling started !!!");
       timeint=clock();
       for (index=1;index < samplemax+1;index++)
        {
         adc1=slot;
         for (delay=1;delay < delaymax;delay++)
          {
           wast=clock();
          }
         adc12(point1,point2,point3);
         array[index] [1] =adc1;
         array[index] [2] =adc2;                    /* Test waves */
```

```
  array[index] [3] =adc3;
 /* array[index] [1] = (int) (4090*sin(6.2*30*index/samplemax));
    array[index] [2] = (int) (4090*cos(6.2*30*index/samplemax));
    array[index] [3] =0;        */
 )
timeint=clock()-timeint;
for (index=1;index < samplemax+1;index++)
 {
  if ( array[index] [1] == 0)
   {
    outofrange=1;
   }
  if ( array[index] [1] == 4095)
   {
    outofrange=2;
   }
 if ( array[index] [2] == 0)
  {
   outofrange=3;
  }
 if ( array[index] [2] == 4095)
  {
   outofrange=4;
  }
 if ( array[index] [3] == 0)
  {
   outofrange=5;
  }
 if ( array[index] [3] == 4095)
  {
    outofrange=6;
   }
 }
if ( outofrange != 0)
 {
  bbc-tab(18,18);
  printf("Data out of range Error number %2d",outofrange);
  bbc-tab(18,19);
  printf("(1) Channel 'A' to low");
  bbc-tab(18,20);
  printf("(2) Channel 'A' to high");
  bbc-tab(18,21);
  printf("(3) Channel 'B' to low");
  bbc-tab(18,22);
  printf("(4) Channel 'B' to high");
  bbc-tab(18,23);
  printf("(5) Channel 'C' to low");
   bbc-tab(18,24);
   printf("(6) Channel 'C' to high");
  }
 rlength=timeint*10;
 bbc-tab(18,14);
 printf("time interval = %6d usec",rlength*1000/samplemax);
 bbc-tab(18,16);
 printf("record length = %6d msec",rlength);
 bbc-tab(18,26);
 printf("Press RETURN to continue");
 ch=getchar();
}
```

```
void load()

{
 int index,ncol;

 FILE *fp;

 char comment[255];
 char buff[255];
 char ch;

 bbc-cls();
 bbc-tab(31,4);
 printf("Load from Disk");
 bbc-move(490,850);
 bbc-draw(720,850);
 box(50,50,1220,975);
 if ((fp = fopen (filename(pathdata),"r")) == NULL)
  {
   bbc-tab(18,12);
   printf("File could not be found");
   bbc-tab(18,14);
   printf("Press RETURN to continue");
   ch=getchar();
  }
 else
  {
   bbc-tab(18,12);
   printf("Data loading");
   fscanf(fp,"%[^\n]s ",&comment);
   fscanf(fp,"%d %d %s %s %s %d\n"
         ,&samplemax,&ncol,&buff,&buff,&buff,&rlength);
   for (index=1; index < samplemax+1; index++)
    {
     fscanf(fp,"%d %d %d\n", &array[index] [1], &array[index] [2]
           , &array[index] [3]);
    }
   bbc-tab(18,14);
   printf("Comment : %s",comment);
   bbc-tab(18,20);
   printf("Press RETURN to continue");
   ch=getchar();
   if (fclose (fp) != 0)
    {
     printf("File did not exist !!!\n");
     ch=getchar();
    }
  }
}

void save()

{
 int index,ncol=3;

 FILE *fp;

 char comment[255];
```

```
char ch;

bbc-cls();
bbc-tab(32,4);
printf("Save to Disk");
bbc-move(510,850);
bbc-draw(700,850);
box(50,50,1220,975);
bbc-tab(18,8);
skipgarb();
printf("Enter comment : ");
scanf("%[^\n]s",&comment);
skipgarb();
if ((fp = fopen (filename(pathdata),"w")) == NULL)
 {
  bbc-tab(18,12);
  printf("File could not be found");
  bbc-tab(18,14);
  printf("Press RETURN to continue");
  ch=getchar();
 }
else
 {
  bbc-tab(18,12);
  printf("Data saving");
  fprintf(fp, "%s\n",comment);
  fprintf(fp, "%d %d ""Channel A ""Channel B ""Channel C ""%d \n"
          ,samplemax,ncol,rlength);
  for (index=1; index < samplemax+1; index++)
   {
    fprintf(fp, "%d %d %d\n",array[index] [1], array[index] [2]
           , array[index] [3]);
   }
  if (fclose (fp) != 0)
   {
    printf("File did not exist !!!\n");
    ch=getchar();
   }
 }
}


void saveplt(int points, int n)

{
 int index,index2;

 FILE *fp;

 char comment[255];
 char ch;

 bbc-cls();
 bbc-tab(31,4);
 printf("Save plot data");
 bbc-move(500,850);
 bbc-draw(710,850);
 box(50,50,1220,975);
 bbc-tab(18,8);
 skipgarb();
```

```
printf("Enter comment : ");
scanf("%[↑\n]s",&comment);
skipgarb();
if ((fp - fopen (filename(pathplt),"w")) -- NULL)
 {
  bbc-tab(18,12);
  printf("File could not be found");
  bbc-tab(18,14);
  printf("Press RETURN to continue");
  ch-getchar();
 }
else
 {
  bbc-tab(18,12);
  printf("Data saving");
  fprintf(fp, ",%s\n",comment);
  for (index=0; index <- points; index++)
   {
    fprintf(fp, "%g",plot[index] [0]);
    for (index2=1; index2<=n; index2++)
     {
      fprintf(fp, ",%g",plot[index] [index2]);
     }
    fprintf(fp, "\n");
   }
  index-fclose(fp);
 }
}
void defaults()

{
 char ch;

 bbc-cls();
 bbc-tab(0,4);
 printf("                                    Signal Analysis Defaults\n");
 bbc-move(400,850);
 bbc-draw(770,850);
 bbc-tab(0,7);
 printf("                              Sample interval delay\n");
 printf("                              Number of samples\n");
 printf("                              I/o slot number\n");
 printf("                              Max correlation time delay\n");
 box(50,50,1220,975);
 skipgarb();
 bbc-tab(14,12);
 switch (ch - toupper(getchar()))
  {
   case 'S' : bbc-tab(14,12);
              printf("Present number %d",delaymax);
              bbc-tab(14,14);
              printf("Enter new delay number");
              bbc-tab(14,16);
              skipgarb();
              scanf("%d",&delaymax);
              break;
   case 'N' : bbc-tab(14,12);
              printf("Present number of samples %d",(int)
```

```
                        pow(2,power));
                bbc-tab(14,14);
                printf("Enter new sample 2↑(power) number, (8-15)");
                bbc-tab(14,16);
                skipgarb();
                scanf("%d",&power);
                samplemax=(int) pow(2,power);
                break;
        case 'I' : bbc-tab(14,12);
                printf("Present slot number %d",slot);
                bbc-tab(14,14);
                printf("Enter new slot number");
                bbc-tab(14,16);
                skipgarb();
                scanf("%d",&slot);
                break;
           case 'M' : bbc-tab(14,12);
                printf("Present correlation time delay = %d msec"
                        ,tdisplace);
                bbc-tab(14,14);
                printf("Enter new time delay in msec");
                bbc-tab(14,16);
                skipgarb();
                scanf("%d",&tdisplace);
                break;
      }
    }


    void display()
    {
     char ch;

     bbc-cls();
     bbc-tab(30,4);
     printf("Display signals");
     bbc-move(480,850);
     bbc-draw(715,850);
     bbc-tab(0,7);
     printf("                        A) Channel 'A'\n");
     printf("                        B) Channel 'B'\n");
     printf("                        C) Channel 'C'\n");
     printf("                        D) Channels 'A' & 'B'\n");
     printf("                        E) Channels 'A' , 'B' & 'C'\n");
     printf("                        F) 'B' Subtracted from 'A'\n");
     printf("                        G) 'C' Subtracted from 'B'\n");
     printf("                        H) 'B-A' & 'C-B'\n");
     box(50,50,1220,975);
     bbc-tab(18,18);
     skipgarb();
     switch (ch = toupper(getchar()))
      {
       case 'A' : disp(1,0,0);
                  break;
       case 'B' : disp(2,0,0);
                  break;
       case 'C' : disp(3,0,0);
                  break;
       case 'D' : disp(1,2,0);
```

```
                    break;
      case 'E' : disp(1,2,3);
                    break;
      case 'F' : disp(4,0,0);
                    break;
      case 'G' : disp(5,0,0);
                    break;
      case 'H' : disp(4,5,0);
     }
}


void disp(int chan1, int chan2, int chan3)
{
 static char *title[] =
  {
   "      ",
   " 'A'  ",
   " 'B'  ",
   " 'C'  ",
   " 'A-B'",
   " 'B-A'",
   };

 int index,point,divider,sigmax=0;

 double scaledx,scaledy,fiddle=100.0;

 char ch;

 for (index=1; index < samplemax+1; index++)
  {
   if (( fabs(array[index] [chan1]) > sigmax ) && (chan1 != 0))
    {
     sigmax = (int) fabs(array[index] [chan1]);
    }
   if (( fabs(array[index] [chan2]) > sigmax ) && (chan2 != 0))
    {
     sigmax = (int) fabs(array[index] [chan2]);
    }
   if (( fabs(array[index] [chan3]) > sigmax ) && (chan3 != 0))
    {
     sigmax = (int) fabs(array[index] [chan3]);
    }
  }
 scaledx = 1000.0/samplemax;
 scaledy = 400.0/sigmax;
 bbc-cls();
 box(100,100,1100,900);
 grid(100,100,1100,900,4,4);
 bbc-move(1100,500);
 bbc-draw(100,500);
 divider=samplemax/200;
 if ( chan1 > 0 )
  {
   point=0;
   bbc-gcol(0,1);
   bbc-move(100,500+(int)(array[1] [chan1]*scaledy));
   for (index = 1; index <= samplemax; index++)
```

```
    {
     bbc-plot(5,100-1+(int)(index*scaledx),500+(int)(array[index]
              [chan1]*scaledy));
     if (index%divider == 0)
      {
       plot[point] [0] = (double)index*(double)rlength
                         /(double)samplemax;
       plot[point] [1] = (20.0*ampgain1*(double)array[index]
                         [chan1])/(4096.0*fiddle);      /* mm h2o */
       point++;
      }
    }
  bbc-move(300,940);
   bbc-draw(400,940);
  }
 else
  {
   point=0;
   for (index = 1; index <= samplemax; index++)
    {
     if (index%divider == 0)
      {
       plot[point] [0] = (double)index*(double)rlength
                         /(double)samplemax;
       plot[point] [1] = 0.0;
       point++;
      }
    }
  }
 if ( chan2 > 0 )
 {
  point=0;
  bbc-gcol(0,2);
  bbc-move(100,500+(int)(array[1] [chan2]*scaledy));
  for (index = 1; index <= samplemax; index++)
   {
    bbc-plot(5,100-1+(int)(index*scaledx),500+(int)(array[index]
             [chan2]*scaledy));
    if (index%divider == 0)
     {
      plot[point] [2] = (20.0*ampgain2*(double)array[index]
                        [chan2])/(4096.0*fiddle);      /* mm h2o */
      point++;
     }
   }
  bbc-move(650,940);
  bbc-draw(750,940);
  }
 else
  {
   point=0;
   for (index = 1; index <= samplemax; index++)
    {
     if (index%divider == 0)
      {
       plot[point] [2] = 0.0;
       point++;
      }
    }
  }
```

```
if ( chan3 > 0 )
 {
  point=0;
  bbc-gcol(0,3);
  bbc-move(100,500+(int)(array[1] [chan3]*scaledy));
  for (index = 1; index <= samplemax; index++)
   {
    bbc-plot(5,100-1+(int)(index*scaledx),500+(int)(array[index]
             [chan3]*scaledy));
    if (index%divider == 0)
     {
      plot[point] [3] = (20.0*ampgain3*(double)array[index]
                        [chan3])/(4096.0*fiddle);     /* mm h2o */
      point++;
     }
   }
  bbc-move(1000,940);
  bbc-draw(1100,940);
 }
else
 {
  point=0;
  for (index = 1; index <= samplemax; index++)
   {
    if (index%divider == 0)
     {
      plot[point] [3] = 0.0;
      point++;
     }
   }
 }
bbc-gcol(0,7);
bbc-tab(1,4);
printf("%5.4g",(sigmax*10.0*ampgain1/(fiddle*2048.0)));
bbc-tab(8,2);
printf("Signal%s",title[chan1]);
bbc-tab(27,2);
printf("Signal%s",title[chan2]);
bbc-tab(49,2);
printf("Signal%s",title[chan3]);
bbc-tab(1,16);
printf("0.00");
bbc-tab(5,29);
printf("0.0000");
bbc-tab(35,29);
printf("Time");
bbc-tab(64,29);
printf("%6.4f sec",(rlength/1000.0));
bbc-tab(6,31);
printf("Press 'P' RETURN to save data points to file or RETURN to
        continue ");
skipgarb();
ch-toupper(getchar());
if (ch == 'P')
 {
  saveplt(point-1,3);
 }
}
```

```
void filter()

{
 char ch;

 static char str1[] = "  Fourier Transform of 'A'   ";
 static char str2[] = "  Fourier Transform of 'B'   ";
 static char str3[] = "  Fourier Transform of 'C'   ";
 static char str4[] = "  Fourier Transform of 'A-B'";
 static char str5[] = "  Fourier Transform of 'B-C'";

 int Freq;

 bbc-cls();
 bbc-tab(25,4);
 printf("Digital filtering of signals");
 bbc-move(430,850);
 bbc-draw(800,850);
 bbc-tab(18,8);
 skipgarb();
 printf("Enter Low Pass Filter Frequency (Hz) : ");
 scanf("%4d",&Freq);
 bbc-tab(18,8);
 printf("                                                    ");
 bbc-tab(0,7);
 printf("                    A)  'A'\n");
 printf("                    B)  'B'\n");
 printf("                    C)  'C'\n");
 printf("                    D)  'A-B'\n");
 printf("                    E)  'B-C'\n");
 box(50,50,1220,975);
 bbc-tab(18,18);
 skipgarb();
 switch (ch = toupper(getchar()))
  {
   case 'A' : fft(1,1,str1);
              filtfft(Freq);
              fft(1,-1,str1);
              break;
   case 'B' : fft(2,1,str2);
              filtfft(Freq);
              fft(2,-1,str2);
              break;
   case 'C' : fft(3,1,str3);
              filtfft(Freq);
              fft(3,-1,str3);
              break;
   case 'D' : fft(4,1,str4);
              filtfft(Freq);
              fft(4,-1,str4);
              break;
   case 'E' : fft(5,1,str5);
              filtfft(Freq);
              fft(5,-1,str5);
  }
}


void filtfft(int Freq)
```

```
{
 int index;

 double n=1.0;

 while ( n*1000.0/rlength <= Freq)
  {
   n++;
  }
 for (index=(int) n; index <= samplemax-1; index++)
  {
   Ff[index] [0] = 0.0;
   Ff[index] [1] = 0.0;
  }
}


void dft()

{
 char ch;

 static char str1[] = "  Fourier Transform of 'A'  ";
 static char str2[] = "  Fourier Transform of 'B'  ";
 static char str3[] = "  Fourier Transform of 'C'  ";
 static char str4[] = "  Fourier Transform of 'A-B'";
 static char str5[] = "  Fourier Transform of 'B-C'";

 bbc-cls();
 bbc-tab(25,4);
 printf("Discrete Fourier Transforms");
 bbc-move(410,850);
 bbc-draw(840,850);
 bbc-tab(0,7);
 printf("                          A)  'A'\n");
 printf("                          B)  'B'\n");
 printf("                          C)  'C'\n");
 printf("                          D)  'A-B'\n");
 printf("                          E)  'B-C'\n");
 box(50,50,1220,975);
 bbc-tab(18,18);
 skipgarb();
 switch (ch = toupper(getchar()))
  {
   case 'A' : fft(1,1,str1);
              break;
   case 'B' : fft(2,1,str2);
              break;
   case 'C' : fft(3,1,str3);
              break;
   case 'D' : fft(4,1,str4);
              break;
   case 'E' : fft(5,1,str5);
  }
}


void rms()

{
```

```
int index;
double msqua=0,msqub=0,msquc=0;
double meana=0,meanb=0,meanc=0;
double factorab,factorac;

char ch;

bbc-cls();
bbc-tab(27,4);
printf("Auto Scaling of signals");
bbc-move(440,850);
bbc-draw(790,850);
box(50,50,1220,975);
for (index=1;index < samplemax+1;index++)
 {
  meana=meana+array[index] [1];
  meanb=meanb+array[index] [2];
  meanc=meanc+array[index] [3];
 }
meana=meana/samplemax;
meanb=meanb/samplemax;
meanc=meanc/samplemax;
for (index = 1; index < samplemax+1; index++)
 {
  msqua=msqua+pow((array[index] [1] -meana),2);
  msqub=msqub+pow((array[index] [2] -meanb),2);
  msquc=msquc+pow((array[index] [3] -meanc),2);
 }
msqua=sqrt((msqua/samplemax));
msqub=sqrt((msqub/samplemax));
msquc=sqrt((msquc/samplemax));
if (msqub > 0)
 {
  factorab=msqua/msqub;
 }
else
 {
  factorab = 1;
 }
if (msquc > 0)
 {
  factorac=msqua/msquc;
 }
else
 {
  factorac = 1;
 }
for (index = 1; index < samplemax+1; index++)
 {
  array[index] [1] = (int) ((double)array[index] [1] - meana);
  array[index] [2] = (int) (((double)array[index] [2]
                     - meanb)*factorab);
  array[index] [3] = (int) (((double)array[index] [3]
                     - meanc)*factorac);
 }
bbc-tab(18,8);
printf("rms of 'A' %9f ",msqua);
bbc-tab(18,9);
printf("rms of 'B' %9f ",msqub);
bbc-tab(18,10);
```

```
 printf("rms of 'C' %9f ",msquc);
 bbc-tab(18,12);
 printf("Scaling factor A/B %9f ",factorab);
 bbc-tab(18,13);
 printf("Scaling factor A/C %9f ",factorac);
 bbc-tab(18,16);
 printf("Press RETURN to continue");
 skipgarb();
 ch=getchar();
}


void crosscorrelation()
{
 char ch;

 static char crossstr1[] = "  Cross Correlation of 'A' with 'B'  ";
 static char crossstr2[] = "  Cross Correlation of 'A' with 'C'  ";
 static char crossstr3[] = "Cross Correlation of 'A-B' with 'B-C'";
 static char crossstr4[] = "        Autocorrelation of 'A'       ";
 static char crossstr5[] = "        Autocorrelation of 'B'       ";
 static char crossstr6[] = "        Autocorrelation of 'C'       ";
 static char crossstr7[] = "       Autocorrelation of 'A-B'      ";
 static char crossstr8[] = "       Autocorrelation of 'B-C'      ";
 static char crossstr9[] = "  Cross Correlation of 'B' with 'A'  ";

 bbc-cls();
 bbc-tab(25,4);
 printf("Cross Correlation of signals");
 bbc-move(410,850);
 bbc-draw(840,850);
 bbc-tab(0,7);
 printf("                          A) Correlate 'A' with 'B'\n");
 printf("                          B) Correlate 'A' with 'C'\n");
 printf("                          C) Correlate 'A-B' with 'B-C'\n");
 printf("                          D) Autocorrelation of 'A'\n");
 printf("                          E) Autocorrelation of 'B'\n");
 printf("                          F) Autocorrelation of 'C'\n");
 printf("                          G) Autocorrelation of 'A-B'\n");
 printf("                          H) Autocorrelation of 'B-C'\n");
 printf("                          I) Correlate 'B' with 'A'\n");
 box(50,50,1220,975);
 bbc-tab(18,18);
 skipgarb();
 switch (ch = toupper(getchar()))
  {
 case 'A' : correlate(1,2,crossstr1);
            break;
 case 'B' : correlate(1,3,crossstr2);
            break;
 case 'C' : correlate(4,5,crossstr3);
            break;
 case 'D' : correlate(1,1,crossstr4);
            break;
 case 'E' : correlate(2,2,crossstr5);
            break;
 case 'F' : correlate(3,3,crossstr6);
            break;
 case 'G' : correlate(4,4,crossstr7);
```

```
                    break;
      case 'H' : correlate(5,5,crossstr8);
                    break;
      case 'I' : correlate(2,1,crossstr9);
     }
}


void pdfunction()

{
 char ch;

 static char str1[] = "  Pdf 'A'  ";
 static char str2[] = "  Pdf 'B'  ";
 static char str3[] = "  Pdf 'C'  ";
 static char str4[] = " Pdf 'A-B' ";
 static char str5[] = " Pdf 'B-C' ";

 bbc-cls();
 bbc-tab(25,4);
 printf("Probability Density Functions");
 bbc-move(410,850);
 bbc-draw(840,850);
 bbc-tab(0,7);
 printf("                    A)  'A'\n");
 printf("                    B)  'B'\n");
 printf("                    C)  'C'\n");
 printf("                    D)  'A-B'\n");
 printf("                    E)  'B-C'\n");
 box(50,50,1220,975);
 bbc-tab(18,18);
 skipgarb();
 switch (ch = toupper(getchar()))
  {
   case 'A' : pdf2(1,str1);
              break;
   case 'B' : pdf2(2,str2);
              break;
   case 'C' : pdf2(3,str3);
              break;
   case 'D' : pdf2(4,str4);
              break;
   case 'E' : pdf2(5,str5);
  }
}


void pdf2(int chan, char title[14])

{
 int index,index2,point,index3=0;
 int pda=0,maxx=10000;

 double maxpd=0.0,scaledpd,scaledx,divider,fiddle=100.0;

 char ch;

 bbc-cls();
 bbc-tab(31,4);
```

```
printf("PDF of signals");
bbc-move(490,850);
bbc-draw(720,850);
box(50,50,1220,975);
bbc-tab(18,6);
printf("Calculating :        percent complete");
for (index = -4096; index <= 4096; index+=2)
 {
  bbc-tab(33,6);
  printf("%3.0f",(double) ((index)*100/(2*4096))+50);
  pda=0;
  for (index2 = 1; index2 <= samplemax; index2++)
   {
    if (array[index2] [chan] >= index-1 && array[index2] [chan]
        < index+1)
     {
      pda++;
     }
   }
  pdf[index3] = pda;
  index3++;
  if (pda >= maxpd)
   {
    maxpd=pda;
   }
 }
for (index = 0; index < index3; index++)
 {
  if ((pdf[index] < (0.001*maxpd)) && (pdf[index+1] < (0.001*maxpd))
      && (maxx > (int) fabs(index-(index3/2))))
     {
      maxx = (int) fabs(index-(index3/2));
     }
 }
scaledpd = 800.0/maxpd;
scaledx = 1000.0/(2*maxx);
bbc-cls();
bbc-tab(28,2);
printf("%14s",title);
box(100,100,1100,900);
grid(100,100,1100,900,4,4);
divider=(2*maxx)/200;
point=0;
bbc-gcol(0,1);
bbc-move(100,100+(int)(pdf[(index3/2)-maxx] * scaledpd));
for (index = (index3/2)-maxx; index <= (index3/2)+maxx; index++)
 {
  bbc-plot(5,100+500+(int)((index-(index3/2))*scaledx)
           ,100+(int)(pdf[index] * scaledpd));
  if ((index+(index3/2)) >= (divider*(int)point))
   {
    plot[point] [0] = (double)((index-(index3/2.0))*20
                      *ampgain1/(4096.0*fiddle));     /* mm h2o */
    plot[point] [1] = (double)pdf[index]/samplemax;
    point++;
   }
 }
bbc-gcol(0,7);
bbc-tab(0,3);
printf("%4.3f",maxpd/samplemax);
```

```
bbc-tab(1,28);
printf("0.00");
bbc-tab(35,29);
printf("0.00");
bbc-tab(3,29);
printf("-%5.4f",(double) maxx*20*ampgain1/(4096.0*fiddle));
bbc-tab(66,29);
printf("%5.4f",(double) maxx*20*ampgain1/(4096.0*fiddle));
bbc-tab(6,31);
printf("Press 'P' RETURN to save data points to file or RETURN to
      continue ");
skipgarb();
ch=toupper(getchar());
 if (ch == 'P')
 {
  saveplt(point-1,1);
 }
}

void subtract()

{
 int index,sigmax=0;

 double scaledx,scaledy;

 char ch;

 static char substr1[] = " Signal 'B' subtracted from signal 'A' ";
 static char substr2[] = " Signal 'C' subtracted from signal 'B' ";

 for (index=1; index < samplemax+1; index++)
  {
   array[index] [4] = array[index] [1] - array[index] [2];
   array[index] [5] = array[index] [2] - array[index] [3];
   if ( fabs(array[index] [4]) > sigmax )
    {
     sigmax = (int) fabs(array[index] [4]);
    }
   if ( fabs(array[index] [5]) > sigmax )
    {
     sigmax = (int) fabs(array[index] [5]);
    }
  }
 scaledx = 1000.0/samplemax;
 scaledy = 400.0/sigmax;
 bbc-cls();
 box(100,100,1100,900);
 grid(100,100,1100,900,4,4);
 bbc-move(1100,500);
 bbc-draw(100,500);
 bbc-gcol(0,1);
 bbc-move(100,500+(int)(array[1] [4]*scaledy));
 for (index = 1; index < samplemax+1; index++)
  {
   bbc-draw(100-1+(int)(index*scaledx),500+(int)(array[index]
          [4]*scaledy));
  }
 bbc-gcol(0,7);
```

```
bbc-tab(1,4);
printf("%3.2f",(sigmax/4096.0));
bbc-tab(19,2);
printf("%s",substr1);
bbc-tab(1,16);
printf("0.00");
bbc-tab(5,29);
printf("0.0000");
bbc-tab(35,30);
printf("Time");
bbc-tab(64,29);
printf("%6.4f sec",(rlength/1000.0));
skipgarb();
ch=getchar();
bbc-cls();
box(100,100,1100,900);
grid(100,100,1100,900,4,4);
bbc-move(1100,500);
bbc-draw(100,500);
bbc-gcol(0,1);
bbc-move(100,500+(int)(array[1] [5]*scaledy));
for (index = 1; index < samplemax+1; index++)
 {
  bbc-draw(100-1+(int)(index*scaledx),500+(int)(array[index]
           [5]*scaledy));
 }
bbc-gcol(0,7);
bbc-tab(1,4);
printf("%3.2f",(sigmax/4096.0));
bbc-tab(19,2);
 printf("%s",substr2);
 bbc-tab(1,16);
 printf("0.00");
 bbc-tab(5,29);
 printf("0.0000");
 bbc-tab(35,30);
 printf("Time");
 bbc-tab(64,29);
 printf("%6.4f sec",(rlength/1000.0));
 skipgarb();
 ch=getchar();
}

void correlate(int chan1, int chan2, char title[39])

{
int index,index2,point,divider,Con=100;

double total,auto1,auto2,max=0,scaledx,scaledy;

char ch;

bbc-cls();
bbc-tab(21,4);
printf("%s",title);
bbc-move(375,850);
bbc-draw(875,850);
box(50,50,1220,975);
bbc-tab(18,6);
```

```
printf("Calculating :          percent complete");
for (index=0; index < (int) (samplemax*tdisplace/rlength); index++)
 {
  bbc-tab(33,6);
  printf("%3.0f",(double) (index*100.0*rlength)
        /(samplemax*tdisplace));
  total=0;
  for (index2=1; index2 < (int) ((samplemax-(samplemax*tdisplace
       /rlength))-1); index2++)
   {
    total = total + (Con*(array[index2] [chan1]*array[index+index2]
          [chan2]))/((samplemax-(samplemax*tdisplace/rlength))-1);
   }
  cross[index] = total;
  if ( fabs(total) > max )
   {
    max=fabs(total);
   }
 }
for (index=1; index < (int) ((samplemax-(samplemax*tdisplace
     /rlength))-1); index++)
 {
  auto1 = auto1 + (Con*(array[index] [chan1] * array[index]
        [chan1]))/((samplemax-(samplemax*tdisplace/rlength))-1);
  auto2 = auto2 + (Con*(array[index] [chan2] * array[index]
        [chan2]))/((samplemax-(samplemax*tdisplace/rlength))-1);
 }
if (max == 0)
 {
  max=1;
 }
scaledx=1000.0*rlength/(samplemax*tdisplace);
scaledy=400.0/max;
bbc-cls();
box(100,100,1100,900);
bbc-move(1100,500);
bbc-draw(100,500);
divider=25;
point=0;
index2=0;
bbc-gcol(0,1);
bbc-move(100,500+(int)(cross[1]*scaledy));
for (index = 0; index < (int) (samplemax*tdisplace/rlength); index++)
 {
  bbc-draw(100+(int)(index*scaledx),500+(int)(cross[index]*scaledy));
  if (index2%divider == 0)
   {
    plot[point] [0] = (double)index*rlength
                      /((double)samplemax*1000.0);
    plot[point] [1] = (double)cross[index]/sqrt(auto1*auto2);
    point++;
    bbc-tab(19,2);
    printf("%3d",point);
   }
  index2++;
 }
bbc-gcol(0,7);
bbc-tab(19,2);
printf("%38s",title);
bbc-tab(1,4);
```

```
printf("%3.2f",(max/sqrt(auto1*auto2)));
bbc-tab(1,16);
printf("0.00");
bbc-tab(5,29);
printf("0.0000");
bbc-tab(32,29);
printf("Time shift");
bbc-tab(64,29);
printf("%6.4f sec",rlength*tdisplace/(rlength*1000.0));
grid(100,100,1100,900,4,4);
curs(scaledx,scaledy,auto1,auto2);
bbc-tab(6,31);
printf("Press 'P' RETURN to save data points to file or RETURN to
        continue ");
 skipgarb();
 ch=toupper(getchar());
 if (ch == 'P')
  {
   saveplt(point-1,1);
  }
}


void curs(double scalex, double scaley, double auto1, double auto2)

{
 int index;

 double offset=0.0;

char direction;

index=0;
bbc-gcol(0,2);
bbc-move(100,500+10);
bbc-draw(100,500-10+(int)(cross[index]*scaley));
while (direction != '\r')
 {
  direction = bbc-get();
  if (direction == '.')
   {
    bbc-gcol(0,4);
    if (cross[index] > 10)
     {
      bbc-move(100+(int)(index*scalex),500+10);
      bbc-draw(100+(int)(index*scalex)
               ,500-10+(int)(cross[index]*scaley));
     }
else
 {
  bbc-move(100+(int)(index*scalex),500-10);
  bbc-draw(100+(int)(index*scalex)
           ,500+10+(int)(cross[index]*scaley));
 }
bbc-gcol(0,2);
index++;
if (index > (int)(1000.0/scalex))
 {
  index--;
 }
```

```
if (cross[index] > 10)
 {
  bbc-move(100+(int)(index*scalex),500+10);
  bbc-draw(100+(int)(index*scalex)
           ,500-10+(int)(cross[index]*scaley));
 }
else
 {
  bbc-move(100+(int)(index*scalex),500-10);
  bbc-draw(100+(int)(index*scalex)
           ,500+10+(int)(cross[index]*scaley));
 }
bbc-tab(10,30);
printf("Time %6.5f sec",((double)(index*rlength
      /(1000.0*samplemax)))-offset);
bbc-tab(57,30);
printf("Roe %6.4f",(double)(cross[index]/sqrt(auto1*auto2)));
}
if (direction == ',')
 {
  bbc-gcol(0,4);
  if (cross[index] > 10)
   {
    bbc-move(100+(int)(index*scalex),500+10);
    bbc-draw(100+(int)(index*scalex)
             ,500-10+(int)(cross[index]*scaley));
   }
  else
   {
    bbc-move(100+(int)(index*scalex),500-10);
    bbc-draw(100+(int)(index*scalex)
             ,500+10+(int)(cross[index]*scaley));
   }
  bbc-gcol(0,2);
  index--;
  if (index < 0)
   {
    index++;
   }
  if (cross[index] > 10)
   {
    bbc-move(100+(int)(index*scalex),500+10);
    bbc-draw(100+(int)(index*scalex)
             ,500-10+(int)(cross[index]*scaley));
   }
  else
   {
    bbc-move(100+(int)(index*scalex),500-10);
    bbc-draw(100+(int)(index*scalex)
             ,500+10+(int)(cross[index]*scaley));
   }
  bbc-tab(10,30);
  printf("Time %6.5f sec",((double)(index*rlength
        /(1000.0*samplemax)))-offset);
  bbc-tab(57,30);
  printf("Roe %6.4f",(double)(cross[index]/sqrt(auto1*auto2)));
 }
if (toupper(direction) == 'O')
 {
  offset=(double)(index*rlength/(1000.0*samplemax));
```

```
        bbc-tab(10,30);
        printf("Time %6.5f sec",((double)(index*rlength
              /(1000.0*samplemax)))-offset);
      }
    }
  }


void calibration()

{
 int adc1=0,adc2=0,adc3=0;
 int *point1,*point2,*point3;
 char ok;

 point1=&adc1;
 point2=&adc2;
 point3=&adc3;
 bbc-cls();
 bbc-tab(32,4);
 printf("Calibration");
 bbc-move(490,850);
 bbc-draw(710,850);
 bbc-tab(20,16);
 printf("Press 'RETURN' to return to main menu");
 box(50,50,1220,975);
 skipgarb();
 while (ok != '\n')
  {
   adc1=slot;
   adc12(point1,point2,point3);
   bbc-tab(6,12);
   printf("Channel 1 %5x   Channel 2 %5x     Channel 3 %5x"
         ,adc1,adc2,adc3);
  }
}


void fft(int chan,int s,char title[39])

{
 int index,point,again=1;
 int i=1,j,k,l,m1,n,n1,freq=0;

 double scaledx,scaledy,con,sigmax=0;
 double a,b,sin,cos,s1=0,c1=-1;

 char ch;

 bbc-cls();
 bbc-tab(31,4);
 if (s == 1)
  {
   printf("DFT of signals");
  }
 else
  {
   printf(" Inverse DFT");
  }
```

```
bbc-move(490,850);
bbc-draw(720,850);
box(50,50,1220,975);
bbc-tab(18,6);
printf("Calculating :        percent complete");
if (s == 1)
 {
  for (index=1; index <= samplemax; index++)
   {
    Ff[index-1] [0] = (double) array[index] [chan];
    Ff[index-1] [1] = 0.0;
   }
 }
n=samplemax;
n1=n/2;
i=1;
for (j=1; j <= n-1; j++)
 {
  if (i > j)
   {
    for (l=0; l <= 1; l++)
     {
      a=Ff[i-1] [l];
      Ff[i-1] [l]=Ff[j-1] [l];
      Ff[j-1] [l]=a;
     }
   }
 k=n1;
 while (i > k)
  {
   i-=k;
   k=(int) floor(k/2.0);
  }
 i+=k;
}
n1=1;
c1=-1;
s1=0;
for (m1=1; m1 <= power; m1++)          /* change for dif samplemax */
 {
  bbc-tab(33,6);
  printf("%3.0f",(double) (m1*100/12));
  k=n1;
  n1=2*n1;
  cos=1;
  sin=0;
  for (i=1; i <= k; i++)
  {
   for (j=i-1; j <= n-1; j+=n1)
    {
     l=j+k;
     a=Ff[l] [0]*cos-Ff[l] [1]*sin;
     b=Ff[l] [0]*sin+Ff[l] [1]*cos;
     Ff[l] [0]=Ff[j] [0] - a;
     Ff[l] [1]=Ff[j] [1] - b;
     Ff[j] [0]=Ff[j] [0] + a;
     Ff[j] [1]=Ff[j] [1] + b;
    }
   a=cos*c1-sin*s1;
   sin=sin*c1+cos*s1;
```

```
    cos=a;
   }
  s1=s*sqrt((1-c1)/2);
  c1=sqrt((1+c1)/2);
 }
if (s == 1)
 {
  con = rlength/(1000.0*samplemax);
 }
else
 {
  con = 1000.0/rlength;
 }
for (i = 0; i <= samplemax-1; i++)
 {
  Ff[i] [0] *= con;
  Ff[i] [1] *= con;
 }
if (s == 1)
 {
  while ( again == 1 )
   {
    sigmax = 0;
    for (index=0; index < n; index++)
     {
      if ( fabs(Ff[index] [0]) > sigmax )
       {
        sigmax = fabs(Ff[index] [0]);
       }
      if ( fabs(Ff[index] [1]) > sigmax )
       {
        sigmax = fabs(Ff[index] [1]);
       }
     }
scaledx = 1000.0/n;
scaledy = 400.0/sigmax;
bbc-cls();
box(100,100,1100,900);
bbc-move(1100,500);
bbc-draw(100,500);
grid(100,100,1100,900,4,4);
bbc-gcol(0,1);
bbc-move(100+500,500+(int)(Ff[0] [0]*scaledy));
for (index = 0; index <= n/2; index++)
 {
  bbc-draw(100+500+(int)(index*scaledx),500+(int)(Ff[index]
           [0]*scaledy));
 }
bbc-move(100+500,500+(int)(Ff[0] [0]*scaledy));
for (index = samplemax; index >= samplemax-(n/2); index--)
 {
  bbc-draw(100+500+(int)((index-samplemax)*scaledx)
           ,500+(int)(Ff[index] [0]*scaledy));
 }
bbc-gcol(0,2);
bbc-move(100+500,500+(int)(Ff[0] [1]*scaledy));
for (index = 0; index <= n/2; index++)
 {
  bbc-draw(100+500+(int)(index*scaledx)
           ,500+(int)(Ff[index] [1]*scaledy));
```

```
 }
bbc-move(100+500,500+(int)(Ff[0] [1]*scaledy));
for (index = samplemax; index >= samplemax-(n/2); index--)
 {
  bbc-draw(100+500+(int)((index-samplemax)*scaledx)
           ,500+(int)(Ff[index] [1]*scaledy));
 }
bbc-gcol(0,7);
bbc-tab(19,1);
printf("%38s",title);
bbc-tab(0,3);
printf("%4.3f",sigmax);
bbc-tab(8,2);
printf("    real                    imag ");
bbc-move(300,940);
bbc-gcol(0,1);
bbc-draw(400,940);
bbc-move(650,940);
bbc-gcol(0,2);
bbc-draw(750,940);
bbc-gcol(0,7);
bbc-tab(0,16);
printf("0.00");
bbc-tab(36,29);
printf("0.0");
bbc-tab(34,30);
printf("Frequency");
bbc-tab(64,29);
printf("%5.2f Hz",(1000.0*n/(rlength*2.0)));
bbc-tab(0,29);
printf("-%5.2f Hz",(1000.0*n/(rlength*2.0)));
bbc-tab(6,31);
printf("Press 'P' RETURN to save data points to file or RETURN
       to continue ");
skipgarb();
ch=toupper(getchar());
if (ch == 'P')
 {
  saveplt(point-1,3);
 }
bbc-cls();
n=1;
bbc-tab(18,8);
printf("Enter Highest Frequency (Hz) or '0' to exit : ");
scanf("%d",&freq);
if ( freq == 0 )
 {
  again = 0;
 }
else
 {
  while ( n*1000/(2*rlength) <= freq )
   {
    n++;
   }
 }
}
else
 {
```

```
    for (index=0; index < samplemax; index++)
     {
      array[index+1] [chan] = (int) Ff[index] [0];
     }
   }
}


void box(int x1,int y1,int x2,int y2)

{
 bbc-move(x1,y1);
 bbc-draw(x2,y1);
 bbc-draw(x2,y2);
 bbc-draw(x1,y2);
 bbc-draw(x1,y1);
}


void grid(int x1,int y1,int x2,int y2,int xsize,int ysize)

{
 int xspace,yspace,index,index2;

 xspace=(x2-x1)/xsize;
 yspace=(y2-y1)/ysize;
 for (index=x1+xspace; index < x2-xspace/2; index += xspace)
  {
   bbc-move(index,y1);
   for (index2=y1; index2 < y2; index2 += 16)
    {
     bbc-draw(index,index2+8);
     bbc-move(index,index2+16);
    }
  }
 for (index=y1+yspace; index < y2-yspace/2; index += yspace)
  {
   bbc-move(x1,index);
   for (index2=x1; index2 < x2; index2 += 16)
    {
     bbc-draw(index2+8,index);
     bbc-move(index2+16,index);
    }
  }
}


void skipgarb()

{
 while (getchar() != '\n')
  {
  }
}


char *filename(char path[12])

{
 char buffer[255];
```

```
 static char *filenm = ".........................";

 while (strlen(filenm) == 0);
  {
   bbc-tab(18,10);
   printf("Enter filename : ");
   scanf("%24s",filenm);
   skipgarb();
  }
 strcpy(buffer,path);
 strcat(buffer,filenm);
 return (buffer);
}
```

LIST OF REFERENCES

Anderson J.L. & Quinn J.A. (1970) Chem. Eng. Sci., Vol 25, pp 373

Aziz K., Govier G.W., & Fogarazi M. (1972) Pressure drop in wells producing oil and gas. The J. of Canadian petroleum, July-September 1972, pp 38-44

Bajpai A.C., Calus I.M. & Fairley J.A. (1978) Statistical methods for engineers and scientists. John Wiley & Sons, Chichester, ISBN 0-47199-644-0

Beck M.S., Green R.G., Hammer E.A., & Thorn R. (1983) On-line multi-component flow measurement. IMC Aberdeen, Instrumentation and control in the offshore oil industry, May 1983

Beck M.S. & Plaskowski A. (1987) Cross correlation flowmeters, their design and application. Adam Hilger, Bristol, ISBN 0-85274-532-X

Bergeles A.E., Lopina R.F., & Fiori M.P. (1967) Critical heat-flux and flow-pattern observations for low-pressure water flowing in tubes. J. Heat Transfer, Vol. 89, pp 69-74

Bergeles A.E. (1969) Two-phase flow structure observations for high pressure water in a rod bundle. Proc. ASME Symp. Two-phase Flow Heat Transfer in Rod Bundles, pp 47-55

Bernier R.J.N. (1981) Unsteady two-phase flow instrumentation and measurement. Report No. E200.4, Division of engineering and applied science, California Institute of Technology

Bradbury L.J.S. (1988) An introduction to the structure of multiphase flows with comments on flows and flow measurement in wellbores. Un-published seminar notes, Schlumberger Cambridge Research, Cambridge

British Standard 1042 (1981) Fluid flow in closed conduits. Part 1, Section 1.1 Orifice plates, nozzles and venturi tube inserted in circular cross-section conduits running full

Butler S.F.J. (1953) Sphere theorem. Proc. Camb. Phil. Soc., No. 49, pp 169-174

Butterfield M.H., Bryant G.F., & Dowsing J. (1961) A new method of strip-speed measurement using a random waveform correlator. Trans. Soc. Instrum. Technology, Vol. 13, pp 111

Clift R., Grace J.R., & Weber M.E. (1978) Bubbles, Drops and Particles. Academic press, New York

Delhaye J.M. & Chevrier C. (1966) The use of resistivity probes for the measurement of local void fraction in two-phase flow. Centre d'Etrudes Nucleaires, de Grenoble, Rep. No. C.E.W. TT - 70

Delhaye J.M. (1969) Hot-film anemometry in two-phase flow. Proc. 11th National ASME/AIChE Heat Transfer Conf. on Two-phase flow instrumentation, Minneapolis, pp 58-69

Denton P. (1987) Schlumberger Cambridge Research internal report

Douglas J.F., Gasiorek J.M., & Swaffield J.A. (1979) Fluid Mechanics. Pitman Books Ltd., London,, ISBN 0-27300-462-X

Farrar B. (1988) Hot-film anemometry in dispersed oil-water flows. Ph.D. Thesis, University of Bradford

Farrar B. & Bruun H.H. (1989) Interaction effects between a cylindrical hot-film anemometer probe and bubbles in air/water and oil water flows. J. Phys. E: Sci. Instruments, Vol. 22, pp 114-123

Govier G.W., Radford B.A., & Dunn J.S.C. (1957) Can. J. Chem. Eng., Vol 35, pp 58

Govier G.W. & Aziz K. (1972) The flow of complex mixtures in pipes. Van Norstrand Reinhold, New York, ISBN 0-88275-547-1

Hammer E.A. (1983) Three component flow measurement in oil/gas/water mixtures using capacitance transducers. Ph.D. Thesis, University of Manchester

Hammer E.A. & **Green R.G.** (1982) The spatial filtering effect of capacitance transducer electrodes. J. Phys. E: Sci. Instruments, Vol. 16, pp 438-443

Harmathay T.J. (1960) Velocity of large drops and bubbles in media of infinite or restricted extent. A.I.Ch.E., Journal No. 6, pp 281

Hewitt G.F. (1978) Meausurement of two phase flow parameters. Academic Press, London

Hewitt G.F. (1986) Flow visualisation. Seminar, School of Mechanical Eng., Exeter University

Hsu Y.Y., Simon F.F., & Graham R.W. (1963) Applications of hot-wire anemometry for two-phase flow measurements such as void fraction and slip velocity. Proc. ASME Multiphase Flow Symp., Philadelphia, pp 26-34

Hunt A. (1986) Deviated gas-liquid flows. paper presented at a seminar on two phase flow and mixing. University of Cambridge, December 1986

Hunt A. (1987) The venturi meter - theory. Report prepared for Schlumberger Cambridge Research, Cambridge

Inoue K. (1983) Pattern recognition approach to human sleep EEG analysis determination of sleep stages. Thesis Kyushu University

Johnson M.A. & **Abou-sabe A.H.** (1952) Heat transfer and pressure drop for turbulent flow of air-water mixtures in a horizontal pipe. Transactions of the ASME, August 1952, pp 977-985

Jones O.C. & **Zuber N.** (1975) The interrelation between void fraction fluctuations and flow patterns in two-phase flow. Int. J. of Multiphase flow, Vol. 2, pp 273-306

Kashap R.L. (1978) Optimal feature selection and decision rules in classification problems with time series. IEE Trans., Vol. IT-24, No. 3, pp 281

Kashiwagi H. (1973) Flow velocity measurement by use of correlation techniques. Kumamoto University, Report No. XIX(i), pp 1-26

King C.H., Ouyang B.S., & Wank Y.W. (1988) Identification of two-phase flow regimes by an optimum modeling method. Nuclear Technology, Vol. 82, pp 211-226

Kondic N.N. & Hahn D.J. (1970) Theory and application of the parallel and diverging radiation beam method in two-phase systems. 4th Int. Heat Transfer Conf., Paris

Kytomaa H.K. (1987) Stability of the structure in multicomponent flows. Dept. of Applied Sci., California Institute of Technology, Report No. 200.24

Lamb H. (1932) Hydrodynamics. Dover publications inc., New York

Lance M. & Bataille J. (1991) Turbulence in the liquid phase of a uniform bubbly air/water flow. J. of Fluid Mechanics, Vol. 222, pp 99-118

Lighthill M.J. & Whitham G.B. (1955) On Kinematic Waves II. A theory of traffic flow on long crowded roads. Proc. Roy. Soc., Vol. 229A, pp 317-345

Lubbesmeyer D. & Leoni B. (1983) Fluid-velocity measurements and flow-pattern identification by noise-analysis of light-beam signals. Int. J. of Multiphase flow, Vol. 9, No. 6, pp 665-679

Lucas G.P. (1987) The measurement of two-phase flow parameters in vertical and deviated flows. Ph.D. Thesis, University of Manchester

Massey B.S. (1968) Mechanics of fluids. Van Norstrand Reinhold, London, ISBN 0-27800-047-9

Matthes W., Riebold W., & deCooman E. (1970) Measurement of the velocity of gas bubbles in water by a correlation method. Review of Scientific Instruments, Vol. 4, No. 6, pp 843-845

Matsui G. (1984) Identification of flow regimes in vertical gas-liquid two-phase flow using differential pressure fluctuations. Int. J. of Multiphase flow, Vol. 10, No. 6, pp 711-720

Matsui G., Aizawa T., & Kumazawa T. (1987) Statistical characteristics of differential pressure fluctuations and flow patterns of gas/liquid two-phase flow in an inclined pipe. Proc. ASME/JSME thermal Eng. Joint Conf., Honolulu Hawii, pp 397-402

Milne-Thomson L.M. (1960) Theoretical Hydrodynamics. 4th Edition, MacMillan & Co Ltd., London

Moore D.W. (1963) The boundary layer on a spherical gas bubble. J. Fluid Mechanics, Vol. 16, pp 161-176

Nishikawa K., Sekoguchi K., & Fukano T. (1969) On the pulsation phenonmena in gas-liquid two-phase flow. Bulletin of JSME, Vol. 12, No. 54, pp 1410-1416

Olszowski S.T., Coulthard J., & Sayles R.S. (1976) Meausurement of dispersed two-phase gas-liquid flow by cross correlation of modulated ultrasonic signals. Int. J. of Multiphase flow, Vol. 2, pp 537-548

Ong K.H. (1975) Hydraulic flow measurement using ultrasonic transducers and correlation techniques. Ph.D. Thesis, University of Bradford

Peebles F.N. & Garber H.S. (1953) Chem. Eng. Progress report No. 49/88

Petrick M. & Swanson B.S. (1958) Radiation attenuation method of measuring the density of a two-phase fluid. The Review of Sci. Instruments, Vol. 29(12), pp 1079-1085

Petrick M. (1962) A study of vapour carry-under and associated problems. Argonne National Laboratories, Report No. ANL 6581, A.I.Ch.E. Journal 9, pp 253

Saffman P.G. (1956) On the rise of small air bubbles in water. J. Fluid Mechanics, Vol. 1, pp 249-275

Sekoguch K., Inoue K., & Imasaka T. (1987) Void signal analysis and gas-liquid two-phase flow regime determination by a statistical pattern recognition method. Bulletin of JSME, Vol. 30, No. 266, pp 1266-1273

Serizawa A., Kataoka I., & Mishigoshi I. (1975) Turbulence structure of air-water bubbly flow. Int. J. Multiphase Flow, Vol 2, pp 221

Shearer C.J. & Nedderman R.M. (1965) Chem. Eng. Sci., Vol. 20, pp 671

Shu M.T., Weinberger C.B., & Young H.L. (1982) A simple capacitance sensor for void fraction measurements in two-phase flow. Ind. Eng. Chem. Fonda., Vol. 21, pp 175-181

Shulman H.L. & Molstad M.C. (1950) Ind. Eng. Chem., Vol. 42, pp 1058

Siemes W. & Kaufmann J.F. (1954) Chem. Eng. Sci., Vol. 5, pp 127-139

Smith A.V. (1985) A fast response multi-beam X-ray absorption technique for identifying phase distributions during steam-water blowdowns. J. Br. Nucl. Energy Soc., Vol. 14, pp 227-235

Tutu N.K. (1982) Pressure fluctuations and flow pattern recognition in vertical two phase gas-liquid flows. Int. J. of Multiphase flow, Vol. 8, No. 4, pp 443-447

Wallis G.B. (1969) One-dimensional two-phase flow. McGraw-Hill Book Co., New York

Wang Y.W., King C.H., & Pei B.S. (1988) Identification of two-phase flow patterns by a single void fraction sensor. Nuclear Technology, Vol. 83, pp 56-64

Ward-Smith A.J. (1980) Internal fluid flow: The fluid dynamics of flow in pipes and ducts. Oxford University press

Xu L.A. (1986) A pulsed ultrasound cross correlation system for velocity measurement in two-component fluids. Ph.D. Thesis, University of Manchester

Yip K.C., Venart J.E.S., & Govier G.W. (1970) Can. J. Chem. Eng., Vol. 48, pp 229

Zuber N. & Findlay J.A. (1965) Average volumetric concentration in two-phase flow systems. Journal of Heat Transfer, November 1965, pp 453-468

Hadamard M.J. (1911) Compt. Rend. Hebd. Seances Acad. Sci., Paris Vol. 152, pp 1735

van Krevelen D.W. & Hoftijzer P.J. (1950) Chem. Eng. Progress, Vol. 46, pp 29

Lance M., Bataille J., & Marie' (1992) Personal communication, Laboratorire de Mecanique des Fluides et d'Acoustique, Lyon

Ryskin G. & Leal L.G. (1985) Numerical solution of free-boundary problems in fluid mechanics. J. of Fluid Mechanics, Vol. 148, pp 1-43

Whitehead L.G, Win L.Y., & Waters M.H.L. (1951) Contracting ducts of finite length. Aeronautical Quarterly, Vol. 2, pt. 4, pp 254-271